



PROCEEDINGS OF THE 3rd INTERNATIONAL
HEAT FLOW CALORIMETRY SYMPOSIUM
FOR ENERGETIC MATERIALS

8th – 11th April, 2002

FRENCH LICK SPRINGS RESORT
FRENCH LICK, INDIANA, USA

Approved for Public Release: Distribution is Unlimited

TABLE OF CONTENTS

TABLE OF CONTENTS	i - iii
PERFACE	v
OVERVIEW OF UK INITIATIVES TO ENHANCE THE WHOLE LIFE ASSESSMENT AND SURVEILLANCE POLICIES FOR MUNITIONS	A1 – A9
P. BARNES	
REVIEW OF PREVIOUS WORKSHOPS ON THE HEAT FLOW CALORIMETRY OF ENERGETIC MATERIALS	B1 – B5
T. GRIFFITHS	
ASSESSMENT OF THE BALLISTIC SERVICE LIFETIME OF A SMALL CALIBER CARTRIDGE BY HEAT FLOW CALORIMETRY	C1 – C29
U. TICMANIS, P. GUILLAUME	
A REPORT ON THE ACCIDENTAL EXPLOSION OF 7.7 TONS OF SMOKELESS POWDERS DURING STORAGE	D1 – D6
J. KIMURA	
APPLICATIONS OF HFC TO EXPLOSIVES, A UK PROSPECTIVE	E1 – E8
C. BAKER, N. TURNER, P. BUNYAN	
IS HEAT FLOW CALORIMETRY THE ULTIMATE METHOD TO DETECT (ALL) STABILITY & COMPATIBILITY RELATED PROBLEMS IN PROPELLANTS?	F1 - F 13
B. VOGELSANGER, R. SOPRANETTI	
THERMAL AND CHEMICAL ANALYSES OF SILICONE POLYMERS FOR COMPONENT ENGINEERING LIFETIME ASSESSMENTS	G1 – G6
R. MAXWELL, B. BALAZS	
COMBINED USE OF ADIABATIC CALORIMETRY AND MICRO- CALORIMETRY FOR QUANTIFYING PROPELLANT COOK-OFF HAZARDS	H1 – H10
P. BUNYAN, T. GRIFFITHS, V. NORRIS	

EVALUATION OF A NEW HIGH-PRESSURE MANIFOLD AND VESSELS FOR A CALVET MICRO-CALORIMETER	II – II4
D. JONES	
A NOVEL MULTI-CHANNEL MICROCALORIMETER FOR LARGE- SCALE STABILITY TESTING OF PROPELLANTS	J1 – J12
L. SVENSSON, J. SUURKUUSK, L. PAULSSON	
HEAT FLOW CALORIMETRY ON OLD 155 MM PROPELLANT CHARGES	K1 - K 10
W. DE KLERK	
SAMPLE GEOMETRY AS CRITICAL FACTOR FOR STABILITY RESEARCH	L1 – L13
W. DE KLERK	
UNDERSTANDING THE TRUE DRIVING FORCE IN THE AUTO-IGNITION OF SINGLE AND DOUBLE BASED PROPELLANTS USING MICRO-CALORIMETRY	M1 – M17
D. ELLISON, A. CHIN	
MECHANISTIC APPROACH TO STUDY THE MOISTURE AND ACIDITY EFFECT ON THE STABILITY OF SINGLE AND DOUBLE BASED PROPELLANTS	N1 – N14
A. CHIN, D. ELLISON	
STABILITY STUDIES OF RED PHOSPHORUS USING HEAT FLOW CALORIMETRY	O1 – O10
T. GRIFFITHS	
THE USE OF DIFFERENTIAL SCANNING CALORIMETRY IN THE ANALYSIS OF PE AS A BURN RATE MODIFIER	P1 – P11
J. DOMANICO	
STUDIES ON THE AGING OF MAGNESIUM PYROTECHNIC COMPOSITIONS CONTAINING POTASSIUM NITRATE USING ISOTHERMAL HEAT FLOW CALORIMETRY & THERMAL ANALYSIS TECHNIQUES	Q1 – Q12
E. CHARSLEY	

THIS PAGE LEFT INTENTIONAL BLANK

STABILITY AND AGING ASSESSMENT OF ROCKET PROPELLANT FORMULATION BATCHES WITH HIGH BURNING RATES	R1 – R15
M. BOHN	
A COMPARISON STUDY ON DECOMPOSITION OF LIQUID NITRATE ESTERS WITH MICRO-CALORIMETER AND CHEMILUMINESCENCE ANALYZER	S1 – S7
J. KIMURA	
HEAT FLOW CALORIMETRY, A TECHNIQUE FOR DETERMINING PROPELLANT STABILITY	T1 – T11
D. WOOD, N. TURNER, R. JEFFREY	
A MICRO-CALORIMETRIC STUDY OF OXIDATION OF POLYBUTADIENES USED IN COMPOSITE PROPELLANTS	U1 – U25
W. BRYANT, G. HUIE, C. PAPPAS	
USES OF CALORIMETRY IN SCALE-UP OF ENERGETIC MATERIALS PROCESSING	V1 – V13
M. LESLEY	
KINETICS OF THE SOLID-SOLID PHASE TRANSITION OF HMX	W1 – W14
R. WEESE, J. MAIENSCHN, C. PERRINO	
MICRO-CALORIMETRIC METHOD TO DETERMINE THE CORROSION RATE OF LIQUID PROPELLANT ON METAL CONTAINERS	X1 – X13
H. FARMER, A. CHIN, D. ELLISON	
THE SUPER SCALE CALORIMETER	Y1 – Y9
D. SHERFICK, S. BACKER	
THE STATUS OF THE HFC STANAG	Z1 – Z18
U. TICMANIS, P. GUILLAUME, S. WILKER, W. DE KERK	
LIST OF ATTENDEES	

THIS PAGE LEFT INTENTIONAL BLANK

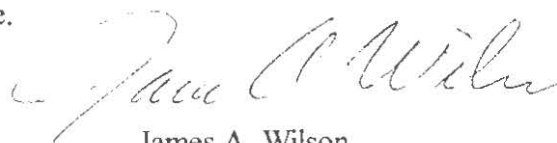
PERFACE

This document is a compilation of the papers presented at the 3rd International Heat Flow Calorimetry Symposium on Energetic Materials which was conducted between the 8th and 11th of April 2002. This meeting was held at the French Lick Springs Resort, French Lick Indiana. The Symposium was organized and sponsored by the Test and Evaluation Branch of the Ordnance Directorate of the Naval Surface Warfare Center, Crane Division. The Symposium was attended by 70 delegates, representing 14 countries and presenting 26 papers. The attendees represented numerous government facilities and laboratories, manufacturers of energetic materials, members of academia and calorimetry manufacturers.

The need to re-schedule the symposium after the events of September 11 represented an extremely critical risk to the very existence of the French Lick meeting. The planning and execution of any meeting requires the work of a great many people, doing it twice require not only work but a great deal of patience from all involved. For this reason there are a number of people I must thank. First and foremost amount this group is the unstinting support of Mr. David Schulte (NSWC Code 40 Director) who was absolutely key to the eventual success of the meeting. His support, both verbal and financial, ultimately lead to the successful meeting in April. Other individuals I would like to thank are Mr. Steve Turpen (Code 405) for his leadership and confidence in the plans once made, Mr. David Sherfick who took on the responsibility of co-chairman and financial lead after my retirement, Mrs. Nancey Meagerlein for her consistent support and innovative ideas, and Dr. Anton Chin for keeping my spirits up and my eyes on the goal.

On behalf of all of the NSWC Crane and SAIC personnel who worked on the symposium, we would like to thank all of the session chairmen and all of the authors who presented their technical papers. Their sharing of expertise and laboratory results made this meeting a significant technical event.

Finally, I would thank all of the non-presenting delegates; it is your participation that makes this type of meeting possible.



James A. Wilson
Symposium Co- Chairman

THIS PAGE LEFT INTENTIONAL BLANK

OVERVIEW OF UK INITIATIVES TO ENHANCE THE WHOLE LIFE ASSESSMENT AND SURVEILLANCE POLICIES FOR MUNITIONS

Peter Barnes

**Defence Ordnance Safety Group
UK MoD
DPA
Abbey Wood, Bristol**

Abstract

This paper summarises the reasons why current munition whole life assessment (WLA) policies and procedures have not been cost effective but then concentrates on ways to improve the situation.

Central to all the initiatives to improve WLA procedures is the use and application of intelligent data, especially the increasing amount of data that is now available to help predict more accurately the end of service life of munitions.

This paper is divided into three main parts. In the first part ways that intelligent data can be used to reduce the uncertainty in current WLA policies and procedures are explained. The consequence of this uncertainty has led to current procedures being slow, expensive and inefficient.

In the second part of the paper emphasis is placed on what added value can thermal analysis techniques and in particular heat flow calorimetry add value to the intelligent data required to predict more accurately the end of service of munitions.

In the third part the recognition that several other technical initiatives are also currently in existence, which in an ever changing world, can significantly effect the total cost of ownership of munitions is also made. The need for improved communications and collaboration between all the WLA stakeholder groups, including the munition manufacturers, to improve the current situation is also emphasised.

Introduction

The theme for this paper is the collection, processing, interpretation and use of intelligent data by competent staff to help develop a new approach to the whole life assessment of munitions.

For this paper intelligent data is defined as data that should be measured or used, instead of what **has been** traditionally measured because it can be. Much of the traditional data **collected** may be of relatively little importance with respect to the important failure mechanisms occurring in munitions. As with many aspects of life the danger is of being swamped by a mass of irrelevant data/information. What is needed is to be able to determine what data is important, and in the case of munitions' lives, what is critical to determining accurately the end of their safe in-service lives.

This paper follows on from the one presented at the last Parari conference in which the problems associated with the MoD not getting best value from the service lives of their munitions were highlighted.

The reasons highlighted for this situation, expressed in terms of science, tools and policy, are tabulated in Table 1 and described in the next section 'basis for the current whole life assessment policies' of this paper. The consequences of the current approach can be summarised as;

- Conservative
- Safe
- Serviceable munitions are destroyed
- Logistical problems are generated
- High reprovisioning (£4.4 Bn over 10 years) cost

In order to provide a central forum for discussion of WLA of munition issues the Munitions Life Assessment Steering Group (MLASG) was established under the chairmanship of DOSG in 1998. The review of the current policies and the proposed new approach to life assessment are two of the deliverables from the MLASG.

Basis for Current Whole Life Assessment Policies

The service life of a munition is controlled by the effects of the environments that the munition is exposed to during its service life, including storage, transportation and operational use. Degradation processes in munitions can be driven by climatic environments, especially temperature for energetic material components, or by mechanical environments, such as fatigue induced by vibration.

In order to predict the life of a munition the most likely failure mode must be established and the munition be tested in such a way that the failure mode is accelerated, in a quantitative way, and the ability of the munition to survive the likely service life is established.

If it is assumed that a temperature sensitive process is the rate-determining step of the likely failure mode, then the munition can be subjected to temperatures higher than those it will (normally) experience in service. Then the rate of reaction can be compared with that expected at the normal service temperatures using a number of thermal models such as Arrhenius, the Berthelot or the Eyring relationships. However there can be problems when using such accelerated ageing techniques. Different failure mechanisms may predominate at different temperatures and the quantitative acceleration of one particular failure mode may result in a completely different mechanism predominating.

Accelerated ageing trials are normally undertaken as part of the Safety and Suitability for Service (S³) testing (or type qualification) of the munition. In calculating the amount of accelerated ageing needed to validate the service life of a munition, two major assumptions are made:

- The expected failure mechanism

- The environments (in particular the temperature) that the munition would experience over the whole of its service life

With the run-down in scientific support, both within MoD and in the UK explosives industry, it has become increasingly difficult to characterise energetic materials sufficiently well for their failure modes to be quantitatively described. In these circumstances, the failure mechanism assumed has had to be a conservative assumption and so long accelerated ageing trials have become the norm. Unless good baseline data is made available then there is no chance of the WLA programmes being optimised. Too often basic important baseline testing such as energetic material characterisation and compatibility testing is either omitted or carried out inadequately.

Over the past 10 to 15 years there has been an increasing move to world-wide deployment of munitions. The environments that munitions now are exposed to varies from good ventilated storage to temporary unventilated storage or exposure to direct solar radiation. Experience has shown that the majority of munitions see environmental conditions less extreme than predicted but some see the extremes of climatic conditions. Extreme environmental conditions are used for designing and qualification testing of munitions.

In addition it should also be recognised that currently manufacturers will design a munition to pass qualification tests, rather than to optimise the life of the munition. On the other hand manufacturers often claim that they are excluded from results and data from the service use of their munitions.

The Solution; A new approach to WLA of munitions

The above section has identified three technical issues, in which the collection and use of non-intelligent data make our current life assessment process slow, expensive and inefficient, these are:

- Uncertainty about actual service environments experienced by individual munitions
- Uncertainty about real life failure modes
- Uncertainty about the acceleration of failure mechanisms

One of the major outcomes from the MLASG is to propose a fundamental change to the way the assessment of munition life is conducted to overcome those uncertainties by the use of intelligent data.

The basis of the proposal is that the S³ assessment should only have a limited accelerated ageing stage, and that the continuing S³ should be confirmed during the service life by means of rigorous in-service surveillance (ISS). This does not mean that munitions would be procured against a requirement of limited life. The contract should still specify the expected service life required by the Equipment Capability Manager. (eg expected 25 years minimum 10 years), but the validation of that life will take place over the course of the service life.

The ISS would include the provision of intelligent data on the temperatures actually seen by the munitions in their service life, as recorded by data loggers. For large,

costly items, such as Guided Missiles, this may be data collected for individual missiles but for cheaper, smaller items, such as small arms ammunition, this may be records of where and when boxes have been at specific locations together with measured temperature data for those locations.

To date despite limited applications the use of data logger temperature data has enabled DOSG to approve the continued use of a number of missiles deployed in the Middle East for which by conventional procedures their lives would have been exceeded.

So the use of logged temperature data has already overcome the use of uncertainty about the service environments. The extension of data loggers to measure humidity and shock and vibration should be encouraged.

The uncertainty about real life failure modes and about acceleration of failure mechanisms will be addressed by the introduction of more vigorous ISS programmes, based on the provision of good baseline data. ISS will involve the breakdown of munitions for chemical/physical/mechanical analysis of the energetic materials. This will enable the monitoring of the properties of the energetic materials when exposed to the (known) in-service environment. In this way the actual failure mechanisms can be accurately monitored and the validity of accelerated ageing can be confirmed.

The number of assets to be destructively tested can be reduced by the use of newer testing techniques which require only very small amounts of energetic material. Therefore maximum information can be obtained from the sectioning of fewer assets than at present. Further reduction of assets lost by destructive testing can be made by the application of non-destructive evaluation (NDE). Coupling NDE with intelligent data of the in-service environment that individual munitions see will enable testing to be carried out 'as required' rather than 'as scheduled' on the most critical assets.

Three testing techniques have been identified, from discussions within MLASG, as potential winners for 'pull through' from research tools in the UK to standard surveillance test techniques, these are the previously mentioned advances in NDE and automatic data logging as well as heat flow calorimetry. These techniques are included in the list of surveillance test methods shown in Table 2.

It must not be forgotten that thermally driven processes are not the only way that munitions age. Vibration induced fatigue can also produce failures in the integrity of energetic (and non-energetic) components of munitions and other mechanical or thermal or thermo-mechanical stressing can result in sudden failure, for example the cracking of warhead high explosive payloads.

Surveillance programmes should, therefore, include as appropriate, some stressing (both thermal and mechanical) on naturally aged munitions to ensure that the S³ will continue for a defined period. This will be particularly important for munitions that will be exposed to high levels of vibration (eg on the wing of an aircraft or in a tracked vehicle). There is the need to define a known life in that environment (eg the number of air carriage hours or number of kilometres for carriage in tracked vehicles).

It is also important to remember that good asset management and tracking is vital to ensure that the lives of munitions are maximised and the life assessment process is optimised. Introduction of data logging and better ISS will improve the ability to optimise munition life, but for the full benefits to be realised, it is vital to know where our munitions are and where they have been. The use of devices such as Radio Frequency Identification Tags can be applied to all natures of defence materiel. WLA munition stakeholders could benefit significantly by 'piggy backing' on developments in other MoD programmes or related industries with asset management problems.

A list of the benefits from the enhanced approach to the WLA of munitions is shown in Table 3.

The role of thermal analysis techniques and particularly heat flow calorimetry

Heat flow calorimetry has been highlighted, in the previous section, as one of three 'potential technology winners' for 'pull through' from a research tool to a standard surveillance technique. Unlike in some other countries in the UK heat flow calorimetry is still used only as a research tool. Within the UK the added value that heat flow calorimetry can add to other surveillance techniques, several of which may be far less expensive to carry out, including other thermal analysis techniques is still being questioned. The debate in the UK is also still open as to the scope of applications to energetic materials that heat flow calorimetry can provide additional intelligent data to predict more accurately the end of life of munitions.

This is the third international heat flow calorimetry conference and in today's economic climatic financial support for scientific studies, rightly or wrongly, have to be concentrated on techniques for which there is a good chance that a tangible deliverable or output can be achieved. In contrast it is increasingly unacceptable for scientists to either study an interesting problem or carry out experiments on a new technique just because one has been developed.

The time for hard decisions to be made as to the added value and applications that heat flow calorimetry has now arrived. This is an ideal forum to make such decision. Where future work areas are proposed their justification will have to stand up to critical scrutiny. During this week there should be a full exchange of positive and critical points to resolve these concerns. For the UK representatives present at this conference the main question is, is the recommendation from MLASG that heat flow calorimetry is a 'potential technology winner' still considered correct. If so, for what applications of energetic materials and subsequently how should the technique be financed for use as a standard surveillance technique.

The changing world

This new approach to the whole life assessment of munitions has to take place in a changing world, with:

- No cold war
- Reduced defence spending
- Strategic defence review

- Flexible & adaptable forces in global role
- Smart procurement
- The use by allied nations of more and more common munitions
- The drive towards the use of international documentation, eg STANAGs
- The MoD being no longer involved with munition or explosive manufacture
- Significant organisational changes within the MoD
- A greatly reduced UK explosives industry

From a purely scientific and technical standpoint the favoured MoD position would be to establish a whole life assessment (surveillance) group which would have overall responsibility to look after the in-service lives of all UK service munitions. However this position is not in favour, with individual integrated project team leaders (IPTLs) or project managers having overall responsibility for the safety of their munitions. Therefore it is important that the policy initiative for the new approach to the life assessment of munitions is advertised and promulgated to all the WLA stakeholder groups, including the manufacturers. Improved collaboration with manufacturers should also ensure that munitions are manufactured to an appropriate build standard to their in-service use that will reduce the number of defects arising during their service lives.

Several other technical initiatives are currently underway which can also significantly effect the total cost of ownership of munitions, in both a negative and positive way, for example, insensitive munitions and increasing environmental (green) regulations. Many of these technical initiatives are inter-related and a coherent and integrated communication strategy to how the project managers (or IPTLs) are approached to comply with the increasing requirements is also needed. In the medium to long term developments in Micro-Electronic Mechanical Systems (MEMS) could also significant effect the design of munitions, their safety considerations and asset management and hence cost of ownership.

The use by allied nations of more and more common munitions necessitates the need for more and more international collaboration on WLA policies. Unfortunately despite the drive to use international standards, such as STANAGs, too often the transfer of information, such as important baseline data is limited due to problems including intellectual property rights. Unless the transfer and exchange of intelligent data is improved between national and international munition stakeholder then nugatory expenditure will continue to occur with unnecessary re-testing and 're-inventing of the wheel'.

It is only competent staff who can tell that data is intelligent data. Important points for intelligent data derived from the contents of this paper are shown in Table 4. In a changing world the important points relating to intelligent data will continue to change.

(a) Science

- Lack of understanding of degradation processes
- Lack of effect of environment on degradation processes
- Lack of energetic material properties
- Application of Arrhenius Kinetics not often relevant

(b) Tools:

- Sub-optimum testing/evaluation techniques often used
- Surveillance testing may not monitor known failures
- Artificial ageing may induce ageing not representative of in-service environment
- Often use tools to measure what can be measured rather than what should be measured

(c) Policy:

- Sub-optimum policies lead to munitions being procured on unit price rather than whole life considerations and often to build standards not adequate to prevent known defects arising during service life (especially at the less expensive end of the munitions market)
- Blanket approach to setting lives – assumes all munitions see same environment
- Poor communication between stakeholders, nationally & internationally – leads to nugatory expenditure
- Poor collaboration with other MoD initiatives, for example effective inventory management and related industries

Table 1: Problems with current whole life assessment policies

Category of Testing	Testing Technology/Methods	
	Testing Technology/Methods	Remarks
Non Destructive Examination (Discrete Testing)	Radiography- (X-ray, gamma and neutron particles)	Used to determine a snapshot of the in-service condition of munitions
	Imaging – (Computerised Axial Tomography (CAT))	
	Ultrasonics – (Laser and Piezo-electric)	
	Inferometry – (Holograph)	
	Boroscope	
Non-Destructive Examination (Continuous Testing)	Automatic environmental monitoring (temperature, humidity, vibration & shock)	a. Used for through life monitoring & asset management.
	Micro-Electric Mechanical Systems (MEMS)	b. MEMS and RFID is applicable to all defence materiel. It provides data on what stock is held, where is it, and its condition.
	Embedded sensors	
	MEMS and Radio Frequency Identification (RFID) systems	
Destructive Testing	Explosive safety testing (charge, scale & small (powder) scale)	Used for baseline testing and, as appropriate, for in-service surveillance testing. Increasingly used for predicting degradation rates in energetic materials.
	Thermal testing (heat flow calorimetry)	
	Chemical Testing (compatibility & analysis)	
	Performance testing (burning rate, closed vessel)	
	Energetic material characterisation (prediction of degradation processes and vulnerability)	
Systems Tests & Modelling	Detailed monitoring of environments seen by munitions during their in-service lives.	Used to predict more accurately the end of life of munitions
	Accelerating ageing (need to compare with real time ageing)	
	Modelling (production of ageing models identified from known life terminating mechanisms)	
	Proof & in-service firings	
	Munition safety tests	

Table 2: Surveillance/WLA testing Technology/Method

- Improved asset visibility
- Enhanced inventory accuracy
- Greater safety
- Increased asset availability
- Improved stockpile management
- Future reduced demilitarisation costs
- Advanced warning of any (potential) in-service problems
- Fewer in-service defects
- Reduced cost of ownership of munitions
- Improved prediction of end of life of munitions
- Increased mission readiness

Table 3: Benefits from enhanced WLA (surveillance) policy

- I. Interpretation, processing, & use of data by competent staff
- N. Non-Destructive Evaluation - return of inspected assets to service use
- T. Total cost of ownership of munitions - minimisation
- E. Effect of in-service environment on degradation processes
- L. Life prediction – accurate - based of knowledge of likely failure processes
- L. Life assessment policy - promulgation to all stakeholders including industry
- I. Individual lives of assets predicted - avoid blanket approach to setting lives
- G. Generation of baseline data (energetic, non energetic materials), proof firing etc
- E. Energetic material characterisation (qualification) & compatibility
- N. Nugatory expenses eliminated, by improved stakeholder communication
- T. Targeted testing/evaluation ‘as required’ rather than ‘as scheduled’

- D. Data logging now, in future MEMS technology
- A. Ageing algorithms – accurately prediction of residual lives
- T. Thermal analysis techniques – including heat flow calorimetry
- A. Asset tracking (of all defence materiel)

Table 4: Highlighted points for intelligent data

THIS PAGE LEFT INTENTIONAL BLANK

Review of Previous Energetic Materials Heat Flow Calorimetry Workshops

T T Griffiths

QinetiQ, Fort Halstead,

Sevenoaks, UK

Abstract

A review of two previous workshops on Heat Flow Calorimetry (HFC) of Energetic Materials held in April 1997 and May 1999 is presented. Both meetings were attended by around 50 delegates and more than 18 papers were presented on each occasion. The majority of the work reported involved studies on propellants but papers were also written on pyrotechnics, compatibility and the curing of binders. Both workshops brought together researchers using HFC to study energetic materials, this allowed them to exchange information and ideas.

Introduction

In 1993, The Technical Co-operation Programme (TTCP) between Australia, Canada, UK and US began a study in a Key Technical Area (KTA 4-21) on the degradation of pyrotechnic fuels. The KTA identified heat flow microcalorimetry (HFC) as an important technique for studying ageing in energetic materials. It recommended that a workshop should be held so that information of recent advances in the use of HFC to study the ageing of energetic materials could be exchanged.

First HFC workshop

The first HFC workshop was jointly organised by Leeds Metropolitan University and the Defence Research Agency under the auspices of KTA 4-21 of TTCP Subgroup WTP4 [1]. The meeting was held between 7th and 9th April 1997 at Chevin Lodge Hotel, Leeds.

Twenty-four papers were presented over the three days of the meeting, 58 delegates from twelve countries were represented. Almost half of the papers were studies on propellants, only three papers included studies of pyrotechnics. Most of the papers were concerned with ageing and the influence of the ambient conditions on the

ageing process. In addition, there were six general papers including those on corrosion of metals, compatibility between materials and curing of polymers.

The Thermometrics Thermal Activity Monitor (TAM) was chosen for most of the work reported but some researchers used calorimeters manufactured by Hart and Setaram. TNO, Netherlands reported experiments performed with their own design of van Geel type calorimeter. Four papers described the results of Differential Scanning Calorimetry (DSC) studies.

The workshop identified that HFC has a number of advantages and some disadvantages compared to other techniques. Modern calorimeters have high sensitivity that allows measurements at lower temperatures but when this is the case, experiments have to take place over relatively large time-scales. All chemical reactions that produce heat are recorded using HFC but the individual reactions cannot be isolated. For propellants, if experiments are conducted at different temperatures, changes in the slope of the Arrhenius curve are often observed. Additionally, HFC enables all reactions to be observed not only those generating gas.

Papers that compared the heat flow from propellants with stabiliser depletion were presented along with information on the effect of sample preparation and environment, particularly those of water and oxygen, had on the HFC data. The results of modelling studies on the heat flow from propellants were presented.

It was noted that HFC cannot be used to evaluate ballistic lifetime of propellants, for studies on the migration of components or changes in the mechanical behaviour. Considerable variation in the heat flow ($\pm 20\%$) was observed in some work reported especially when the experiments were conducted at lower temperatures.

Studies on pyrotechnics included papers on the protection of magnesium, compatibility studies and a preliminary study on ageing of pyrotechnic compositions using the TAM flow through cell.

A novel use for the HFC involved a study on the corrosion of metal by red fuming sulphuric acid. The work resulted from an accident when a tank, designed to safely store the acid, ruptured unexpectedly. A special ampoule was manufactured for the TAM from the same stainless steel as was used for making the tank. The lid was constructed so

that a pressure transducer could be fitted. This allowed the pressure change inside the ampoule to be monitored during the experiments. The work successfully allowed the reason for the tank bursting to be explained.

Two other uses of HFC were reported. The first was a study on the curing of fluorinated polyether rubbers and the second was a comparison of the heat flow from solid and powdered samples and an adhesive. The results were used to estimate the interaction profile thickness.

There were a number of outputs from the workshop including:

- A 'Round Robin' on propellants to allow a comparison of results by different laboratories;
- The requirement for a new design of TAM flow through cell;
- A second workshop on the HFC of Energetic Materials.

Second HFC workshop

The second workshop held between 17th and 19th May 1999 at Chevin Lodge Hotel, Leeds [2]. It was jointly organised by the University of Huddersfield and the Defence Evaluation and Research Agency. Eighteen papers were presented during the workshop, 50 delegates from twelve countries were represented. Almost half of the papers were studies on propellants with the remainder covering a range of topics including high explosives, ageing of plasticisers, sample preparation, corrosive liquids and calibration of the TAM.

A wider range of equipment was described in the paper, but once again most researchers were using the Thermometrics TAM. One calorimeter made by Calorimetric Scientific Corporation with ampoule dimensions of 12cm x 12cm x 30cm was capable of holding a 6Kg sample. An automated sampling system for the TAM was described. The system maintained 36 samples contained in 4cm³ ampoules at the correct temperature between measurements.

Research on propellants included studies on sample the sizes and form. The results of the 'Round Robin' experiments on double-based propellants were presented. A novel approach to reduce the volume of the sample ampoule using a glass rod was

described. It was also noted that the large (20cm³) cell of TAM had higher heat loss than 4cm³ one. This could affect the heat flow measurements especially for propellants.

Problems of stability with the flow through cell system of the TAM were reported and a description of how improvements could be made to the flow through cell was presented. A comparison of DSC and HFC for a study of compatibility was described.

Output from second workshop included:

- Alternative techniques for calibrating the TAM;
- A Second 'Round Robin' on propellants;
- A third workshop.

Conclusions

The papers presented at the previous workshops concluded that the reactions studied by HFC are influenced by the sample environment. In particular:

- The sample ampoule size;
- The free space in the ampoule;
- The size of the sample;
- The packing of the sample;
- Pre-treatment of the sample e.g. grinding
- Sealing of the ampoule cap;
- Pressure generated in the sample ampoule during the experiment;
- Depletion of atmosphere i.e. oxygen during the experiment;
- The humidity in the ampoule and the amount of water in the starting material.

The research also showed that:

- No single test can provide complete service life data for propellants
- For propellants, DSC is suitable for identifying adverse behaviour, HPLC gives a measure rate of stabiliser depletion and HFC can be used to determine Arrhenius data;

- Increased heat production is observed for propellants when the atmosphere in the sample ampoule is at high humidity and/or contains oxygen.
- Identical results can be obtained by different laboratories or equipment if the samples are prepared in a similar way.
- Problems occur with the TAM flow through cell especially when it is operated at high temperature and humidity.
- A database of the behaviour of different propellant types is required;
- Techniques for the calibration for temperature, humidity and energy are a problem area that is shared with the pharmaceutical industry.

References

1. Proceeding of the First Workshop on the Heat Flow Calorimetry of Energetic Materials, published by the Defence Research Agency, 1997.
2. Proceeding of the Second Workshop on the Heat Flow Calorimetry of Energetic Materials, published by the Defence Evaluation and Research Agency 1999.

Copies of these publications are available from QinetiQ Ltd, Building R47, Fort Halstead, Sevenoaks, Kent, TN14 7BP, UK.

Copyright © QinetiQ Ltd 2002

THIS PAGE LEFT INTENTIONAL BLANK

ASSESSMENT OF THE BALLISTIC SERVICE LIFETIME OF A SMALL CALIBER CARTRIDGE BY HEAT FLOW CALORIMETRY

*Uldis Ticmanis, Gabriele Pantel, Stephan Wilker, Lutz Stottmeister
WIWEB, Großes Cent, 53913 Swisttal, Germany*

*Pierre Guillaume, Jean-Pierre Marchandise, André Fantin
PB Clermont S.A., Rue de Clermont 176, 4480 Engis, Belgium*

Presentation on the 3rd International symposium on Heat Flow Calorimetry and it's applications for Energetic materials, French Lick, Indiana, April 2002

ABSTRACT

The thermal decomposition kinetics of both built-in explosives – a double base ball propellant and a primer composition – were established from HFC and DTA/TGA measurements. Using these data a thermal safety simulation of the cartridge indicated a infinite safety life time at ambient temperatures below 130°C.

The ballistic behaviour of the systems was studied in details by ageing

- ◆ Complete ammunitions
- ◆ Cartridges which only contain the primer
- ◆ Propellant alone in closed and completely filled ampoules

The aged cartridges were loaded with fresh propellant and the aged propellant was loaded in fresh cartridges. The three series of experiments were fired and the gas pressure and the bullet velocity were recorded.

No decrease of both ballistic parameters was found from the separate ageing of the primers. Ageing of the propellant caused a decrease when compared to unstressed complete cartridges. Ageing of the complete ammunitions presents a greater decrease of ballistic results than expected from the two other series.

To find out the component limiting the ballistic life time, the compatibility of the components was studied by HFC at different temperatures. The process limiting the service life time (to a still more than sufficient period of time) is a gas phase reaction of solvent vapour from the propellant with the primer composition.

These results show that ageing of only one component in a whole system can lead to wrong predictions of the service lifetime of ammunitions.

This paper is divided into four parts. The first part describes general aspects of the investigated materials and their stability including the test methods. The second part describes the ballistic studies, whereas part III of this work gives details about the compatibility studies of the primers with the propellant. Part IV of this paper shows the results of the analyses of the aged components.

INTRODUCTION

The service life of a propellant is one of the most important factors that describes their usability. On the one hand, there is the possibility of self-ignition leading to disastrous destruction of the surroundings. On the other hand, there is the problem of the ballistic stability, the period of time during which the ammunition can be safely used and/or during which the interior ballistic requirements remain fulfilled.

The main factors leading to a change of the interior ballistic behaviour are the loss of energy content due to slow decomposition reactions and the migration/diffusion process.

Most of the time, the functional life time of the ammunitions is assessed from the calculated lifetime of the propellant.

The aim of this work was to correlate the lifetime of the ammunition with the life time determined from the components (mainly the propellant). For this purpose, we have used a double base spherical propellant that has been extensively studied in the recent past years [1]. That propellant (K6210) is dedicated for the 9mm x 19 ammunition. Parts of this work have already been published [2].

PART I – GENERAL REMARKS

EXPERIMENTAL CONDITIONS

1. BALLISTICS

The following ballistic parameters were recorded: The velocity, the case mouth pressure, the chamber pressure and the action time (when available).

A NATO EPVAT [3] barrel was used for the case mouth pressure and 20 cartridges were fired for each series. A pressure barrel was used for the chamber pressure and 10 cartridges were fired for each series. The complete ammunitions were fired only in the NATO EPVAT barrel.

2. HFC

The HFC experiments were performed with a TAM 2277 from Thermometrics AB (Sweden) using 3 ml glass ampoules for the propellant between 89°C and 50°C and a steel ampoule for the complete ammunition and the propellant alone at 89°C. HFC measurements of primers were also done at different temperatures (89, 80 and 70°C). Compatibility measurements were mostly performed at 89° and at 50°C.

3. CHEMICAL ANALYSIS

The chemical analysis was performed with a Gynkotek HPLC system. For the propellant analyses a methanol/water mixture (67/33) was used as mobile phase (flow rate 1.2 ml/min). The detection occurred at 225 nm with a diode array detector. For the primer analyses a methanol/water mixture (40/60), adjusted to pH 3 by acetic acid, was used as mobile phase (flow rate 1.0 ml/min). The detection occurred at 280 nm.

4. HEAT OF EXPLOSION

The heat of explosion was determined according to literature procedures [4].

CARTRIDGE STUDIED

Explosives and materials of the cartridge and the primer, including the primer composition, are presented in figures 1 and 2. For this study, the ammunition was filled with the same propellant lot whose stability was tested alone.

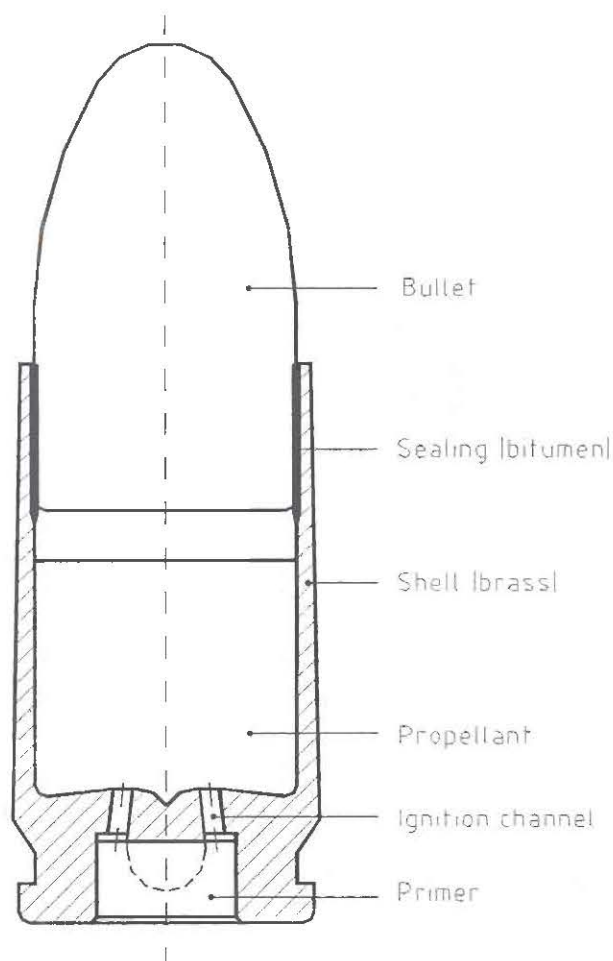


Figure 1. Cartridge 9 mm - 19

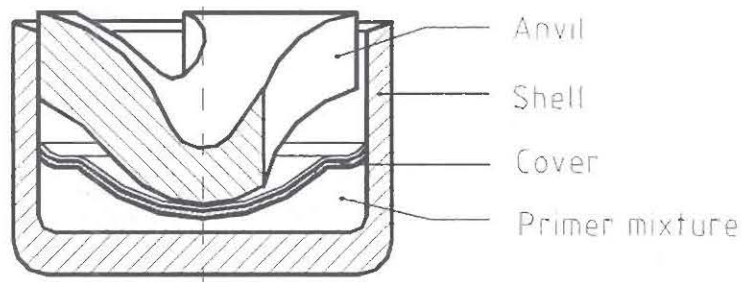


Figure 2. Detailed drawing of the primer
(the primer mixture contains tetracene, diazole, oxidizer, titanium and propellant)

ASSESSMENT OF THE LIFETIME OF THE PROPELLANT

Recent studies have shown that the lifetime of the propellant can markedly differ according to the test conditions [5] used to calculate the lifetime of the propellant. Therefore, the ageing of the propellant has been done under ammunition-like conditions, ie that means, the same filling grade and the same closure of the vessels.

From the HFC curves of the fresh propellant aged in full and sealed ampoules, one can calculate the activation energy and then estimate the time at lower temperature to reach a given value of decomposition of the propellant (figure 3) [6].

For measurements between 89 and 50°C, an activation energy of 140 kJ/mole was found (see figure 4). If we use that value for the range between 90 and 50°C and an activation energy of 80 kJ/mole between 50 and 20°C [7], the lifetime of the propellant can be estimated for different heat losses of the propellant due to its slow decomposition (see figure 5).

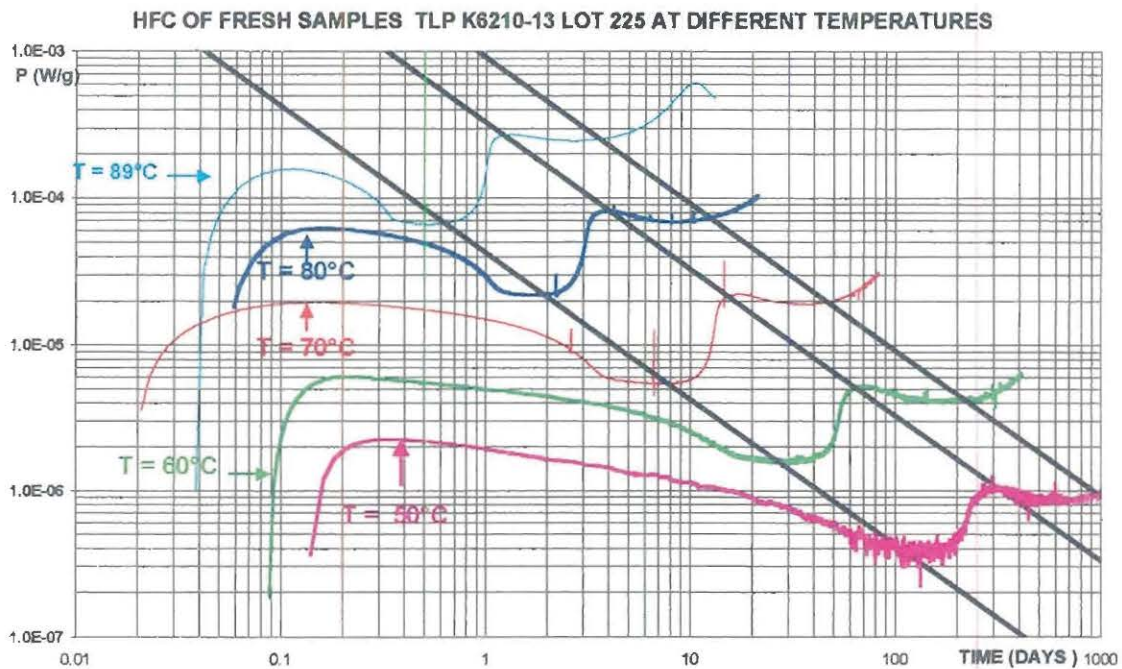


Figure 3. Heat flow measurements of propellant K 6210 at 89°C, 80°C, 70°C, 60°C and 50°C with fresh samples (each sample 3.50 g; ampoules filled and closed, propellant non-conditioned)

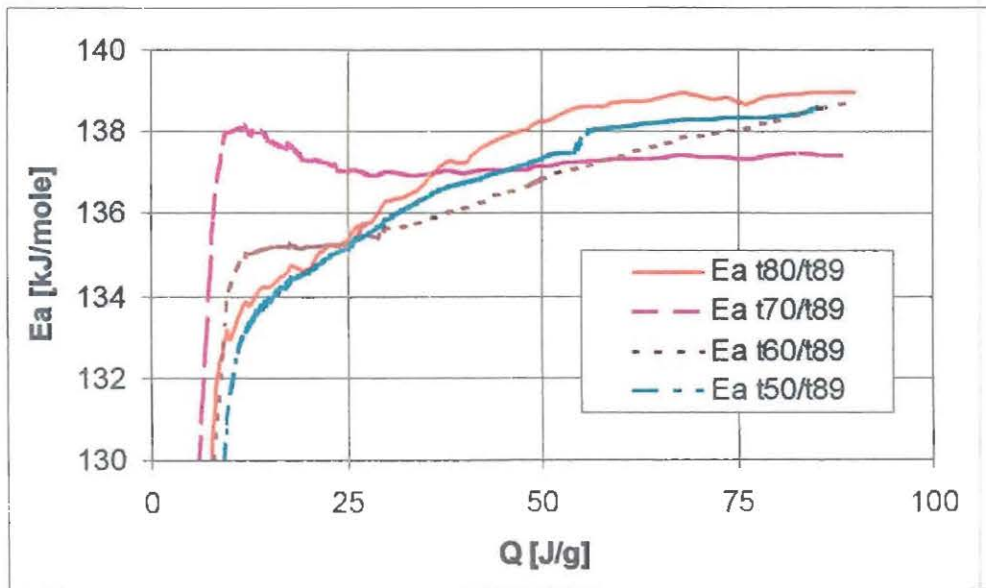


Figure 4. Activation energies of the decomposition of propellant K 6210 at temperatures between 89°C and 50°C in dependence of the released energy. The calculation refers to the times when a certain energy release is reached.

If the loss of energy is the sole parameter considered for the loss of ballistic performance, the lifetime of the ammunition can be estimated from the same graph.

From ballistic requirements, the ammunition should not have a velocity drop of more than 30 m/s [3]. This drop of velocity can be estimated by lowering the charge weight of the ammunition. A

lowering of about 7.5% of the charge weight will give a drop of the velocity of about 30 m/s. This means a heat loss of about 300 J/g (the heat of explosion being around 4125 J/g) and the lifetime of the ammunition will be estimated to 200 years at 20°C.

Other phenomena to be taken into account for the assessment of the ballistic lifetime are the diffusion/migration of the deterred layers of the propellant and the compatibility of all the components of the ammunition. Those phenomena can not be estimated from HFC curves of the propellant.

$P, \mu W/g$ at 89°C

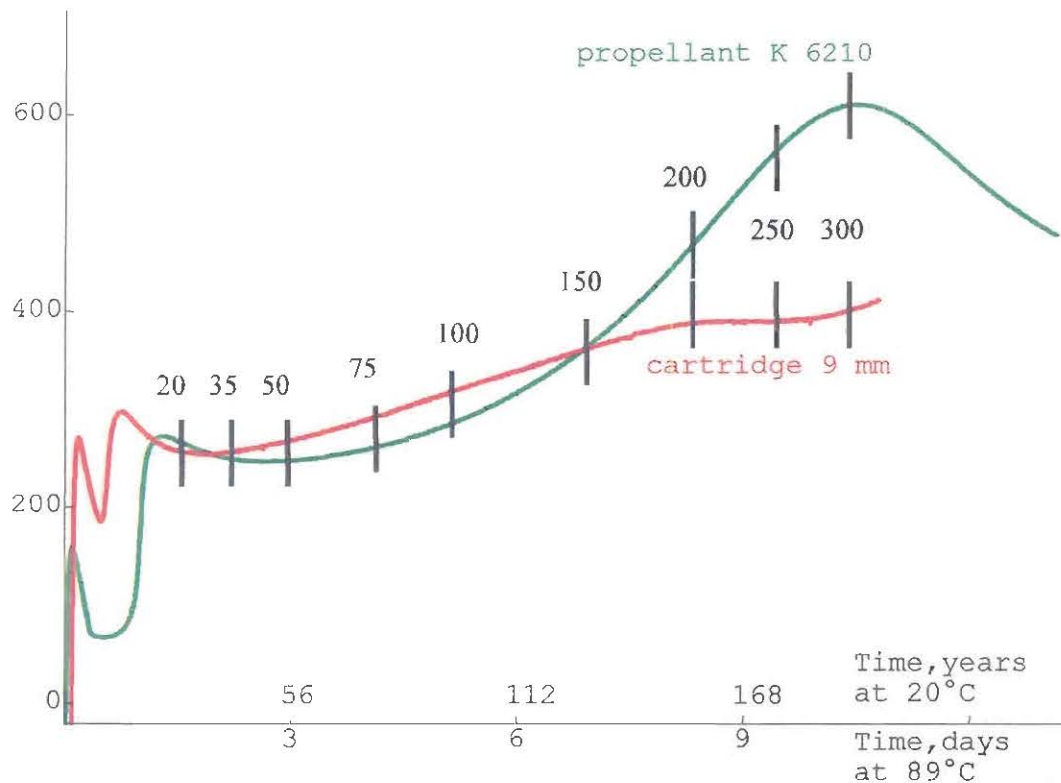


Figure 5. HFC curves of propellant K6210 and 9-mm-cartridges at 89°C including the ageing times (black bars with numbers, which refer to the energy release of the propellant until each measuring point) and an x-axis with extrapolated time at 20°C according to [7].

ASSESSMENT OF THE SERVICE LIFE TIME OF THE PRIMER

Assessments of thermal („chemical“) stability have been performed earlier [8] by DTA/TGA of a closely related primer which differs from the cartridge's primer only by being a little bit larger. A measurement with a heating rate of 1 K/min showing three exothermal steps is presented in fig. 3. TGA curves at different heating rates (fig. 4) can be used for the estimation of the activation energy of the individual (independent) reactions e.g. by using the Kissinger equation (1) [9].

$$\ln(H/T_{\text{dyn}}^2) = A' - E_a/RT_{\text{dyn}} \quad (1)$$

H = heating rate [K/min]

T_{dyn} = temperature for reaching a certain reaction degree

A' = constant, only for the same reaction degree

E_a = activation energy [kJ/mole]

R = gas constant (0,0083143 kJ/(K*mole))

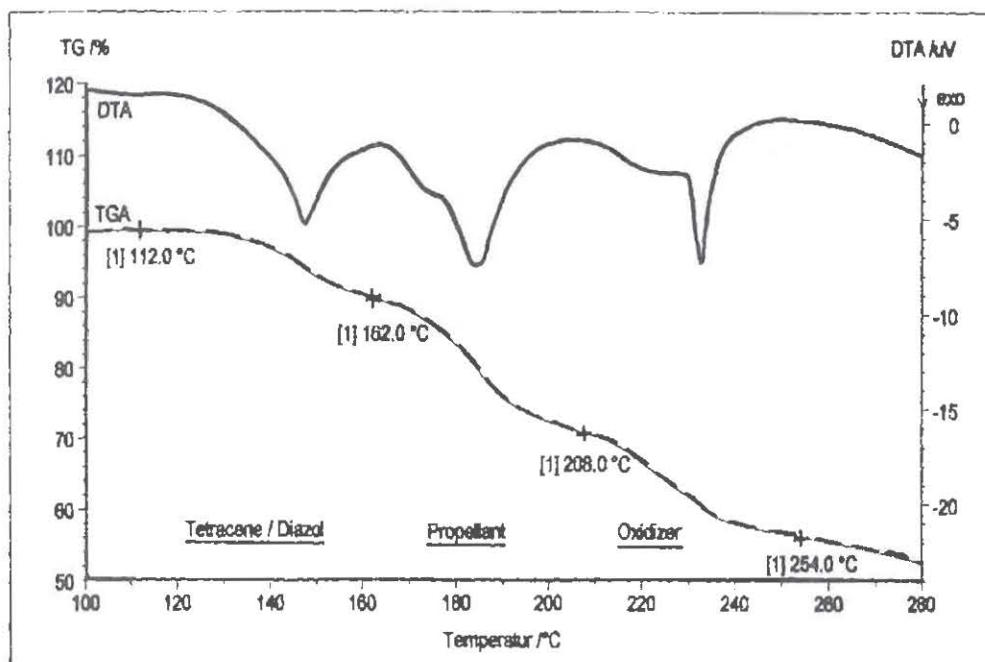


Figure 6. DTA/TGA measurement of a primer composition at 1K/min

For primer mixtures relative large decomposition degrees can be assumed before the function of them decreases. We believe that 20 % is „conservative“ enough. Calculations for this point (E_{20}) and that of the highest reaction rate (E_{max}) in the step (DTGA maximum) are listed up in table 1.

Step	$E_{a\ 20}$ [kJ/mole]	$E_{a\ max}$ [kJ/mole]
1 Tetracene/Diazole	148,6	255,5
2 Propellant	168,8	154,5
3 Oxidizer	158,5	152,7

Table 1: Activation energies at 20% and in the maximum of the decomposition reaction.

The large difference in the values for both evaluation points in the case of step 1 demonstrates that something is wrong and the individual reactions of tetracene and diazole are too equal to be separated by dynamic TA. For the propellant and the oxidizer eqn. (2) can be used to calculate isothermal storage times leading to the same reaction degree as the dynamic measurement [10].

t_{iso} = isothermal storage time [min]

$$t_{iso} = \frac{1}{H} * e^{\frac{E}{RT_{iso}}} * \int_0^{T_{dyn}} e^{-\frac{E}{RT}} dT \quad (2)$$

T_{iso} = isothermal storage temperature [K]

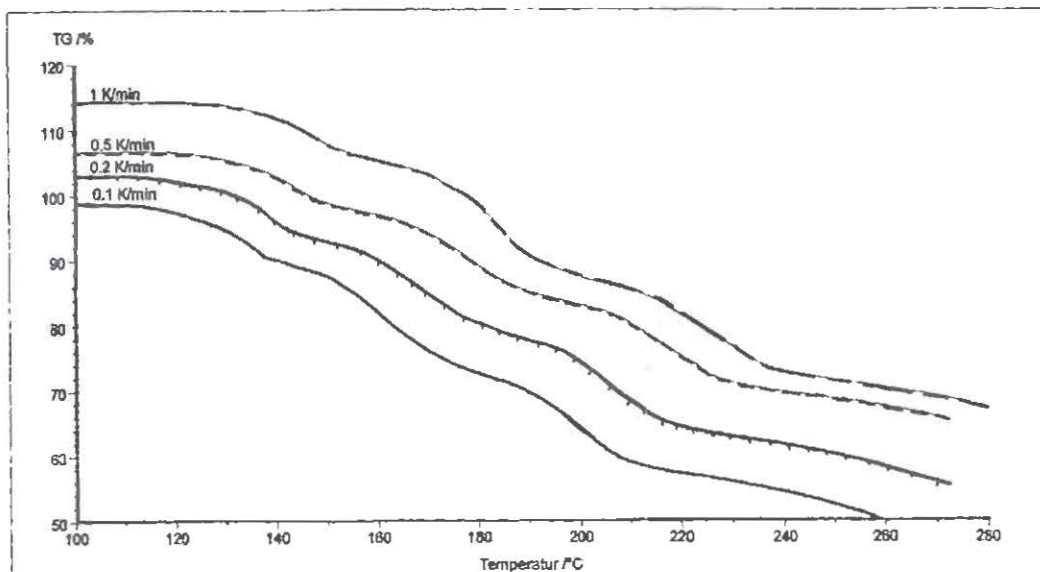


Figure 7. TGA curves of a primer mixture at different heating rates

At 89°C the times for a decomposition of 20% can be calculated. The propellant loses 20% after 330 days (0,90 years) whereas the oxidizer lasts about 24 years. Since the longest storage time for cartridges and primers used in this study was only 10,5 days we are sure that these components will cause no problems concerning thermal stability.

The same related primer was stored at 90°C and analyzed by HPLC. The results indicate a time for 20 % decomposition at 89°C of

tetracene:	9 days
diazole:	13 days

The activation energy is assumed to be about 180 kJ / mole [11].

SUMMARY OF PRIMER STABILITY TESTS

At ambient temperature the thermal stability of the primer will not be the limiting component for the ballistic lifetime. Under the highest chosen ageing conditions (10,5 days at 89°C) some problems may occur from decomposition of tetracene and/or diazole.

PART II - BALLISTICS

EXPERIMENTAL PLAN

The complete ammunition, the primed cases and the propellant alone were aged for the same times.

The propellant was aged in sealed ampoules at temperatures of 70°C, 80°C and 89°C for defined periods of time corresponding to different total heat release. The values were chosen according to the HFC measurements of the propellant at those temperatures (see figure 5).

The ageing plan is given in table 2.

	T = 89°C	T = 80°C	T = 70°C
Heat release (Q)	t	t	t
[J/g]	[days]	[days]	[days]
20	1.55	5.4	19.4
35	2.21	7.1	27.7
50	2.94	10.3	36.9
75	4.13	13.4	51.6
100	5.15	18.0	64.5
150	6.95	24.3	87.0
200	8.35	29.2	104.5
250	9.47	33.1	118.6
300	10.44	36.5	130.7

Table 2: ageing plan applied to the propellant, the primed cases and the ammunition

The following experimental series were investigated:

- The propellant alone was aged in fully loaded and sealed vessels. The effectiveness of the sealing was checked by measuring the weight loss after the ageing. The aged propellant was then loaded into fresh primed cases for the ballistic tests and samples were taken for chemical analysis.
- The ammunitions were weighted individually before and after ageing to determine their tightness. Some cartridges were dismantled for chemical analysis of the components.
- The primed cases were aged similarly and loaded with fresh propellant for the ballistic tests. The primer composition was chemically analysed after ageing.

EXPERIMENTAL RESULTS

1. Weight loss

After ageing the weight loss for the propellant vessels varies from 0.06% (20 J/g) to 3.9% (300 J/g) at 89°C, till 6.0% at 80°C and till 3.4% at 70°C.

The weight loss of the ammunitions was at the maximum 0.016%. So they can be regarded as being tightly closed through all the ageing.

2. Ballistics

2.1. Primed cases

The primed cases have been aged at 89°C and 70°C according to the test plan and then loaded with 0.4 g of fresh propellant. The firing was performed in the 2 tubes (NATO EPVAT and pressure tube). The results are given in tables 3-6 (pressure tube results) and in figure 8 (NATO EPVAT).

It appears from the results that the ageing of the primer has only a weak influence on the ballistics. For ageing over 200 J/g, one can notice a slight increase of the action time and an increase in the standard deviation.

E (J/g)	Pmo (89°C)	s	Vmo (89°C)	s	t4	s
0	2021	87,5	395	3,5	0,832	0,076
20	2044	74,4	395	3,5	0,839	0,025
35	2027	81,2	395	3,3	0,844	0,023
50	2073	65,2	396	3,2	0,834	0,021
75	2013	66,8	394	3,2	0,855	0,026
100	1940	107,5	388	5,3	0,930	0,029
150	1937	127,4	391	6,4	n.m.	n.m.
200	1964	93,7	393	4,4	0,896	0,058
250	1908	167,9	389	9,9	0,993	0,231
300	1900	118,5	390	6,4	1,266	0,259

Table 3: ballistic results in the NATO EPVAT tube of the primed case aged at 89°C

The following abbreviations are used throughout all following tables: E = energy release [J/g], Pmo = mouth pressure in NATO EPVAT barrel [bar], s = standard deviation, Vmo = velocity in NATO EPVAT barrel at 10 m distance [m/s], t4 = action time [ms], Pch = chamber pressure in the pressure tube [bar], Vch = velocity in the pressure tube at 10 m distance [m/s], n.m. = value was not measured

E (J/g)	Pch (89°C)	s	Vch (89°C)	s
0	2801	159,7	398	3,4
20	2501	95,6	391	3,9
35	2570	135,0	392	3,9
50	2556	153,4	393	3,2
75	2558	116,7	394	3,2
100	2567	146,0	392	4,7
150	2445	85,6	391	2,4
200	2406	95,3	391	2,7
250	2415	116,9	392	3,9
300	2417	205,3	393	5,3

Table 4: ballistic results in the pressure tube of the primed case aged at 89°C

E (J/g)	Pmo 70°C)	s	Vmo (70°C)	s	t4	s
0	1940	107,5	387,7	5,30	0,935	0,03
20	2008	92,8	393,9	4,42	0,896	0,02
35	1954	68,5	391,6	3,58	0,919	0,03
50	2009	59,3	394,1	2,55	0,922	0,04
75	1984	77,6	389,3	4,80	0,903	0,02
100	1976	78,6	391,6	5,62	0,902	0,02
150	1968	90,2	391,8	4,10	0,912	0,02
200	1952	69,0	391,0	3,41	0,915	0,03
250	1964	82,5	392,9	4,17	0,907	0,02
300	1917	96,6	391,3	4,45	0,914	0,02

Table 5: ballistic results in the NATO EPVAT tube of the primed cases aged at 70°C

E (J/g)	Pch (70°C)	s	Vch (70°C)	s
0	2801	159,7	398,0	3,40
20	2699	173,9	397,2	3,58
35	2668	153,2	396,8	4,35
50	2669	130,6	397,0	3,10
75	2612	182,7	394,3	4,03
100	2500	122,5	393,5	3,93
150	2528	278,4	390,3	5,79
200	2593	84,7	394,6	3,66
250	2498	122,4	392,6	3,75
300	2481	173,2	393,2	5,30

Table 6: ballistic results in the pressure tube of the primed cases aged at 70°C

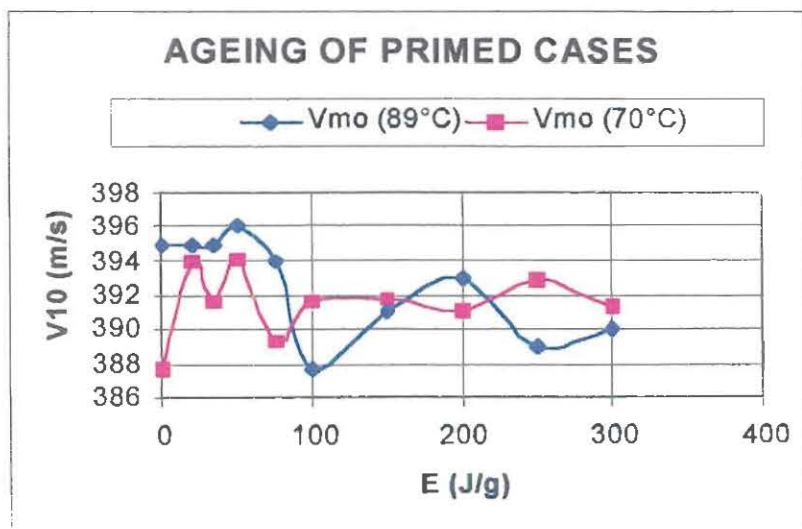


Figure 8: evolution of the velocity in the NATO EPVAT tube with the ageing of the primed case.

2.2. Propellant

The propellant has been aged at 89°C, 80°C and 70°C in fully loaded and sealed ampoules and then loaded into fresh cartridges. The cartridges were fired in the 2 tubes and results are presented in tables 7 to 10 (pressure tube) and figures 10 and 11 (velocity tube).

At first, the charge weight was adjusted according to the weight loss measured in the ageing vessel. This was done because we forecasted a similar weight loss in the ammunition. However, after ageing of the ammunition, no weight loss was observed. Therefore, we have repeated the series at 70°C with the same charge weight for all the ageing. By taking into account an additional drop of velocity due to the lowering of the charge weight (see fig. 9), the loss of velocity is nearly directly related to the energy loss of the propellant up to 200 – 250 J/g for all three series.

E	Charge weight [g]	P ch (89°C)	s	V ch (89°C)	s
0	0,400	2667	184,66	398,3	4,24
20	0,400	2659	103,26	395,6	3,47
35	0,400	2590	188,66	390,0	6,38
50	0,399	2689	124,76	393,4	3,60
75	0,400	2669	118,97	387,8	5,55
100	0,396	2548	122,04	386,7	3,74
150	0,392	2423	79,74	377,7	4,67
200	0,389	2256	117,98	366,6	5,04
250	0,386	2098	239,53	359,5	8,87
300	0,384	1773	92,05	340,1	5,28

Table 7: ballistic results in the pressure tube of the propellant aged at 89°C

E	Charge weight [g]	P ch (80°C)	s	V ch (80°C)	s
0	0,400	2603	184,35	389,3	4,67
20	0,400	2759	156,63	393,0	6,49
35	0,400	2757	133,02	394,0	4,71
50	0,399	2620	198,11	387,0	5,21
75	0,398	2585	155,69	386,0	4,84
100	0,394	2467	74,31	379,0	3,65
150	0,393	2390	123,41	373,0	5,34
200	0,390	2096	111,73	360,0	6,64
250	0,385	1866	99,65	345,0	6,85
300	0,382	1794	179,52	334,0	11,46

Table 8: ballistic results in the pressure tube of the propellant aged at 80°C

E	Charge weight [g]	P ch (70°C)	s	V ch (70°C)	s
0	0,400	2945	166,76	400,7	3,59
20	0,400	2839	166,44	397,0	3,83
35	0,400	2809	148,85	397,7	4,64
50	0,399	2885	152,37	396,7	5,21
75	0,400	2857	160,13	397,3	4,52
100	0,395	2779	134,29	391,8	4,10
150	0,394	2613	113,22	383,9	3,38
200	0,391	2356	133,92	371,2	5,61
250	0,389	2300	155,93	365,7	7,75
300	0,387	2159	98,59	356,3	6,24

Table 9: ballistic results in the pressure tube of the propellant aged at 70°C

E	Charge weight [g]	P ch (70°C)	s	V ch (70°C)	s
0	0,400	2945	166,76	400,7	3,59
20	0,400	2839	166,44	397,0	3,83
35	0,400	2809	148,85	397,7	4,64
50	0,400	2885	152,37	396,7	5,21
75	0,400	2856	160,13	397,3	4,52
100	0,400	2810	100,97	395,0	2,45
150	0,400	2805	121,15	393,0	6,82
200	0,400	2409	71,64	374,8	3,11
250	0,400	2318	63,41	368,8	1,64
300	0,400	2265	192,70	362,2	8,23

Table 10: ballistic results in the pressure tube with a constant loading charge weight of the propellant aged at 70°C

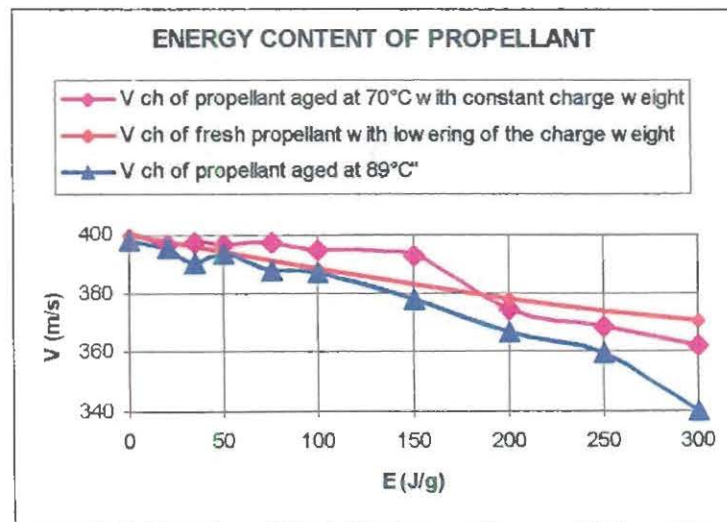
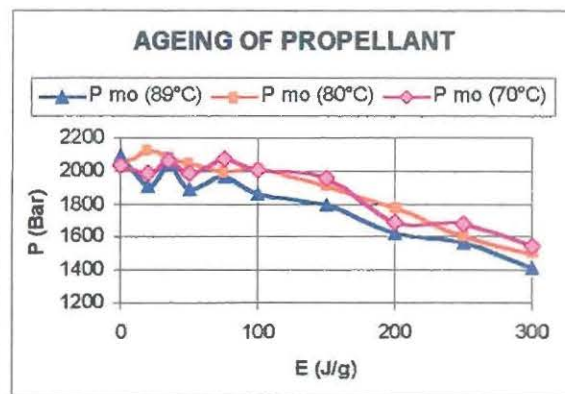
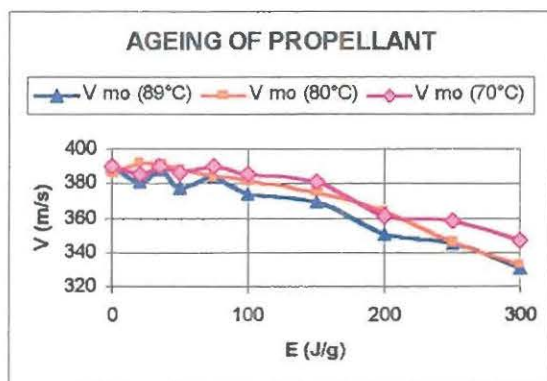
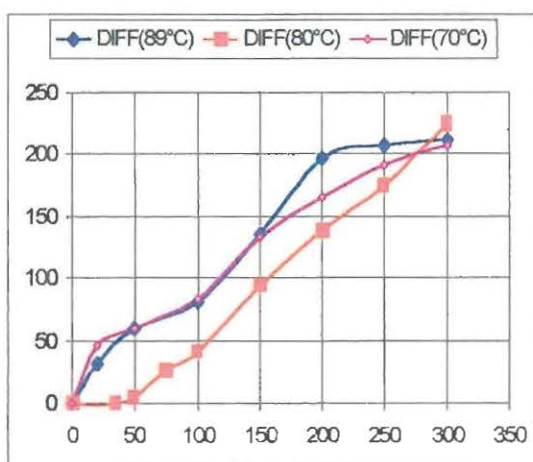
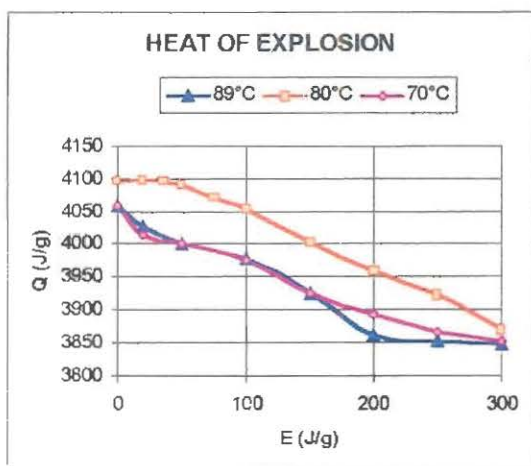


Figure 9: Influence of the reduction of the energy on the velocity



Figures 10 & 11: Velocity (left) and pressure (right) in the NATO EPVAT tube of the propellant aged at different temperatures



Figures 12 & 13: Evolution of the heat of explosion of the aged propellant (left) and difference to $Q = 0$ J/g (right)

From the results on the ageing of the propellant, one can conclude that the main factor determining the loss of performance is the loss of energy of the propellant.

2.3. Ammunition

The ammunition was aged at 89°C, 80°C and 70°C. The cartridges were fired in the NATO EPVAT tube. The NATO EPVAT results are presented in tables 11-13 and the pressure barrel results are shown in figures 14 and 15.

E	P (89°C)	s	V (89°C)	s	t4	s
0	1957	100,98	387,0	5,27	n.m.	n.m.
12	1833	104,77	379,7	4,54	0,944	0,0293
20	1782	73,12	376,0	4,70	n.m.	n.m.
35	1674	140,48	368,8	8,68	1,145	0,154
50	1667	76,86	368,0	4,80	n.m.	n.m.
75	1042	394,91	297,3	53,99	6,247	2,825
100	1207	194,26	324,0	20,90	n.m.	n.m.
150	768	307,8	251,8	51,88	n.m.	n.m.
200	623	374,46	218,0	71,07	n.m.	n.m.
250	564	223,7	201,7	53,03	n.m.	n.m.
300	553	304,5	205,1	59,30	n.m.	n.m.

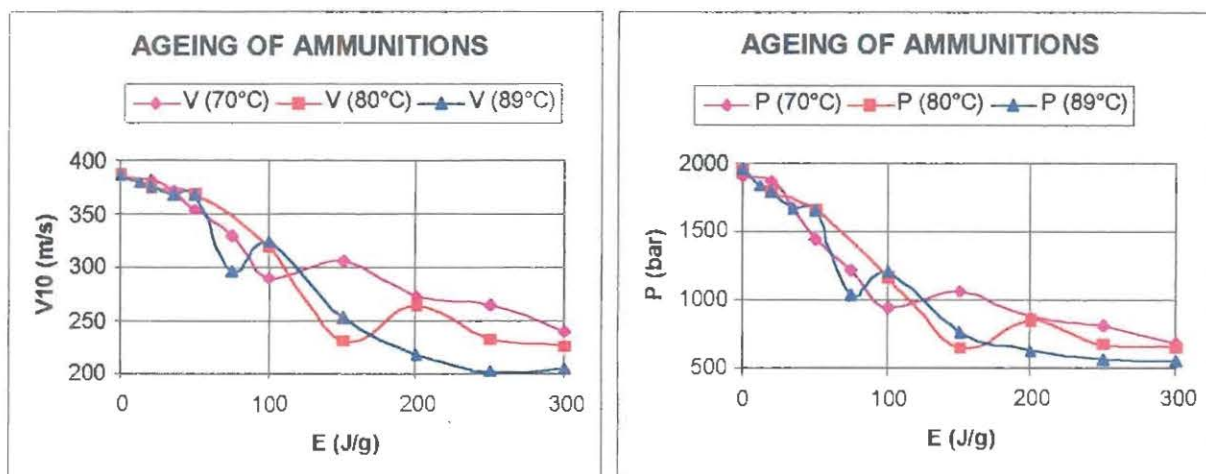
Table 11: ballistic results in the NATO EPVAT tube of the ammunition aged at 89°C

E	P (80°C)	s	V (80°C)	s
0	1950	78	388	2,9
20	1792	110	375	6,1
50	1668	78	369	5,5
100	1178	217	319	25,7
150	649	310	230	57,5
200	854	295	265	47,0
250	675	309	231	56,7
300	649	328	225	59,8

Table 12: ballistic results in the NATO EPVAT tube of the ammunition aged at 80°C

E	P (70°C)	s	V (70°C)	s	t4	s
0	1915	106,4	385,1	5,5	n.m.	n.m.
20	1876	85,5	382,0	4,9	n.m.	n.m.
35	1671	93,3	371,0	6,1	1,000	0,038
50	1449	164,3	353,2	15,1	1,591	0,326
75	1230	249,4	329,7	33,4	3,021	3,200
100	948	279,3	291,2	42,5	7,133	3,648
150	1060	233,6	306,8	30,9	7,875	7,082
200	870	318,9	273,6	56,3	13,722	8,652
250	809	275,6	265,3	46,5	12,850	3,210
300	682	316,5	240,0	57,1	13,271	2,969

Table 13: ballistic results in the NATO EPVAT tube of the ammunition aged at 70°C



Figures 14 & 15: Velocity (left) and pressure (right) evolution in NATO EPVAT tube for the ammunition aged at different temperatures

The drop of velocity is quite larger than for the previous case. In addition, during the firing we have noticed some abnormal pressure/time-curves as shown in figure 17. The abnormal curves were observed for ageing of 150 J/g and above. Also some misfiring occurred for those ageing times of the ammunition.

For the series of firing of the aged ammunitions, we can conclude that the ammunition will meet the ballistic requirements up to an ageing time corresponding to an energy release of about 60J/g. However, this value will still give a lifetime of the ammunition of around 50 years at 20°C.

A summary of the results is given in figure 16.

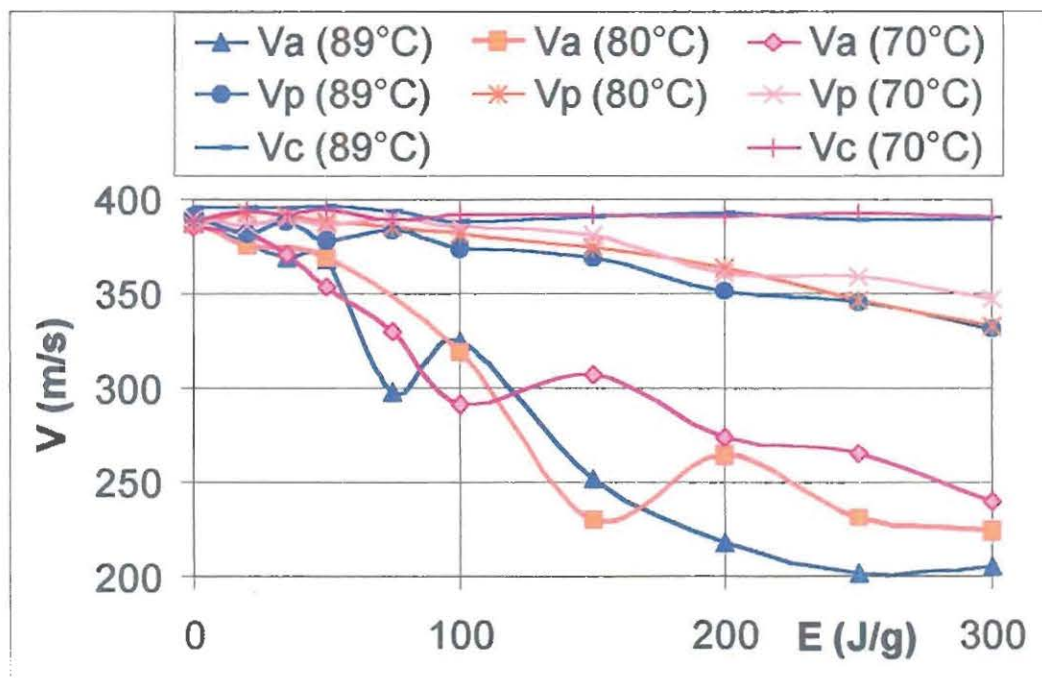
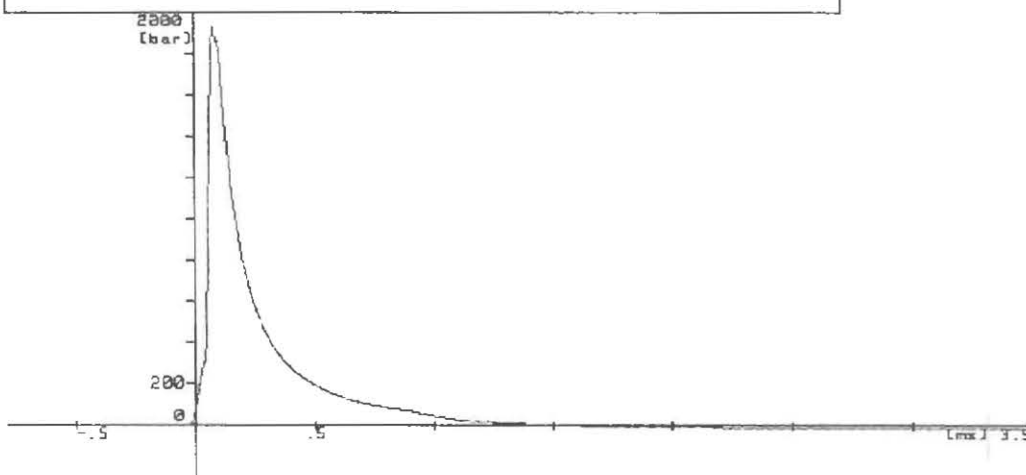


Figure 16: Summary of the velocity results in the NATO EPVAT tube for all the series tested; "a" is for ammunition, "p" is for propellant, "c" is for primed cases.

Kurvendaten									
Nr	K	Maximum	Int.	t1	t2	tx	tmax	t4	pt4
31	1	1930	0.000	0.000	0.000	0.000	0.000	0.000	0.000



Kurvendaten									
Nr	K	Maximum	Int.	t1	t2	tx	tmax	t4	pt4
25	1	125.0	0.000	0.000	0.000	0.000	0.000	0.000	0.000
14	1	500.0	0.000	0.000	0.000	0.000	0.000	0.000	0.000
30	1	655.0	0.000	0.000	0.000	0.000	0.000	0.000	0.000

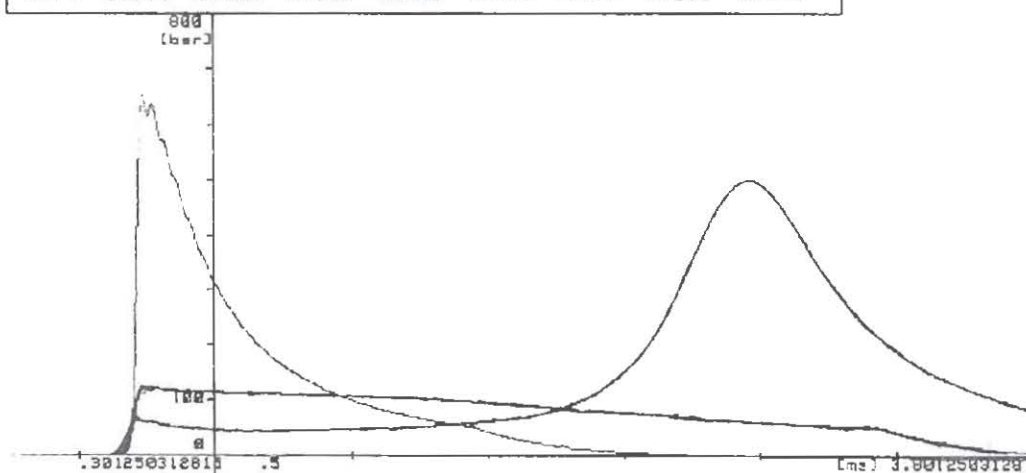


Figure 17: pressure – time curves for an non stressed cartridge (top) and highly stressed cartridges (bottom). These experiments were performed in the NATO EPVAT tube.

Assessment of the ballistic lifetime from shooting

The mean value for the bullet velocity of the unstressed cartridges was 386,7 m/s. The technical specification of the cartridge demands a minimum mean value of 370 m/s.

To find these „iso- α -points“ from the data of the stressed cartridges testing the following empirical equation was used for interpolation:

$$v = v_0 + c \cdot t^n \quad (3)$$

v = bullet velocity [m/s]

v_0 = bullet velocity of the unstressed cartridge [m/s]

t = storage times [d]

c, n = constants

Table 14 summarises the extrapolated times for 370 m/s.

T [°C]	time [d]	v [m/s]	t_{370} [d]	E_a [kJ/mole] ¹⁾
70	0	385	28,1	110,4 (70/80)
	19,4	382		
	27,7	371		
80	0	388	9,39	152,6 (80/89)
	5,4	375		
	10,3	369		
89	0	387	2,58	129,3 (70-89)
	1,55	376		
	2,94	368		

1) calculated from $\ln t_{370} = A + E/(RT)$

Table 14. Extrapolated times for 370 m/s

Using the lower value of the activation energy (110,4 kJ/mole) 57 years at 20°C are calculated as „ballistic lifetime“.

SUMMARY OF BALLISTIC TESTS

The ballistics of the ammunition is no longer related only to the diminishing of the energy content of the propellant or the ageing of the primer as separated events. The reason for the drastic drop of the ammunition's function seems to be a reaction between the propellant (or one of its components) and the primer. Why there was this huge difference between aged propellant samples / aged primed cases and aged cartridges we performed a series of thermoanalytical and chemical investigations described in the following chapters.

PART III - COMPATIBILITY OF THE CARTRIDGE EXPLOSIVES

EXPERIMENTAL SETUP

The following HFC compatibility experiments were performed:

- ♦ propellant with bitumen sealing
- ♦ propellant with primer composition admixture
- ♦ propellant with primer in gas phase contact
- ♦ primer in solvent atmospheres
- ♦ primer loaded with single compounds of the composition in isopropanol atmosphere

RESULTS OF COMPATIBILITY TESTS

Influence of the bitumen lacquer in the sealing of the cartridge

The bitumen sealing (see fig. 1) reacts considerably with the DB propellant of the cartridge if 1 : 1 mixtures are tested. In fact this incompatibility can be neglected because the contact area is not existing or very small [12].

Propellant with primer composition in admixture

HFC measurements of the primer or the primer composition show a considerable dependence on the amount of the locked-in air. Therefore when testing the compatibility of the propellant with the primer composition in the ratio of the cartridge (about 3 g propellant and 0,13 g primer composition) a mixture with small glass balls was used. Fig. 18 shows the faster increasing of the heat flow after the minimum in the admixture when compared with the propellant (this means an accelerated consumption of the stabilizer). The inflection points of the HFC measurement can be better seen as peaks in the derivated curves (fig. 19).

P, $\mu\text{W/g}$

T = 89°C

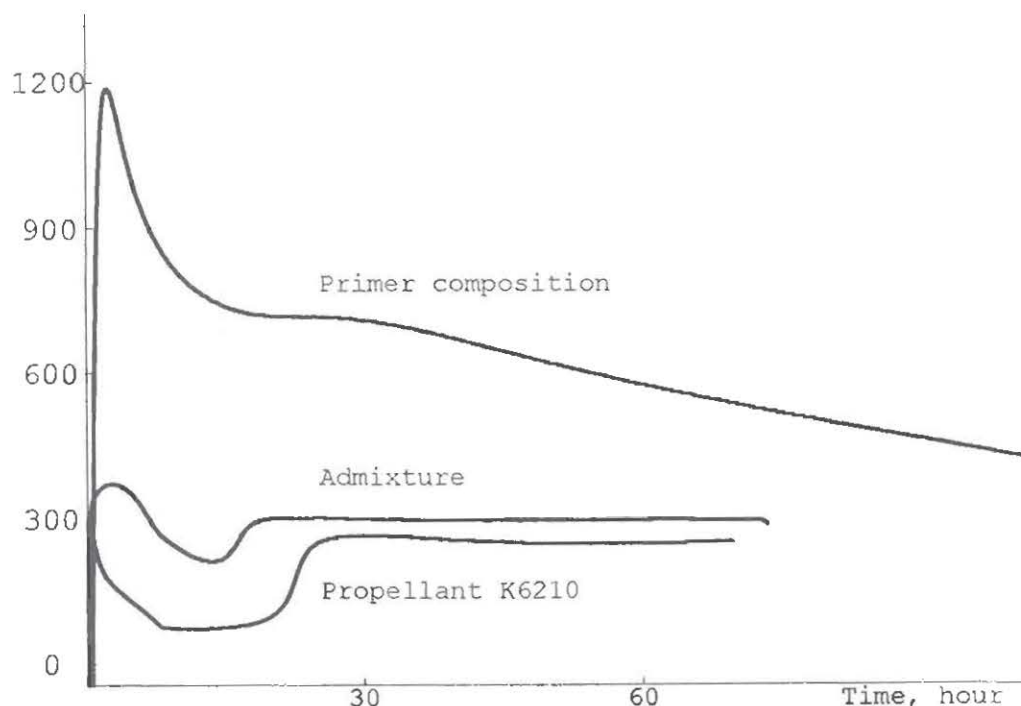


Figure 18. HFC curves of propellant, primer composition and admixture

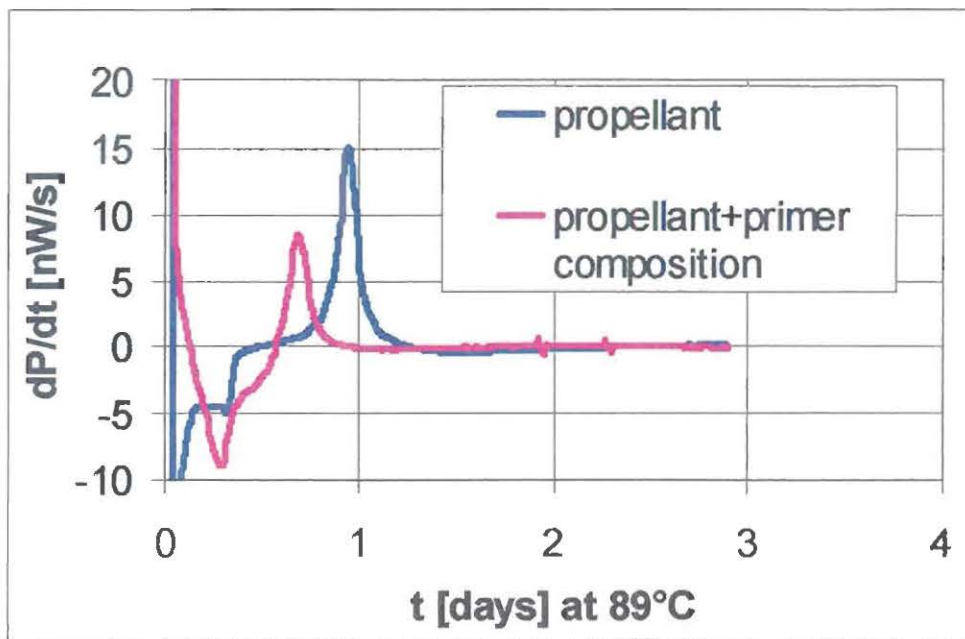


Figure 19. Derived HFC curves of propellant K6210 and its admixture with primer composition

Propellant with primer in gas phase contact

Direct contact of propellant and primer composition does not occur in reality, this test is in principle too hard. A gas phase contact through the ignition channels however is real. We reproduced this situation for HFC using the following setup:

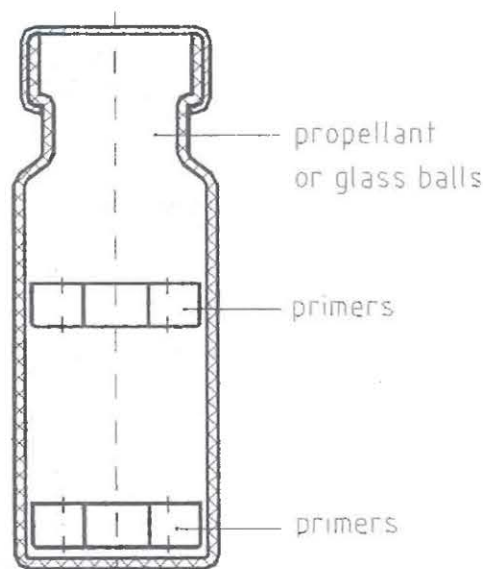


Figure 20. Experimental setup for compatibility tests by HFC

The derived HFC curves for 89° and 70°C are presented in the figures 21, 22 and 23. A summary of the effects is given in table 15.

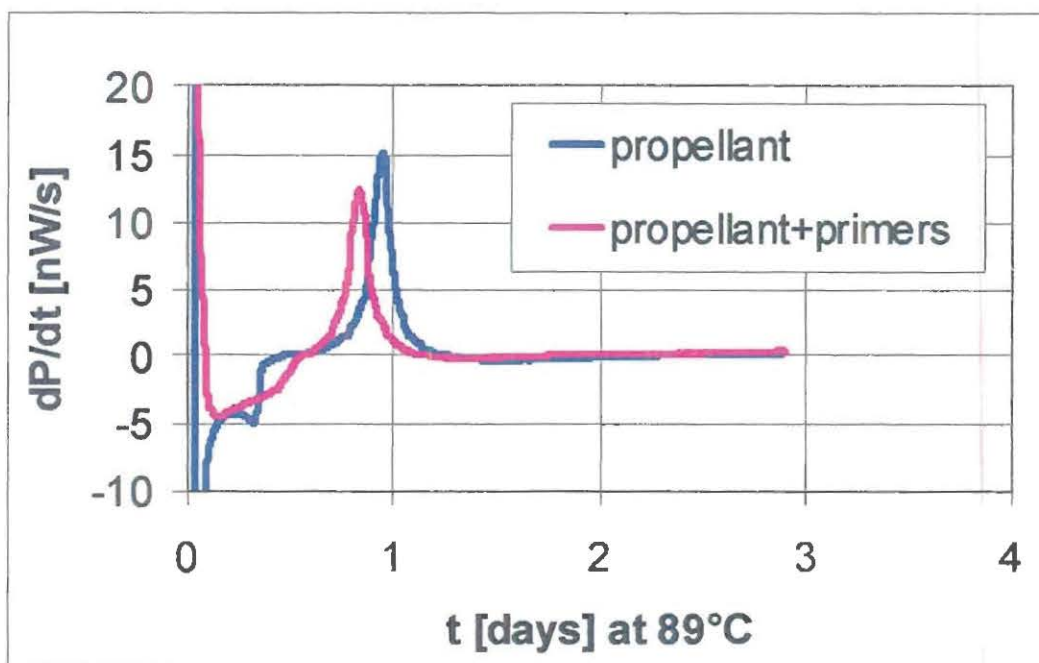


Figure 21. Derived HFC curves of propellant and propellant in gas phase contact with primers at 89°C

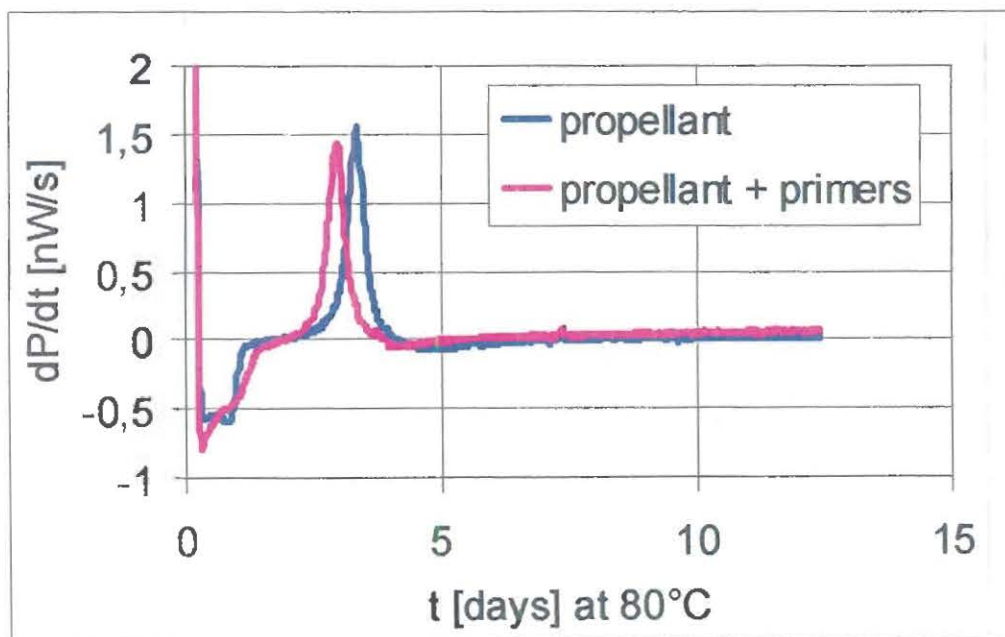


Figure 22. Derived HFC curves of propellant and propellant in gas phase contact with primers at 80°C

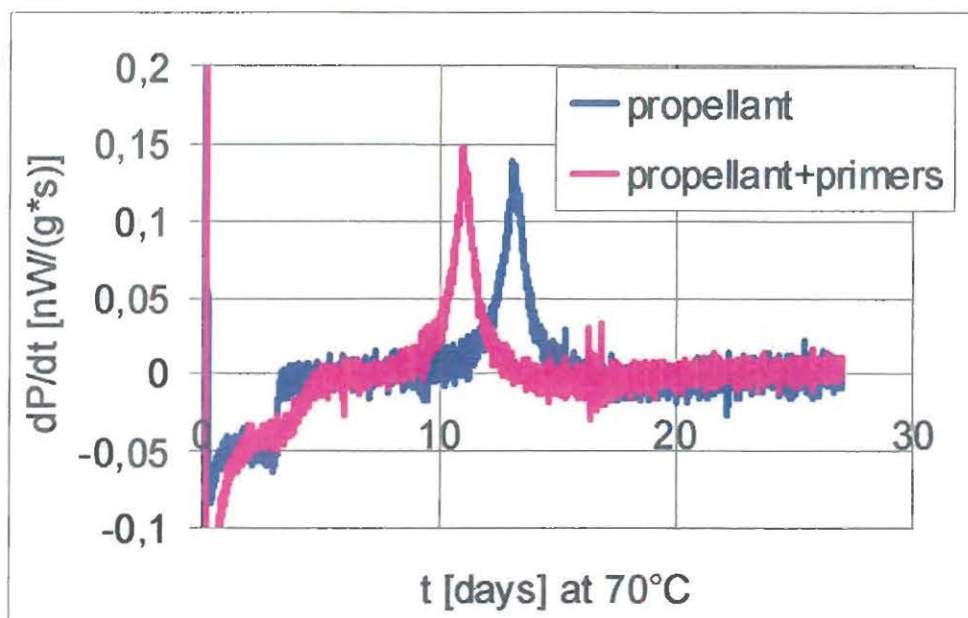


Figure 23. Derivated HFC curves of propellant and propellant in gas phase contact with primers at 70°C

The reaction can be characterized as follows: The interreaction is fast. It does not disappear at lower temperatures. At the same time it is limited, and the calculated interreaction heats are small.

Tested system	T [°C]	$t_{i,p}$ [d]	$t_{i,m}$ [d]	$t_{i,p}-t_{i,m}$ [d]	$t_{i,m}/t_{i,p}$ [%]
Propellant mixed with primer composition	89	0,945	0,694	0,251	27
Propellant with primer mixture in gas phase contact	89	0,945	0,834	0,111	12
	80	3,31	2,91	0,40	13
	70	13,16	11,03	2,13	16

Table 15. Evaluation of derivated HFC curves at different temperatures

$t_{i,p}$ = time until inflection point of the propellant

$t_{i,m}$ = time until inflection point of the propellant in contact with primers

Primer in solvent atmospheres

A possible reaction of isopropanol with diazole was discussed earlier [13]. Besides traces of this solvent and ethyl acetate the DB propellant of the cartridge contains about 0,5 % water. To increase the effects we used solvent atmospheres in the following setup:

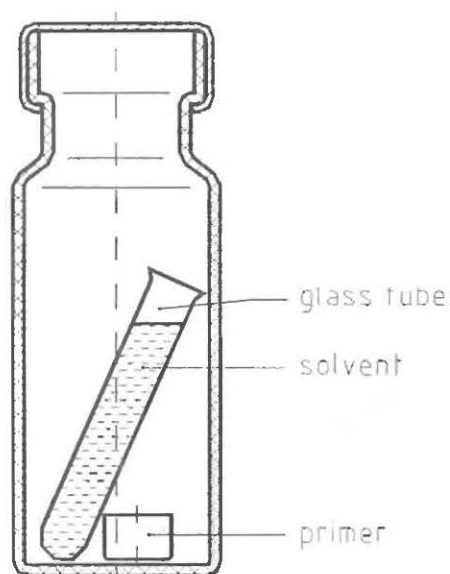


Figure 24: Experimental setup for the HFC measurements of primer composition(s) in solvent atmospheres

The results (see fig. 25) can be summed up as follows:

Isopropanol (iPrOH) vapor causes an extremely fast exothermic and autocatalytic reaction. In comparison water or ethyl acetate are much less effective. Surprisingly the amount of the primer composition of 1 primer (about 20 mg) when loaded in a TAM glass ampoule shows nearly no reaction, whereas copper and brass shells are equally effective as the original nickel plated surface (fig. 26).

P, mW/g

T = 50 °C

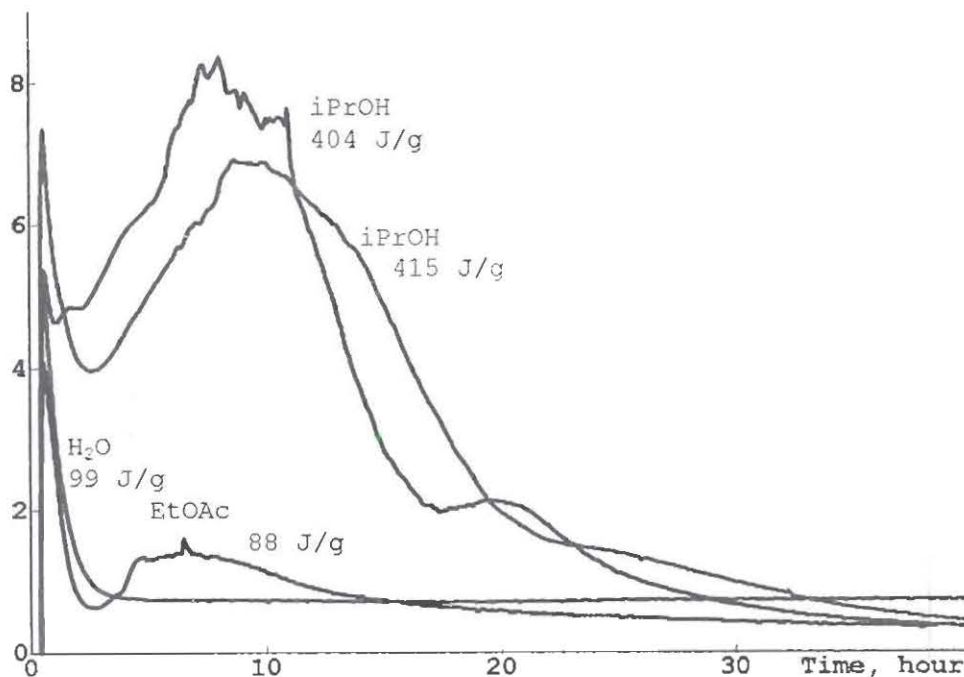


Figure 25. Reaction of primer composition in solvent atmospheres

P, mW/g

T = 50°C

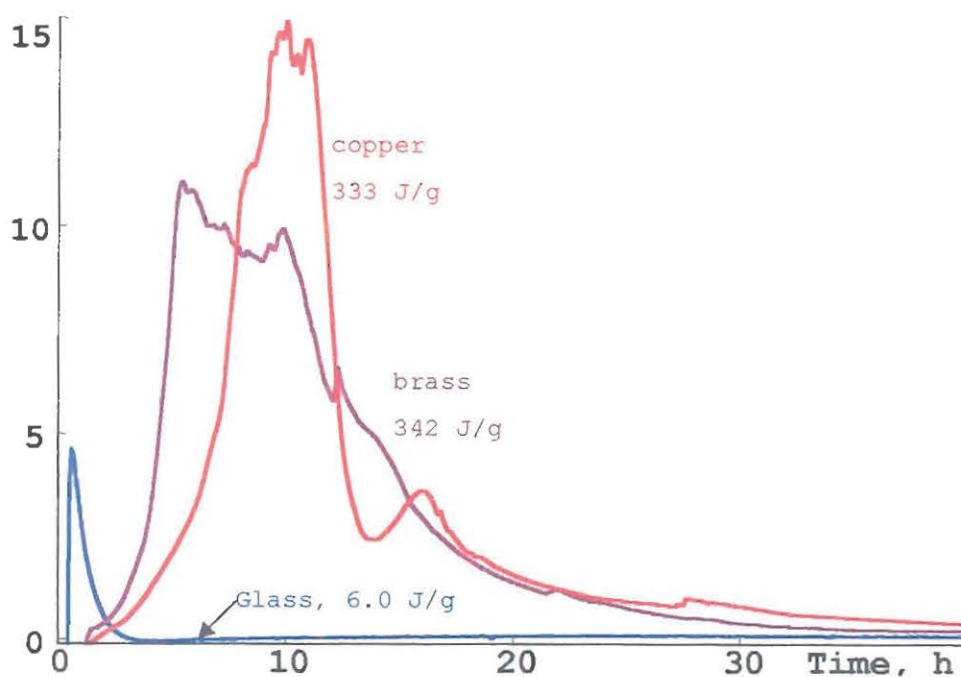


Figure 26. Reaction of primer composition in solvent atmospheres loaded in different materials

P, mW/g

T = 50°C

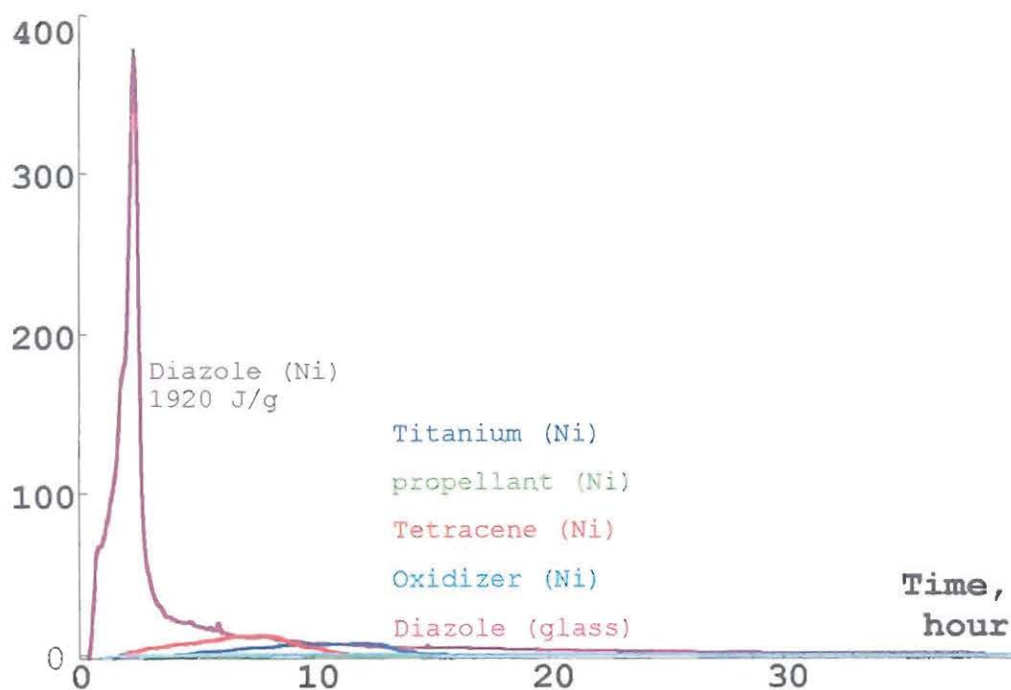


Figure 27. HFC of components of the primer composition loaded in nickel shells in iPrOH atmosphere

Primer shell loaded with single compounds of the composition in isopropanol atmosphere

In this series the same setup as before was used, but the original shell was loaded with a single component of the composition corresponding to the amount in one primer only. Fig. 27 proves that the reacting component is indeed diazole, however, metal is necessary as a catalyst. Nothing happens on glass surfaces.

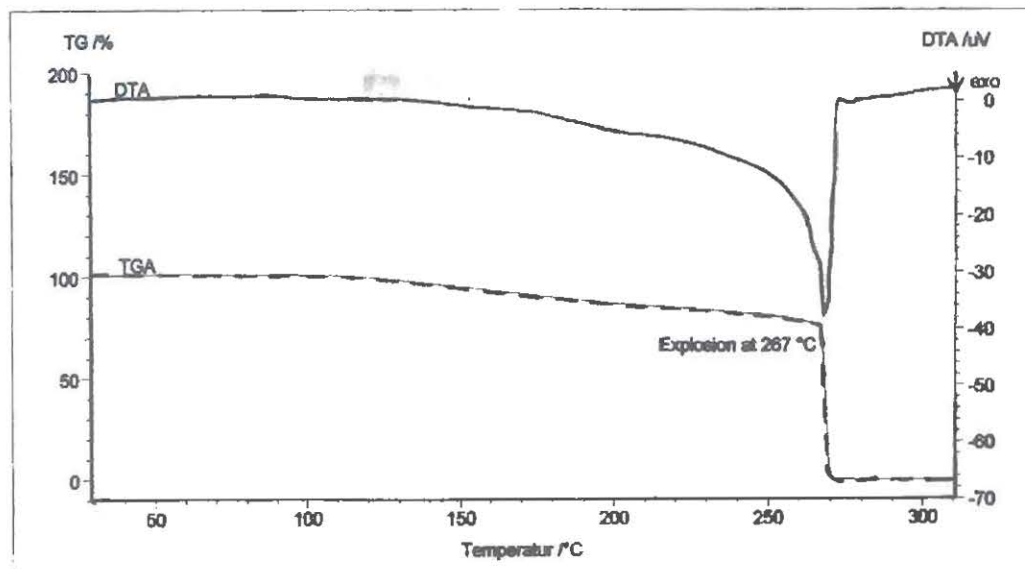


Figure 28. DTA / TG curve of the reaction product of Diazole and isopropanol

In the same way we produced about 10 mg of the nearly black reaction product of diazole with isopropanol, which has not been identified yet. DTA/TGA of a 15 mg sample of this black material ends up in a vigorous explosion at 267°C (see fig. 28).

Comparison of HFC curves of different compounds of the cartridge

The following figure summarises all measurements that were performed with different compounds from the cartridge.

As can be seen the heat generation rate of the propellant increases when it is mixed with primers. Also a slight reduction of the time of the second maximum is visible. This time shift is much bigger if propellant which is delaborated from cartridges is measured alone. A comparable time-shift, but a higher heat flow is observed when the complete ammunition is measured.

All these changes of the heat generation rates are connected with incompatibilities between the components of the propellant, the primer and the cartridge (if applicable).

P, $\mu\text{W/g}$

80°C

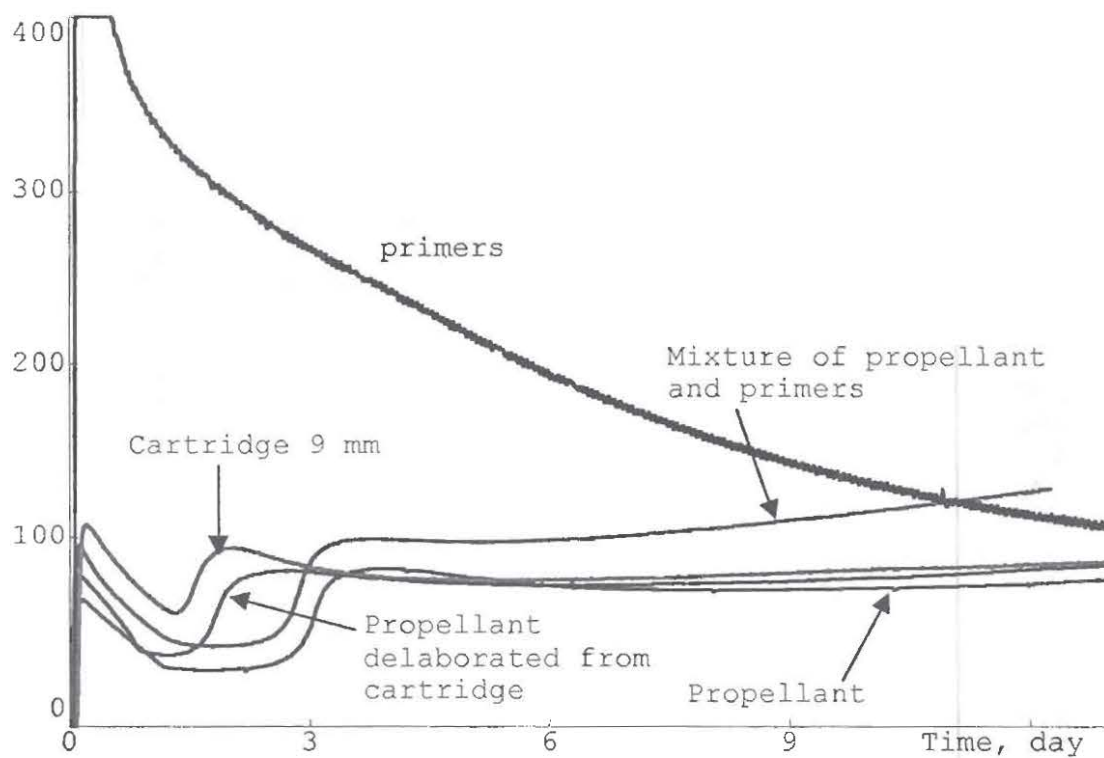


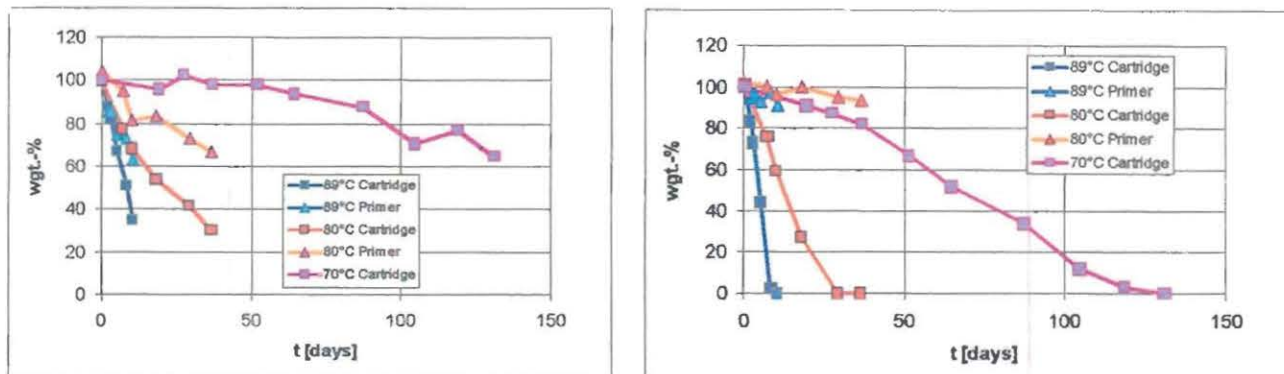
Figure 29. Comparison of HFC curves of different compounds of the cartridge

PART IV – ANALYSES OF AGED COMPONENTS

This part of the paper describes the changes of the primer after ageing in cartridges or alone and the changes of the propellant (mainly stabiliser depletion).

ANALYSIS OF PRIMER MIXTURE AFTER AGEING

The two compounds tetracene and diazole were analysed by HPLC as described above. The analyses occurred after the ageing of primed cases and after the ageing of cartridges. In the latter series there was a gas phase contact of primer and propellant. The results are presented in figure 30 and 31. At the manufacturer's request the true initial contents were set at 100%.



Figures 30 and 31. Tetracene (left) and diazole (right) depletion in primed cases and in cartridges.

The depletion curve of tetracene in cartridge shows a weak, that of diazole a moderate autocatalytic characteristics. By fitting of a first order reaction with autocatalysis kinetic parameters as listed in table 16 were obtained.

$$P = 100 * a / (e^{akt} - 1 + a) \quad (4)$$

$$k = A * e^{-E_a / (RT)} \quad (5)$$

P = content [%]

a = autocatalytic constant

k = reaction rate constant [s⁻¹]

A = frequency factor [s⁻¹]

T = temperature [K]

Compound	Storage of	T [°C]	E _a [kJ/mole]	A [s ⁻¹]	a	SD [%]
tetracene	cartridge	80/89	112,148	1,3663E10	1,31	3,7
tetracene	cartridge	70/80	243,770	4,2169E29	1,31	6,1
tetracene	primer	80/89	164,580	2,7419E17	1,31	4,9
diazole	cartridge	80/89	120,022	1,1152E11	12,24	3,8
diazole	cartridge	70/80	158,682	5,8910E16	12,24	3,8
diazole	primer	80/89	177,779	2,9814E18	12,24	2,9

Table 16. Kinetic parameters of tetracene and diazole depletion

The reaction rate of both tetracene and diazole decreases considerably as indicated by higher values of E_a calculated from 70 and 80°C. We suppose that the „Arrhenius“ is supported by decreasing vapour pressure of the solvents.

ASSESSMENT OF BALLISTIC LIFETIME FROM SHOOTING AND FROM DEPLETION KINETICS

Again as 'worst case' we assumed our lowest activated kinetics (80/89°C) to be valid at lower temperatures. Then, using the '370 m/s' times extrapolated from ballistics (see table 14) the corresponding contents of tetracene and diazole were calculated (table 17).

T [°C]	t	P _{tetr} [%]	P _{diaz} [%]
89	2,58 d	81,1	78,2
80	9,39 d	74,2	66,8
70	28,1 d	74,6	71,3

Table 17. Critical content of tetracene and diazole

Using the marked highest values (= lowest decomposition) extrapolation for T = 20°C gives 45 years for tetracene and 84 years for diazole.

ANALYSIS OF PROPELLANT AFTER AGEING

Detailed analyses of the propellant after ageing are presented in [2]. Here we only want to give a summary of results with the aim of a comparison of the behaviour between the aged propellant in HFC ampoules and the aged propellant in the cartridge. In the following figure the results of stabiliser depletion at 80°C is presented. Ageing of propellant and ammunition at 89°C or at 70°C leads to nearly identical analytical results.

One further comment has to be made: In the graph the sums of mono-N-DPAs, of N-NO-mono-N-DPAs, of DNDPAs and TNDPAs are collected to make it look clearer. For experimental reasons we were not able to quantify 4,4'-DNDPA in all cases. So this compound is not included in the DNDPA-sum.

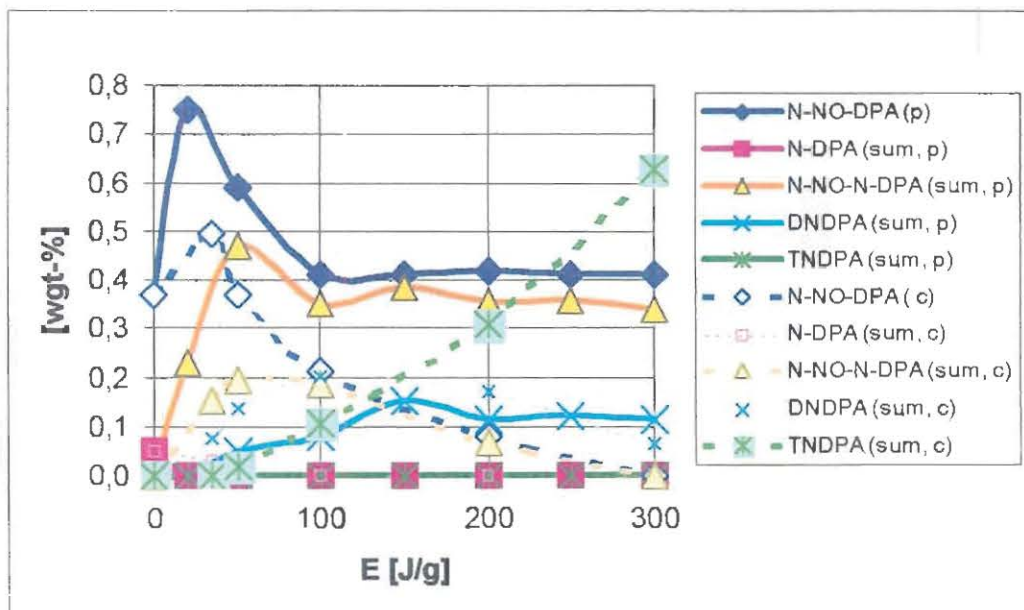


Figure 31. HPLC results of aged propellant (p) and aged propellant in the cartridge (c)

There is a big difference in the appearance of the stabiliser products. Whereas in HFC ampoules N-NO-DPA and N-NO-N-DPAs dominate until 300 J/g (there are only traces of TNDPAs present) the propellant which was aged in cartridges shows after 300 J/g nearly no N-NO-DPA and nearly no N-NO-N-DPAs, but mainly TNDPAs as stabiliser depletion product. This seems to show that there are slightly different ageing conditions in both cases. In HFC ampoules (they seem to be closed very tight) there is no oxygen access to the propellant. In cartridges (which from their

weight loss also do not appear as being untight) there seems to be more oxygen available. The DPA depletion is faster (which is obvious from the earlier 2nd HFC maximum, see figure 5) and so is the N-NO-DPA depletion which follows the depletion of the original stabiliser. Also the NG content has dropped down to about 15 % (compared to 17 % when the propellant was aged in HFC ampoules). The main reaction product of this is 1,3-dinitroglycerin (when aged in cartridges), compared to the formation of N,N-diphenylformamid as a side reaction which only occurs if the ageing happens in tightly closed and completely filled ampoules.

So, not all of the differences in stabiliser depletion between ageing in HFC ampoules and ageing in cartridges could be cleared. But the results show that the ageing conditions are not identical.

SUMMARY

Ballistic and analytical evaluation give comparable minimum life-times of about 50 years at ambient temperature.

At the test temperatures diazole shows a large, tetracene a moderate incompatibility.

The rapid decrease of tetracene and diazole depletion at 70°C may indicate a much longer life time.

CONCLUSIONS

As a result of the work performed in our laboratories several conclusions can be drawn:

- ◆ In many cases compatibility - not stability - will determine the service life of ammunition.
- ◆ reducing compatibility testing to several couples of explosive/contact material may not always be sufficient.
- ◆ The test setup should be as close as possible to reality. If volatile compounds are present in a closed explosive device open test arrangements may be misleading.
- ◆ A combination of different test techniques (TGA/DTA, HFC, ballistic tests and chemical analysis) helps to detect incompatibilities and helps to find out which reactions are responsible for unwanted effects. But we also know that this huge amount of work and effort can not be performed for every weapon system which is in use.

The detected incompatibility of the metal catalyzed reaction of diazole with isopropanol has no severe influence on the service life time of the cartridge as demonstrated by storage and shooting of the cartridge. Reasons for this may be the small available amount of this solvent or the suitability of the reaction product as component of the primer composition.

REFERENCES AND NOTES

- [1] M. Rat, P. Guillaume, S. Wilker, G. Pantel, „Stability Studies of Spherical Propellants“, *ICT-Jahrestagung* 27, 16 (1996); P. Guillaume, M. Rat, S. Wilker, G. Pantel, „Practical Application of Microcalorimetry to the Stability Studies of Propellants“, *TTCP Workshop Leeds* 4/1997; S. Wilker, P. Guillaume, „International Round Robin Test to Determine the Stability of DB Ball Propellants by Heat Flow Calorimetry“, *ICT Jahrestagung* 29, 132 (1998).
- [2] U. Ticmanis, P. Guillaume, A. Fantin, G. Pantel, J.-P. Marchandise, L. Stottmeister, S. Wilker, „Ballistische Untersuchungen an thermisch belasteten TLP“, 3. *WIWEB-Forum Explosivstoffe* **2000**.
- [3] STANAG 4090: "SMALL ARMS AMMUNITION (9 mm PARABELLUM)", MOPI (Manual of Proof and Inspection Procedure for NATO 9 mm Ammunition (AC/225 (Panel III/SP.1) D/170)).
- [4] DIN 51900-1, „Bestimmung des Brennwertes mit dem Bombenkalorimeter und Berechnung des Heizwertes“, Draft June 1998; German TL 1376-0600, 3.41, „Bestimmung der Explosionswärme“.
- [5] S. Wilker, U. Ticmanis, L. Stottmeister, P. Guillaume, B. Vogelsanger, C. Balès, P. Bisogni, W. de Klerk, D.J. Wood, D.S. Tucker, „Influence of atmospheric conditions on the ageing of single and double base propellants“, *Symp.Chem.Probl. Connected Stabil.Explos.* 12th, (2001).
- [6] P. Guillaume, M. Rat, G. Pantel, S. Wilker, „Heat Flow Calorimetry of propellants – Effects of sample preparation and Measuring Conditions“, *Propellants, Explosives, Pyrotechnics* 26, 51-57, **2001**.
- [7] STANAG 4582, „Explosives, Nitrocellulose Based Propellants, Stability Test Procedure and Requirements using Heat Flow Calorimetry“, WG Draft (2/02); U. Ticmanis, S. Wilker, G. Pantel, M. Kaiser, P. Guillaume, C. Balès, N. van der Meer, „Principles of a STANAG for the estimation of the chemical stability of propellants by heat flow calorimetry“, *ICT-Jahrestagung* 31, 2 (2000); U. Ticmanis, S. Wilker, P. Guillaume, W. de Klerk, „The Status of the HFC STANAG“, 3rd *International symposium on Heat Flow Calorimetry and it's applications for Energetic materials*, French Lick, Indiana, April **2002**.
- [8] W. Scheunemann, U. Ticmanis, „Investigation of qualification samples of percussion cup“, *WIWEB-Report* 330/13762/99.
- [9] H.E. Kissinger, *Anal. Chem.* 29 1702-1706 (1957).
- [10] M. Kaiser, W. Scheunemann, U. Ticmanis, „Fortschrittliche Methoden zur Bestimmung der Stabilität von Zünd- und Anzündstoffen und Munitionskomponenten“, *ICT-Jahrestagung* 26, 30 (1995).
- [11] S. Wilker, G. Pantel, M. Kaiser, U. Ticmanis, „Wärmeflußmessungen an Anzündhütchen“, *ICT-Jahrestagung* 26, 84 (1995).
- [12] S. Wilker, G. Holl, U. Ticmanis, A. Sommer, G. Pantel, „Chemische Verträglichkeit von TLP mit Kontaktmaterialien“, *ICT-Jahrestagung* 28, 17 (1997).
- [13] W. Scheunemann, U. Ticmanis, M. Kaiser, M. Künstlinger, „Zersetzungskinetik von Anzündmitteln“, Vortrag 3. *WIWEB Forum Explosivstoffe* **2000**.

HFCS 2001/2 SESSION MINUTES

SESSION #1:

Question asked by: Dr. Bohn, Fraunhofer-Intitut für Chemische Technologie

Question directed to: Dr. Uldis Ticmanis and Dr. Pierre Guillaume, WIWEB, Germany and PB Clermont, Belgium

Question: You have shown a correlation between the decrease of Q_{ex} with aging and the increase in heat elevation measured by HFC. There is a correlation but I mean one can recognize a systematic deviation. Do you agree? How to explain the deviation?

Answer: The correlation is made between the heat released in the calorimeter and the difference of Q_{ex} between a fresh and an aged propellant. The latter operation means calculating a difference between two large numbers which is always a source of errors. So we're not sure whether there is a systematic deviation in the comparison of both curves.

Question asked by: Dr. Indu B. Mishra, CPIA, Johns Hopkins University

Question directed to: Dr. Uldis Ticmanis, WIWEB, Germany

Question: Your study shows propellant is 20% destroyed in 333 d. You did studying at 89°C. It is known from earlier studies that accelerated aging at high temperatures does not reflect a real decomposition scenario, as DPA breaks down to N-nitroso DPA, 2N-DPA, 4N-DPA, and further nitrated DPA products. Storage at room temperature shows no performance reduction in 50 years! You also show fast decomposition for tetracene and diazole are 89°C.

Answer: The 20% decomposition in 333 days was calculated for the small percentage of propellant in the primary mixture of the primer. This cannot be compared with storage of pure propellants. After our experience there's no change in the decomposition mechanism of propellants between at least 60°C and 90°C, except perhaps in some cases (see last presentation = STANAG 4582).

Question asked by: Dave Schulte, NSWCR Crane

Question directed to: Dr. Uldis Ticmanis and Dr. Pierre Guillaume, WIWEB, Germany and PB Clermont, Belgium

Question: Are you aware of any research that parallels your work on larger cartridges?

Answer: None to our knowledge.

Question asked by: Dave Schulte, NSW Crane

Question directed to: Dr. Uldis Tiemanis and Dr. Pierre Guillaume, WIWEB, Germany and PB Clermont, Belgium

Question: What parameters drive the incompatibility to be the service life determinants?

Answer: In all cases, where an explosive reacts faster with a contact material than it decomposes by itself, the incompatibility will dominate the service lifetime.

THIS PAGE LEFT INTENTIONAL BLANK

**APPENDIX: REPORT ON INVESTIGATION INTO THE ACCIDENT WHICH
OCCURRED IN EXPLOSIVES TEMPORARY STORAGE PLACE NO. 12 OF
TAKETOYO PLANT, NOF CORPORATION (OFFICIAL SUMMARY)**

**Jun-ichi Kimura Ph. D., Representative of JK Research, jkr@ym.catv.ne.jp
A Member of Investigation Committee for the Accident at Taketoyo Plant, NOF Co. Ltd.**

1. SUMMARY OF THE ACCIDENT

(1) Time of Occurrence, Place and Weather Conditions

Around 22:09 on Tuesday, August 1, 2000, an explosion occurred at the Explosives Temporary Storage Place No. 12 of Taketoyo Plant, Aichi Works, NOF Corporation, Aichi Prefecture, Japan in which 7.7 tons of smokeless gunpowder and other items were kept.

Weather data of the day recorded by Taketoyo Municipal Hall (22:00) was fine, temperature 26.3℃, relative humidity 84%, average wind velocity 3.1 m/sec and mean direction of the wind south-east.

(2) The Extent of the Damage

This accident resulted in 79 injuries and 888 cases of physical damage such as houses affected by the explosion blast. The scale of the accident was large and it had a big social impact.

2. An Outline of Taketoyo Plant (Conditions for Handling of Smokeless Gunpowder)

(1) Implementation of the Stability Test

It was necessary to perform the stability test for a total of 662 lots of smokeless gunpowder in the whole Taketoyo Plant (of which 180 lots of smokeless gunpowder were kept in Explosives Temporary Storage Place No.12), according to laws and regulations, but the test was not performed at all for 520 of these lots (78.5%) (including 171 lots kept in Explosives Temporary Storage Place No.12 or 95% of the total kept there).

The results of the stability tests which were performed, were not reported to the prefectural governor.

(2) Storage Period

When the storage time of smokeless gunpowder kept in Explosives Temporary Storage Place No. 12 was investigated, 4 lots had a storage time of more than 4 years and the longest storage time was 4 years and 4 months.

(3) Containers

In Explosives Temporary Storage Place No. 12, 5 kinds of containers such as wooden containers with an inner aluminum surface (capacity: 465 kg) and wooden containers (capacity: 71 kg or 82 kg) were used. About 65 % of the storage quantity of smokeless gunpowder was kept in the wooden containers with an inner aluminum surface.

(4) Conditions for Keeping Material, Other Than Intermediates in the Manufacturing Process, in the Temporary Storage Place and Disposal

Explosives such as leftover products after the packaging and returned products were kept in Explosives Temporary Storage Place No. 12. But, as these were not intermediates in the manufacturing process, their being kept in the temporary storage place was inappropriate and these should have been stored in magazines, from the standpoint of ensuring security. Moreover, since there were no disposal standards for waste explosives, which are necessary for the disposal of these explosives, they were not disposed of properly.

(5) Measure to Shade Sunlight

As measures of window shading for Explosives Temporary Storage Place No. 12, only the measure of painting over the window glass with red paint was performed, instead of putting up shading curtains, which had been done in the past, and there was insufficient technical verification for that change.

(6) Reuse of Leftover Products after the Packaging, and Returned Products

On the occasion of reuse of leftover products after the packaging, which were produced a long time ago, and returned products, a stability test was not performed in many cases and the degree of deterioration could not be detected fully.

3. The State of the Accident (Damage to Explosives Temporary Storage Place No. 12)

After the accident, Explosives Temporary Storage Place No. 12 was transformed into merely a steel skeleton. The roof and wall materials of it scattered entirely and the storage place collapsed completely. Various sizes of 13 funnel-shaped holes were formed on the ground. The largest one (the longest diameter: 310 cm, the shortest diameter: 280 cm and the depth: 130 cm) was formed at the far-east part.

4. The Results of the Investigation and the Analysis

(1) Process for Ignition and Explosion

It is estimated that the smokeless gunpowder called MJ-B (2 cases each of 2kg double base gunpowder), which were produced 4 years ago and were kept for 2 years in a black synthetic resin container, were exposed to sunlight because the storage point was close to the window facing west. Such an environment resulted in spontaneous combustion, for it was placed in an atmosphere of high temperature and high humidity in the summer season and the stability deteriorated remarkably.

On an other aspect of this accident, it has been found that part of the smokeless gunpowder kept in Explosives Temporary Storage Place No. 12, brought about a heavy explosion and the successive high-velocity combustion of the containers themselves caused the bigger damage. The reason why part of the gunpowder exploded almost instantly within a very short time period is that the whole building was in flames due to the initial combustion or explosion and the temperature for all of the smokeless gunpowder went up rapidly. Thus it is estimated that the conditions became very susceptible to explosion and shifted from combustion to explosion almost instantly.

(2) Compliance with the Laws and Regulations

□ Storage in Explosives Temporary Storage Place No. 12

Non-PVC, which was not permitted to be kept in the place, was actually stored there. The maximum storage weight by permission in the place was 8.8 tons, but in the past, up to max. 19,731.31 kg of storage weight was kept there.

Furthermore, smokeless gunpowder other than intermediates in the manufacturing process (i.e. leftover products after the packaging, returned products, et al.) was kept for a long time in the place.

□ Storage situation in facilities other than the Temporary Storage Place No. 12

In 13 facilities such as manufacturing buildings more explosives were kept than the

maximum storage weight permitted. Furthermore, in 9 facilities such as manufacturing buildings, explosives other than the permitted explosives were kept.

□ Implementation of stability test

For smokeless gunpowder, for which a stability test should be performed, 78.5% was not tested at all by the stability test required by laws and regulations and the test results were not reported to the prefectural governor, either.

□ Disposal

Gunpowder et al. of 117.96 kg was disposed of without the permission of the prefectural governor.

□ Documentation

There were problems in the contents of the book in which the bringing-in and carrying-out of explosives at Explosives Temporary Storage Place No.12 were recorded.

5. Actions to Prevent Recurrence

(1) A Lesson from the Accident

Observing the cause of this accident, we are forced to conclude that the handling of smokeless gunpowder was insufficient, as we know of such facts as that the explosives temporary storage place was used as a substitute for magazines by Taketoyo Plant, putting priority on productivity. NOF Corporation should reexamine its present safety control system, in order to never cause such an accident again, and make every effort to establish a proper safety control system.

(2) Actions to Prevent Recurrence by Taketoyo Plant

It is necessary for Taketoyo Plant to take the following actions to prevent recurrence.

The measures which this investigative committee evaluated as appropriate in the mid-term report have already been taken for the following items □.

□ Items for production of explosives, in general

Intensification of safety education, strengthening of safety control system, orderly preparation of company rules for safety, and improvement of the structure of buildings such as window shading

□ Items for smokeless gunpowder

- Shading measure of light, installment of recording thermometer and hygrometer and conditioning for temperature and humidity at the temporary storage place of smokeless gunpowder

- Installation of automatic fire-extinguishing equipment such as sprinklers at the temporary storage place for smokeless gunpowder
- Adoption of smaller size for containers of smokeless gunpowder, restrictions on container material, and clarification of storage methods at the temporary storage place
- Reexamining of safety distance at the temporary storage places of some smokeless gunpowder
- Exact implementation of the stability test
- Proper treatment of smokeless gunpowder and proper usage of temporary storage place for explosives

(3) Proposal of Reexamination for Enforcement Regulations of Explosives Controlling Act

The administrative authorities also should consider reexamination of technical standards of the following items:

- Standards for the temporary storage place of smokeless gunpowder
 - Shading measure of light, installment of recording thermometer and hygrometer, and conditioning for temperature and humidity
 - Installation of automatic fire-extinguishing equipment such as sprinklers
 - Adoption of smaller size for containers, material restrictions on containers and clarification of storage methods at the temporary storage place
 - Clarification of the storage period
- Reexamination of safety distance at the temporary storage places of smokeless gunpowder

The accident occurred by the spontaneous ignition originating from inappropriate handling of smokeless gunpowder at the temporary storage place. Thus explosion accidents can be prevented by setting standards of □ on the temporary storage place of smokeless gunpowder. Nevertheless, with the aim of preparing for the worst, it is necessary to reexamine the safety distance of smokeless gunpowder at the temporary storage place at the same level as high explosive. However, propellant and some smokeless gunpowder, which are judged as having a very low probability of explosion by DDT test (50/60 steel tube test), are appropriate to be excluded from the subject of reexamination for distance.

It is also desirable for the validity of the DDT test (50/60 steel tube test) to be studied, based on technical progress for the future.

- Appropriate implementation of the stability test
- Clarification of the legal duty of the person in charge of safety matters in the production process

Member of the Investigation Committee

Dr. Hideyo Osada Professor Emeritus, Kyushu Institute of Technology.
(Chairperson)

Dr. Terushige Ogawa Professor, Yokohama National University
Material Technology, Dept of Engineering.

Dr. Junichi Kimura Chief-in-Propellants and Explosives Laboratory
Guns and Ammunition Division, First Research Center
Technical Research and Development Institute
Japan Defense Agency (resigned on July 1, 2001).
Representative of JK Research (at the present time).

Dr. Masamitsu Tamura Professor, Graduate School of Tokyo University
Environmental Study, Research Dept. for New Regional
Creative Science.

Michio Nakajiku Senior Managing Director, Explosives Safety Association of
Japan.

Dr. Masatake Yoshida Head of Research Office for High Energy Chemistry
Dept. of Extreme Reaction
National Institute of Materials and Chemical Research
Agency of Industrial Science and Technology.

THIS PAGE LEFT INTENTIONAL BLANK

Application of heat flow calorimetry to high explosives

Carole Baker¹, Neil Turner¹ and Paul Bunyan²

¹DOSG, Abbey Wood, Bristol, United Kingdom.

²QinetiQ, Centre for Environmental Technology, Fort Halstead, Sevenoaks, Kent, United Kingdom.

Abstract

Based on examples of life terminating processes in high explosives during storage and use, it is clear that decomposition of the energetic material is not invariably the cause of system failure. It is also by no means the only reaction that may take place in, and be observed by, a microcalorimeter.

This paper will describe some thermal analysis experiments conducted on high explosive samples. These employ differential scanning calorimetry to monitor thermal effects at elevated temperatures (around 200°C) and microcalorimetry to record thermal effects at much lower temperatures (below 100°C).

The work shows that, due to the generally high thermal stability of many high explosive compositions, Heat generation rates are very low, if detectable at all, at normal storage temperatures, even with a very sensitive instrument like the TAM. The measurement of very low levels of heat generation is difficult, time consuming and therefore expensive. If the assumption is made that the life limiting process is invariably the slow decomposition of the energetic component, this will frequently lead to very long service lifetime predictions.

A number of possible complications are identified. Firstly, a sensitive calorimeter will detect other reactions which may not lead to failure, but which may still dominate the heat flow signal. Secondly, the true failure process may generate little energy and be overlooked. In view of these considerations, at present it seems unwise to rely on HFC as the only tool for the assessment of the life of high explosive energetic systems.

1 INTRODUCTION AND BACKGROUND

All processes (physical or chemical) are accompanied by the generation or consumption of energy, usually in the form of heat. It follows that, in principle, all processes can be studied using some sort of calorimeter. The very high sensitivity of modern microcalorimeters means that the technique can be considered as a way to look at some very slow reactions. For example, single, double and triple based propellants, containing nitrate esters, will undergo thermal decomposition, even at normal magazine storage temperatures, and this process can be observed directly by microcalorimetry. It is known that, in addition to loss of energy leading to changes in reliability and performance, the decomposition reaction in this type of explosive is autocatalytic and can lead to self ignition in systems containing old propellant. Microcalorimetric techniques have been used increasingly over the last two decades for weapons system surveillance and lifetime prediction [1, 3]. Much work has been done recently to standardise microcalorimetry test procedures to allow unambiguous interpretation and pass/fail criteria to be established [4].

Modern weapon systems contain many other unstable materials including:

- High explosives (RDX, HMX, TNT)
- Composite propellants (AP/AL/polymeric binder)
- Non energetic materials (structural components)

In view of the success of the microcalorimetric approach to surveillance testing in cordites etc., it would be an attractive proposal to apply a similar approach to devices containing these unstable materials as well. Indeed, some countries have already proposed the use of microcalorimetry in this way [5].

In the United Kingdom, at the present time, there is no rigidly defined set of procedures which are applied to all

systems. Instead, the current practice is to apply past experience to decide what the failure mechanisms are likely to be on an individual, case by case, basis. A testing regime tailored specifically to observing and quantifying the critical failure process is devised [6]. Some (but by no means all) of the techniques which may be included in the test programme for a weapon system are:

Empirical full scale tests – ability to survive a feasible hazard

- Slow cook off test
- Fuel fire test
- Shaped charge attack

Examination of physical integrity of whole device

- Dismantling/Visual examination
- X-ray, Ultrasound scans

Mechanical tests

- Dynamic mechanical analysis
- Tensile strength

Chemical analysis of energetic components

Vacuum stability tests

Thermal analysis of energetic components

Whilst clearly essential, surveillance and lifetime tests comprise a significant part of the total cost of a weapons system. Given the recent availability of very sensitive microcalorimeters, coupled with the fact that calorimetry is a universal technique – i.e. whatever process will eventually be life limiting will invariably be associated with some thermal activity, it is an attractive proposition to see if some, or even all, of the various techniques in the above list can be replaced by heat flow calorimetry.

This paper will examine this proposition further. Section 2 reports attempts to study the thermolysis reaction of an in-service PBX composition based on an RDX-filled polypropylene glycol rubber by calorimetry. Sections 3 and 4 discusses the results in the light of experience of known life limiting processes which have been encountered in systems containing PBX in the past.

2 EXPERIMENTATION AND RESULTS

Studies at elevated temperatures were carried out using isothermal differential calorimetry and at moderate temperatures by microcalorimetry. The heat generation rate expected at moderate temperatures (60 – 90°C) was found by calculation, using the high temperature data and compared with the results observed experimentally at lower temperatures.

Differential Calorimetry Studies

Table 1 *Isothermal Differential Calorimetry – Time to Reach 50% Evolution of total Decomposition Peak Energy*

Temp /°C	Temp /K	$t_{(50\% \text{ conversion})}$ /min	1/T /Kelvin	$-\ln [t_{(50\% \text{ conversion})}]$
215	488.15	432	0.002049	-6.06843
215	488.15	426	0.002049	-6.05444
210	483.15	606	0.00207	-6.40688
210	483.15	666	0.00207	-6.50129
205	478.15	1062	0.002091	-6.96791
205	478.15	968	0.002091	-6.87523
200	473.15	1590	0.002113	-7.37149
200	473.15	1760	0.002113	-7.47307

All experiments were carried out using the Mettler DSC-30 differential calorimeter, using small PBX samples (<20mg) contained in 40µl aluminium crucibles.

The decomposition exotherm was recorded under isothermal conditions at temperatures of 200, 205, 210 and 215°C. In each case the decomposition has a complicated appearance and is characterised by 2 major peaks and a total decomposition enthalpy of $2539 \pm 150 \text{ J.g}^{-1}$ (Fig 1). However, as the general shape of the curves is comparable, isoconversion techniques will allow an estimate of apparent activation energy at constant degrees of advancement of the reaction [7]. The tabulated data and resulting Arrhenius plot are shown in table 1 and figure 2.

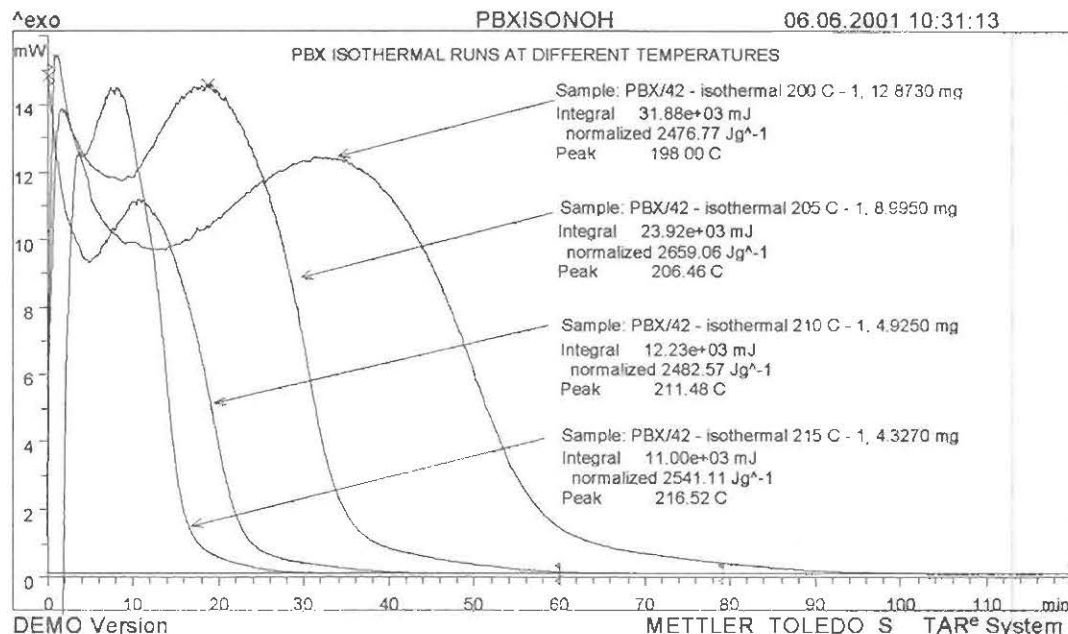


Fig 1 Isothermal DC runs on PBX Sample

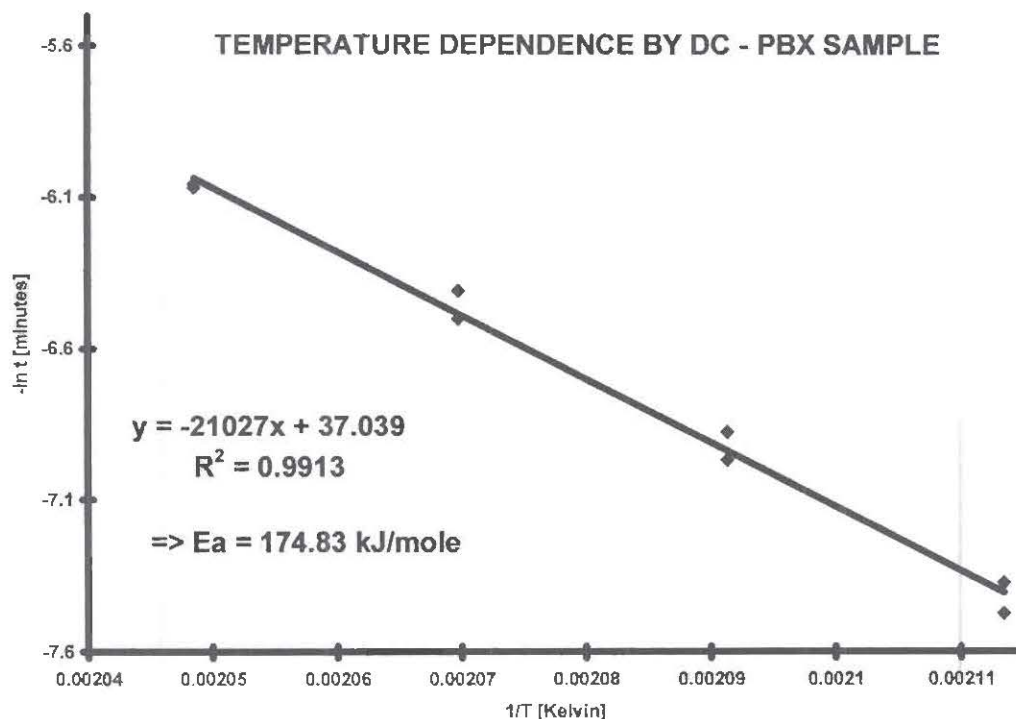


Fig 2 Temperature Dependence of PBX Decomposition From Isothermal DC Data

Extrapolation Checks by DC

The validity of extrapolating this plot down to lower temperatures was tested as follows.

Extrapolating the temperature dependence plot shown in figure 2 would suggest that the corresponding time to achieve 50% extent of reaction at an isothermal temperature of 160°C would be 1836 minutes. Since the instrument is not sensitive enough to measure the anticipated exotherm at such a low temperature directly, a 'one point' ageing experiment with retrospective determination of residual energy was conducted as follows:

- 1 Heat a sample of known weight in the DSC-30 to 160°C at 20°C.min⁻¹.
- 2 Maintain temperature at 160°C for 1836 minutes.
- 3 Raise temperature to 210°C at 20°C.min⁻¹.
- 4 Record (attenuated) exotherm while holding temperature constant at 210°C until the signal has decayed.
- 5 Determine reduction in peak area resulting from earlier thermal history – i.e. storing at 160°C for 1836 minutes.

The resulting DC/DSC trace is illustrated in figure 3.

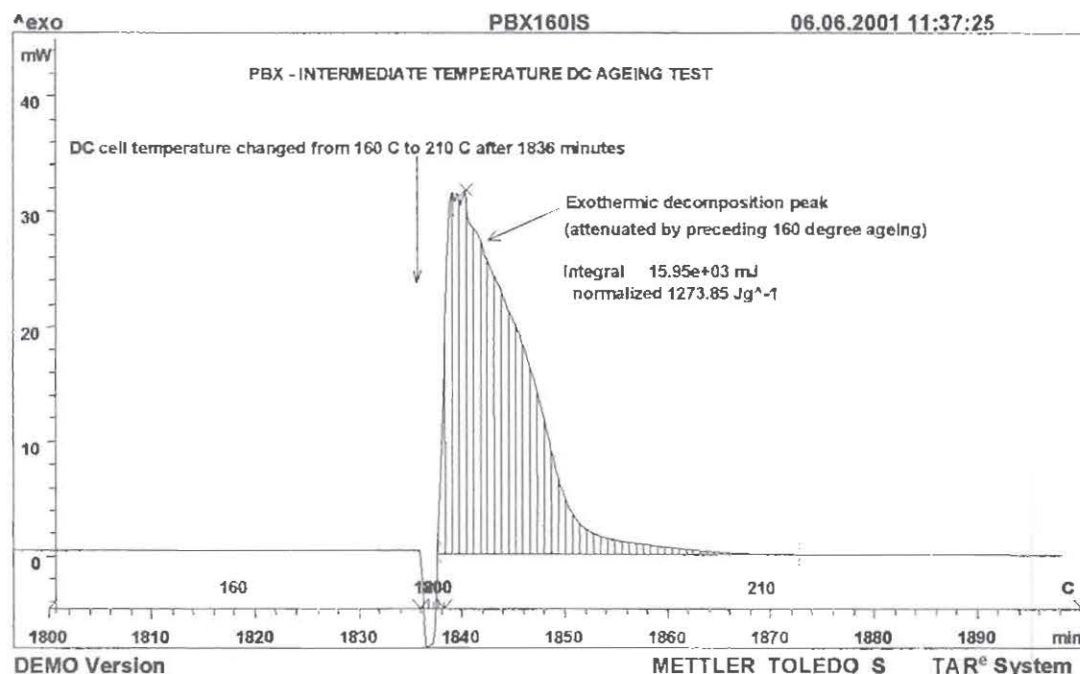


Fig 3 Intermediate Temperature Ageing Test to Validate PBX Decomposition Kinetics Plot

The percentage reduction was 52% compared to a PBX sample heated directly to 210°C (very close to expected 50%) suggesting that the plot describes the temperature dependence of the decomposition from 215°C down to 160°C satisfactorily. Alternatively, using the time for a 52% reduction at 160°C (1836 minutes) and to reach the same point in the reaction at 215°C (7.4 minutes) suggests a similar activation energy of 176.2 kJ/mole at this stage in the reaction.

The maximum heat generation rate at 215°C recorded was 3.23 mW/mg (or 3230000 µW/g). If Fig 2 was valid down to the temperature region generally used for HFC studies, this would predict rather low values of heat generation at moderate temperatures (Table 2).

Table 2 Anticipated Maximum Heat Generation From Heat Flow Calorimetry Experiments at Moderate Temperatures

Experimental Temperature/°C	Expected Heat Generation Rate $\mu\text{W/g}$	Comments
90	1.0	Should be detectable
80	0.2	Barely detectable
70	0.03	Not detectable above noise
60	0.005	Not detectable above noise

Microcalorimetry Studies

All microcalorimetry experiments were performed on $1.5 \pm 0.1\text{g}$ samples of PBX sealed in 3cm^3 glass ampoules, using a Thermometric type 2277 thermal activity monitor (TAM).

Heat generation was recorded on freshly prepared samples at thermostat temperatures of 90, 80 and 70°C. The experiments were allowed to continue until at least 0.5 J.g^{-1} had been evolved. The resulting traces are illustrated in figure 4. In each case heat generation was small, but detectable and also higher than anticipated from a consideration of the earlier DC studies. Data from each TAM experiment was used to construct a plot of \ln (time to evolve 0.5 J.g^{-1}) against $1/T$ (Fig 5). The deduced apparent activation energy was around 64 kJ.mol^{-1} . However the plot was a very poor fit to a straight line – the curved plot suggesting that the apparent activation energy was becoming lower as the temperature was reduced. Extrapolating such data to estimate an equivalent time at room temperature could give extremely erroneous values.

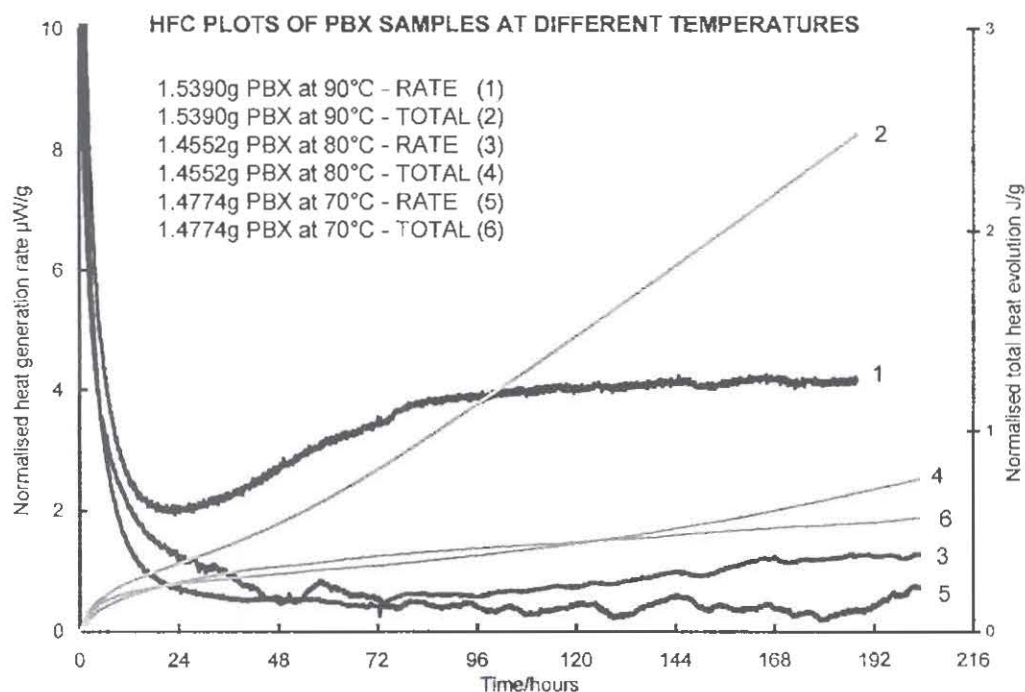


Fig 4 Heat Generation from PBX at 90°C, 80°C and 70°C

Extrapolating the HFC temperature dependence plot suggested that heat generation should be of the same order as instrumental noise at 60°C. Time constraints meant that leaving a PBX sample on at 60°C for long enough to evolve measurable quantities of heat was not feasible and so measurements were attempted at 60°C on the samples previously used for the TAM experiments at 90, 80 and 70°C (i.e. their initial extent of reaction could be taken as that reached at the end of the initial, higher temperature test). If an accurate signal could be measured, this would allow activation energy in this temperature range to be determined by the 'step principle' [8].

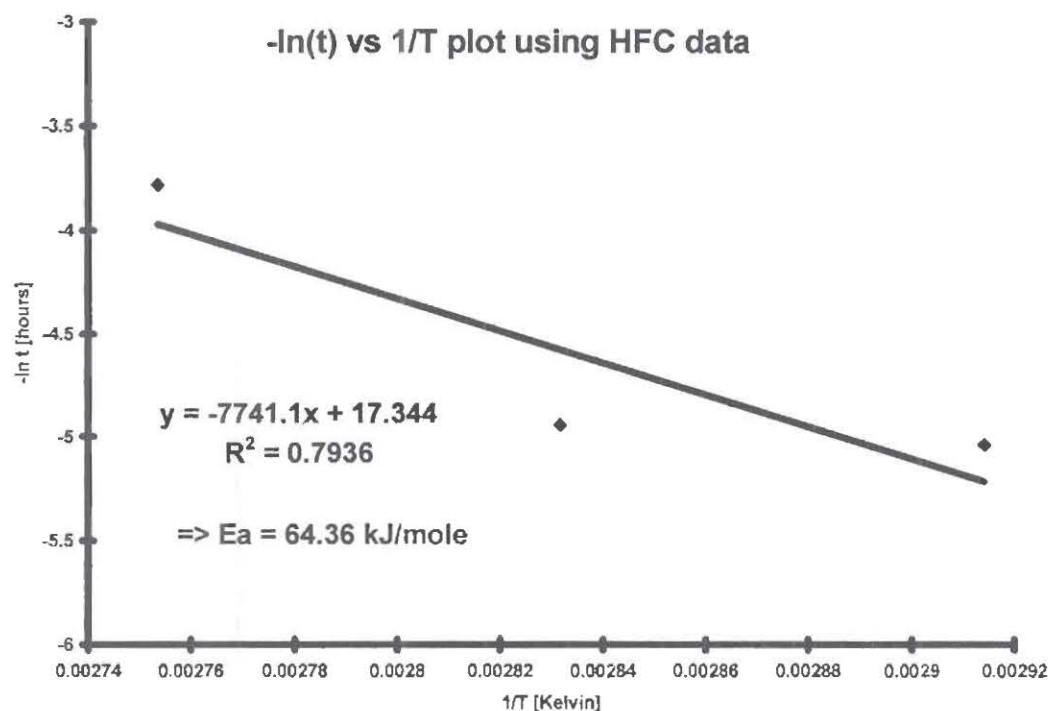


Fig 5 Temperature Dependence of PBX Decomposition Constructed From Microcalorimetry Data at 90, 80 and 70°C

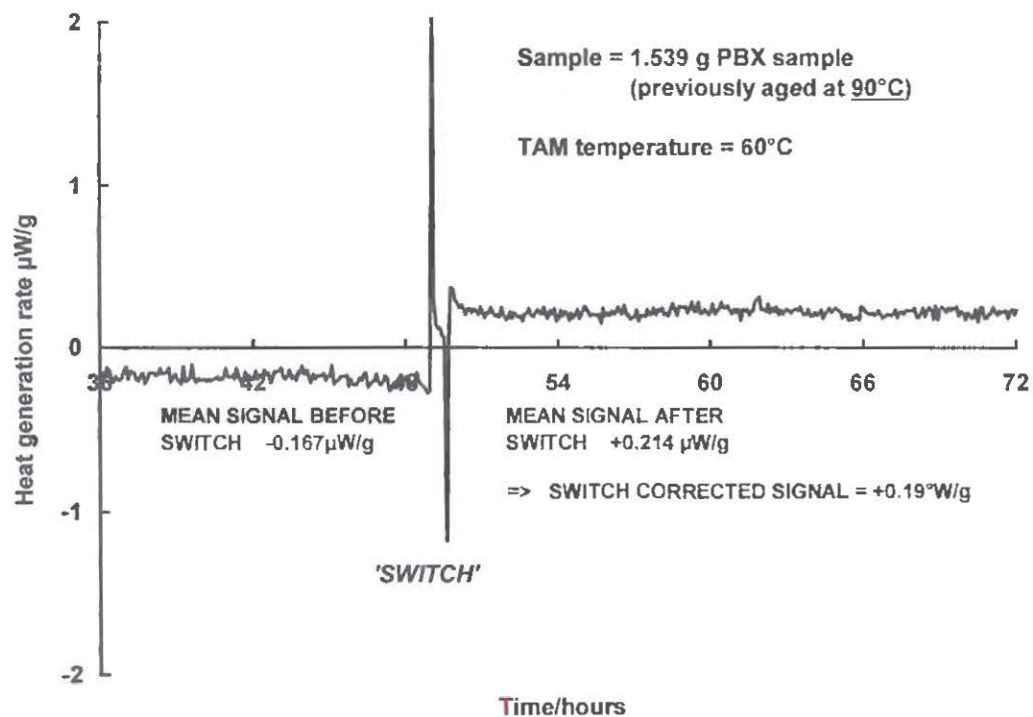


Fig 6 Heat Generation at 60°C from PBX sample previously used for 90°C Microcalorimetry experiment – 'switch' technique used to confirm true baseline position

Heat generation did appear to be just detectable above noise, although due to the fact that the heat generation was so close to zero a 'switch' experiment [9] was required in each case to confirm this (e.g. figure 8 showing the switch experiment on a sample previously monitored at 90°C). Taking the mean values for 12 hours before and after switch and deducing true baseline position to be half the difference leads to the estimates of 0.190, 0.189 and 0.124 $\mu\text{W/g}$ for the samples formerly measured at 90, 80 and 70 °C respectively.

While consistent with activation energy being low (somewhat less than 100 kJ.mol^{-1}), since it is difficult to show that the exotherm is there at all and it would not be sensible to quote a more exact figure.

3 DISCUSSION

Heat generation rates from Nitramine high explosives are very low in comparison to nitrate ester propellant compositions. They may be difficult to detect at all, at moderate temperatures, even with a very sensitive instrument like the thermal activity monitor. The measurement of very low levels of heat generation ($< 1\mu\text{W}$) is difficult, time consuming and therefore expensive.

The fact that the microcalorimeter is so sensitive coupled with the relatively high stability of most high explosives and composite propellants will mean that other thermally-active effects may overwhelm the heat flow signal due to thermolysis of the energetic material itself. If the heat generation from another, non-life limiting process such as post curing of a polymeric binder, corrosion of a metal component or surface oxidation processes, are attributed to thermolysis of the explosive itself, this may lead to over pessimistic forecasts.

On the other hand, some processes which could shorten the life of a device significantly, may generate very small quantities of heat which are undetectable, even with a microcalorimeter. For example, a small number of chain breaks in a polymer, or the formation of a small number of crosslinks will represent very little chemical activity – and therefore generate very little heat. However, these may result in a major change in molecular weight and this will, in turn, have a marked effect on physical properties. In cases where changes in physical properties could be life limiting, it appears sensible to use techniques which measure mechanical properties directly as the main tool for identifying critical age-related changes. In cases such as this, relying on microcalorimetric evidence too heavily might lead to over optimistic forecasts.

If the assumption is made that the life limiting process is invariably the slow decomposition of the energetic component, this will frequently lead to very long service lifetime predictions – hundreds or even thousands of years. Any prediction that 'proves' that a complex chemical system will last virtually for ever, should be treated cautiously.

4 RECOMMENDATIONS AND CONCLUSIONS

It is recommended that a critical appraisal of available data is made before reliance is made on heat flow calorimetry data when used for in service surveillance and lifetime prediction. This is to ensure that the process responsible for any observed heat flow and the process which might lead to failure of the weapon are the same.

Experiments should be examined retrospectively by asking questions such as:

- Is the kinetic evidence consistent with the reaction assumed to be taking place?
- Are the results believable in the light of experience, the results of other experiments and common sense?
- Are the results born out by any available ageing data at lower temperatures?
- Is there supporting evidence that the observed heat generation is really due to a likely lifetime limiting process at all?

Of course, for research purposes, yes or no are both useful answers to each of those questions as further critical experimentation can always follow. However, for general, standardised surveillance purposes, it is a requirement that the answer to each question is yes!

In the case of nitrate ester propellants, the situation appears promising since each of those questions can be answered with a 'yes'. Therefore the approach appears potentially very useful.

In the case of some of the more chemically stable ingredients found in weapon systems, the situation is less clear due to potential complications:

- Thermolysis of the explosive components will be more difficult to detect and therefore more time consuming and expensive.
- Calorimeter will detect other reactions which may dominate the heat flow signal, but be unimportant with regard to reliability and safety of the system.
- True failure process may generate little energy and remain undetected, especially in the case of failures due to changes in mechanical properties.

With the present state of knowledge, it is considered premature to rely on HFC as the only tool for the assessment of the life of high explosive energetic systems. It is proposed that the existing approach of devising a test programme tailored specifically to observing and quantifying the critical failure process should continue for the foreseeable future in the UK.

5 ACKNOWLEDGEMENT

This work was supported and funded by UK MOD (DOSG).

6 REFERENCES

1. B Vogelsanger and R Sopranetti, Safety, Stability and Shelf Life of Propellants – the Strategies used at Nitrochemie Wimmis AG, Proc. Symp. Chem. Probl. Connected Stabil. Explos., 1998, 361.
2. J Wilson, The use of Heat Flow Calorimetry to Optimize the Service Life Evaluation of Gun Propellant, Proc. 2nd International Workshop on Microcalorimetry, Otley, Yorkshire, UK, 17-19th May 1999.
3. S Wilker and P Guillaume, International Round Robin Test to Determine the Stability of DB Ball Propellants by Heat Flow Calorimetry, Proc. 2nd International Workshop on Microcalorimetry, Otley, Yorkshire, UK, 17-19th May 1999.
4. U Ticmanis, S Wilker, G Pantel, M Kaiser, P Guillaume, C Balés and N van der Meer, Principles of a STANAG for the Estimation of the Chemical Stability of Propellants by Heat Flow Calorimetry, Proc. 31st Int. Conf of ICT, Paper V2, Karlsruhe, Germany, 27-30th June 2000.
5. A Chin, Explosives Manual, Safety Assessment for Explosives (SAFE), Quality Evaluation of Explosives, Test and Evaluation Department, Ordnance Engineering Directorate, Crane, Indiana, April 2000.
6. Ordnance Board, Proceedings P 123(1), The Scientific Basis For The Whole Life Assessment Of Munitions - Pillar Proceeding, 1996.
7. M Reading, D Dollimore, J Rouquerol and F Rouquerol, Journal of Thermal Analysis, 29 (1984), 775.
8. Swedish Defence Standard FSD 0214, Environmental Resistance Testing of Ammunition, Test Method 113.1, 1991.
9. S Wilker, G Pantel, U Ticmanis and Pierre Guillaume, Microcalorimetric Investigation of Energetic Materials – A review of Methodic Development at BICT, Proc. of TTCP Workshop on Calorimetry, Otley, Yorkshire, April 6-8th 1997.

© Copyright QinetiQ Ltd 2002.

THIS PAGE LEFT INTENTIONAL BLANK

Is Heat Flow Calorimetry the Ultimate Method to Detect (all) Stability and Compatibility Related Problems in Propellants ?

Beat Vogelsanger and Ruth Sopranetti

NITROCHEMIE WIMMIS AG, CH-3752 Wimmis, Switzerland

Tel: +41 (0) 33 228 13 00 Fax: +41 (0) 33 228 13 30

During the last years, heat flow calorimetry (HFC) established itself as an excellent technique for the investigation of chemical ageing of propellants and other explosives.

With the implementation of STANAG 4147 and STANAG 4582, internationally standardised procedures and requirements for the assessment of chemical stability and compatibility become available for the first time.

This might lead to the impression that the HFC method, applied according to the two STANAGs: (i) might be the ultimate method to detect all stability and compatibility problems in propellants; (ii) is able to replace all other, more conventional test methods; (iii) might even allow to estimate the functional life of the propellant under investigation.

The experience, however, clearly shows that ageing and incompatibility processes of propellants are very complex. One single method will never be able to give a complete picture of all relevant ageing processes taking place (not even if the method is backed up by a STANAG).

In case of stability assessment of an unknown propellant, stabiliser depletion, nitrocellulose molecular mass reduction and nitrogen oxide (or gas) evolution should be measured in addition to the HFC testing. For surveillance of production and storage of well investigated propellants, however, a single HFC analysis is often sufficient to ensure that 'everything is running well'.

In case of compatibility measurements, similar problems might appear. It is therefore suggested to support the HFC assessment with data such as stabiliser consumption and pressure built-up – these additional data can be easily obtained from the samples already used in the HFC investigation.

1. Introduction

During the last 10 to 20 years, heat flow calorimetry (HFC) established itself as an excellent technique for the assessment of chemical stability and compatibility of propellants and other explosives.

Main advantages of the HFC-technique are:

- Extremely **high sensitivity**, which allows to directly measure the heat production of double base propellants down to temperatures of 40°C, in special cases even to 30°C (if a low noise amplifier is used [1]).

- Good **reproducibility** of measurements (repeated 'in-house' measurements of reference sample over 3 years yielded a relative standard deviation of 2.2% regarding total heat production; whereas an international round robin test showed a relative standard deviation of between 2.7% and 9% [2]).
- Heat flow curves **contain a large amount of information**: The shape of the curve is characteristic for the composition of the propellant. Propellants stabilised with diphenylamine (DPA) show a broad, 'belly-type' minimum, whereas the minimum is very sharp for akardite-2-stabilised propellants. For the DPA-propellants, even the time at which all parent stabiliser is consumed can be seen from the HFC curves (rise of heat flow following first minimum).
- **Ease of use** – modern HFC instruments are easy to operate with.

The main disadvantages of HFC are:

- **High cost of equipment.**
- Results are sometimes **difficult to interpret** (in particular for propellants of new recipes).
- Measures '**sum parameter**' – usually it is not known which reactions contribute to which extent to the total heat generation.
- Relative **small sample size** (at least with TAM HFCs) might reduce precision in particular for larger grain propellants.

Until recently, the main problem in HFC testing of explosives was the **lack of standardised procedures and requirements**. This, however, **is changing with the implementation of STANAG 4147 for compatibility testing** and the **development of STANAG 4582 for stability assessment**.

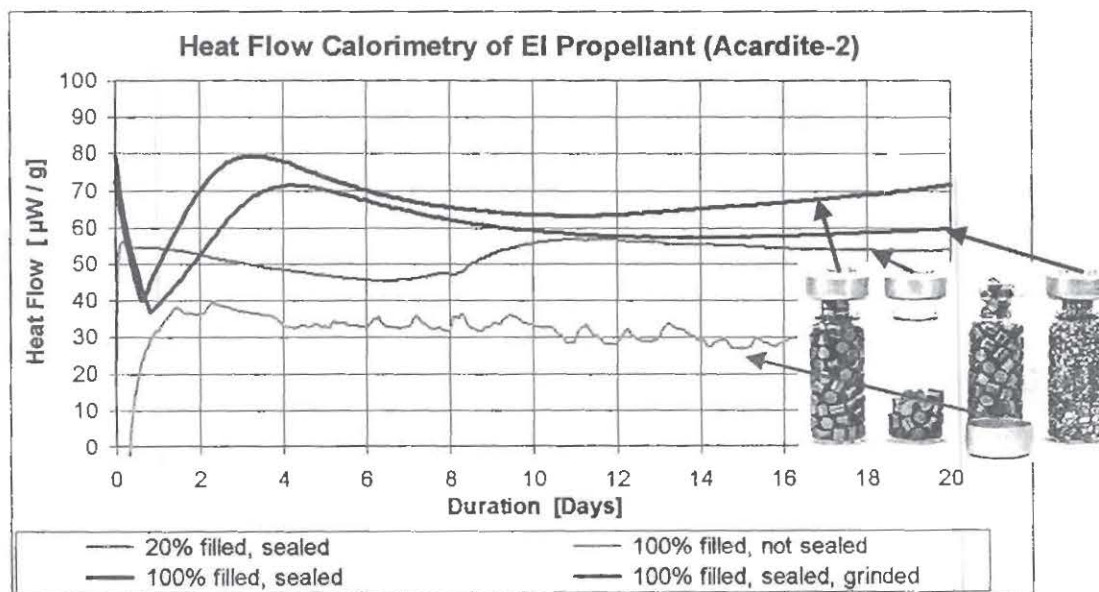


Figure 1: Dependence of heat flow curves on experimental conditions.

An other general problem with HFC testing is that the recorded **heat flow curve depends on sample preparation and conditioning as well as on loading density and sealing tightness of the HFC ampoule** (see Figure 1). This, however, also applies to other stability tests. As a consequence, sample preparation and experimental set-up have to be kept as constant as possible, preferably by using a standardised procedure.

2. Stability Testing of Propellants (Draft STANAG 4582)

2.1 Characteristics of STANAG 4582

The draft of STANAG 4582 ('Explosives, Single, Double and Triple Base Propellants, Stability Test Procedure and Requirements using Heat Flow Calorimetry'):

- defines sample preparation (grinding only if necessary);
- defines ampoule set-up (fully filled, tightly closed);
- bases on isothermal measurements of heat flow;
- allows to choose temperature between 60°C and 90°C, resulting in test times between 123 days (at 60°C) and 3.5 days (and 90°C) – a convenient sequence is 10.6 days at 80°C;
- gives upper heat flow limit (for each test temperature; e.g. 114 µW at 80°C),
- which will guarantee chemical stability for at least 10 years at 25°C.

2.2 Limitations of STANAG 4582

Even if it is very useful to have a STANAG which standardises test conditions and sentencing criteria in HFC stability testing of propellants, it has to be taken into account that:

- Using the same sentencing criteria for all propellant types makes life easier, but increases the risk of misjudging.
- Propellant ageing is very complex – several processes contribute to the ageing (the processes can compete with each other).
- The heat release is not always 'proportional' to the over-all propellant ageing.

2.3 'Universal' Sentencing Criterion

In most other stability tests, different criteria or different ageing conditions are applied to the individual propellant classes. Typical examples are the STANAGs basing on stabiliser depletion: According to STANAG 4117, the effective stabiliser concentration has to be above 0.6% after 60 days at 65.5°C for a single base propellant stabilised with DPA, whereas in case of a double base propellant stabilised with 2-nitro-diphenylamine, a stabiliser concentration of 0.2% is still tolerated after 35 days of ageing at 60°C. These differences are mainly due to historic reasons – from a modern point of view it is hard to understand why more severe stability requirements should be applied to a certain propellant class just because this class is inherently more stable than an other. This applies in particular for the qualification of a propellant,

where the requirements necessary to fulfil the propellant's tasks have to be met irrespective of the propellant type which is finally chosen.

The HFC STANAG 4582 makes no such difference – test sequence and requirements are the same for all nitrocellulose based propellants. This, of course, makes stability testing and assessment using the HFC method much easier.

As a consequence, it appears that propellants belonging to different classes can show huge differences in heat flow, even if all of them are regarded as being of 'good stability' within their individual classes. This is demonstrated in Figure 2: The heat flow values of several chemically stable double base propellants are about one order of magnitude higher than the heat flows of typical single base propellants.

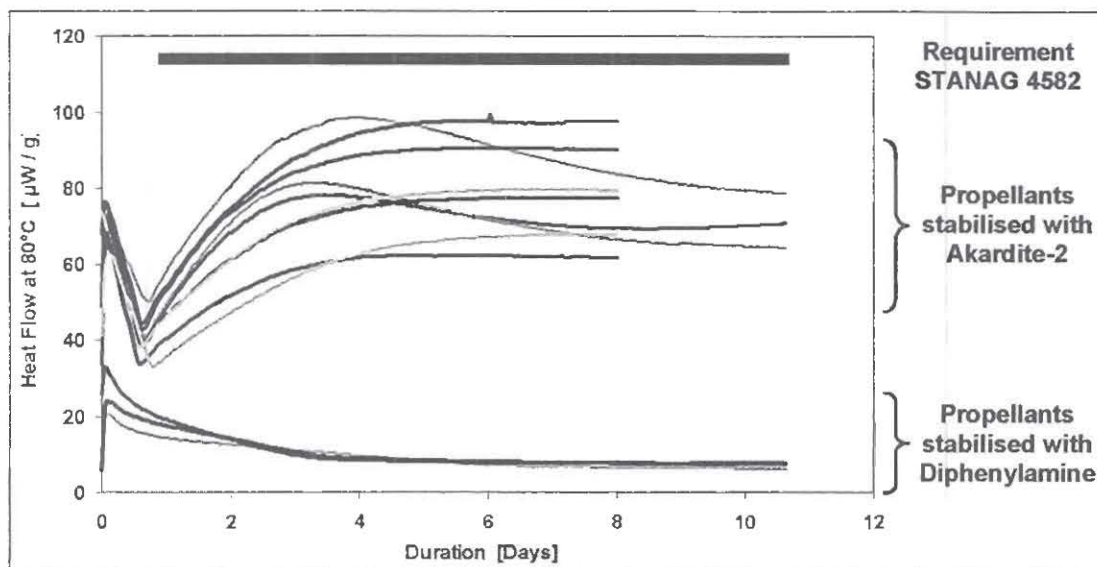


Figure 2: Heat flow curves of different single base propellants (stabilised with DPA) and double base propellants (stabilised with akardite-2) at 80°C.

Therefore, the 'universal' sentencing criterion of STANAG 4582, which is well suited for propellant qualification, is often not useful for quality control or surveillance. In particular for propellants with heat flow values far below the STANAG limit, individual criteria should be used if a constant quality has to be assured.

2.4 Comparison of Main Ageing Phenomena

As can be seen from Figure 3, different phenomena appear during chemical ageing of propellants. Ageing of propellants usually starts with slow thermal decomposition of the nitric esters (usually nitrocellulose NC and nitroglycerine). In this initial reaction and in the consecutive reactions with air or humidity, different reactive compounds, such as nitrogen oxides and nitrogen acids, are produced. These products can either

- (i) be chemically trapped by a stabiliser,
- (ii) react with the cellulose backbone of the NC, or
- (iii) diffuse out of the propellant grains.

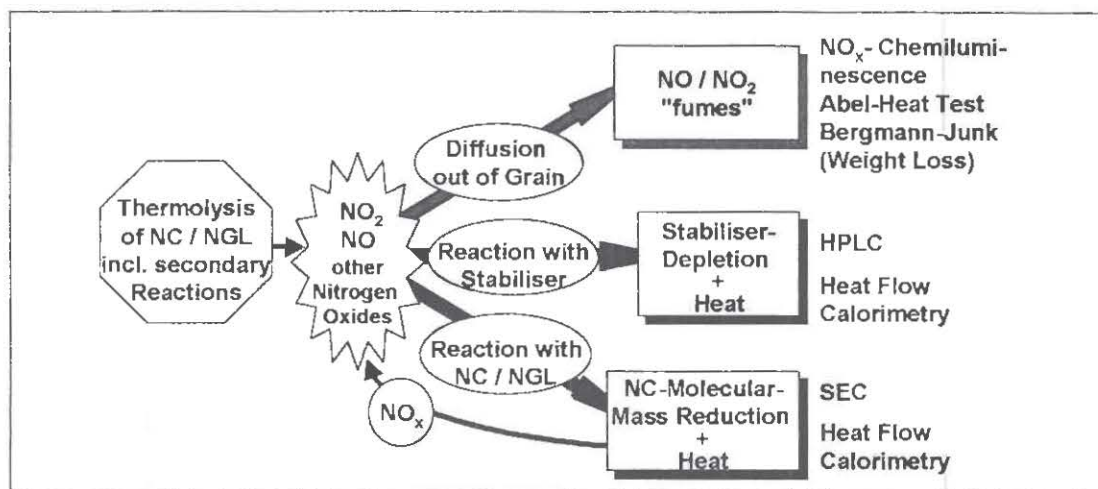


Figure 3: Overview of ageing phenomena in nitro-cellulose based propellants [3].

As all three primary phenomena (stabiliser depletion, NC molecular mass reduction and NO_x -evolution) are used for stability assessment, it appears to be very interesting to compare the extent of these effects with the amount of heat production. Such a comparison, using different propellant types, is shown in Figure 4.

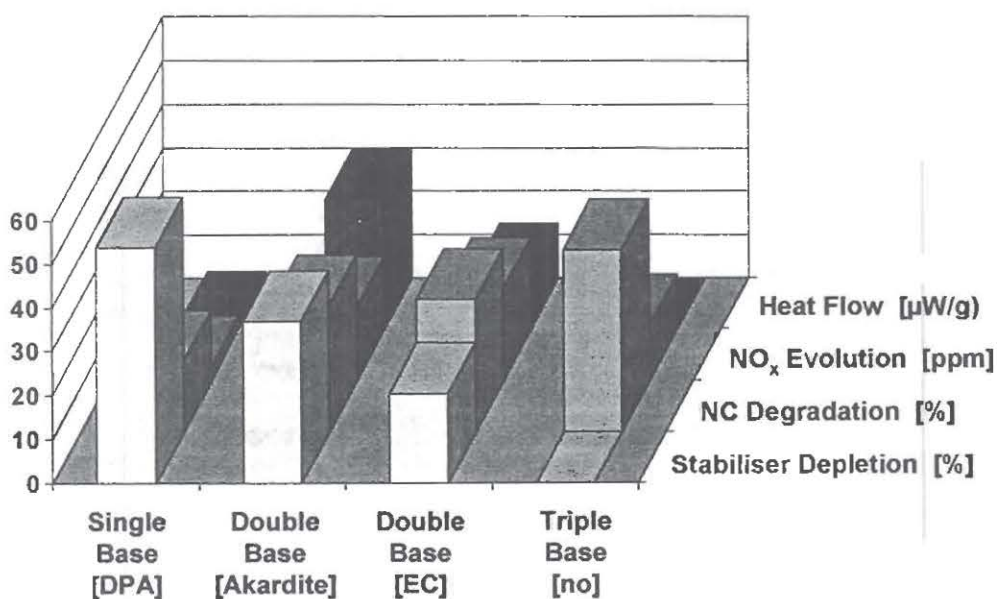


Figure 4: Stabiliser depletion, NC degradation, NO_x -evolution and heat production of four different propellants after 4 weeks at 71°C .

The results of this comparison shows **no direct correlation between the heat flow and the other ageing phenomena** (at least if different propellant types are tested):

- In the **single base propellant**, 54% of the initial stabiliser **DPA** is converted, and the NC molecular mass is reduced by 16% after 4 weeks at 71°C. Both NO_x-evolution and heat production are at a very low level.
- The **double base propellant** stabilised with **akardite-2** shows a slightly slower stabiliser depletion rate but a slightly higher NC depletion if compared to the single base propellant. NO_x-evolution and heat production, however, are tremendously higher (by factors of 5.4 and 18) than in the single base reference.
- In case of the **double base propellant** stabilised with **ethyl-centralite** (EC), stabiliser depletion is slightly lower and NC depletion is slightly higher than in the previous case. Again, NO_x-evolution and heat production are much higher (by factors of 6.8 and 7.5) than for the single base propellant.
- The **triple base propellant** contains **no stabiliser** and therefore does not show any stabiliser depletion. For this specific propellant type, also heat production is close to zero (or even endo-thermal in certain cases). If the stability is judged from stabiliser depletion or heat flow only, it has to be concluded that this propellant does not age chemically at all. However, from the amount of NC degradation and NO_x-evolution, it becomes clear that the triple base propellant's chemical ageing rate must be in the same range as for the two double base propellants.

From these results it becomes evident that it is very dangerous to judge the chemical stability of an unknown propellant by only one ageing effect. In order to exclude the possibility of serious misjudgements, all possible ageing processes have to be investigated at least once in the propellant's life-cycle. We therefore recommend to use HFC and other methods of stability / shelf life testing over the life-cycle of propellants according to the scheme shown in Figure 5.

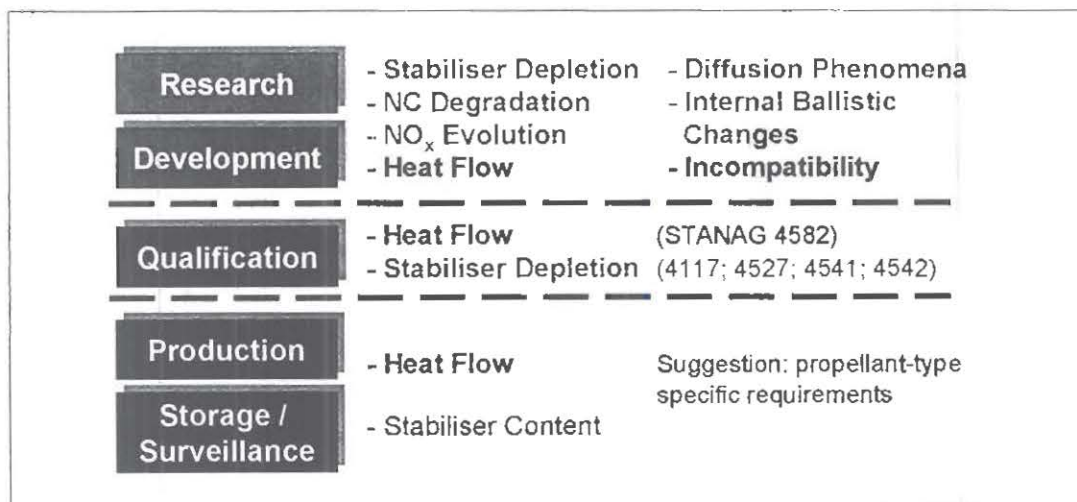


Figure 5: Recommended test scheme for stability / shelf life testing over the entire life-cycle of a propellant [3].

2.5 Assessment of Functional Life

The functional life (ballistic life) of a propellant is mainly determined by

- the energy loss of the propellant (due to chemical ageing),
- the nitro-cellulose degradation (embrittlement of propellant grains),
- different diffusion processes (surface coatings, nitro-glycerine, etc.),
- incompatibility and other processes.

The HFC stability test only detects the energy loss of the propellant (which, of course, also contains a part originating from NC degradation). Therefore, the prediction of functional life from HFC stability test data is, if at all, only possible for propellants in which the interior ballistic changes are dominated by the energy loss.

2.6 Conclusions / Recommendations Regarding HFC Stability Testing

- HFC is an excellent technique for stability testing of propellants.
- For routine stability testing of known propellants (e.g. for surveillance and quality control), the use of 'HFC solely' is sufficient in most cases.
- For basic investigations of propellants with new / unknown ingredients, however, all possible ageing phenomena which might contribute to the chemical ageing must be analysed (stabiliser depletion / NC degradation / heat release / NO_x evolution).
- In most cases, judging of functional life is impossible from HFC data solely.
- For HFC stability testing of propellants, the STANAG 4582 sequence generally should be used (e.g. 10.6 days at 80°C).
- In case of surveillance and quality control, the use of an 'universal' sentencing criterion might be inappropriate – in order to detect unwanted changes in product quality between different batches or during propellant storage, propellant specific criteria should be applied.

3. Compatibility Testing of Propellants (STANAG 4147)

3.1 Characteristics of STANAG 4147

STANAG 4147 ('Chemical Compatibility of Ammunition Components with Explosives', Test 2, 'Heat Flow Calorimeter Test'):

- defines sample preparation (grinding / sieving to < 0.2 mm is recommended);
- does not define ampoule set-up (e.g loading density, confined condition, carrier gas, etc.; but: experimental conditions have to be reported);
- bases on isothermal measurement of heat flow values of explosive, of contact material, and of a 1:1 mixture of both;
- recommends a sequence of 7 days at 85°C;
- lays down assessment basing on 'relative increase in heat generation'.

3.2 Limitations of STANAG 4147

Again, it has to be stated that it is very important to have a STANAG which standardises test conditions and sentencing criteria in HFC compatibility testing of propellants. But there are some problems:

- The test condition of STANAG 4147 differ from the ones in the 'stability' STANAG 4582. In particular, STANAG 4147 does not allow to choose the test temperature.
- The stipulated temperature of 85°C is not optimal for the most often used type of calorimeters (TAM; built by Thermometrics), since long-term operation at 85°C - 89°C will damage these instruments.
- Grinding of propellants does often not make sense.
- The interpretation of results is often difficult: On one hand, the 'relative increase in heat generation' is not always the best criterion. On the other hand, measuring only one 'incompatibility phenomenon' means that we have no data to support the assessment. Since misinterpretations will have serious consequences, it would be advantageous to have the opportunity to confirm the assessment.

3.3 Sentencing Criteria in Compatibility Assessment

Two different approaches are commonly used to assess the compatibility – relative and absolute compatibility. The two approaches are described in the following table.

STANAG 4147 is basing on the **relative incompatibility**. Here, the amount of heat release of the mixture is divided by the heat release of the isolated components, resulting in the so-called D-value.

As an alternative, the **absolute incompatibility** (amount of additional heat release of the mixture, which is due to incompatibility reactions) can be directly used for the assessment.

Method of assessment:	<u>Relative Incompatibility</u>	<u>Absolute Incompatibility</u>
Equation for calculation of 'incompatibility' (1:1 mixture)	$D = \frac{2 \cdot Q_M}{Q_E + Q_S}$	$Q_R = Q_M - \frac{Q_E + Q_S}{2}$
Perfectly compatible	$D = 1.0$	$Q_R = 0.0$
Slight but acceptable incompatibility ('compatible')	$1.0 < D \leq 2.0$	e.g. $Q_R \leq 30 \text{ J/g [4]}$ (in 10.6 days 80°C)
Compatibility should be checked with another method	$2.0 < D \leq 3.0$	
Incompatible	$D > 3.0$	$Q_R > 30 \text{ J/g}$
D = relative compatibility according to STANAG 4147		
Q_R = specific heat release due to incompatibility ('absolute incompatibility')		
Q_S = specific heat release of contact material		

Q_E = specific heat release of explosive
 Q_M = specific heat release of mixture (1 : 1)

Each of the two methods has its advantages and drawbacks. The relative incompatibility approach of STANAG 4147 can be used for a wide range of explosives: The D-criterion is, in principle, equally applicable for very stable secondary explosives as for relatively unstable nitrocellulose-based propellants.

There are, however, cases where the STANAG criterion is too conservative. This is the case for example, when explosive and contact material both deliver only marginal heat release, whereas the mixture shows a short initial exothermal reaction. Here, the high D-value predicts incompatibility even when the heat flow of the mixture is still small. In such cases, the alternative assessment method basing on the absolute incompatibility seems to be more appropriate.

3.4 Survey Regarding Test Sequences and Sentencing Criteria

In order to obtain an overview regarding compatibility test procedures used all over the world, a survey was performed [5]. The results of this survey are listed in the following table:

Na-tion	HFC sequence	Criterion for assessment 'compatible'		Additional criteria	Additional methods / comments
		Relative incompatibility	Absolute incompatibility		
B	14 days 80°C	STANAG 4147	—		
CH	8 days 80°C	STANAG 4147	$\leq 20 \text{ J/g}$	No auto-catalysis	
D	10.6 days 80°C	—	$\leq 30 \text{ J/g}$	STANAG 45824	
FIN	7 days 70°C		$\leq 5 \text{ } \mu\text{W/g}$; $\leq 10 \text{ J/g}$	No auto-catalysis	VS/TG/DSC
GB	3.75 days 77°C	STANAG 4147	—		VS
NL	7 days 85°C	STANAG 4147	—	No auto-catalysis	TG/DSC/VS
S	7 days 65°C	—	$\leq 10 \text{ J/g}$		Explosives
	> 7 days 70°C	Problem-specific requirements			Propellants
USA	66°C – 80°C	Arrhenius-evaluation / problem-specific requirements			DSC / others

To our knowledge, HFC is not yet used for compatibility testing in Canada, Denmark and Italy. HFC was not used in France for compatibility testing until 2001 (neither at ETBS nor at SNPE); ETBS, however, started HFC compatibility testing with the round robin test organised by WIWEB, Germany, in 2002. The experts from USA and from company Bodycote (Sweden) do not rely on fixed procedures but choose test conditions and criteria on a case to case basis.

Even if this table is incomplete and simplified, it allows to draw the following conclusions:

- (i) Almost no one does completely follow the procedure provided in STANAG 4147. Within this survey, only TNO from the Netherlands uses both test sequence and criteria such as described in STANAG 4147.
- (ii) Different test temperatures and durations are applied in the different nations. Very promising and logical seems the suggestion of WIWEB, Germany, to use the same range of test sequences as given in the 'stability STANAG' 4582.
- (iii) About one half of the nations apply the relative incompatibility criterion of STANAG 4147, whereas the others prefer an absolute criterion. In Switzerland both criteria are used – if they give contrary results, additional investigations have to be done.
- (iv) In some nations, the heat flow curves are also inspected for indications of auto-catalysis. Auto-catalysis takes place if the curve of incompatibility rises continuously with time. WIWEB, Germany, suggests to demand that all three samples (explosive, contact material and mixture) also fulfil the requirements of the 'stability STANAG' 4582.
- (v) Several nations do not solely rely on HFC results for compatibility assessment but also consult the results of thermogravimetric analysis (TG), differential scanning calorimetry (DSC), or vacuum stability (VS) testing. This increases the certainty of the assessment but causes additional costs.

3.5 Suggestion for Expanded HFC Compatibility Test

In order to improve test conditions, to increase reliability of assessment and to obtain additional information to support the assessment without excessive rise in cost, we suggest to perform / expand the HFC compatibility test as follows:

- Sample preparation (grinding of sample, filling and closing of ampoules) should be performed analogous to the description in STANAG 4582.
- An appropriate test sequence has to be chosen from the list given in STANAG 4582; e.g. 10.6 days at 80°C.
- The assessment should be done using both relative (D-value) and absolute criteria. As absolute incompatibility criterion, 30 J/g can be used for all STANAG 4582 sequences, as suggested by WIWEB, Germany [4].
- After the sequence, pressure build-up of ampoules and stabiliser depletion of propellant might be measured in order to confirm the compatibility assessment. Thereby, the relative increase in pressure build-up and stabiliser depletion in the mixture should not exceed 50% (this in accordance with STANAG 4147, Test 5A, which demands for stabiliser depletion $D \leq 1.5$ in order to be assessed as 'compatible').

An example of such an extended study is given in Figure 6: Thereby, the compatibility of a double base propellant with a red varnish was tested. HFC curves of grinded propellant, of varnish and of a 1:1 mixture of both were measured during 8 days at 80°C (see Figure 6). Both STANAG 4147 (requirement: $D \leq 2$) and absolute criterion

(absolute increase ≤ 20 J/g in 8 days at 80°C) have been fulfilled. At the end of the sequence, pressure build-up was measured in all three ampoules. No excessive increase in pressure build-up appeared in the mixture, which supports the HFC compatibility assessment. HPLC analysis of the extracts of propellant and mixture (non-aged and aged in the ampoules for 8 days at 80°C) indicated that the stabiliser depletion rate is reduced in the mixture if compared to the pure propellant. This in fact was confirmed in a repeated analysis of samples aged for 8 days and 20 days at 80°C. These results further support the compatibility assessment. The reduced stabiliser depletion rate (reduction by 43%) in the mixture might be explained by the fact that part of the stabiliser diffuses from the propellant into the varnish during accelerated ageing. The results of this study are given in the following table.

	Propellant	Contact material	Mixture	D-value	Relative increase	Absolute increase
Heat generation [J/g]	18.3	62.3	50.0	1.24 4	24%	9.7 J/g 4
Vial pressure [mbar]	176	334	265	1.04 4	4%	10 mbar
Stabiliser deplet. [%]	46%	—	26%	0.57 4	-43%	

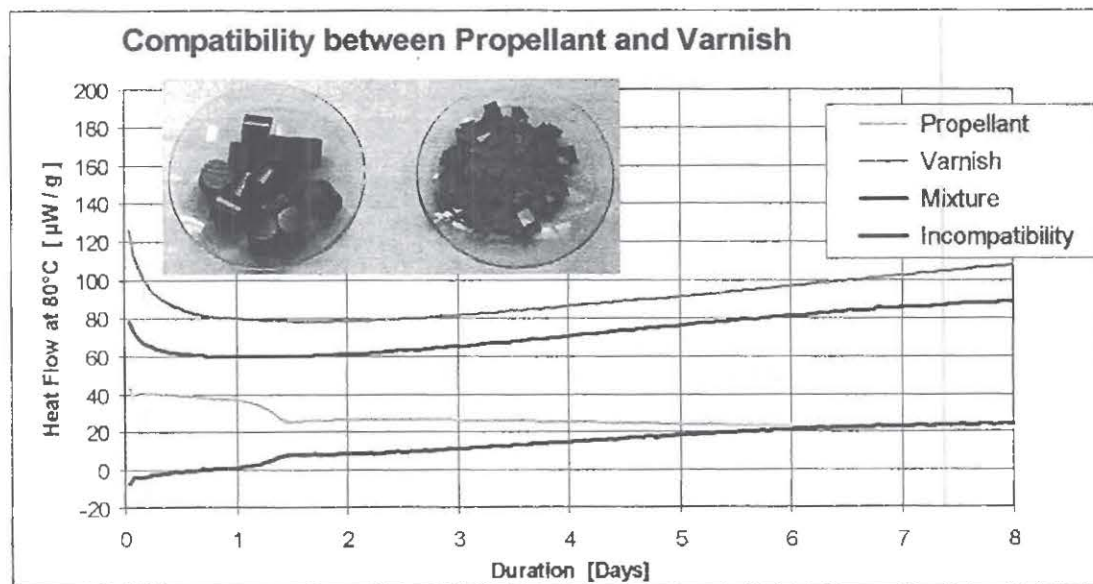


Figure 6: Extended compatibility study for double base propellant and a red varnish; HFC curves for 8 days at 80°C.

3.6 Conclusions / Recommendations Regarding HFC Compatibility Testing

- HFC is an excellent technique for compatibility testing of propellants.
- HFC compatibility testing is standardised in STANAG 4147, Test 2.
- This STANAG, however, is neither fully accepted nor implemented in the 'HFC community'.
- Whereas the basic principles of this STANAG can be maintained, the following details should be revised:
 - Allowance for use of different temperatures (such as in STANAG 4582); Important: The temperature dependence of incompatibility has to be carefully investigated first.
 - Application of both 'relative' and 'absolute' incompatibility criteria.
 - Adoption of sample preparation procedures of STANAG 4582.
- Incompatibility can cause different reactions. It is therefore risky to judge compatibility from HFC measurements solely.
- In fact, each compatibility assessment should be backed up by results from other 'incompatibility phenomena':
 - Additional information can easily be obtained from stabiliser depletion or pressure build-up of the samples used in the HFC test.
 - As a more costly but better accepted alternative, some of the other tests described in STANAG 4147 can be applied (e.g. vacuum stability test, thermogravimetric analysis or differential scanning calorimetry).

4. Final Conclusions

- HFC has proven to be an excellent tool in the field of stability and compatibility assessment.
- The two 'HFC STANAGs' are very helpful guidelines to perform our task.
- Nevertheless, we should never forget that the stability / compatibility issue is extremely complex.
- No single technique is capable of detecting all stability / compatibility related problems – HFC makes no exception.
- Our competence and experience is still needed ! and can not be replaced by two STANAG's.

Acknowledgements

The authors thank all co-workers who have contributed to this work, in particular Nathalie Lüdi, Bruno Bärtschi and Jürg Kislig. Special thanks go to Dr. Stephan Wilker, Gabriele Pantel, and Dr. Uldis Ticmanis from WIWEB, Germany, to Dr. Pierre Guillaume from PB Clermont, Belgium, as well as to Dr. Wim de Klerk from TNO, Netherlands, for numerous interesting discussions. We thank all who have contributed to our survey, see [5]. Financial support by the Swiss Procurement Agency ('Gruppe Rüstung') is gratefully acknowledged (LFP-Project 135-15). The authors thank Dr. Hansruedi Bircher for supporting this project.

References

1. Dr. Pierre Guillaume, PB Clermont, Belgium; private communications.
2. S. Wilker and P. Guillaume: *International Round Robin Test to Determine the Stability of Double Base Ball Propellants by Heat Flow Calorimetry*, internal report WIWEB 810/22621/98 (1998) / Poster 132 at the 29th International Annual Conference of ICT, Karlsruhe, June 30 – July 3, 1998.
3. B. Vogelsanger and R. Sopranetti: *Safety, Stability and Shelf Life of Propellants*, 11th Symposium on Chemical Problems Connected with the Stability of Explosives, Båstad, 1998.
4. Dr. Stephan Wilker, WIWEB, Germany; private communications.
5. Contributions to the survey came from: Pierre Guillaume (B); Louis-Simon Lussier (CAN); Stephan Wilker (D); Jesper Nielsen (DK); Corrine Balès (F); Maija Hihkio (FIN); David Tucker (GB); Renzo Cabrino (I); Wim de Klerk (NL); Lars-Gunnar Svensson (SE); David Lee and Bruce Thomas (USA).

THIS PAGE LEFT INTENTIONAL BLANK

THERMAL AND CHEMICAL ANALYSES OF SILICONE POLYMERS FOR COMPONENT ENGINEERING LIFETIME ASSESSMENTS.

Bryan Balazs and Robert S. Maxwell

Weapon Materials Compatibility and Aging Group
Lawrence Livermore National Laboratory
Livermore, CA 94551

Introduction

Accurate predictions of a polymer component's functional lifetime at best are tenuous when one has only relatively short term chemical or mechanical property data to extrapolate. We have analyzed a series of silica-filled siloxanes to determine the chemical and microstructural signatures of aging, and we are incorporating these data into rational methodologies for assessing a component's lifetime measured against as-designed engineering properties. We are monitoring changes in mechanical properties, crystallization kinetics, cross-link density changes, and motional dynamics with a variety of analysis methods: Modulated DSC, Dynamic Mechanical Analysis, and Solid-State Nuclear Magnetic Resonance.

Previous work has shown that the addition of phenyl side groups to polydimethylsiloxane (PDMS) polymer chains reduces the rate and extent of crystallization of the co-polymer compared to that of pure PDMS^{1,2}. Crystallization has been observed in copolymer systems up to 6.5 mol % phenyl composition by DSC and up to 8 mol % phenyl by XRD.^{1,2} The PDMS-PDPS-silica composite materials studied here are silica reinforced random block copolymers consisting of dimethyl and diphenyl monomer units with 11.2 mol. % polydiphenylsiloxane. Based on this previous work, it is not expected that this material would exhibit crystallization in the polymer network; however, these silicones do, in fact, exhibit crystallization phenomena. This report focuses primarily on our efforts to assess the information content of the crystallization phenomena with respect to aging signatures and mechanisms that may be limiting the functional lifetime of the composite materials.

Experimental

The PDMS-PDPS-silica composite material was a random block copolymer consisting of 90.7 wt.% dimethyl (DMS), 9.0 wt.% diphenyl (DPS), and 0.31 wt.% methyl vinyl (MVS) siloxane monomer units. The polymer was milled with a mixture of 21.6 wt. % fumed silica,

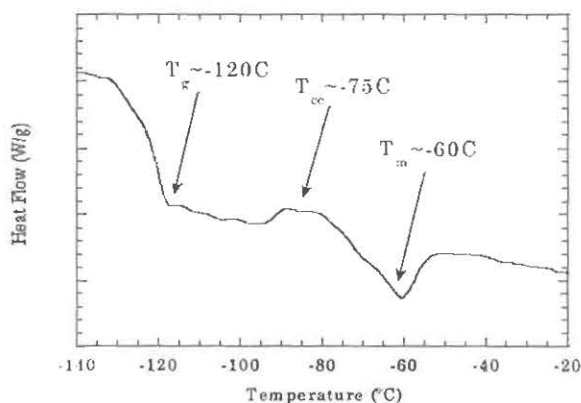


Figure 1. MDSC trace for pristine PDMS-PDPS-silica composites foam. Relevant thermodynamic events are indicated.

4.0 wt. % precipitated silica, and 6.8 wt. % ethoxy-endblocked siloxane processing aid. The resulting gum was then milled with 50 or 60 volume percent of 25-40 mesh prilled urea spheres. Heat was applied to activate the peroxide curing agent in the base gum, after which the urea was washed out with water. Control samples were irradiated for various periods of time in a stainless steel container (volume ~ 2 l) exposed to a ^{60}Co gamma source ($E_{\text{avg}} \sim 1.2$ MeV, 0.5 Mrad/hr). All dosing experiments were performed at the same dose rate.

DMA testing was performed (Rheometrics RMS-800 Dynamic Mechanical Spectrometer, Piscataway, NJ) in parallel plate geometry with a static compression force of 400g. The sample was sheared at a frequency of $f=6.3$ rad/sec and using a ramp sequence of 20°C from -150°C to 20°C at a rate of $2^\circ\text{C}/\text{min}$. MDSC analyses were performed (TA Instruments, MDSC 2920, New Castle, DE) by cooling the sample at a rate of $6^\circ\text{C}/\text{min}$ to -150°C , followed by heating at $3^\circ\text{C}/\text{min}$ with a modulation frequency of $\pm 0.4^\circ\text{C}/50$ sec. Isothermal x-ray diffraction measurements were done at -85°C on a Siemens D500 Diffractometer with an Anton Paar TTK Heizregler subambient stage, using a primary beam monochromator.

^1H NMR T_2 measurements were performed at 500.13 MHz on a Bruker DRX-500 spectrometer using a HCX 5mm probe. ^1H $\pi/2$ excitation pulses of 7 μs and relaxation delays of 10 seconds were used. In all cases, small (0.5 cm x 0.5 cm) squares of foam were cut from the larger foam and set in the portion of a 5 mm NMR tube that would be within the coil volume of the probe.

Results

MDSC analyses, shown in Figure 1, show a glass transition temperature (T_G) at -120°C and a melting point (T_M) at -60°C ($\Delta H_M \sim 2.5\text{J/g}$). The presence of a crystallization phenomena was indicated by the presence of an exothermic peak at -80°C with a heat of cold

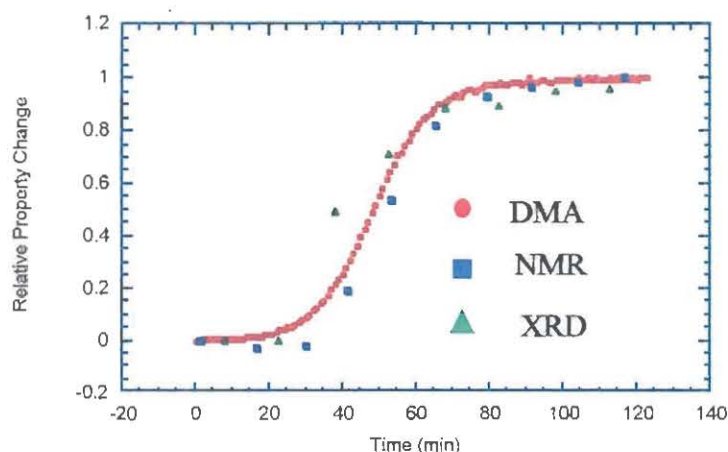


Figure 2. Relative changes in G' (DMA), T_2 (NMR) and %crystallinity (XRD) for foam.

crystallization (ΔH_C) of $\sim 1.5\text{J/g}$. DMA data (not shown) showed similar results: The glass transition was evidenced by a drop in G' and a peak in $\tan \delta$ at -120°C , and crystallization was also evidenced by the peak in G' at -75°C where the formation and melting of the crystalline phase causing an increase in the shear modulus.

We used low temperature X-ray diffraction to measure the degree of crystallinity in the copolymer composite. This data showed that $\sim 15\%$ of the polymer was crystallizing after 2 hours at -85°C . In order to see how crosslink density might affect the degree of crystallization in these materials, a series of samples with variable crosslink density were prepared and subject to crystallization and the % crystallinity was measured (data not shown). The data show that at sufficiently high crosslink density ($\sim 1.5X$ the nominal density studied here), the degree of crystallization after 2 hours at -85°C began to decrease.

To examine the kinetics of polymer crystallization, isothermal DMA experiments were performed on pristine, variable crosslink density, and irradiated materials. These experiments were performed by rapidly cooling samples to -85°C and tracking G' as a function of time. We have also investigated the kinetics of crystallization by MDSC, XRD and NMR analysis. Results of ^1H relaxation measurements by NMR and the ratio of crystalline peak area to

amorphous halo by XRD as a function of time at $-85\text{ }^{\circ}\text{C}$ are normalized and plotted along with the DMA data in Figure 2. MDSC could also track the kinetics by changes in ΔH_c with time. The precision of these latter thermal measurements, however, were quite poor and further investigation is ongoing to improve these measurements. The results of our kinetic experiments show that, by all measurement methods, crystallization in the pristine material took place over a 1.8 hour period. We are currently investigating the nature of the slow crystallization kinetics.

Isothermal DMA crystallization kinetic measurements were then performed on materials with variable crosslink density (produced by altering the concentration of vinyl monomer units that produce the crosslinks during the curing process) to assess the variability

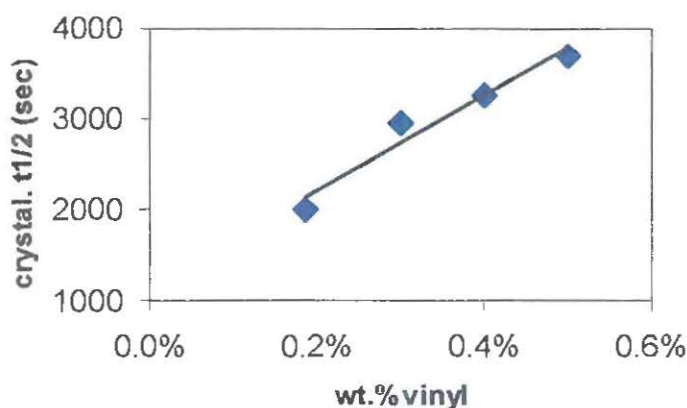


Figure 3. Time to half crystallization as a function of wt.% vinyl monomers (and thus, crosslink density).

of the kinetics with simulated aging signatures. The results of these measurements are shown in Figure 3 and show that as the crosslink density increased, the crystallization kinetics slowed considerably.

In an effort to assess the applicability of measurements of crystallization kinetics to assess changes in actual aged material, we studied the crystallization kinetics for a series of radiatively aged samples. Results from isothermal DMA studies of these samples is shown in Figure 4. For an unirradiated sample, approximately 1.8 hours were required for full crystallization, while a sample dosed to 25 Mrads took 10 hours to crystallize to the same extent. For all model samples, DMA curves suggest that the ultimate amount of crystallization does not change with exposure to radiation, but the time to the onset of crystallization and the

rate at which crystallization occur does change. Our results suggest that monitoring crystallization kinetics by MDSC, DMA, NMR or XRD may provide a sensitive method to assess structural changes occurring due to polymer crystallization.

Conclusions

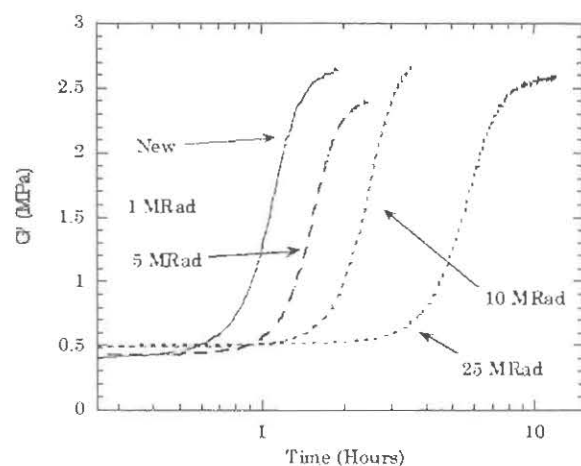


Figure 4. Results of isothermal DMA experiments on gamma-irradiated polymer composite materials.

We have presented preliminary data on crystallization phenomena in PDMS-PDPS-silica composite foam materials. A crystallization event is clearly seen for these materials by DSC, DMA, XRD, and NMR methods despite a concentration of diphenyl monomer units above the threshold at which crystallinity had previously been shown to be precluded^{1,2}. The time to crystallization onset and the rate at which the crystallization occurs have been shown to be sensitive to changes in crosslink density induced by artificial aging mechanisms. Naturally aged material also show subtle changes in crystallization behavior. We are still investigating the origins of this phenomenon and investigating the value of such measurements to assess aging signatures for lifetime prediction efforts.

Acknowledgments

This work was performed under the auspices of the U.S. Department of Energy by the University of California, Lawrence Livermore National Laboratory under contract # W-7405-ENG-48. The authors would like to thank Albert Shields (LLNL) for performing DMA

testing, Aaron May (Honeywell KCP) for DSC testing, Todd Alam (SNL-NM) for the isothermal ^1H NMR measurements, and Cecil Rayborn and Don Carpenter (BWXT Y-12 LLC) for the XRD work.

References

- 1) S. Chistov, O. Levina, N. Lebedeva, and I. Skorokhodov, Poly. Sci. U.S.S.R., 1984, 26, 2911.
- 2) K. Andrianov, G. Slonimskii, A. Zhdanov, V. Levin, Y. Godovakii, and V. Moskalenko, J. Poly. Sci. A, 1972, 10, 13 (1972).
- 3) "Crystallization Behavior of PDMS-PDPS-SILICA COMPOSITES Series Silicone Cushions," Allen Chien, Steve DeTeresa, Rebecca Cohenour, Jim Schneider, James LeMay and Bryan Balazs, UCRL- ID-140376 Sept 2000.
- 4) M. Avrami, J. Chem. Phys., 1939, 7, 1103.
- 5) J. M. Schultz, "Polymer Materials Science," pg. 385, Prentice-Hall, Inc., Englewood Cliffs, New Jersey, 1974.

THIS PAGE LEFT INTENTIONAL BLANK

Combined Use of Adiabatic Calorimetry and Microcalorimetry for Quantifying Propellant Cook-off Hazards

P F Bunyan¹, T T Griffiths¹ and V J Norris²

¹ QinetiQ, Centre for Environmental Technology, Fort Halstead, Sevenoaks, Kent, TN14 7BP, UK.

² QinetiQ, Centre for Environmental Technology, Bishopton, Scotland, PA7 5NJ.

Abstract

Recent work performed at DERA (now QinetiQ) has shown how accelerating rate calorimetry (ARC) can be used to obtain time to maximum rate (tmr) curves using larger samples of energetic materials. The use of larger samples reduces the influence of thermal inertia, permitting experimental data to be gathered at temperatures closer to those likely to be encountered during manufacture, transportation or storage of an explosive device. However, in many cases, extrapolation of the time to maximum rate curve will still be necessary. Because of its high sensitivity compared to the ARC, heat flow calorimetry (HFC) can be used to obtain data points at, or below, the region where an explosive system might exceed its temperature of no return and undergo a thermal explosion.

Paired ARC and HFC experiments have been conducted on some energetic material samples to explore this possibility further. Examples of where both agreement and disagreement are found between the two techniques are reported and the significance of these discussed. Ways in which combining ARC and HFC experiments can enhance, complement and validate the results obtained from each technique are examined.

1 INTRODUCTION AND BACKGROUND

Assessment of the safety of munitions when subjected to extreme environmental conditions is of great importance to the MOD, justifying the expenditure of considerable time and effort on safety trials. However, comprehensive hazard trials are very expensive, especially if they need to be repeated, for example, in response to a minor change in the manufacturing process for a qualified system. It is therefore highly desirable to obtain an improved general understanding of the physical and chemical processes involved in thermal runaway to complement and enhance the existing tests and possibly allow a reduction in the number of expensive large scale tests required to assess cook off safety hazards accurately. An approach which may help to address this requirement is the application of calorimetric tests such as accelerating rate calorimetry (ARC) and heat flow calorimetry (HFC).

The ARC is an automated laboratory instrument which experimentally determines the temperature, pressure and time relationships of exothermic reactions in a confined, adiabatic environment. It has been used extensively by the chemical industry to evaluate the risk of thermal explosions in containers of self heating materials under a variety of conditions. In principal, we can regard a weapon such as a rocket motor as a system of this type and therefore suitable for study by ARC. However, the extremely high energy released during the decomposition of military explosives will mean that special attention must be paid to certain aspects of ARC technique and data handling which were of less importance, and could be ignored, when systems containing less energetic materials have been studied. It has been reported that, in order to get fully controlled runaway curves from explosives and propellants, far smaller sample masses had to be used than would be satisfactory for less energetic systems¹. Thermal inertia (ϕ) values were therefore rather high, leading to a reduced volume of data and higher onset temperature detection thresholds. This was undesirable, since the results had to be extrapolated over a relatively large temperature range.

However, it is possible to record the early part of the runaway reaction using a larger energetic material sample, before ignition occurs, under far more favourable conditions (lower ϕ , lower onset temperature etc.). In many cases involving decomposition reactions in highly energetic materials of high activation energy, a plot of \ln time to maximum rate (θ_m) vs. $1/T$ is straight, whereas a plot of \ln (incorrect θ_m) vs. $1/T$ plots as a positive curve if the assumed time of maximum rate is too long, or a negative curve if the assumed time of maximum rate is too short. It follows that it would be possible to obtain valid time to maximum rate plots even in the absence of an experimentally measured time of maximum rate by trial and error; plotting a series of time to maximum rate curves for different assumed times of maximum rates and then choosing the straightest plot as the correct one. It has been reported that a valid estimate of what the time to maximum rate would have been if no transition to ignition reaction had intervened can be obtained and used to construct valid time to maximum rate plots using this iterative approach².

With the use of this technique, it is possible to obtain quantitative adiabatic calorimetry data commencing at lower temperatures than in the past. However, the technique is still only moderately sensitive and in many cases some extrapolation will be required to describe self heating behaviour of many explosive containing systems at the temperature of interest.

If a straight line law is seen from the t_{mr} plot, obviously it can be extrapolated. However, a number of physical or chemical processes could potentially intervene at intermediate temperatures which might invalidate the extrapolated values. e.g. phase transitions, loss of volatiles in open systems, autocatalysis by volatile products which are lost from porous systems, domination of the heat generation in the system at low temperatures by a reaction of low activation energy and at high temperatures by a reaction of high activation energy. These have been discussed by Whitmore and Wilberforce³.

Therefore, in order to have confidence in the extrapolated ARC result, its validity should be checked by critical experiment, at, or below the temperature of interest.

A heat flow calorimeter such as the Thermal Activity Monitor [TAM] measures low levels of heat generated by a thermally active material under isothermal conditions. It is far more sensitive than the ARC and can detect heat evolution rates of less than 1 μW. In practical terms this means that the heat generated by cordites, for example, can be monitored at temperatures well below those that might cause critical storage temperatures to be approached. It is therefore ideally suited to validating extrapolated ARC time to maximum rate plots.

Self heat rate and heat generation rate can be easily interconverted, although direct comparison of experimental ARC and HFC data is often not possible in practice, since the different sensitivities associated with the two techniques mean that data collection temperature ranges, used to study the same material, rarely overlap.

The strengths and weaknesses of the TAM and the ARC are to some extent mutually exclusive. Unlike the ARC, the TAM is unable to reach higher temperatures or record entire explosive decomposition reactions. However, its greater sensitivity makes it ideal for single point checks at moderate temperatures

This paper describes combined studies where both ARC and TAM techniques have been used to examine identical materials. One example where the extrapolation appears valid and one example where the extrapolation fails, are described in detail.

2 THEORY AND CALCULATIONS

Providing the appearance of the experimental time to maximum rate curve is a straight line, equation 1 can be solved and used to predict the time to maximum rate at any other temperature⁴.

$$\ln(\theta_m) = -\ln A + \frac{E}{R} \left(\frac{1}{T} \right) \quad 1$$

Where: θ_m = Time to maximum rate at temperature T
 A = Pre exponential factor
 E = Activation energy
 R = The gas constant
 T = Absolute temperature

A prediction of expected heat generation rate at temperature T can be obtained using equation 2, as described by Wilberforce⁵.

$$q = \frac{RT^2 C_v}{\theta_m E} \quad 2$$

Where: q = Heat generation rate at temperature T
 C_v = Specific heat

Conversely, if heat generation rate and activation energy are measured from heat flow calorimetry experiments an adiabatic time to maximum rate can be estimated from microcalorimetry data, by rearrangement of equation 2 to give equation 3.

$$\theta_m = \frac{RT^2 C_v}{q E} \quad 3$$

From a series of microcalorimetry studies conducted at different temperatures, a series of temperature/time to maximum rate data pairs can be generated and an analogous equation to 1 obtained from the regression line of a plot of \ln (time to maximum rate) vs. reciprocal of absolute temperature.

Obviously the two time to maximum rate plots would coincide if the reaction responsible for the heat generation process followed the same chemical mechanism over both ARC and TAM temperature ranges and obeys an Arrhenius law variation of rate with temperature. It follows that a single TAM experimental result can be compared with a result calculated from extrapolated ARC data. If the extrapolation is valid, the expected and observed rates should be comparable.

Once an estimate of heat generation rate of the self heating material has been made and validated, whether or not a system incorporating it will be stable will depend on the environment it experiences. The heat generation rate will be one variable which, when considered along with other relevant parameters (including heat loss characteristics of the container, temperature of the surroundings, specific heat and in the case of solids, thermal conductivity) will allow critical conditions to be assigned.

For example, a simple, useful, approximate relationship of practical value and directly applicable to ARC experimental data has been derived by Townsend⁶. They showed that, for pseudo zero order reactions, the adiabatic time to maximum rate is equal to the cooling time constant of the system at the critical temperature of no return (equation 4).

i.e. At the maximum stable system temperature:

$$\theta_{T_{NR}} = \frac{MC_v}{Ua} \quad 4$$

Where: M = Sample mass
 U = Heat transfer coefficient of container
 C_v = Specific heat
 $\theta_{T_{NR}}$ = Time to maximum rate at the temperature of no return

The temperature of no return (T_{NR}) – the highest temperature that can be experienced by the system while remaining stable – can be determined from the intersection of the equipment time line and zero order time to maximum rate curves graphically. The associated ambient temperature which will lead to this condition developing is another important factor to consider and is referred to as the self accelerating decomposition temperature (T_{SADT}). This is typically a few degrees lower than T_{NR} and is simply related to it by equation 5⁷.

$$T_{SADT} = T_{NR} - \frac{R(T_{NR} + 273.15)^2}{E} \quad 5$$

Where: E = Activation energy for the exothermic process

Note that this simple treatment will give optimistic estimates for critical conditions for systems where significant thermal gradients can develop (e.g. large solid systems of low thermal conductivity). The model used must clearly be appropriate to the type of system being studied.

3 EXPERIMENTATION AND RESULTS

An ARC experiment was conducted on each of the selected materials. After estimating the time of maximum rate iteratively², a time to maximum rate plot of $\ln(\text{time to maximum rate})$ vs. the reciprocal of the absolute temperature, was constructed. The adiabatic time to maximum rate at a lower temperature, within the operating range of the TAM, was calculated by extrapolation and an expected heat generation rate at this temperature calculated using equation 2.

Heat generation was measured experimentally at this lower temperature by microcalorimetry and the rate observed compared with the rate anticipated from the earlier ARC experiment. One example where the extrapolation appears valid (a double base propellant, section 3.1) and one example where the extrapolation appears invalid (ammonium dinitramide, section 3.2) are described in detail. Results from all materials studied are summarised in table 1.

3 Example 1 – Double Base Rocket Propellant

The first example uses a double base rocket propellant containing; nitrocellulose 53%, nitroglycerine 42.2%, 2-nitrodiphenylamine 2.0% and dibutylphthalate 2.8%. Specific heat was determined by DSC at 80°C to be $1.58 \text{ J.g}^{-1}.\text{K}^{-1}$.

A scanning heat-wait-search (HWS) ARC experiment was performed. Experimental conditions were:- Sample mass: 4.6867g, Bomb type: 2.54 cm diameter spherical titanium, Initial temperature: 100°C, Final temperature: 140°C, Self-heat detection threshold: $0.015 \text{ }^{\circ}\text{C.min}^{-1}$, Step: $3 \text{ }^{\circ}\text{C}$, Wait time: 10 minutes, Data step temperature: $1 \text{ }^{\circ}\text{C}$, thermal inertia: 2.32, Atmosphere: nitrogen.

The raw data plot of temperature vs. time is shown in Fig 1.

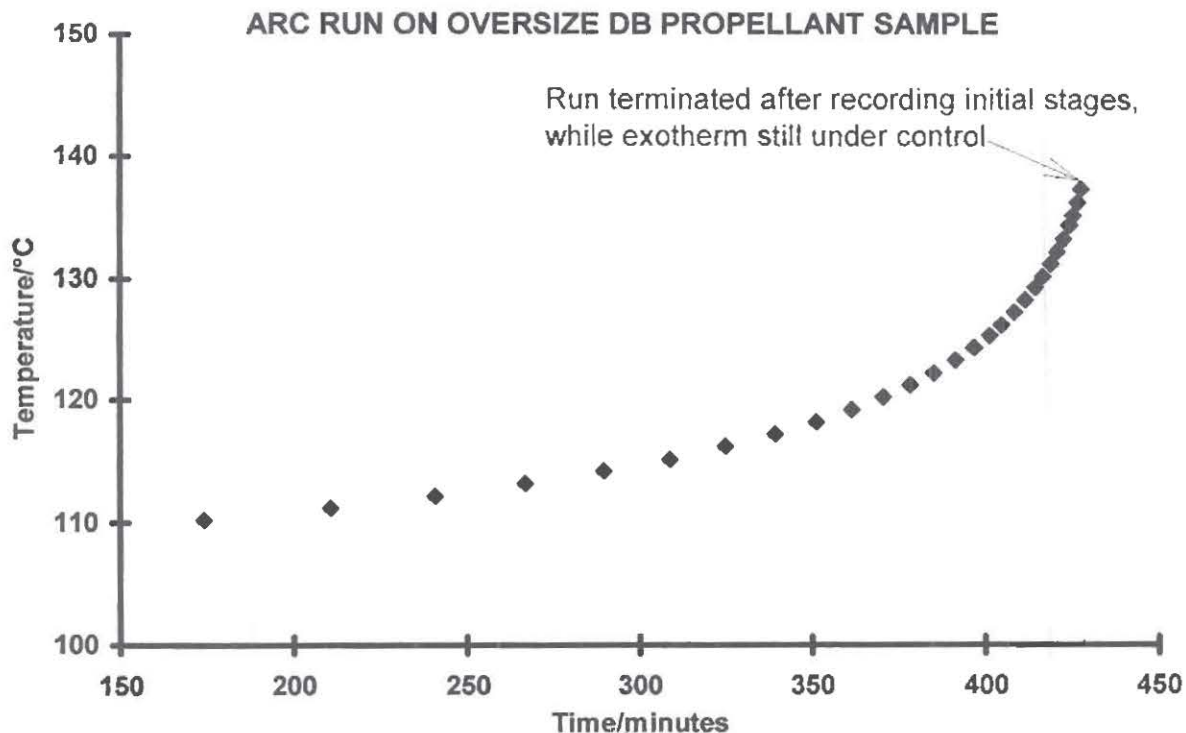


Fig 1 Double Base Propellant – Adiabatic Temperature vs. Time Curve

A time of maximum rate was estimated iteratively as described in reference 2 and used to construct a ϕ corrected time to maximum rate plot (Fig 2).

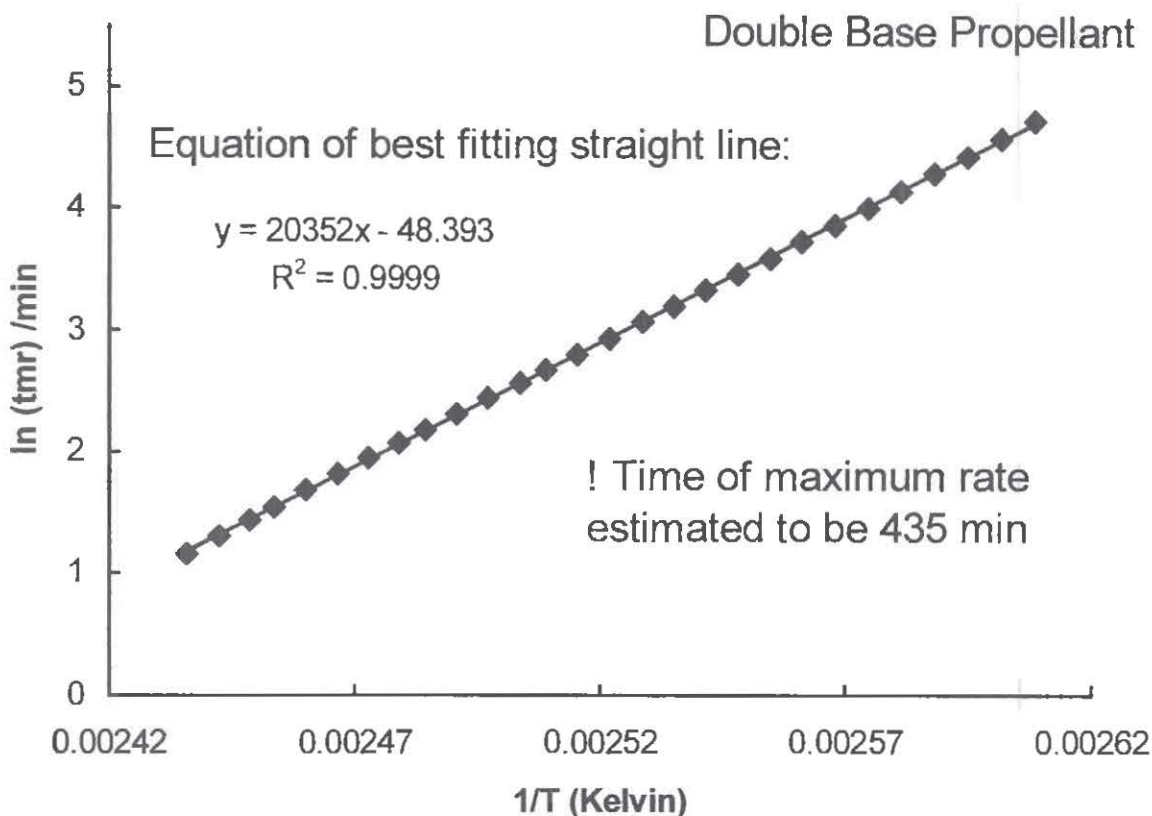


Fig 2 Double Base Propellant – Time to Maximum Rate Plot

Extrapolating the equation of the best fitting straight line to a starting temperature of 353.15 K gives an estimated adiabatic time to maximum rate of 10269 minutes (from equation 1), indicating an expected heat generation rate of $15.8 \mu\text{W} \cdot \text{g}^{-1}$ at 80°C (by equation 2).

A 2.4638g sample of the double base propellant was sealed in an atmosphere of nitrogen in a 3cm^3 glass ampoule, lowered into the detection region of the TAM and the heat flow resulting from the exothermic decomposition reactions monitored until a constant signal was observed. The TAM thermostat was set at 80°C . A plot of heat generation rate and total heat evolved against time are illustrated in figure 3. It can be seen that, once thermal equilibrium had been achieved, a reasonably constant heat generation rate of $16.4 \mu\text{W} \cdot \text{g}^{-1}$ was recorded i.e. very close to the value expected by calculation from the ARC experiment.

4 Example 2 – Ammonium Dinitramide

The second example used ammonium dinitramide (ADN). This has been proposed for use as an oxidiser in high energy, low signature propellant compositions. Specific heat was determined by DSC at 70°C to be $1.4 \text{ J} \cdot \text{g}^{-1} \cdot \text{K}^{-1}$. TAM experiments were conducted at a lower temperature of 70°C . This was to avoid any complications introduced by working at temperatures close to the melting point of ADN and also because ARC studies suggested that heat generation at 80°C might exceed the measuring range of the TAM.

A scanning heat-wait-search (HWS) ARC experiment was performed. Experimental conditions were:- Sample mass: 0.3623g, Bomb type: 2.54 cm diameter spherical titanium, Initial temperature: 100°C , Final temperature: 155°C , Self-heat detection threshold: $0.015^\circ\text{C} \cdot \text{min}^{-1}$, Step: 3°C , Wait time: 10 minutes, Data step temperature: 1°C , thermal inertia: 20.06, Atmosphere: nitrogen.

The raw data plot of temperature vs. time is shown in Fig 4.

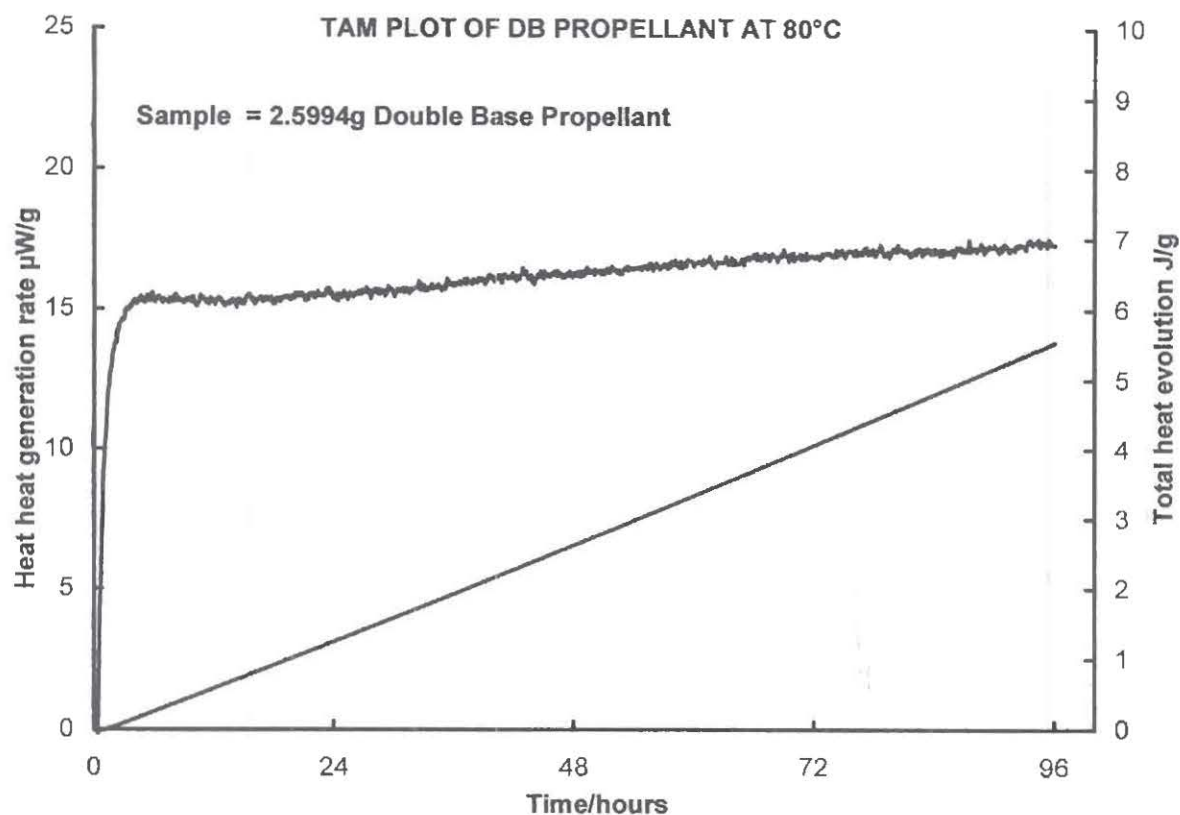


Fig 3 Double Base Propellant – Heat Generation at 80°C by Microcalorimetry

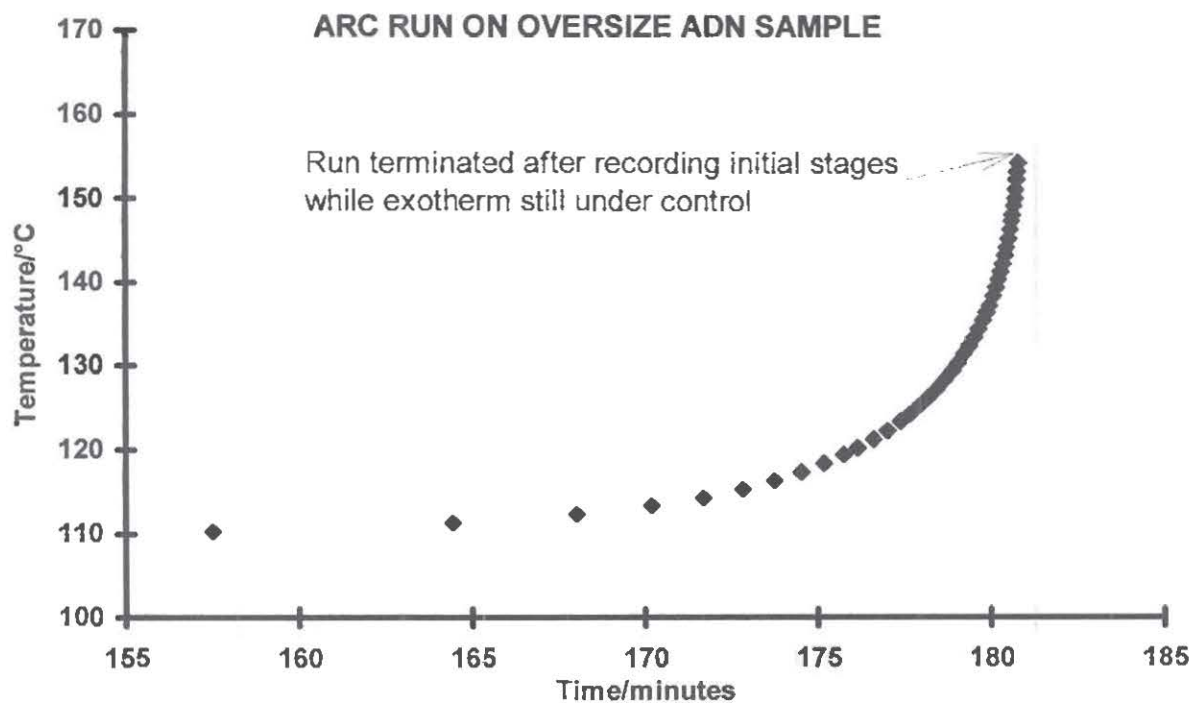


Fig 4 Ammonium Dinitramide – Adiabatic Temperature vs. Time Curve

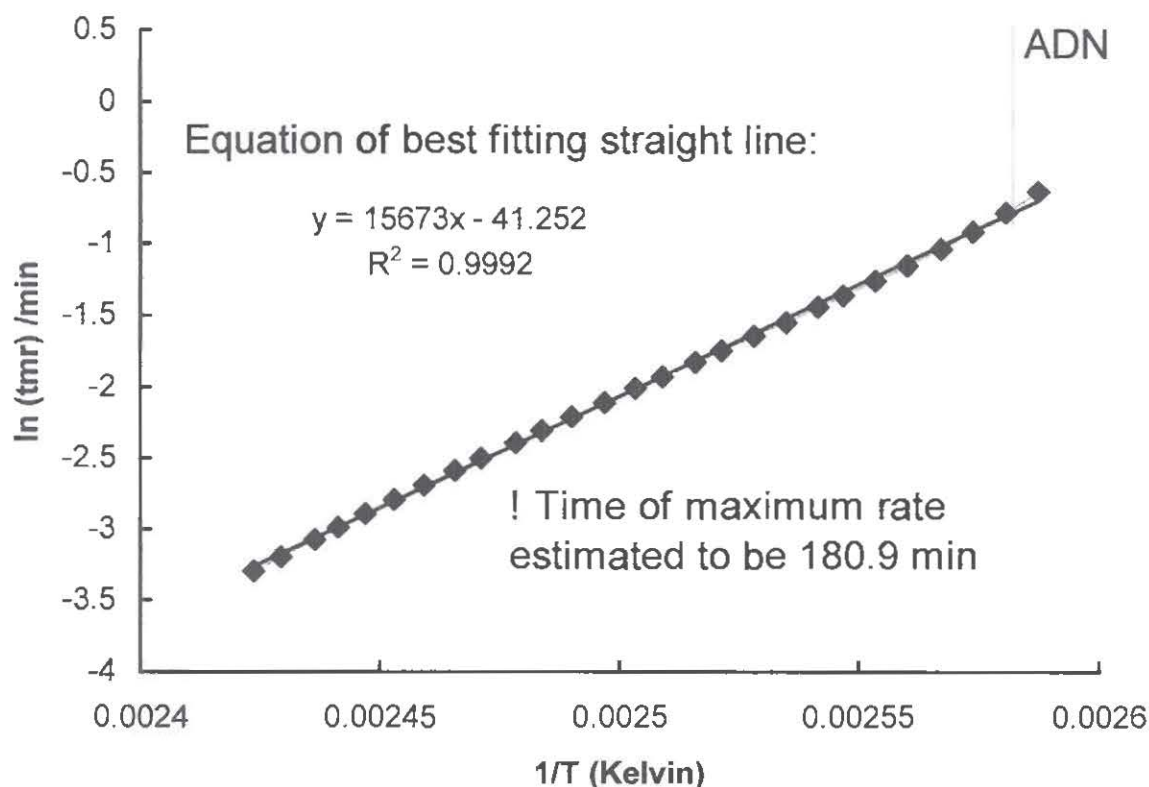


Fig 5 Ammonium Dinitramide – Time to Maximum Rate Plot

A time of maximum rate was estimated iteratively² and used to construct a ϕ corrected time to maximum rate plot (Fig 5).

Extrapolating the equation of the best fitting straight line gives an estimated adiabatic time to maximum rate of 83.25 minutes (from equation 1), indicating an extremely high expected heat generation rate of $2105 \mu\text{W}\cdot\text{g}^{-1}$ at only 70°C (by equation 2).

A 1.2546g sample of ammonium dinitramide was sealed in an atmosphere of nitrogen in a 3cm^3 glass ampoule, lowered into the detection region of the TAM and the heat flow resulting from the exothermic decomposition reactions monitored until greater than 0.5 J/g total heat energy had been generated. The TAM thermostat was set at 70°C . A plot of heat generation rate and total heat evolved against time are illustrated in figure 6. It can be seen that, once thermal equilibrium had been achieved, a reasonably constant heat generation rate of $2\mu\text{W}\cdot\text{g}^{-1}$ was recorded i.e. over 1000 times less than anticipated by calculation from the ARC experiment! Note that, if the original high prediction obtained using the ARC had been confirmed, it is difficult to see how this material could ever be considered for use as a propellant ingredient for service use!

3.3 Other Energetic Materials Examined

3 energetic, rubbery binders, PolyNIMMO [Poly(3-nitratomethyl-3-methyloxetane)], PolyGLYN [Poly(Glycidynitrate)] and GAP [Glycidyl azide polymer] and a single base gun propellant [Nitrocellulose 98.5%, diphenylamine 0.85-1.5%, calcium carbonate 0.2-0.6% and graphite glaze 0.1-0.3%], were also studied by ARC and TAM, employing a similar procedure to that described for the double base rocket propellant and ADN. Results are summarised, along with those from the double base propellant and ADN, in table 1.

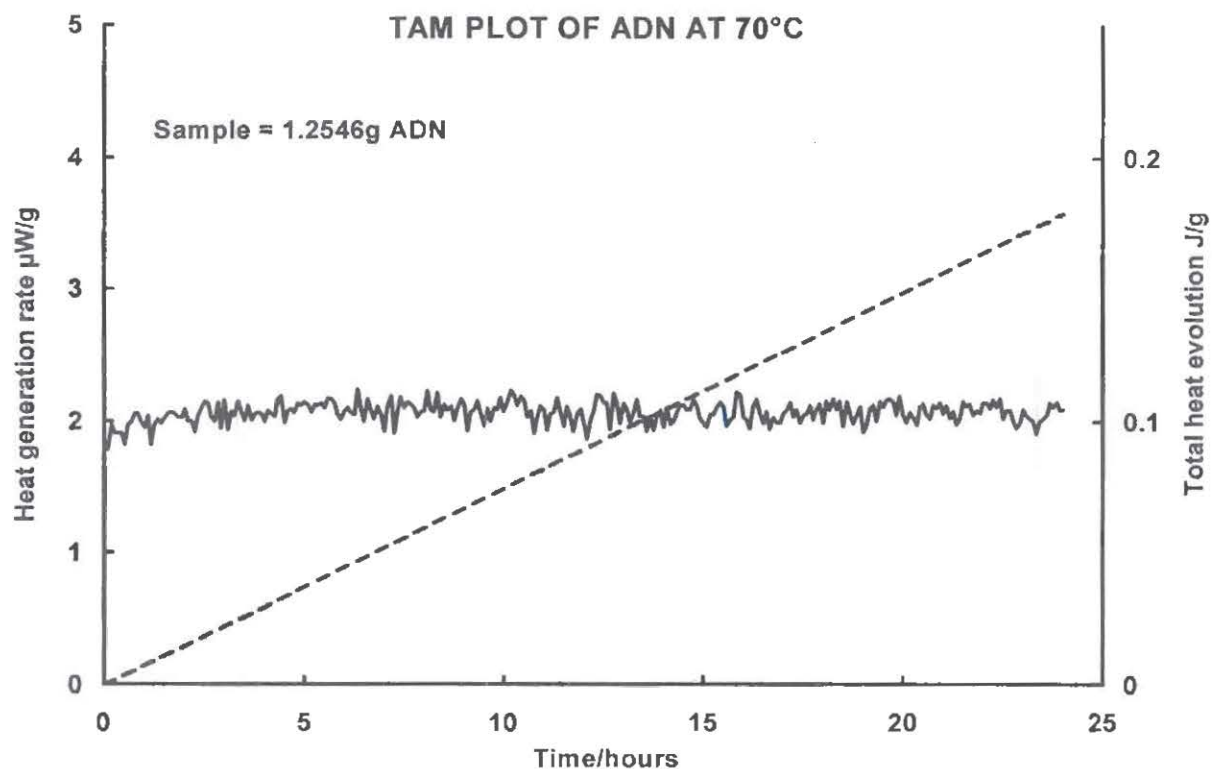


Fig 6 Ammonium Dinitramide – Heat Generation at 70°C by Microcalorimetry

Table 1 Comparison of Extrapolated ARC data with 80°C Microcalorimetry Experiments

ARC Experiment	Predicted rate at moderate temperature (ARC ¹)/μW.g ⁻¹	Observed rate at moderate temperature (microcalorimetry ²)/μW.g ⁻¹
Run 333 (PolyNIMMO) ²	4.9	9.0
Run 340 (PolyGLYN) ²	13.7	21.2
Run 344 (GAP) ²	0.36	1.64
Run 348 (Single base propellant) ²	35.5	9.2
Run 350 (Double base propellant) ²	15.8	16.4
Run 392 (Ammonium dinitramide) ³	2105	2.0

¹ Predicted self heat rate at lower temperature obtained by extrapolation of time to maximum rate plot from low ϕ ARC experiment. This can then be converted to heat generation rate using equation 2

² Moderate temperature = 80°C

³ Moderate temperature = 70°C

4 GENERAL DISCUSSION

In these cases, all of the nitrate ester containing materials – both traditional propellants and new energetic binders, give broad agreement between the two techniques.

Although it is obviously better to look at the temperature of interest directly, this may not always be possible; e.g. if the relevant temperature is above 90°C, but below the detection region of the ARC. In these cases, a decision has to be made as to whether a value for heat generation calculated by extrapolation is accurate enough to permit a useful decision about whether the system will be stable or not under designated environmental conditions.

If the critical extrapolation test survives to below that of the conditions of interest, the calculated heat generation rate under those conditions may be used with greater confidence in calculations to specify critical conditions. Just how close the agreement must be between expected and observed results at that temperature for the description to be judged valid will inevitably be a subjective decision based on experience and will depend on the perceived seriousness of a runaway and how large safety margins are deemed acceptable.

An example of where agreement is not found is provided by ADN where the observed heat generation rate measured at 70°C by microcalorimetry is over 2 orders of magnitude smaller than anticipated by calculation from the ARC experiment conducted at elevated temperature. In this case, examination of the DSC curve of ADN points to a likely explanation (Figure 7).

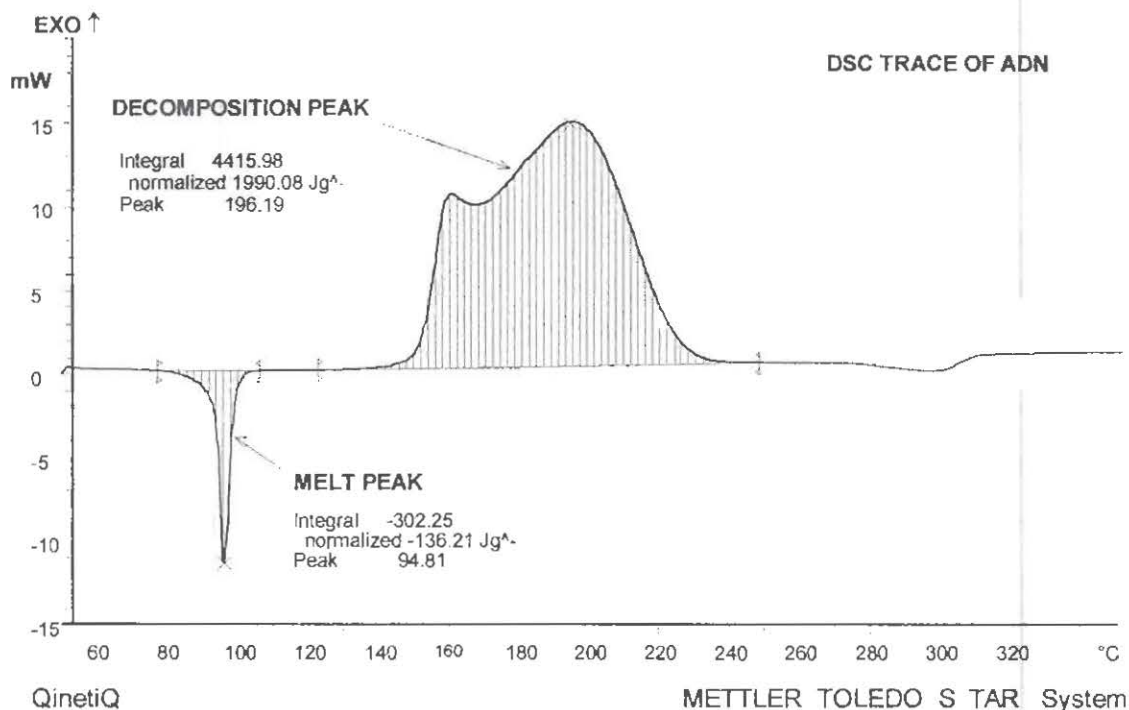


Fig 7 Ammonium Dinitramide – Differential Scanning Calorimetry trace

It can be seen that ADN melts between 90 and 100°C and the discrepancy between ARC and HFC is consistent with a different, faster decomposition mechanism when ADN is molten compared to the crystalline material..

Obviously, the poor thermal stability of ADN above 80°C is not ideal and if an alternative smoke-free, high energy oxidant was available it would be preferable to use it. However, there are only very few alternatives to ADN for use as oxidants in high energy/low smoke propellants, and all have limitations at least as inconvenient as the high temperature stability of ADN. If it is considered that the advantages of ADN warrant its use, it can at least be used with an understanding of the operational constraints its use would impose; i.e. the risk may be managed, if properly understood. Obviously data gathered at temperatures below 80°C would be relevant for 'normal' lifetime prediction, while assessing what might happen in the event of accidental heating; for example resulting from a nearby fire, would require the use of experimental data gathered above 90°C.

4 CONCLUSIONS AND RECOMMENDATIONS

The self-heating characteristics of a number of energetic materials have been described using the techniques of accelerating rate calorimetry and microcalorimetry in combination. It has been shown that the two techniques are largely complimentary and that their strengths and weaknesses are mutually exclusive. Although ARC and TAM data can be interconverted (i.e. self heat rate to/from time to maximum rate), direct comparison of experimental data gained over the same temperature range is often not possible, due to these techniques having very different sensitivities. However, once a general description of the self heating characteristics of an energetic material has been made using the ARC, the high sensitivity of the TAM makes it an ideal way to confirm or deny the validity of extrapolating the ARC data to lower temperatures.

All of the nitrate ester energetic materials studied here show a reasonably good level of agreement between results from the two techniques and it seems reasonable to assume that the heat generating decomposition reactions may be described by a single Arrhenius equation with sufficient accuracy to allow practical hazard assessments to be made.

In contrast, in the case of ADN, comparison of heat generation expected from extrapolated ARC studies and microcalorimetric measurements made at 70°C show that the ARC data clearly cannot be extrapolated to lower temperatures. The reason for this appears to be the intervening melting transition causing a mechanism change between 80 and 90°C. Obviously data gathered at temperatures below 80°C would be relevant for 'normal' lifetime prediction, while assessing what might happen in the event of accidental heating; for example resulting from a nearby fire, would require the use of experimental data gathered above 90°C.

It is recommended that data obtained from high temperature ARC experiments should be validated by the use of heat flow calorimetry experiments conducted at temperatures below the temperature where the self heating hazards of the system of interest are being considered.

5 ACKNOWLEDGEMENT

This work was supported and funded by UK MOD (DOSG).

6 REFERENCES

- 1 P F Bunyan, D A Tod and G Kavanagh, *Characterisation of Thermal Runaway Reactions in Energetic Solid Materials Using Accelerating Rate Calorimetry*, Proc. 30th Int. Conf of ICT, Paper P62, Karlsruhe, Germany, 29th June - 2nd July 1999.
- 2 P F Bunyan and D A Tod, *Accelerating Rate Calorimetry Experiments on Energetic Materials: Obtaining Time to Maximum Rate Plots on Larger Samples*, Proc. 31st Int. Conf of ICT, Paper V4, Karlsruhe, Germany, 27-30th June 2000.
- 3 M W Whitmore and J K Wilberforce, *J. Loss Prev. Process Ind* 6 (2), (1993), 95.
- 4 D I Townsend and J C Tou, *Thermochimica Acta*, 37 (1980), 1.
- 5 J K Wilberforce, *Journal of Thermal Analysis*, 25 (1982), 593.
- 6 D I Townsend, *Accelerating Rate Calorimetry, Runaway Reactions, Unstable Products and Combustible Powders*, Chem E Symposium Series No 68 3/Q, Chester England, 1981.
- 7 H G Fisher and D D Goetz, *J. Loss Prev. Process Ind* 4 (5), (1991), 305.

© Copyright QinetiQ Ltd 2002.

THIS PAGE LEFT INTENTIONAL BLANK

THE CONSTRUCTION AND EVALUATION OF A NEW HIGH PRESSURE MANIFOLD AND VESSELS FOR A CALVET MICROCALORIMETER

D.E.G. Jones , A.M. Turcotte and R.C. Fouchard
Canadian Explosives Research Laboratory, Natural Resources Canada
555 Booth St., Ottawa, Ontario K1A 0G1 Canada
E-mail: djones@nrcan.gc.ca

SUMMARY:

Precision heat flow calorimetry, using a Tian-Calvet instrument (Setaram C-80) has been an integral part of our laboratory studies of the thermal properties of energetic materials for some time. Our ability to study the effects of high pressure on the decomposition characteristics, with a high degree of sensitivity, has been limited. We therefore undertook to design, construct and evaluate a high pressure manifold capable of operation up to 69 MPa for our Setaram C-80 instrument.

This report will describe, in detail, the high pressure manifold construction, safety assessment, calibration as well as a brief description of the initial trials with energetic materials.

INTRODUCTION:

The effect of high pressure on the decomposition characteristics of explosives is an important safety consideration for explosives manufacturing, transportation and blasting. Several other researchers have adapted the Setaram C-80 for high pressure applications [1-8]. Until now, our laboratory did not have the capability to analyze energetic materials with a high degree of sensitivity at pressures above 6.9 MPa. We therefore undertook to design, construct and evaluate a high pressure manifold capable of operation up to 69 MPa for our existing Tian-Calvet instrument (Setaram C80).

The Setaram C80 consists of a massive aluminum block, with two identical cylindrical cavities located symmetrically about the center; a thermopile surrounds each cavity. The design results in a sensitivity to heat flow of about 10 μW . This sensitivity, as well as the ability to heat at very low heating rates (0.01 to 2.00 $^{\circ}\text{C min}^{-1}$) and the ruggedness of the C80 make it an ideal candidate for high pressure applications.

All components of the high pressure manifold, designed and constructed at CERL, were rated at > 69 MPa. Presently, a 41.3 MPa argon cylinder is being used as a pressure source and a maximum pressure of 33 MPa is being used. Following a complete evaluation of the system, a pressure source capable of reaching 69 MPa will be incorporated.

A detailed operating procedure and a safety assessment were carried out for the completed system before any experimental work was started. The system was then leak tested, calibration of the temperature and heat flow were carried out, followed by blank runs at various pressures, a repeatability study and verification. Preliminary studies with ammonium nitrate (AN) and pentaerythritol tetranitrate (PETN) were then carried out. The results of these studies show that the high pressure manifold system, in conjunction

with a Setaram C80 heat flow calorimeter, is useful and well adapted for testing energetic materials at high pressures.

EXPERIMENTAL:

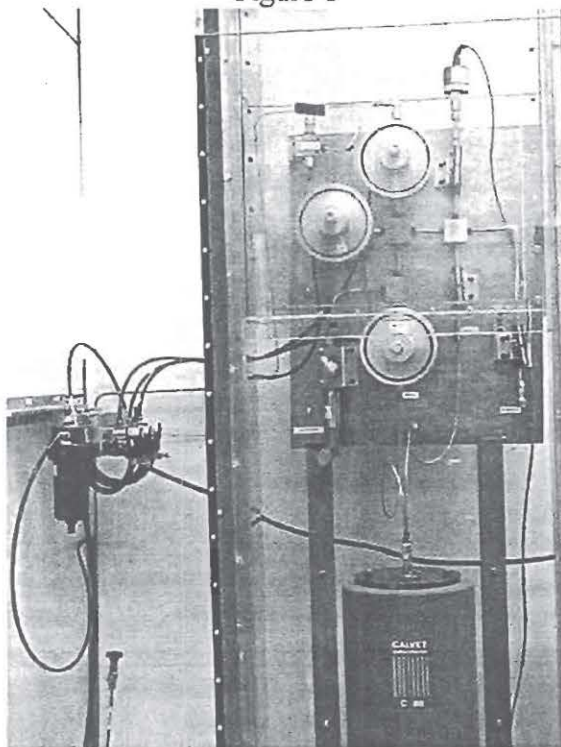
Materials:

Alumina (synthetic sapphire), indium and tin (SRM) were purchased from The National Bureau of Standards (NBS). Ammonium nitrate (AN) was ACS reagent grade (Sigma Chemical Co.) and was dried overnight in an oven at 80 °C, then stored in a dessicator. Pentaerythritol tetranitrate (PETN) was removed from "liteline" detonating cord (Austin Powder Co.).

Design and Construction of the C-80 High Pressure Manifold:

Extensive modifications to our Setaram C-80 heat-flux calorimeter system were necessary to allow the study of the thermal decomposition of explosives at pressures up to 69 MPa. A picture of the completed system is shown in Figure 1.

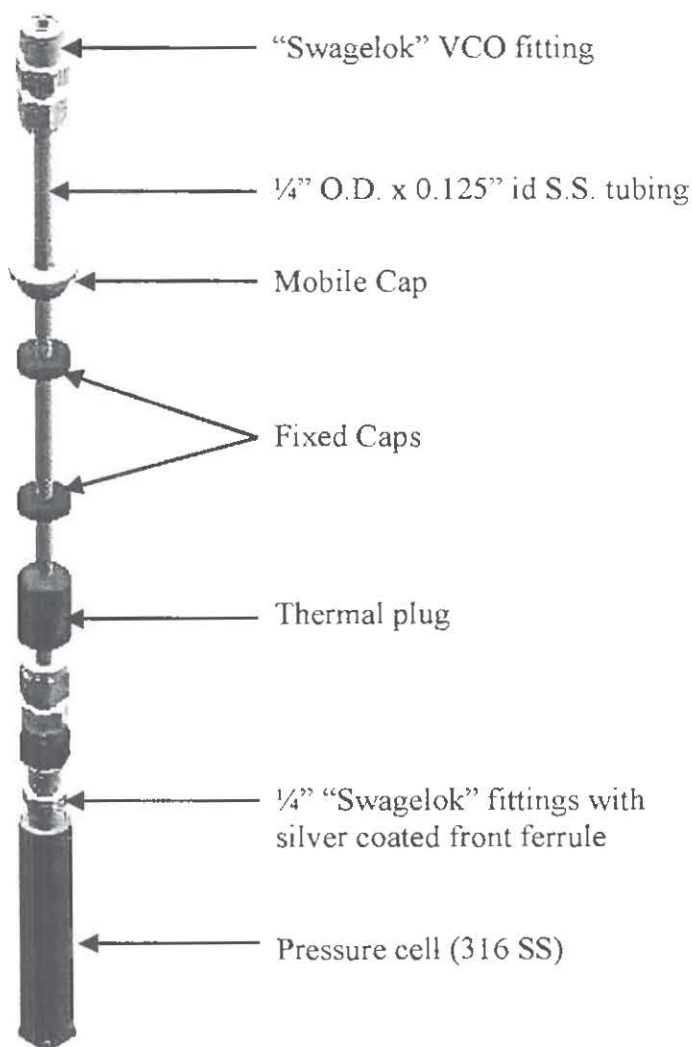
Figure 1



A 13 mm thick "Lexan" cage was constructed around the apparatus, with an exhaust vent. This cage protects the operator from mishaps and/or fumes. Pressure sample/reference vessels are available from Setaram, however, these vessels have a wall thickness of 3.1 mm and are limited to a maximum pressure of 10 MPa. Therefore high pressure sample/reference vessels and transfer tubes were manufactured by our machine shop.

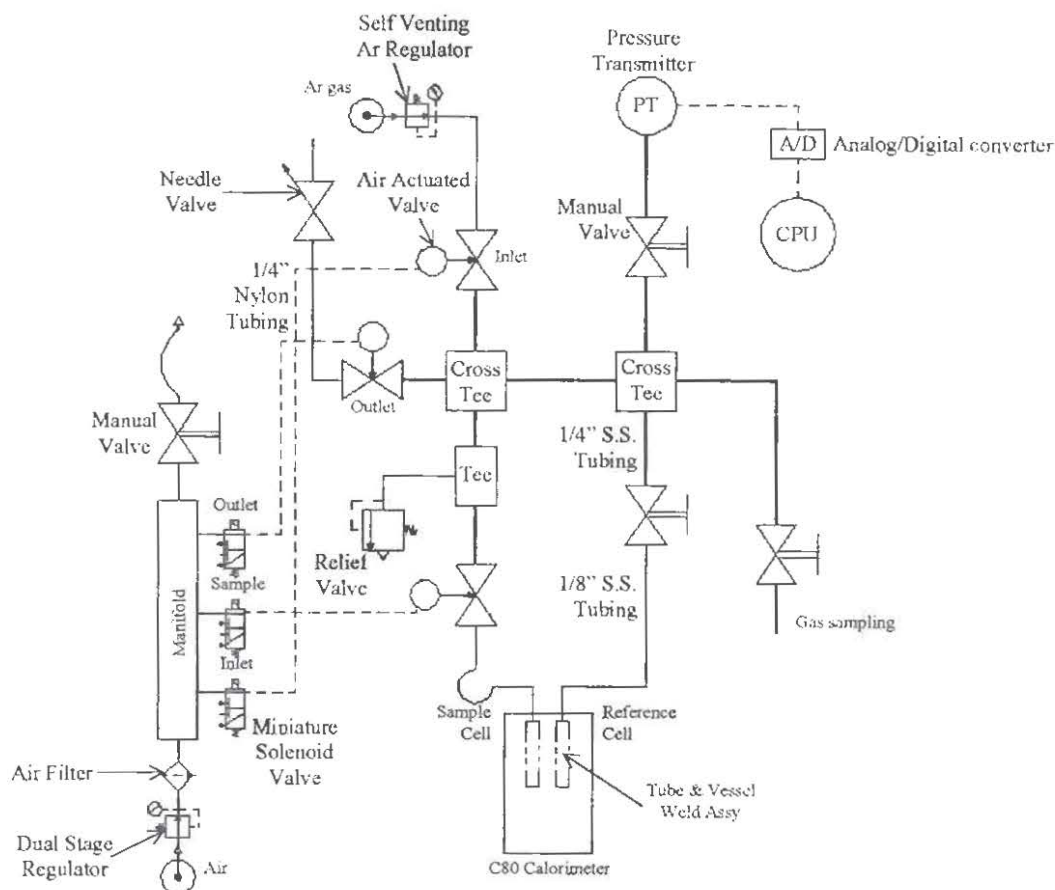
These vessels were made from 316 stainless steel with a wall thickness of 5.25 mm, and a volume of 3.26 mL. The transfer tubes were constructed using 6 mm 316 stainless steel tubing with a wall thickness of 2 mm capable of withstanding a maximum pressure of 80 MPa. The vessels and transfer tubes were connected with 6 mm "swagelok" fittings using silver coated front ferrules. This system gave an excellent seal over 8-10 experiments, at which point, a new fitting and ferrule could be installed without replacing the entire transfer tube. Figure 2 shows details of the vessels and transfer tubes designed and

Figure 2



constructed at our facility. The transfer tubes were connected to the high pressure manifold using 3 mm o.d. by 1 mm i.d. tubing. This allowed a "flexible" connection between the sample/reference and manifold without compromising the pressure limits. A schematic for the high pressure manifold is shown in Figure 3.

Figure 3



The total volume of the system (vessels, transfer tubes plus the manifold) was calculated to be 28.3 mL. All components of the manifold have maximum pressure ratings greater than 69 MPa. As an added safety precaution, air actuated valves (Autoclave Engineers) were installed for the gas inlet, outlet and sample vessel. These valves are controlled using solenoid valves (Snap-Tite) connected to a control box with a long cable to allow remote manipulation. Flushing and pressurization of the manifold/ vessels, can therefore be carried out at a safe distance from the apparatus. A pressure relief valve (Autoclave Engineers) set at 70 MPa was installed as a further safety precaution.

A series of pressure transducers with 4-20 mA output, (Setra Systems Inc.) were purchased to cover the pressure range from 0 to 69 MPa. These transducers can easily be interchanged to cover the pressure range of interest. The pressure transducer was connected to a digital panel meter (Alpha Control & Instruments). In order to store the pressure data, the digital meter was connected to a "Strawberry Tree" data shuttle (Dalimar Instruments Inc.) then to a computer utilizing the "Workbench PC for Windows" software. At the end of an experiment the C80 heat flow data and pressure data files were combined using "Sigma-Plot" software.

To protect the sample vessel from corrosion, alumina liners (99.7%) (Arklay S. Richards Co. Inc.) were used. The liners were 6 mm o.d. by 4 mm i.d. and 90 mm high. For very fine samples 6 mm o.d. extra coarse (170-220 μm) fritted discs were placed on top of the sample liner to contain the sample during the experiment.

A detailed operating procedure, and a safety assessment were developed for the completed system before any experimental work was started. Detailed calculations of the effects of overpressure in the system as well as an evaluation of fragmentation hazards were carried out as part of the safety assessment and are discussed in the results and discussion section of this report.

Leak Testing:

The system was first pressurized to 3.4 MPa with argon and monitored for leaks. Once the system was leak tight the system was pressurized to 34.5 MPa and monitored. This procedure was repeated until the system was free of leaks. During the initial testing, leaks developed at the fitting between the cell and transfer tubes. The stainless steel front ferrules were replaced with silver coated ferrules. With these ferrules a leak-free connection could be maintained for eight or nine experiments before needing replacement.

Calibration:

The first step of calibration was verification of the thermocouples. A 45 cm type K thermocouple (Omega) was calibrated against a temperature calibrator (Fluke 701). This thermocouple was placed in the sample well of the C-80. The instrument was heated to 25 °C and held there for 2 hours. Readings of the block, furnace and sample thermocouple were recorded at the end of the 2 hour wait time. This procedure was repeated at 100, 200, and 300 °C. The difference between the block temperature and the corrected sample temperature values were used as temperature correction factors in the C-80 software.

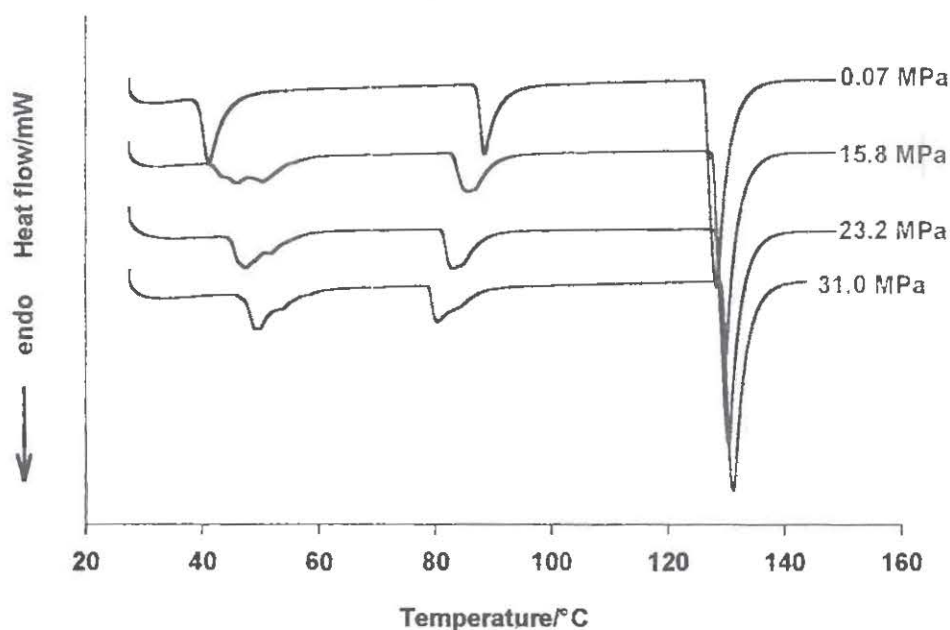
Blank runs at ambient and 33.2 MPa of argon, and a run of 3.6 g of synthetic sapphire (SRM) at 0.07 MPa argon were carried out from 25-300 °C at 0.3 °C min⁻¹. Heat flow calibration values were calculated and entered into the software. Three runs of indium alone were also carried out at a heating rate of 0.3 K min⁻¹ and starting pressure of 0.07 MPa argon to test the calibration of the system. It was found that due to the large thermal mass of the new cells that calibration of the temperature and heat flow were necessary to correct the existing calibration using sapphire.

Calibration with indium and tin reference materials (SRM) was performed as follows; 100 mg of indium was placed in an alumina liner, about 75 mg of alumina powder was placed on top of the indium and 100 mg of tin was placed on top of the alumina. In this way both materials could be analyzed in one run. These materials were run at 0.1, 0.3, 0.5, 0.7, and 1 °C min⁻¹ at 0.07 MPa pressure of argon. Each melting peak was integrated and the onset T (T₀) and heat of fusion (ΔH_f) recorded at each of the 5 heating rates. The temperature correction and sensitivity coefficients were calculated from the average of the five heating rates and entered into the software. A final verification run of indium and tin produced onset temperatures and enthalpy values that were in close agreement with literature values.

AN Trials:

As an initial test of the pressure manifold, a study was undertaken to examine the effect of pressure on the phase transitions of AN. Samples of 0.8 g dry AN were heated from 28 to 150 °C at 0.3 °C min⁻¹ at pressures of 0.07, 15.8, 23.0, and 31.0 MPa of argon. An overlay graph of representative runs is shown in Figure 4.

Figure 4
Comparison of C-80 results for AN
at various pressures of Argon



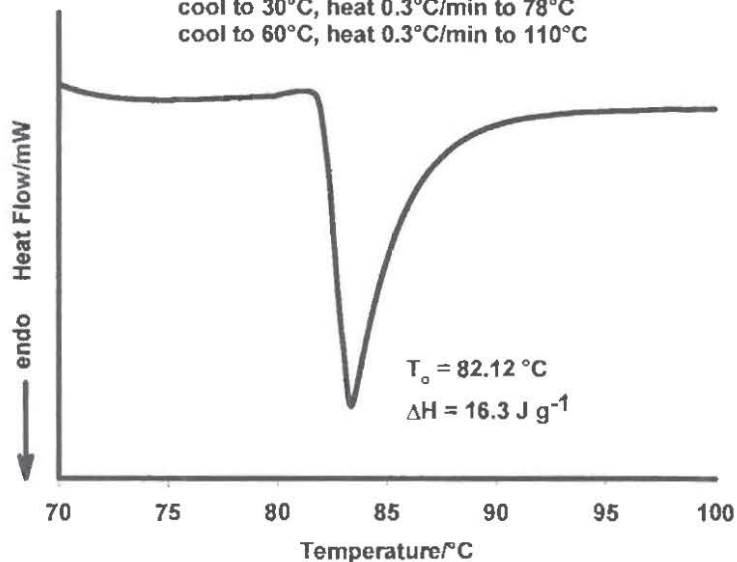
The AN IV to III and III to II phase transition peaks at higher pressures were very irregular in shape, unlike those at ambient pressure. These transitions are known to be very slow because of the drastic crystallographic changes occurring [9]. Hence, it was felt that an annealing period would allow structural relaxation and a sharper transition might occur. In order to test this idea, a run of 0.8 g AN at 31.1 MPa of argon was carried out with "conditioning" steps before the measurement of the AN III to II phase transition as follows:

0.3 °C min⁻¹ to 45 °C, isothermal 1 hour
cool to 30 °C, heat 0.3 °C min⁻¹ to 78 °C
cool to 60 °C, heat 0.3 °C min⁻¹ to 110 °C

The results of this experiment are shown in Figure 5. As can be seen from the figure, the "conditioning" produced a smooth and regular peak..

Figure 5
Ammonium Nitrate
0.8053 g 31.1 MPa argon

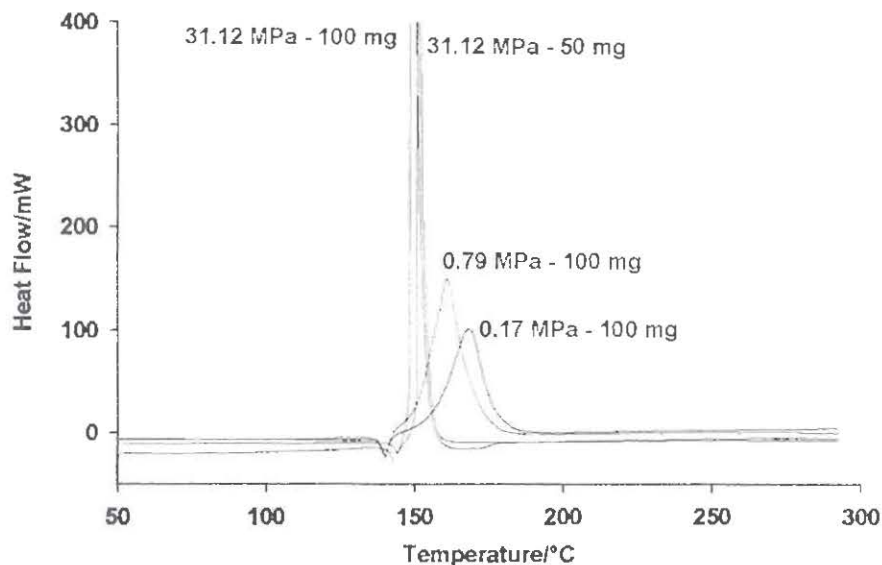
0.3°C/min to 45°C, iso 60 min
cool to 30°C, heat 0.3°C/min to 78°C
cool to 60°C, heat 0.3°C/min to 110°C



PETN Trials:

To evaluate the high pressure manifold at higher temperatures, during decomposition of explosives, a study was undertaken using PETN. Samples of 100 mg of PETN were heated from 28-300 °C at 0.3 or 1.0 °C min⁻¹. At higher pressures the C-80 detector signal was saturated, therefore the sample size was reduced to 50 mg. Samples were run at 0.07, 0.17, 0.79, and 31 MPa of argon. A graphical comparison of the results at different pressures is show in Figure 6.

FIGURE 6
Comparison of C-80 Runs of PETN
At Various Pressures of Argon



RESULTS & DISCUSSION:

As part of the safety assessment of the system, detailed calculations of overpressure likely to be generated if a sample of explosive were to burn to completion in the C80 while operating at high pressure were completed. At the present time, we are limiting the system to a maximum sample mass of 0.1 g of energetic material. Under these conditions, at a starting pressure of 69 MPa the calculations show that the overpressure from the reaction would be 80 MPa. This is slightly above the 79.2 MPa setting for the relief valve and within the limits of the system.

Calculations were also carried out to ascertain the fragmentation hazard of a failure of a part of the system. These calculations show that the Lexan cage should be more than capable of stopping any projectile. The connection between the sample vessel and the transfer tube is the most critical since it must be opened and retightened for every run. It was difficult to maintain a leak-free connection for more than one or two experiments with stainless steel front ferrules. Switching to silver coated front ferrules gave a much better seal that could be maintained over eight or nine runs. At that point, a whole new fitting was installed. The "VCO" fittings between the transfer tubes and 1/8" tubing to the manifold also has to be opened and retightened for every run. However, this connection, which is not heated, could be reused over many runs with only occasional replacement of the "O" ring.

Calibration:

The results of the verification and calibration of the C80 thermocouples are shown in Table 1.

Table 1

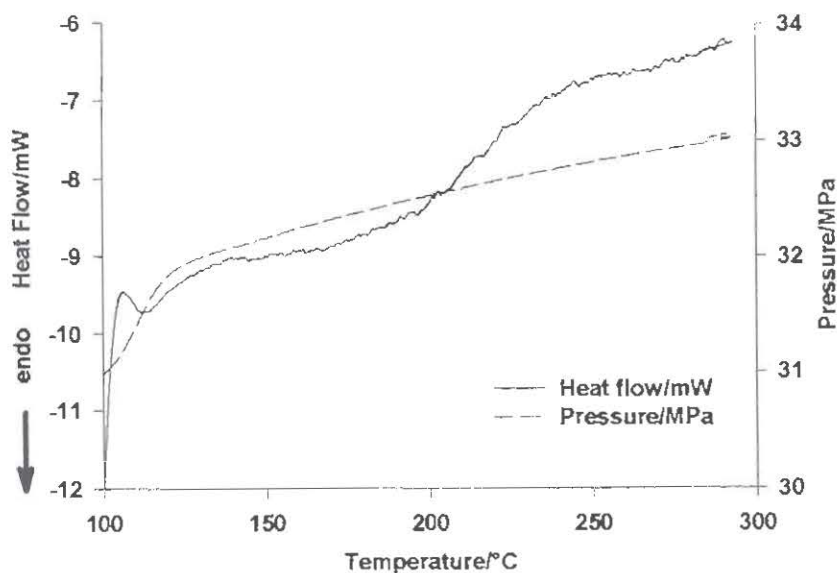
Program T/°C	Block T/°C	Furnace T/°C	Sample T/°C	Sample T Correction/°C
25	24.97	25.45	24.9	-0.07
100	98.86	99.99	99.6	+0.74
200	197.97	200.00	198.6	+0.63
300	297.12	300.00	297.9	+0.78

The sample temperature (T) correction is the difference between the block temperature and the sample temperature measured by placing a calibrated thermocouple in the sample vessel well. These values were used to adjust the C80 temperature calibration for the new high pressure sample/reference vessels.

Baseline runs with empty vessels at $0.3\text{ }^{\circ}\text{C min}^{-1}$ and 0.07 and 33.2 MPa argon were then carried out, as well as a run with sapphire (4 g) at the same heating rate and ambient pressure. The graph for the blank run at 33.2 MPa argon is shown in Figure 7. The baseline drift over the temperature range 100 – 300 $^{\circ}\text{C}$ was less than 4.0 mW.

Figure 7

Blank Run
0.3 K/min to 300 $^{\circ}\text{C}$ ~33 MPa argon



The thermal mass of the new pressure cells is quite high (140 g vs. 75 g for standard cells), therefore the system is probably not at equilibrium using a heating rate of 0.3 K min⁻¹. Results of a repeatability study using indium at 0.3 K min⁻¹ and 0.07 MPa argon to verify the calibration of the high pressure system are shown in Table 2. Three samples of indium were run and the results compared. The onset temperature values are too high and the enthalpy values low.

Table 2

$T_o/^\circ\text{C}$	$\Delta H_f/\text{J g}^{-1}$
159.05	26.2
158.88	26.4
159.21	26.3

(Literature values, 156.6 °C and 28.7 J g⁻¹)

It was then decided that the original Setaram factory calibration would be used, then corrected using runs of indium and tin at five different heating rates as described in the experimental section of this report. The values of the onset temperature (T_o) and heat of fusion (ΔH_f) for both indium and tin at the five heating rates are given in Table 3.

Table 3

<u>Indium</u> Rate/ $^\circ\text{C min}^{-1}$	$T_o/^\circ\text{C}$	$\Delta H_f/\text{J g}^{-1}$
1.0	163.2	25.0
0.7	161.4	26.0
0.5	159.9	27.7
0.3	158.7	26.1
0.1	157.2	26.1
<u>Tin</u>		
1.0	238.6	53.0
0.7	236.6	53.9
0.5	235.2	55.4
0.3	233.9	57.3
0.1	232.3	55.6

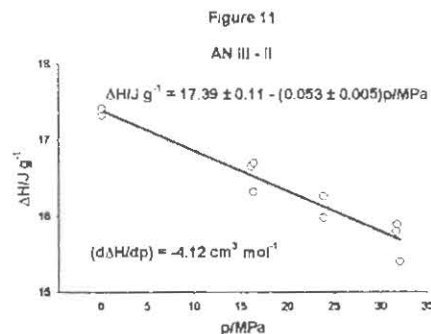
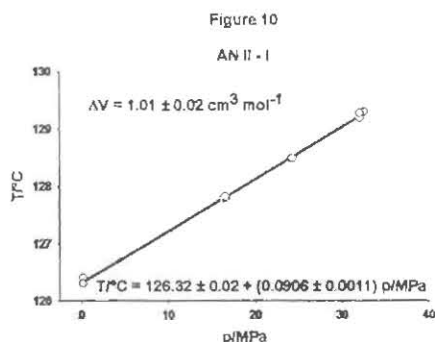
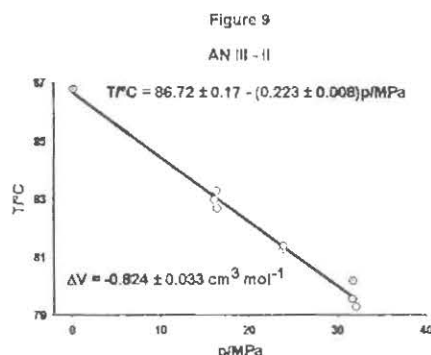
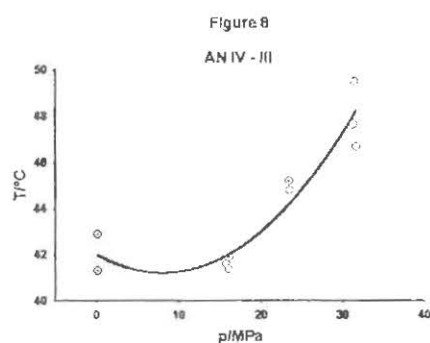
The average heat of fusion, based on the five heating rates for each metal was used to calculate a factor (F) using the equation: $F = \text{true melting point} / \text{experimental melting point}$. The factors for the two metals were then averaged and each sensitivity coefficient was divided by the factor to determine new coefficients.

In the same way, the onset temperatures were used to correct the temperature coefficients in the C80 software. A run of indium and tin at 0.3 K min⁻¹ and 0.07 MPa

argon was then carried out to verify the temperature and heat flow calibration values. The onset temperature and enthalpy values for indium (156.7°C and 29.0 J g^{-1}) were in good agreement with the literature values of 156.6°C and 28.7 J g^{-1} . Likewise the values for tin (231.8°C and 60.1 J g^{-1}) agreed well with the literature values of 231.97°C and 60.2 J g^{-1} . The large thermal mass of the high pressure cells was compensated for with the calibration technique described above and the system was now ready for trials with energetic materials.

AN Trials

The initial trials to examine the effect of pressure on the phase transitions of ammonium nitrate showed substantial shifts in the onset temperature of the transitions with pressure (Figure 4). The ammonium nitrate trials were limited to a maximum temperature of 150°C , which is below the melting and decomposition temperature using a sample mass of 1.0 g . Plots of onset temperature versus pressure for the three phase transitions of AN are shown in Figures 8-10.



The onset temperature versus pressure relationship of the AN IV - III phase transition is not linear and there is significant scatter in the data (Figure 8). It is possible that there is a significant amount of IV - II transition occurring at ambient starting pressure, while this transition is inhibited at elevated pressures. The onset temperature of the AN III - II transition shows a linear decrease with increasing pressure (Figure 9). The equation for the onset temperature from the line of best fit is $T/^{\circ}\text{C} = (86.72 \pm 0.17) - (0.223 \pm$

0.008)p/MPa. The change in bulk volume (ΔV) was calculated to be $\Delta V = -0.824 \pm 0.033 \text{ cm}^3 \text{ mol}^{-1}$ for the AN III – II transition using the Clausius Clapeyron equation. The AN II – I phase transition showed a linear increase in onset temperature with increasing pressure (Figure 10). The equation for the onset temperature from the line of best fit is $T/^\circ\text{C} = 126.32 \pm 0.02 + (0.0906 \pm 0.0011) p/\text{MPa}$. The change in bulk volume was calculated to be $\Delta V = 1.01 \pm 0.02 \text{ cm}^3 \text{ mol}^{-1}$. There is an increase in bulk volume for both the IV – III and II – I transitions and a decrease in volume for the III – II transition. The observations for the II – I transition are opposite to that obtained from crystallography, but the other two volume changes are in agreement with the crystallographic results [9]. A plot of $\Delta H/J \text{ g}^{-1}$ versus pressure for the AN III – II phase transition is shown in Figure 11. The equation for $\Delta H/J \text{ g}^{-1}$ was calculated to be $17.39 \pm 0.11 - (0.053 \pm 0.005) p/\text{MPa}$. The value of $d\Delta H/dp$ was calculated to be $-4.12 \text{ cm}^3 \text{ mol}^{-1}$.

PETN Trials:

The thermal behaviour of PETN was determined up to 300 °C to test the high pressure manifold during decomposition. At various pressures of argon, substantial differences in the onset temperature and enthalpy of melting and decomposition were observed (Figure 6). Plots for the melting endotherm and decomposition exotherm of PETN at the various heating rates and pressures are shown in Figures 12 to 19.

Figure 12

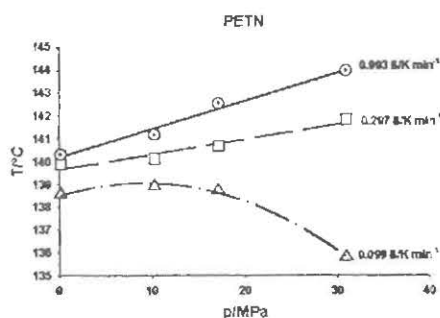


Figure 13

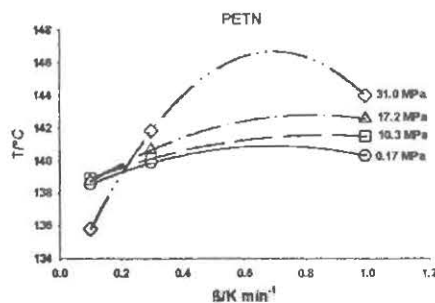


Figure 14

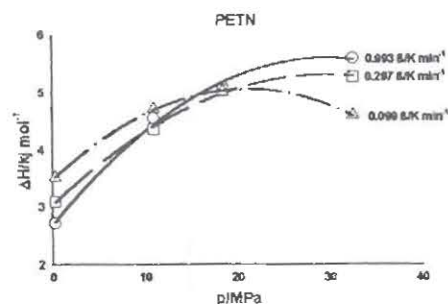


Figure 15

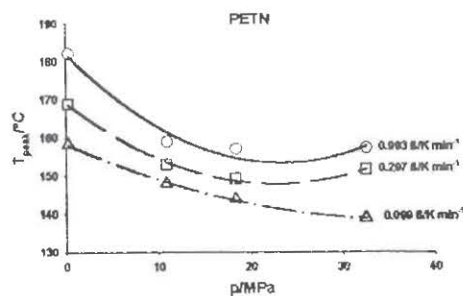


Figure 16

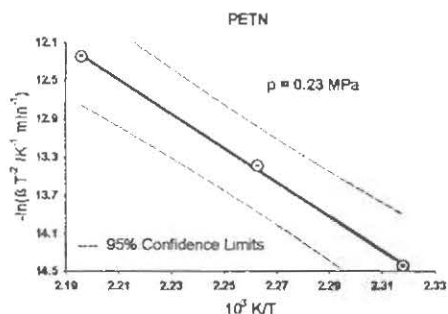
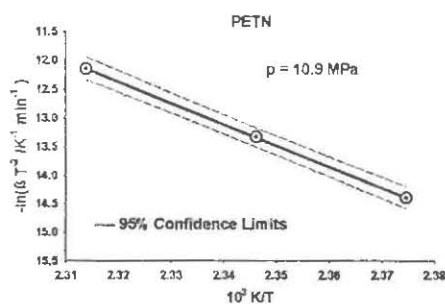


Figure 17



The onset temperatures of melting of PETN show a linear increase with increasing pressure at heating rates of 0.993 and $0.297 \text{ }^\circ\text{C min}^{-1}$, however, at a heating rate of $0.099 \text{ }^\circ\text{C min}^{-1}$ the onset temperature of melting appears to decrease with increasing pressure (Figure 12). A plot of the onset temperature of melting versus heating rate at the various pressures is shown in Figure 13. The ΔH values for the melting endotherm versus pressure at the three heating rates are shown in Figure 14.

For the decomposition exotherm of PETN, Figure 15 shows a plot of the peak temperature versus pressure at the three heating rates used. Example plots of $-\ln(\beta T^2 / \text{K}^2 \text{ min}^{-1})$ versus 10^3 K/T at two pressures are shown in Figures 16 and 17.

CONCLUSIONS:

The high pressure manifold designed and constructed at our facility has enhanced our research and testing capabilities. By carefully choosing components that exceeded the pressure limits we require, carrying out a detailed safety assessment of the system and testing and verifying the system in stages, we have shown that the manifold can be operated safely and effectively.

The large mass of the sample/reference vessels necessary at high pressures means that calibration of the system to account for thermal lag and use of lower heating rates are necessary to take full advantage of this system.

This instrumentation allows us to examine the pressure effect on phase transitions, allowing the determination of ΔV values as demonstrated with the experiments carried out in this study using AN.

The onset temperature of melting of PETN increases with pressure except at very low heating rates. The enthalpy values for the decomposition of PETN increase with increasing pressure and the peak temperature decreases with increasing pressure.

Initial testing of energetic materials, at pressures up to 31 MPa , have shown that this system can produce accurate and meaningful data without compromising safety in the laboratory.

ACKNOWLEDGMENTS:

Ettore Contestabile and Don Wilson of The Canadian Explosives Research Laboratory (Natural Resources Canada) provided valuable information for the vessel design and commissioning of the manifold.

The authors would also like to thank Al Vaillancourt and Sal Alaimo from Technical Services at Natural Resources Canada, for their valuable assistance in assembling the manifold.

REFERENCES:

1. Grolier, J.-P. E., "Solution Calorimetry at High Temperatures and Elevated Pressures", *Pure & Appl. Chem.*, vol. 62, no. 11, pp 2115-2120, 1990
2. Coxam, J.-Y., et al., "Modification of a C-80 Setaram Calorimeter for Measuring Heat Capacities of Liquids at Temperatures up to 548 K and Pressures up to 20 MPa," *J. Chem. Thermodynamics*, vol. 23, pp 1075-1083, 1991
3. Baba, M., Dordain, L., et al, "Calorimetric Measurements of Heat Capacities and Heats of Mixing in the Range 300-570 K and up to 30 Mpa", *Indian Journal of Technology*, vol. 30, pp 553-558, 1992
4. Handy, B.E., Sharma, S.B., et al "A Tian-Calvet Heat Flux Microcalorimeter for Measurement of Differential heats of Absorption", *Meas. Sci. Technol.*, vol 4, pp 1350-1356, 1993
5. Dordain, L., Coxam J.-Y., et al., "Measurements of Isobaric Heat Capacities of gases from 323.15 to 573.15 K up to 30 MPa", *Rev. Sci. Instrum.* Vol 65, no. 10, pp 3263-3267, 1994
6. Handa, Y. P., et al, "High-Pressure Calorimetric Study of Plasticization of Poly(methyl methacrylate) by Methane, Ethylene, and Carbon Dioxide", *Journal of Polymer Science: Part B: Polymer Physics*, vol 34, pp 2635-2639, 1996
7. Dordain, L., Coxam, J.-Y., et al, "Isobaric Heat Capacities of Multicomponent gases between 323 and 423 K and at Pressures up to 25 Mpa: Comparison with Some Equations of State", *Chemical Engineering Science*, vol 52, no. 20, pp 3593-3597, 1997
8. Bessieres, D., et al, "Apparatus for Simultaneous Determination of the Densities and Heat Capacities of Liquids With Dissolved Gas Under an Extended Range of Pressure (0.1-100 MPa)", *Meas. Sci. Technol.* vol 11, pp 69-72, 2000
9. Sorescu, D.C. and Thompson, D.L., "Classical and Quantum Mechanical Studies of Crystalline Ammonium Nitrate", *J. Phys. Chem*, vol 105, pp 720-733, 2001.

THIS PAGE LEFT INTENTIONAL BLANK

A novel multi-channel microcalorimeter for large-scale stability testing of propellant

Lars-Gunnar Svensson, Bodycote CMK AB, Box 431, S-691 27 Karlskoga, Sweden

Jaak Suurkuusk, Thermometric AB, Spjutvägen 5A, S-175 61 Järfälla, Sweden

Lars-Erik Paulsson, Bodycote CMK AB, Box 431, S-691 27 Karlskoga, Sweden

INTRODUCTION

The use of heatflow microcalorimetry (HFC) as a tool for testing the storage stability of nitrate ester propellant has grown rapidly over the past decade. In contrast to the commonly employed liquid chromatographic (HPLC) technique for determination of stabiliser(s) and stabiliser derivatives in propellant samples¹ HFC techniques provide a means for direct measurement of the primary critical factor for storage safety, namely the heat production from the propellant degradation process. Knowledge of the heat generation function $P(T, \alpha)$ that describes the propellant's exothermic properties as a function of temperature T (Arrhenius' equation) and chemical state (kinetic function $f(\alpha)$, α = progress parameter 0 to 1), and the heat dissipation from the propellant charge allows calculation of the risk for a thermal runaway situation to occur. From such calculations maximum heatflow limits for safe storage of propellants can be defined for various storage conditions. HFC can provide data for the assessment of temperature influence (activation energy E_a) as well as the influence of the progress of the degradation (α) on the heatflow. However, only the temperature influence will be discussed in this paper.

As a first step towards a future standardisation of a HFC method for propellant stability a Round Robin test² was initiated a few years ago at a number of test laboratories. The aim of this test was to compare calorimetric results for one specific propellant type when tested under prescribed experimental conditions in different instruments and by different individuals. Results from the Round Robin test have subsequently been summarised and used as the basis for a proposed new HFC standard³.

ASPECTS ON MEASURING CAPACITY IN PROPELLANT SURVEILLANCE TESTING

The basic principle for HFC as a method for propellant surveillance testing is to continuously observe the heat generation in the propellant at some elevated temperature for a period of time that simulates a given storage time under natural conditions. During this observation time the propellant must fulfil certain stability criteria in terms of maximum heatflow, and possibly also maximum rate of heatflow increase³. Somewhat simplified one can say that the HFC instrument emulates a small climatic chamber for accelerated ageing with on-line monitoring of the sample stability.

Optimization of the combination test temperature - test time is a well-known dilemma in the design of accelerated ageing programs. By selecting a high ageing temperature the test time can be reduced, but unfortunately often at the expense of an increasing uncertainty in the test result. This is due to the risk for triggering of undesired side reactions in the propellant degradation process that would have played a minor role at the real storage temperature. A too

low temperature, on the other hand, increases the test time and thus the need for extended HFC resources to maintain the sample flow-through capacity of the laboratory.

In Sweden a typical flow-through level of propellant samples in a surveillance test laboratory is, say, 2000 samples per year. For stabiliser analysis with HPLC this sample volume is no big problem. With an auto-sampler and a retention time normally well below 1 hour¹ one single HPLC instrument is fully sufficient for this task. A HFC-based surveillance method, as previously outlined, requires much more instrumental resources as shown by the following simple example:

Assume that the activation energy for degradation of a propellant is 100 kJ/mol, a typical value for this type of reactions³. Using a modified form of Arrhenius' equation

$$k_T = \exp\left(\frac{E_a}{R} \cdot \left[\frac{1}{T_1} - \frac{1}{T_2}\right]\right) \quad (1)$$

with T_1 = natural storage temperature = 293 K (20°C) and T_2 = HFC test temperature = 343 K (70°C, a standard test temperature at CMK) we obtain a temperature acceleration factor $k_T \approx 400$. This implies that the observation time in HFC for simulation of, say, 5 years under natural storage conditions amounts to approx. 4.6 days. A simple calculation shows that 30 parallel calorimeter channels would be needed to meet a 2000 sample/year capacity requirement (based on 300 measuring days per year). This corresponds to 8 four-channel instruments of the standard TAM type. The number of channels can of course be reduced by selection of a higher test temperature, but on the other hand, some propellants might require a longer measuring time than 4.6 d due to E_a values below 100 kJ/mol.

The example above clearly emphasizes the need for HFC instruments with multi-channel capacity in large-scale routine propellant surveillance testing. Two years ago Thermometric AB and Bodycote CMK AB therefore initiated a cooperation project with the aim to develop a 48-channel microcalorimeter for such purposes. A working prototype of this calorimeter is now available for evaluation. Instrument design, together with results from basic performance testing of baseline stability and noise, interchannel cross-talk and thermal equilibration time constant are summarised in this paper. The presentation also includes some results from measurements on selected propellant samples for demonstration of the instrument's capabilities in a real application, and for comparison with the corresponding data generated in a standard 4-channel TAM.

INSTRUMENT DESIGN

The 48 Channel TAM is a high measuring capacity microcalorimeter system designed for highly sensitive multisample measurements. These features make the instrument an ideal tool for multisample stability screening, compatibility measurements and quality control. Figure 1 shows a schematic picture of the instrument.

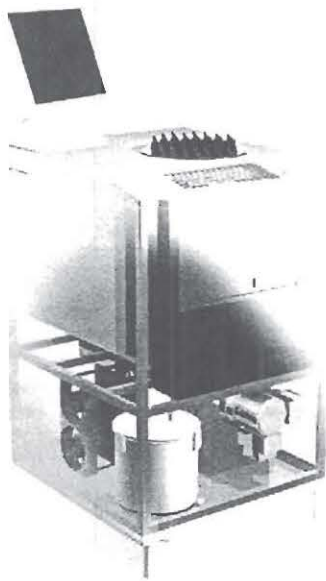


Figure 1 - A schematic picture of the thermostat showing the individual components of the 48 Channel TAM. At the top the inlets to the 48 Mini Calorimeters are shown.

The instrument houses 48 individual and independent, highly sensitive 4 ml Mini Calorimeters. Different types of experiments can be conducted at the same time. All channels are individually controlled through the Lab Assistant™ software. The calorimeters are immersed in a precisely temperature controlled liquid thermostat. A user-defined temperature profile determines the type of calorimetric measurement, i.e. isothermal, scanning or step-wise scanning. By software control, the calorimeters can either operate as heat flow or power compensation calorimeters. The heat flow mode is used for slow reactions and optimal resolution. Power compensation is used for monitoring rapid processes.

Samples are contained in various types of ampoules that are subsequently loaded into the calorimeter. All closed ampoules currently available for the 4 ml TAM system from Thermometric can be used. All necessary cooling/heating, control, measuring and computing units, including software, are integrated into the 48 Channel TAM. A local network can be used to enable remote PC control and data analysis.

Thermostat

The 48 Channel TAM liquid thermostat can operate in the temperature range of 15°C to 150°C (optionally 200°C). Under isothermal conditions the short-term temperature control of the thermostat is better than $\pm 50 \mu\text{K}$ and temperature drift during 24 hours is within $\pm 100 \mu\text{K}$. The high accuracy and stability of the thermostat makes the calorimeter well suited for heat flow measurements on very low levels over extended periods of time, e.g. hours to weeks. The detection limit is $\pm 0.5 \mu\text{W}$ and the baseline stability over 24 hours is $\pm 1.0 \mu\text{W}$. The dynamic measuring range is up to 50 mW.

The unique, precise temperature control system and the close thermal contact between the calorimeters and surrounding liquid enables experiments to be performed under very slow temperature scanning conditions, from $\pm 0.01 \text{ K}\cdot\text{h}^{-1}$ up to $\pm 2 \text{ K}\cdot\text{h}^{-1}$.

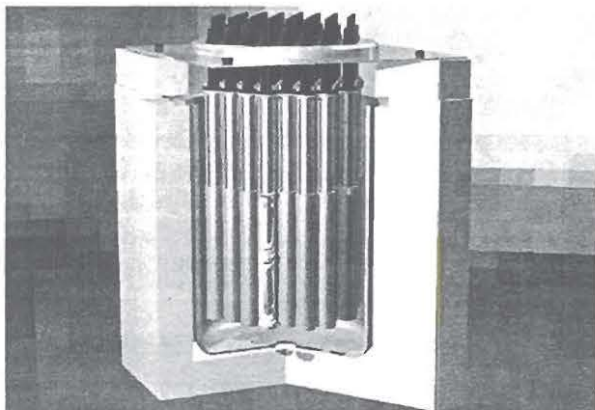


Figure 2 - A schematic picture of the thermostat containing 48 Mini Calorimeters. In each Mini Calorimeter the sample ampoule is positioned above its reference.

Calorimeter Design

The individual calorimeters are of the twin differential type, i.e. two measuring units are used. One holds the sample ampoule and the other holds an inert reference ampoule. The two measuring units are positioned above one another, on each side of a small intermediate heat sink. Both units are surrounded by cylindrical heat sinks. The measuring assembly is positioned in a cylindrical steel container, which is at the same temperature as the surrounding thermostat. The calorimetric unit is permanently submerged in the liquid thermostat with the sample unit at the top, easily accessible for the user. The mass of the sample can be adjusted to balance the heat capacity of the reference ampoule for optimal performance. This principle reduces the short-term noise and increases the sensitivity of the system. The difference in heat flow between the sample and the reference is continuously monitored.

Data acquisition system

Lab Assistant™ is a user-friendly and powerful software developed for the complete control and evaluation of data. Experimental design is facilitated using a library of customisable wizards that guide the user through the appropriate settings used for a particular type of experiment. Data analysis programs as well as advanced report facilities have been included in the software for convenient interpretation and visualisation of data.

The software can be used within a network enabling the user to control and evaluate both ongoing and completed experiments from a remote computer. **Advanced mathematical** and graphical functions account for convenient data modelling and **advanced data analysis**. An interface for the exchange of data between other analysis packages is also available.

Application Areas

For complex systems, 48 different mixtures of a formulation can be studied simultaneously for the evaluation of interactions between the constituents. The evaluation of shelf life of propellants as well as the quality control of hazardous materials such as sodium percarbonate are application areas where the throughput is dramatically increased by the use of the 48 Channel TAM.

The 48 Channel TAM can also be used for performing experiments under extremely slow temperature-scanning conditions in order to study physical processes under virtually isothermal conditions. A user-defined temperature profile controls the temperature during the complete experiment. Isothermal as well as dynamic sections during which the temperature is changed in a stepwise or in a linear way can be combined. The slow scanning rate is compensated by the amount of substance (1 – 4 g) and the high-sensitivity, which enables the study of phase transitions with much better resolution than conventional Differential Scanning Calorimetry (DSC) can provide. The slow scanning rate ensures that the sample virtually remains in thermal, physical and chemical equilibrium.

INSTRUMENT PROPERTIES

3206 4ml Mini Calorimeter

Mode of operation	Isothermal	Scanning (3)	STANAG 4582 requirements
Number of calorimetric units	48	48	
Total volume	< 5 ml	< 5 ml	≥ 2 ml
Measuring range	± 50 mW	± 100 J·K ⁻¹ (4)	≤ 0.5 mW/g
Limit of detectability	0.5 µW	1 mJ·K ⁻¹	
Precision	< ± 1 µW (1)	< ± 2 mJ·K ⁻¹	
Accuracy	< 1 %	0.1 % (5)	≤ 2% (6)
Noise short time (0.1Hz)	< ± 0.5 µW	1 mJ·K ⁻¹	
Baseline over 24 hours			
Drift	< 1 µW		
Deviation	< ± 0.8 µW		
Error	< ± 1 µW		
Time constant empty	120 s		
Time constant 2 ml glass beads	350 s		

- 1) Baseline reproducibility. Repeated loading experiments with a 3 ml glass ampoule containing 2 g glass beads
- 2) 3 ml glass ampoule containing 2 g glass beads
- 3) Scanning rate 2 K·h⁻¹
- 4) Maximum apparent heat capacity difference between measuring sample and reference sample
- 5) Calibrated against standard sample
- 6) Includes all types of measuring errors

3102 48 Channel TAM Thermostat

Operating temperature	15 - 150°C (200°C)
Fluctuation (0.02Hz)	< ± 50 µK
Stability over 24 hours	± 100 µK
Scanning rate	± 2 K·h ⁻¹

General specifications

Power requirement	110/220 V \pm 10% 50/60 Hz
Power consumption	1000 VA (max load)
Ambient temperature range	20 - 30°C
Ambient temperature stability	\pm 1°C
Humidity	< 65 %
Dimension (w x d x h)	595 x 670 x 980 mm (excl. screen)
Net Weight	110 kg

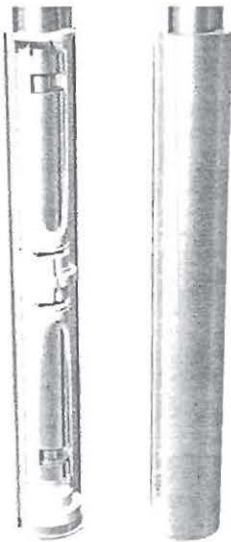


Figure 3 - Schematic design of a Mini Calorimetric unit containing a sample ampoule positioned above a reference ampoule containing an inert reference sample of known heat capacity.



Figure 4 - A Mini Calorimeter attached to a data interface.

MEASUREMENTS ON PROPELLANT

Samples and sample preparation

Four different kinds of nitrate ester propellant were used for the preliminary heatflow measurements in the calorimeter. Two of the propellants were of single-base and the others of double-base type. Standard 3 ml glass vials with crimp lids were used as sample ampoules in all measurements.

Three ampoules with different amounts of sample were prepared for each propellant type in order to study the influence on the free air volume (amount of O₂) on the heatflow curve. All samples were tested as received except ÅKB204 that had to be cut in small pieces from large foils of 0,5 mm thickness to fit into the ampoule. No preconditioning was used and all measurements were carried out in air atmosphere.

Sample data are summarised in Table 1.

TABLE 1 – Survey of sample data

Sample code	Sample	Sample amount (g)	Sample form	Remarks
A1	ÅKB204 (double base)	1,005	2 x 2 x 0,5 mm	
A2	"	2,000	"	
A3	"	2,770	"	Completely filled
A4	"	2,001	"	Standard TAM
B1	NC1066 (single base)	1,001	Rods, L 5 mm, D 2,5 mm	
B2	"	2,004	"	
B3	"	2,736	"	Completely filled
B4	"	2,003	"	Standard TAM
C1	JK6B (single base)	1,001	1,5 x 1,5 x 0,3 mm	
C2	"	2,002	"	Completely filled (a)
C3	"	1,501	"	
C4	"	2,002	"	Standard TAM
D1	NK700 (double base)	1,002	4 x 4 x 0,5 mm	
D2	"	2,005	"	
D3	"	2,883	"	Completely filled
D4	"	2,008	"	Standard TAM

(a) Low bulk density, sample amounts exceeding 2 g not possible

Stability measurements using fixed temperature steps

Heatflow curves for measurements using the temperature sequence 78 → 68 → 58°C are shown in Figures 5 through 8 for each separate propellant type. All curves are normalised to unit mass (1 g) to facilitate direct comparison. A reference curve from measurements on a 2 g sample at 80°C in a standard 4-channel TAM is also included in each diagram. Originally the

intention was to use the sequence $80 \rightarrow 70 \rightarrow 60^\circ\text{C}$ but a temperature calibration error in the thermostat bath resulted in a $2.0 \pm 0.3^\circ\text{C}$ temperature reduction.

Figure 5 summarises the HFC results for the double base propellant ÅKB 204. During the first 12 h all three 48 Channel TAM curves coincide fairly well at a heatflow level of $25 \mu\text{W/g}$, a fully normal value for a double base propellant at 78°C . After 1.5 days the heatflow for the completely filled ampoule (2.77 g) drops abruptly from 29 to $15 \mu\text{W/g}$ due to lack of O_2 in the ampoule. For the 2 g sample with access to more O_2 due to the larger free air volume, this heatflow drop is delayed to approx. 2.5 d and for the 1 g sample no drop at all is obtained during the observation time. The higher noise level for the 1 g curve is a pure normalisation effect. The 48 Channel TAM and standard TAM curves for the 2 g samples are very similar in shape and noise level, but deviate in signal level as a consequence of the temperature difference. The fast thermal response of the 48 Channel TAM previously discussed is clearly illustrated in the two temperature steps. Within less than 3 h after changing the bath temperature the heatflow signal can be considered as fully reliable again. The subsequent drift in the heatflow curves shall thus be ascribed to real physical and/or chemical effects rather than to thermal equilibration. The equilibration time for a standard TAM with ampoule cylinders is typically 10 to 12 h.

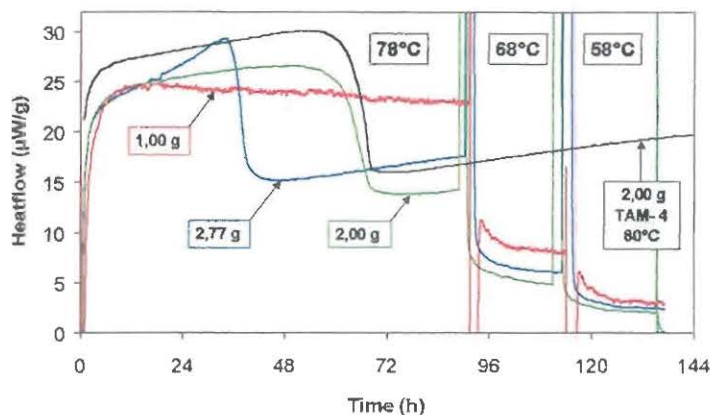


Figure 5 – Normalised HFC curves from 48 Channel TAM measurements on three different amounts of propellant ÅKB 204 at 78, 68 and 58°C . A reference curve from a measurement in a normal 4-channel TAM at 80°C is also included.

Figure 6 shows the corresponding HFC curves for the single base propellant NC 1066 using the same experimental conditions as in Figure 5. Also in this case the heatflow depends on the free volume but to a lesser extent than for ÅKB 204. No abrupt changes in the heatflow level are observed. The sample with the smallest free volume has the most rapidly decreasing curve probably due to the faster decline in

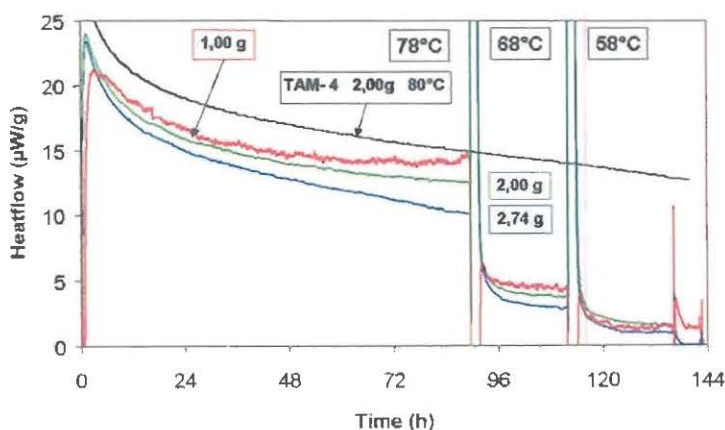


Figure 6 – Normalised HFC curves from 48 Channel TAM measurements on three different amounts of propellant NC 1066 at 78, 68 and 58°C . A reference curve from a measurement in a normal 4-channel TAM at 80°C is also included.

O₂ concentration. The results for the single base propellant JK6B in Figure 7 has a certain resemblance with Figure 6. The free volume effect, however, is even smaller than for NC 1066 indicating a minimal interaction of the JK6B propellant with O₂. All three curves attain fairly constant and close heatflow levels within 3 days at 78°C. No significant difference between the 48 Channel TAM and standard TAM curves is obtained for the 2 g samples, neither for NC 1066 nor for JK6B, except for the pure temperature effect.

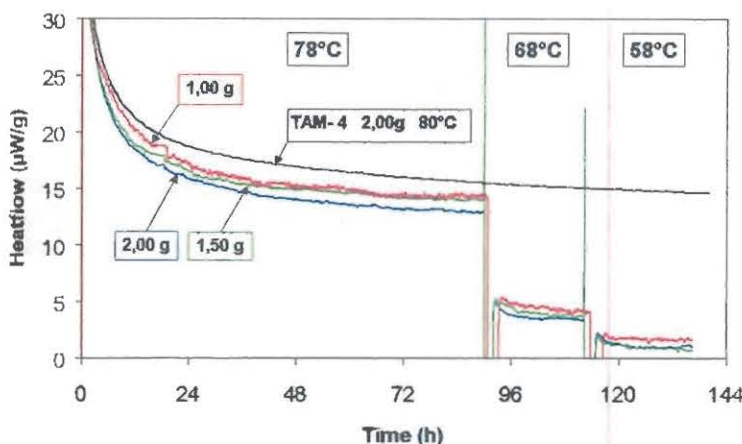


Figure 7 – Normalised HFC curves from 48 Channel TAM measurements on three different amounts of propellant JK6B at 78, 68 and 58°C. A reference curve from a measurement in a normal 4-channel TAM at 80°C is also included.

The fourth sample in this study, NK 700, is a highly energetic double base propellant with a nitroglycerine content around 40%. It shows a higher exothermicity than any of the other propellant samples, both regarding the initial interference with the air oxygen and in the subsequent

decomposition under anaerobic conditions. As shown in Figure 8 the peak heatflow value from the O₂ interaction amounts to 130 µW/g for the 1 g sample, with a subsequent decline to an almost constant level at 33 µW/g. The 2 g and 2.88 g (completely filled) samples yield lower and narrower peaks but also higher anaerobic heatflow compared to the 1 g sample. A similar observation was made for ÅKB 204 in Figure 5.

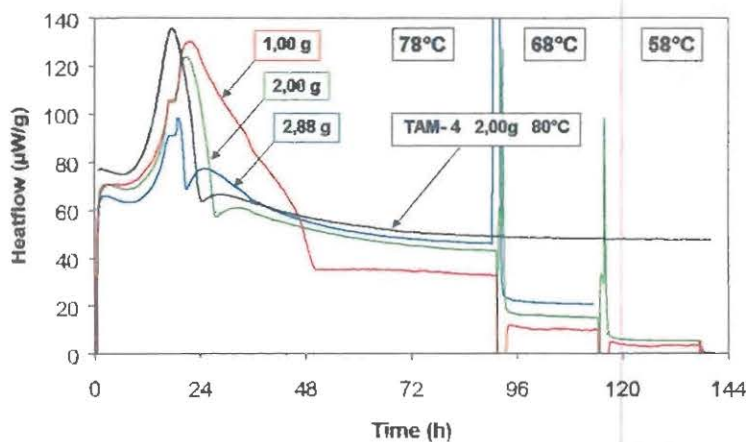


Figure 8 – Normalised HFC curves from 48 Channel TAM measurements on three different amounts of propellant NK 700 at 78, 68 and 58°C. A reference curve from a measurement in a normal 4-channel TAM at 80°C is also included.

Activation energy

The evaluation of activation energy for propellants from HFC measurements using temperature steps shall preferably be evaluated from steady-state conditions, i. e. based on constant heatflow parts of the curve. However, experience from stability testing of propellants at CMK's laboratory has revealed that such steady-state conditions can take long time to attain, especially at low temperatures. The activation energies in Table 2 are therefore based on a faster "step" technique with linear extrapolation of the heatflow curve backwards to the starting point of the temperature change, using the relative change of the heatflow in this point for the E_a calculation. In large-scale routine stability testing of propellant with determination of E_a the step method might be the only realistic alternative due to time limitations.

TABLE 2 – Summary of activation energies (kJ/mol) according to step method

Propellant	M = 1 g	M = 1.5 g	M = 2 g	Filled up
ÅKB 204	84	-	72	80
NC 1066	97	-	80	96
JK6B	86	108	-	109
NK 700	100	-	90	(75)

No obvious correlation seems to exist between the amount of sample (free volume) and the activation energies listed in Table 2. The scattering in the E_a values is at least partly a result of the increasing influence of the signal and baseline reproducibility errors on the measuring accuracy at the lowest temperature. Due to the special calorimeter design without direct access to the reference ampoule the so-called switch technique⁴ for baseline error corrections is not applicable here. One alternative to the switch technique is to temporarily raise the sample ampoule to the equilibration position to obtain a baseline, another is to temporarily replace the sample ampoule by an ampoule with an inert substance. Both techniques will be further investigated during the future evaluation of the TAM-48 prototype.

For propellant ÅKB 204 it shall be emphasized that the E_a value for the 1 g sample is based on the oxygen interference reaction and thus not directly comparable with the activation energies for the other two samples with purely anaerobic reactions.

The use of temperature scanning mode in propellant testing

Except for access to classical DSC application areas the 48 Channel TAM scanning mode also provides a powerful tool for measurement of the temperature influence on propellant degradation rate under dynamic conditions with simultaneous determination of the absolute heat capacity. Both these parameters are crucial input data for the evaluation of propellant storage safety, using conventional calculation models based on the balance between heat production and heat dissipation. Heatflow data from slow scanning experiments are in this respect very realistic due to the non-steady state conditions prevailing during a real self-heating process. The scanning rate must of course be in reasonably good conformity with the actual rate of temperature rise in the stored propellant.

Figure 9 shows the HFC curve from a slow scanning experiment with propellant NC1066 over the temperature interval 30 to 95°C, using a scan rate of 1°C per hour. The scan rate is chosen at random — whether it is the best choice for a self-heating process in a propellant

bulk has not been considered here. Much lower scan rates can be used if necessary, of course at the expense of the measuring time. The y-axis is given in apparent specific heat capacity (C_p) units ($\text{J}\cdot\text{K}^{-1}\cdot\text{g}^{-1}$), obtained as the quotient between the heatflow dq/dt and the scan rate dT/dt in accordance with Eq. (2).

$$\frac{dq}{dt} = C_p \cdot \frac{dT}{dt} \quad (2)$$

It shall be emphasized that Figure 9 represents the pure raw data curve, i. e. no corrections have been made to compensate for C_p contributions from the sample ampoule, the reference body, the sample holders and the heatflow sensors, nor for the temperature dependence of the Seebeck effect. All these factors are specific for each individual ampoule and channel. However, since they are very reproducible their impact on the curve can be determined in one single blank experiment with the empty ampoule and stored in a "blank curve" library for corrections of all subsequent experiments.

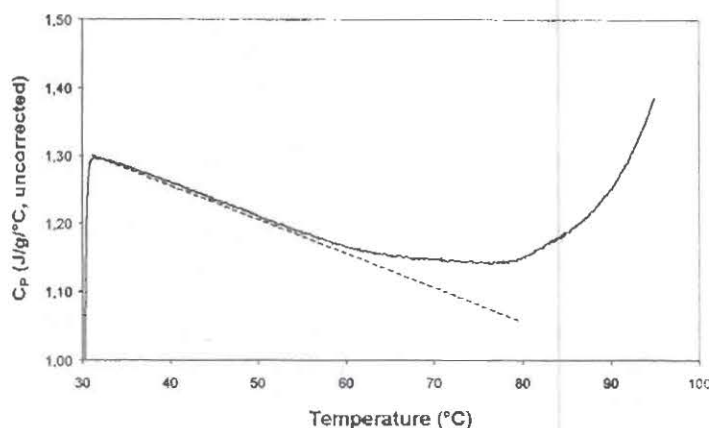


Figure 9 – Heat capacity vs. temperature curve for propellant NC1066 recorded at a scan rate of $1^\circ\text{C}/\text{h}$. No corrections for C_p contributions from ampoules, sample holders etc have been carried out. The starting point of the curve is arbitrarily adjusted to $1.3 \text{ J}\cdot\text{K}^{-1}\cdot\text{g}^{-1}$, a typical C_p value for a nitrate ester propellant.

The starting point of the curve in Figure 9 has arbitrarily been set to $1.3 \text{ J}\cdot\text{K}^{-1}\cdot\text{g}^{-1}$ which is a reasonable C_p value for a nitrate ester propellant. Despite the disturbing initial slope of the curve the exothermic contribution from the accelerating propellant decomposition is clearly distinguishable from approx. 60°C and onwards. With blank correction the onset point is likely to appear at a slightly lower temperature. Due to the uncorrected baseline no attempt has been made to derive an activation energy from the exothermic part of the curve.

SUMMARY AND DISCUSSION

The prototype version of the 48 Channel TAM described in this paper fulfils the basic requirements stated in the STANAG 4582 (draft) for use in stability testing of propellant. The estimated throughput capacity of typically 2000 samples per year makes it an ideal tool for large-scale propellant surveillance applications. Rapid thermal equilibration of the calorimetric cells account for minimum waiting time before reliable heatflow data are available, e. g. in conjunction with temperature changes.

A routine procedure for qualification of propellant for safe storage, using the 48 Channel TAM, is suitably based on one single and relatively high temperature. The requisite measuring time for simulation of future storage under natural conditions is based on the

acceleration factor calculated from the activation energy. The STANAG 4582 procedure for propellant stability testing suggests two, fixed E_a values for this purpose. Additional experimental determination of E_a can anyway be motivated, at least in the build-up phase of a surveillance routine, for subsequent introduction of "generalized" E_a values on a statistical basis. With regard to the proposed breakpoint in the Arrhenius curve³ around 60°C the temperature interval for E_a measurements should preferably extend from, say, 80°C down to at least 50°C (40°C if possible) in 10°C steps. However, according to the results from the preliminary measurements on propellants in this study the 48 Channel TAM might not be sufficiently sensitive for this task at temperatures below 60°C. This is partly a consequence of the fixed reference ampoule that does not allow baseline corrections based on "switch" measurements. An instrument with higher sensitivity, e. g. a 4-channel TAM nanocalorimeter, is therefore recommended for the lowest temperatures.

The propellant results presented in this paper clearly illustrate the influence of the sample vessel free volume on the HFC signal. This is particularly evident for the double base propellants showing a strong initial interaction with the air oxygen. The more propellant in the vessel the smaller is the O_2 reaction, a fact that is considered also in the STANAG 4582.

The temperature scanning mode of the 48 Channel TAM offers an interesting tool for determination of activation energies under conditions similar to those obtained during self-heating processes in bulk quantities of propellants. Absolute heat capacity data for the propellant sample can be derived from the same experiment. Both parameters are important input data for the calculation of storage safety.

REFERENCES

1. NATO Standardisation Agreement (STANAG) 4541
2. S. Wilker, P. Guillaume, *International Round Robin Test to Determine the Stability of DB Ball Propellants by Heat Flow Calorimetry*, ICT Jahrestagung **29**, 132 (1998)
3. NATO Standardisation Agreement (STANAG) 4582 (draft version)
4. L. G. Svensson, L. E. Paulsson, T. Lindblom, *A Microcalorimetric Study of the Temperature and Stabilizer Effects on the Heat Generation in Gun Propellants*, Proc. 4:th Gun Propellant Conference, Mulwala, Australia (1990)

THIS PAGE LEFT INTENTIONAL BLANK

Heat Flow Calorimetry and Functionality of old 155 mm propellant charges

Wim P.C. de Klerk

Researchgroup Pyrotechnics and Energetic Materials

e-mail : klerk@pml.tno.nl

TNO Prins Maurits Laboratory

P.O. Box 45, 2280 AA Rijswijk, The Netherlands

Abstract

Within the Netherlands, the Dutch Army has substantial amounts of gun propellants in storage for the 155-mm Howitzer. These propellants lots differ significantly in year of production and therefore in age. These lots have a variation of production year from the middle of 1950's until the early 1990's.

Because of economic reasons, a strong reduction of the amount of stored 155-mm Howitzer gun propellant is needed. Therefore TNO-PML was asked to give a well-funded advice which propellant lots are the most suited to be safely stored and used for another 10 years, with a minimum amount of tests.

The first part of the project was to collect all available data (also Heat Flow Calorimetry (HFC) measurements) to select a smaller group of propellants which then will be investigated. In the second part, 25 lots were investigated by microcalorimetry and GPC.

During the HFC investigations the heat generation was measured during two weeks, and afterwards the safe diameter was calculated in combination with an indicative value for the decrease of the amount of energy in the propellant for the artificial ageing period (i.e. 15 years). Comparison of these new results with the earlier measurements (since 1972), lead to a good foundation to select 6 lots for ballistic research.

Introduction

In peacetime, with the decrease of consumption of stock ammunition, and the increase of stock time, the safety problem of the ammunition in long stock becomes increasingly important. The propellant powder of ammunition in long-term stock process undergoes slow decomposition reaction and exothermic processes. When the decomposition reaches a certain degree, a self-acceleration effect will appear, which intensifies the decomposition and produces a great amount of heat. If the heat can not be conducted away in time, its accumulation will lead to spontaneous combustion of propellant powder, which will pose a great threat to the safety of the stock.

Decomposition of NC, however, not only leads to heat production that can finally result in run-away reactions, but the decomposition also causes a break-down of the nitrocellulose polymeric chains [4, 5]. This results in a decrease of the mechanical integrity of the propellant grains [2, 6]. In case of gun propellants the mechanical properties affect the ignition behavior of the propellant

grain bed. Embrittlement may lead to enhanced breakage of grains, which in turn leads to an increase of the burning surface area, finally resulting in an accelerated pressure rise and a diminished porosity of the propellant bed during firing. Consequences may be an irregular pressure build-up, pressure waves or increased peak pressures [2].

The Dutch Army has a large amount of 155 mm Howitzer ammunition, from quite old periods. The oldest are from just after the Second World War (Marshall Help). At this moment a significant amount of these charges are in stock. The MoD has asked TNO-PML to predict the remaining lifetime of this ammunition. In principle a quite simple question, but in reality very complicated.

Analysing the complete stock, it gives the following distribution of the 99 propellant lots;

M3-serie	NOV-code 4401	17 propellant lots
M4-serie	NOV-code 4411	48 propellant lots
Nr 13-serie	NOV-code 4421	34 propellant lots



The age of the propellant also introduce an extra problem, namely it varies from 5 to 45 years. In principle it's a long term project, but the question was to perform it in two years, and with a minimum amount of money, so clustering the different lots, to keep the effort as low as possible.

The whole project was divided in three phases, namely:

Phase A : Analysing all available information related to surveillance control

Phase B : Ageing program of 25 propellant lots for a prediction time of at least 10 years

Phase C : Performing ageing on four types viscose or silk bags, followed full firing tests

This papers deals about the work what is performed for phase A and B. The work for phase C is still in process, and will be reported at a later stage.

Available information

Before making a choice of the 25 propellant lots for phase B, the following aspects have to be taken into account;

- number of viscose or silk bags of one propellant lot
- usage for training purposes during the coming five years
- results of periodic control from Ammunition Department

Even the information of accidents with these viscose or silk bags influences the choice of the final propellant lots. One of the problems, which were reported by the troops, was the strength of the

viscose or silk bag itself. In a separate project this aspect was investigated by mechanical tests on the fibers after ageing these fibers in contact with the propellant for a specific period of time.

Also the information from earlier performed tests at TNO-PML were used for selecting the propellant lots for phase B. The used database contains the information of all the surveillance test results (based on HFC measurements), and if available also the chemical information. This last point may be helpful for clustering the propellant lots.

Results of Phase A

Collecting all the available data shows also the drawbacks of the periodic control system over the years. There was a minimum of data available about the functional lifetime related to the ballistic performance as investigated by the Army. In the TNO-database not all the chemical information was available, especially not from the oldest lots, because these propellant were delivered without any paperwork. All these aspects make a right choice for Phase B quite complex.

The HFC data was available from the point on that the system was introduced in The Netherlands (early 1970's). One assumption was made during the whole study, namely that the propellant who were thermally aged also has a major ballistic decrease.

The parameters, which were used from the HFC database, were the safe diameter [10, 14], the decrease in calorific values as calculated from the curves and the changes in the shape of the curves.

Examples of the results are given in Table 1.

Table 1: Overview of the trend in HFC data for a long period of time.

NOV code	Propellant lot	Year of HFC	D344 [m]	Year of HFC	D344 [m]	Year of HFC	D344 [m]
4401	6357	1981	0.58	1989	0.52	1997	0.45
4411	6245	1979	0.74	1987	0.59	1998	0.48
4421	6927	1989	0.78	1997	0.51		

Only focussing on the values is not safe, also the shape of the curves is of influence. For the above three mentioned propellant lots these curves are presented.

Results Phase B

Heat Flow Calorimetry

In the following figures the results of three 155-mm propellants are presented. It deals about KB 4379 (production year 1957), KB 6245 (production year 1972) and KB 6527 (production year 1982). All three investigated propellants are single base. The last two are stabilized with DPA, and from the oldest one, no chemical information is available.

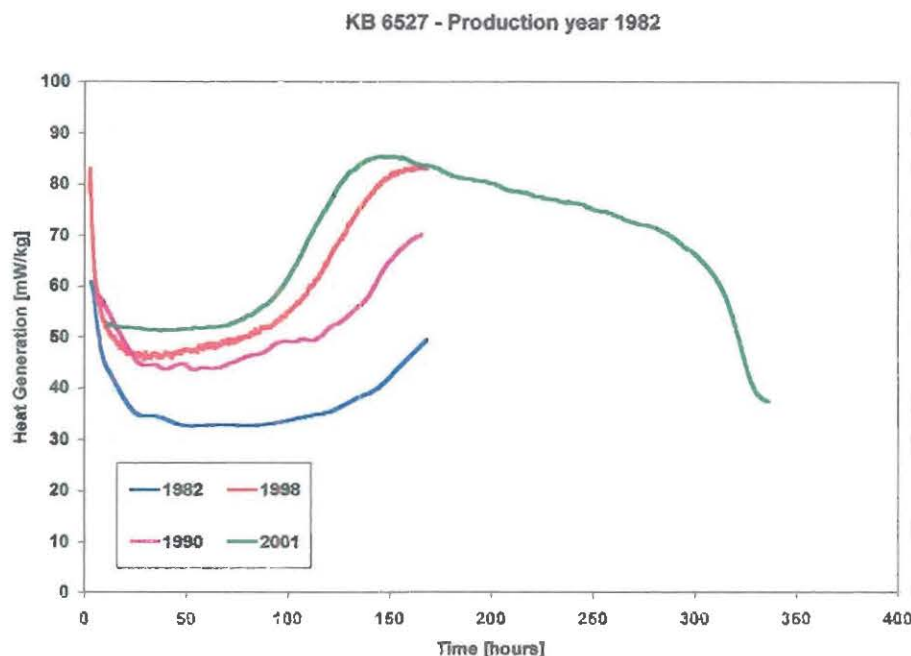


Figure 1: HFC curve of KB 6527.

In figure 1, the measurements from the earlier years (one week measurements), shows a slight increase in the heat generation at the end of the curve. Comparing the measurement of 2001 with the earlier ones it may be concluded that the shape is the same and the maximum is reached after 150 hours. The heat generation is low, as may be expected from 20 years SB propellant, and there is no indication that there will be any problem the coming fifteen years.

In figure 2, the increase in total heat generation over all the years is quite large. The first measurement (1979) results in a low heat generation, which is normal immediately after the production of the propellant. The three measurements afterwards show an increasing Q-level, and the last one from 2001 results in a much higher heat generation. This is an indication for instability, but looking to the amount of heat that is produced there is no reason for any danger (run-away reaction).

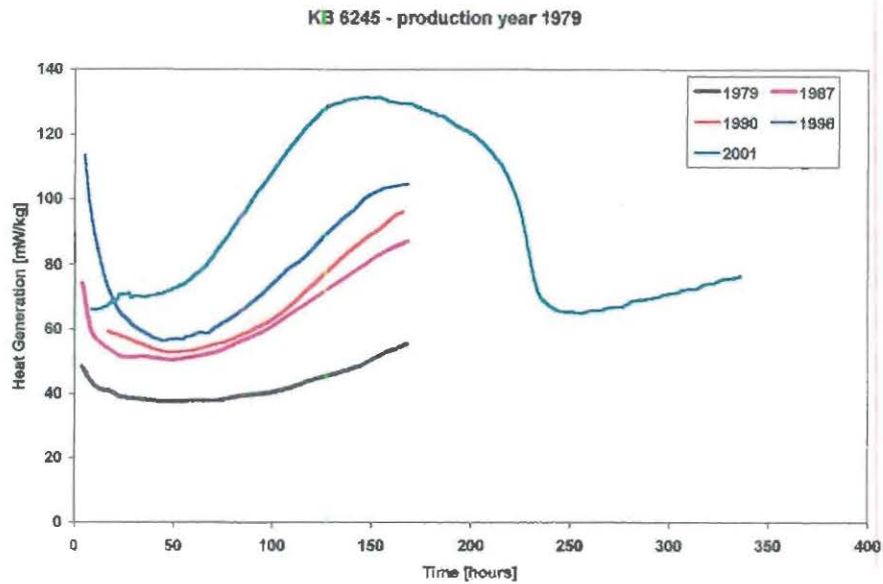


Figure 2: HFC curve of KB 6245.

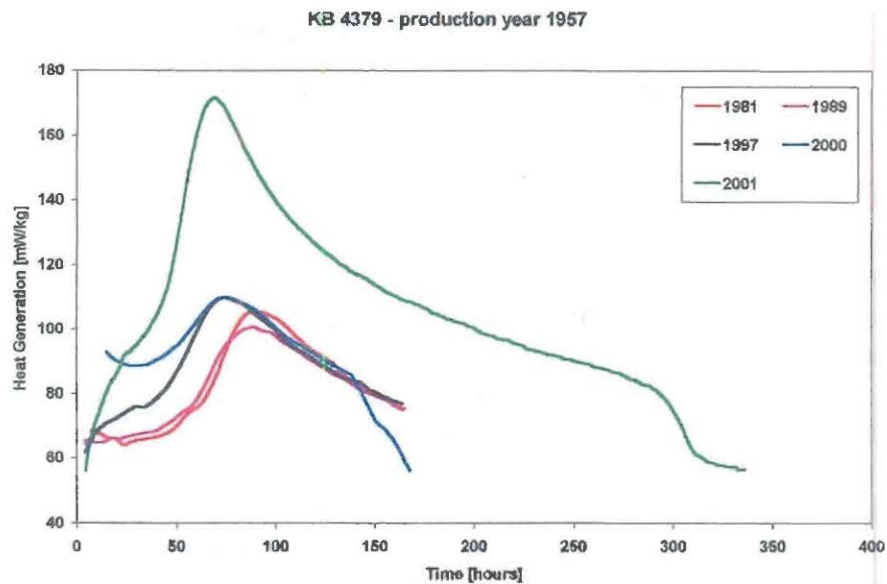


Figure 3: HFC curve KB 4379.

Figure 3 shows the effect on the heat generation by an old propellant. The propellant is already 45 years old, which may be an indication that the propellant becomes in the dangerous region. These curves indicate that the maximum is shifted to an earlier time, in combination with a higher energy content. These both aspects inform about the condition of the propellant. This charge needs further investigation in the stability aspects but also the functional aspects.

Mechanical integrity of viscose or silk bags

One of the other problems for safe handling of the charges was the strength of the viscose or silk and/or viscose bags with the propellant. Figure 4, shows the condition of some of the bags, which is really bad. The structure of the fibers is affected by the decomposition products of the propellant, in combination with the environmental parameters. During the decomposition of the gun propellant NO_x is formed, and in combination with moisture it will lead to the production of nitric acid. This acid destroys the fiber-structure of the viscose or silk bag

The moisture which is needed for the reaction comes from the decomposition step, but also from the surrounding. The charges were stored for quite a long period in a non-climate controlled storage facility, which explains the penetration of moisture in the bags.



Figure 4: Photo of the damage on the viscose or silk bag

The ageing experiments followed by mechanical analysis of the bags, result in an accelerating factor of 2.75 pro 10 °C temperature difference for the silk bags. For the viscose bags, it was more complicated to determine this factor, also because of the difference in quality of the used materials (bags and sewing material). These differences caused a variation of the results. For the calculations of the remaining lifetime (based on strength measurements), a general acceleration factor of 2.5 is used for all kind of bags. Taking into account this acceleration factor, it's not clear for all investigated bags or they will be safe to handle the coming 10 years. A limitation of this part, is that all the investigated bags came from one ammunition box. For a better statistical foundation, additional mechanical measurements on bags from different boxes are proposed.

Mechanical strength of charges

To simulate the first part of the firing process, a compression of a propellant bed and subsequent firing of the fractured grains in a Closed Vessel [7, 8] are performed. Quasi-static compression is relatively simple and provides good indications with respect to propellant bed behavior during the first stages of ignition and combustion in a gun.

For the quasi-static compression test, 300 grams of propellant is quasi-statically pressed for 4 seconds at 300 Bars. The compression is performed at -40°C . After acclimatization CV tests are performed with a loading density of 0.214. Extrapolation of the change in linear vivacity between

0.2 and 0.7 P_{\max} to $P/P_{\max} = 0$ results in a value that is a measure of the destruction of the propellant grains. This value corresponds to the relative surface area at the beginning of combustion due to the fractured grains [8], and is sometimes called 'relative surface area'. For various applications one can use specific criteria for the 'relative surface area'.

The change of polymeric chain length of the propellant samples was determined by means of gel permeation chromatography (GPC). Polystyrene standard samples were used as references for the calculation of the molecular weights. Although the obtained molecular weights are therefore not absolute but relative values, the results provide a good indication of the ageing effect [3, 6]. The results of the GPC measurements are given in Figure 5. Important data with respect to the polymeric chain length of NC are the (weight average) molecular weight (M_w) as well as the molecular weight distribution. The latter can be determined from the ratio between weight average and number average molecular weight (M_w/M_n). These results of the GPC-measurements are given in Table 2.

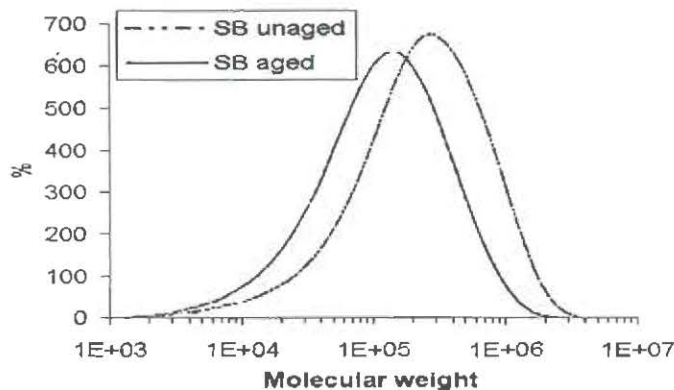


Figure 5: Results of GPC-measurements: molecular weight distributions of unaged and aged SB propellant from the I55 mm charge.

Table 2: Results of GPC-measurements.

Sample	Molecular weight		Width of weight distribution	
	M_w (dupl.)	ratio aged/unaged	M_w/M_n (dupl.)	Ratio aged/unaged
SB unaged	331000	0.53	4.3	0.85
	328000		4.1	
SB aged	176000	0.53	3.6	0.85
	173000		3.6	

The result show that the chain lengths of propellant grains, which were aged for a period that is equivalent to 20 – 30 years, is shortened by 50%. Further the width of the mole weight distributions is decreased as well, by 15%. It is reasonable to assume that both factors affect the mechanical properties of the propellant grains.

These results show that the mechanical properties of NC propellant grains significantly change as a result of ageing. The consequence of this change, in terms of the propellant bed behavior during the first stages of ignition and combustion in a gun, can hardly be predicted.

The results of CV tests that were performed after quasi-static compression of SB propellant at -40°C are plotted in Figure 6.

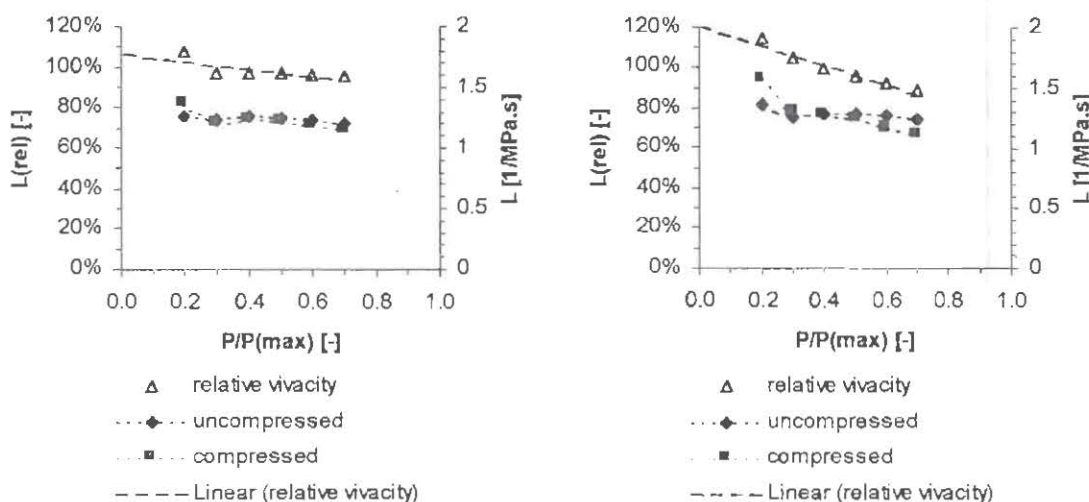


Figure 6: Vivacity curves of unaged (left) and aged (right) SB gun propellant.

The 'relative surface areas' that are derived from the extrapolated relative vivacity's are given in Table 3.

Table 3: Results of quasi-static compression: relative surface areas.

	Unaged	Aged	Relative increase
SB propellant	107%	121%	+ 13%

The data in Table 3 show that the mechanical integrity of the propellant decrease significantly due to ageing. The increased surface area of the propellant bed will lead to an accelerated pressure rise during firing while the increased fines fraction results in a diminished porosity. Consequences may be an irregular pressure build-up, pressure waves or increased peak pressures [2].

Criteria for the 'relative surface area' depend greatly on the weapon system for which the propellant is developed. Further, loading density and design peak pressure determine whether problems will arise due to increased 'relative surface area' caused by ageing. Unsafe situations or damage to the weapon as a result of the change in burning behaviour can obviously be expected in the case of high loading densities and when ammunition operates at the maximum allowable peak pressure. In these cases gun simulator tests are recommended to rule out the danger of unsafe application of the propellant.

Criteria for the 'relative surface area' depend greatly on the weapon system for which the propellant is developed. Further, loading density and design peak pressure determine whether problems will arise due to increased 'relative surface area' caused by ageing. Simulations show that the peak pressure strongly rises at increasing 'relative surface areas' in case of at high loading densities, while the muzzle velocity is hardly affected (fig. 7).

Unsafe situations or damage to the weapon as a result of the change in burning behaviour can obviously be expected in the case of high loading densities and when ammunition operates near the maximum allowable peak pressure. In these cases gun simulator tests are recommended to rule out the danger of unsafe application of the propellant.

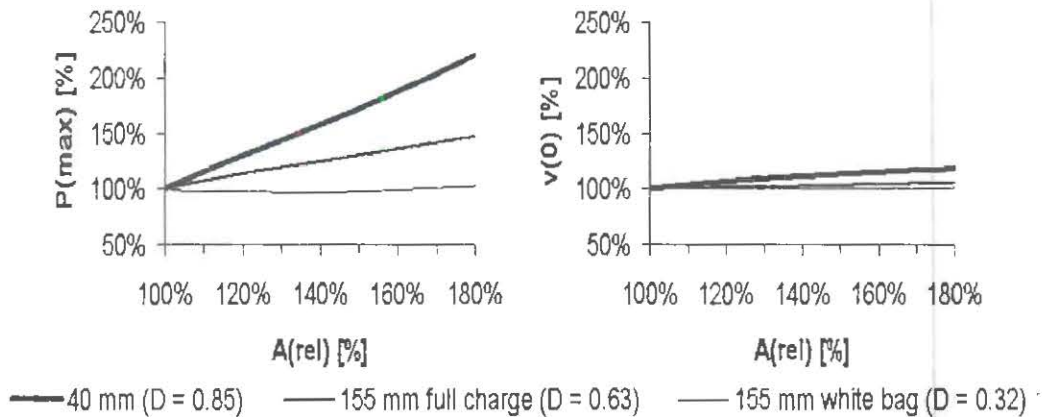


Figure 7: Peak pressure and muzzle velocity plotted as a function of the 'relative surface area', $A(\text{rel})$, for some weapon configurations (D = loading density [kg/dm^3]).

heat development and energy content

The thermodynamic property of the SB propellant hardly change when aged under confined conditions as shown in Table 4.

Table 4: Change of calorific values due to ageing.

	Microcalorimetry	Bomb calorimeter
SB propellant	- 3%	(change not significant)

The change of calorific value is often used to determine whether an aged propellant meets the ballistic criteria. Usually the calorific decrease is very small, theoretically resulting in a minor decrease of the muzzle velocity [9]. This is, however, only true if other propellant parameters that are related to the burning behaviour, like the mechanical properties, are unchanged.

Discussion/Conclusion

- The safe lifetime of conventional gun propellants is generally derived from propellant parameters that are closely connected to thermal properties. Especially heat generation caused by NC degradation due to the reduction of the stabilizer content is connected to the safe

storage lifetime of a gun propellant.

The results of this study show that besides “safe *storage* lifetime” also a decrease of mechanical integrity as a result of ageing can lead to unsafe application of propellants. In other words, the safe *ballistic* lifetime may be limited due to loss of mechanical quality. In order to be able to provide the user with complete information about the conditions of propellant with respect to its lifetime, both the safe storage lifetime and the safe ballistic lifetime should be considered.

- In order to be able to provide the user with complete information about the conditions of propellant with respect to its lifetime, both the safe storage lifetime and the safe ballistic lifetime should be considered.
- The change of polymeric chain-length of NC, caused by degradation of NC during ageing, results in a loss of mechanical integrity of propellant grains, while thermal properties and burning behaviour may hardly have changed. The loss of mechanical integrity leads to increased grain fracture during ignition and the first stages of combustion in the weapon. Depending on loading density and design peak pressure, this may lead to unsafe situations with respect to pressure build-up.

Acknowledgement

The author thanks the Dutch Ministry of Defense for financing this project.

References

1. E.W. Lindeijer, F.A.J.T. Kraak, Onderzoek oorzaak van het verteren van natuurzijde kardoeszakken, in aanraking met zwart buskruit, en met rookzwak buskruit (in Dutch), PML rapport TL 1971-6, opdracht 8670, A67/KM/052, mei 1971.
2. E.A. Brönnimann, A. Sopranetti, and Ch. Stalder, A universal test procedure to predict the shelf life of propellants, Symposium on Chemical Problems connected with the stability of explosives, part 7, Sweden, 1985.
3. C.A. van Driel, W.P.C. de Klerk, Functional Lifetime of Gun Propellants, Proceedings 19th International Symposium on Ballistics, 7 – 11 May 2001, Vol. 1, p. 139.
4. M.A. Bohn and F. Volk, ‘Bestimmung der sicheren Lagerzeit einer plastifizierten Nitro-cellulose’, 25th International Annual Conference of ICT, June 28 – July 1, 1994, Karlsruhe, Germany.
5. F. Volk and M.A. Bohn, ‘Ageing behaviour of propellants determined by mass loss, heat generation, stabiliser consumption, and molar mass decrease’, 87th Symposium of the Propulsion and Energetics Panel of the AGARD, 1996, Athens, Greece.
6. F. Volk, M.A. Bohn, and G. Wunsch, ‘Determination of chemical and mechanical properties of double base propellants during ageing’, in: Propellants, Explosives, Pyrotechnics 1987, Vol. 12, p. 81–87.
7. STANAG 4115, ‘Definition and Determination of Ballistic Properties of Gun Propellants’.
8. W.W. Stein and H. Jahnk, ‘Determination of the grain fracture behaviour of propellant beds’, 4th Int. Gun propellant & propulsion symposium, 1988, p. V-363.
9. H.P.J. Jongeneelen, ‘Ballistic Stability. The relation between the decrease in calorific value and in muzzle velocity’, PML report, 1971.

THIS PAGE LEFT INTENTIONAL BLANK

Sample geometry as critical factor for stability research

Wim P.C. de Klerk^a & Marco N. Boers^b

^a Researchgroup Pyrotechnics and Energetic Materials
e-mail : klerk@pml.tno.nl

^b Researchgroup Properties Energetic Materials
TNO Prins Maurits Laboratory
P.O. Box 45, 2280 AA Rijswijk, The Netherlands

Abstract

Stability research on gun propellants is widely performed by microcalorimetry since the 1980's. TNO Prins Maurits Laboratory has already a broad experience since the early 1970's. In the past many studies were performed, to investigate the influence of oxygen, humidity etc. Less attention is paid to two other important aspects, namely the sample geometry and filling degree during the microcalorimetric test.

A statement in the old Dutch military literature presents the following *"It's a well known fact that the free surface influences the decomposition rate of the gun powder, i.e. ungrounded propellant decomposes slowly in opposite to ground propellant. This all for the same type of propellant (Amsterdam, February 1924),* which implies research on this topic, related to the stability prediction measured by microcalorimetry.

Because of the fact that the decomposition of nitrocellulose is influenced by the amount of oxygen and the reactive places, the best way to investigate the stability of gun propellants is to measure it 'ammunition like'. This means a combination of the propellant grains and the filling degree of the vessel. For small caliber ammunition it's mostly close above 95 %, and for large caliber bag ammunition (e.g. 155 mm) it's around 60 %.

In this paper an overview is given of the influences of different grain sizes and atmospheres, implicit the filling degree of the sample vessel. As a result on this important aspects, TNO has developed three different sizes of sample vessels, to investigate the propellant grains in the most 'ammunition like' condition. For some propellants it's still a problem, for example igniter propellants for large caliber.

Introduction

Propellants are notorious because of their intrinsic instability. Where in history the disasters led to storage outside inhabited area's (powder explosions in Delft (NL), 1654), nowadays accidents with solid propellants lead to an increase in research topics. The first efforts in the development of guncotton were studded with disasters. In 1847, an explosion in the first year of operation destroyed the first factory for the manufacture of guncotton at Faversham (UK) [1].

In the earlier years the surveillance was based on the 65.5 °C red fume-test. This method indicates the stability of the propellant in a closed glass bottle, which contains the propellant grains in its original form. The drawback of this methodology was and still is the interpretation by

the human-eye. An improvement in the stability research-techniques was the introduction of the HPLC method.

Comparing the different STANAG's related to stability research by HPLC (4117, 4527, 4541 and 4542), the ageing of the propellant is performed, without grinding the grains, except for the stick propellants, they will cut into fit lengths. After the ageing period the grains will grind into particles of less than 2 mm to facilitate extraction. The propellant is aged in its original sample geometry, but with a low filling-degree (~ 30 %), which is still on the safe side. These methods only give information on the expected stabilizer depletion for 5 or 10 years.

In all well-known literature it's announced that the decomposition of the propellants generates a temperature increase inside the propellant caused by the decomposition energy. This is a result of the sum of all chemical processes which occur during the ageing (and storage) of the gun propellant, directly related to the decrease in calorific value and possibly a run-away reaction.

After an extensive research [4,9,10,18-20] on the ageing process of NC based gun propellants, the surveillance in the Netherlands is based on the heat generation of gun propellants. Since the beginning of the nineteen-seventies the heat generation in an accelerated ageing process is carried out with the Heat Flow Calorimeter (TNO-HFC). The heat generation is measured for a non ground sample stored during one week at 85 °C (358 K). The result will be used to calculate two parameters; the first parameter to be determined is the safe diameter [5,6,7] of the propellants, a parameter which is characteristic for the self-ignition hazard, the second parameter is the expected decrease in calorific value for judging the ballistic stability [8]. Both the safe diameter and the decrease of calorific value are being established for a future storage period of 10 years.

Usually, surveillance of nitrocellulose (NC) based propellants is performed without paying much attention to the environmental conditions of the stored propellant, except for the storage temperature. Effects of other major aspects like relative humidity (RH), amount of oxygen (filling degree of the test-vessel) and the particle size (ground/unground) are quite often discussed in the literature, but not adopted for test procedures [12,13,14,17].

The RH will vary with location and time. The relative humidity may change from day to day in coastal areas or from season to season, making incorporation in a standard test procedure complicated. STANAG 2895 [21] has covered most of the external effects. An overlooked aspect is, for instance, that propellants for surveillance purposes can be stored in a magazine different from the magazines containing the munition articles, as is the case in the Netherlands.

One of the factors that influences the chemical stability is the available oxygen and in some investigations the stoppers of glass tubes containing the ageing propellant are lifted regularly to keep the oxygen content at a more or less constant level. The effects of the oxygen content as well as the effects of grinding will be discussed in this paper.

Equipment

The HFC used for these investigations at TNO-PML is of the van Geel type [2]. It consists of an aluminium block, which acts as a large heat sink to keep the temperature constant. A Peltier element in good thermal contact with the bottom of a stainless steel vessel, measures the heat

generated by the sample in the passive mode. The volume of the standard vessel is 70 cm³ and other sizes for performing HFC experiments are available.

The HFC technique, with a relative large measuring vessel (large sample sizes, see figure 1), has the great advantage of the propellant being measured in its original form (no cutting or other pre-treatments), and in the condition as-ammunition-like, with respect to the loading density of the ammunition article.

The temperature to perform measurements has a range from 40 till 150 °C, which gives the possibility for shorter ageing periods. Other stability determination techniques such as DSC or DTA are not used for surveillance of gun propellants, anymore in The Netherlands. The propellants are inhomogeneous and the mentioned technique use very small sample quantities.

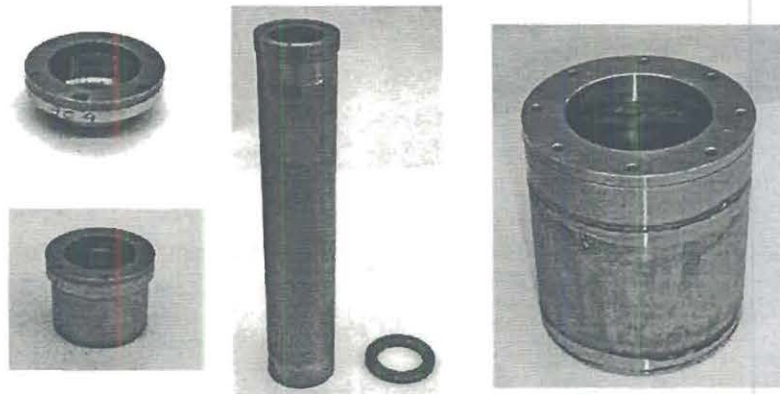


Figure 1: Available sample vessels for propellant stability research.

Background

Safe diameter

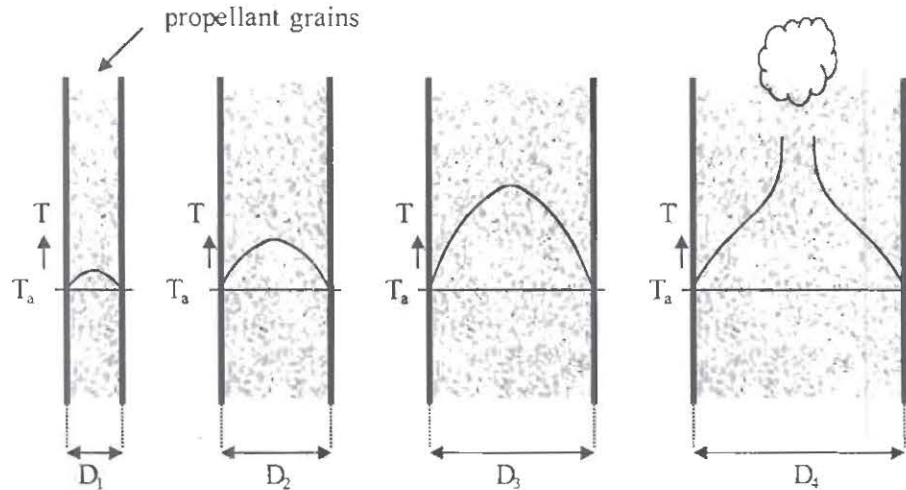
Definition: maximum diameter of a cylindrical filled container with propellant for which self-ignition is just excluded

If a propellant has been stored, no self-ignition will occur as long as equilibrium exists between heat generation and heat transfer to the surroundings. Whether this equilibrium will establish depends among others on the storage temperature. One of the other factors is the resistance encountered by the heat flow on its way to the surroundings. This resistance depends on the heat conductivity of the propellant and the dimensions of the propellants mass (package size). At a certain diameter the heat transfer will lag behind and the temperature will continue to rise, resulting in self-ignition (figure 2).

Also the ageing of the propellant plays a role, because the heat generation depends on the presence of stabilizer (derivatives). Based on this consideration the self-ignition hazard, for each storage temperature may be characterized by calculating the safe diameter [7]. The definition is not only valid for cylindrical shapes but also for other geometry's.

For the calculation of the safe diameter it is assumed, that during the considered storage period of 10 years the propellant will be exposed to extreme storage conditions for 2 weeks, the storage

conditions are ambient in the magazine during the rest of the period. During the extreme storage conditions the propellant is assumed to be exposed for a period of two weeks, the following daily temperature profile: 9 hours at 35 °C; 5 hours at 40 °C; 5 hours at 60 °C and 5 hours at 71 °C.



Selfheating increases with increasing diameter;
safe storage, when $D \leq$ safe diameter.

Figure 2: Schematic overview of the meaning of the safe diameter.

According to Merzhanov [15] and Barendregt [16], the formula to calculate the safe diameter, D_{344} , is as follows;

$$D_{344} = \frac{2.7 \cdot \lambda}{2} + \sqrt{\frac{(2.7 \cdot \lambda)^2}{4} + \frac{4 \cdot R T_a^2 \cdot \delta_c \cdot \lambda \cdot \exp\left(\frac{E_a}{R} \left(\frac{1}{T_a} - \frac{1}{T_m}\right)\right)}{\rho_b \cdot E_a \cdot Q_{\max}}} \quad [\text{m}]$$

The following parameters are used [6]:

E_a	activation energy		[kJ/mol]
R	gasconstante	8.31	[J/mol.K]
T_a	ambient temperature	344	[K]
T_m	measured temperature	358	[K]
δ_c	shape factor	2.00	[-] for a cylinder
λ	thermal conductivity		[W/m.K]
ρ_b	bulk density		[kg/m ³]
Q_{\max}	maximum heat generation		[mW/kg]

Lambda (λ) and bulk density depends on each propellant lot.

Ballistic stability

Based on theory and confirmed with closed vessel tests, a proportional relation exists between the decrease of calorific value of the propellant and the decrease in muzzle velocity. In formula $\Delta V_0 = a \cdot \Delta Q$ [8], where it has been experimentally found that the factor, a , varies between 0.1 and 2. A decrease in calorific value of the propellant during the storage period of the propellants is a result of the exothermal decomposition of the propellant. This decrease is equal to the total quantity of heat released during the storage period. During the accelerated ageing in the HFC, the heat generation is measured.

It can be concluded from the above-mentioned that the decrease in muzzle velocity after 10 years of storage in the Netherlands is in the order of a few tenths of percent. And after 10 years of storage in the tropics it will be in the order of a few percents. The acceptable decrease depends on the actual application of the propellant.

Surveillance process

The surveillance process in The Netherlands is split-off in two parts, namely the acceptance of new propellants and the stability control (surveillance) of old propellant lots. During the acceptance and surveillance control the safe diameter of the propellant is determined for a temperature of the surroundings of 71 °C (344 K). In accordance with NATO requirements such a temperature must be reckoned with. It should be remarked in this connection that it has been established experimentally that the temperature of a propellant container can really run up to as high as 344 K when exposed to direct radiation of sunlight. In actual practice, however, such storage will only occur incidentally (for instance after dropping ammunition during or UN-missions).

Experimental results

Influence of humidity

It can be expected that the RH will have an influence on the chemical stability of NC based propellants. During decomposition of these propellants, NO_x is released which reacts with water to nitric acid. Nitric acid is considered [3] to react with the hydrolysed propellant giving nitrous acid, which catalyses the decomposition reaction of NC-propellants.

In general for single, double base and rocket propellants results the higher the relative humidity in a larger heat production rate. Also the moisture content of the propellant is expected to be of influence to the heat production.

In a surveillance procedure a sample preconditioning is not yet performed as a standard. The samples are aged in vessels or glass tubes closed under "atmospheric conditions" (e.g. STANAG 4117).

It is evident from the HFC data that the RH increases the heat production, as measured by the HFC, of all considered types of propellants. The heat production at highest RH's is about 2 - 3 times the heat production at the lowest RH (at 85 °C, figure 3). The data indicate that this increased heat production is due to an acceleration of the decomposition. The curvature of the heat production shifts in time but maintains it's original shape.

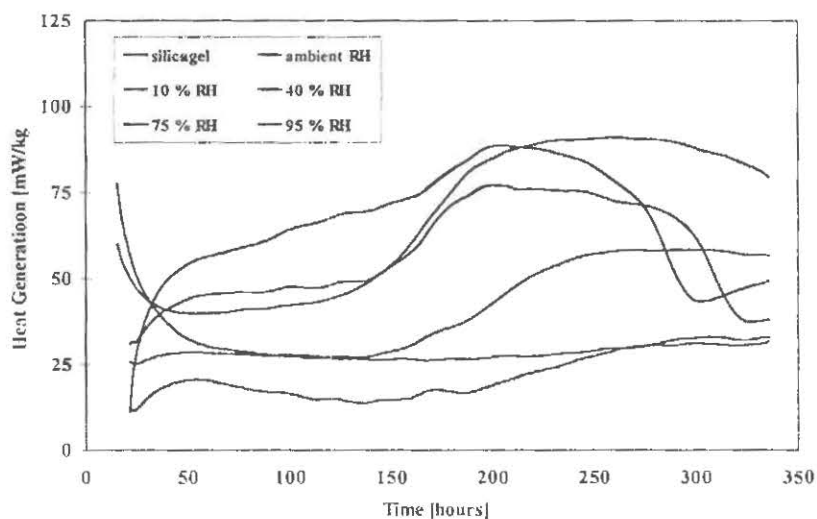


Figure 3: Heat Generation of a DB propellant as a function of time for different relative humidity's

Influence of amount of oxygen

Another factor that influences the chemical stability is oxygen and in some investigations the stoppers of glass tubes containing the ageing propellant are lifted regularly to keep the oxygen content at a more or less constant level [11].

The presence of excess of oxygen is reported to increase the heat production of the propellant as NO can be oxidized to NO₂ which catalysis the decomposition of the propellant [3].

In figure 4 an overview of the relation between the amount of oxygen in the vessel the heat generation is given [11].

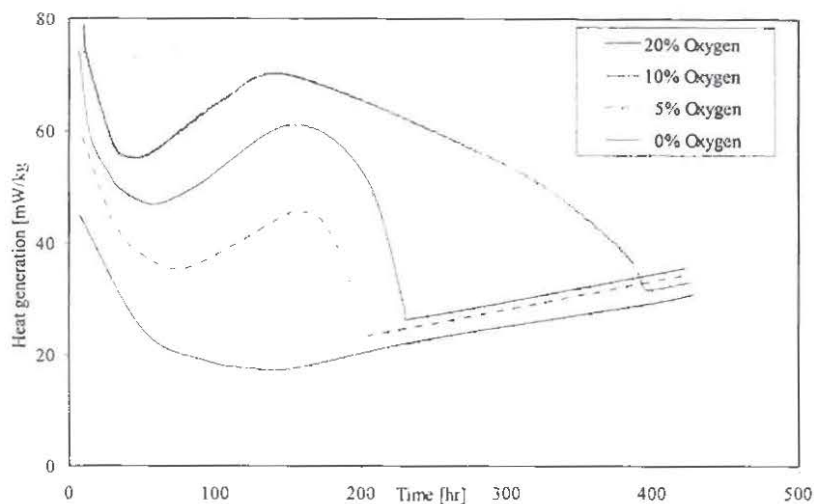


Figure 4: Heat generation in smokeless powder at 85 °C with variable oxygen concentration

Indirectly the filling degree of the test vessel determines the amount of available oxygen. In case of a complete filled sample vessel, the amount of oxygen, available for the oxidation reaction is less, in correlation with the amount of reaction surfaces. This will lead to less heat generation. In figure 5, the effect of filling degree is presented for a double base propellant (3 % EC).

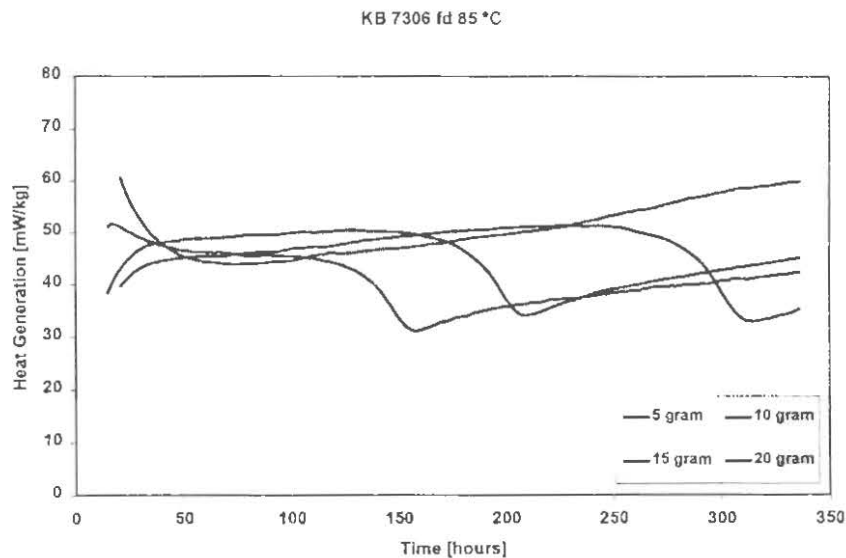


Figure 5: Heat generation as function of filling degree for a double base propellant at 85 °C.

To check if these effects depend on temperature, the same investigation was performed at 75 °C (figure 6). The same tendency in the curves occurs so it could be expected that it is more or less a temperature independent effect.

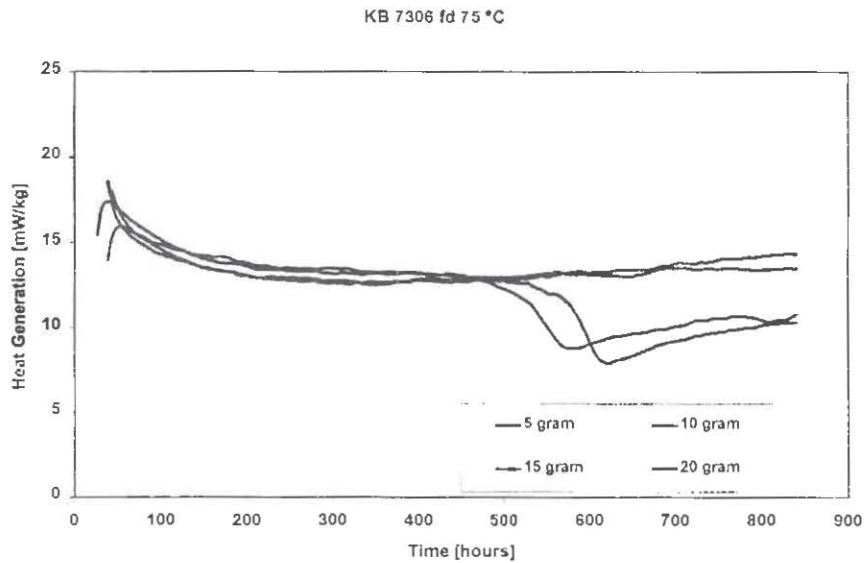


Figure 6: Heat generation of a DB propellant at 75 °C for different filling degrees.

In figure 7 the influence of the filling degree on a single base propellant is presented. The red curve is the situation with 5 gram of a propellant in a vessel of 70 cm³, which means a loading density of 0.071 g/cm³. When the vessel is complete filled with 20 gram propellant (original grains, purple curve) the loading density is 0.285 g/cm³. In relation to the original ammunition article with a filling degree of 0.292 g/cm³, it's in a good agreement.

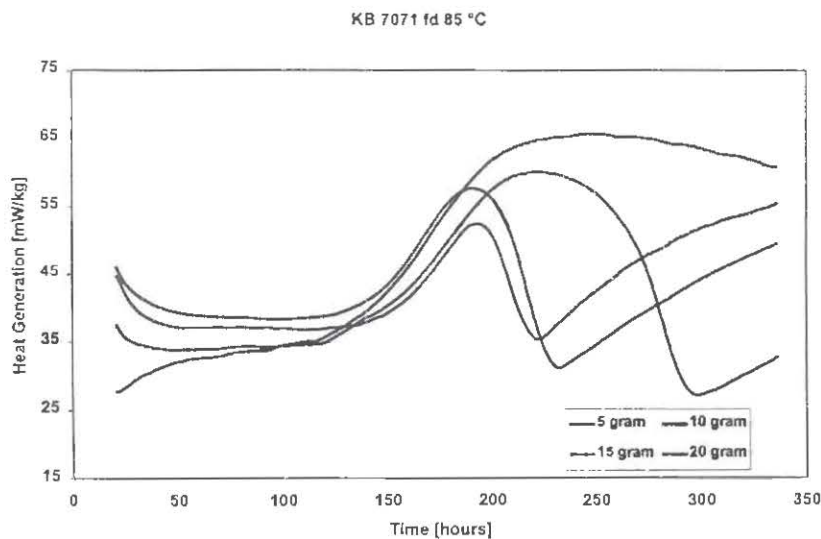


Figure 7: Heat generation as function of filling degree for a single base propellant at 85 °C.
Sample vessel was closed under ambient conditions.

The above mentioned figure shows clearly that the effect of the filling degree is also present in single base propellant measurements.

In an earlier version of STANAG 4582, a preconditioning at a relative humidity of 69 % was prohibited. To subscribe the effect of the relative humidity in combination with the filling degree, the same propellant as in figure 7, is investigated at a higher RH-value.

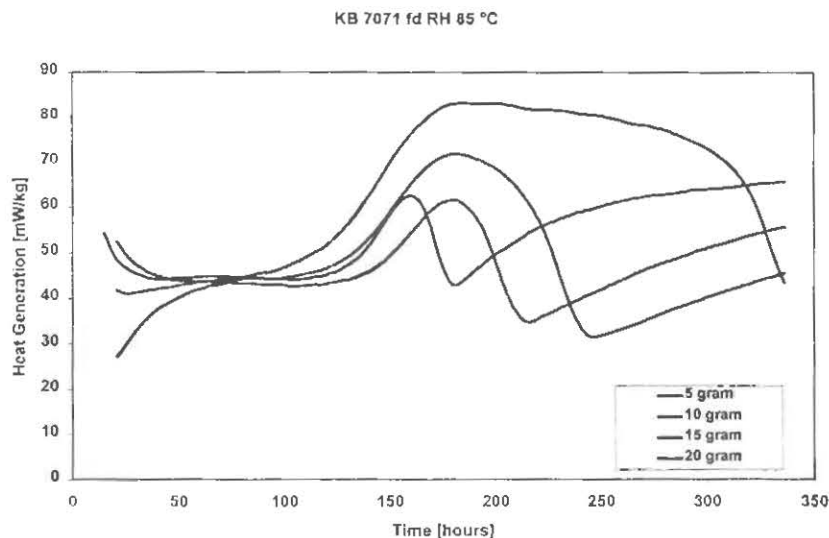


Figure 8: Heat generation as function of filling degree for a single base propellant at 85 °C.
Sample vessel was closed after 24 hours pre-conditioning at a relative humidity of 69 %.

In figure 8, all reactions are influenced by the higher relative humidity. The resulting enthalpies are in the same range, only the reaction takes place in a shorter period.

Surface effects & particle sizes

During the experimental program it was observed that from part of the propellants the heat generation was relatively high during the first days of the experiment. This initial effect was not observed for triple base propellants [9]. The NQ-group has a stabilizing effect resulting in hardly any red fumes in the 65.5 °C test.

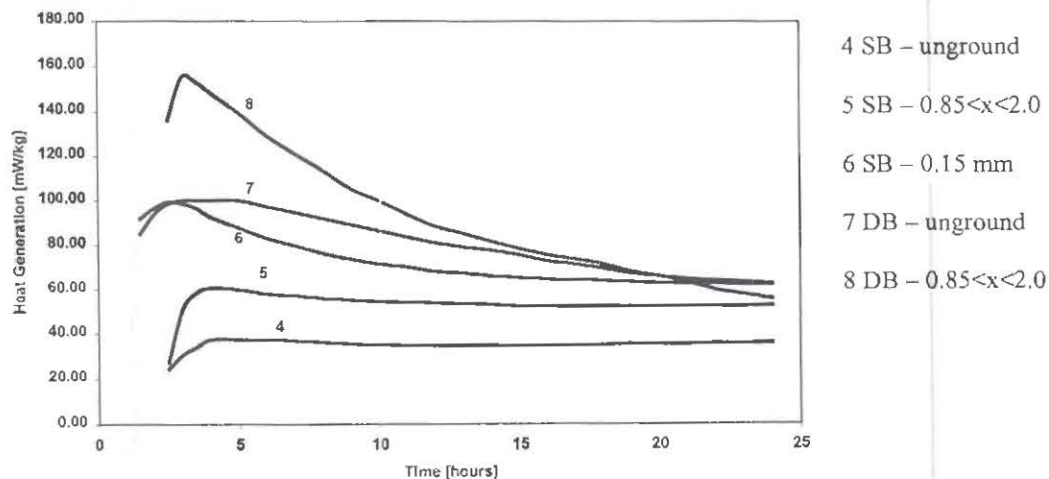


Figure 9: HFC measurements with the different initial effects caused by particle size.

The influence of the surface area of propellant grains has been investigated with HFC experiments of different propellant particle sizes. Besides experiments with ungrounded propellant grains also experiments were carried out with ground samples of varying particle sizes: about 1 mm and about 0.15 mm at the average.

The chemical composition of the investigated propellants is as follows. Curve 4, 5 and 6, single base propellant with 83 % NC and 1 % DPA. Curve 7 and 8 are from a double base propellant with 55 % NC, 41 % NG and 1.7 % stabilizer (EC + MC + AKII).

From the curves mentioned in Figure 9 it could be concluded that the surface area of the propellant effect the initial heat effect. The initial heat effect of ungrounded propellant is only small, while for propellant that had been ground to small particles (about 0.15 mm) this effect is about a factor 2 larger for the investigated propellants. The surface area of the propellant is increased by grinding, so more surface is available for reaction with oxygen.

Besides the aspect that the particle size influences the initial effect, it also has a strong influence on the whole heat generation curve. These effects are observed in the measurements.

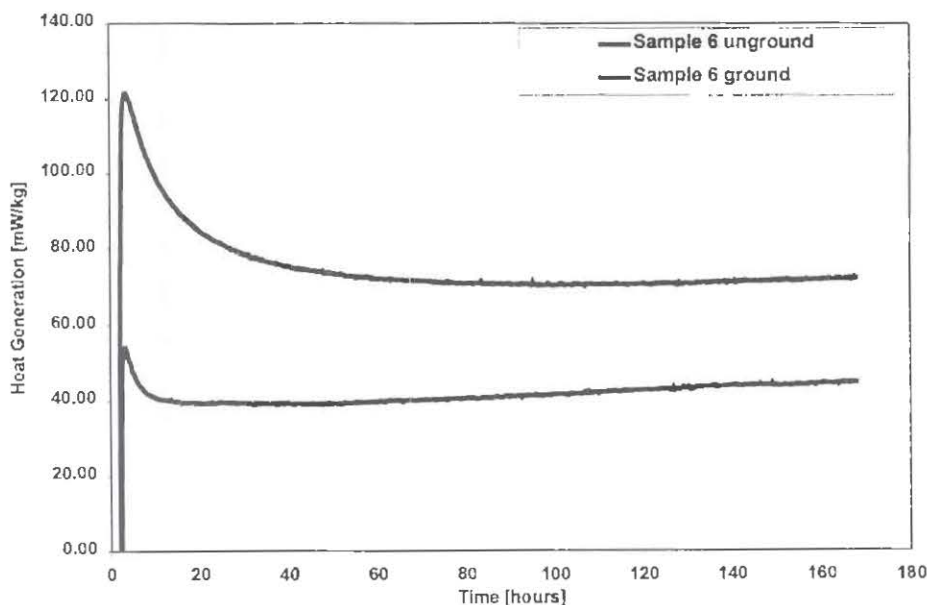


Figure 10: HFC measurement on a double base propellant, with the effect of pretreatment.

In figure 10, sample 6 (54 % NC, 26 % NG and 3.1 % EC), besides the initial effect also the level of the heat generation is a factor two as high for the grounded sample (~ 2 mm) as the ungrounded sample (tubes with a diameter of 5.3 mm). This will affect the calculated safe diameter (parameter from TNO calculations) or the acceptance level (according STANAG 4582), leading to too conservative values.

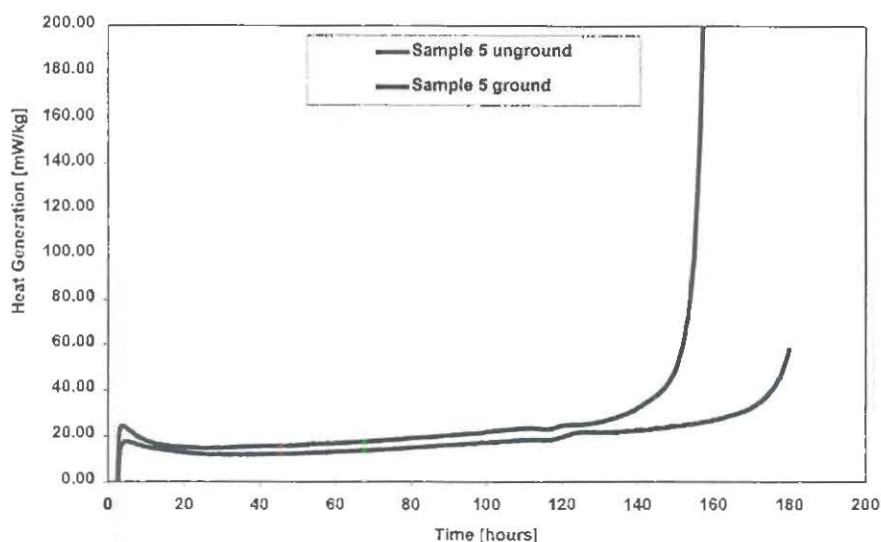


Figure 11: HFC measurement on a triple base propellant with the effect of pretreatment.

In figure 11, sample 5 (30 % NC, 21 % NG, 49 % NQ and 0.4 % m-nitro-aniline), the initial effect is very small, which was expected according to prior studies [9], but the curve shows a run-away which is ~ 40 hours earlier for the ground sample as the ungrounded sample (diameter 11 mm). In practice it means that the expected lifetime of the grounded sample is 2 to 3 years shorter, calculated from the year of measurement. This has economical (buy new ammunition) and environmental consequences (decommissioning of the ammunition) in an earlier stage.

Discussion & Conclusion

- Based on the results of the HFC measurements of propellant samples for acceptance and/or surveillance control it has been shown that in case the grains are treated (grinding) the heat curves have the same shape, but are shifted or stretched. Mostly leading to a too conservative safe diameter and decrease in calorific value.
- In case the propellant grains will not fit the sample vessel, the best way is to adapt the vessel. If this is impossible, try to minimize the grinding activities.
- The amount of available oxygen influences the reaction rate and as a result, the heat generation. So a 'not ammunition like' filling degree implies incorrect predictions for the safe lifetime corresponding to the different types of ammunition.
- Related to this it is advisable to carry out the heat flow calorimetry test with ungrounded propellant grains in the condition, as the propellant grains are stored, so "ammunition like".
- The TNO-HFC is designed to facilitate these measurements to a large extent.

Acknowledgement

The authors thank the Dutch Ministry of Defence for financing this project.

Reference list

1. N.E. Beach, N.S. Garman, Propellant Surveillance, Weapons Technology, 199-201, september-october 1964
2. J.L.C. Van Geel, Industrial Engineering Chemistry, 58, 24, 1966
3. E. Camera, G. Modena, B. Zotti, Propellants, Explosives, Pyrotechnics, 8, 70, 1983.
4. A.J. der Weduwen, Testing and surveillance of gun propellants (in Dutch), TNO-report, 1956
5. J.L.C. van Geel, The determination of the explosion hazards of propellants in storage. The heatflow and pressure test, TNO-report, 1963
6. J.L.C. van Geel, The safe radius of heat generating substances, TNO-report, 1965
7. J.L.C. van Geel, The heat generation test for the determination of the self-ignition hazard and the ballistic stability of nitrate ester propellants, TNO-report, 1971
8. H.P.J. Jongeneelen, Ballistic stability. The relation between the decrease in calorific value and the muzzle velocity, TNO-report, 1971
9. W. Verbeek, Improvement of the acceptance and surveillance control of nitrate ester propellants. Part 3, Comparative investigation of stability tests for nitrate ester propellants, TNO-report, 1974
10. E. Jilderda, Improvement of the acceptance and surveillance control of nitrate ester propellants. Part 8, The rate of heat generation as a function of time of three propellants under isothermal conditions at a temperature between 45 and 95 °C, TNO-report PML 1979-079, 1979
11. P. vd Meij, A.H. Heemskerk, Stability of Nitrocellulose propellants by thermal decomposition and stabilizer composition, Sciences et Techniques de l'Armement – Memorial de l'Artillerie française, tome 60, Paris, 1986
12. W. de Klerk, N. vd Meer, Influence of environmental factors on the lifetime of gun propellants investigated with heat flow calorimetry, 1st Workshop on the microcalorimetry of Energetic Materials, Leeds (UK), 1997
13. R. Eerligh, W. de Klerk, N. vd Meer, Influence of relative humidity on ageing of propellants, 11th Symposium on chemical problems connected with the stability of explosives, Zweden, 1998
14. W. de Klerk, N. vd Meer, Influence of storage on ageing of gun propellants in munition articles or in glass bottles, 2nd Workshop on the microcalorimetry of Energetic Materials, Leeds (UK), 1999
15. A.G. Merzhanov, V.G. Abramov, Thermal explosion of explosives and propellants. A review, Propellants and explosives, 6, 130-148, 1981.
16. R.B. Barendregt, Thermal investigations of unstable substances, including a comparison of different thermal analytical techniques, PhD thesis, Delft, Technical University, 1981
17. U. Ticmanis, S. Wilker, P. Guillaume, W. de Klerk, Influence of the atmospheric conditions on the ageing of single and double base propellants, 12th Symposium on chemical problems connected with the stability of explosives, Zweden, 2001
18. M.N. Boers, W. de Klerk, E. Krabbendam, Life time predictions of propellants, TNO-report, PML 2001-A18, 2001

19. J.L.C. van Geel, Self-ignition Hazard of Nitrate Ester Propellants, PhD thesis, Delft Technical University, 1969.
20. J.L.C. van Geel, J. Verhoeff, Heat generation measurements for the stability control of nitrate ester propellants, 4th Symposium on Chemical Problems connected with the stability of explosives, Sweden, 1976.
21. NATO Standardization Agreement STANAG 2895, "Extreme climatic conditions and derived conditions for use in defining design/test criteria for NATO forces material", February 1990.

THIS PAGE LEFT INTENTIONAL BLANK

Understanding the True Driving Force in the Auto-ignition of Single and Doublebase Propellants using Microcalorimetry

Daniel S. Ellison and Anton Chin
Test & Evaluation Department
NSWC
Surface Warfare Center Division
Crane, In 47522-5001 USA

A reliable assessment of the storage and handling safety of nitrate-ester based gun propellants is a prime consideration. Unexpected auto-ignition of propellants has been feared since the earliest days of propellant production. Magazines have exploded; propellants under thermal aging tests have exploded under conditions that appear unexplainable. There has always been a basic assumption that knowing the critical parameters of a propellant (i.e. size, heat generation, thermal heat transfer, grain size and other related kinetic parameters) is all that is necessary to predict safety. By using the correct kinetics, one should be able to predict whether the propellants will either cook-off or gradually decompose. However, there are many examples that clearly demonstrate that the thermal degradation processes in single and double-based propellants are not definitively understood.

This paper will show by actual example how low temperature auto-ignition can occur at conditions one would not expect. Microcalorimetric data will be presented on propellant samples under controlled conditions. This data will show that a well known autocatalytic driving force can account for most observed variability within propellant lots. Data will be presented that give an explanation for the observed change in mechanism near 60°C reported by many researchers.

Introduction and Background

Energetic materials by their very design are a storage medium of thermal energy that when hit by proper stimuli releases this stored thermal energy. In high explosives the rate is very rapid. In propellants the energy release must be at a specific and controlled rate that depends upon the usage of the propellant. Due to this higher requirement, there are several basic concerns and problems associated with the use of the propellants. They are:

- reliability (readiness, performance)
- safety (storage, handling, transport and operational)
- useful life span (shelf and service life)
- environmentally compatible formulation without compromising the performance.

To fully address the problems one must:

- Understand the processes that affect the product
- Fingerprint the propellant composition for that process or processes.
- Incorporate characteristics into the manufacturing process to optimize the performance and service life of the propellant.

The Life Assessment Process

A reliable assessment of the storage and handling safety of nitrate-ester based gun propellants is the prime consideration. Unexpected auto-ignition of propellants has been feared since the earliest days of propellant productions. Magazines have exploded; propellants under thermal tests have exploded under conditions that appear unexplainable. Figure 1 shows what happens when a propellant is exposed to critical conditions due to its size, its shape, and its thermal conductivity and related parameters.^{1,2} The assumption in figure 1 is that if one knows the critical parameters of a propellant one can predict long-term stability. By using the correct kinetics, the propellants will either cook-off or gradually decompose. Calculations of stability begin to fail when exothermic events illustrated in Figure 2 are encountered.

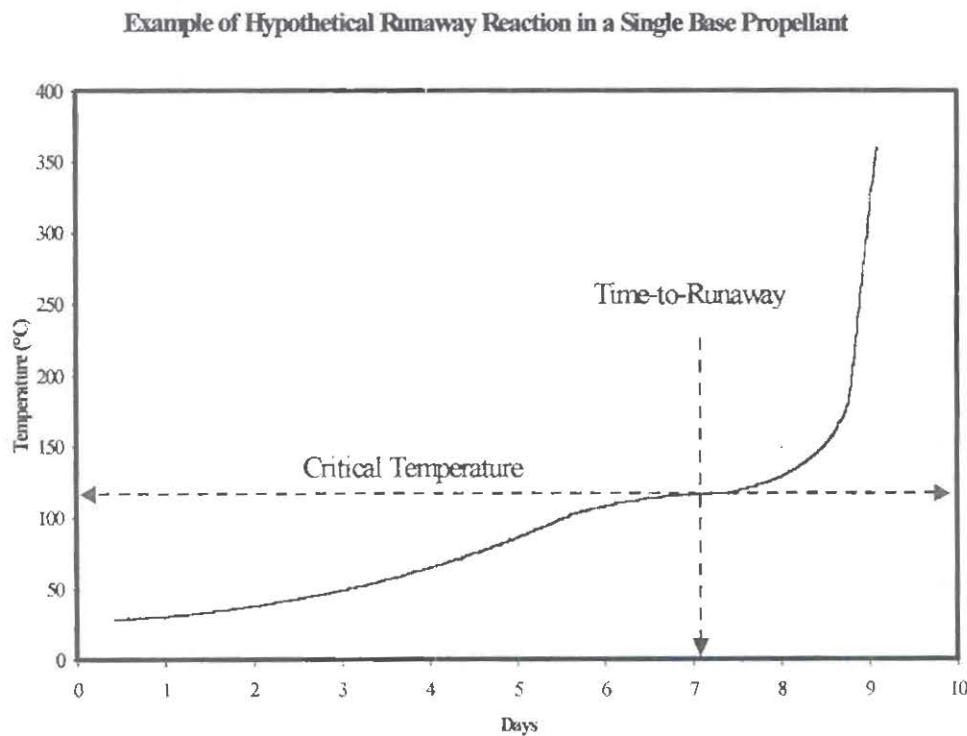


Figure 1. This is an example of a hypothetical thermal runaway event for a single base propellant.

Figure 2 shows two tests of NACO single base propellant from the same lot but with two significantly different outcomes. Obviously, there is a difference due to an autocatalytic event. Understanding the driving forces behind this event is the key to most propellant stability related problems.

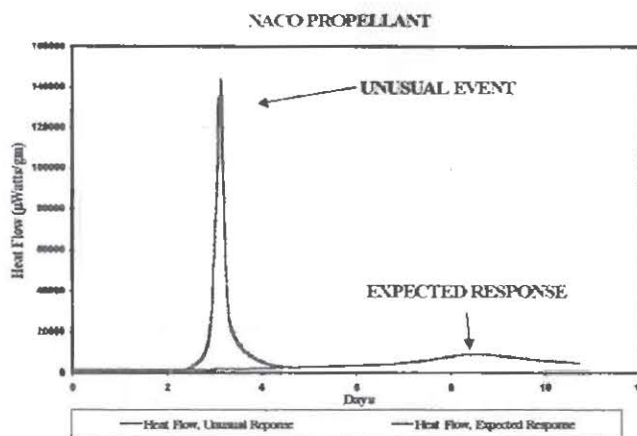


Figure 2. Unusual exothermic event observed in NACO Propellant compared to expected microcalorimetric heat

Before you can assess stability, you must understand the process that drives the event

The factors that cause heat generation in nitrocellulose must be identified. These will include but are not limited to water, acid or any impurity that may serve as an inhibitor. This measurement must be done under controlled conditions. The variables must be isolated and observed (i.e.; the proper test should not allow too many variables to interact with the sample at once). The testing process must allow for separation of variables as well as simultaneous measurements of all. The tool of choice in this case is microcalorimetry. One can fingerprint the process and then begin to separate the variables that critically affect safety and performance.

A considerable amount of work has been done in the area of propellants using microcalorimetry.^{3,4,5,6} Using the basic principles of kinetics, the service life of propellants could be established if the manufacturing process for propellants were controlled. However, small changes in manufacturing processes affect the long-term stability of the propellant. It will be shown how most of the conventional test methods such as the fume test and stabilizer depletion

are actually evaluating the effect of just one parameter. It will be shown that the configuration of the sample changes the stability of the propellant. Changing the sample configuration changes the concentration effect of this critical parameter.

There seems to be one common observation by those involved in the surveillance of propellants: Every lot of propellant should be monitored because of the wide variability of the apparent stability of propellants.

Several investigators have observed that varying the sample weight of propellant from the same lot in a fixed volume will have marked different decomposition heat flows (μ Watts/gram).^{7,8} Initially it was thought that this effect was dependent on the difference in the mass of the sample. It can now be shown that this is actually caused by changes in the headspace above the sample. It will be shown that the water content of the propellant sample is changing due to saturation vapor pressure above the sample. Changing the water content changes the effectiveness of the acid in the propellant. This work is derived from observations made by many researchers into how water control of the test propellant samples affects the results of stability tests.

Studies on the affects of humidity on propellants have shown that nitric acid of various concentrations have predictable results to the thermal stability and kinetics of propellants.⁹ In one study, unstabilized nitrocellulose was subjected to heat flow microcalorimetric analysis at 70°C. Water and acid concentrations were varied to study the effects of the water and nitric acid on the nitrocellulose. Figures 3 and 4 show the raw data taken from reference 9 re-plotted to emphasize the dramatic affect that different water and acid concentrations have on nitrocellulose. In Figure 3, one sees that the time to peak is reduced as the nitric acid concentration drops. In Figure 4 the peak height of the microcalorimetric heat flow curve increases with water content. This indicates a rate order change from first to zero order. The reaction will proceed more rapidly.

The samples and nitric acid concentrations are extreme in the previously cited research. The issue facing us is the connection to what one finds in conventional propellant studies which depend on only red fume formation, weight lost, and stabilizer content to determine the safety and performance. Figure 5 shows that the heat flow characteristics of a standard ball propellant used in 20-mm can be changed dramatically by drying. Figure 5 is the same propellant of equivalent weight in the sample volume. The only difference is that by reducing the water content from 0.8% to 0.3% the thermal decomposition pathway has been extended. In other words the rate of decomposition is reduced. The obvious reason is that the acid and water can inhibit the normal function of the stabilizer (a limiting factor to control the decomposition rate of nitrate esters). This results in the rate order changes as can be seen in the decrease of the heat flow slope (rate curve) as the water content decreases in Figure 5. The peak height decreases because as the rate decreases the heat flow curve has to extend to cover the same amount of energy release. This is the first Law of Thermodynamics - The Law of Conservation of Energy. For the same reason, the time to peak will increase. This effect is consistent with changes in

water and acid content as noted above. However, there must be an optimal pH range for the water and acid effect. More studies are urgently needed to determine this range.

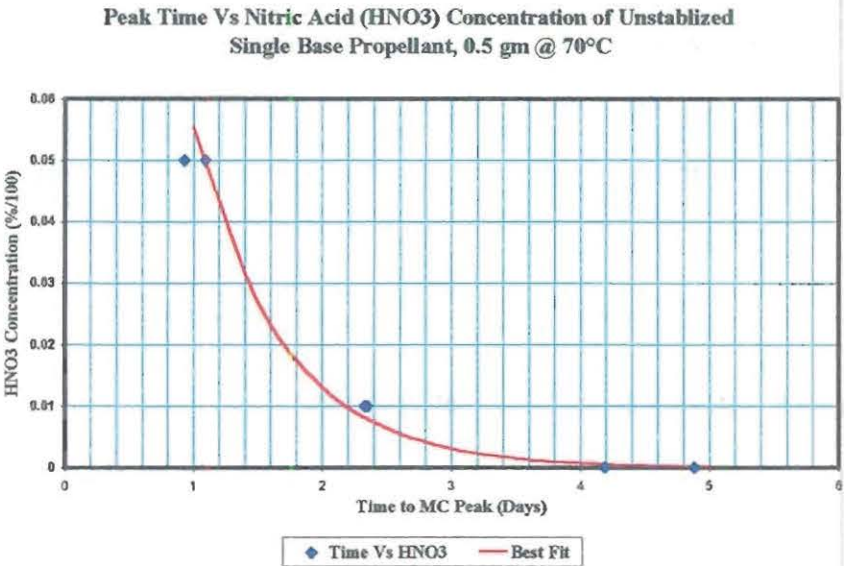
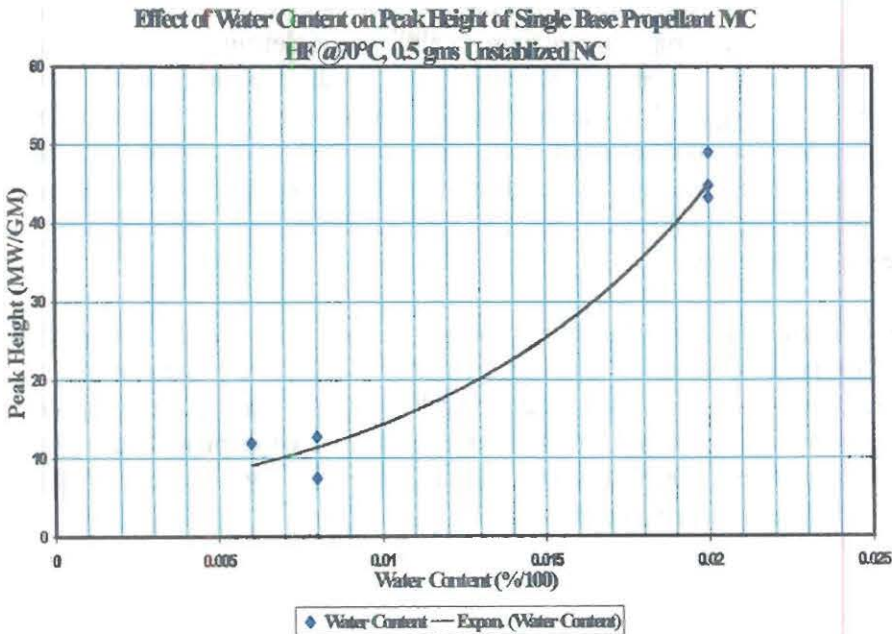


Figure 3. Plot of microcalorimetric peak position versus acidity for unstabilized nitrocellulose @ 70°C



Approved for Public Release; Distribution is Unlimited

Figure 4. Plot of water content vs. microcalorimetric maximum peak height @

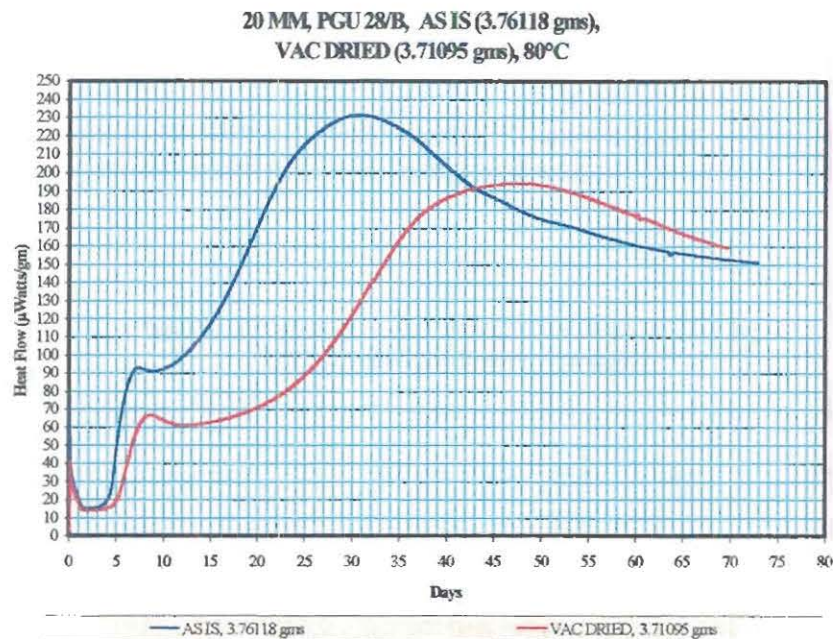


Figure 5. Effects of drying 20-mm ball propellant

The water content changes are due to the physical process of saturation vapor phase density. This can be demonstrated in Figures 6 and 7. Figure 6 is a plot of the water vapor density versus temperature (°C). This means that in any closed system the water will move into the vapor phase. If too much water is present, the extra water will condense as liquid. The amount of water in the vapor phase will then equilibrate with the liquid phase.

When this same data is plotted as a log function one immediately notices a change in slope near 60°C. It is this change in slope that appears to give an apparent change in mechanism to those researchers that attempt to measure stabilizer depletion for predictive purposes. The main problem with using stabilizer depletion for predictive analysis is that no one finds reproducibility in this change. The reason is quite simple. In the process of doing experiments, the researcher fails to take into account how water content will change under the conditions of the test. In some cases, the test is conducted without sealing the test ampoule to keep the original water within the container. As the test proceeds the water is lost and the rate of stabilizer depletions is affected.

In reality, there is no change in mechanism at 60°C. It is only a basic change across the whole temperature range due to the quantity of water that can be present in the vapor phase. At low temperatures, such as 65.5°C, less water can be in the vapor phase compared to tests run at 80°C where more water can move into the vapor phase. If the propellant sample has a limited amount of water, then the amount of water may all be in the vapor phase and the propellant acts as if it has been dried as shown in figure 5.

SATURATION VAPOR DENSITY OF WATER

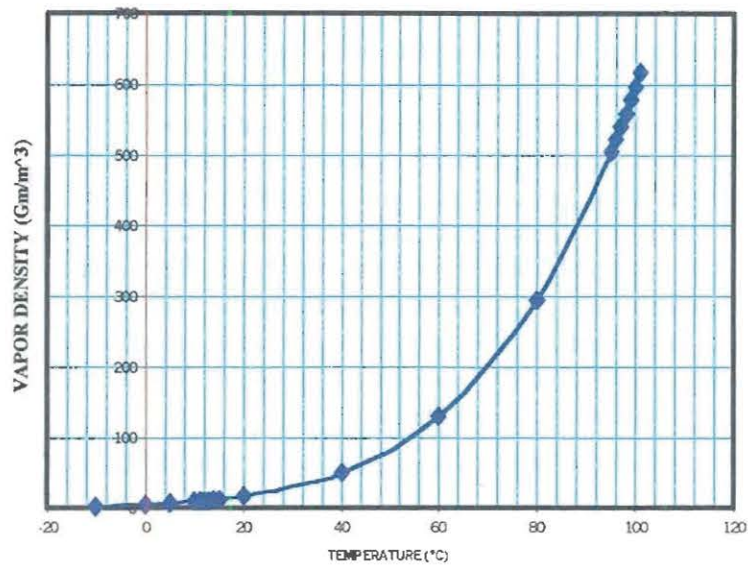


Figure 6. Water saturation vapor as a function of temperature

SATURATION VAPOR DENSITY OF WATER

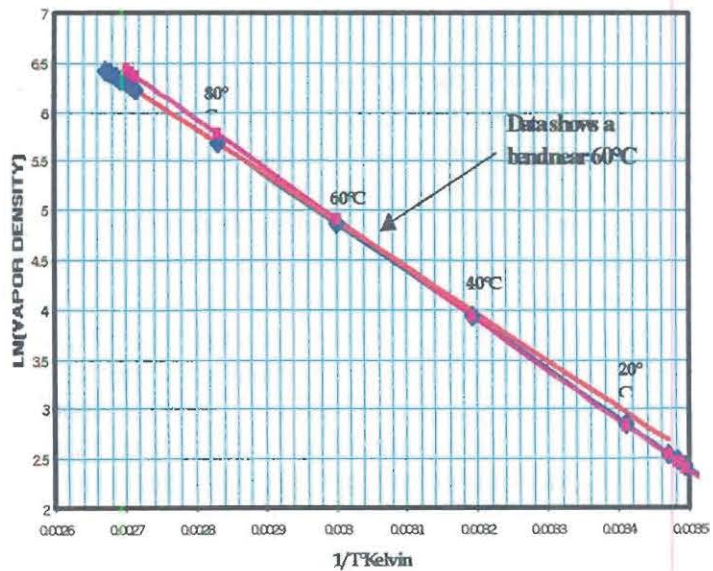
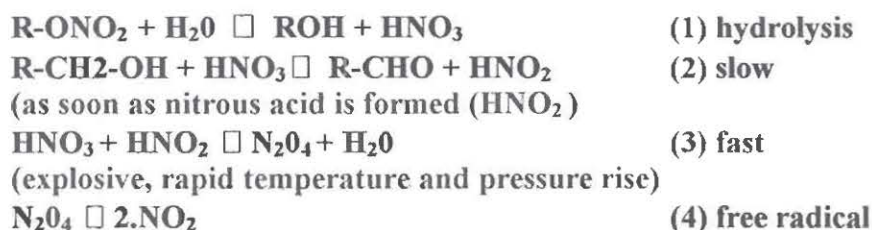


Figure 7. Log Plot of Water Saturation Vapor Phase versus Temperature in (1/T° Kelvin)

Explaining the Unpredictable: The thermal runaway reaction of propellants

Nitrocellulose, being a nitro ester, has the potential of thermal runaway. The conditions that cause this have always been a mystery. Much effort is ongoing now by the Navy surveillance community to continuously monitor the safety of propellants by testing control batches and using this data to warn of potential problems with a lot. Once propellant is manufactured using current techniques it becomes immediately subject to degradation as a function of its water content. This factor is so significant that if the water concentration is allowed to drop to almost dry conditions, the potential of rapid thermal runaway is created. This chemical process is possible because of the basic underlying chemical equilibrium that exists with water and the nitric acids that are always present in nitrocellulose from manufacturing processes. In fact, to remove these nitric acid products would almost certainly make nitrocellulose less or even ineffective as a propellant.

The chemistry behind the process: the nitrate ester (R-ONO_2) acts in following manner:



Equations 1, 2, 3 and 4 show the basic chemical processes occurring in propellants. Rapid thermal runaway is the result of driving the chemical reaction to formation of nitrous acid and water.^{10,11} When the water content is low, the nitrous acid formation is favored. When the propellant is dry, the acids are not activated. A small amount of water from some external source such as humid air will quickly drive the formation of the nitrous acid. This leads to the free radical N_2O_2 . The free radical causes the rapid thermal runaway. This runaway process is not dependent in its early stages on the amount of propellant. It is controlled by the water content. If the water content is high, estimated at more than 1%, the reaction is driven back to the nitric acid and the propellant behaves in a normal and expected manner. The nitric acid content controls the time of the reaction in high water content conditions, but the overall peak energy release is controlled by the amount of water present as was stated before. If the water content is very high, the performance becomes degraded because the nitric acid content is too dilute to drive the reaction exothermically. This will result in poor output power. This is what makes shipping propellant in water a safe practice.

Where is this thermal runaway actually observed? If it is that well understood, why has it not been known before this?

Although the chemistry is understood, the missing factor is the influence of water. This is how the connection between water and the thermal runaway process was established:

Figure 8 shows microcalorimetric heat flow curves for NACO run at 115°C. There is one notable observation. The times to peak are variable although the samples came from the same lot of propellant. If the safety of a propellant lot is determined by samples from this lot, which result do you use to make a judgement about the safety of the lot? Figure 9 clearly indicates that this lot could be dangerous if it has the potential to ignite as the microcalorimeter data show. Even within the container of the bulk propellant, not all the samples are going to retain the same amount of water. This establishes a connection of the peak times to water content that makes the variability understandable.

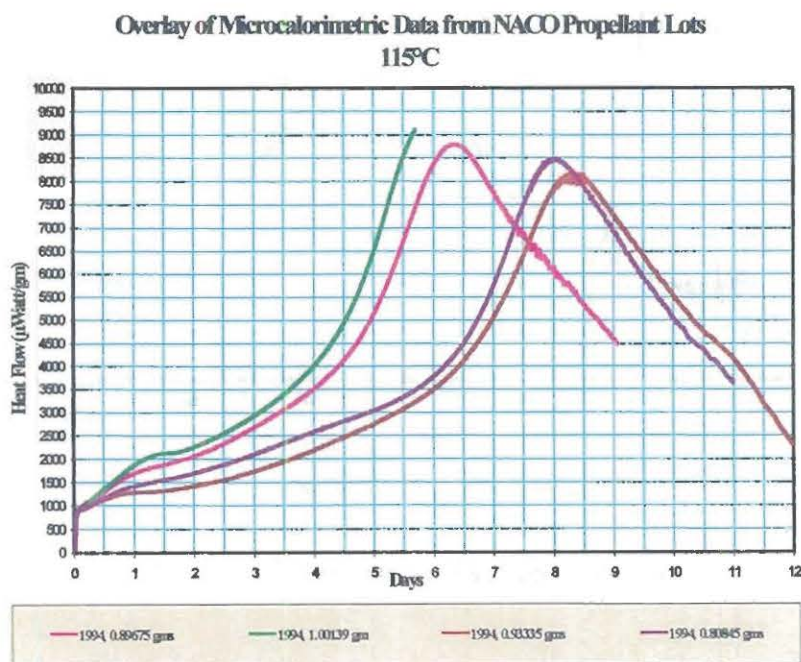


Figure 8. The same lot of NACO propellant with different induction times at 115°C

The autocatalytic event in Figure 9 occurred because the propellant grain is dry. There is water within the grain but the majority of the water is lost from basic transport mechanisms as the temperature changes and through poor seals in the storage container. NACO is a single base propellant containing large amounts of ether. Ether is residual from the manufacturing process. Ether will absorb water from the grain. If the ether escapes the container, water will be removed with it and the grains will be even dryer than usual. This results in the event shown in Figure 9. The normal thermal path at 115°C causes the peak to occur in 8 to 10 days. The autocatalytic event occurred in 2 days. It was driven by the chemical processes already discussed. The exothermic was detected in other as-is (not dried) NACO propellant samples. The difference was a change in time caused by difference in water content. Figure 10 shows another highly exothermic event.

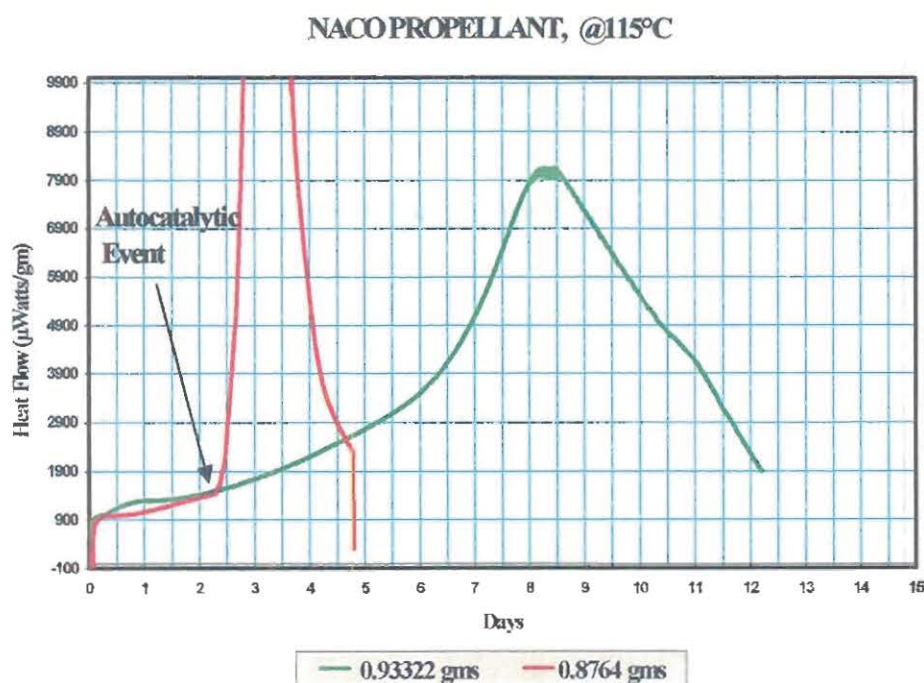


Figure 9. Close-up of autocatalytic event in NACO Propellant at 115°C

These microcalorimetric tests begged the question: "What happens if you attempt to remove water?"

The question led to the relationship of water and the highly exothermic events. The amount of water is variable (up to 4%). Under ambient temperature condition samples of NACO propellant were dried under static vacuum (26 inches Hg) for 3 days. By that, the process used was to pull a vacuum down to 26 in Hg, turn the pump off and allow the samples to lose any volatiles at that reduced pressure. The samples were conditioned at ambient temperature conditions for 3 days. The samples were then placed in a specially designed high pressure test ampoule with a threaded cap and O-ring seal as shown in Figure 11. The conventional low-pressure test ampoule is depicted next to the improved ampoule.

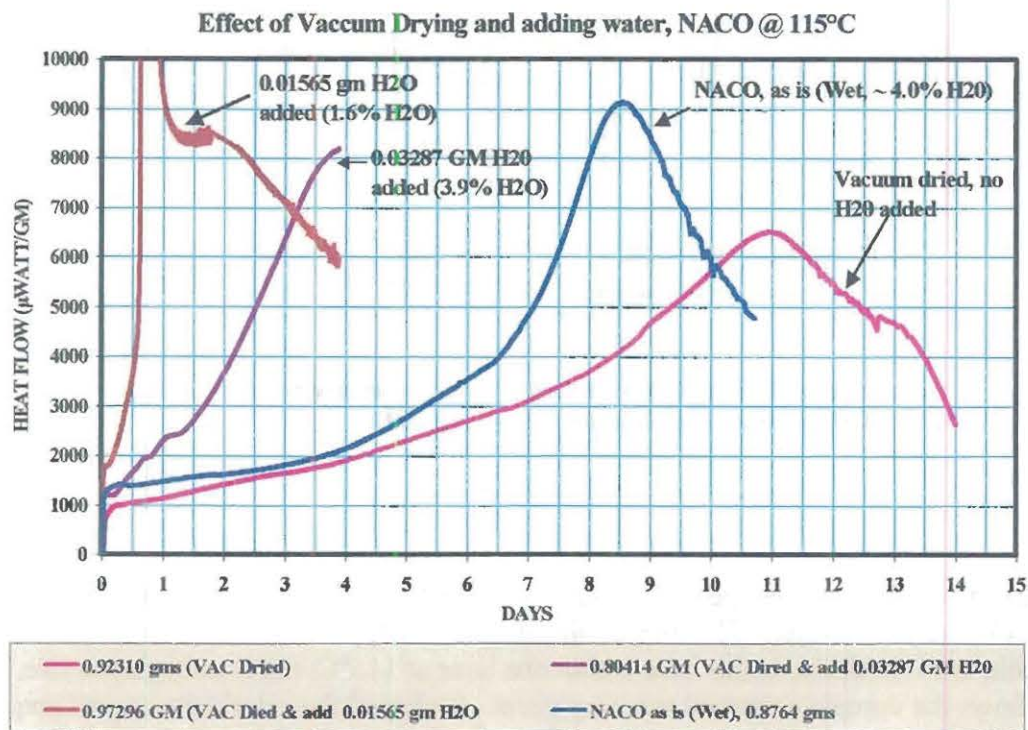


Figure 10. Effect of adding water to vacuum dried NACO propellant samples.

Water was added in different amounts to each test sample. One sample was analyzed as dried. Each test sample was placed in high-pressure ampoules. The samples were run in a Calorimeter Sciences Model 4400 high temperature microcalorimeter operating at 115°C. The results are shown in Figure 12. As can be seen, the lower the water content the farther the heat flow curve moves to the longer decomposition time. This is because the vacuum drying causes residual acid to concentrate on the surface of the grain. Since the propellant is dry, the acids

become inhibited. Adding water causes the acid to become active again and a violent reaction can develop. This is evident by the sharp spike in the sample with 0.01564 grams of water added. This reaction was exothermic initially, but stopped and returned to the normal decomposition heat flow. It is suggested here that it stopped because the water content within the grain was higher than that on the surface and the potential runaway reaction stopped as the acid became diluted again. If the internal water content of the grain is very low, then thermal runaway could occur. This is exactly what happened in the next example.

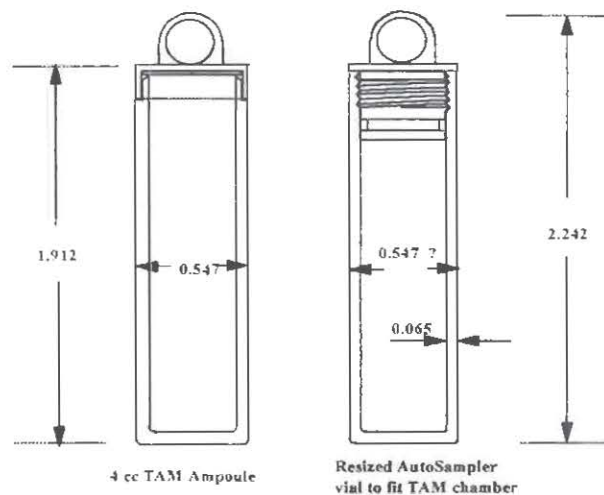


Figure 11. Standard microcalorimeter test ampoule and high-pressure modification with o-ring seal.

Figure 12 shows what happens when another NACO propellant sample was dried and exposed to a low level of water. The thermal decomposition appears to follow a normal expected path, until suddenly, in this case within one hour at 115°C, the heat begins to rise. Figure 13 shows the complete thermal runaway event. It clipped the calorimeter signal amplifier at over 150 milliwatts.

NACO PROPELLANT, 0.89708 GMS WITH 0.13346 GMS H2O ADDED, @ 115°C

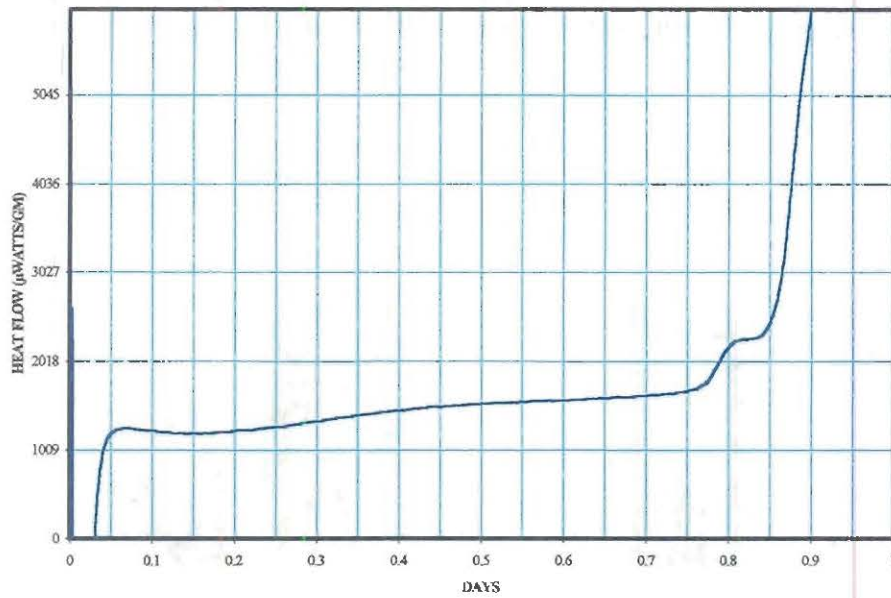


Figure 12. Violent thermal runaway induced by drying NACO propellant grain and then adding water into the closed vessel.

NACO PROPELLANT, 0.89708 GMS WITH 0.13346 GMS H2O ADDED, @ 115°C

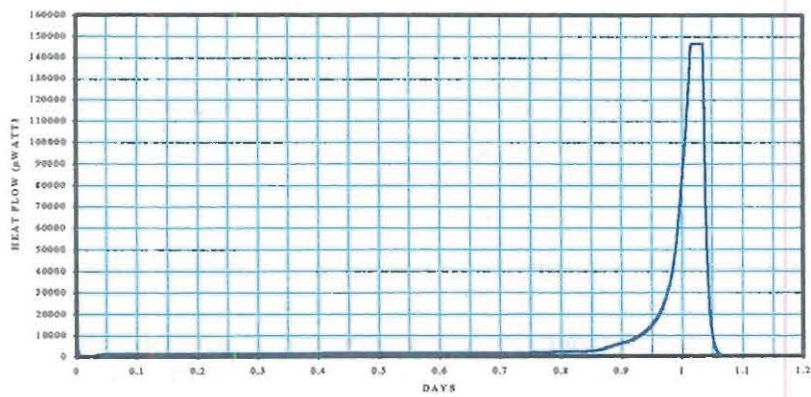


Figure 13. Complete heat flow curve for thermal runaway

The damage to the calorimeter and the test ampoules was noticeable. The pressure release was high enough to jam internal heat shunts in the calorimeter caused by the force of the screw top of the test ampoule hitting the shunt as it separated from the body of the test ampoule.



Figure 14. Test ampoules and NACO propellant samples before and after thermal runaway.

In comparing a sample of the NACO propellant grain as received with the one retrieved from the test (Figure 14), there are indications the grain had begun to burn. This is further evident from the enlargement of the perforation holes in the grain.

One could assert that the temperature was close to critical conditions and the runaway was accidental. That issue was addressed by the following test: Under routine analysis, as shown in Figure 15, the time to reach any high exothermic values would have to take more than 80 days at 80°C. At 80 days, the peak heat flow was less than 100 μ watts/gram. In Figure 16, a dried sample of NACO propellant was treated with water and in less than 10 days its heat flow was over 5500 μ Watt/gram. If enough of these grains were together, they would generate enough heat flow to cause a violent reaction.

Overview of NACO Propellant after aging at 80°C

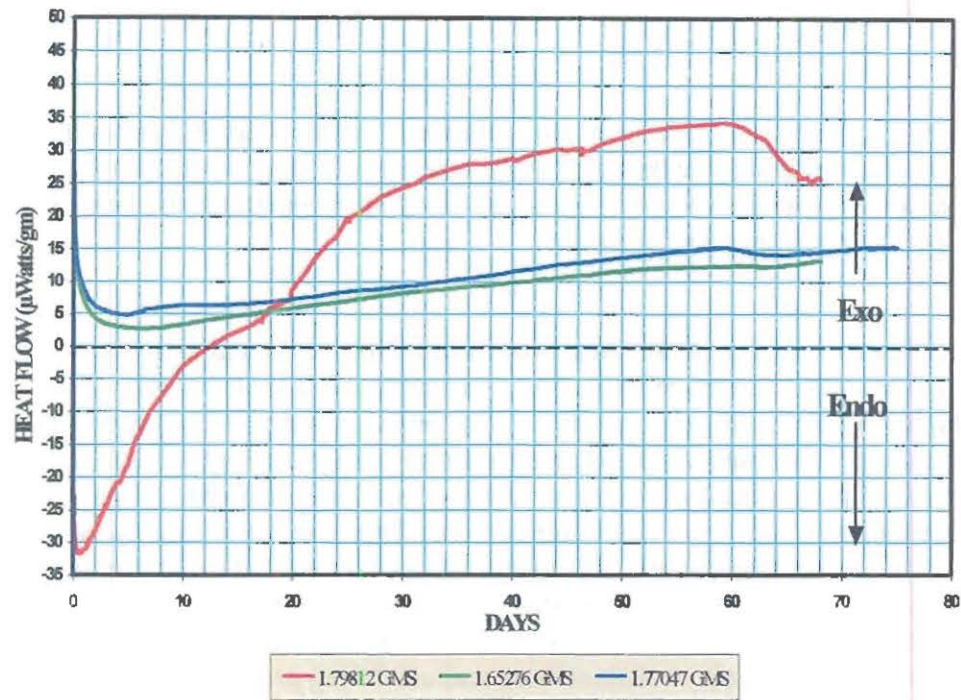


Figure 15. Expected microcalorimetric heat flow curve for wet NACO propellant.

NACO PROPELLANT, 0.7554 GMS, VAC DRIED AND THEN 0.02845 GMS H₂O ADDED, 80°C

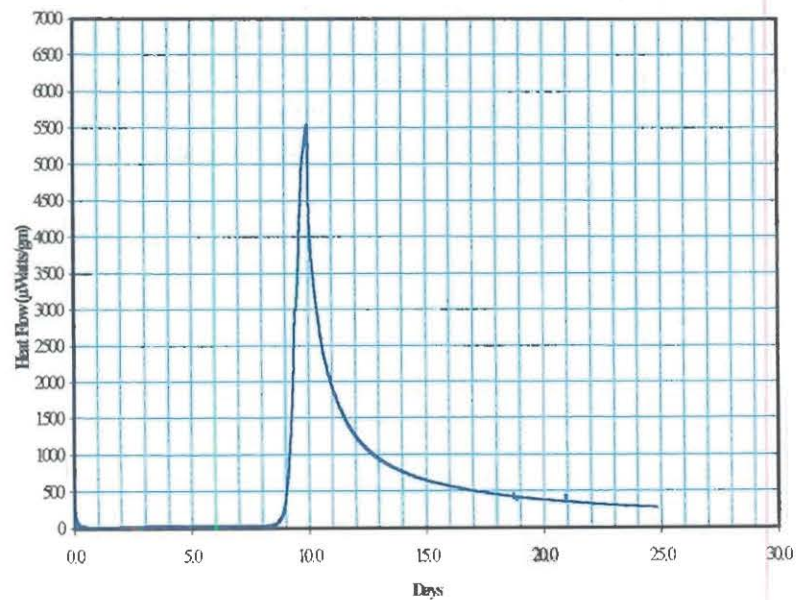


Figure 16. Very exothermic event when NACO propellant grain was dried and water added into test ampoule at 80°C

SUMMARY

Munition Propellants are made from nitrocellulose. Nitrocellulose is commonly manufactured in single base, double base and triple base forms. Much of the problem with using propellant is that it is unable to survive the wide variability of the environments without serious degradation in both performance and/or safety.

Using test methodologies, a preliminary connection has been established between the water content and pH value of nitrocellulose-based propellants and their stability. This connection is highly controlled by the saturation vapor phase of water and pH changes at the variable temperature and atmospheric pressure changes that the propellant will see throughout its lifetime. Once propellant is manufactured using current techniques it becomes immediately subject to degradation as a function of its water content. This is so significant that if the water concentration is allowed to drop to very dry conditions, the potential of rapid thermal runaway is created when exposed to moisture later in its storage or use. The thermal runaway conditions are possible because of the basic underlying chemical equilibrium that exists with water and the nitric acids that are always present in nitrocellulose from manufacturing processes. In fact, to remove these nitric acid products would almost certainly make nitrocellulose ineffective as a propellant.

Propellant stability, in addition to natural environmental stimuli, is highly controlled by the concentration of its acid and water content (pH value). Nitrate esters in acid solutions are subject to hydrolytic reactions with the formation of nitric and nitrous acids. As soon as the latter is formed, fast free radical chain reactions will then take place to give rise to the violent decomposition. The stabilizers are added to destruct the nitrous acid and/or any nitrogen oxide radicals as soon as they are formed. Most stabilizers are weak bases and their effectiveness is a function of acid concentration in the propellant system. Using too much stabilizer will increase the pH value of the composition which will destabilize the nitrate ester. Too much acid (lower pH) will neutralize the normal function of the stabilizer. Therefore, there must be an optimum pH range for each individual stabilizer to perform to its highest efficiency so the most dangerous stage of propellant decomposition "thermal runaway" can be prevented. We will need to determine this optimum pH range.

-
- ¹ A. Duswalt, "Hazards Model for Autocatalytic Reactions," *Proc. 18th NATAS Conference* 1989.
- ² A. Fabre, J. Bataillet, "Self-Ignition Modeling Method based on Microcalorimetry Measurements". *Proceedings Workshop Microcalorimetry of Energetic Materials, Leeds, UK* 1999.
- ³ D. Ellison, A.Chin "The Application of Microcalorimetry for obtaining the correct heat generation rates for predicting Thermal Runaway in Nitrocellulose based propellants. *Proceeding of the Workshop on the Microcalorimetry of Energetic Materials, Leeds, United Kingdom, May 1999.*
- ⁴ D. Ellison, A.Chin "A study of the Thermal Stability and Performance of Energetic Materials using Heat Flow Calorimetry", *Proc. Workshop Microcalorimetry of Energetic Materials, Leeds, UK* 1999.
- ⁵ D. Ellison, A.Chin "Recent Developments in Microcalorimetry using automated and large scale sampling systems", *Proc. Workshop on the Microcalorimetry of Energetic Materials, Leeds, UK* 1999.
- ⁶ D. S. Ellison, A. Chin, "20 mm Gun Propellant Safety Service Life Study using Microcalorimetry/HPLC correlation Diagram", *Predictive Technology and Stockpile Life Symposium* 1997
- ⁷ M. Rat, P. Guiliaume, S. Wilker, G. Pantel, "Practical Applications of Microcalorimetry to the Stability Studies of Propellants", *Proc. TTCP Workshop, Leeds UK* 1997
- ⁸ A. Chin, D. Ellison, "Factors that affects the results of Microcalorimetric Data", *Proc. Workshop on the Microcalorimetry of Energetic Materials, Leeds, UK* 1997.
- ⁹ L. Paulsson, "Influence of Humidity on the stability of propellants", *Proc. Eleventh symposium on the Chemical Problems Connected with the Stability of Explosives* 1999
- ¹⁰ E. Camera, G. Modena, B. Zotti, "On the Behavior of Nitrate Esters in Acid Solution II. Hydrolysis and Oxidation of Nitroglycol and Nitroglycerin", *Propellants, Explosives, Pyrotechnics*, 7, 66-69 1982
- ¹¹ E. Camera, G. Modena, B. Zotti, "On the Behavior of Nitrate Esters in Acid Solution III. and Oxidation of Ethanol by Nitric Acid in Sulfuric Acid", *Propellants, Explosives, Pyrotechnics*, 8, 70-73 1983

THIS PAGE LEFT INTENTIONAL BLANK

Mechanistic Approach to Study the Moisture and Acidity Effect on the Stability of Single and Double Based Propellants

Anton Chin and Daniel S. Ellison
Test & Evaluation Department
NSWC
Surface Warfare Center Division
Crane, In 47522-5001 USA

Abstract

Single and double-base propellants typically use DPA, 2-NDPA, EC or AK as stabilizers to slow down the aging and degradation processes. The functional group (reactive site) of the stabilizer is the amino group attached to at least one conjugated pi electron system (i.e. aromatic benzene, etc.). It is a well-known fact that the amino group with an available lone pair of electrons will trap the nitrogen oxides produced during the decomposition of nitrocellulose. The reactivity and basicity of the lone pair of electrons depend mainly on the aromaticity (resonance effect) and electronegativity (inductive effect) of the groups attached to the amino group. Due to this reason, the effectiveness of this type of stabilizer is highly pH dependent.

Results from Heat Flow calorimetric analysis strongly indicates that the effectiveness of the stabilizer falls within a certain but yet undefined pH range. This might mean even a slight change of the acidity of the propellant composition could seriously affect the effectiveness of the stabilizer and subsequent safety of the propellants. From a reaction mechanistic point of view, whether the intermediate of stabilization process is an "adduct" at higher moisture content or an ammonium ion at a lower pH value, the protection power of the stabilizer will be hindered. In this paper, we will explain the effects of moisture and acidity to the shelf life of propellant composition based on very fundamental reaction mechanisms. Correlation of real time heat flow curve and stabilizer depletion mechanism is also discussed.

INTRODUCTION

Nitrocellulose (NC) based propellants require routine chemical stability testing since the inherent instability of NC leads to self-ignition. During the last century, enormous numbers of tests has been devised to survey their stability. The Time-To-Fume (Red Fume) test is among one of the earliest methods and is still being used today to determine

Approved for public release; distribution is unlimited

the safety of gun propellants. However it was found that although the test is rather simple and empirical in nature it sometimes can not represent the real aging process. During the last three decades, modern analytical techniques such as HPLC (High Performance Liquid Chromatography) and HFC (Heat Flow Calorimetry) have been developed to improve the accuracy of predicting the safe storage life of gun propellants.

A Combination of traditional and modern methods gives more helpful information about the component studied. The correlation and translation of the results into terms of stability, compatibility and remaining useful shelf life of the complex mixture of ingredients in a gun propellant is still a problem. The major problem is that the results produced from each method often do not agree and have huge standard deviations. The differences are probably caused by so many variables involved in the nitrate ester decomposition processes (i.e., moisture and acid content, oxygen level, presence of strong nucleophiles and electrophiles, quantity of stabilizers, plasticizers and inhibitors, sample geometry and loading density, etc.). Since most of the current testing methods do not specifically aim to detect both quantity and effects of all these factors, the prediction of service life mainly depends upon how we interpret the kinetic effect of these variables. It should be noted that it is not just the stabilizer depletion kinetics plays an important role in the degradation mechanism of propellant aging processes. Acid, water, inhibitors and many other components mentioned above are also key factors that affect the overall kinetics. Therefore, a test without well-controlled conditions will seriously affect the reproducibility and accuracy of the test data.

It is the objective of this paper to understand more about the mechanism how acid and water may affects the kinetics of the nitrate ester decomposition reaction and the linearity of the Arrhenius plot below 60°C. It is also our goal to demonstrate how through the understanding of the true reaction mechanisms, a more accurate method can be chosen to predict the shelf life of gun propellants.

MECHANISMS OF CHEMICAL DECOMPOSITION AND STABILIZATION OF NITRATE ESTERS

I. DECOMPOSITION

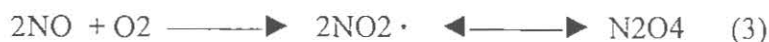
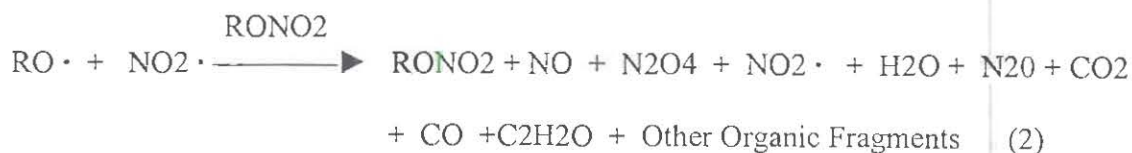
Degradation of nitric esters generally involves two major routes: the thermolysis and the hydrolysis. To illustrate this, a simple schematic of degradation and stabilization equations is listed below:

A. Thermolysis – dissociation induced by heat usually resulted in free radical products

Initiation Step



Propagation Steps



B. Hydrolysis – dissociation induced by acid hydrolysis

Initial Steps



Propagation Steps



In this paper we will focus the discussion on the very basic decomposition mechanism published by the literature [1,2,3]. It will not be surprising that the actual mechanism could be far more complicated than these. In all of the above reactions, only the N_2O_4 ($2\text{NO}_2 \cdot$) produces a red and brownish color. The $\text{NO}_2 \cdot$ is the key factor to initiate the chain reaction (Equation 2) that leads to more degradation. However, despite the decomposition route, the rate of formation of $\text{NO}_2 \cdot$ is always controlled by the amount of water and acids (Equation 6), precursor NO and oxygen (Equation 3) present in the system.

In a microcalorimetric study of the influence of moisture and a small amount of nitric acid on nitrocellulose, Paulsson reported that with the addition of water the onset time of accelerated degradation of nitrocellulose will be longer, but the maximum heat released will be higher than that of drier nitrocellulose. With the addition of small amounts of

nitric acid, the onset time will be earlier [4] (Figure 1). Crane scientists found similar results by a separate experiment with double base gun propellants [5] (Figure 2).

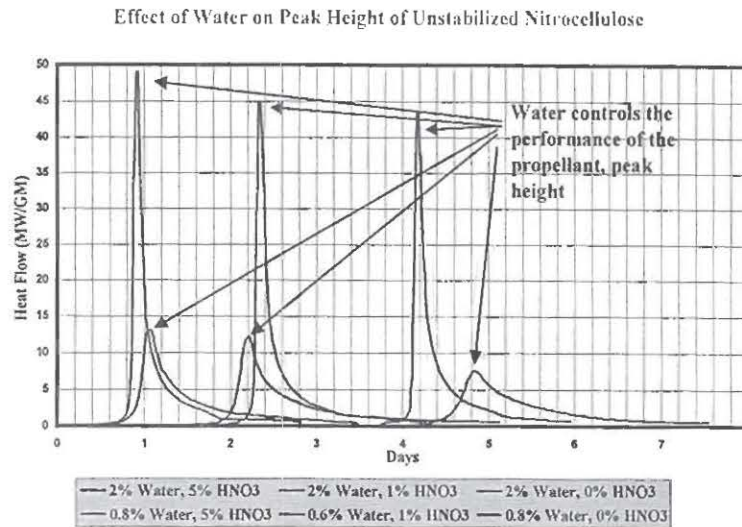


Figure 1. Influence of acid and water on the stability of propellants (Paulsson)

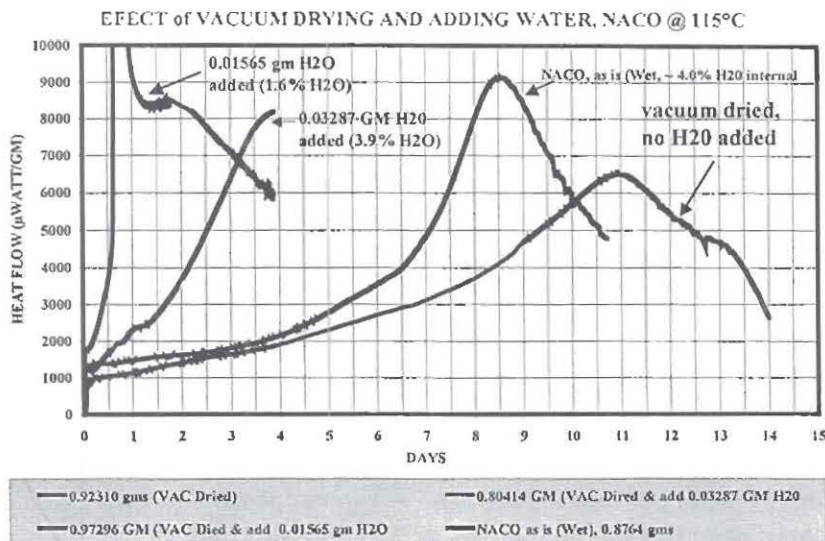


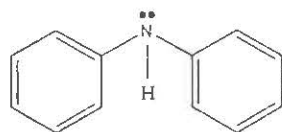
Figure 2. Effect of adding water to dried NACO propellant (Ellison & Chin)

It should be noted that there is a very delicate balance among nitrocellulose decomposition mechanisms. Even a small change in concentration of moisture, acid, oxygen, stabilizer, etc, will shift the direction of chemical equilibrium of the decomposition reactions.

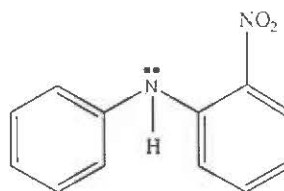
For example, if the propellant is getting drier, the relatively more concentrated nitric acid will begin to inhibit the normal function of the stabilizer. With increasing acidity, the nitrate ester will become more stable even without the protection of the inhibited stabilizer because at high concentrated acid condition the equilibrium favors the formation of nitrocellulose. When a small amount of water (<2% by weight)) is added, the condition of the dry propellant will quickly reach the critical point that a rapid acid hydrolysis may occur. With excess of water (>>>>2%), the stabilizer will be inhibited by solvation. The rate of acid hydrolysis of NC will also be reduced because of massive dilution by water. With this in mind, we know there must a delicate balance point between the quantity of acid/water and safety/performance of the propellant.

II. STABILIZATION

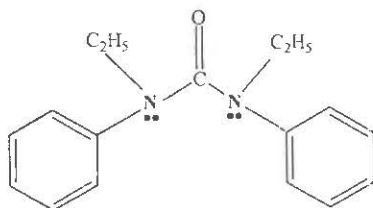
Four stabilizers are of interest for application in gun propellants in the United States; diphenylamine (DPA), 2-nitrodiphenylamine (2-NDPA), ethylcentralite (EC), and Akardite (AK).



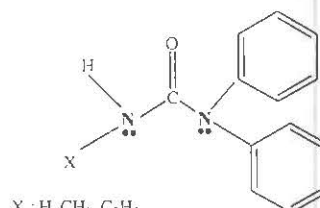
Diphenylamine



2-Nitrodiphenylamine



Ethyl Centralite



X = H, CH₃, C₂H₅

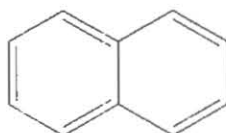
Akardite

DPA is used in single-base propellants but is incompatible with nitroglycerin and so can not be used in double-base and triple-base compositions. EC or 2-NDPA is used for double-base and triple-base propellants that use nitroglycerin as the gelatinizing agent for the nitrocellulose. Akardites are used in propellants that contain diethyleneglycol dinitrate (DEGN) rather than nitroglycerin. The details of the stabilizer depletion mechanism are well known and widely published in the literature [1]. An ideal, effective stabilizer should have a reaction rate fast enough to trap the nitrogen oxides before the later has a chance to react with nitrocellulose. However, the reactivity of the stabilizer must be controlled within a range so it will be compatible with the other ingredients in the propellant composition. There are three major factors that control the kinetics and mechanism of the stabilization reaction.

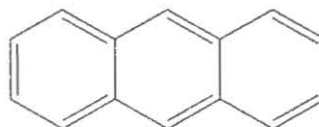
A. Aromaticity (Resonance Effect): An ideal stabilizer usually has its active site (functional amino group) attached to at least one aromatic group. Monocyclic pi system of $4n + 2$ electrons (where n is an integer) have the special stability associated with filled orbital shells. For benzene, $n = 1$; whereas for naphthalene, $n = 2$; and anthracene, $n = 3$. Such systems are said to be aromatic and to have aromatic stability (aromaticity). Aromatic compounds with high aromaticity should better control the reactivity of the stabilizer and accommodate more nitrogen oxides. The following are few commonly used aromatics.



Benzene

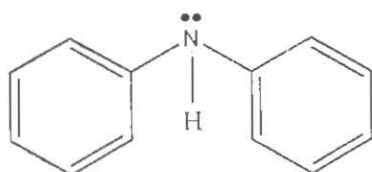


Napthalene

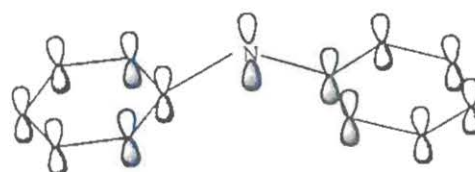


Anthracene

With two phenyl rings attached to the amino group of DPA, the lone pair electrons are further stabilized by more resonance energy generated by the p orbital overlapping in the aromatic ring. Because of the p orbital delocalization, the partial pyramidal structure of the amino orbital is forced to become more planar and therefore can conjugate with the phenyl pi system more effectively. Conjugation with the phenyl ring also decreases the basicity of the amino group in DPA that brings the reaction rate to a desirable range.

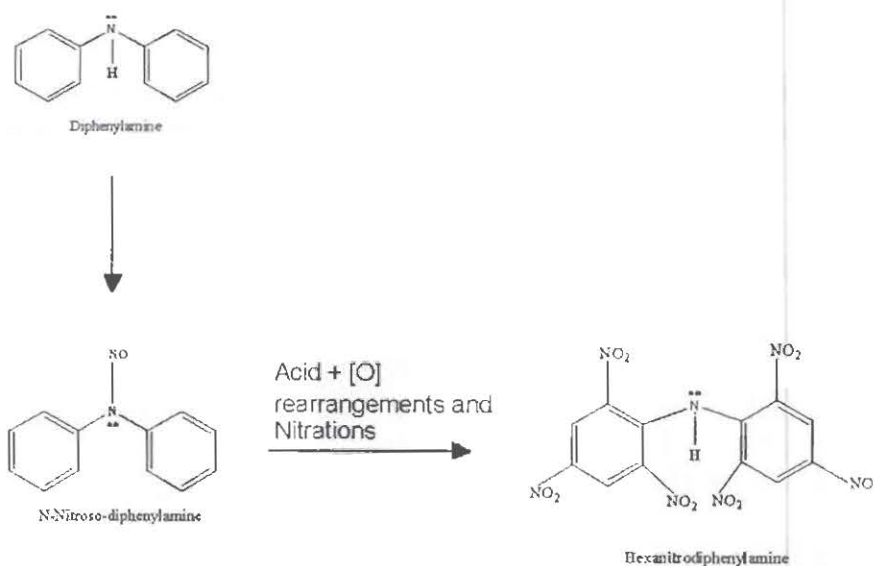


Diphenylamine

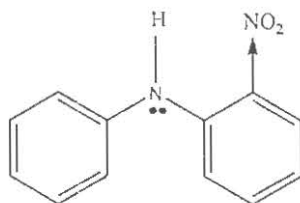


Diphenylamine

In addition to the rate controlling function, the aromatic group can accommodate more nitro groups rearranged from the N-nitroso intermediate. This multiple number of equivalents make the stabilizer much more effective than the non-aromatic one. The number of aromatic groups on the stabilizer affects the reactivity and effectiveness of that stabilizer.



B. Electronegativity (Inductive Effect): An element with full s and p orbitals in the outer electron shell is known as an octet. An octet is the electron configuration of an atom consisting of 2 s subshell and 6 p subshell electrons. Elements with this configuration are known to have exceptional stability (i.e. inert gas family). The power of an atom or a group of atoms to attract a shared pair of electrons to satisfy the octet rule is called its relative electronegativity. The elements in fluorine and oxygen families need only one and two electrons, respectively, to fill the p orbitals (to fulfill the octet rule). Therefore the electronegativity of these elements is relatively higher than the rest of the elements in the periodic table. For example 2-NDPA is less reactive than DPA because the electronegative NO₂ attached to the number two carbon of one the phenyl rings pulls back the electrons from the active amino group. This pullback action is called the “inductive effect”. Because of this, 2-NDPA with less electron density on the amino group is less reactive and therefore more compatible with nitroglycerine in the double-based propellants.



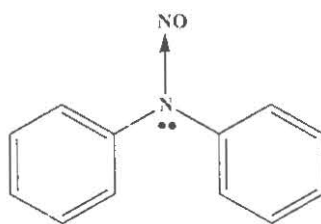
The first generation of daughter products of DPA are still effective to attract nitrogen oxides but at a slower rate. Based on the principle of aromaticity and electronegativity, the effectiveness of commonly used stabilizers to trap nitrogen oxides are in the following order:

DPA > 4-NDPA, 2-NDPA, EC > AK*, 2,2'-DNDPA, NEC > TNDPA, DNEC, etc.....

DPA = diphenylamine, 2-NDPA = 2-nitrodiphenylamine,
 4-NDPA = 4-nitrodiphenylamine, 2,2'-DNDPA = 2,2'-dinitrodiphenylamine,
 TNDPA = trinitrodiphenylamine, EC = ethylcentralite, NEC = nitrocentralite,
 DNEC = dinitroethylcentralite, AK = Akardite

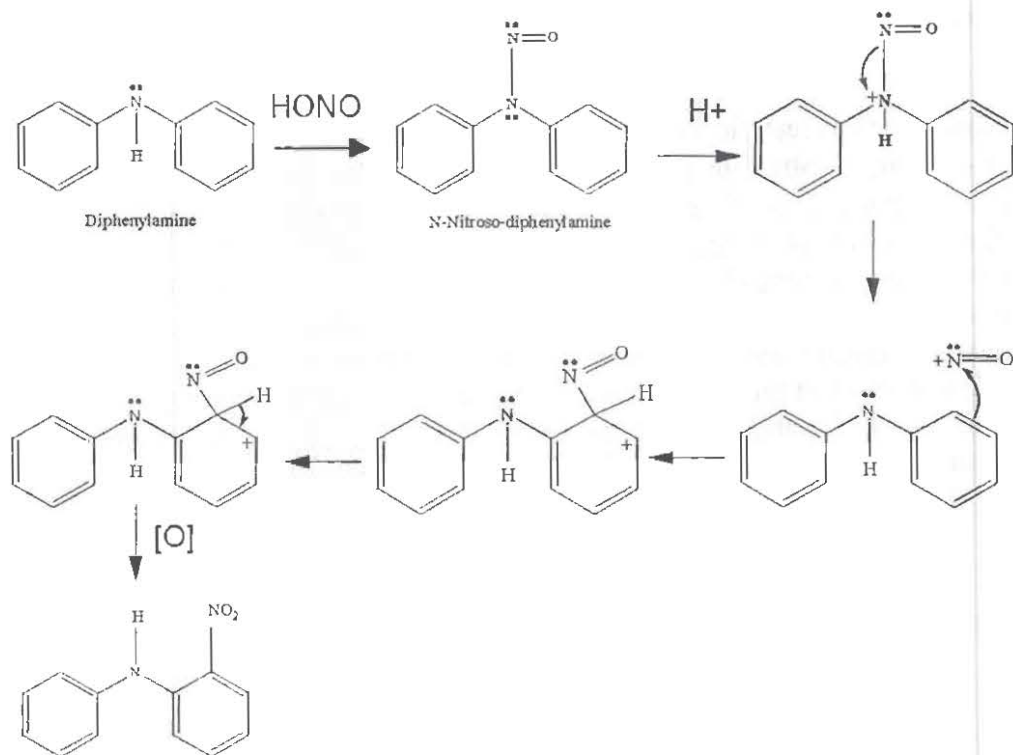
*(note: The rate could be changed if more NG is in the composition)

The higher the nitration, the less reactive is the stabilizer. An amino group of less electron density will have lower basicity and nucleophilicity to trap nitrogen oxides that have a partial positive charge on the nitrogen atom. On the other hand, the nitroso intermediate (NO) on the amino group of DPA is also an electron-withdrawing group. The NO pulls the electrons away from the benzene group that deactivates the electrophilic aromatic substitution. For example, N-nitroso-diphenylamine is unable to react with nitrogen oxides at neutral condition (~pH 7).

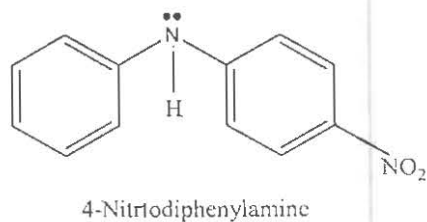
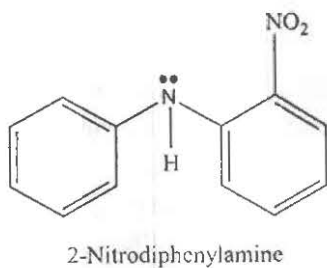


N-Nitroso-diphenylamine

Only under the right acidic condition will the NO rearrange to the aromatic ring by either intra-molecular or inter-molecular pathway. Since the amino group is an ortho, para director, the first generation products are predominantly 2-NDPA and 4-NDPA.

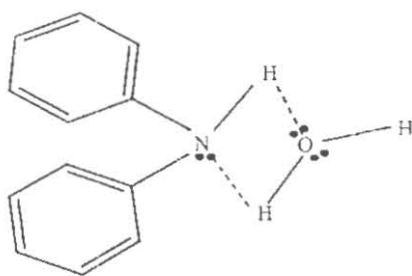


It should be noted that steric hindrance also plays an important role on the reactivity of the stabilizers. 2-NDPA is slightly less reactive than 4-NDPA in trapping nitrogen oxides because the lone pair electrons is blocked by the nitro oxide on the # 2 carbon nearby.



The cycle of nitrosation, rearrangement and electrophilic aromatic substitution (nitration) will continue until all the available positions on the aromatic ring are filled. Since the concentration of acid is critical for the rate of nitration, the effectiveness of stabilizer is highly pH dependent.

C. Inhibition: Results from Heat Flow Calorimetric analysis strongly indicated that the effectiveness of the stabilizer falls within a certain but not yet defined pH range. This might mean even a slightly change of the acidity of the propellant composition could seriously affect the effectiveness of the stabilizer and safety of the propellants. From a reaction mechanistic point of view, whether the intermediate is solvation adduct at higher moisture content, or ammonium ions at a concentrated acid condition (at a pH much lower than acid catalyzed rearrangement in the abovementioned electronegativity section), the protection power of the stabilizer will be hindered. Under a much higher moisture condition, the reactive amino center of the stabilizer will be completely solvated by the water molecule. Solvation is the formation of an adduct mainly by charge attraction between the amino group (in our case) and water molecule through hydrogen bonding, etc..



Solvation of DPA

Although the active amino group of a solvated stabilizer is inhibited and unable to trap the nitrogen oxide effectively, the rate of degradation of NC is decreasing with increasing water content. The reason is the hydrolysis of NC is pH dependent, and a very diluted acid will not be strong enough to catalyze the decomposition. This is a part of the reason that many sensitive propellants are shipped in water. With the protection by solvation, the rate of depletion of stabilizer is also very slow. Paulsson and Leffers both reported

the exceptional stability of DPA stored under high water condition [4,6]. The normal reactivity of the stabilizer resumes when water is removed from the system.

One important thing worthwhile to mention is that people tend to increase the stabilizer content (i.e. >3%) to attain a longer shelf life. On the contrary, too much stabilizer will decrease the shelf life of propellant by increasing its pH value to relatively more basic conditions. It is a well-known fact that rearrangement of the nitroso intermediate to the aromatic ring requires an acidic condition to catalyze the electrophilic aromatic substitution. Under more basic conditions, the rearrangement is not favored. This will cause the active amino group of the stabilizer to be blocked by the nitroso group. The hindered stabilizer will no longer be able to take any more nitrogen oxides until rearrangement occurs again. Propellant compositions with a higher pH value will also destabilize the nitric ester (note: nitric esters are not stable in basic condition) by a SN2 reaction (Nucleophilic Substitution of the Second Order). Therefore, maintaining a delicate balance of water and acid content (pH value) is extremely important for a long safe storage life and performance of the propellants.

DISCUSSION AND CONCLUSION

Nitrocellulose based propellants often have a fixed acid and water content during the manufacturing time. After manufacture the quantity and ratio of acid /water will continue to vary depending upon the aging conditions of storage and operation. The level of variation depends on many factors such as: loading density, temperature, volume of ullage and sealing condition of the containing cartridge, etc. just to name a few. As described in this paper and many other literatures, the degradation mechanism and aging processes involving acid and water are extremely complicated and very little is known as of today. Therefore an integral test method that can truly represent the entire aging process must be used to determine the safe shelf life of the propellants. Heat Flow Calorimetry (HFC) is the only method that can meet all these requirements. Without the need to know the complicated mechanisms, anyone can easily see the aging and safe condition of the propellant through a simple HFC heat flow curve. The complete life cycle of aging profiles including the depletion of parent and daughter stabilizers, as well as the effects of acid/water, etc., will be shown entirely by one heat flow curve (Figure 3).

As mentioned in the Introduction Section of this paper, the effect by acid and water is tremendous. Based on microcalorimetric analysis of the influence of acid and water on the stability of propellant, Paulsson [4] found with the addition of a small amount of water the rate of degradation drastically increases (from first to zero order, a performance issue). On the contrary, addition of an excess amount of water will decrease the rate of degradation [5]. With the addition of acid the onset time of auto-ignition will start much sooner (a safety issue). However, there must be an optimal but not yet defined pH range that can give the propellant maximum safe shelf life and superior performance. This range could be very narrow.

In a study of vapor density as a function of temperature, we found the linearity of Arrhenius plot of vapor density vs. $1/T$, has changes at 60 °C. This nearly coincides with the HPLC analysis of stabilizer depletion reported by Bohn that the rate of depletion changes at 60 °C [7,8,9]. The two different slopes mean that there may be two different mechanisms involved in the depletion of DPA: one above 60°C and one below. This finding will seriously affects the accuracy of prediction of the safe shelf life that depends on the linear extrapolation from high to ambient temperature. After careful analysis, we believe that this change of slope is most likely due to the water effect. If there is ullage in the test ampoule, the vapor density will be lower in the ullage than expected at below 60 °C (figure 4). This also means the quantity of moisture will be relatively higher inside the propellant. If this is the case, the rate of depletion of DPA will increase as a result of faster NC decomposition [4,5].

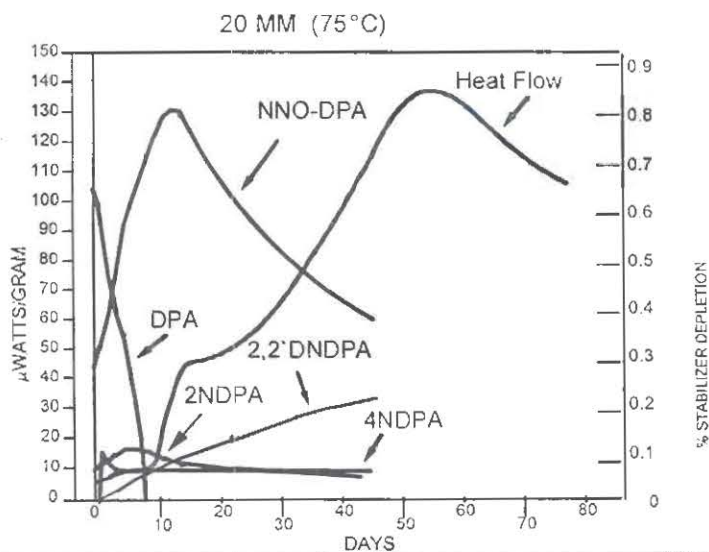


Figure 3. . Heat Flow Curve of 20 mm Gun Propellant vs. HPLC Stabilizer depletion Analysis. DPA is the Parent stabilizer. NNO-DPA is the Intermediate Which Will be Rearranged After Oxidation to the Daughter Products (2NDPA, 4NDPA, and 2,2' DNDPA, etc.).

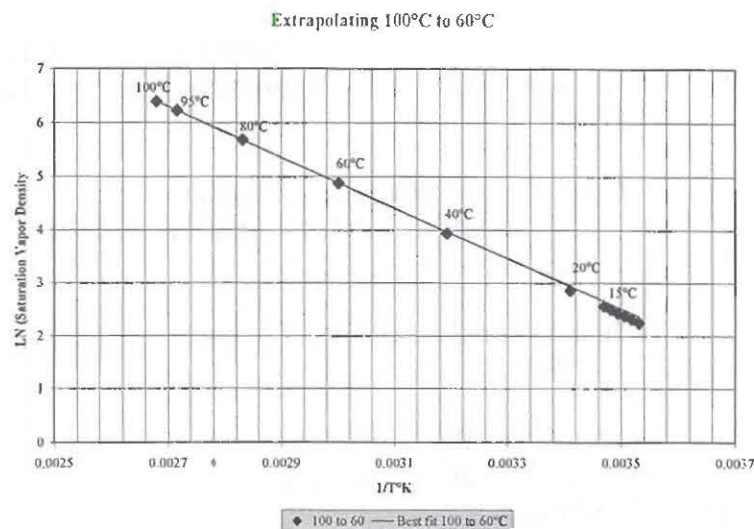


Figure 4. Vapor density versus temperature

With good control of the experiments, both Bofor [10] and Crane [11] found almost perfect linearity from 80 to 40 °C in the Arrhenius plot use heat flow data. However, we do occasionally obtain data that produces a non-linear plot below 60 °C. We believe this is probably caused by inconsistent test conditions where water and ullage play an important role to the kinetics. Therefore, in order to obtain more accurate data, the test condition must be as close as possible in representing the true condition of the actual devices. For example, in 20-mm gun ammunition there is 36 grams of doublebase propellant. Our tests indicate that the actual water content in the propellant controls the stability. The test must reflect the differences in a typical 4 gm test sample used in the microcalorimeter and that of the actual sample.

REFERENCES

1. L. Druet and M. Asselin, "A Review of Stability Test Methods for Gun and Mortar Propellants". Defence Research Establishment, Valcartier, Quebec Canada. J. of Energetic Materials, (1986), and references therein.

2. E. Camera, G. Modena and B. Zotti, "On the Behaviour of Nitrate Esters in Acid Solution. II. Hydrolysis and Oxidation of Nitroglycol and Nitroglycerin". *Propellants, Explosives, Pyrotechnics* 7, 66-69 (1982).
3. E. Camera, G. Modena and B. Zotti, "On the Behaviour of Nitrate Esters in Acid Solution. III. Oxidation of Ethanol by Nitric Acid in Sulphuric Acid". *Propellants, Explosives, Pyrotechnics* 8, 70-73 (1982).
4. L. E. Paulsson, "Influence of Humidity on the Stability of Propellants". *Symp Chem Probl Connected Stabil Explos*, 11th (1998).
5. D. S. Ellison and A. Chin, "Understanding the True Driving Force in the Auto-Ignition of Single and Doublebase Propellants using Microcalorimetry". *Symp Chem Probl Connected Stabil Explos*, 14th (2001).
6. R. Leffers, R. Scheibel and H. Jahnk, "Propellant Surveillance in the Scope of Ammunition Surveillance". WTD 91 (federal Armed Forces Technical Center for Weapons and Ammunition), Meppen, Germany, June 22-24 (1993).
7. M. A. Bohn and F. Volk, *Propellants, Explosives, Pyrotechnics* 17, 171-178 (1992).
8. M. A. Bohn, *Propellants, Explosives, Pyrotechnics* 19, 266-269 (1994).
9. M. H. Sammour, *Propellants, Explosives, Pyrotechnics* 19, 82-86 (1994).
10. L. G. Svensson, L. E. Paulsson and T. Lindblom, "A Microcalorimetric Study of Temperature and Stabilizer Effects on the Heat Generation in Gun Propellants". 4th Gun Propellant Conference, Mulwala, Australia (1990).
11. A. Chin and D. S. Ellison, "20 mm Gun Propellant Safety Service Life Study Using Microcalorimetry/HPLC Correlation Diagram". 1997 International Workshop on Microcalorimetry, Leeds, UK, April 7-9th (1997).

HFCS 2001/2 SESSION MINUTES

Session 3

Question asked by: Lars-Gunnar Svensson, Bodycote Materials Testing CMK, SWEDEN

Question directed to: Anton Chin, NSWC Crane

Question: What type of reaction in the complex degradation of the propellant is expected to contribute most to the total heat output measured in HFC?

Answer: The heat generated from bond formation of the products of NO_x and acid catalyzed decomposition of Nitrocellulose (NC) are contributing to most of the total heat output. It is well known that the nitration of NC and stabilizers are slightly endothermic. However, the products formed from the decomposition are exothermic and net enthalpy is slightly positive at the beginning of the decomposition reaction. The rate and magnitude of total heat output increase rapidly (autocatalysis) when most of the effective stabilizers are nearly consumed.

THIS PAGE LEFT INTENTIONAL BLANK

Stability Studies of Red Phosphorus using Heat Flow Microcalorimetry

T T Griffiths
QinetiQ,
Fort Halstead, Sevenoaks,
Kent, TN14 7BP, UK.

E L Charsley and S J Goodall
Centre for Thermal Studies, University of Huddersfield,
Queensgate, Huddersfield HD1 3DH, UK.

P Barnes
Defence Ordnance Safety Group,
Abbey Wood, Bristol, BS34 8JH, UK.

Abstract

Red phosphorus is widely used for the production of smoke and obscurant munitions particularly when a multi-spectral performance is important. A preliminary study has been carried out on the ageing behaviour of red phosphorus in air and in argon at 50°C and at a range of relative humidities using isothermal heat flow microcalorimetry.

The experiments in air and argon confirmed that the presence of oxygen was required for the reaction to proceed at a significant rate. In addition, the rate of reaction in air was found to increase with increasing relative humidity. However, it was established that the reaction could also proceed in the absence of an external source of moisture.

The addition of a stabiliser and microencapsulant was found to have a marked effect on the reactivity of red phosphorus. Tin hydroxide appeared to be a more effective stabiliser than aluminium hydroxide and two of the samples containing tin hydroxide were found to have a 3 day cumulative heat value approximately 1% of that given by the red phosphorus sample containing only a dust suppressant.

Introduction

Phosphorus is too reactive to be found free in nature and is obtained primarily by the reduction of phosphate rock, essentially calcium phosphate, with coke and silica in an electric furnace. Phosphorus shows extensive allotropy, the three main forms, which have distinctive appearances and properties, are white (or yellow), red and black.

Red phosphorus is used as a flame retardant in the plastics industry and in the production of safety matches and metal phosphides. It is produced from white phosphorus by a thermal conversion process. It is also used in the manufacture of smoke and obscurant munitions particularly when a multi-spectral performance is important. Two main problems are associated with its use as a pyrotechnic ingredient. The first is the flammability of the material that can cause fires during processing; the second is the instability of the phosphorus and the resultant evolution of phosphine during storage. The fire hazard is countered by the use of an anti-dusting agent and stabilisers are used to suppress the reactivity.

Red phosphorus burns in air to produce a dense cloud of phosphorus oxides. Phosphorus pentoxide (P_4O_{10}) is formed in an excess of air and phosphorus trioxide (P_4O_6) is formed when the air supply is restricted. These acid anhydrides readily absorb and react with atmospheric water to form products such as phosphorous acid H_3PO_3 .

In excess air the reactions are:



and



Red phosphorus undergoes an important series of degradation reactions at room temperature in the presence of oxygen and moisture to produce phosphoric, phosphorous and hypophosphorous acids and small quantities of the highly toxic gas phosphine. The mole fraction of the acids vary slightly with the duration and conditions used but the ratio is reported [1] as being approximately 0.40:0.55:0.05, with ratio of phosphorus in the acids and the phosphine being approximately 13 to 1. The overall reaction was described by the equation:



The mechanism of the reaction is not fully understood but both oxygen and water are reported to be necessary for the reaction to take place. The reaction can be catalysed by traces of certain metal ions including copper and iron [2]. Phosphine is a colourless gas with the odour of garlic; it is a strong reducing agent. It is possible that hydrogen may also be produced by the oxidative hydrolysis of phosphorus, although this is uncertain and the mechanism is unclear.

There are concerns over the toxicity of phosphine especially if it collects in an enclosed area for example, in a magazine, on-board ship. The reliability of munitions containing phosphorus can be reduced if they contain copper components that can be attacked by phosphine, or ingredients like magnesium that degrade in the presence of phosphoric acids. The hydrogen formed in the magnesium degradation reaction is itself a safety hazard and the formation of any gas in a sealed system can result in pressurisation and subsequent swelling or bursting of munitions.

Understanding the underlying mechanisms causing the degradation of red phosphorus and determining ways of overcoming the problem is currently the subject of TTCP KTA 4-27. Academia, Government Departments and Industry from Australia, UK and the US are participating in the programme.

This paper describes a preliminary study on the degradation of red phosphorus using heat flow calorimetry, experiments were performed on five different commercial grades obtained from two manufacturers.

Experimental

The ageing behaviour of red phosphorus has been studied by isothermal heat flow calorimetry in air and argon at 50°C and a range of relative humidities. Most of the work was carried out on a commercial grade of red phosphorus (99% purity) which had been coated with a dioctyl phthalate dust suppressant but other samples coated with a range of stabilisers and microencapsulants were also examined (Table 1). Samples RP4, which was supplied by a different manufacturer, was stabilised and encapsulated with the same materials as RP3.

The measurements were performed using a Thermometric Model 2277 Thermal Activity Monitor. Each sample (100 mg) was sealed in a 3 cm³ glass ampoule along with a small glass tube containing water or a saturated salt solution. This maintained the relative humidity at the required level during the experiments which, in general, continued for three days.

Table 1. Red Phosphorus Samples Examined

Sample Number	Stabiliser	Microencapsulant	Dust Suppressant
RP1	None	None	Diethyl phthalate
RP2	Aluminium hydroxide	Epoxy resin	Diethyl phthalate
RP3	Tin hydroxide	Epoxy resin	Diethyl phthalate
RP4	Tin hydroxide	Epoxy resin	Diethyl phthalate
RP5	Tin hydroxide	Melamine- formaldehyde resin	Diethyl phthalate

Results and Discussion

Duplicate heat flow curves obtained in air and in argon at 50°C and 100% RH for a red phosphorus sample RP1, which had been coated with a diethyl phthalate dust suppressant, are compared in Figure 1. In air, the curves exhibited good reproducibility and the maximum heat flow in the region of $1450 \mu\text{Wg}^{-1}$ was observed after approximately 6 hours, followed by a rapid decrease in the signal. In argon, once equilibrium between the water in the liquid and gas phase had been established, essentially no heat flow was observed.

The lack of any significant reaction in argon confirms that oxygen is necessary for the degradation of red phosphorus. Therefore it appeared likely that the rapid decrease in the heat flow signal in air, once the peak maximum had been reached, could be attributed to the depletion of oxygen in the sealed ampoules. In order to investigate this effect, the experiments in air at 50°C and 100% RH were repeated and after three days the ampoules were transferred to a heated dry block at 50°C. The ampoules were then opened and exposed to laboratory air, before resealing and replacing in the microcalorimeter. The signals were monitored for a further period and the heat flow curves obtained between 2 and 4 days are given in Figure 2. Opening the ampoule and replenishing the atmosphere can be seen to have resulted in an increased heat flow, thus confirming that oxygen was consumed during the degradation reaction.

However, the rate of heat flow observed after opening and resealing the ampoule was similar to that observed after two days in the initial experiments and was well below the maximum value. Although an increased heat flow was given when the ampoules were purged with a stream of air before resealing, the signals were still markedly below the peak maximum. An additional factor in the drop in the reaction rate may be therefore be due to a protective effect of the reaction products. It is proposed to investigate this effect using a relative humidity perfusion cell, where the effect of oxygen depletion can be eliminated.

The influence of humidity on the rate of reaction of the unstabilised sample RP1 has been investigated. Measurements have been carried out in air at 50°C and RH values of 30.5%, 50% and 74% RH. In addition, experiments were performed on samples which had been sealed in laboratory air i.e. in the absence of a salt solution. The heat flow and cumulative heat curves are shown in Figures 3 and 4, together with measurements made earlier at 100% RH and the heat flow and cumulative heat values are summarised in Table 2.

Table 2. Microcalorimetry Heat Flow and Cumulative Heat Values for Sample RP1 in Air at 50°C and at Different Humidities

RH / %	Heat Flow / μWg^{-1}		Cumulative Heat / Jg^{-1}
	Maximum	At 3.0 days	At 3.0 days
Lab Air	192 ± 4	146 ± 10	45 ± 3
30.5	261 ± 15	196 ± 7	55 ± 4
50	382 ± 15	226 ± 13	62 ± 7
74	1201 ± 17	139 ± 18	143 ± 5
100	1450 ± 21	96 ± 0	135 ± 1

In general the rate of reaction can be seen to increase with increasing humidity and this increase becomes particularly marked when the humidity was raised above the 50% level. Comparison of the results obtained at 74% and 100% RH show that although the experiments at the higher humidity gave a higher maximum signal ($1450 \mu\text{Wg}^{-1}$ compared with $1201 \mu\text{Wg}^{-1}$), after approximately 0.7 days the signals decreased below those observed at 74% RH. The cumulative heat curves show that a similar amount of heat has been generated in both cases after 2 days.

The results obtained in laboratory air, show that the red phosphorus can degrade in the absence of an external source of moisture. However, the amount of moisture in the untreated phosphorus is not at present known, although flushing the sample and ampoule with dry air before sealing had little influence on the rate of reaction, compared to a sample sealed in laboratory air. The increase in the heat flow signal on increasing the humidity to 30.5% RH was relatively small and at 3 days the cumulative heat had only increased from 45 Jg^{-1} to 55 Jg^{-1} . The rapid decrease in the heat flow signals obtained at 74% and 100% RH, after the maximum has been reached, has resulted in the signals falling below those obtained in laboratory air after 2.4 and 2.7 days, respectively. This is probably a result of the oxygen depletion in the ampoules.

The stabilised red phosphorus samples have been compared by experiments carried out at 50°C and 74% RH. It was found that the addition of a stabiliser and microencapsulant to the red phosphorus had a marked effect on its reactivity. This is illustrated in Figure 5 where the heat flow curves for the RP1 sample is compared with that obtained for RP2 which was the most reactive of the stabilised samples. The heat flow and cumulative heat curves for the stabilised samples are plotted on an enlarged scale in Figures 6 and 7. It can be seen that the heat flow for sample RP2, which was stabilised with aluminium hydroxide, was essentially constant over the three days at around $50 \mu\text{Wg}^{-1}$. The heat flows for samples RP3 and RP5, which were stabilised with tin hydroxide, showed lower heat flow signals in the region of $18 \mu\text{Wg}^{-1}$. Sample RP4, which also contained tin hydroxide, showed the highest reactivity in the initial stages of the reaction but after three days it had decayed to a similar level to samples RP3 and RP5.

The cumulative heats, measured after three days ranged from 3 Jg^{-1} to 12 Jg^{-1} for the stabilised samples compared to 150 Jg^{-1} for the sample that only contained a dust suppressant. The ranking, from lowest to highest cumulative heat flow, was $\text{RP3} < \text{RP5} < \text{RP4} < \text{RP2} < \text{RP1}$. It

would therefore appear that aluminium hydroxide is a less effective stabiliser than tin hydroxide but that the choice of microencapsulant had less effect on the heat flow curves.

In view of the small heat flow signals obtained at 74% RH for the samples containing a stabiliser, experiments were also performed at 100% RH. The results were essentially the same as those observed at the lower RH. The exception was the sample of RP2, which showed a significantly increased heat flow. This resulted in an increase in the cumulative heat at the end of 3 days from 12 Jg⁻¹ at 74% RH to 38 Jg⁻¹ at 100% RH.

Conclusions

The comparison of the results from the heat flow experiments in air and argon on the unstabilised red phosphorus coated with the dust suppressant dioctyl phthalate showed that the presence of oxygen was required for the reaction to proceed at a significant rate. The rapid reduction in the heat flow as the experiments in air progressed was attributed to the depletion of the limited amount of oxygen in the microcalorimetry ampoule.

The studies on the unstabilised red phosphorus RP1 at different humidities showed that the degradation reaction could proceed at 50°C in the absence of an external source of moisture. However, the amount of moisture in the untreated phosphorus is not at present known, although flushing the sample and ampoule with dry air before sealing has had little influence on the rate of reaction, compared to a sample sealed in laboratory air.

The rate of reaction was markedly increased when the relative humidity was raised above the 50% level. However, the rapid decrease in the heat flow signals obtained at 74% and 100% RH, after the maximum has been reached, meant the signals fell below those obtained in laboratory air after 2.4 and 2.7 days, respectively, presumably due to oxygen depletion. Further work to determine the effect of humidity on the rate of reaction will be carried out using a relative humidity perfusion cell where the effect of reduced oxygen concentration can be avoided. This approach would also allow the possible protective effect of the degradation products to be evaluated.

The addition of a stabiliser and microencapsulant has been shown to have a marked effect on the reactivity of red phosphorus. Aluminium hydroxide appeared to be a less effective stabiliser than tin hydroxide but the choice of microencapsulant appeared to be less important. The differences in stability, observed for samples RP3 and RP4, could result from the quantity of stabiliser or microencapsulant that has been used on the samples.

The cumulative heat for sample RP3 after three days at 50°C and 74% RH, was just over 1% of the sample that only contained a dust suppressant. The ranking, from lowest to highest cumulative heat flow, for the red phosphorus samples examined, was RP3 < RP5 < RP4 < RP2 < RP1.

Increasing the relative humidity to 100% gave essentially the same results as those at 74% RH, the exception was sample RP2 which exhibited a higher heat flow over the period of the experiment. The cumulative heat flow after three days at 100% RH was more than twice as great as the cumulative heat flow at 74% RH.

The studies need to be extended to establish if similar improvements in stability are observed for pyrotechnic compositions containing stabilised red phosphorus. Additionally, the relationship between the heat flow from red phosphorus and the amount of phosphine released needs to be investigated.

References

1. Silverstein, M S, Nordblom, G F, Dittrich, C W and Jakabcin, J J, *Stable Red Phosphorus*, Ind & Eng Chem, 1948, 40, 301.
2. Tarantino, P, *Red Phosphorus Literature Review*, Proceedings of the 1986 Red Phosphorus Symposium, CRDEC, Aberdeen Proving Ground, 1986.

Copyright © QinetiQ 2002

Figures

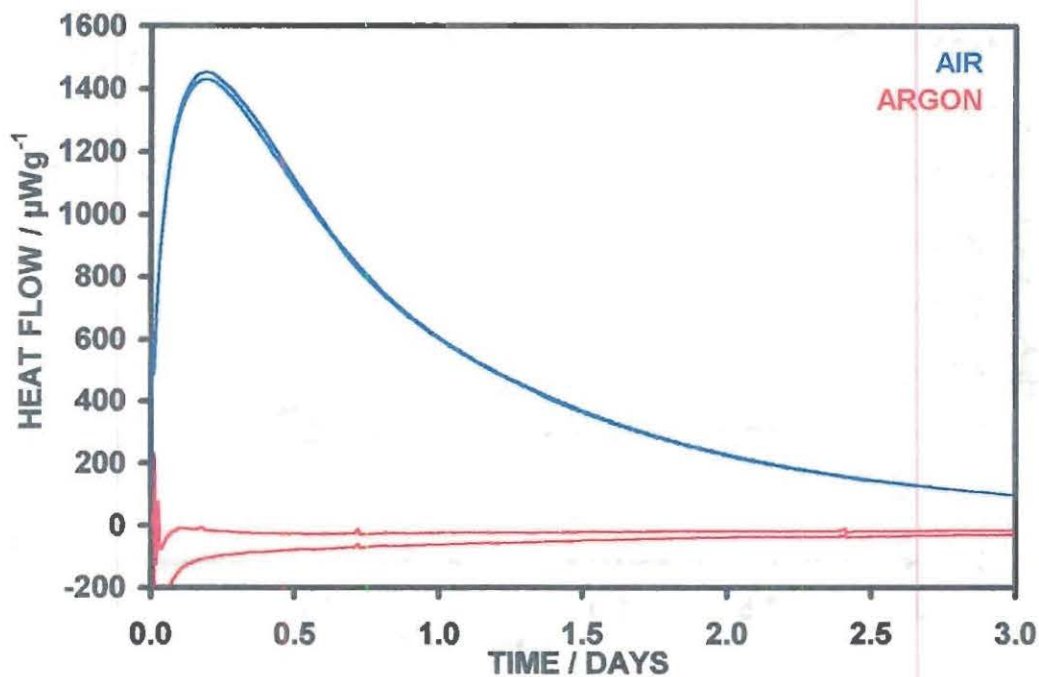


FIGURE 1. MICROCALORIMETRY CUMULATIVE HEAT CURVES FOR RED PHOSPHORUS SAMPLE RP1 IN AIR AND IN ARGON (Sample mass, 100mg; 50°C; 100% RH)

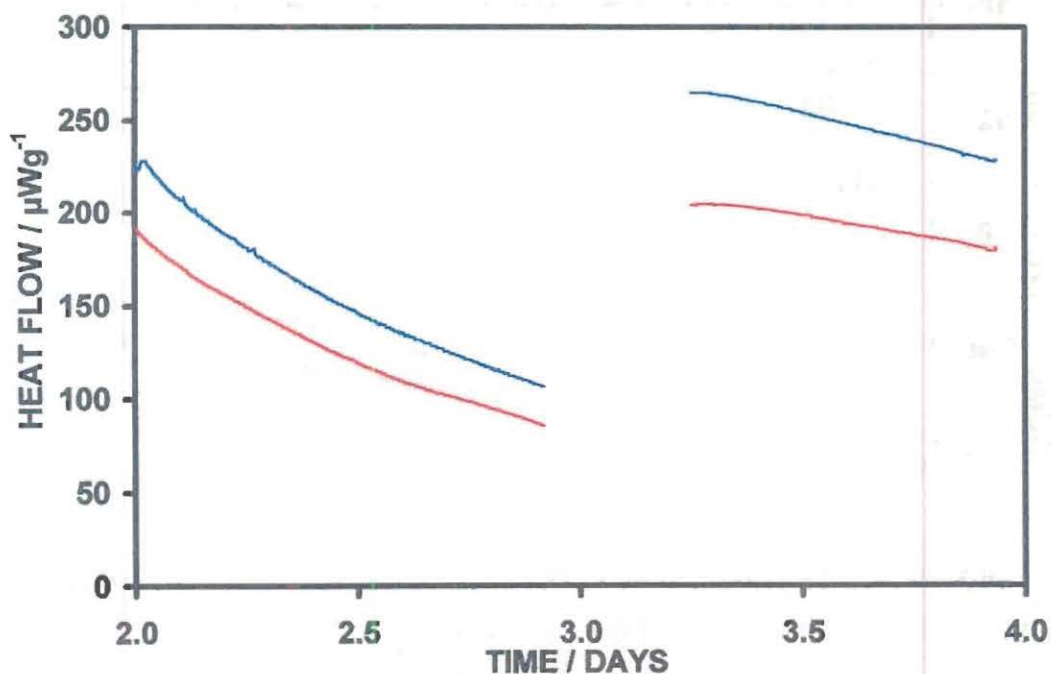


FIGURE 2. MICROCALORIMETRY HEAT FLOW CURVES FOR RED PHOSPHORUS SAMPLE RP1 OPENED AND RE-SEALED DURING EXPERIMENT (Sample mass, 100mg; 100% RH; 50°C; atmosphere, air)

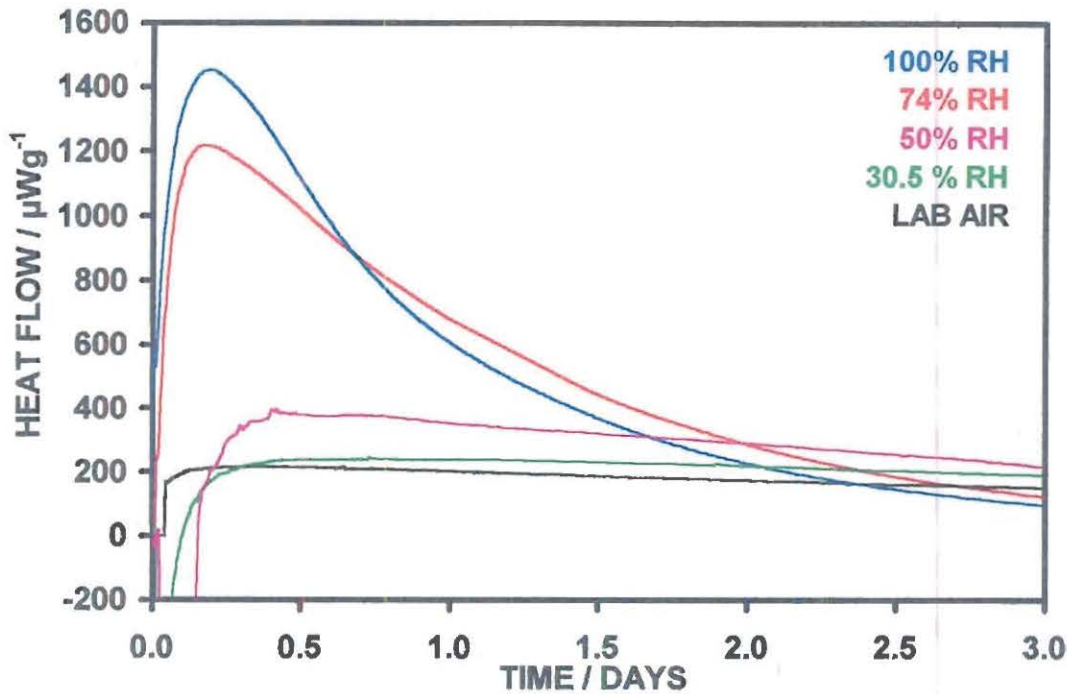


FIGURE 3. MICROCALORIMETRY HEAT FLOW CURVES FOR RED PHOSPHORUS SAMPLE RP1 AT DIFFERENT RH VALUES
(Sample mass, 100mg; 50°C; atmosphere, air)

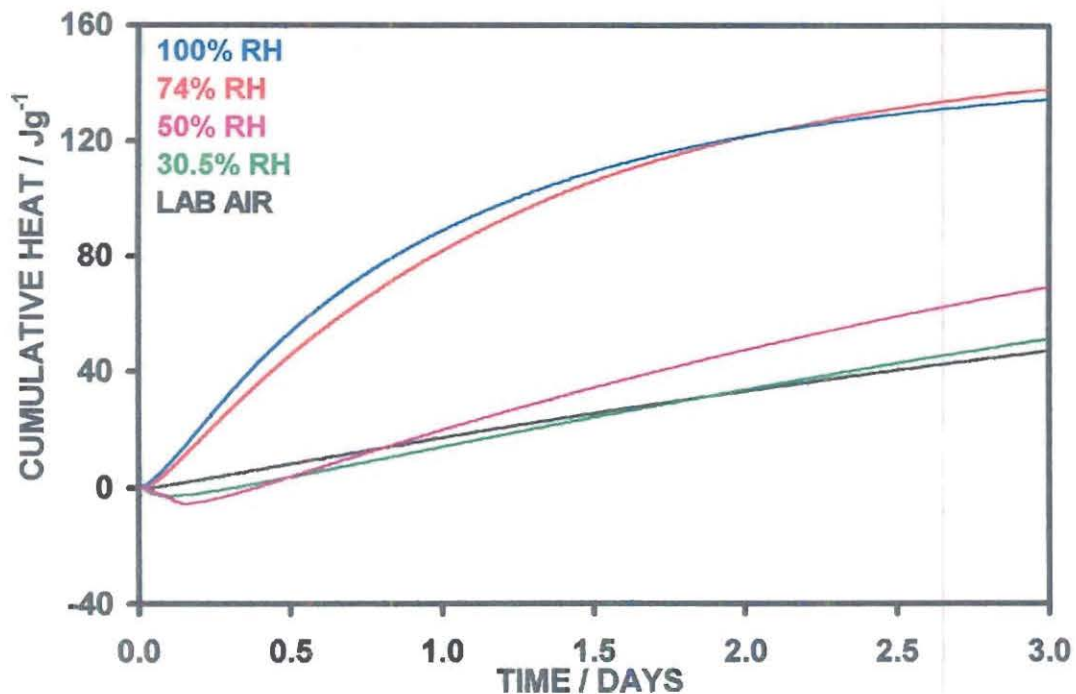


FIGURE 4. MICROCALORIMETRY CUMULATIVE HEAT CURVES FOR RED PHOSPHORUS SAMPLE RP1 AT DIFFERENT RH VALUES
(Sample mass, 100mg; 50°C; atmosphere, air)

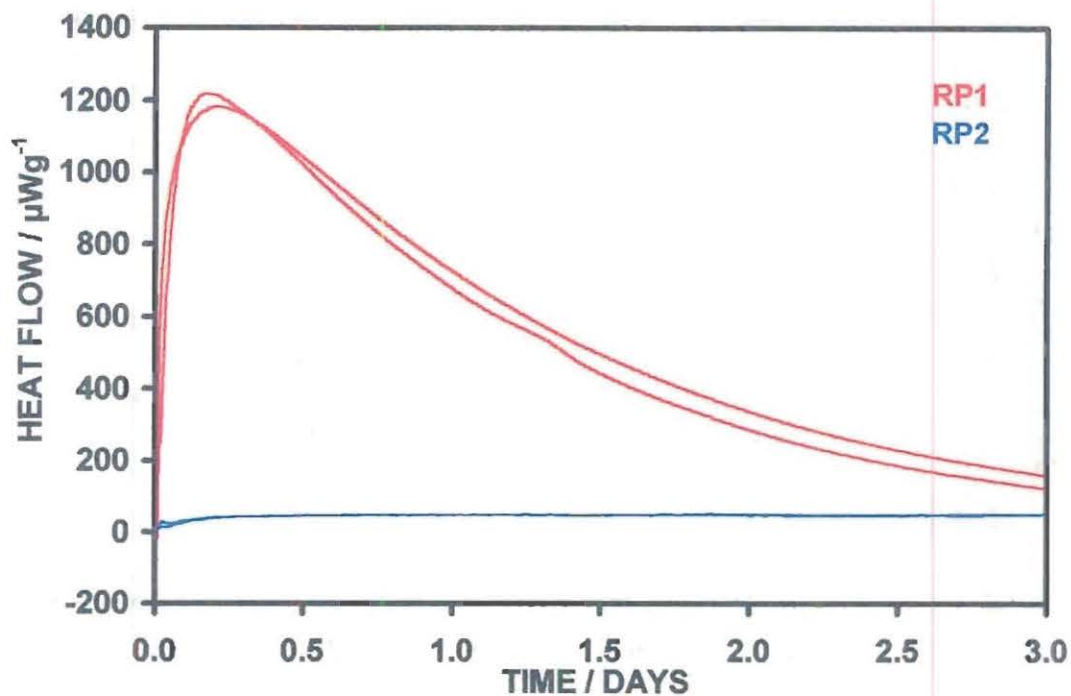


FIGURE 5. MICROCALORIMETRY HEAT FLOW CURVES FOR RED PHOSPHORUS SAMPLES RP1 AND RP2
(Sample mass, 100mg; 50°C; 74% RH; atmosphere, air)

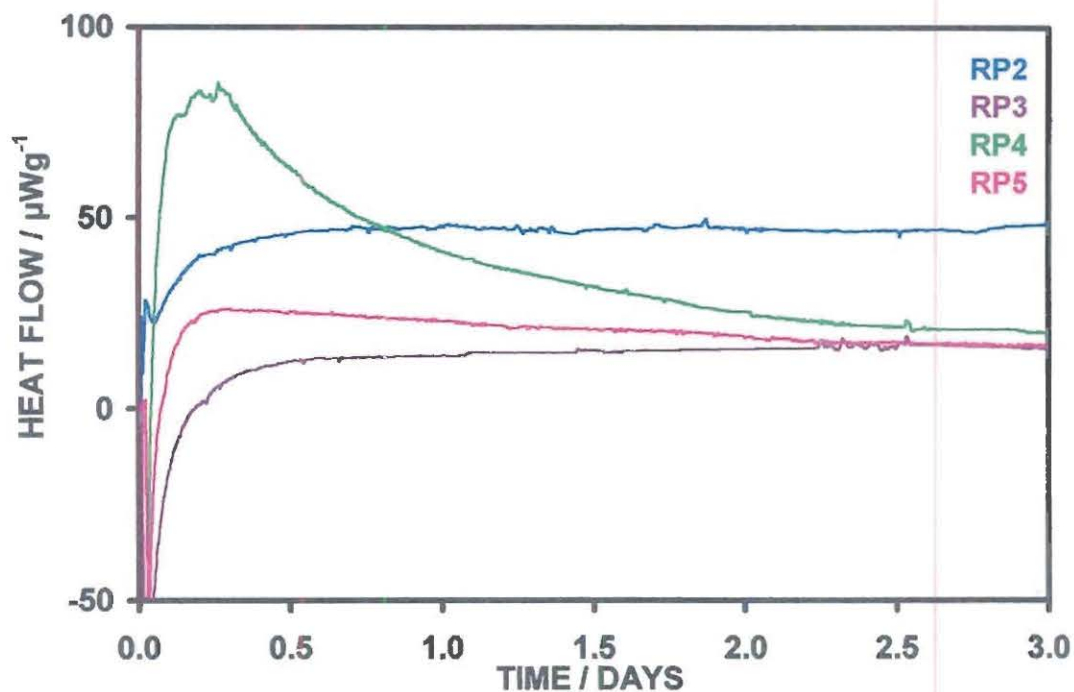


FIGURE 6. MICROCALORIMETRY HEAT FLOW CURVES FOR STABILISED RED PHOSPHORUS SAMPLES
(Sample mass, 100mg; 50°C; 74% RH; atmosphere, air)

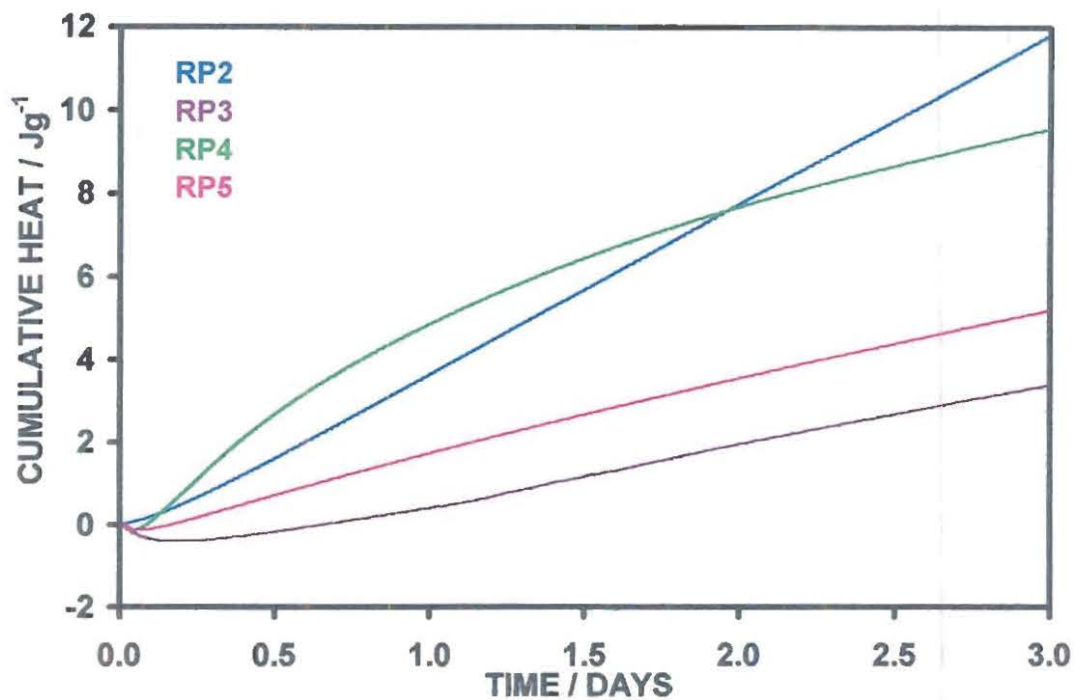


FIGURE 7. MICROCALORIMETRY CUMULATIVE HEAT CURVES FOR STABILISED RED PHOSPHORUS SAMPLES
 (Sample mass, 100mg; 50°C; 74% RH; atmosphere, air)

THIS PAGE LEFT INTENTIONAL BLANK

The Use of DSC in the Analysis of PE as a Burn Rate Modifier

**Joseph A. Domanico
Gene V. Tracy**

**Pyrotechnics Team
Building E3580 Beach Point Road
AMSSB-REN-SP
Edgewood Chemical Biological Center
Aberdeen Proving Ground, MD 21010-5424 USA
410-436-2180**

Abstract

Currently, pentaerythritol is being evaluated as an additive for pyrotechnic smoke formulations that are based on the vaporization of terephthalic acid for their effect. Initial experiments using pentaerythritol as an additive have demonstrated its ability to function as a burn rate retardant for this type of pyrotechnic smoke formulation. While the initial experiments have revealed that pentaerythritol is a burn rate retardant when present in significant quantities, the work also indicated that small amounts of pentaerythritol seemed to function as an accelerant. The work presented in this paper describes the attempt to correlate this observation, based on the burn times of smoke grenades, with DSC results. Several formulations were examined with pentaerythritol contents that ranged from 0 to 12 % by weight.

1. Introduction

Pyrotechnic smoke formulations based on terephthalic acid (TA) are currently used in several smoke items deployed by the U.S. Army for both training and tactical missions. These formulations are essentially a mixture of potassium chlorate, sucrose, TA, and lesser amounts of other ingredients added to improve the performance and handling characteristics. When ignited, the heat generated by the exothermic reaction between KClO₃ and sucrose is used to vaporize the TA, which condenses into a dense smoke once outside of the hot reaction zone. While these formulations have performed well in their intended roles, in some applications the burning rate of the item, particularly smoke pots, was higher than desired. It was discovered that the substitution of pentaerythritol (PE) for a portion of the TA could reduce the burning rate significantly without adversely affecting smoke quantity or quality. Typical TA based smoke grenades contain 57% TA and burn for approximately 45 seconds. Using formulations containing a blend of PE and TA that totaled 57%, it was possible to double this burn time using the same grenade configuration. Currently, work is underway to incorporate PE into the formulations used for both the M83 (Grenade, Hand, Smoke, Screening, Practice, TA) and the M8 (Smokepot, Floating, Screening, Practice, TA). Figure 1 shows

a typical smoke screen produced by a small device approximately 2.5" in diameter by 4.5" in height.

One of the objectives of the early experiments was to quantify the effect of substituting PE for TA. Some of these initial experiments, accomplished with grenade size items, seemed to indicate that small amounts of PE had little effect, and it was not until the percentage in the formulation reached approximately 12% that the burning rate started to decrease. In two consecutive series of experiments, the formulations containing approximately 5% PE actually yielded slightly higher burning rates than those without PE. It was thought that at low concentrations, because of its lower melting and boiling points relative to TA, the PE vapor generated actually functioned as tinder, promoting ignition. Then, as the quantity of the PE was increased, a point was reached where the endothermic processes involved in generating the PE vapor negated this tinder effect and the PE then functioned as a coolant in the mix. Both the number of experiments and the effect was small, however, and could have been the result of normal variations resulting from the experimental errors associated in weighing, mixing, assembling, and timing the burns.

In an effort to acquire a better understanding of the ignition characteristics of the TA/PE blends and their relationship to the burning rate, particularly at lower percentages of PE, batches of several different TA/PE formulations were made. Grenades were assembled and tested for burn times and DSC runs were made with samples of each formulation. The DSC data was then examined to determine if trends were present that associated particular exotherms or endotherms with burn rate trends.

2. Experimental Procedures

The base line formulation (Table 1) used in this series of experiments is the same as that used in the original work in developing the performance characteristics of the TA/PE blend.

Table 1. Base Line Pyrotechnic Smoke Formulation

KClO ₃	-	23 % by weight
Sugar (sucrose)	-	14
Terephthalic acid (TA)	-	57
MgCO ₃	-	3
Polyacrylic Rubber	-	2
Graphite	-	1

Based on this formulation, five batches of smoke mix were made using ingredients of the same lots that had been treated identically. The batches were all made on the same day with the mixing conditions as uniform as possible. In all cases, the percents of KClO₃, sugar, MgCO₃, polyacrylic rubber, and graphite were as listed in Table 1. Portions of the TA were substituted with PE, but the sum of the TA and PE was always 57 %. Table 2 describes the formulations used in this series of experiments.

Table 2. Formulations Used In This Experiment

Batch Number	% TA	%PE
01062601	57.0	0
01062602	54.5	2.5
01062603	52.0	5.0
01062604	49.5	7.5
01062605	47.0	10.0
01062606	44.5	12.5

Each batch was 700g, which was sufficient to fabricate two grenades and provide a sample for DSC analysis. The mixes were carefully blended for 45 minutes in a planetary mixer using the polyacrylic rubber binder dissolved in acetone as the mixing medium. Additional acetone was added as necessary to adjust the consistency. At the conclusion of the mixing process, the batches were placed in conductive trays and transported to a forced air oven to dry.

Two grenades were fabricated out of each batch in a typical core-burning configuration. The mixtures were consolidated into the grenade cans using a force of 15,000 pounds and increments of 150, 120, and 70 grams. The last increment (70 g) had 7.5 grams of an ignition composition placed on its top surface prior to consolidation. Ignition was achieved by using 1½ inches of quickmatch attached to an electric match inserted into an aluminum fuze body.

Two small samples were taken from each of the batches and carefully ground with a mortar and pestle to increase their homogeneity. Two DSC analyses were performed on each of these samples and then two more analyses were performed on the combined and blended samples. As a result, a total of 6 DSC analyses were run on each of the batches. In addition, DSC analysis was performed on terephthalic acid, pentaerythritol, KClO_3 , sucrose, as well as the stoichiometric blends of TA + KClO_3 , PE + KClO_3 , and sucrose + KClO_3 . The sample sizes used in the DSC runs ranged between 0.71 mg and 1.22 mg with an average of 0.96 mg. The DSC was programmed to equilibrate at 50 ° C and then ramp up at 20° per minute to 400 ° C.

3. Results And Discussion

Typical DSC runs with sugar / potassium chlorate as the fuel / oxidizer system are not normally heated much beyond the ignition point of about 175 degrees Centigrade. Once the pyrotechnic composition is ignited, the components are consumed. It was thought that there would be no reason to continue to heat the composition higher. Heating a sample beyond the ignition point was also considered to put undue stress on the equipment and would also consume much more time per individual sample. This, of course, would reduce the number of samples that could effectively be run in a given allocation of time.

Figures 2 to 5 shows the typical DSC curves for the reactive components in a typical composition. They include sugar (sucrose), potassium chlorate, pentaaaaaaaa, and terephthalic acid, respectively. Notice that it is necessary to heat only the potassium chlorate above 350 degrees centigrade to obtain a usable graph. Typically, the melted fuel results in an exothermic reaction at a much lower temperature.

Figure 6 shows a typical DSC curve from another project that used ammonium perchlorate as the oxidizer. Not that there is an endothermic reaction which occurs at 243 degrees centigrade and a pair of exothermic reactions at 290 degrees centigrade and 450 degrees centigrade. Typically, DSC runs made with ammonium perchlorate as the oxidizer have higher ignition temperatures and are also run only to the ignition point.

To assist in further understanding the reaction between sucrose and an oxidizer, a pyrotechnic blend of sucrose and ammonium perchlorate was prepared and a sample ran in the DSC. Figure 7 shows the reaction curve. It was interesting to notice the "dual hump" for the exothermic portion of the curve. This result lead to preparing additional pyrotechnic blends to determine if this situation was true for other fuel / oxidizer combinations. Figures 8 through 11 show the results for the low temperature heating of sucrose / potassium chlorate, the higher temperature heating of sucrose / potassium chlorate, the terephthalic acid / potassium chlorate, and the PE / potassium chlorate mixtures. The dual exothermic curves for the sucrose / potassium chlorate blend showed that there were two competing reactions which may have an effect on burn rates of the same composition when used inside a device such as a grenade.

In an attempt to determine if there was indeed, a second reaction between the PE and the potassium chlorate that may have a greater affect on the burn rate for a specific smoke composition, a series of test samples was made and placed into the DSC for analysis. Figure 12 shows a comparison of several DSC curves overlaid on each other. It was interesting to note that while the first curve has an increasing area under the curve, the second curve has a decreasing area under the curve. It is believed that this second exotherm was responsible for the success of the PE in reducing the burn rate without significantly reducing the amount of smoke produced. Using more that 12.5% of paaaaaaaa in similar compositions merely resulted in a pyrotechnic compositions that did not perform as well.

4. Conclusions

Although not fully understood, the effect of the addition of PE to terephthalic acid smoke compositions produced the desired effects. The burn rates for pyrotechnic smoke compositions containing increasing percentages of PE did, indeed, slow down considerably. The quality of the smoke produced by such compositions was consistently high when compared to using other diluents.

Figure 13 shows the reduction in burn rate with the addition of several percentages of PE..

The success of this experiment has lead to the development of white smoke producing compositions which provide more smoke for longer periods of time, with the added benefit of low toxicity to both individuals and the environment.

Figure 1
Typical smoke cloud from a grenade sized device

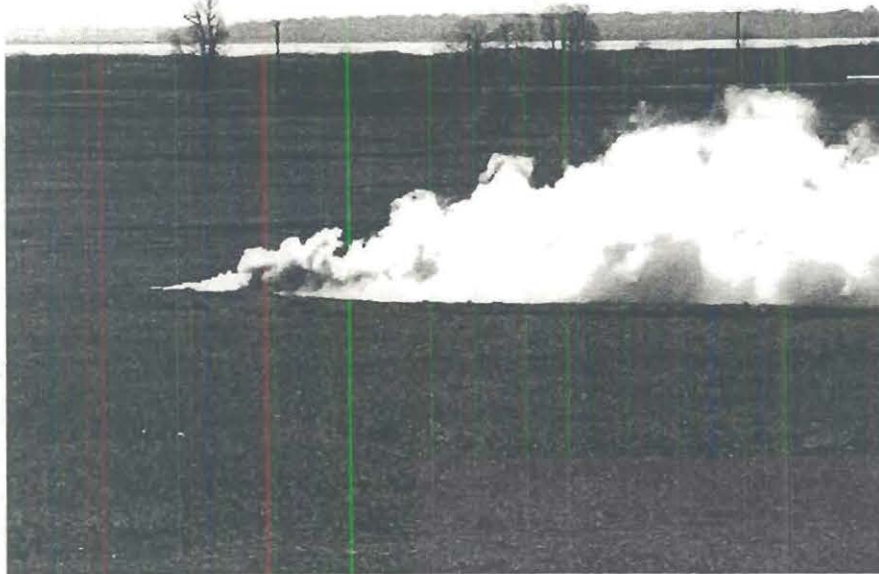


Figure 2
DSC curve for sugar

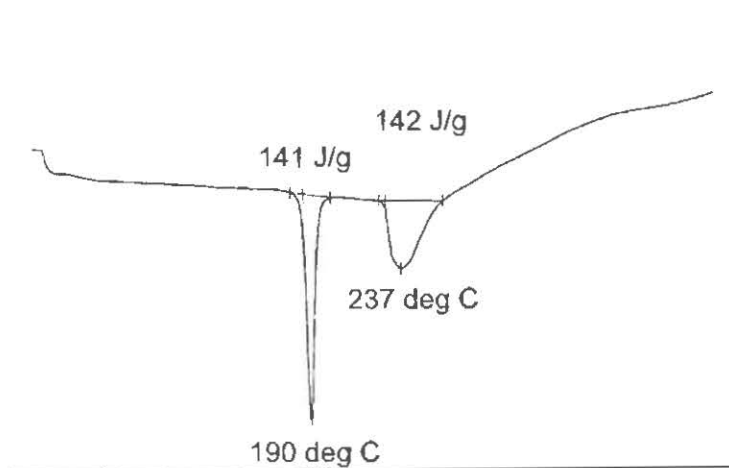


Figure 3
DSC curve for potassium chlorate

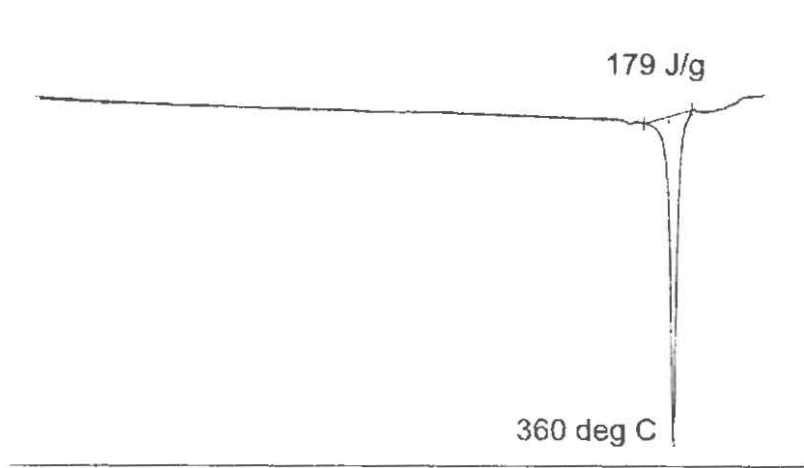


Figure 4
DSC curve for PE

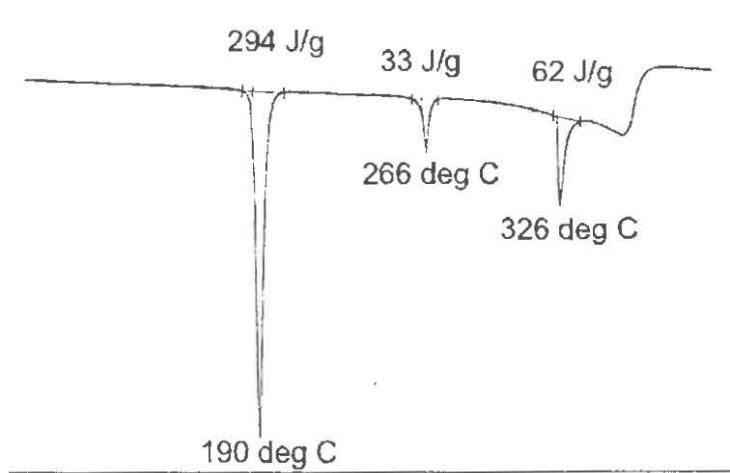


Figure 5
DSC curve for terephthalic acid

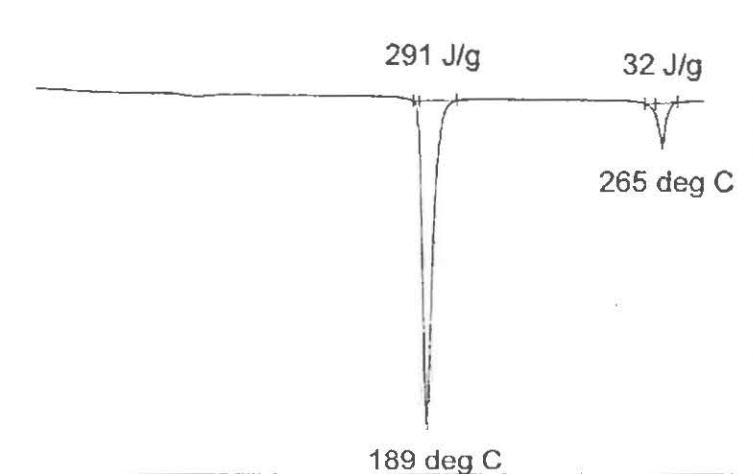


Figure 6
DSC curve for ammonium perchlorate

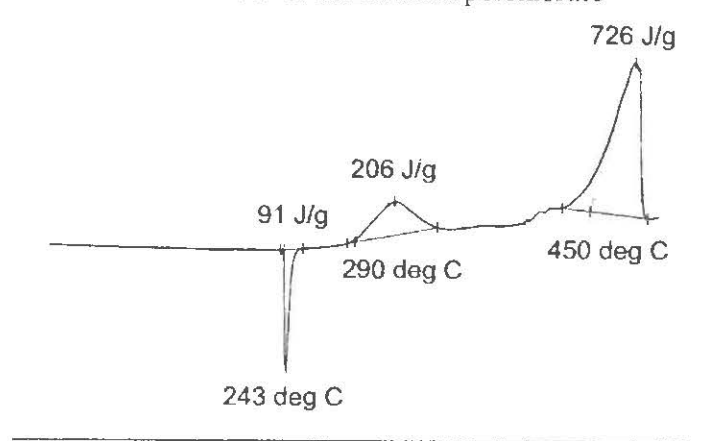


Figure 7
DSC curve for sugar and ammonium perchlorate

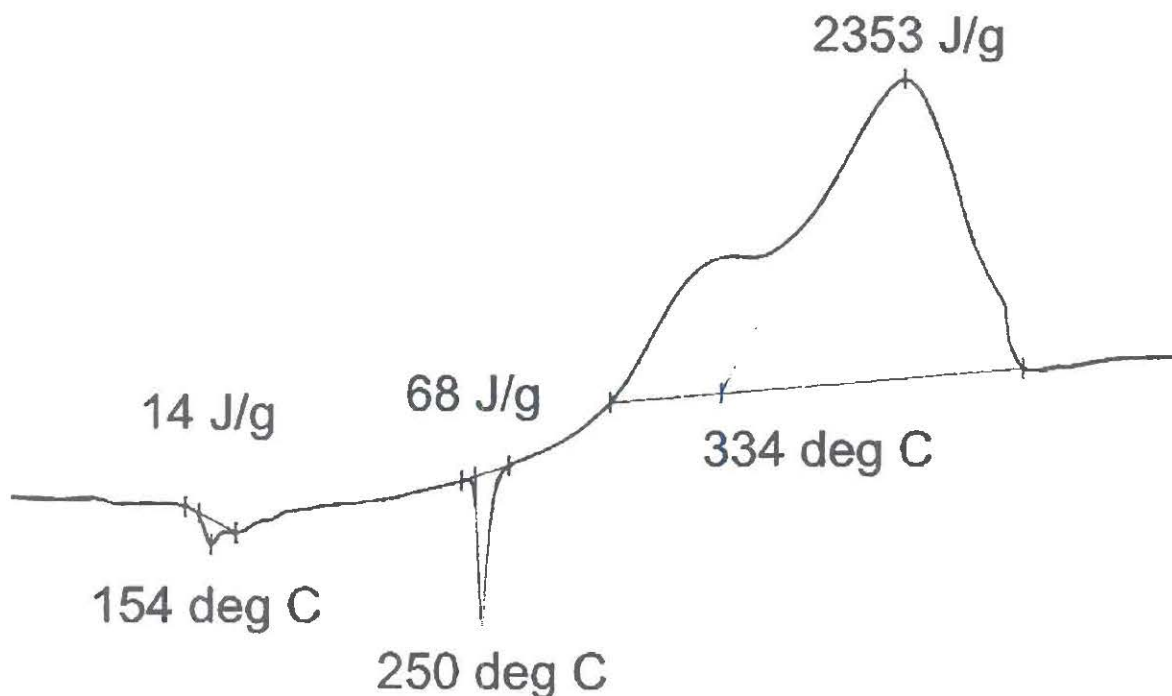


Figure 8
Low temperature DSC curve for sugar and potassium chlorate

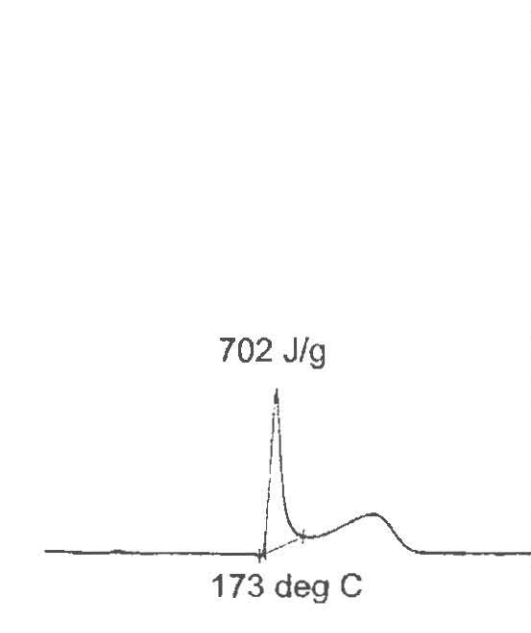


Figure 9
High temperature DSC curve for sugar and potassium chlorate

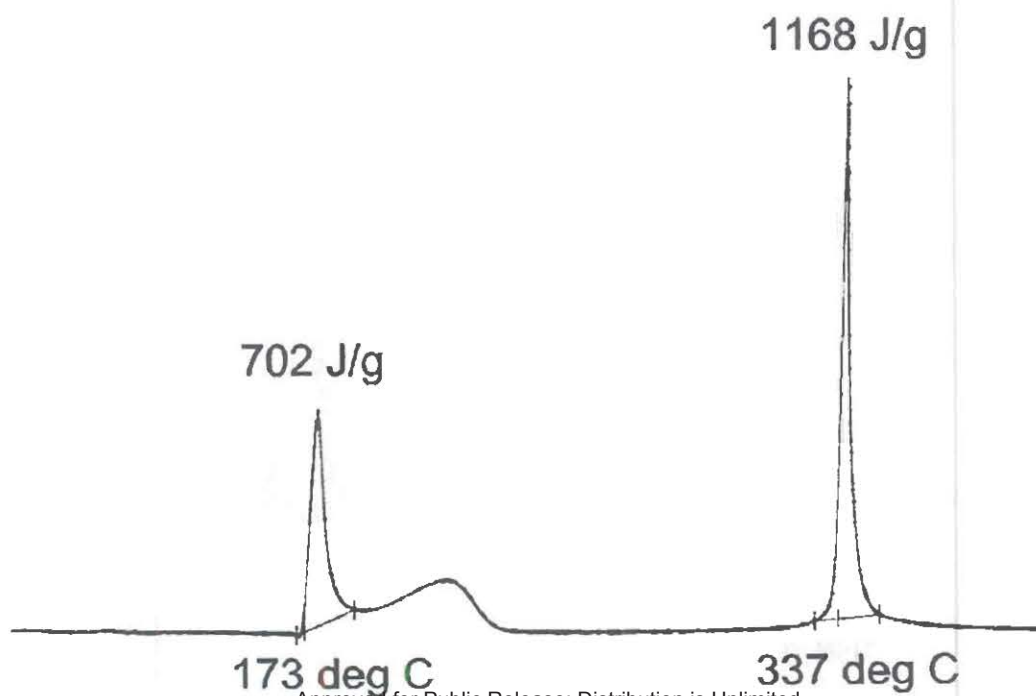


Figure 10
DSC curve for terephthalic acid and potassium chlorate

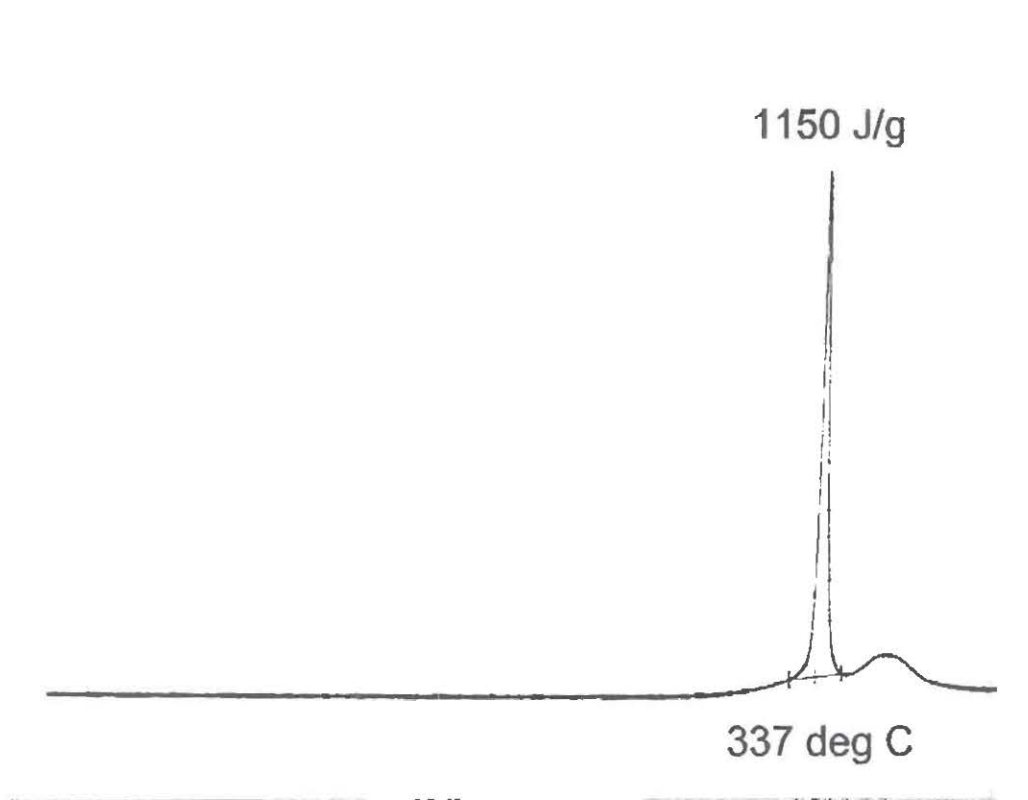


Figure 11
DSC curve for PE and potassium chlorate

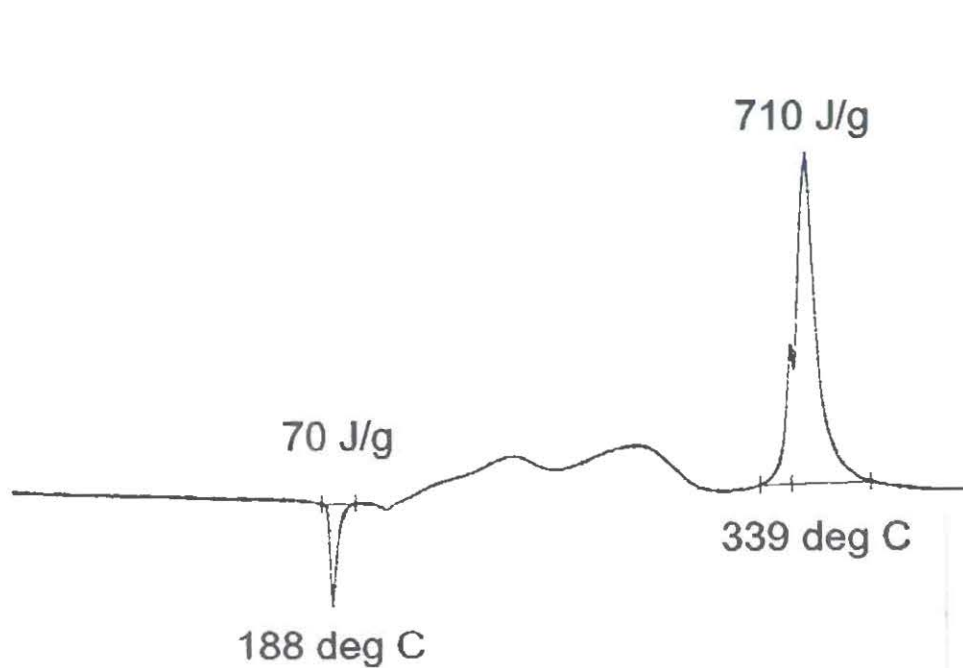


Figure 12
DSC curve overlay for 0% PE through 12.5% PE

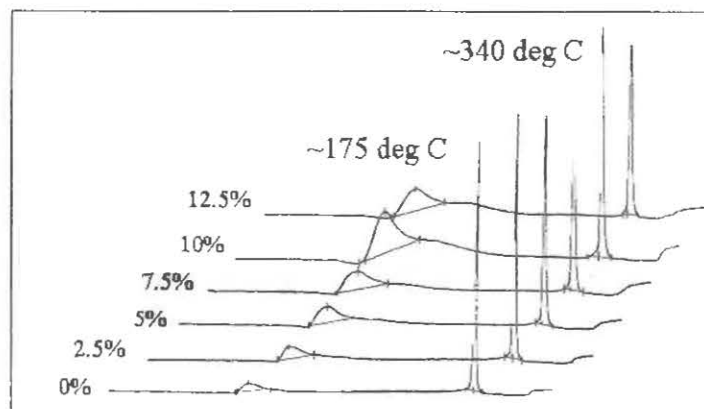
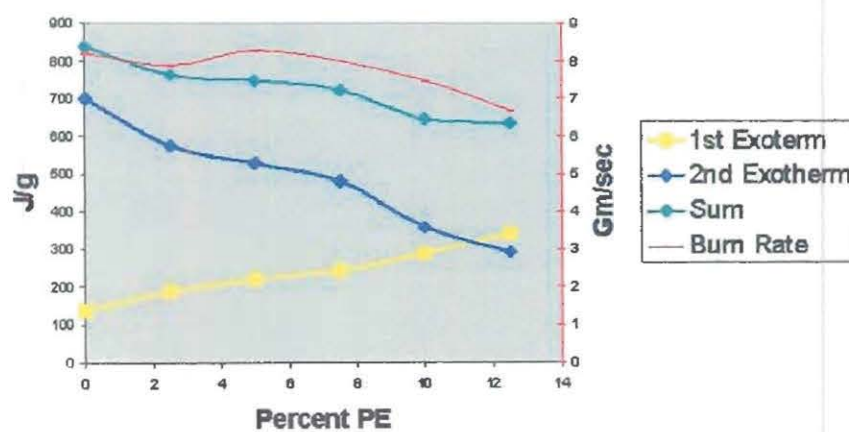


Figure 13
Burn rate reduction vs. percent of PE



THIS PAGE LEFT INTENTIONAL BLANK

STUDIES ON THE AGEING OF MAGNESIUM-POTASSIUM NITRATE PYROTECHNIC COMPOSITIONS USING ISOTHERMAL HEAT FLOW CALORIMETRY AND THERMAL ANALYSIS TECHNIQUES

S.D.Brown, E.L.Charsley, S.J.Goodall, P.G.Laye and J.J.Rooney,
Centre for Thermal Studies, School of Applied Sciences, University of Huddersfield,
Queensgate, Huddersfield HD1 3DH, UK.

T.T.Griffiths, QinetiQ, Fort Halstead, Sevenoaks, Kent TN14 7BP, U.K.

ABSTRACT

The ageing behaviour of pyrotechnic mixtures of magnesium and potassium nitrate has been followed at 50°C and 65% relative humidity by isothermal heat flow calorimetry. Measurements have been carried out with samples in air and in an inert atmosphere. The main reaction product was found to be magnesium hydroxide. This has been determined quantitatively by thermogravimetry and the amount formed correlated with the measured cumulative heat of ageing. The results have been compared with those obtained for magnesium powder studied under the same conditions. In addition the influence of the ageing process on the pyrotechnic reaction has been studied by high temperature differential scanning calorimetry under ignition conditions and modulated temperature differential scanning calorimetry.

INTRODUCTION

Thermal techniques provide powerful methods for the characterisation of pyrotechnic compositions. Typically these compositions are based on finely divided mixtures of metallic or non-metallic elements with inorganic oxidising agents (1). We have used thermal techniques to study the influence of ageing on pyrotechnic systems, at temperatures in the range 40 to 70°C and relative humidities (RH) from 50 to 100%. Two approaches have been adopted. In one, the indirect approach, the samples are aged in a humidity cabinet for different times and then characterised by thermal analysis and calorimetric techniques. A recent example of this approach is a study of the boron-potassium dichromate pyrotechnic delay system, where the ageing has been followed by high temperature differential scanning calorimetry under ignition conditions, time to ignition measurements and isothermal microcalorimetry (2). It is also possible to perform pyrotechnic tests, such as burning rate, light output and exothermicity measurements on the aged compositions.

In the other approach, the samples are aged in an isothermal microcalorimeter. This enables the ageing process to be monitored directly since the technique is sufficiently sensitive to measure the small amount of heat released during ageing. The aged products can then be characterised by thermal and analytical techniques but since the sample masses are normally in the range 100-500mg there is insufficient material for the standard pyrotechnic tests.

In the present paper preliminary results are reported for the ageing of the magnesium-potassium nitrate pyrotechnic system in the presence of water vapour using isothermal microcalorimetry. The results have been compared with those obtained for magnesium powder under the same conditions. Since magnesium hydroxide was found to be the main product of ageing, a method was developed using thermogravimetry (TG) to enable the amount formed to be determined quantitatively. These studies have been supplemented by examination of the aged samples by high temperature differential scanning calorimetry (DSC) under ignition conditions and modulated temperature DSC (MTDSC). A preliminary study on the magnesium-sodium nitrate system has been reported previously (3).

EXPERIMENTAL

The studies have been carried out on a magnesium-potassium nitrate pyrotechnic composition containing equal masses of the components. The potassium nitrate was to Interim DEF STAN 68-63/1 and the Grade 4 magnesium to DEF STAN 13-130/1. The composition was prepared by blending the components in a Turbula mixer.

Microcalorimetric measurements were carried out on 100mg samples at 50°C and 65% RH using a Thermometric Model 2277 Thermal Activity Monitor (TAM). The samples were sealed into 3cm³ glass ampoules. The humidity was maintained using a saturated solution of potassium iodide in a small tube in the ampoule. Samples of the residues were analysed for magnesium hydroxide by thermogravimetry and characterised by high temperature DSC under ignition conditions and MTDSC.

Thermogravimetry was carried out using a Stanton Redcroft TG1000 thermobalance. A method was devised for determining magnesium hydroxide by heating a 10mg sample in a platinum crucible in an atmosphere of argon according to the following programme:

- [a] The temperature was maintained at 25°C for 10 min to establish the initial mass reading.
- [b] The temperature was raised to 150°C at 30°C min⁻¹ and held constant for 10 min.
- [c] The temperature was raised to 320°C at 30°C min⁻¹ and held constant for 30 min.

Magnesium hydroxide was determined from the mass loss accompanying the dehydration reaction in step [c]. The mass change in step [b] enabled the amount of moisture present in the sample to be determined.

High temperature DSC under ignition conditions was carried out using a specially developed apparatus (4). Measurements were made on 10mg samples, which were heated in argon at 50°C min⁻¹. MTDSC experiments were carried out using a TA Instruments Model 2920. The measurements were made on 5mg samples contained in platinum crucibles in an atmosphere of helium with an underlying heating rate of 3°C min⁻¹, a period of 30s and an amplitude of 0.1°C (5).

RESULTS AND DISCUSSION

MICROCALORIMETRIC STUDIES

Magnesium Powder

Typical heat flow and cumulative heat curves for the magnesium sample are shown in Figure 1. It can be seen that following a rapid rise to give a peak after 0.3 days, the heat flow decreased to a minimum after about 5.5 days. The signal then increased slowly for the remainder of the experiment.

The possible role of oxygen in the ageing process was assessed by carrying out experiments on samples sealed in ampoules under an atmosphere of argon. It can be seen from Figure 2 that no significant difference was found from the result obtained in air. This indicates that under these closed conditions the ageing of magnesium is due to the reaction with water vapour alone. X-ray diffraction studies showed that magnesium hydroxide was the main product of the ageing reaction. This was measured quantitatively using the thermogravimetric method already described. A typical experimental curve is shown in Figure 3. The moisture and magnesium hydroxide contents were determined from the TG curve after the application of a small buoyancy correction.

The results of duplicate TG measurements on the residues from two calorimetric experiments after 28 days are shown in Table 1. It can be seen that there is good reproducibility between the individual duplicate measurements. The cumulative heats are also given in the Table 1. The similarity between the calorimetric results together with the closeness of the TG measurements indicates that a similar amount of ageing has taken place in the two calorimetric experiments.

Further determinations of magnesium hydroxide were carried out on samples aged in the TAM for periods ranging from 3.5 to 14 days. The amount of magnesium hydroxide formed is plotted against the time of ageing in Figure 4. Also included are the results from the 28 day experiments. The results show that the magnesium hydroxide content increases in a linear manner with the time of ageing. Measurements on the unaged sample showed that this already contained a significant amount of magnesium hydroxide (2.7%).

The amount of magnesium hydroxide formed is plotted against the cumulative heat in Figure 5. The increase in the amount of magnesium hydroxide with time of ageing correlates well with the corresponding increase in the cumulative heat. The results point to the reaction,



being the major component of the ageing process.

Table 1

TG Determination of Magnesium Hydroxide Content of Magnesium Powder Aged in
Air for 28 days at 50°C and 65%RH

Experiment	Mass Loss /	Mg(OH) ₂ / %	Heat / Jg ⁻¹
1	2.74	8.88	415
	2.73	8.84	
2	2.64	8.54	410
	2.68	8.69	
Mean	2.70 ± 0.05	8.74 ± 0.15	413 ± 3

50% Mg-50% KNO₃ Composition

The heat flow and cumulative heat flow curves obtained by microcalorimetric studies on the 50% Mg-50% KNO₃ composition over a 28 day period are shown in Figures 6 and 7 respectively. The curves are compared with those for the same amount of magnesium as present in the composition. It can be seen that the heat flow from the pyrotechnic composition is markedly greater than that given by the magnesium alone. This is particularly significant in the initial stages of ageing. Calorimetric experiments with potassium nitrate alone in the presence of water vapour gave a negligible heat output (Figure 8). It is clear that the ageing process in the composition in the presence of water vapour must involve interaction between magnesium and potassium nitrate.

A series of microcalorimetric experiments was carried out to age the pyrotechnic composition for time periods ranging from 3.5 to 21 days. The amount of magnesium hydroxide formed is plotted against the time of ageing in Figure 9, together with the results obtained after 28 days. Also shown is the amount of magnesium hydroxide formed by the equivalent amount of magnesium. The quantity of magnesium hydroxide given by the pyrotechnic composition is markedly greater than that formed by magnesium alone and this difference is particularly significant in the initial stages of ageing. This reflects the increased heat observed in the pyrotechnic system compared with magnesium alone. The rate of formation of magnesium hydroxide by the pyrotechnic composition slows appreciably after 14 days and appears to be similar to that given by magnesium.

The relationship between the amount of magnesium hydroxide formed and the heat evolved for the Mg-KNO₃ composition is shown in Figure 10. The results have been fitted to a second order curve and show a good correlation between the amount of hydroxide formed and heat evolved.

HIGH TEMPERATURE DSC STUDIES

High temperature DSC studies were carried out under ignition conditions to investigate the influence of the ageing process on the high temperature pyrotechnic reaction. The ignition temperature of samples aged from 1 to 14 days is shown in Table 2. The values increase rapidly over the first 5 days of ageing and then remain unchanged on further ageing. The DSC curves for the compositions aged for 1 and 2 days (Figure 11) show that the pre-ignition exothermic reaction given by the unaged composition is significantly reduced after only 1 day of ageing. The proximity of the ignition temperature after 5 days of ageing to the melting temperature of magnesium (650°C) suggests that fusion of unreacted magnesium may be the trigger for ignition in these compositions.

Table 2

Ignition Temperatures Determined by DSC for a 50% Mg-50% KNO₃ Composition Aged in Air for Different Times at 50°C and 65% RH

(DSC conditions: sample mass, 20mg; heating rate, 50°C min⁻¹; atmosphere, argon)

Age / days	0	1	2	3	5	7	14
Ignition	627	633	639	643	647	645	647
Temperature / °C	±3	±0	±1	±1	±1	±1	±1

MODULATED TEMPERATURE DSC STUDIES

An important relatively recent development in the field of DSC has been the introduction of modulated temperature DSC where a sinusoidal wave is superimposed on the linear heating rate normally used in conventional DSC experiments (6). The power of the technique is that it allows the total heat flow, which is analogous to a normal DSC signal to be resolved into two components. These are the "reversing" or heat capacity component, which is heating rate dependent and the "non-reversing" or kinetic component which is temperature dependent. The technique has been shown to have a number of advantages in the study of pyrotechnic systems and has enabled the fusion of an oxidant to be distinguished from the strongly exothermic reaction between the oxidant and a fuel (5).

In the present work, MTDSC measurements showed that the pre-ignition reaction in the 50% Mg-50% KNO₃ composition started at about 330°C. This is in the region of the fusion of potassium nitrate, which is shown by a sharp endothermic peak. The influence of ageing is clearly demonstrated in Figure 12, where the total heat flow signal after ageing for just 1 day shows no sign of this low temperature pre-ignition reaction. A comparison between the reversing signals for unaged and aged samples shows that ageing for 1 day produces a broader melting peak with a reduced melting temperature. The endotherm at 275°C observed in the total heat flow signal for the aged composition, is due to the decomposition of magnesium hydroxide and hence does not appear in the reversing signal.

CONCLUSIONS

Microcalorimetric studies of the ageing of 50% Mg-50% KNO₃ in air at 50°C and 65% RH have shown that potassium nitrate plays an essential role in the increased rate of ageing compared with that of magnesium alone. The major product of ageing is magnesium hydroxide and a good correlation has been found between the heat evolved in the ageing process and the amount of magnesium hydroxide formed. High temperature DSC and MTDSC studies have shown that the high temperature reaction between magnesium and potassium nitrate is affected directly by the ageing process at 50°C.

Work is in progress to make additional quantitative measurements of the components of aged samples including total magnesium, nitrate and nitrite contents. In addition, a technique has been developed for free magnesium determination with samples in the mass range 10 to 20mg. It is hoped that these methods, in conjunction with the thermal studies, will provide a better insight into the ageing process of the magnesium-potassium nitrate system and other nitrate-based pyrotechnic compositions.

REFERENCES

1. E.L.Charsley, T.T.Griffiths and B.Berger, Proc. 24th International Pyrotechnics Seminar, IIT Research Institute, Chicago, USA, 1998, 133.
2. E.L.Charsley, H.Fieldhouse, T.T.Griffiths, J.J.Rooney and S.B.Warrington, Proc. TTCP Workshop on the Microcalorimetry of Energetic Materials, Defence Evaluation and Research Agency, Fort Halstead, Kent, UK, 1997, Q1.
3. E.L.Charsley, S.J.Goodall, T.T.Griffiths and P.G.Laye, Proc. 12th Symposium on Chemical Problems Connected with the Stability of Explosives, Karlsborg, Sweden, 2001, in press.
4. E.L.Charsley, S.B.Warrington and T.T.Griffiths, Proc. 26th Int. ICT Conference, Fraunhofer-Institut, Germany, 1995, 23-1.
5. E.L.Charsley, J.J.Rooney, H.A.Walker, T.T.Griffiths, T.A.Vine and B.Berger, Proc. 24th International Pyrotechnics Seminar, IIT Research Institute, Chicago, USA, 1998, 147.
6. M.Reading, Trends in Polymer Science, 8, 1993, 248.

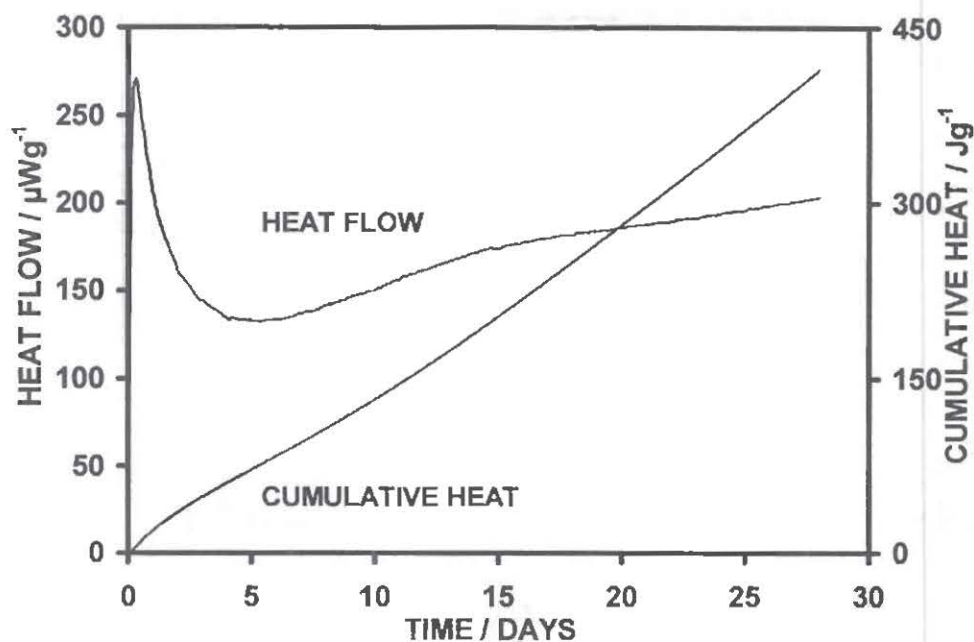


FIGURE 1. MICROCALORIMETRY CURVES FOR MAGNESIUM
(Sample mass, 100mg; 50°C; 65% RH; atmosphere, air)

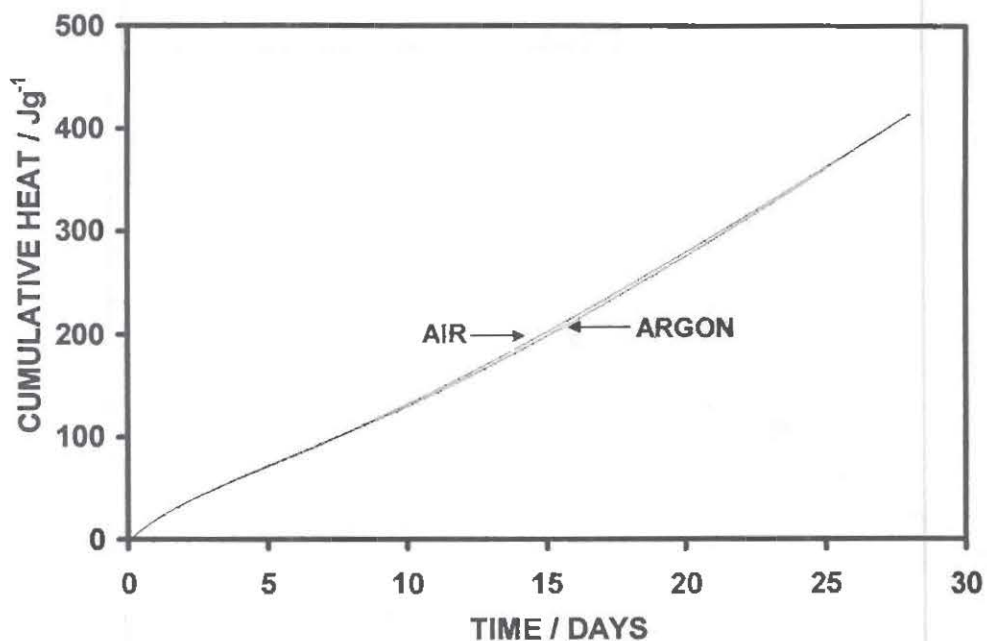


FIGURE 2. COMPARISON OF CUMULATIVE HEAT CURVES FOR MAGNESIUM
IN AIR AND IN ARGON
(Sample mass, 100mg; 50°C; 65% RH)

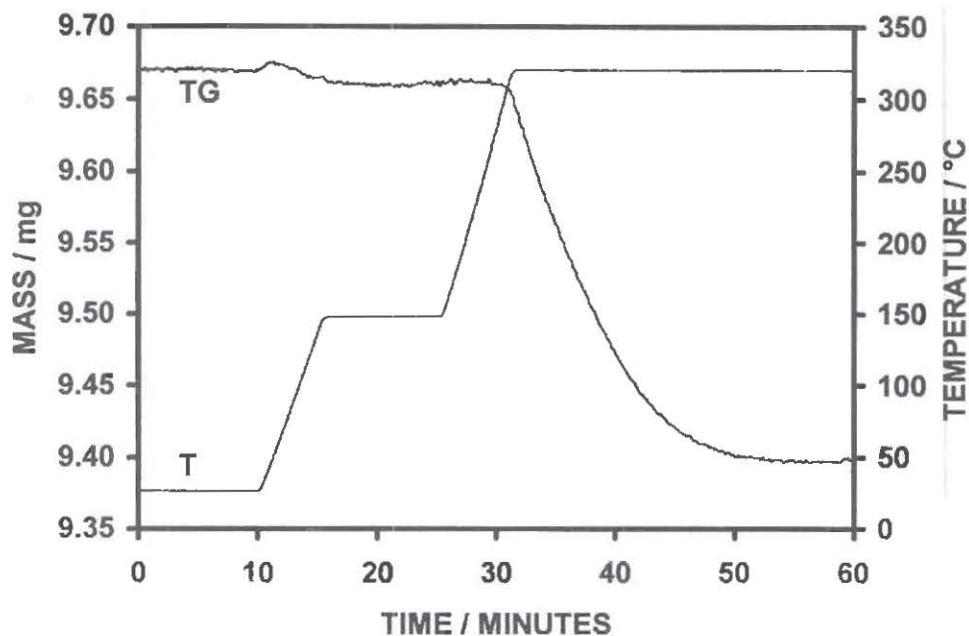


FIGURE 3. THERMOGRAVIMETRIC METHOD FOR DETERMINATION OF MAGNESIUM HYDROXIDE CONTENT
(Sample mass, 10mg; heating rate, 30°C min⁻¹; atmosphere, argon)

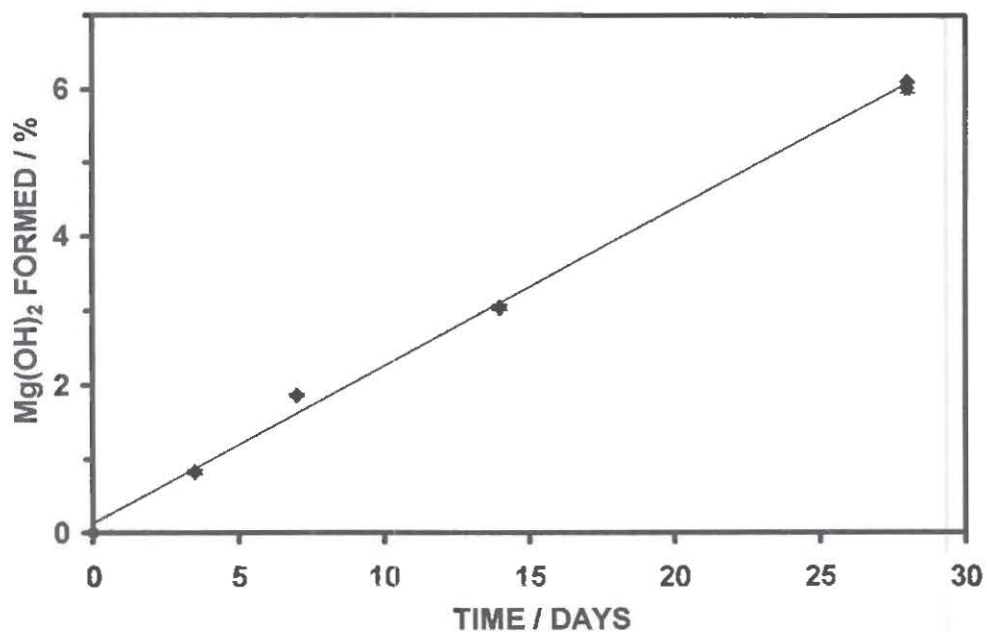


FIGURE 4. PLOT OF Mg(OH)₂ FORMED AGAINST TIME OF AGEING FOR MAGNESIUM SAMPLES IN AIR AT 50°C AND 65%RH

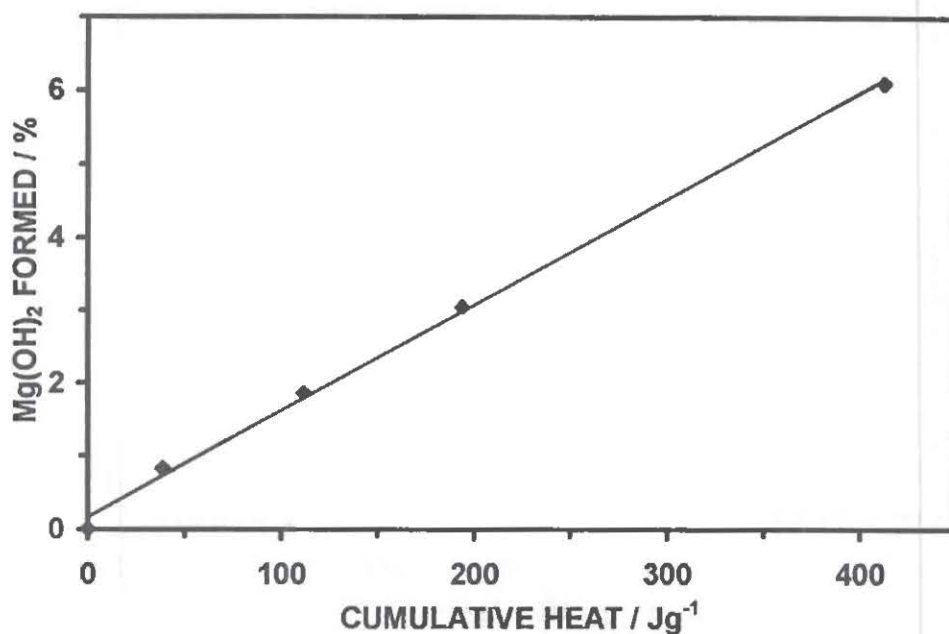


FIGURE 5. PLOT OF Mg(OH)_2 FORMED AGAINST CUMULATIVE HEAT FOR MAGNESIUM SAMPLES AGED IN AIR AT 50°C AND 65% RH

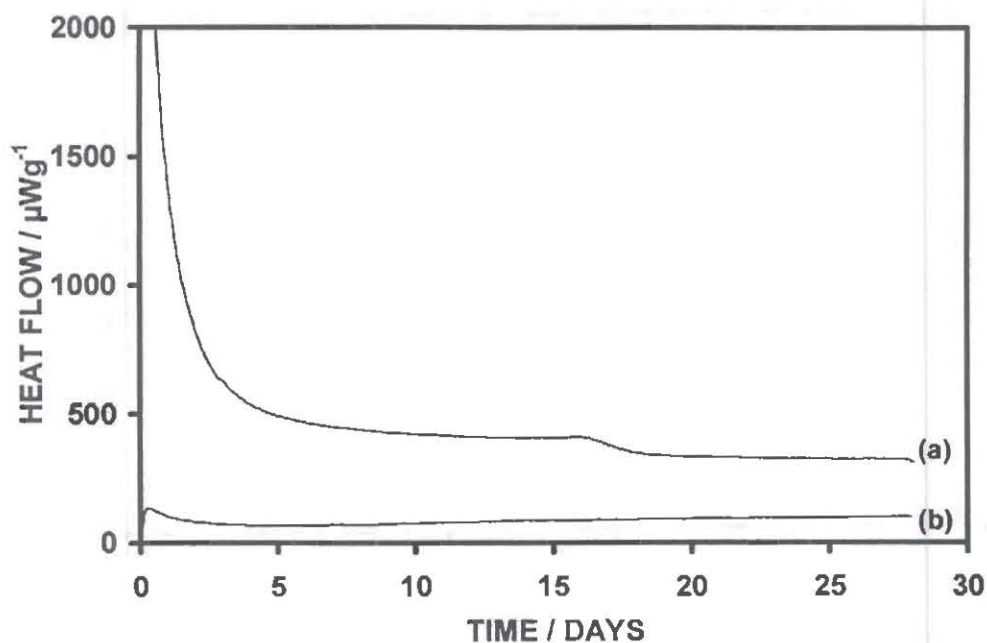


FIGURE 6. HEAT FLOW CURVES FOR (a) A 50% Mg -50% KNO_3 COMPOSITION AND (b) MAGNESIUM (x 0.5)
(Sample mass, 100mg; 50°C ; 65% RH; atmosphere, air)

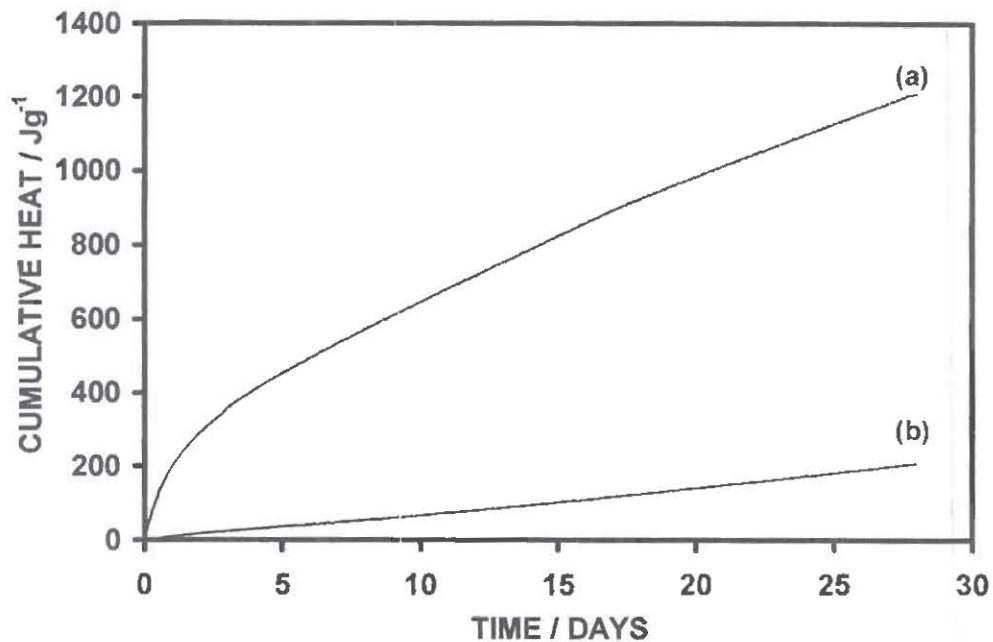


FIGURE 7. CUMULATIVE HEAT CURVES FOR (a) A 50% Mg-50% KNO₃ COMPOSITION AND (b) MAGNESIUM (x 0.5)
(Sample mass, 100mg; 50°C; 65% RH; atmosphere, air)

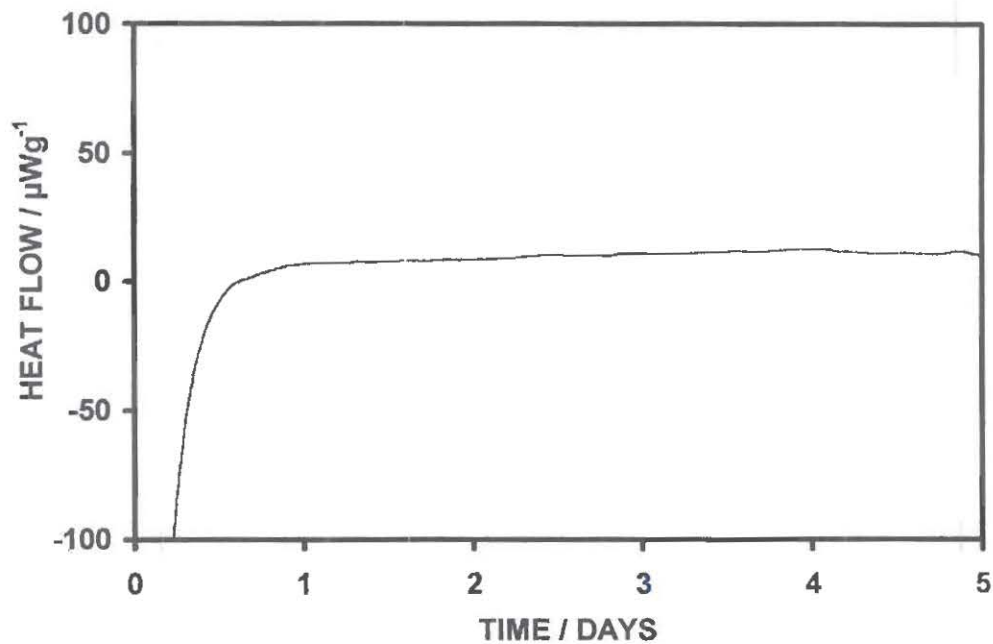


FIGURE 8. HEAT FLOW CURVE FOR POTASSIUM NITRATE
(Sample mass, 100mg; 50°C; 65% RH; atmosphere, air)

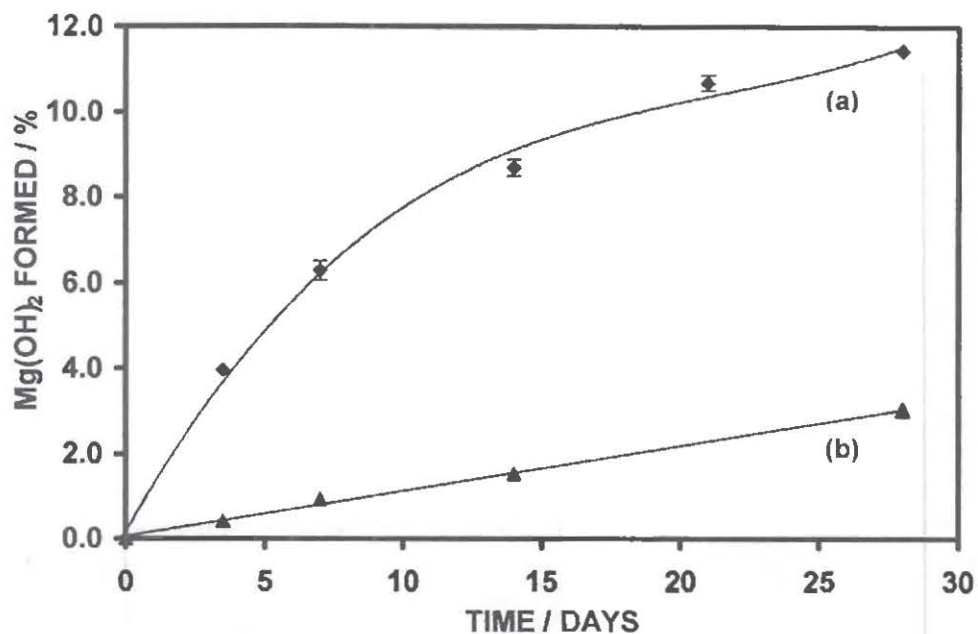


FIGURE 9. PLOT OF $\text{Mg}(\text{OH})_2$ FORMED AGAINST TIME OF AGEING IN AIR AT 50°C AND 65% RH FOR (a) A 50% Mg-50% KNO_3 COMPOSITION AND (b) MAGNESIUM ($\times 0.5$)

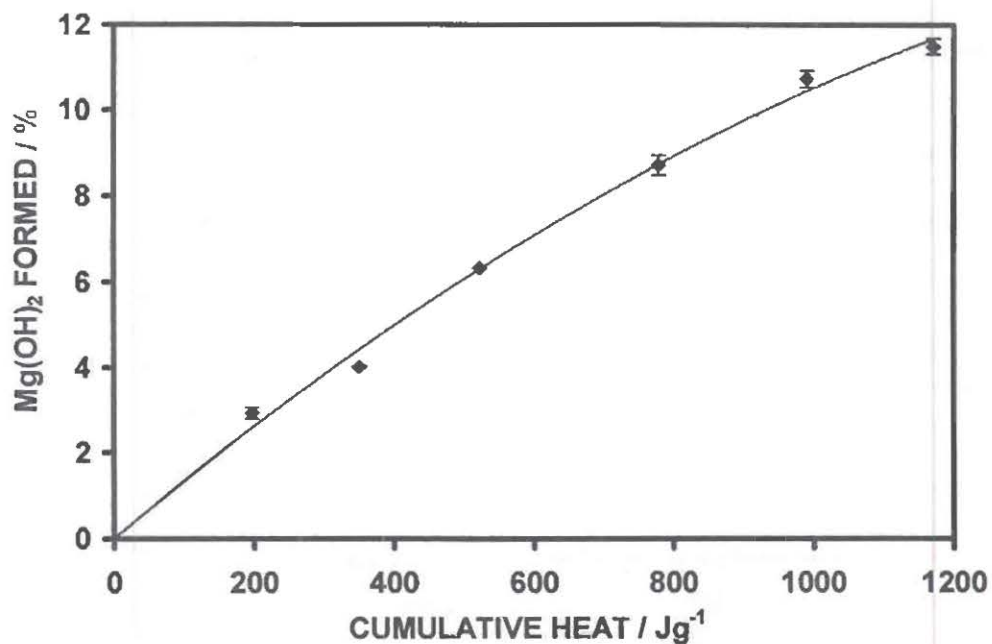


FIGURE 10. PLOT OF $\text{Mg}(\text{OH})_2$ FORMED AGAINST CUMULATIVE HEAT FOR A 50% Mg-50% KNO_3 COMPOSITION AGED IN AIR AT 50°C AND 65% RH

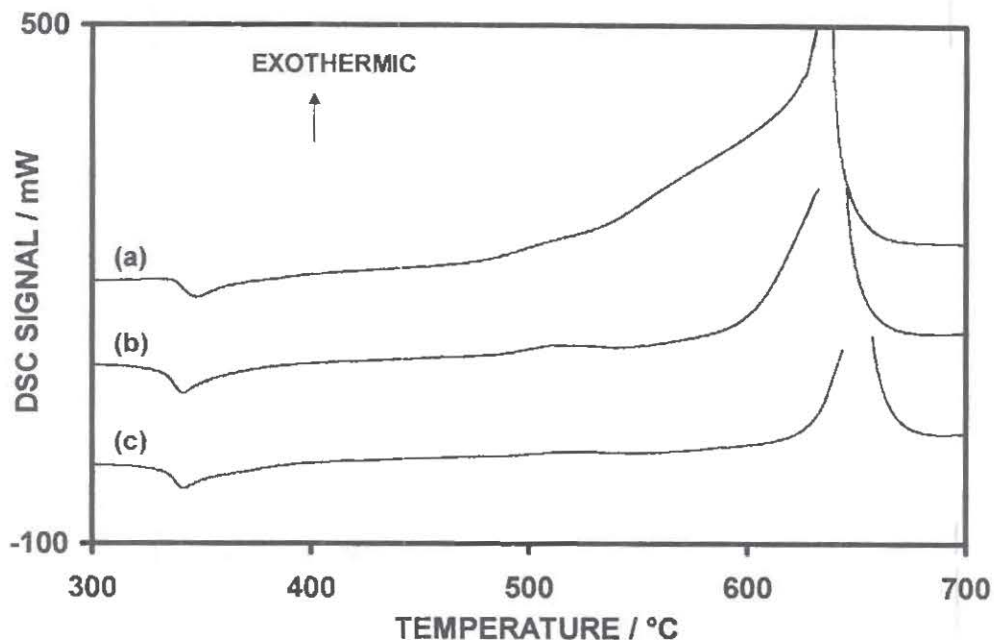


FIGURE 11. DSC CURVES FOR A 50% Mg-50% KNO₃ COMPOSITION
(a) UNAGED AND AGED FOR (b) 1 DAY, (c) 2 DAYS
IN AIR AT 50°C AND 65% RH
(Sample mass, 10mg; heating rate, 50°C min⁻¹; atmosphere, argon)

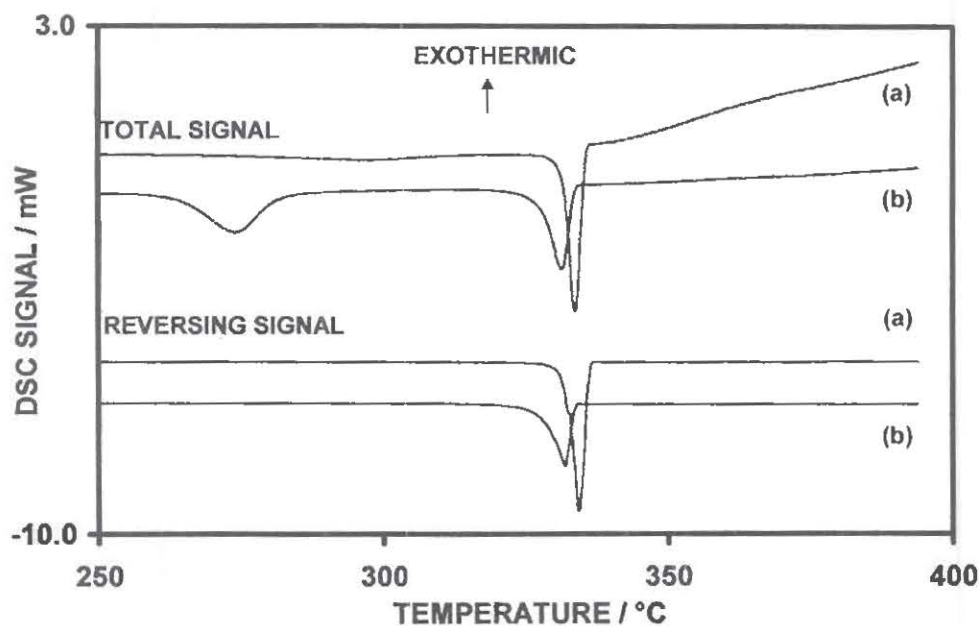


FIGURE 12. MTDSC CURVES FOR A 50% Mg-50% KNO₃ COMPOSITION
(a) UNAGED AND (b) AGED IN AIR AT 50°C AND 65% RH FOR 1 DAY
(Sample mass, 5mg; heating rate, 3°C min⁻¹; atmosphere, helium;
period, 30s; amplitude, 0.1°C)

THIS PAGE LEFT INTENTIONAL BLANK

Stability and Ageing Assessment of Rocket Propellant Formulation Batches with high Burn Rates

Manfred A. Bohn

Fraunhofer-Institut für Chemische Technologie (ICT)
Postfach 1240, D-76318 Pfinztal-Berghausen, Germany
e-mail: Manfred.Bohn@ict.fhg.de

Abstract

To achieve higher burning rates with rocket propellants some batches have been formulated, for which the main ingredients are (1) the energetic plasticizers GAP-A (short chain GAP with azide end groups), TMETN (trimethylol-ethane trinitrate) and BTTN (1,2,4-butanetriol trinitrate), (2) the energetic substances ammonium perchlorate (AP) and ϵ -CL20 (ϵ -HNIW, hexanitro-hexaza-iso-wurtzitane, crystallized in ϵ -phase). The binder was GAP-N100. From the point of view of stability and ageing, the interesting fact is that the formulations contain none of the typical stabilizers for the nitric acid ester components TMETN and BTTN, although their contents range up to 21 mass-%. One reason for doing so is to increase the content of the high energy ingredients. To assess basic stability, a series of tests and investigations were performed. These are the autoignition temperature test (AIT), Dutch Mass Loss Test (DMLT) and Vacuum Stability Test (VST). To investigate ageing, two measurement quantities are used: heat generation rate (heat flow) as function of time at 70°C, 80°C and 89°C and mass loss as function of time at the temperatures of 70°C, 80°C and 90°C. The evaluation of the measurements is based on reaction kinetic models.

1. Introduction

The objective of this investigation is to evaluate these types of ingredient mix named HFK # as possible rocket propellants and to correlate the stability and ageing behaviour with their composition, which is shown in Table 1 for seven HFK batches. The compositions are designed to get high burning rates. Information about the burning behaviour can be found in /1/. Using the data from typical stability tests, it is not possible to predict the ageing caused by decomposition reactions. The purpose of these tests is to get basic stability data in a short time, because the applied test temperatures of about 100°C and more are much higher than the meteorologically determined in-service temperatures, which according to /2/, are not higher than 71°C. This is the possible maximum induced daily temperature in the material beneath its surface in hot and dry areas. To assess ageing one needs time-temperature data of the properties between 50°C and a maximum of 90°C. For unknown formulations simplified methods using reduced measurement data sets are not applicable due to the lack of the necessary data base. To establish such a data base, heat generation rate and mass loss as function of time and temperature are determined. With unknown formulations at least two methods with a different probing of the material should be used. The two types of probing here are the split-off of decomposition gases and the heats of reactions. The heat generation rate was measured using a TAM (Thermal Activity Monitor), produced by Thermometric AB, Sweden. The mass loss was determined by weighing of samples stored in vials inserted in

PID-controlled ovens, whereby the weighing intervals were adjusted to the decomposition rate.

Table 1 also lists some performance data of the formulations. The specific impulses and heats of explosion for gaseous and liquid water in the burning products have been calculated using the ICT Thermodynamic Code and the data from the ICT Thermochemical Data Base [3].

Table 1: Composition and some performance data of the HFK batches investigated.

		178	180	181	182	184	185	189
GAP-A	[m.-%]	12.25	14	9	-	-	10.5	9
TMETN	[m.-%]	12.25	14	9	18	21	10.5	2.25
BTTN	[m.-%]	-	-	-	-	-	-	6.75
GAP-N100	[m.-%]	10.5	7	12	12	14	14	12
ϵ -CL20	[m.-%]	42	42	47	47	42	42	47
AP	[m.-%]	20	20	20	20	20	20	20
others	[m.-%]	3	3	3	3	3	3	3
O ₂ -balance	[%]	-28.7	-27.8	-27.1	-20.0	-22.9	-31.2	-25.8
I _{SP} (70:1, eq.flow)	[Ns/N]	251	252	253	258	255	249	254
I _V (70:1, eq.flow)	[Ns/l]	4290	4330	4420	4580	4450	4240	4440
Q _{EX} (gaseous water)	[J/g]	4540	4670	4700	5050	4880	4510	4750
Q _{EX} (liquid water)	[J/g]	4840	4940	4960	5370	5200	4750	5020

2. Results

2.1 Basic stability test data

The results of the autoignition temperature test and of the Dutch mass loss test fulfil the corresponding limit criteria, Table 2. The data of the vacuum stability test (determines gas evolution) are all above the limit value but this is caused by the high test temperature. With formulations containing nitric acid ester compounds a temperature of 90°C is generally used. This reduces the evolved gas amount approximately by a factor of 3 to 4.

Table 2: Results of the stability tests.

		limit value	178	180	181	182	184	185	189
autoignition temperature, 5°C/min	[°C]	≥ 170	172	173	175	172	170	176	177
Dutch ML test, 105°C, 4g, ML at 72h - ML at 8h	[%]	≤ 2	0.78	0.75	0.68	0.90	1.11	0.80	0.75
vacuum stability, 100°C, 40h, 2.5g	[ml/g]	≤ 1.2	1.55	1.56	1.32	1.74	2.06	1.49	1.54

2.2 Mass loss data

As an example of all investigated HFK batches the mass loss data of HFK 178 at 90°C are shown in Fig. 1 as function of time. The data of both parallel samples coincide, which was the case for all batches at all measurement temperatures. In Fig. 2 the averaged ML data at 90°C of each of the seven HFK batches can be seen. HFK 184 with 21 mass-% TMETN as the only plasticizer has the highest decomposition rate k_{ML} , followed by HFK 189 with TMETN+BTTN and GAP-A. This is followed by HFK 182 with 18 mass-% TMETN. HFK 180 and 181 show the lowest decomposition rate. In Fig. 2 the curves obtained according to model 'ML: linear + exponential' are also included, see section 3.1. All data descriptions are very good, which is also documented by the high correlation coefficients. The ML curves show an initial flexure, then a linear increase. In terms of reaction kinetics, the linear increase means a global decomposition reaction of zero order. In detail, the decomposition course is much more complex, and therefore this linear part of the mass loss is named decomposition reaction of pseudo zero order. Figs. 3 and 4 show the ML data and modelling at 80°C and 70°C. Qualitatively the behaviour is identical to that found at 90°C. But HFK 189 changes its ageing behaviour at lower temperature, it is now the batch with the highest mass loss rate.

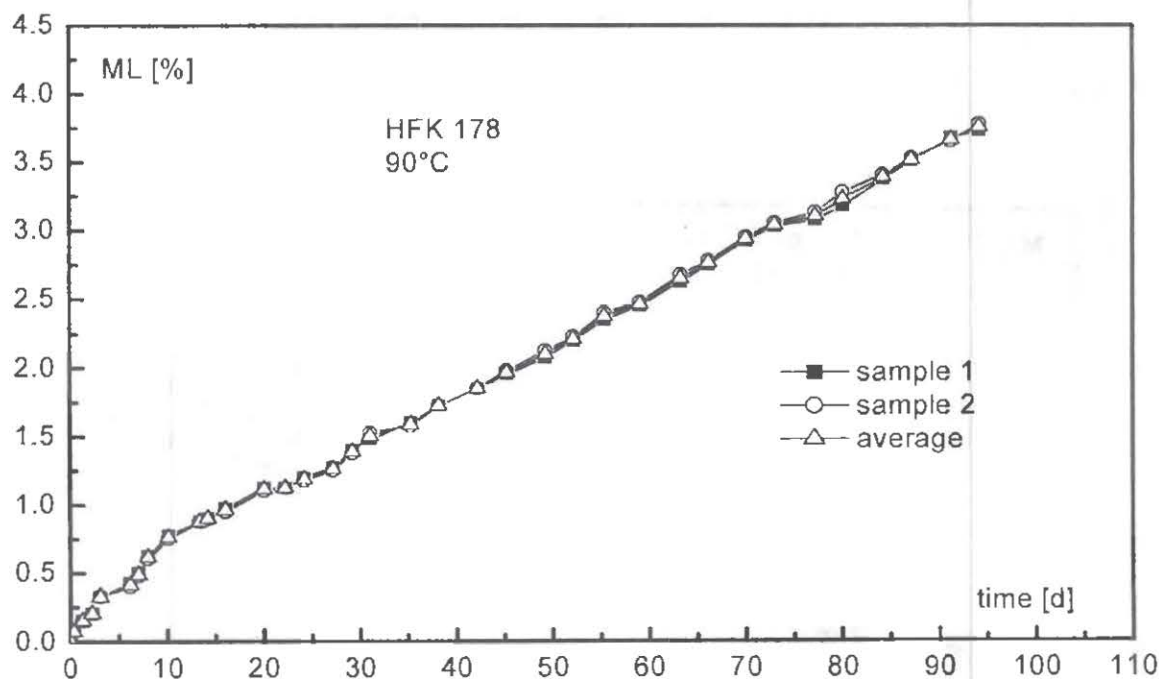


Fig. 1: Mass loss data of HFK 178 at 90°C. The data of both parallel samples coincide.

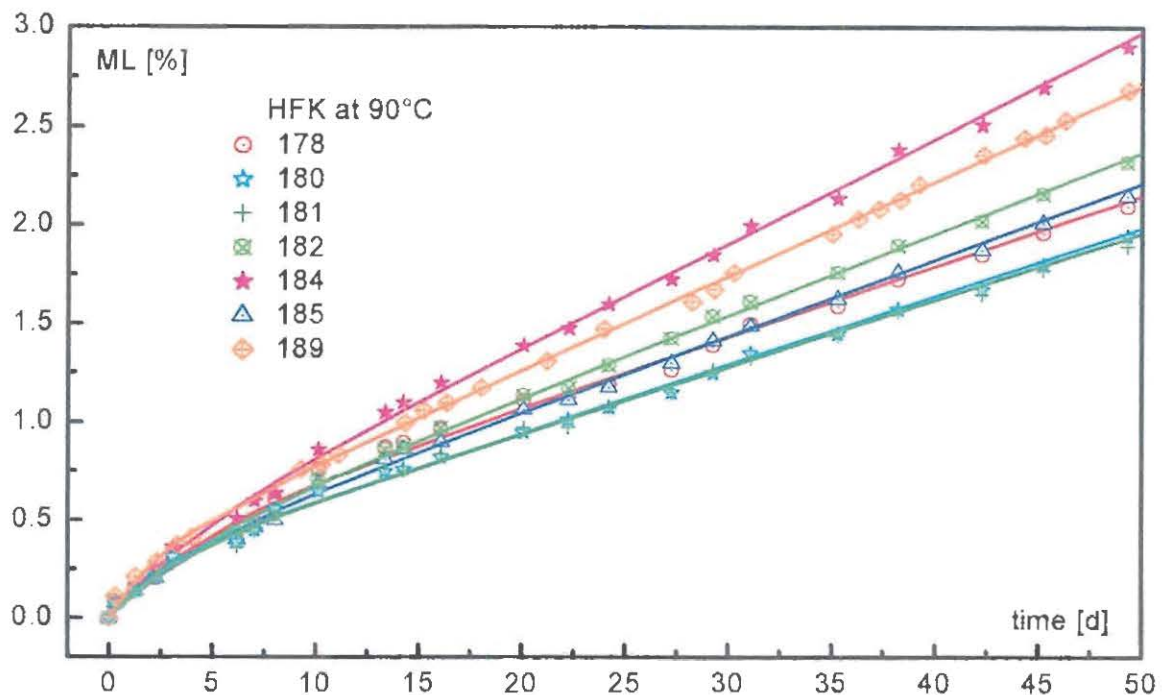


Fig. 2: ML data of seven HFK batches at 90°C. The lines are the model 'ML: linear + exponential'.

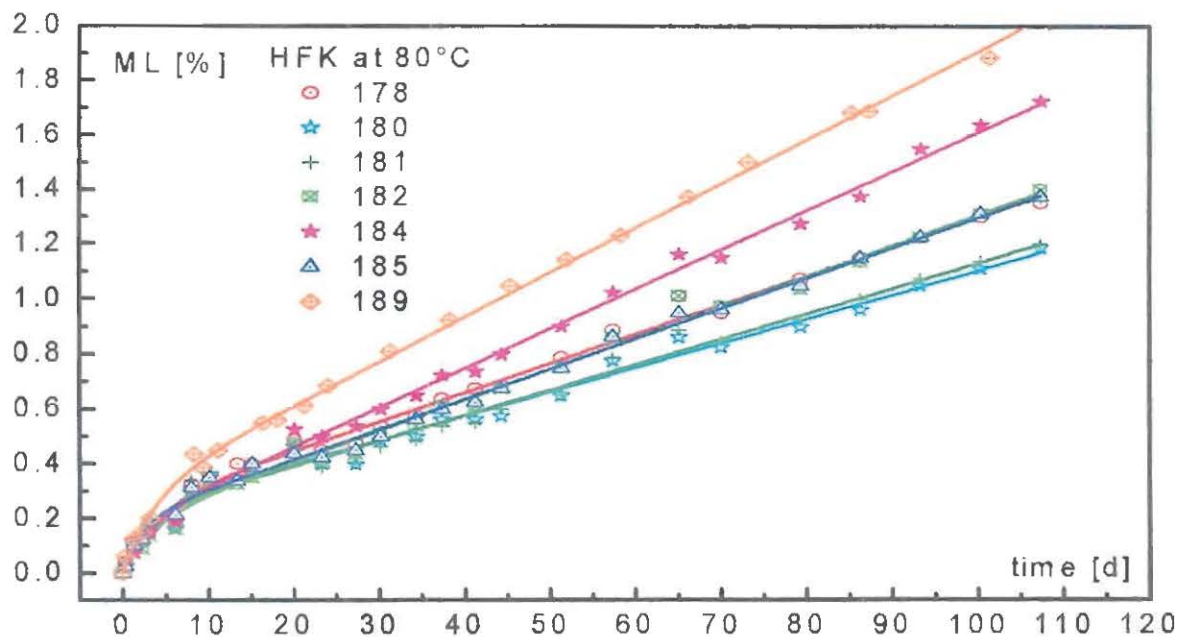


Fig. 3: ML data of seven HFK batches at 80°C. The lines are the model 'ML: linear + exponential'.

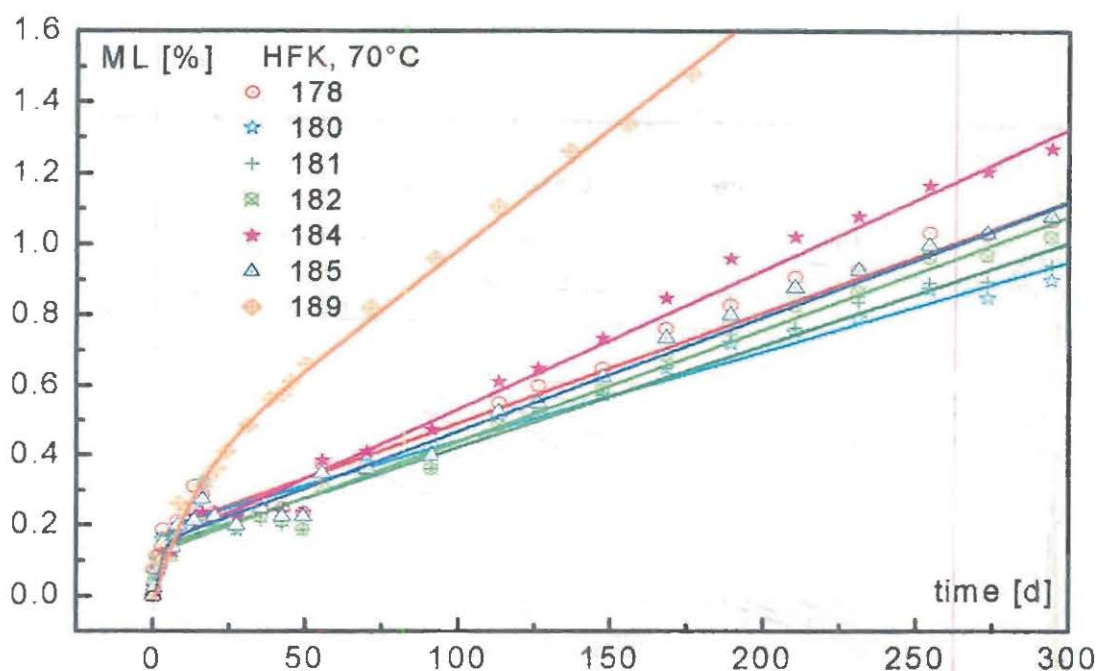


Fig. 4: ML data of seven HFK batches at 70°C. The lines are the model 'ML: linear + exponential'.

2.3 Heat generation rate data

The heat generation rates (HGR) dQ/dt of the HFK batches at 89°C, 80°C and 70°C are shown in the Figs. 5, 6 and 7. By integration over time, the heat generations (HG) Q are obtained, which are also presented in the figures with bold lines, correlating with the right ordinates. The measurement procedure used is different compared with the one used for the mass loss measurements. In that case, new sample material was taken at each temperature. Here the measurements start in measuring series I with unstressed material at 80°C, Fig. 6. Then using the same samples the measurements continued at 70°C, Fig. 7, and then the measurements were taken at 89°C, Fig. 5. This procedure is named 'pseudo-iso-conversion' method, also abbreviated to 'pic mode'. The conversion achieved at 80°C is nearly not changed at 70°C because of the lower decomposition rate and the short measurement times. At 89°C one has again nearly the same conversion state as at 80°C. At this state of conversion the Arrhenius parameters can be obtained in a much shorter time than using unstressed material at all measurement temperatures. This method works good if the sample decomposes with one defined reaction. In the case of a defined reaction of zero order this method is even free of error. One measures just the HGR, which is directly proportional to the reaction rate constant. With autocatalytic systems the HGR will not scale correctly in pic mode.

There is one obvious difference in the HGR curves measured using unstressed material and in pic-mode. At the beginning, the unstressed material shows a peak in the curves. This is the HGR caused by the residual curing reaction of the binder, which does not occur in pic mode measurements.

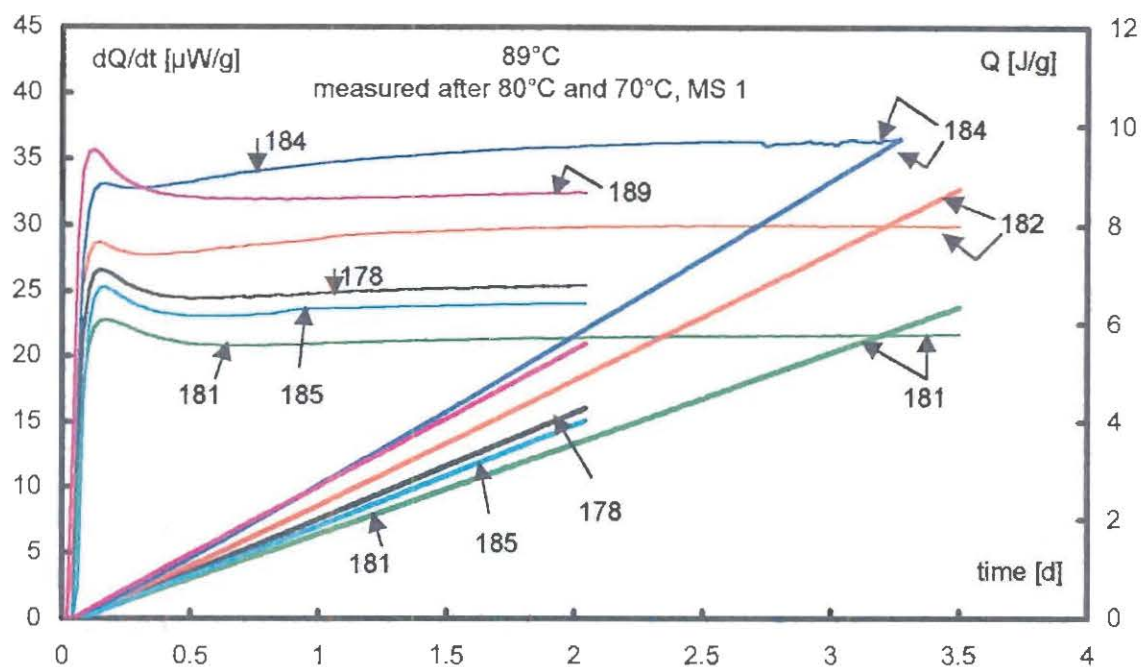


Fig. 5: HGR dQ/dt and HG Q (bold lines) of HFK batches at 89°C, determined in pseudo-iso-conversion mode after measurements had been taken at 80°C and 70°C.

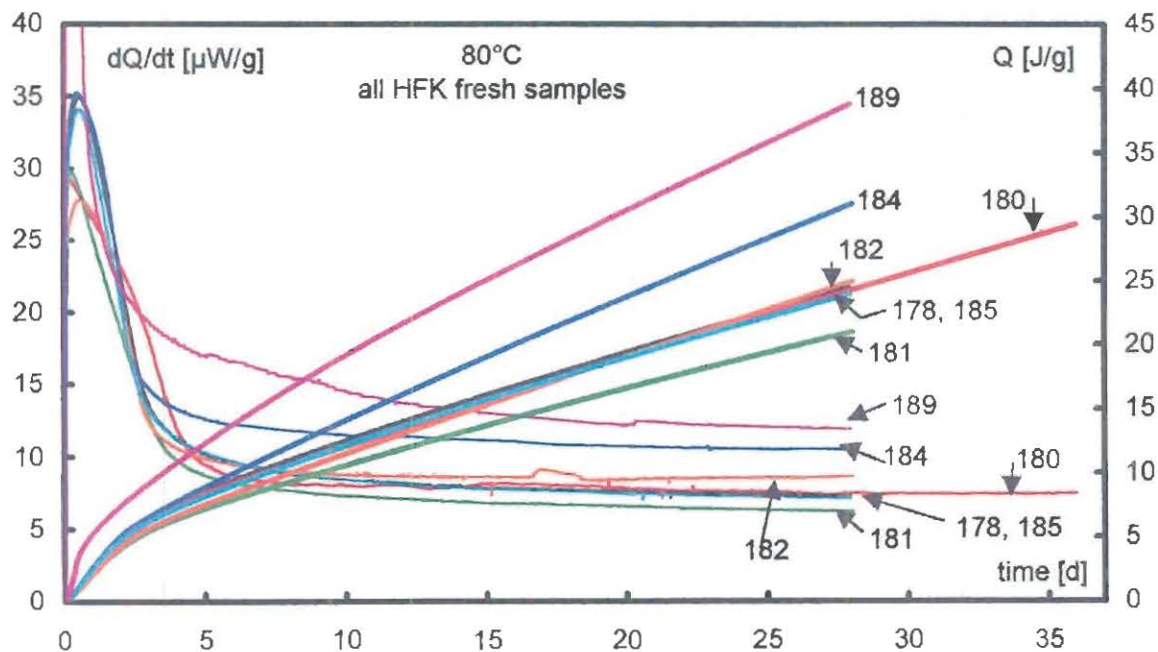


Fig. 6: HGR dQ/dt and HG Q (bold lines) of HFK batches at 80°C, determined using fresh samples.

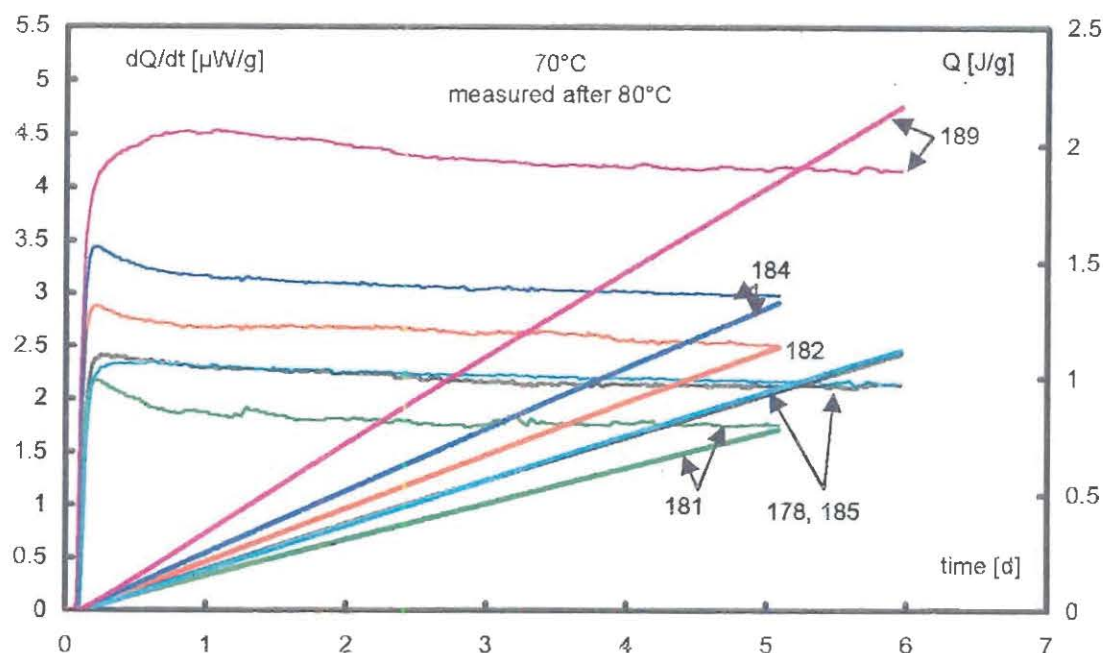


Fig. 7: HGR dQ/dt and HG Q (bold lines) of HFK batches at 70°C, determined in pseudo-iso-conversion mode after measurements had been taken at 80°C.

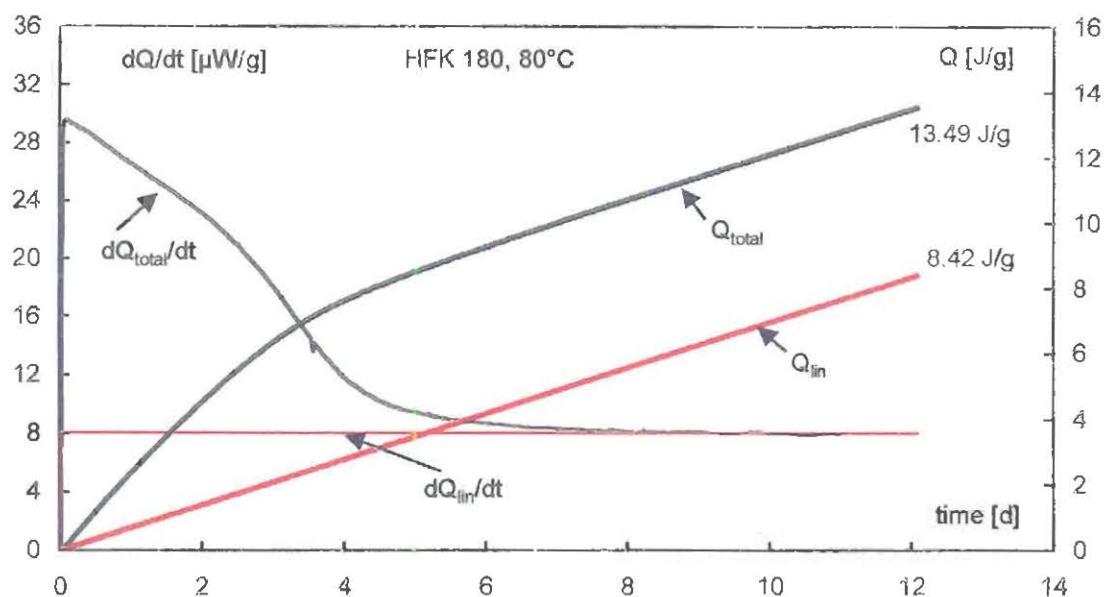


Fig. 8: Separation between initial and long term behaviour in HGR and HG for HFK 180.

For all HFK batches the HG has an analogous course to the ML: the initial flexure (with unstressed material) is followed by a linear increase, which again is indicative of a global decomposition reaction of pseudo zero order. Both measurement quantities mass loss and heat generation rate lead to the same interpretation of the data. However, the residual curing as an

addition reaction to form the polyurethane binder is not recognized by mass loss, but this is an advantage of this method in the context of stability and ageing assessment.

Fig. 8 shows the separation in both HGR and HG into the initial range and into the range relevant for the assessment, also named 'linear'. In Figs. 6 and 8 the initial courses are determined by a residual curing reaction of the binder and furthermore by a decomposition reaction as the ML data indicate. In Table 3 HGR data are compiled. All data are taken in the region with a pseudo zero order behaviour, that means the HGR is nearly constant with time.

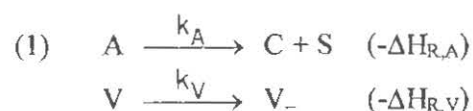
Table 3: Heat generation rate data from the linear part in HG of HFK batches obtained after the given times. 'pic' mode means measured in 'pseudo-iso-conversion' mode.

		dQ/dt [μ W/g]						
<i>Meas. Series 1</i>	time	178	180	181	182	184	185	189
70°C, pic mode after 80°C	3.0 d	2.16	./.	1.76	2.62	3.04	2.22	4.25
80°C new samples	27.5 d	7.38	7.46	6.26	8.69	10.55	7.16	11.95
89°C, pic mode after 80°C, 70°C	2.0 d	25.43	./.	21.42	29.87	35.95	24.08	32.48
<i>Meas. Series 2</i>	time							
70°C, pic mode after 89°C	5.0 d	2.94	2.64	2.62	./.	4.34	2.9	4.96
80°C, pic mode after 89°C, 70°C	4.5 d	8.84	8.41	7.58	./.	13.21	8.67	14.37
89°C new samples	16.5 d	26.77	27.13	22.79	34.4	41.45	26.13	36.72

3. Discussion

3.1 Mass loss

The mass loss data are analysed using the model 'ML: linear + exponential', corresponding to 'zero order reaction + first order reaction'. The reaction scheme is shown in Eq.(1), it is formulated in molar concentrations with $(-\Delta H_{R,i})$ as reaction enthalpies.



The global main component A of a formulation decomposes in gaseous products C (in the scheme C summarizes over all gaseous products) and in the residue remaining products S (S summarizes over all remaining products). The main component A is assigned to a reaction of zero order. The minor component V can evaporate or decompose into gaseous products

according to a reaction of first order. The initial mass of V in the sample is expressed as part of the total sample mass M, $M_V(0) = a \cdot M(0)$. The detailed formulation can be found in the literature /4, 5/. Using the following model settings, Eq.(2) results, formulated for the mass loss ML.

- $M_S(0)$ is zero
- the mass M_N of a non-reacting ingredient is small
- the molar mass ratio m_C/m_A is set approximately to one

$$(2) \quad ML(t, T) = OF_{ML} + 100\% \cdot \left(\frac{m_C}{m_A} \cdot (1-a) \cdot \underbrace{k_{ML}(T) \cdot t}_{\text{zero order reaction}} + a \cdot \underbrace{(1 - \exp(-k_V(T) \cdot t))}_{\text{first order reaction}} \right)$$

$$(3) \quad k_{ML}(T) = k_A(T) \cdot \frac{m_A}{M_A(0)}$$

$k_{ML}(T)$ is connected with the reaction rate constant $k_A(T)$ from Eq.(1) via Eq.(3). In the experimental data the offset OF_{ML} was always zero. Then only three model parameters remain to be determined: a , k_V and k_{ML} , which is done with a non-linear fit algorithm.

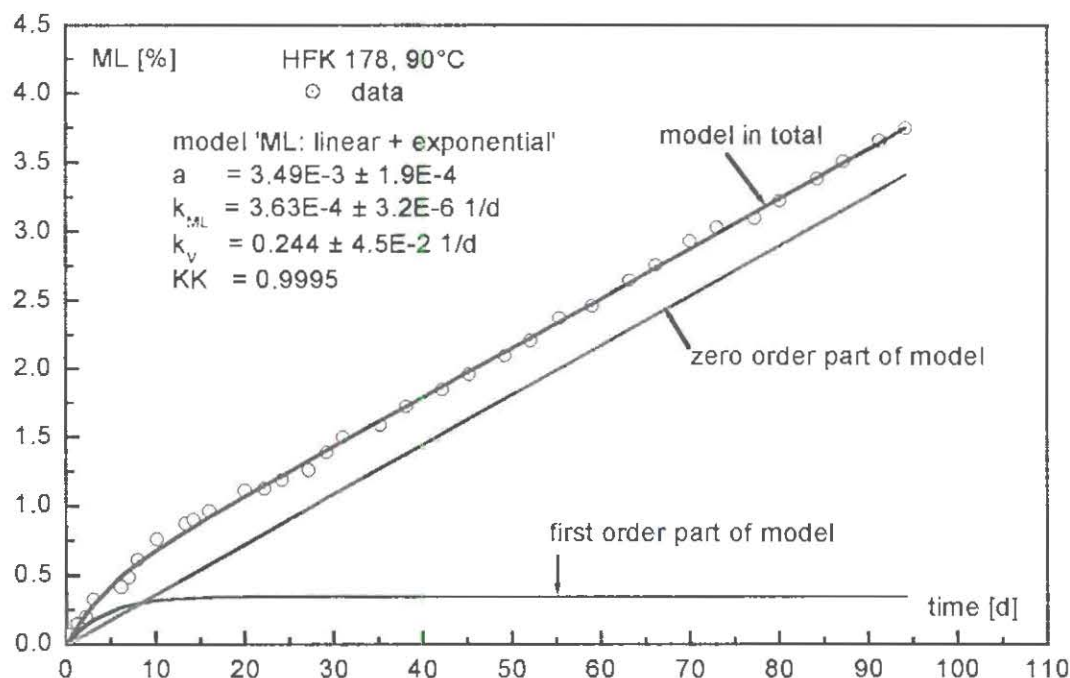


Fig 9: Application of model 'ML: linear + exponential'. For all seven HFK the description was equally good. The separation of the sum curve into both model parts 'zero order' and 'first order' is shown.

In Fig. 9 the description with Eq.(2) is shown with HFK 178 at 90°C as example. The model results are summarized in Table 4. The reaction rate constant k_{ML} and the mass fraction a are scaled by 100%. The correlation coefficients KK of the model descriptions of the seven batches are high at all temperatures. Qualitatively, all HFK batches show identical ageing behaviour, see Figs. 2 to 4. The Arrhenius parameters of $k_{ML}(T) \cdot 100\%$ are given in Table 5. Also a step by step evaluation was performed, that means the calculation of the Arrhenius parameters using pairs of temperatures. From this, one can conclude that the activation energies decrease with decreasing temperatures. This effect is pronounced with HFK 189, the lower value of 86.3 kJ/mol is about 26% less than the higher value.

Table 4: The model parameters k_{ML} , k_V and a , and the correlation coefficients KK of the model fits. k_{ML} and a are scaled by 100%.

90°C		178	180	181	182	184	185	189
$k_{ML} \cdot 100\%$	[%/d]	0.036	0.035	0.034	0.042	0.054	0.039	0.048
k_V	[1/d]	0.24	0.41	0.34	0.22	0.24	0.25	0.43
$a \cdot 100\%$	[%]	0.35	0.25	0.26	0.29	0.31	0.27	0.30
KK	[-]	0.9995	0.9996	0.9995	0.9993	0.9993	0.9996	0.9997
80°C								
$k_{ML} \cdot 100\%$	[%/d]	0.0106	0.0089	0.0093	0.0114	0.0145	0.0111	0.0160
k_V	[1/d]	0.244	0.297	0.352	0.275	0.322	0.419	0.23
$a \cdot 100\%$	[%]	0.24	0.22	0.21	0.18	0.17	0.19	0.30
KK	[-]	0.997	0.995	0.996	0.997	0.999	0.999	0.9994
70°C								
$k_{ML} \cdot 100\%$	[%/d]	0.00315	0.00255	0.00291	0.0032	0.00395	0.00325	0.00679
k_V	[1/d]	0.656	0.396	0.558	0.719	0.415	0.542	0.080
$a \cdot 100\%$	[%]	0.18	0.19	0.14	0.12	0.14	0.15	0.31
KK	[-]	0.995	0.994	0.996	0.997	0.997	0.997	0.999

Table 5: Arrhenius parameters of the reaction rate constants $k_{ML}(T) \cdot 100\%$. A calculation of the parameters using pairs of temperatures is shown, indicating a change in the parameters going from higher to lower temperatures.

T. range [°C]		178	180	181	182	184	185	189
90 - 70	E_{aML} [kJ/mol]	126.2	135.6	127.2	133.3	135.4	128.7	101.1
	$\lg(Z_{ML} \text{ [%/d]})$	16.70	18.03	16.82	17.79	18.20	17.09	13.21
	KK	0.9997	0.9982	0.9977	0.9994	0.9996	0.9995	0.9923
pairs of temperature evaluation								
90 - 80	E_{aML} [kJ/mol]	130.4	146.0	138.2	139.1	140.2	134.0	117.1
	$\lg(Z_{ML} \text{ [%/d]})$	17.31	19.55	18.41	18.62	18.90	17.86	15.53
80 - 70	E_{aML} [kJ/mol]	122.3	125.9	117.1	128.0	130.9	123.7	86.3
	$\lg(Z_{ML} \text{ [%/d]})$	16.11	16.58	15.28	16.99	17.53	16.34	10.97

To assess the in-service time periods one defines an allowed limit value of a quantity. With mass loss generally 3% is taken. The degree of mass change is y_{ML} and given in Eq.(4). With Eq.(5) the times $ty_{ML}(T)$ or $ty_{ML,L}(T)$ to reach the given limit value M_L or the limit degree $y_{ML,L}$ can be calculated. The times at 50°C to reach 3% ML are listed in Table 6.

$$(4) \quad y_{ML} = \frac{M(ty_{ML}(T))}{M(0)} = M_r(ty_{ML}(T)) = 1 - k_{ML}(T) \cdot ty_{ML}(T)$$

$$y_{ML,L} = \frac{M_L}{M(0)} = M_{r,L} = 1 - k_{ML}(T) \cdot ty_{ML,L}(T)$$

$$(5) \quad ty_{ML}(T) = \frac{1 - y_{ML}}{k_{ML}(T)} \quad ty_{ML,L}(T) = \frac{1 - y_{ML,L}}{k_{ML}(T)}$$

Table 6: Times $ty_{ML,L}(T)$ in years to reach a mass loss of 3% at 50°C, calculated according to Eq.(5) with the corresponding Arrhenius parameters for $k_{ML}(T)$.

<i>T. range [°C]</i>		178	180	181	182	184	185	189
90 - 70	ty_{ML} (3% ML, 50°C) [a]	41.1	63.6	45.2	46.9	39.9	42.5	11.1
90 - 80	ty_{ML} (3% ML, 50°C) [a]	48.2	92.1	69.7	60.1	47.5	51.8	20.6
80 - 70	ty_{ML} (3% ML, 50°C) [a]	37.5	48.5	36.6	41.2	35.0	37.1	7.8

3.2 Heat generation rate

The two parts of the model for mass loss, Eq.(2), are given with heat generation by Eq.(6) for the pseudo zero order reaction and by Eq.(7) for the first order part. OF_Q is as OF_{ML} a possible offset. A third contribution to the total HG is shown by Eq.(8). It stands for the residual curing reaction of the binder. This curing reaction is no longer present in the materials measured in pic mode.

$$(6) \quad Q_A(t, T) = OF_Q + (k_{Q,A}(T) \cdot t) \quad \text{with} \quad k_{Q,A}(T) = k_A(T) \cdot (-\Delta H_{R,A})$$

$$(7) \quad Q_V(t, T) = OF_Q + (-\Delta H_{R,V}) \cdot a \cdot (1 - \exp(-k_V(T) \cdot t))$$

$$(8) \quad Q_{curing}(t, T) = OF_Q + (-\Delta H_{R,curing}) \cdot F_{curing}(t, T)$$

In Table 7 the Arrhenius parameters determined using the data from Table 3 are presented. As a reminder, index G indicates the global type of heat generation measured in complex systems such as the HFK batches. Also an evaluation was made using pairs of temperatures. The same results are achieved here as are achieved with the mass loss. As temperature decreases, the activation energy decreases.

The second series of measurements shows lower activation energies than the first one. This is interpreted with the order of temperature measurements. Here an initial temperature of 89°C was used, this was followed by a temperature of 70°C, which was followed by a temperature of 80°C. Because measurement periods at 89°C were relatively long, up to 17 days, sample ageing was stronger than in measurement series 1. The reason for such a long measurement time was the surprising complexity of the HGR curves at 89°C with fresh samples, which caused longer times to reach the pseudo zero order state. The therefore higher degree of conversion results in a higher decomposition activity at lower temperatures, which results in lower activation energies by the Arrhenius parameter determination. This interpretation would not be valid in a system with one defined decomposition reaction according to zero or first order. It is applicable because of the complex reaction courses in these batches.

Table 7: Arrhenius parameters calculated from the pseudo zero order HGR data given in Table 3. A calculation of the parameters using pairs of temperatures is shown, indicating a change in the parameters going from higher to lower temperatures.

Measurement Series 1		178	180	181	182	184	185	189
T. range [°C]								
89 - 70	Ea _{Q,G} [kJ/mol]	134.8	./.	135.4	134.2	135.0	130.6	111.5
	lg(Z _{Q,G} [μW/g])	20.84	./.	20.84	20.81	21.02	20.20	17.58
	KK	0.9981	./.	0.9985	0.9980	0.9986	0.9975	0.9990
		pairs of temperatures evaluation						
89 - 80	Ea _{Q,G} [kJ/mol]	146.2	./.	145.3	145.9	144.9	143.3	118.1
	lg(Z _{Q,G} [μW/g])	22.49	./.	22.29	22.52	22.45	22.05	18.55
80 - 70	Ea _{Q,G} [kJ/mol]	125.7	./.	127.3	124.7	127.0	120.3	106.1
	lg(Z _{Q,G} [μW/g])	19.46	./.	19.62	19.39	19.81	18.65	16.77
Measurement Series 2								
T. range [°C]								
89 - 70	Ea _{Q,G} [kJ/mol]	119.9	126.4	117.3	./.	122.4	119.3	108.8
	lg(Z _{Q,G} [μW/g])	18.70	19.65	18.26	./.	19.26	18.61	17.26
	KK	0.9977	0.9976	0.9969	./.	0.9971	0.9977	0.9999
		pairs of temperatures evaluation						
89 - 80	Ea _{Q,G} [kJ/mol]	130.9	138.4	130.1	./.	135.1	130.4	110.9
	lg(Z _{Q,G} [μW/g])	20.31	21.39	20.12	./.	21.10	20.22	17.55
80 - 70	Ea _{Q,G} [kJ/mol]	110.9	116.7	107.0	./.	112.2	110.4	107.2
	lg(Z _{Q,G} [μW/g])	17.35	18.19	16.71	./.	17.71	17.26	17.01

The in-service time periods based on HGR and HG respectively can be determined analogously to the same way as with mass loss. But there is one essential difference. For mass loss the easily determinable initial value M(0) is available as the reference. For HG the corresponding reference value would be the value obtained after the complete decomposition

reaction of the substance, *but at the temperatures of interest*. These data are practically not obtainable on formulations investigated here. It would take many years of measurement. Therefore the heat of explosion Q_{EX} is taken as $Q_{reference}$. This may result in a systematic error, because the decomposition reactions are different when obtaining Q_{EX} compared with the slow ageing at temperatures between 30°C and 90°C. In the first case thermodynamics nearly completely controls the reaction channels, in the second case kinetic control is dominant. Eq.(9) gives the definition of the degree of energy change in the formulation. The permitted limit value Q_L is typically 97% of the reference. For the standard case, the times $ty_{Q,L}(T)$ must be determined using Eq.(10).

$$(9) \quad y_{Q,L} = \frac{Q_L}{Q_{reference}} = 1 - \frac{Q(ty_{Q,L}(T))}{Q_{reference}}$$

$$(10) \quad (1 - y_{Q,L}) \cdot Q_{reference} = \int_0^{ty_{Q,L}(T)} (dQ(t, T)/dt) \cdot dt$$

For a zero order reaction Eq.(10) simplifies to Eq.(11). According to Eq.(12) the needed HGR values can be calculated at the required temperatures with the Arrhenius parameters. Table 8 shows the times necessary to reach an energy loss of 3% at 50°C.

$$(11) \quad ty_{Q,L}(T) = \frac{(1 - y_{Q,L}) \cdot Q_{reference}}{(dQ(T)/dt)}$$

$$(12) \quad \ln(dQ(T)/dt) = \ln(k_{Q,G}(T)) = \ln(Z_{Q,G}) - E_{a,Q,G} / RT$$

Table 8 also contains additional data for the thermal critical radius of the HFK batches, calculated according to the Frank-Kamenetzskii description of thermal explosion caused by self heating in stationary phases, Eq.(13). The meaning of the symbols is given with the equation. The value of the critical Frank-Kamenetzskii parameter δ_c is 2.0 for a cylinder with infinite length. The values of 0.2 W/m/K and 1.6 g/cm³ have been taken for heat conductivity and mass density. The results on the values of $r_{C,FK}$ show that problems may arise if heating of the propellant cannot be avoided when the rocket system is at high speed.

$$(13) \quad r_{C,FK} = \sqrt{\frac{\delta_c \cdot \lambda}{\rho} \cdot \frac{RTw^2}{E_{a,Q,G}} \cdot \frac{1}{Z_{Q,G}} \cdot \exp(+E_{a,Q,G} / RTw)}$$

δ_c	critical Frank-Kamenetzskii parameter (FKP _C), its value is shape dependent [-]
$r_{C,FK}$	thermal critical radius [length] at given wall temperature Tw
ρ	mass density [mass/volume]
λ	heat conductivity [energy/time/length/K]
Tw	storage temperature (wall temperature of the sample) [K]
R	general gas constant (8.3144 J/mol/K)
$E_{a,Q,G}$	activation energy of the global heat generation rate [energy/mol]
$Z_{Q,G}$	pre-exponential factor of the global heat generation rate [energy/mass/time]

Table 8: Times $ty_{Q,L}$ in years to reach 3% energy loss at 50°C calculated using Eq.(11). The reference quantity $Q_{reference}$ is the heat of explosion with gaseous water. Furthermore the critical radius $r_{C, FK}$ (values in meters) is listed according to Frank-Kamenetzki for a cylindrical shape (infinite length) at several environmental temperatures T_w between 50°C and 110°C, calculated using Eq.(13).

	178	180	181	182	184	185	189
$Q_{EX, gw}$ [J/g]	4540	4670	4700	5050	4880	4510	4750
Measurement Series 1							
$ty_{Q,L}$ (3% $Q_{EX, gw}$, 50°C) [a]	38.4	./.	49.7	36.6	29.4	34.9	12.5
$r_{C, FK}$ (50°C) [m]	3.78	./.	4.22	3.51	3.19	3.68	2.32
$r_{C, FK}$ (71°C) [m]	0.87	./.	0.97	0.81	0.73	0.89	0.70
$r_{C, FK}$ (90°C) [m]	0.27	./.	0.30	0.25	0.23	0.28	0.27
$r_{C, FK}$ (110°C) [m]	0.09	./.	0.10	0.08	0.07	0.10	0.11
Measurement Series 2							
$ty_{Q,L}$ (3% $Q_{EX, gw}$, 50°C) [a]	20.7	26.9	22.4	./.	15.5	20.2	9.6
$r_{C, FK}$ (50°C) [m]	2.95	3.22	3.05	./.	2.44	2.93	2.06
$r_{C, FK}$ (71°C) [m]	0.80	0.82	0.86	./.	0.65	0.80	0.64
$r_{C, FK}$ (90°C) [m]	0.28	0.27	0.31	./.	0.22	0.29	0.25
$r_{C, FK}$ (110°C) [m]	0.11	0.10	0.12	./.	0.08	0.11	0.10

4. Conclusion

The ranking of the HFK batches corresponding to their ageing rate is:
according to mass loss, evaluated with k_{ML}

90°C : 184 > 189 > 182 > 185 > 178 > 180 ≈ 181
80°C : 189 > 184 > 182 ≈ 185 > 178 > 181 ≈ 180
70°C : 189 >> 184 > 185 ≈ 182 > 178 > 181 > 180

according to heat generation rate, evaluated with HGR in the linear region
measurement series 1

89°C : 184 > 189 > 182 > 178 > 185 > 181 (no data for 180)
80°C : 189 > 184 > 182 > 180 > 178 > 185 > 181
70°C : 189 >> 184 > 182 > 185 ≈ 178 > 181 (no data for 180)

measurement series 2

89°C : 184 > 189 > 182 > 180 > 178 ≈ 185 > 181
80°C : 189 > 184 > 178 ≈ 185 > 180 > 181 (no data for 182)
70°C : 189 >> 184 > 178 ≈ 185 > 180 ≈ 181 (no data for 182)

The main sequence is determined by the nitric acid esters BTTN and TMETN which explains the series of 189, 184 and 182. After the position of HFK 182 the differences in the rates are quite small, and the more detailed ranking following the position of HFK 182 seems to be co-influenced by the reactive interaction between GAP and ϵ -CL20 /6/. A different temperature dependence is indicated for HFK 189. It shows a lower activation energy than the other batches. However, based on the summarized chemical decomposition reactions, the thermal ageing behaviour of all investigated HFK batches is favourable, in spite of the lack of stabilizers for the nitric acid ester plasticizers. Both measurement methods mass loss and heat generation rate provide a congruent information on the ageing of the HFK batches.

5. Acknowledgment

Dr. Klaus Menke and Mr. Siegfried Eisele, both at ICT, have designed and manufactured the HFK batches.

The work was financed by the German Bundesministerium für Verteidigung (BMVg).

6. References

- /1/ S. Eisele, K. Menke
About the Burning Behaviour of Smoke Reduced Composite Propellants based on AP / CL20 / GAP
Proceed. 32nd International Annual Conference of ICT, pages 149-1 to 149-18, July 3-6, 2001, Karlsruhe, Germany. Fraunhofer-Institut für Chemische Technologie (ICT), Postfach 1240, D-76318 Pfinztal-Berghausen, Germany.
- /2/ STANAG (Standardization Agreement) 2895
Extreme climatic conditions and derived conditions for use in defining design and test criteria for NATO forces material
1990, NATO Headquarters, Military Agency for Standardization, Bruxelles, Belgium.
- /3/ H. Bathelt, F. Volk, M. Weindel
The ICT Thermochemical Data Base
Proceed. 30th International Annual Conference of ICT, pages 56-1 to 56-12, June 29 - July 2, 1999, Karlsruhe, Germany. Fraunhofer-Institut für Chemische Technologie (ICT), Postfach 1240, D-76318 Pfinztal-Berghausen, Germany.
- /4/ M.A. Bohn
Modelling of the stability, ageing and thermal decomposition of energetic components and formulations using mass loss and heat generation
Proceed. 27th International Pyrotechnics Seminar, pages 751 to 770, July 16-21, 2000, Grand Junction, Colorado USA.
- /5/ M.A. Bohn
Kinetic Description of Mass Loss Data for the Assessment of Stability, Compatibility and Aging of Energetic Components and Formulations Exemplified with ϵ -CL20
Propellants Explosives Pyrotechnics 27, issue 3 (2002), in press.
- /6/ V. Thome, P.B. Kempa, M.A. Bohn
Erkennen von Wechselwirkungen der Nitramine β -HMX und ϵ -CL20 mit Formulierungskomponenten durch Computersimulation
Proceed. 31st International Annual Conference of ICT, pages 63-1 to 63-20, June 27-30, 2000, Karlsruhe, Germany. Fraunhofer-Institut für Chemische Technologie (ICT), Postfach 1240, D-76318 Pfinztal-Berghausen, Germany.

THIS PAGE LEFT INTENTIONAL BLANK

A Comparison Study on Decomposition of Liquid Nitrate Esters with Microcalorimeter and Chemiluminescence (CL) Analyzer

Jun-ichi Kimura, CL Advisor, Tohoku Electronic Industry Co. Ltd.

Tohoku Electronic Industrial Co., Ltd. 6-6-6 Shirakasadai, Rifu, Miyagi, Japan 981-0134

Fax: +81-22-356-6120, e-mail: jkr@vm.catv.ne.jp or rie@tohokudensi.co.jp

1. Introduction

Chemiluminescence (CL) is classified into three different types; autonomous chemiluminescence (ACL), oxyluminescence (OXL) and enhanced chemiluminescence (ECL). ACL is originated from thermal decomposition of oxygen-rich compounds such as organic peroxides and explosives, which emit ultra weak light even under an inert atmosphere. OXL is the luminescence due to autoxidation of organic materials. ECL uses oxidizer (OX: H_2O_2) and light-emitting material (LEM: luminol or aldehydes) in liquid phase. Consequently CL emission from ECL is normally strong compared to other two CL. ECL has been practically used to analyze lipid peroxides and natural antioxidants combined with HPLC.

CL is light emission phenomenon due to highly exothermic chemical reaction, where some products are excited electronically by heat of reaction. The light emitting-species should be conjugated systems, carbonyl compounds, and molecular oxygen. CL techniques have become one of the most sensitive method to evaluate the aging of almost all the organic compounds. There is advantage to the selectivity of CL: characteristic groups and oxygen may be recognized in molecules of widely varying complexities. Because of the low luminescence efficiency ($\sigma = 10^{-6}$ to 10^{-10}) for ACL and OXL compared to that of fluorescence and phosphorescence ($\sigma = 1$ to 10^{-4}), very weak emission of light is normally not observed in routine measurements of conventional emission spectrometers. Light detection sensitivity of CL analyzers and CL spectrometers normally ranges from pW to nW per cm^2 of a sample.

2. Experimental

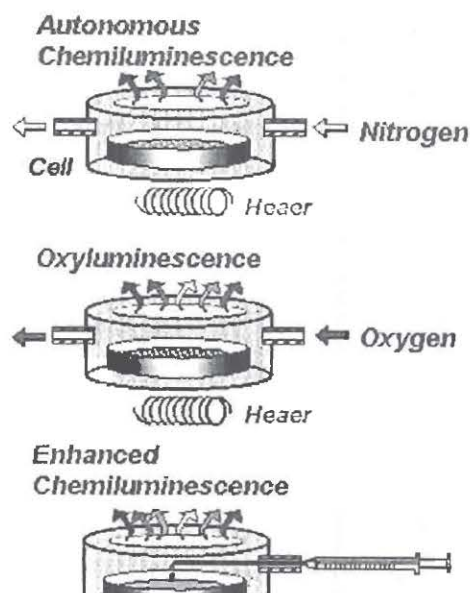


Figure 1 General experimental setups for three different types of chemiluminescence

Apparatus

The low-level luminous intensity of CL was measured with a CL analyzer CLD-100 and CLA FC-2 spectrometer, which are the products of Tohoku Electric Industry, Sendai, Japan. Cut-view of CL apparatus and experimental set-up is shown in Fig. 2. A test sample of approximately 3g was set in a stainless steel pan with a diameter of 50mm (height: 10mm) and heated up to a predetermined temperature below 160°C in nitrogen with a flow rate of 60 ml min⁻¹. The sample pan was set into a closed cell equipped with a quartz window on the top.

The detection range of luminous intensity for these CL apparatus apparatus were estimated to be from a few pW to a few nW at a wavelength of 420nm, where their photo multiplier tubes exhibit the highest sensitivity. It should be pointed out that the CL intensity depends on the surface area but not the sample weight. Graphite coating of propellants grains, however, did not affect the CL intensity probably due to the porosity of the coated grain.

In the calorimetric measurements Micro DSC III made by Setaram in France were employed. Sample and reference vessel are made of Hastelloy C (pressure-resistance: 20 bar; volume: 1.2ml). Micro DSC III has a detection sensitivity of 0.2 μW and the heating temperature ranges from -20°C to 120°C.

Samples

Three liquid nitrate esters were used as the test samples for comparison between heat generation rates and CL intensities. These are trimethylolethane trinitrate (TMETN), triethyleneglycol dinitrate (TEGDN) and diethyleneglycol dinitrate (DEGDN). All the samples were degassed in vacuum oven at room temperature to reduce signal noise. In the CL measurements these samples were used without degassing.

3. Results and Discussions

The three liquid nitrate esters exhibited the similar temperature dependence of heat

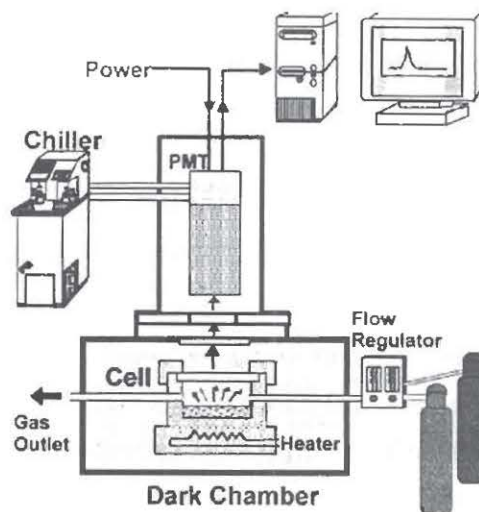


Figure 2 Experimental set-up of a CL apparatus with a gas flow control system.

generation rate as depicted in Fig. 3 and Fig. 4. In the Arrhenius plots the ordinate is heat generation rate in a unit of $\mu\text{W/g}$ in Fig. 3, in a unit of $\mu\text{W/mol}$ in Fig. 4. As can be seen in Fig. 4, all the data points at the same temperature were overlapped. Activation energy for heat generation rate was obtained to be $12.5 \text{ kcal mol}^{-1}$ (52.5 kJ mol^{-1}). This value is rather low compared to that ($23.0 \text{ kcal mol}^{-1}$ (96.6 kJ mol^{-1})) from NO_x evolution rate for DEGDN and TEGDN. If NO_2 act as an oxidizer in the self-oxidation of nitrate esters, the activation energy for heat generation rate should be the same value with that for NO_x generation rate. The O/F ratio for these three nitrate esters is the order as follows: $\text{TMETN} > \text{DEGDN} > \text{TEGDN}$. It should be pointed out that the two dinitrate esters and the one trinitrate ester exhibited the same heat generation rates in a unit of $\mu\text{W/mol}$. This coincidence implies that two nitrate ester groups ($-\text{O}-\text{NO}_2$) react with each other to generate another oxidizer, which is probably oxygen.

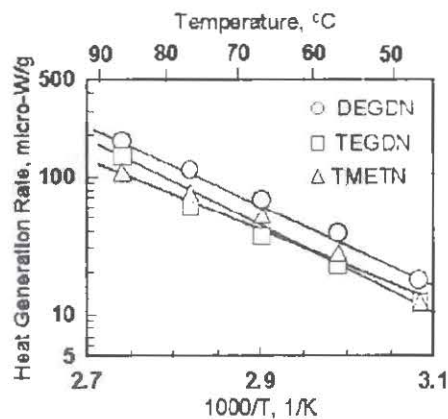


Figure 3 Arrhenius plots of heat generation rate in a unit of $\mu\text{W/g}$ for three liquid nitrate esters.

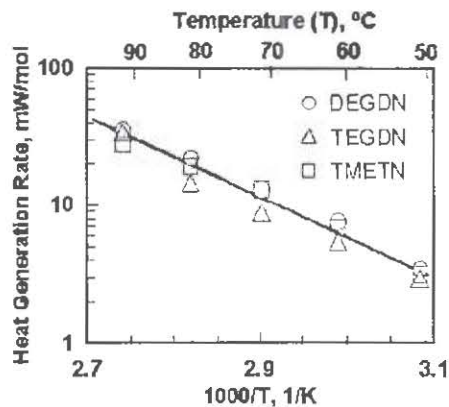


Figure 4 Replot of the Arrhenius plots (Fig. 3) in a unit of mW/g . Activation energy was obtained to be $12.5 \text{ kcal mol}^{-1}$ (52.5 kJ mol^{-1}).

CL intensities for the three nitrate esters were measured in flowing nitrogen atmosphere at a flow rate of 60 ml/min in the temperature range from 50°C to 90°C . Figure 5 shows the Arrhenius plots for CL intensities for DEGDN and TEGDN. CL emission arises from the surface but not from the bulk. Thus it is difficult to convert the CL intensities in a unit of count/sec per surface area of the sample pan with a diameter of 5 cm to that in a unit of count/sec per number of molecules on the surface.

Activation energy of CL emission for DEGDN was 11.3 kcal/mol and 10.4 kcal/mol for both TEGDN and TMETN, whose values are close to the value of 12.5 kcal/mol obtained with calorimetric measurements (Fig. 4). DEGDN exhibited high CL emission probably due to the contracted conformation of DEGDN estimable with MM and MO calculation. Density of DEGDN (1.38 g/cm³) is higher than TEGDN (1.335) despite the lower molecular weight. Consequently it can be thought the difference in number of molecules between DEGDN and TEGDN would be higher than that estimated based on the difference in molecular weight.

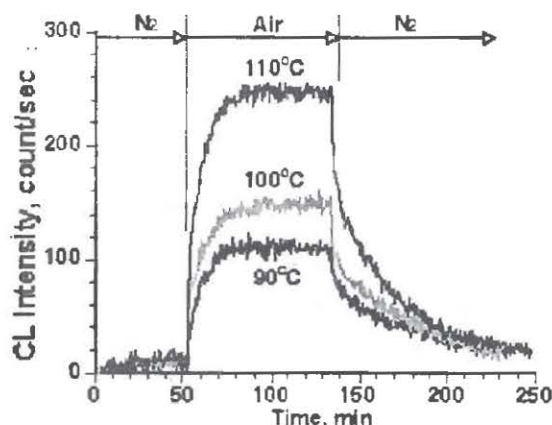


Figure 6 CL intensity-time profiles for DEGDN obtained by gas-switching from nitrogen to air and then to nitrogen. Flow rates of the gases were 60 ml min⁻¹.

Effect of air on CL intensities of nitrate esters has been investigated. Figure 6 illustrates the air effect on the CL intensities for DEGDN by using fast gas-switching technique. From the transient CL curves we can deduce kinetics parameters and reaction order. Figure 7 shows Arrhenius plot of CL intensities for DEGDN heated in air and nitrogen. A significant difference in the CL intensities was observed. Activation energy for the CL

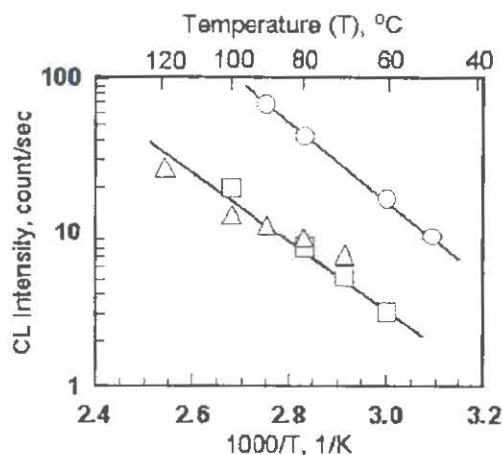


Figure 5 Arrhenius plots of CL intensities for DEGDN, TEGDN, and TMETN. Activation energies were 11.3 kcal mol⁻¹ for DEGDN and 10.4 kcal mol⁻¹ for TEGDN and TMETN.

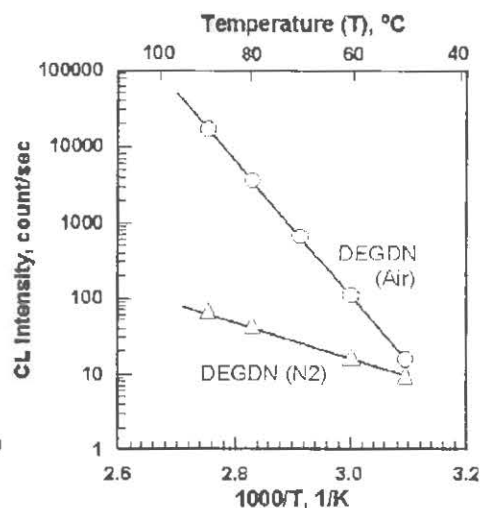


Figure 7 Arrhenius plots of CL intensities for DEGDN measured in air and nitrogen. Activation energies were 11.4 kcal mol⁻¹ for CL in nitrogen and 40.7 kcal mol⁻¹ for CL in air.

intensity in air was $40.7 \text{ kcal mol}^{-1}$, which is as high as 3 times compared with that ($11.4 \text{ kcal mol}^{-1}$) for the CL intensity in nitrogen. This result strongly suggests that the liquid nitrate esters tend to decompose rapidly above 60°C in air. Nitrocellulose (NC) did not show such a big difference in CL intensity over the same range of temperatures; NC exhibited an increase in CL intensities several times but the value of activation energy remained almost unchanged despite change in atmosphere. These results may suggest that a double base propellant would be more susceptible to air than a single base propellant.

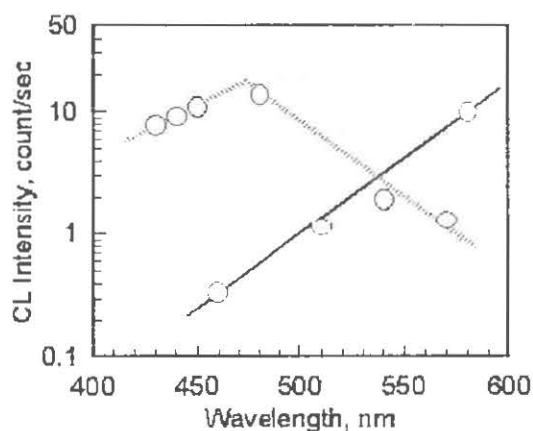


Figure 8 CL spectrum for DEGDN heated at 80°C in flowing nitrogen (60 ml/m). One peak at 470 nm and left branch of singlet oxygen ($^1\text{O}_2$) appeared.

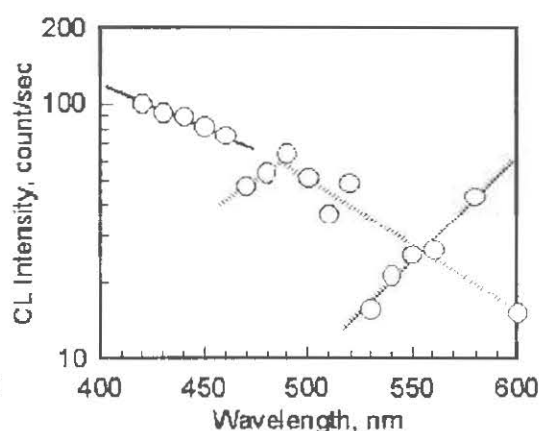
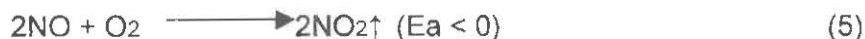


Figure 9 CL spectrum for DEGDN heated at 80°C in flowing air (60 ml/m). In addition to the peak at 490 nm and singlet oxygen ($^1\text{O}_2$), right branch of a peak appeared at shorter wavelength.

CL spectroscopic measurements were conducted for DEGDN heated in both air and nitrogen with a CL spectrometer CLA-FC2. This kind of emission spectra could not be detected with fluoro-spectrometers because of their extremely low emission intensities. Fig. 8 shows the CL spectrum for DEGDN heated in nitrogen at a temperature of 80°C . Light-emitting species will be an excited carbonyl compound having the peak at 470 nm and singlet oxygen ($^1\text{O}_2$). The singlet oxygen will show the emission peak at around 1,270 nm. Fine structure in the spectrum (discrete lines) can be used to identify the formation of singlet oxygen. Fig. 8 shows three discrete lines at 460 (480) nm, 510 (520) nm, and 580 (580) nm where theoretical values are noted in the brackets. When DEGDN was heated in air, emission intensities of central peak and singlet oxygen increased but the spectral positions remained unchanged. In addition to these CL emissions a new CL emission appeared at lower wavelength range as a right branch of an unidentified peak.

Based on the CL spectrum, one can propose a decomposition and autoxidation mechanism. From the spectrum of DEGDN shown in Fig. 8, peroxy radicals (ROO^\cdot) could be the precursor, which are possibly formed through oxidation of alkoxy radicals (RO^\cdot) by nitrogen dioxide (NO_2) (Reaction 1). These radicals are formed by homolysis of nitrate ester groups (RO-NO_2) (Reaction 1). NO_2 could be reduced to nitrogen monoxide (NO). An observed activation energy for evolution of NO_2 from DEGDN was a small negative value indicating that the observed NO_2 was regenerated NO_2 from NO and O_2 (Reaction 5). Nitrocellulose (NC) exhibited only one CL peak at 490 nm below 70°C . Light-emitting material must be excited carbonyl compounds formed by the thermal decomposition of hydroperoxides (R-OOH). All the NO_x evolved from NC was NO gas below 70°C . These new CL and NO_x data naturally lead us to establish a basic reaction scheme (Scheme 1) for the decomposition of liquid nitrate esters as below:

**Scheme 1 Basic reaction scheme for decomposition
(self-oxidation) of liquid nitrate esters.**



In order to confirm the Scheme 1, CL measurements were conducted for oxygen-sorbed triethylene glycol (TEG) in nitrogen. Fig. 10 shows Arrhenius plot for the O_2 -sorbed TEG. Activation energy was $14.2 \text{ kcal mol}^{-1}$, which agrees with $14.4 \text{ kcal mol}^{-1}$ for TEGDN heated in nitrogen. Reaction 3 in Scheme 1 might occur. Activation energy for the decomposition of peracids is known to be about 15 kcal mol^{-1} . Reaction 4 might predominate the CL and

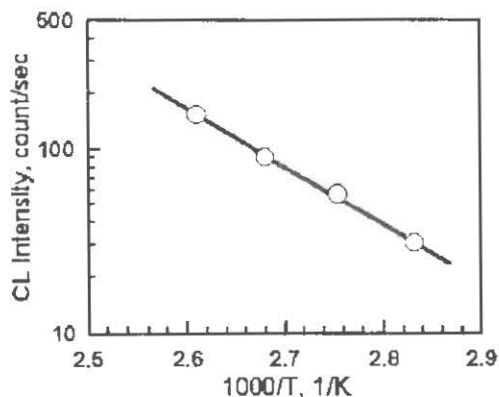


Figure 10 Arrhenius plot of CL intensities for O_2 -sorbed triethylene glycol (TEG). Activation energy $14.2 \text{ kcal mol}^{-1}$ agrees with $14.4 \text{ kcal mol}^{-1}$ for TEGDN.

the heat generation.

4. Summary

CL techniques have been demonstrated to be one of the most sensitive diagnostic methods to investigate the decomposition of energetic materials at near ambient temperatures. CL data frequently coincides with microcalorimetric data. CL intensity and CL spectrum from EM principally originated from the surface; heat generated from EM is basically occur in the bulk. Both techniques will compensate defects in each technique. Coherent interpretation of new findings brought by CL and microcalorimetry will be the advent of new age in the study of propellants, explosives and pyrotechniques.

Totally new theory on the thermal decomposition and autoxidation of energetic materials must be established by making the best use of chemiluminescence and microcalorimetry as early as possible.

5. References (not cited in the paper)

- 1) S. S. Stivala, J. Kimura, and L. Reich, Chap. 1, "The Kinetics of Degradation Reactions, pp. 1-65, in "Degradation and Stabilization of Polymers, ed. H. H. J. Jellinek, Elsevier, New York (1983).
- 2) G. A. George, Chap. 3, "Chemiluminescence of Polymers at Nearly Ambient Conditions", in "Luminescence Techniques in Solid State Polymer Research", ed. L. Zlatkevich, Marcel Dekker, New York (1989).
- 3) Kimura J, "Chemiluminescence Study on Thermal Decomposition of Nitrate Esters", 14, pp. 89-92, Prop. Explos. and Pyrotech. (1989).
- 4) Kimura J, "Nitrocellulose", Vol. 6, pp. 4582-4587, Ed. J. C. Salamone, Polymeric Materials Encyclopedia, CRC Press, Boca Raton, FL (1996).
- 5) Kimura J, "Application of Chemiluminescence to Mechanistic and Kinetic Studies of Explosives -Nitrocellulose and Diethyleneglycol Dinitrate (DEGDN)", 11th Symposium on Chemical Problems Connected with the Stability of Explosives, pp. 205-219, Båstad, SWEDEN (1998).
- 6) Kimura J, "Investigation into the Thermal Decomposition of Energetic Materials by Direct Chemiluminescence", 5th Life Cycle of Energetic Materials, pp. 356-365 (1999).

Appendix: introduction of CL spectrometer

Tohoku Electronic Industry (TEI) is the only one company to manufacture commercially available CL spectrometers in the world. TEI has been working for more than 30 years in the field of CL apparatus. The know-how accumulated during long-term experience has successfully developed an inexpensive and high-performance CL spectrometer CLA-FS1 employing cut-off (edge) filters. Detectable wavelength ranges from 340 nm to 720 nm. Model CLA-FS1 enables an inexperienced operator to measure reproducible CL spectrum within a short time. This universal CL spectrometer was exhibited as a new product in PITTCON 2002 held in New Orleans in March 17-22, 2002.

HFCS 2001/2 SESSION MINUTES

Session 4

Question asked by: Anton Chin, NSWC Crane

Question directed to: Dr. Jun-Ichi Kimura, Japan Kayaku Research: JK Research, JAPAN

Question: If peroxide is an important intermediate during the aging of nitrate ester; Would NGT increase its shock sensitivity and become more dangerous?

Answer: Liquid nitrate esters does not form peroxide intermediate as much as the solid nitrate esters. So there will be no concern for increase in shock sensitivity as a dangerous level.

THIS PAGE LEFT INTENTIONAL BLANK

HEAT FLOW CALORIMETRY

A Technique for Determining Propellant Stability

Dr David J Wood^a, Mr N Turner^b & Mr R G Jeffrey^a

a. QinetiQ, Bishopton, Station Road, Bishopton, Renfrewshire, PA7 5NJ, UK

b. DOSGST, Ash 2b, MOD Abbeywood #3212, Bristol, BS34 8JH, UK

Abstract

Considerable effort has been directed in recent years into establishing and validating procedures for the routine use of Heat Flow Calorimetry in colloidal propellant procurement and surveillance programmes. This paper presents results and findings of work undertaken within the UK QinetiQ Bishopton Laboratory. Recent work is reported on characterising and understanding the critical effect of sample nature and environment on measured heat flow behaviour and includes an evaluation of the proposed new STANAG 4582. Particular emphasis is placed on the importance of ambient environment on measured heat flow and the paper discusses ways of controlling this to allow representative measurement of propellant stability. Overall it is concluded that HFC is and remains a powerful and potentially very useful additional research tool for the characterisation of the propellant ageing process but that certain limitations remain to be overcome before it can be considered for use in routine surveillance programmes.

1 Introduction

This paper discusses some of the more recent findings and conclusions of our studies into the use of Heat Flow Calorimetry (HFC) for determining the stability of propellants.¹³

Earlier work¹ had established that HFC was potentially a powerful additional tool for the characterisation of the propellant ageing process. However it was found to have severe limitations that, it was concluded at that time, would limit its use for routine surveillance. HFC results were found to be highly dependent on the microenvironment within the sample during ageing. Moisture content and the presence, or absence of air, in particular, were found to have a very marked effects on heat flow. It appeared that early heat flow behaviour was dominated by reactions with these species and that once consumed a more steady state heat flow resulted. These earlier results confirmed the findings of other workers in this area². Aspects of this previous and subsequent work were presented at the previous "Workshop on the Microcalorimetry of Energetic Materials" held Leeds, UK 17th – 19th May 1999³.

All HFC testing discussed in the paper was undertaken using a four channel Thermal Activity Monitor (TAM) Type 2277 system from ThermoMetric Ltd. configured with Bomic software developed by Bofors, Sweden. Details of the equipment, its operation and calibration are as previously reported¹.

2 Analysis

2.1 Microenvironment & the Importance of Sample Preparation

2.1.1 Preconditioning of Samples

Our initial HFC studies followed a strict preconditioning procedure prior to testing. All tests were carried out on 1–2g samples in standard 3ml glass ampoules. The ampoules and propellant samples were conditioned at a specific humidity prior to sealing the ampoules with caps. The

samples were then heated to the temperature of the calorimeter in an oven for 2 hours, prior to being quickly transferred to the calorimeter and lowered to the upper stop position. The samples were left in this position for about 30 minutes to allow them to come to equilibrium. The ampoules were then fully lowered into the measuring position and the monitoring of the heat flow commenced once equilibrium was attained.

Similar conditioning procedures were recommended in a European study to ensure that the original moisture content of the propellant is known⁴. They also recommended that the loading density of the propellant within the sample vial was kept constant. Their study concluded that the propellant should be conditioned before measurement or the moisture content of the propellant should be fixed. Filling of the ampoules should be kept constant, with the preference for a fully filled vial as this more closely matched the situation in a cartridge case. They found that HFC measurements showed excellent reproducibility between different laboratories if these parameters, loading density and moisture content, were fixed.

Subsequent to this report the results of a "Round Robin Test" carried out in 1998 on a double base ball propellant indicated that preconditioning of the propellant was not really necessary⁶. This conclusion was reached as a result of an in-depth study carried out by a number of different laboratories all using carefully conditioned and unconditioned propellant samples.

Work in the US on diphenylamine stabilised double base gun propellant samples has also examined the effect of loading density^{6,7}. Their work was aimed at ensuring the calorimeter was loaded with propellant in a similar way to the loading pattern of the actual propellant cartridge. By this means they hoped to better mirror the actual ageing experienced within the charge. Preconditioning of the sample at elevated temperatures was achieved inside the calorimeter so that early heat flow patterns could be recorded.

2.1.2 Grain Size

Small arms powders come in the form of ballpowders, flake or granular shapes and preparation for testing by conventional techniques or by HFC is minimal. Samples are now, generally, transferred directly from the store to the test apparatus so as to allow testing of the propellant in the same environmental condition as occurred within the charge. This allows for the analysis to determine round to round variation and for the more critical comparison of stores, which have seen adverse storage conditions or are approaching the end of their predicted shelf life.

Larger calibre gun and rocket propellants, however, generally require sample pre-treatment prior to analysis. Usually this involves some form of size reduction process so as to ensure the portion of the sample selected for testing is truly representative of the bulk. The most common form of pre-treatment involves grinding or milling the propellant to produce a course powder form that can be blended, so as to ensure a representative sample, and is suitable for chemical analysis by extraction techniques. However it is recognised that this process of sample size reduction and grinding not only puts work into the propellant, inducing localised heating and possible degradation, but more importantly allows the release of trapped species, the re-introduction of moisture air into the matrix of the propellant and fundamentally changes the microenvironment of the test material. This has major implications for any subsequent stability or ageing testing.

To establish the criticality of sample preparation on propellant stability, a solid block and a ground sample of a double base rocket motor stabilised with 2NDPA was analysed by stabiliser depletion measurements and by HFC to assess their stability.

Six NATO tubes were prepared for ageing comprising three tubes containing ground propellant and three containing a single solid block of propellant, which had been machined to just fit into a NATO Test tube. It had been determined using thermocouples placed into a solid block sample that the time to reach 80°C throughout the test piece was only two hours and hence temperature lag

between the two tests types would have little overall influence on the ageing behaviour. The results are given in Table 2-1.

days @ 80°C	Block sample %2NDPA	Chopped sample %2NDPA
0	1.78	1.78
6	0.72	0.91
10	0.30	0.35
15	0.06	0.14

Table 2-1: Effect of Grain Size on Stabiliser Depletion

As can be seen there is a significant difference for the solid and ground samples with the block sample showing the higher rate of stabiliser loss.

The experiment was duplicated but using HFC. To keep the sample conditions similar to those used for the stabiliser consumption trial, a 1 gram solid block and a 1 gram ground sample were placed in vials and conditioned at 20°C and 50% relative humidity overnight. The sample vials were then sealed and placed in the calorimeter at 80°C and after a period of equilibration their heat output measured by HFC, Figure 1.

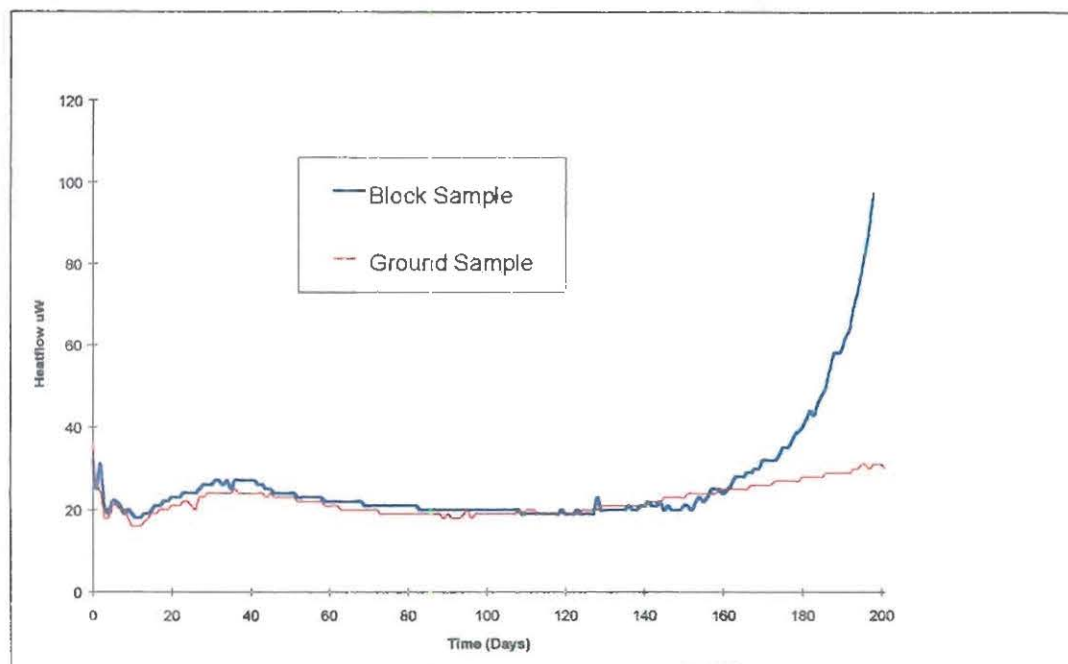


Figure 1: HFC of Ground and Block Propellant Samples

The results, Figure 1, show a substantial drop in heat output during the first 15 days for both samples. From the results in Table 2-1 it can be seen that this drop in heat output coincides with the depletion of 2NDPA. There is then a slight rise in output which eventually levels off to give a relatively steady output of 20 μ W. This relative stability, which occurs once all the primary stabiliser is consumed, we believe, demonstrates that the degradation process is now in a steady state condition during which relatively consistent reactions and reaction products (energetically speaking) are being produced within the matrix. This we believe is due to reaction with the degradation products of the primary stabiliser which in themselves act as stabilisers.

However at a point further down this degradation path, presumably at the point when all possible stabilising reactions have occurred, we see a steep rise in heat flow indicative of the onset of autocatalytic breakdown. Interestingly this occurs first in the block sample.

Hence both stabiliser depletion studies and HFC indicate that using prepared ground samples will give an over optimistic assessment of stability.

It is assumed this result reflects the ease with which the initial products of decomposition can be lost to the atmosphere within the sample container from the grains of the ground sample. In the solid block it is suspected that these breakdown products are retained in the bulk for longer giving rise to either acceleration of the degradation process or enhanced reaction with the remaining active stabilising species. This result has important implications for all stability testing of propellants.

Recent work being carried out on a variety of rocket motor formulations has highlighted this effect still further. Solid blocks of propellants aged at elevated temperatures, have been analysed across their web to determine the levels of stabiliser and stabiliser degradation products. It appears that not only are the degradation reactions occurring at the surface different from those occurring in the bulk but also that the profile of these reactions varies between propellant types and from stabiliser to stabiliser. This potentially has major implications in the assessment of propellant stability using HFC as well as for more traditional methods of analysis.

Examination of the heat flow profile in Figure 1 indicates a marginally higher heat flow from the block sample compared to the ground sample up until around 120 days but the level of this difference is thought to be such as to not clearly highlight the major difference found in stabiliser consumption rate unless the experiment is run until the onset of autocatalysis.

2.1.3 Sealing of Sample Ampoules

An examination of the rate of stabiliser depletion for a single base (NC200) and a double base (PU) propellant heated at 50, 60 @ 65.5°C, under different conditions has been undertaken. All samples following ageing were analysed for stabiliser loss and weight change. The heat outputs at 80°C of the material prepared for analysis was also determined by HFC. The results supported development of the STANAG agreement for testing by HFC⁸ and only key findings are summarised here.

The NC200 propellant grains were small enough to be used in this trial without additional preparation. The PU samples were subject to grinding to produce a 2mm ground sample for testing. At each temperature, and for each period of ageing three samples, in the ageing containers listed below, were prepared:

- Glass container 10ml (filled and sealed).
- Glass container 10ml (filled, but unsealed).
- NATO Test Tube at loading density as detailed in STANAG 4117.

The results for ageing in accordance with STANAG 4117 agree with stabiliser depletion work carried out by C. McPherson in 1994⁹ on PU propellant.

The colour change (from fawn to brown) in the PU samples suggested that the sealed samples of PU experience the greatest change on ageing, this was confirmed by the higher loss in stabiliser for these samples.

The unsealed container, which contained 5g of ground PU propellant, experienced the least loss in stabiliser. It is suspected that this is due the fact that both NG and the gases produced during degradation of the propellant can escape but clearly indicates the importance of controlling the propellant environment during testing.

As expected, at higher temperatures there was greater loss in stabiliser. Overall there was little difference in the stabiliser loss for the sealed "full" container and the NATO tube.

Also as expected the greatest weight loss occurred in the unsealed PU sample. This weight loss was significantly higher than for the sealed samples, presumably due to the loss of NG at elevated temperatures. Also as expected the higher the temperature and the longer the time, the greater the loss of weight.

A similar pattern was obtained for NC200 although being a single based propellant the weight loss was less marked. It was found that the unsealed sample experienced the least loss in stabiliser. The loss of stabiliser for the sealed and NATO samples was similar. The weight loss in the NC200 samples increased with time, reaching a maximum after 20 days in the unsealed sample at ~1.5%. This weight loss was at a level at which it is thought to be dominated by loss of volatile matter from the propellant.

Heat flow experiments mirrored those used to assess stabiliser and weight loss. However to allow measurement at a reasonable energy output level the STANAG loading density experiment used a part filled tube that contained 1 gram of material. This is a higher loading density than is used in the NATO Test. Experiments on sealed and unsealed tubes were conducted using tube that were fully filled with propellant. The experimental configuration is summarised in Table 2-2.

Experiment	NC200	PU
Sealed Full Tube	1.38g	1.9g
Unsealed Full Tube	1.38g	1.9g
Part Filled Sealed Tube	1.0g	1.0g
Sealed Full Tube (Pieces of Propellant)	-	1.7g

Table 2-2: Sealing of Ampoules – HFC Experimental Configuration – PU & NC200

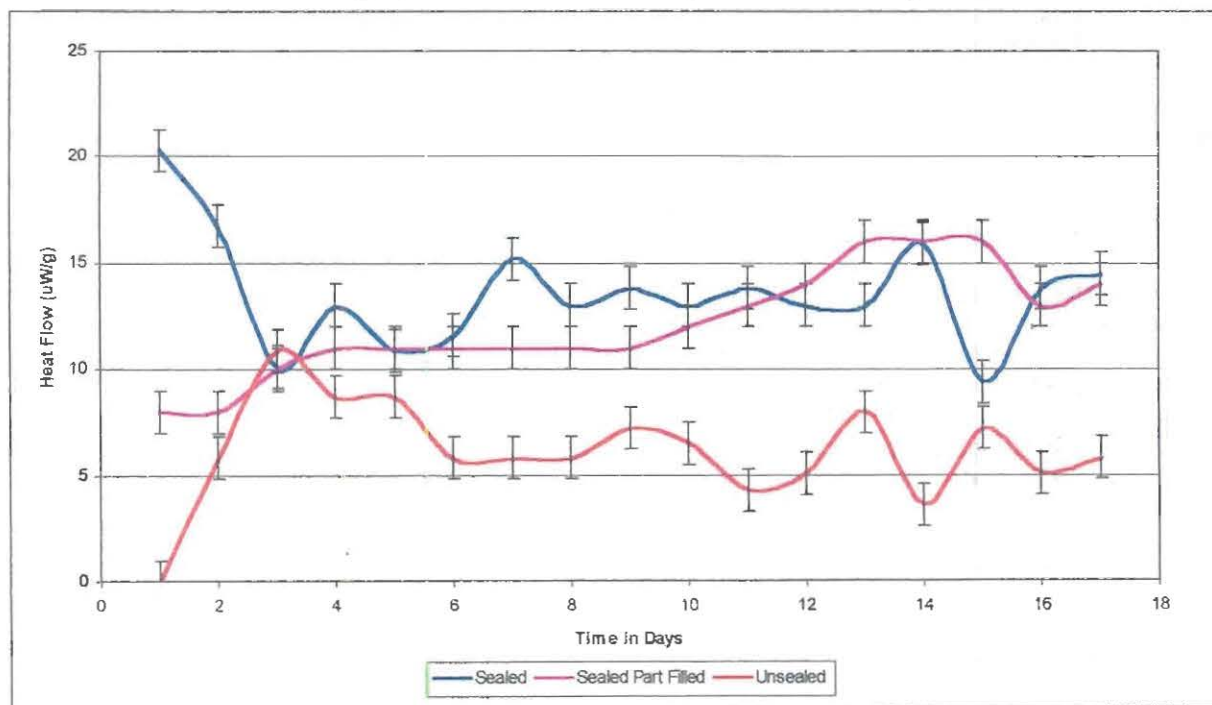


Figure 2: Sealing of Ampoules – HFC of NC200

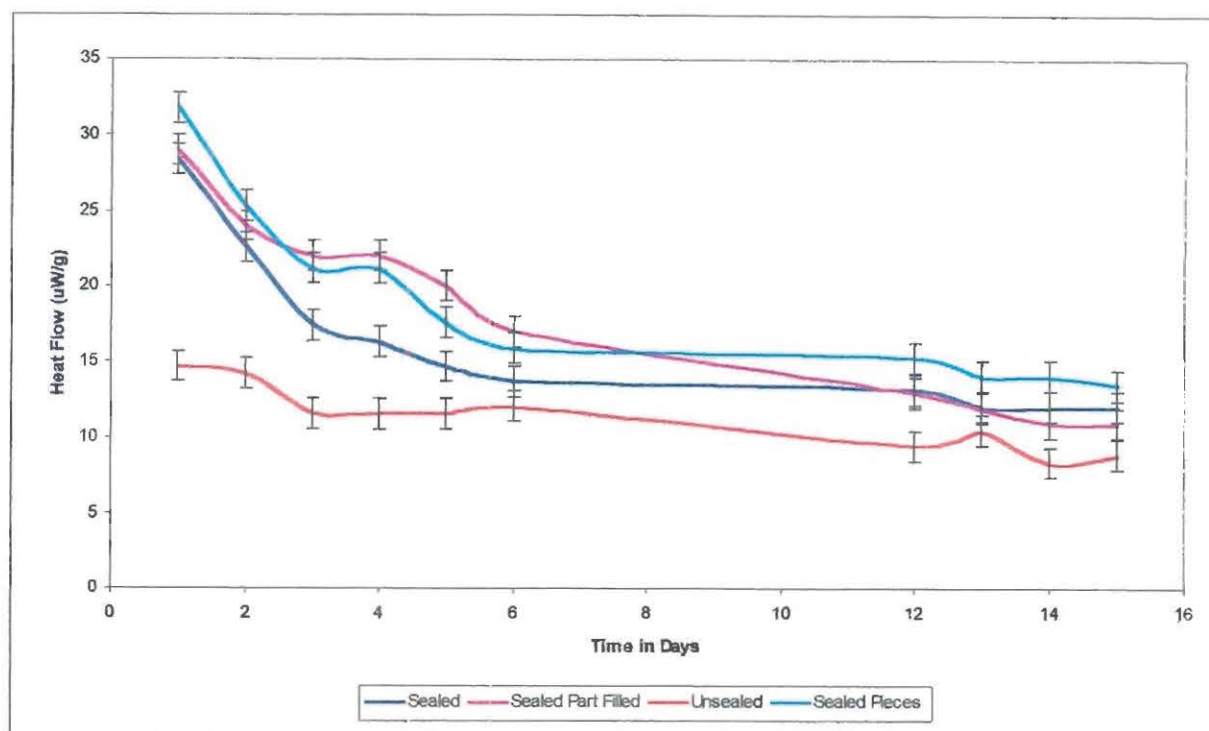


Figure 3: Sealing of Ampoules – HFC of PU Propellant

Heat flow data for the experiments is shown in Figure 2 & Figure 3. As can be seen the HFC trace for the unsealed PU and NC200 samples gave the lowest heat output. This presumably reflects the loss of material from the propellant which being generally an endothermic process will show as a lowering of the heat output from what is in the main an exothermic decomposition and reaction process within the propellant. Comparison of the sealed and partially filled samples presents a more interesting picture. For the NC200 initially the part filled sealed tube appears to show a lower heat flow than the filled sealed tube. This increases with time in contrast to the heat flow from the sealed filled sample, which decreases with time. After a period of 3 to 4 days the heat flow appears to stabilise although the heat flow from the sealed filled tube appears to remain higher until after approximately 12 days when the overall heat flow is similar.

The opposite effect appears to occur for the PU propellant. Here the part filled tube appears to show a higher heat output than the filled sealed tube until after 12 days when heat outputs become similar. The tube filled with large pieces of PU propellant appears to relatively consistently give a higher heat output irrespective of time.

It is interesting to note that both propellant types show a change in behaviour after approximately 3 days. Prior to this time heat output is variable whilst after this time a more stable state appears to be establish.

The results clearly demonstrate the importance of sample loading. It is our understanding that the overall trends found in this work agree well with the initial results from the WIMMIS NC (Switzerland) and WIWEB (Germany) laboratories that are conducting similar experiments but on other types of propellant.¹⁰

2.2 Characterisation and Interpretation of HFC Traces

Clearly there are a number factors which affect the heat output from propellant samples in the HFC. To obtain a meaningful measurement of heat output, these factors must be understood and controlled.

Experimentally it is found that when a sample vial is initially placed in the HFC, the system must be allowed to reach equilibrium, whereby the sample vial and its contents attain the temperature conditions of the HFC, before any meaningful measurement can be taken. Experience has shown that HFC traces in the initial stages can vary greatly with the thermal activity rapidly increasing or decreasing to varying degrees in the first few hours of measurement. The factors affecting this initial heat output appear to include preconditioning, the temperature at which the experiment is conducted, the surrounding headspace (atmosphere) and the stability of the material.

Numerous studies have shown that during the first three days for certain propellant compositions a trough appears, whereby the heat flow curve falls to a minimum then increases to a second maximum. For propellants stabilised with DPA, it has been argued that this is due the depletion of DPA and the production of N-NO-DPA ¹¹.

Our experiments on single based DPA stabilised propellants have shown that at 80°C a peak in the heat flow trace appears between 2 and 6 days. This coincides with formation of N-NO-DPA due to the degradation of DPA. A similar pattern emerges for double-based propellants stabilised with 2NDPA, with a peak in the HFC trace occurring during the formation of 2,4'-Dinitro-DPA and loss of 2NDPA.

The post 2-6 day HFC trace at 80°C for what would generally be classed as normal "stable" propellants now enters a region of relative stability with uniform heat output with the thermal activity remaining reasonably constant or rising only slowly. This generally continues reasonably steady until a point at which the propellant heat flow starts to rise exponentially. This final rise is thought to represent the point at which autocatalytic breakdown of the nitrate-esters occurs and is believed to occur once all active stabilising species have been consumed. This point is generally reached after many weeks ageing at 80°C.

2.3 STANAG 4582

A major study has been undertaken within Europe in recent years aimed at development of a STANAG for a stability test procedure and requirements for single and double based propellants that uses HFC. The agreement, STANAG 4582, is now at Working Group Draft level ⁸ and the work supporting its development has been reported in various publications ^{5, 8 & 11}.

The concept for STANAG 4582 developed out of discussion held during and following the TTCP Subgroup W meeting held at Leeds during 7th – 9th April 1997. Early work was led by Wilker and Guillaume and involved eight separate laboratories within Europe. QinetiQ Bishopton has been involved in supporting subsequent work leading to finalisation of the draft but due to funding restrictions was not involved in the earlier work. The finalisation work is scheduled for publication at the Symposium on Problems Connected with the Stability of Explosives to be held Karlsborg, Sweden 14-18th May 2001.

Work underpinning the STANAG has reconfirmed and demonstrated the importance of sample preparation. Although some conflicting results have been reported, it is recommended that samples be conditioned prior to testing at a constant humidity (60 to 70% at ambient temperature being recommended). If necessary to ensure a representative sample is tested, cutting or grinding to 1-2 mm size range is also recommended.

However the most important recommendation is that samples are tested at as high a loading density as practicable, 0.9 to 1.0. This is to minimise the volume of air trapped within the sample as work has demonstrated that the level of trapped air has a very marked effect on the resultant HFC trace. Further it is considered that this state is more representative of the filling condition within service charges or rounds.

Testing is made in the range 60 to 90°C with test duration dependent on the test temperature. Criteria of acceptance are based on the maximum heat flow during a defined time period. This

maximum heat flow has been calculated from first principles as the heat flow that would be necessary, generated within a propellant cartridge of 23 cm inner diameter (assumed to equate to polyethylene of 3.5 cm thickness), to cause a 1.5°C temperature rise in the centre of the charge when the charge is heated at a constant temperature of 71°C. At this temperature the limiting heat flow is calculated to be 39 µW/g.

Test times are based on assumed worst case kinetics for decomposition of the propellant and assume activation energies for decomposition of 120kJ/mole >60°C and 80kJ/mole <60°C. These activation energies have been determined from actual experiment.

As experiment has shown that early decomposition behaviour is dominated by atmosphere effects the initial part of the decomposition, up until a total heat generation of 5J/g, is ignored for both measurement and timing purposes. For completeness the total energy release during the measurement period is recorded. This serves as an indication of the level of degradation of the propellant during the test period. The test period, after a total energy release of 5J/g is set to be equivalent to 10 years storage at 25°C.

The method is therefore similar to the UK Silver Vessel test in that the measured parameter is a heat output level that is necessary to produce a defined temperature rise within a defined bulk of propellant.

At first sight the test appears to be based on sound principles. However although the test is based on such principles it does assume that the sample is tested in a condition that is wholly representative of the propellant in service stock. The test's assumption is that propellant in service stock is hermetically sealed within rounds. Clearly this will not always be the case. Large calibre munitions often use combustible cartridge cases, some propellant stocks are stored loose, whilst sealing of rounds can fail and give rise to a different internal environment than is assumed within the test condition. Work reported by the group responsible for the test development clearly indicates that the presence of moisture and/or air increases heat flow. Further if we explore the analogy with the UK Silver Vessel test we find that the acceptable time limit for a 10 year life at 25°C is 10.6 days. This equates to ~ 254 hours at 80°C. This is considerably lower than the 2000 hours limit set within the UK Silver Vessel test. Finally the criteria is based on storage at 25°C. UK practice sentences based on storage at 32°C. The method does however include a calculation for determination of safe storage time at other storage temperatures or for combinations of storage temperatures.

3 Discussion

3.1 Micro-environment

Our work and the work of others within the field have emphasised the critical importance of sample size, preconditioning and ampoule sealing on the results obtained by HFC. Significant nugatory effort was expended in the early part of our work in attempting to develop a procedure that would allow propellant to be tested in a constant humidity environment throughout the period of the test. Previous work ¹ had shown that initial heat output was directly related, in particular, to the initial moisture content of the propellant with the highest heat output obtained from propellant conditioned at higher RH conditions.

One of the objects of our work had therefore been to examine heat output under controlled humidity conditions. This work was in part carried out at QinetiQ Fort Halstead using a flow through cell arrangement. Work carried out at Bishopton centred on incorporation of vials containing humidity standard solutions, either glycerol/water or saturated salt solutions. Both approaches to the work have, however, proved unsuccessful. It is our understanding that the sensitivity of the flow through cell is such as to require higher and less representative ageing temperatures and that there is also

a problem with condensation within the equipment ¹⁰. Experiments have shown that in the Bishopton approach, in particular for nitroglycerine containing propellants, migration of species into the solution within the inner vial dominates the heat flow output rendering the experimental output meaningless.

It therefore appears that potentially the only meaningful way ahead is to precondition the sample to a controlled humidity and, as recommended in the STANAG, control both form and vial loading density if a reproducible result is to be obtained. In doing this it must be accepted that, in part, the resultant heat flow trace will reflect the reaction and consumption of trapped moisture and oxygen but that once consumed a lower (or higher) heat flow will result due to the lack of availability of these species for exothermic (or endothermic) reactions. As a consequence it is possible that wrong conclusions on the heat flow from a "real" propellant situation may be drawn. Alternatively it is necessary to devise a test protocol that allows testing under specified environmental conditions.

It has been argued by Wilker et al ¹¹ that the resultant heat flow will give a better measure of the stability of propellant in sealed round propellants and this is the basis of STANAG 4582. Although this might well be the case, the assessment of propellant stability within any given round or munition must always consider the significance of the worse possible scenario. Unless it is established, therefore, that the worse possible scenario is ageing within a sealed system results from HFC should be treated with some caution. This is particularly the case if used to assess propellant used in combustible cartridge cases. Experiments should therefore be constructed in such a way as to indicate the likely effect of ready access to moisture and oxygen, as might occur in a round or charge with a sealing failure or for loose stored propellant. However experimentally this is not trivial and will require careful design of experimental protocol. Further work is required to establish such a protocol and one possible way ahead is discussed in more detail in the next Section of this paper.

3.2 Use of HFC within Propellant Surveillance Programmes

As should be clear from the aforesaid discussion on the importance of controlling and understanding the critical micro-climate to be used in HFC testing, design of such experiments may not be trivial but will be crucial if HFC is to be used to predict stability and safety in anything other than fully sealed conditions. Such experiments will further be critical if maximum heat flow or ageing occurs in the presence of air and/or moisture. Current work on the effect of Web thickness on the ageing of propellant ¹² suggests that depletion of carbamate is higher in the outer regions of the propellant most exposed to ambient environmental conditions and thus adds weight to this conclusion. However, it has yet to be established if this results in a higher or lower heat flow and/or if this is actually a consequence of exposure to air/moisture or is purely the consequence of propellant breathing. It should be noted however that it has been established that no such effect is found for 2NDPA stabilised propellants.

One possible experimental approach, to establish likely HFC behaviour under ambient environmental conditions, would be to monitor heat flow after propellant has been aged for given periods under various environmental conditions. Such experiments could be used to establish the optimum ageing environment so as to record the worst possible example for either stabiliser consumption, gassing or heat flow. So as to record a meaningful trace under or near prevailing "ambient" conditions within the propellant, it will be necessary to measure heat flow in the early stages of the heat flow experiment during the time when heat flow is still affected by the presence of trapped moisture and air. This will almost certainly require ampoules to be only part filled if measurement is to be completed during the region 1-3 days at 80°C.

Previous work in our Laboratory ¹ has demonstrated that this approach will work and is potentially a viable method for obtaining kinetic data. The approach would complement that proposed by Wilker et al ¹¹ adopted in STANAG 4582 as it would allow for measurement of heat flow under conditions other than fully sealed with all moisture and oxygen consumed.

The Wilker et al ¹¹ approach reflected in STANAG 4582 is an attempt to use HFC to predict the safe storage life of propellant based on demonstration that the resultant maximum heat flow rate at any given temperature, as measured by HFC, is less than that required to cause autocatalytic ignition in a charge system. This level as discussed earlier is based on both kinetic and thermal conductivity considerations. The approach proposed here would use the same criteria as in STANAG 4582 but base the assessment on heat flow as measured after 1-3 days in the HFC at say 80°C. Propellant samples would be aged externally to the HFC under controlled environment conditions. It is believed that this approach could give a much clearer indication of true safety in storage should maximum heat flow not be obtained under sealed conditions.

The other advantage of this approach, which could be used to study any environmental condition, including fully hermetically sealed, is that it would require far less HFC time and would therefore open the potential to use the technique for more routine monitoring of stability.

3.3 The Way Ahead

It is perhaps appropriate to address the question of where we go from here. Clearly HFC is a very powerful tool if used correctly and is a useful aid for assessing the safety and stability of propellant. However unless reliable and robust equipment can be found that allows the heat flow to be recorded under controlled and variable environmental conditions such measurement will always potentially be compromised. Indeed it is likely if not probable that any attempt to record heat flow from any double-based propellant at greater than say 50°C will be affected or potentially dominated by volatilisation of nitroglycerine. Experiments to date suggest several orders of magnitude higher sensitivity equipment will be required to allow measurement at such temperatures and would necessitate significantly higher cost equipment than that which currently exists. The question therefore exists as to whether this would be cost effective if compared to alternative assessment procedures or to alternative methods of stability assessment. Only time and further experiment will allow this question to be answered.

4 References

1. Evaluation of Heat Flow Calorimetry for the Assessment of Propellant Stability.
DRA/DWS/WX4/CR95983/1.0, Feb 1996.
2. Proceedings of the Workshop on the Microcalorimetry of Energetic Materials.
7-9th April 1997, Leeds UK, WX3 DERA Fort Halstead.
Various papers therein.
3. Microcalorimetry: A Technique for Determining Propellant Stability.
R G Jeffrey, M Elliot, D J Wood, P Barnes & N Turner.
Proceedings of the Workshop on the Microcalorimetry of Energetic Materials.
17-19th April 1999, Leeds UK, WX3 DERA Fort Halstead.
4. Practical Application of Microcalorimetry to the Stability Studies of Propellant.
M Rat, P Guillaume, S Wilker & G Pantel.
Proceedings of the Workshop on the Microcalorimetry of Energetic Materials.
7-9th April 1997, Leeds UK, WX3 DERA Fort Halstead.
5. International Round Robin Test to determine the Stability of DB Ball Propellant by Heat Flow Calorimetry.
S Wilker & P Guillaume.
Proceedings of the Workshop on the Microcalorimetry of Energetic Materials.
17-19th April 1999, Leeds UK, WX3 DERA Fort Halstead.
6. 20mm Gun Propellant Safety Service Life Study using Microcalorimetry/HPLC Correlation Diagrams.
A Chin & D S Ellison.
Proceedings of the Workshop on the Microcalorimetry of Energetic Materials.
7-9th April 1997, Leeds UK, WX3 DERA Fort Halstead.

7. Common Factors that may affect the accuracy of Microcalorimetric Data.
D S Ellison & A Chin.
Proceedings of the Workshop on the Microcalorimetry of Energetic Materials.
7-9th April 1997, Leeds UK, WX3 DERA Fort Halstead.
8. NATO Standardisation Agreement (STANAG)
Explosives, Single and Double Based Propellants, Stability Test Procedure and
Requirements using Heat Flow Calorimetry.
STANAG 4582.
9. Stabiliser Consumption Trials on Various Propellant Stores.
C McPherson, Bishopton Laboratory Report No. BN/92/29, May 1994.
10. Private Communication.
11. Heat Flow Calorimetry – Effects of Sample Preparation and Measuring Conditions.
P Guillaume, M Rat, G Pantel & S Wilker.
Proceedings of the Workshop on the Microcalorimetry of Energetic Materials.
17-19th April 1999, Leeds UK, WX3 DERA Fort Halstead.
12. Effect of Web Thickness on the Ageing of Propellants
DERA/LWS/WS3/CR010105/1.0, Feb 2001
13. Microcalorimetry – A Technique for Determining Propellant Stability
DERA/LWS/WS3/CR000491/1.0, Feb 2001

© Copyright QinetiQ Ltd 2001.

THIS PAGE LEFT INTENTIONAL BLANK

A MICROCALORIMETRIC STUDY OF A CARBOXYL-TERMINATED POLYBUTADIENE (CTPB) AND A CTPB COMPOSITE PROPELLANT

William Bryant Jr.

Gene Huie

Chris Pappas

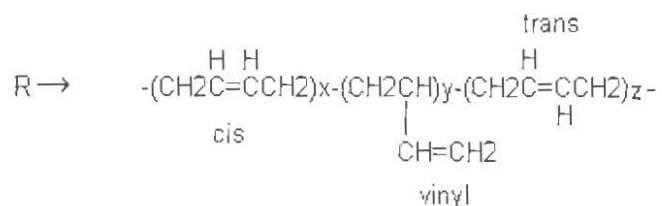
ABSTRACT

Isothermal high-pressure differential scanning calorimetry (HPDSC) and isothermal microcalorimetry were used to study accelerated aging in HC434, a carboxyl terminated polybutadiene (CTPB), and a composite propellant formulated from this polymer. Both methods show in general that the heat flow rate increases with increasing iron content of the material and concomitantly that the stability toward oxidation decreases. With one apparent exception, in general, the increasing propensity for propellant 'A', which is formulated from HC434, to form cracks upon hot/cold temperature cycling with increasing age, seems to show some correlation with increased heat flow rate in the propellant as measured at 75°C. The calculated activation energies for the propellant and the polymer, 84 ± 3 kJ/mole and 87 ± 2 kJ/mole, respectively, are in agreement.

1. INTRODUCTION

As part of lot acceptance testing, rocket motors containing propellant formulation 'A' are aged at 165° F for a period of 84 days. Every 28 days units are withdrawn, subjected to a hot/cold temperature cycle, and x-rayed while cold to detect the presence of cracks. Recently, a composite propellant formulated from a carboxyl-terminated polybutadiene that is crosslinked with an epoxy, failed to pass accelerated aging tests as a result of prematurely forming cracks in the grain. Testing showed that an increase in the modulus as well as a decrease in strain capability had occurred prior to crack formation during the accelerated aging. Composite propellants containing polybutadiene binders, either carboxyl-terminated or hydroxyl-terminated, are known to be susceptible to oxidation, which can lead to hardening and crack formation resulting from crosslinking reactions involving oxygen and the formation and recombination of free radicals. The basic thermo-oxidation scheme for polymeric and organic compounds, shown below, has been described in a number of studies.¹⁻³

R \equiv polybutadiene polymer chain shown below



- I. $\text{RH} + \text{O}_2 \longrightarrow \text{R}\bullet + \text{HO}_2\bullet$ initiation (free radical formation)
 $\text{R} + h\nu \text{ or heat} \longrightarrow \text{R}\bullet$
- II. $\text{R}\bullet + \text{O}_2 \longrightarrow \text{ROO}\bullet$ conversion (peroxy radical formation)
- III. $\text{ROO}\bullet + \text{RH} \longrightarrow \text{R}\bullet + \text{ROOH}$ propagation (peroxide formation)
- IV. $\text{ROOH} \longrightarrow f(\text{RO}\bullet + \text{OH}\bullet) + (1-f)(\text{RO} + \text{H}_2\text{O})$ degenerate chain branching
- V. $2 \text{R}\bullet \longrightarrow \text{R}-\text{R}$ termination (crosslink formation)
 $\text{R} + \text{ROO}\bullet \longrightarrow \text{ROOR}$ termination (crosslink formation)

This oxidative free radical crosslinking reaction is known to be catalyzed by various metals and metal containing compounds, viz., iron, copper, and chromium in particular.^{4,5}



M \equiv catalytic metal

The decomposition of the hydroperoxide of step IV, which can be catalyzed by trace metals, is the step that is also inhibited by the antioxidant as seen in the reaction below:



where InH = hydrogen donating class of antioxidants

The catalysis of step IV would lead to the increased rate of production of hydroperoxy radicals and an increased rate of consumption of antioxidant, assuming the antioxidant can react quickly enough. Even in the presence of antioxidant, some hydroperoxy radicals go on to participate in deleterious reactions such as step 5, which results in oxidative crosslinking and a possible shortening of the service life of ordnance containing these binders. Using heat flow microcalorimetry, the relative heat flow rates of propellants and the polybutadiene polymers used to formulate them can be determined in as little time as 24 - 36 hours, thus distinguishing lots that may have relatively high heat-flow rates. This tool can be used to quickly assess whether potential propellant or polymer additives will adversely affect binder stability or improve stability by inhibiting oxidation. We have applied heat flow microcalorimetry to determine the relative heat flow rates of different lots of the carboxyl-terminated polybutadiene, HC-434. Data obtained from sealed and unsealed vials and data obtained in oxygen and nitrogen atmospheres suggest that a major contribution to the heat flow of some polybutadiene composite propellants is oxidation. The data also indicate that iron contamination can catalyze the reactions contributing to the heat flow. The potential for heat flow microcalorimetry to be a valuable tool in optimizing energetic materials for maximum service life is demonstrated.

2. EXPERIMENTAL

2.1 SAMPLES

The polymer used in this study is a carboxy-terminated polybutadiene with the trade name designation HC434.

The propellant used in this study, designated propellant 'A', is a composite propellant containing the following ingredients:

HC434 polymer, epoxy curative, aluminum, ammonium perchlorate, iron oxide, dioctyladipate, and a chromium salt cure catalyst.

2.2 ACCELERATED AGING AND X-RAYING OF MOTORS

Motor units containing propellant 'A' are x-rayed prior to accelerated aging and put into ovens at approximately 75° C. Every 28, 42, 56, 70, and 84 days units are withdrawn from the oven, subjected to a hot/cold temperature cycle and x-rayed to detect the presence of cracks.

2.3 INSTRUMENTATION

A Calorimetry Sciences Corporation Model 4500 and Model 4400 microcalorimeter were used for heat flow measurements. Each unit uses a large aluminum block heat sink and thermoelectric type sensors for differential heat flow measurement. The Model 4500 has a coupled sample and reference cell, which can accommodate samples up to 11 mm in diameter and 40 mm in height, and can measure heat flows as low as 0.5 microwatts in its present environment. The model 4400 has a reference cell coupled with three sample cells, which can accommodate samples up to 38 mm in diameter and 78 mm in height, and can measure heat flows as low as 2 to 3 microwatts in its current environment.

All high-pressure DSC measurements were conducted on a Dupont Model 910 differential scanning calorimeter with a model 900830-902 high-pressure cell.

2.4 DIFFERENTIAL SCANNING CALORIMETRY

Samples of HC434 polymer weighing approximately 4 milligrams were weighed to the nearest 0.01 mg into uncoated aluminum DSC sample pans. A sample was then placed into a Dupont high-pressure DSC cell, pressurized to 550 psi with air and the temperature ramped rapidly from room temperature to 125°C within about 2 minutes. The sample heat flow was monitored isothermally at 125°C until an exotherm was detected. The time from the point at which 125°C is reached to the onset of the exotherm, defined as the induction time, and the time to reach the peak of the exotherm, were recorded.

2.5 MICROCALORIMETRY

Polybutadiene samples weighing 0.208 g were used for all microcalorimetric measurements on the CSC Model 4500. The 0.208 gram samples were put into 1.9 ml glass vials. The vials were sealed by wiping the top of the vial with a very thin film of polydimethylsiloxane vacuum grease and placing a small square of aluminum foil over the top. The vial was then crimped with an aluminum cap having a silicone rubber insert. Some samples were run uncapped to determine the affect of unlimited free-volume on the heat flow rates. Polybutadiene samples of 1.00 gram mass in open 40 ml vials were used when making microcalorimetric measurements on the CSC Model 4400. All propellant samples were weighed to 0.821 grams. For activation energy determinations, microcalorimetric measurements were conducted at 75°, 65°, and 55° C.

Propellant samples measured in an oxygen or nitrogen atmosphere were first placed under vacuum for 24 hours followed by equilibration in a vacuum dessicator filled with the appropriate gas (nitrogen or oxygen). The sample in oxygen was equilibrated for 24 hours while the sample in nitrogen was only equilibrated for 4 hours. After removal from the dessicator, the sample was briefly exposed (about 10 minutes) to the atmosphere followed by purging in the sample vial for about 2 minutes with either oxygen or nitrogen, after which it was immediately capped and sealed as previously described.

The polybutadiene samples for the iron chelation studies were prepared by mixing lot 341M with 0.67 millimoles of either glutaric acid, EDTA, or 8-hydroxyquinoline, which would yield mixtures of 0.59, 1.28, and 0.65 weight percent, respectively. Since the HC-434 was known by previous analysis, using ICAP, to contain 47 ppm of iron, the molar ratio of chelating compound to iron was constant at 53 to 1.

2.6 ANTIOXIDANT ANALYSIS USING HPLC

HC434 samples containing the antioxidant AO2246 [2,2-methylene-bis(4-methyl-6-tert-butylphenol)] were analyzed using HPLC. Samples weighing 0.4 ± 0.1 g were chopped into small pieces and put into 25 ml scintillation vials with 20 ml of unstabilized THF and allowed to sit over night in a dark drawer. Standards of AO2246 were dissolved in acetonitrile. Samples of the solution containing HC434 and AO2246 were analyzed using a Hewlett-Packard 1100 HPLC under the following conditions:

95/5 acetonitrile/water
Supelco C-18 column 250 x 46 mm 5 μ
35°C oven temperature
281 nm wavelength 10 μ L injections
10 minute run time

3. RESULTS AND DISCUSSION

3.1 ACCELERATED AGING AND X-RAYING OF MOTORS

Records of lot acceptance testing of a small rocket motor using propellant 'A' indicate that motors made with different lots of polybutadiene have different failure rates. For this particular test, failure is indicated by the appearance of a crack, detected by x-ray, in the propellant grain before or after the start of accelerated aging and cold/hot temperature cycling. The historical lot acceptance testing records are shown in Table 1a and are plotted in Figure 1 for motors made with polybutadiene lots 322M, 341M, and 336M. The polymer lots seem to produce motors with resistance to cracking increasing in the following order 336M < 341M < 322M. According to the data, polymer lot 336M produces motors so vulnerable to cracking that cracks are even observed upon x-raying prior to the start of accelerated aging in some motors grains. More motor lot acceptance data are shown in Table 1b and Figure 2 for motors more recently produced, i.e., with propellant used in this study. These data are shown separately, since they were obtained during the time that microcalorimetric data were obtained for the polymer lots and

propellant mixes used in the manufacture of these motors. The polymer lots used to make these motors are 322M, 341M, 336M, and the most recently manufactured polymer lot 354M. No microcalorimetric data are available for propellant made from polymer lot 336M. The polymer lots are shown in order of propellant motor grains with increasing resistance to cracking: 336M < 341M, 354M < 322M.

3.2 HIGH PRESSURE DSC

The thermograms for a series of different lots of HC434 polymer were obtained isothermally at 125°C and 550 psi in air. A typical thermogram of a sample of HC434 polymer at 125°C and 550 psi in air is shown in Figure 3. The induction time, which is defined as the time interval from the moment the sample reaches the test temperature to the onset of the exotherm, was measured for each polymer lot. The reciprocal of the induction time, which can be considered an average rate for the steady-state oxidation of the polymer, increases as a function of the iron content of each sample as shown in Figure 4 and Table 2. The data for polymer lot 336M indicates that this material is the least stable and also has the highest iron content, 144 ppm, of any of the polymer lots. The most stable material, lot MJH, also has the lowest Fe concentration at 5 ppm. Although the induction time is probably also a function of the antioxidant concentration, this concentration is generally fairly constant between 0.7 and 0.8 % as measured by high performance liquid chromatography (see Table 3). The exceptions are lots 341M and lot MJH, which have antioxidant concentrations of 0.5% and 1.16 %, respectively. The data point labeled no. 14 on the plot does not appear to fit the linear trend of the data, however this sample is originally lot no. 322M (labeled 13) to which 100 ppm of soluble iron in the form of ferric acetylacetonate has been added. This form of iron may be different from the form of iron that might be catalyzing oxidation in the original sample. This could account for the deviation of this sample (point labeled 14) from the trend of the other samples. The point labeled 15 is a sample that originally had an iron content of about 60 ppm, but after chelation with a sodium salt of ethylenetriaminetetraacetic acid, the iron had been reduced to about 5 ppm. The use of HPDSC to determine the relative oxidative stability of materials has been reported in the literature by several workers.⁶⁻⁹ The observed decrease in the induction time (increase in the reciprocal induction time) as a function of increasing iron content is expected based on observations by others that iron compounds catalyze oxidation of polybutadiene.⁶

3.3 OVEN AGING OF DIFFERENT HC434 POLYMER LOTS

Lots 322M, 341M, 354M, and 336M of HC434 polymer were each put into 400ml beakers and placed in an oven at 77°C. Six weeks later the samples were inspected and the following observations were noted:

- 1) Lot 322M remained in a liquid state.
- 2) Lot 341M was mostly gelatinous.
- 3) Lot 354 had been knocked over and spilled, however the part remaining in the beaker was cured solid. The material that had seeped under the beaker was gelatinous, while the material which was more exposed to the air was cured solid.

- 4) Lot 336M had cured solid.

These results are generally consistent with the level of iron known to be present in the different HC434 lots, which are listed in order of increasing iron concentration: 322M < 341M < 354M < 336M.

3.4 HEAT FLOW MICROCALORIMETRY

3.4.1 SEALED AND OPEN VIALS

Power-time curves for samples of HC434 polymer lot 322M and for a sample of propellant 'A' formulated from lot 322M polymer were obtained at 75° C in open and sealed vials as shown in Figures 5 and 6. The results for the HC434 polymer are as expected for a reaction mechanism involving the consumption of oxygen. In the closed vial the heat flow rate decreases with time presumably because the limited supply of available oxygen is being depleted in the closed system as the reaction proceeds. Conversely, in the open system the availability of oxygen is unlimited - particularly if the reaction rate is not diffusion limited - and the reaction can become autocatalytic. The measured heat flow rate in the propellant seems to be lower in the open vial than in the sealed vial. If this result is significant it could possibly be due to loss of volatile components in the propellant, such as plasticizer, which would result in some endothermic activity, or it could be due to heat loss to the environment from the opening in the vial. The heat flow rates in either case remain constant throughout the course of the experiment.

3.4.2 PROPELLANT HEAT FLOW IN OXYGEN AND NITROGEN ATMOSPHERES

Power-time plots for mix 051B of propellant 'A', obtained in oxygen and nitrogen atmospheres, are shown in Figure 7. The total heat evolved after 40 hours is 60% less in nitrogen than in oxygen. Apparently, some oxygen or some other reactive species has remained after exposure to vacuum for 24 hours. These data provide further support for an oxidative mechanism contributing to the heat flow. It is interesting to note that the short burst of exothermic activity that occurs under oxygen gas at about 14 hours and under nitrogen at about 30 hours appears in both samples after about 0.4 joules of heat have been evolved.

3.4.3 HC434 POLYMER

The power-time curves for different lots of HC434 polymer at 75° C in sealed vials (1.8 ml) are shown in Figure 8. These data are characterized by a decreasing heat flow rate which in the case of lot 322M and 330M appears to level off to a steady state heat flow rate after about 5 to 10 hours. The remaining lots seem to be continuing to decrease in heat flow well after 10 hours. These initial experiments were run for short duration in an

effort to maximize the number of samples run in relatively short period of time, but long enough to observe differences between the different lots of HC434. Studies of longer duration and under conditions of unlimited oxygen supply are needed to further characterize any differences that may be manifested with continued aging. The total heat evolved from the exothermic reaction of different lots of HC434 polymer at 76°C was measured by integrating the heat flow rates as a function of time up to 15 hours at 76° C and is shown plotted in Figure 9. As was the case with the HPDSC results, the microcalorimetric data generally show an increase in the rate of heat generated with increasing iron content. The nonlinearity may be due, at least in part, to the affects of the limited oxygen supply, particularly with the faster reacting samples. Although conceivably some increase in heat flow might be attributed to an increase in the thermal conductivity of the sample, most is probably attributable to the catalytic activity of the iron, particularly since the levels of iron are so low. Heat flow rates that are measured within 0 to 8 hours for these samples probably exhibit some thermal equilibration effects as well as effects due to chemical reaction. For an as yet unknown reason, lot 354M does not appear to fit the general trend of the data. These samples contain soluble and insoluble iron, which may be different in their effect on the heat flow and catalysis of oxidation. It is not known how much of the iron in lot 354M is soluble iron. There are other factors such as the distribution of trans, cis, and vinyl isomers in polybutadienes that could effect the rates of oxidation.

3.4.4 POLYBUTADIENE IN LARGE OPEN VIALS

Power-time data for 1.0 gram samples of lots 336M, 341M, and 322M of HC434 polymer in large 40 ml vials were obtained at 75°C and are shown in Figures 10 and 11. The heat flow rates for all lots are constant up to about 150 to 175 hours; the time is not clearly defined because data was lost due to a brief power failure just as the samples became autocatalytic. The data might have revealed whether or not the onset of autocatalysis differed for the three polymer lots. It is apparent that the total heat evolved over the course of the experiment increased with increasing iron content. Unlike lots 322M and 336M, where heat flow rates reached a maximum and then declined, the heat flow rate of lot 341M continues to increase throughout the time of measurement. As a sample becomes harder due to crosslink formation, the rate of oxygen diffusion into the material decreases and the rate of oxidation may become diffusion controlled. Diffusion effects were not studied in this work. In agreement with the microcalorimetric data in small sealed vials, the heat flow rates during the period of steady-state, increase with increasing iron content. At some point between 150 and 175 hours the heat flow rates of lots 336M and 341M increase sharply. The magnitude of the autocatalytic activity increases with increasing iron content of the polymer.

3.4.5 PROPELLANT MIXES

Power-time curves, shown in Figure 12 for a series of propellant mixes, viz., 0470, 0472, and 0475 prepared from polymer lots 341M, 354M, and 322M, respectively, were

obtained at 75°C in sealed glass vials. The curves are characterized by gradually decreasing heat flow rates over the 30 hours during which the data were collected. Note that the relative heat flow rates among the different propellant mixes seem to correlate qualitatively with the relative heat flow rates among the corresponding polymer lots from which the propellants were formulated. The propellant mixes 0470 and 0472 have heat flow rates of about the same magnitude and are approximately twice those of mix 0475. Similarly, the corresponding polymer lots 341M and 354M have heat flow curves of about the same magnitude and are both also significantly greater than lot 322M. The total heat evolved for lots 341M and 354M is approximately no more than 1.5 times greater than that of lot 322M. The apparent correlation between the heat flow rates of the different polymer lots with the heat flow rates of the corresponding propellant lots suggests that the same mechanism contributes to the heat flow in both materials. However, the potential for other reaction mechanisms to contribute to the propellant heat flow must also be considered, particularly the hydrolysis of the ester crosslink in the propellant, since this reaction cannot occur in the neat polymer. Other potential reactions in the propellant could involve oxidation of the aluminum, or additional catalysis of polymer oxidation by chromium, which is a component of the cure catalyst. Because of the potential for additional reactions in the propellant, the relative heat flow rates of the different propellant mixes might not be the same quantitatively as the relative heat flow rates among the different corresponding polymer lots from which the propellants are made. However, the qualitative correlation does suggest that the polymer reaction mechanism makes a significant contribution to the propellant heat flow.

Propellant mix 0487 was prepared from polymer lot MJH. MJH was prepared by chelating the soluble iron from a blend of polymer lot 354 and another lot using the sodium salt of EDTA. The EDTA and chelated iron were then removed by washing the polymer with water followed by a drying process. Although this propellant mix was prepared from polymer lot MJH, which had the lowest heat flow rates of any of the polymers tested (see Figure 8), the resulting propellant (mix 0487) yielded a power-time plot having heat flow rates slightly higher than propellant mix 0475 (see Figure 13), which was prepared from the less stable lot 322M. This was contrary to expectations since polymer lot 322M yielded heat flow rates higher than that of lot MJH. The removal of the iron impurities in lot MJH by chelation resulted in a polymer with the lowest heat-flow rates of any of the polymer lots tested. This was expected to produce a propellant with the lowest heat flow rates. It was also expected that motors manufactured using this propellant would have the lowest grain cracking rates, but this did not occur as shown in Figure 2. The propellant prepared with HC434 lot MJH was more susceptible to grain cracking than the propellant prepared with HC434 lot 322M. This example was the only exception to the general observation more stable polymer (polymer with lower heat flow rates), yields more stable propellant (propellant with lower heat flow rates). At this point we have no explanation for this apparently anomalous result. It could be possible that some type of contamination occurred during the manufacture of mix 0487, or that we have reached a lower limit for heat flow in this formulation due to possible reactions of other propellant components. It is not known at this time how much the other components in the propellant contribute to the heat flow and to the stability of the binder.

Iron oxide, which is used as a burn rate modifier in the propellant, could contribute to the catalysis of binder oxidation, particularly if some of it dissolves in the polymer. This could possibly account for the higher than expected heat flow and grain cracking in propellant mix 0487. The iron oxide could also contain catalytic metal impurities.

Perhaps some instability in HC434 lot MJH might be revealed in a longer-term heat flow experiment. Unlike some lots that have initially low iron levels, lot MJH originally contained high levels of iron, although this would not be expected to have an adverse effect on the oxidative stability after the iron is removed. Also, it is not known if the iron chelation procedure had any effect on the polymer that would effect the aging properties of the propellant from which it was formulated. In hindsight the aging properties of propellants prepared from lot MJH before chelation should have been determined. This data could then have served as a control for propellant prepared with lot MJH after the chelation procedure. Perhaps some processing parameters, which we have not identified, also affect cracking propensity of the resulting propellant.

3.4.6 CHELATION EXPERIMENTS

The catalytic activity of metals is known in some cases to be inhibited by the formation of a chelate. If iron is catalyzing reactions contributing to the heat flow in the HC434 polymer, as the previous high-pressure DSC and microcalorimetric data suggest, deactivation of the iron via chelation should significantly reduce the rate of heat flow as measured by microcalorimetry. Several compounds, viz., glutaric acid, ethylenediaminetetraacetic acid (EDTA), and 8-hydroxyquinoline (8HQ), were tested because of their known potential for forming complexes or chelates with metals. The results of the heat flow measurements at 75° C on mixtures of HC434 with each of the chelating compounds are shown in and Figure I4. The power vs time curves of Figure I4 show significant reductions in the heat flow rates of some of the mixtures. The reduction in heat flow achieved by the chelating compounds is shown in increasing order of effectiveness: EDTA < glutaric acid < 8HQ. The greater apparent effectiveness of the 8HQ can possibly be attributed at least in part to its complete solubility in the polymer. The glutaric acid was only partially soluble and very little, if any, of the EDTA was soluble in the polymer. Thus, the limited solubility of EDTA in the polymer may account for its minimal effect in reducing the heat flow rather than its chelating ability, since it is known to be an effective chelating agent for iron. The heat flow data were obtained from neat 8HQ and no significant heat flow was observed, suggesting that the interaction of 8HQ with the HC434 sample is responsible for the reduction in the heat flow of the HC434.

3.4.7 ACTIVATION ENERGIES

Heat flow data for polybutadiene lot 322M and propellant 'A' prepared with lot 322M polymer were obtained at 55°, 65°, and 75° C, and are shown for the polymer and

propellant in Figures 15 and 16, respectively. The heat flow rate after 15 hours at the specified temperatures was chosen to calculate the Arrhenius activation energy:

$$R = Ae^{-E_a/RT}$$

where R is the rate of the measured process or some quantity proportional to the rate; 'A' is the pre-exponential factor; 'E_a' is the activation energy; 'R' is the gas constant; and 'T' is the absolute temperature. This method was chosen, rather than an isoconversional method because (1) it is assumed equilibration effects are insignificant after 15 hours, and (2) that the reaction is approximately in a steady-state condition. This would allow the rate at the same time increment to be used at all three temperatures to determine the Arrhenius activation energy, rather than taking the rate at some isoconversional point. It is not known how much, if any, diffusion effects contribute to the observed rates. Although diffusion effects are considered to be negligible since increasing the mass of the sample increases the heat flow rate proportionally, even though the area of the air-sample interface, where diffusion of oxygen could occur, remains constant. The agreement between the propellant and polymer activation energies again suggests a common mechanism. The activation energy of 20 kcal/mole is in good agreement with the range of activation energies (27 - 17 kcal/mole) determined by Celina, et. al., for a polyurethane crosslinked binder over a temperature range of 125 to 25°C.¹⁰

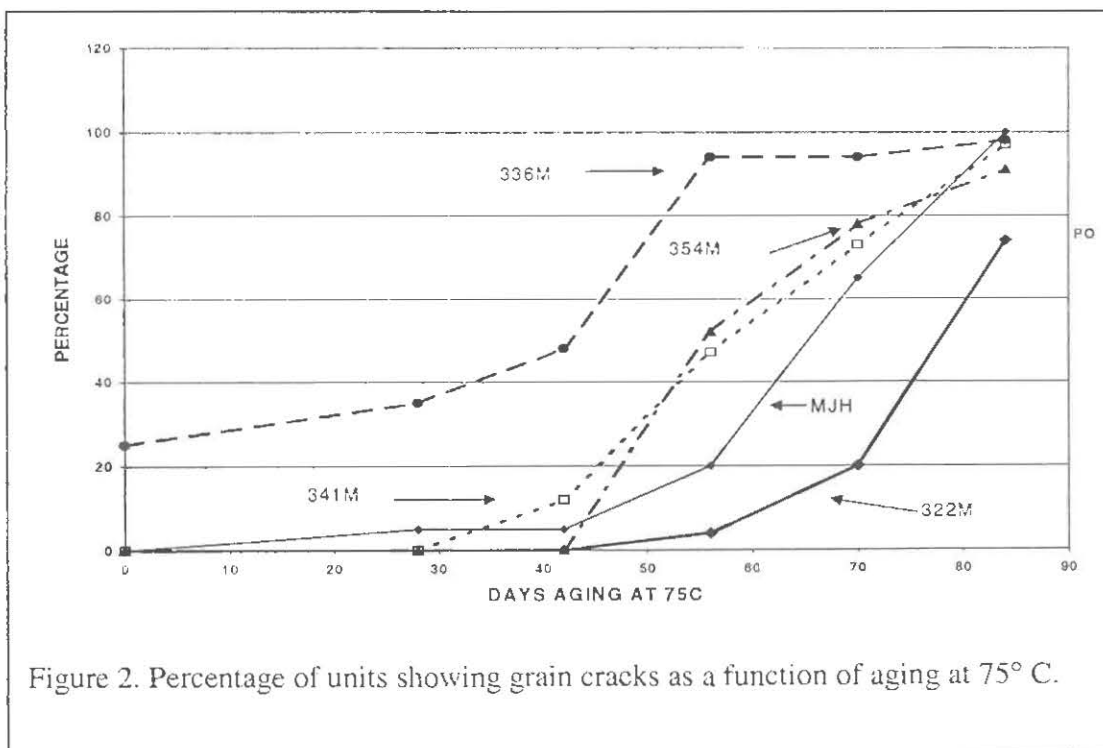
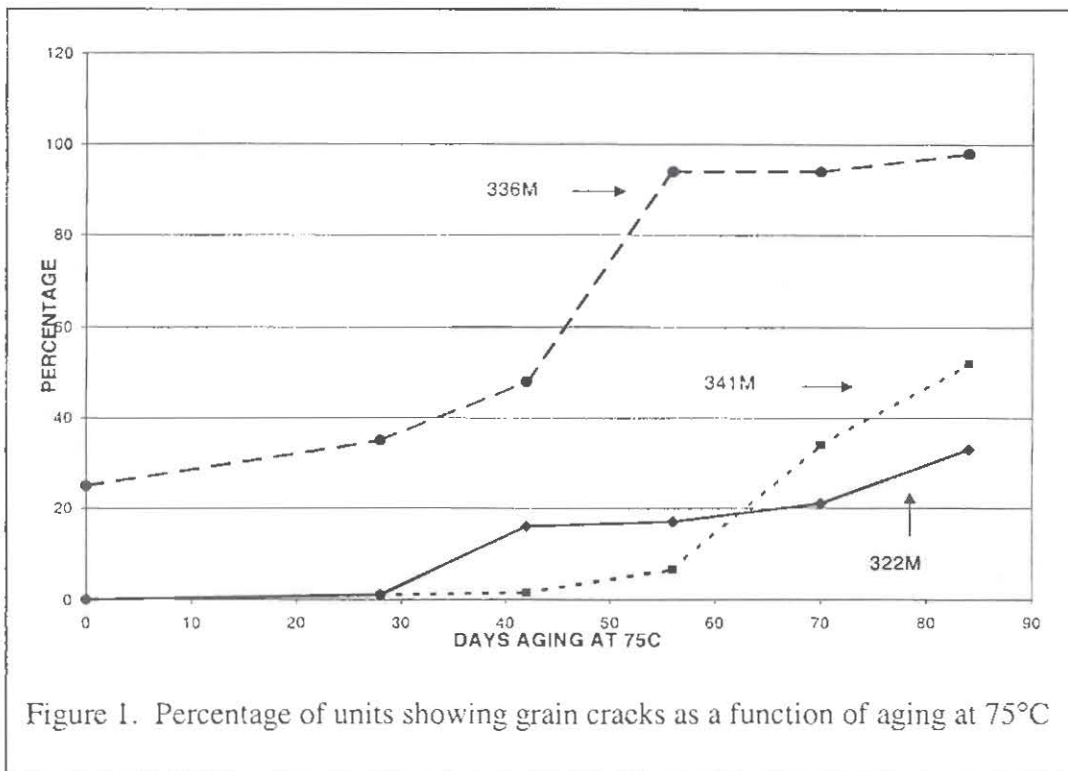
4. CONCLUSIONS

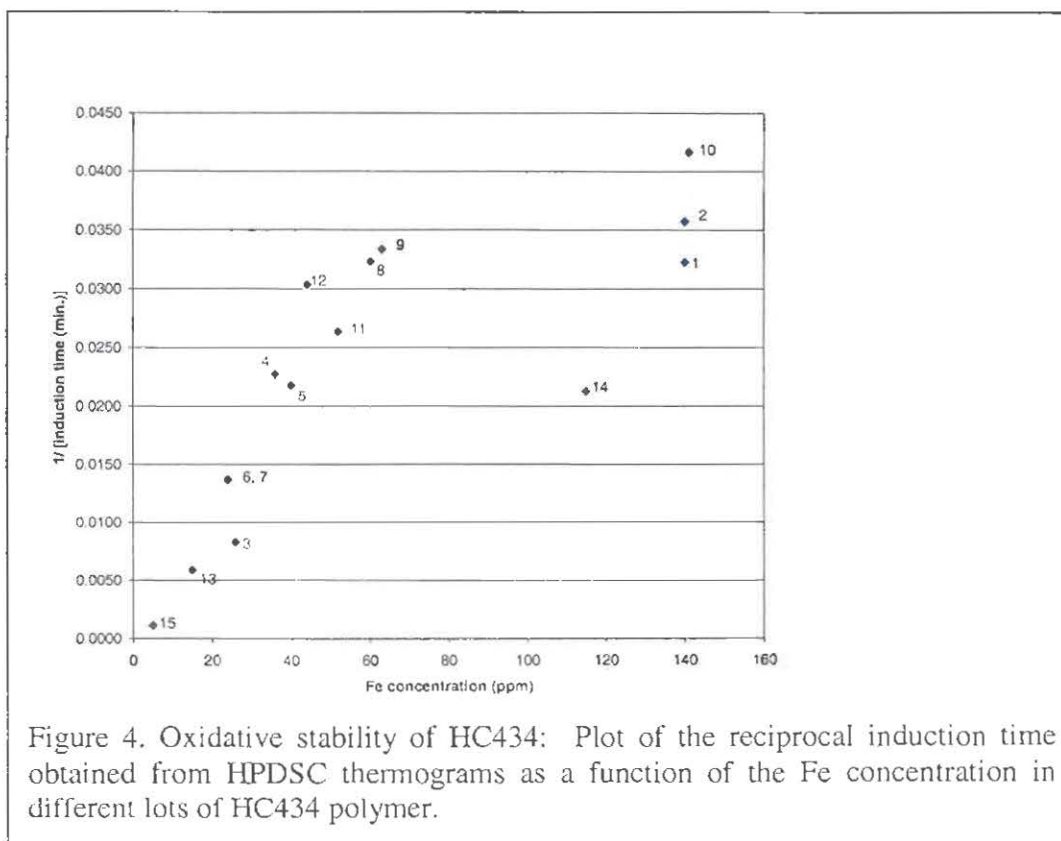
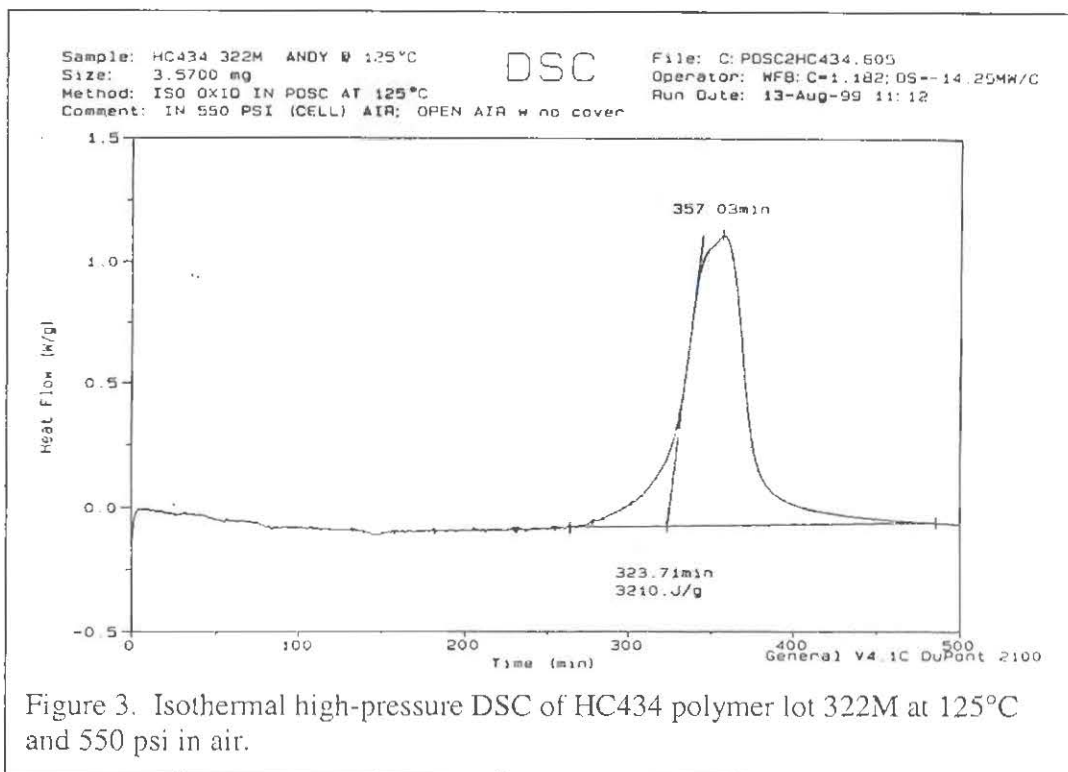
The results of this study indicate that aging of a composite propellant can be observed using microcalorimetry and that polymer oxidation contributes significantly to the observed reaction. In the case of HC434, the presence of trace iron impurities catalyzes the rate of oxidation in the polymer and the propellant from which it is formulated. The possibility of other reactions in the propellant, such as ester hydrolysis and additional catalysis of oxidation by the chromium cure catalyst are not known at this time and need to be investigated. These results corroborate the many studies in the literature, which indicate that oxidative reactions are a significant mechanism in polybutadiene aging. Longer-term microcalorimetric studies should be conducted on propellant and polymer. The effect of other propellant ingredients on the heat flow rate and oxidation of neat polymer and propellant, as well as the effect of polybutadiene structure on oxidative stability need further investigation. Although we have shown a correlation between iron impurity levels and oxidative stability as well as some correlation with propellant cracking propensity, we can not account for the high cracking propensity of propellant mix prepared with lot MJH polymer. There are a number of factors that could account for the poor aging characteristics of the propellant prepared from the lot MJH polymer: 1) processing variables; 2) unidentified impurities in the polymer or other propellant

ingredients; 3) Solubilized iron from the iron oxide burn rate modifier; 4) differences in the microstructure of the polymer; or 5) effects of the chelation process used to remove iron impurities from the HC434 polymer.

REFERENCES

1. Tibor Kelen, *Polymer Degradation*, (Van Nostrand Reinhold, New York, 1983), p.108.
2. R. L. Pecsok, P. C. Painter, J. R. Shelton and J. L. Koenig, *Rubber Chem. and Technol.* 49 (4), (1976), p. 1010.
3. R. T. Conley, ed., *Thermal Stability of Polymers*, "Fundamental Reactions in Oxidation Chemistry"; P. M. Norling and A. V. Tobolsky, vol. 2, (Marcel Dekker, New York, 1970), p. 114.
4. Tibor Kelen, p. 183.
5. R. T. Conley, p. 138.
6. H. Berg, B. Stenberg, and R. Sanden, *Plastics and Rubber Processing and Applications*, **12** (1989), p. 235-239.
7. J. Minn, *Thermochnica Acta*, **91**, (1985), p. 87-94.
8. J. A. Walker and W. Tsang, *Soc. Auto Eng.*, **801**, (1980), p. 1.
9. Marshall, et. al., *Polymer Engineering and Science*, **13** (6), (1973).
10. M. Celina, A graham, R. Assink, and L. Minier, "Polymer Aging Techniques Applied to Defradation of a Polyurethane Propellant Binder", *Proc. 1999 Life Cycles of Energetic Materials*, 9/26 - 9/29, Orlando, FL (1999).





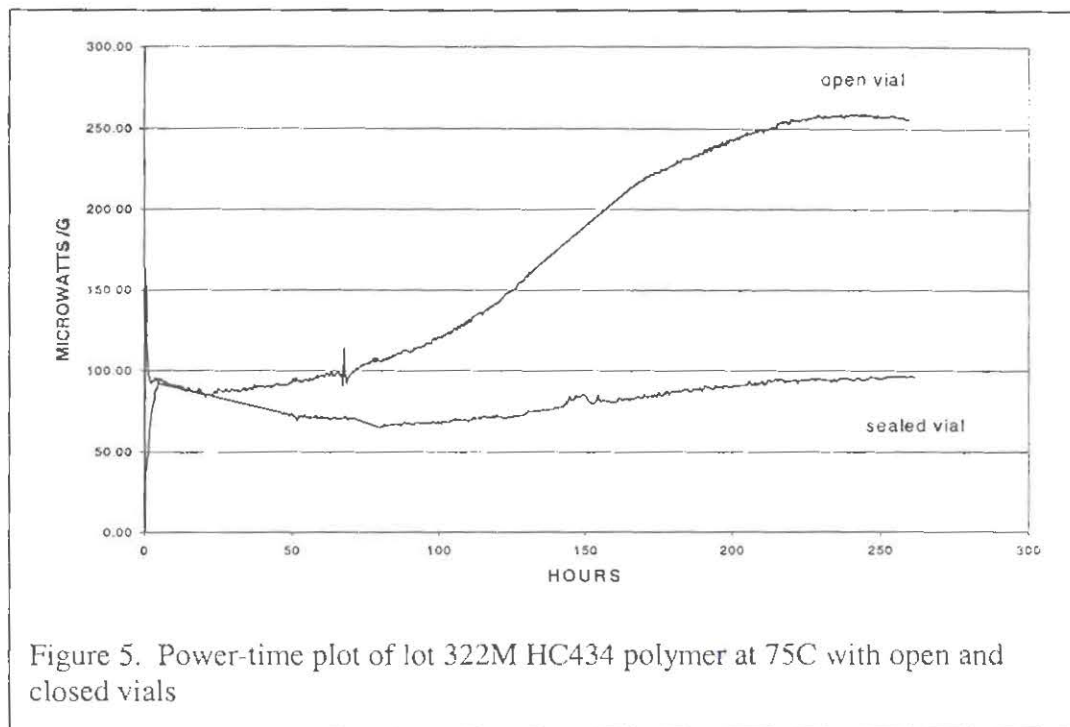


Figure 5. Power-time plot of lot 322M HC434 polymer at 75C with open and closed vials

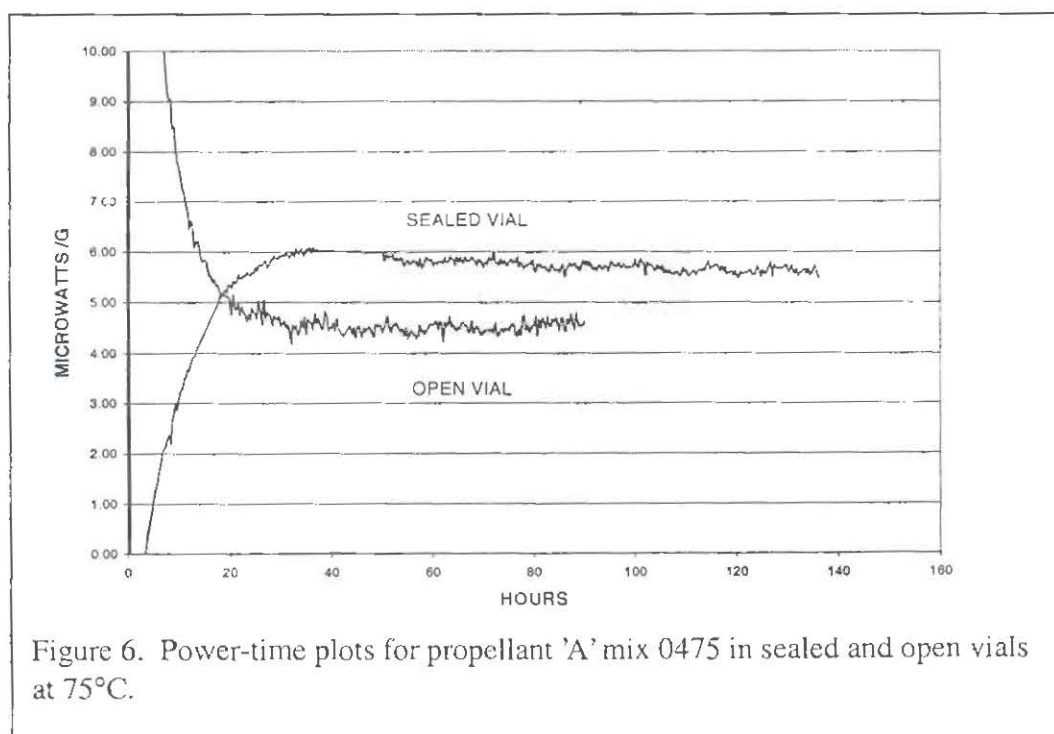


Figure 6. Power-time plots for propellant 'A' mix 0475 in sealed and open vials at 75°C.

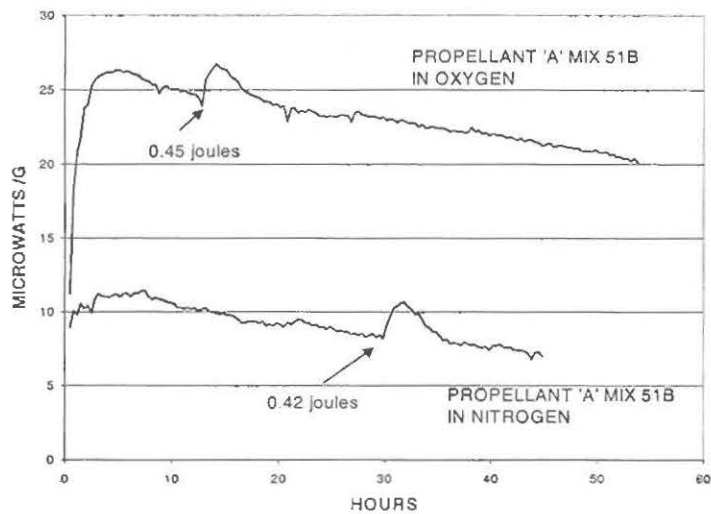


Figure 7. Power-time plots for propellant 'A' in oxygen and nitrogen atmospheres

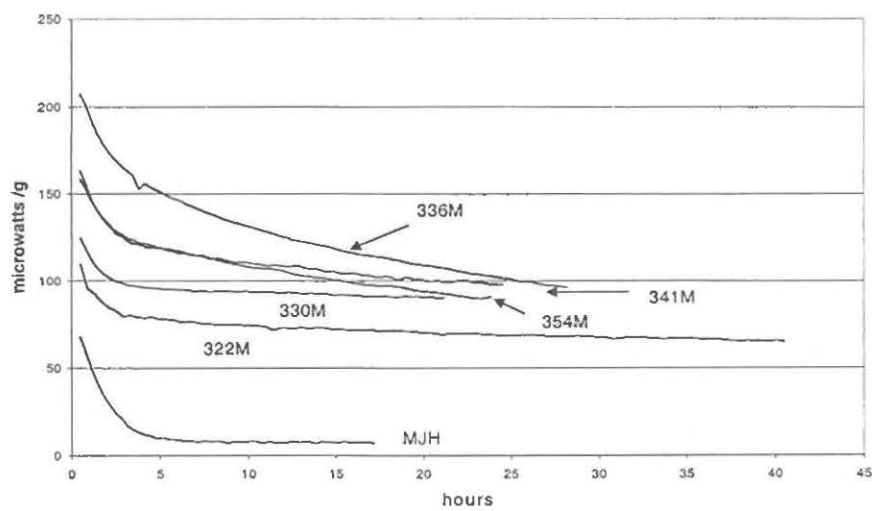
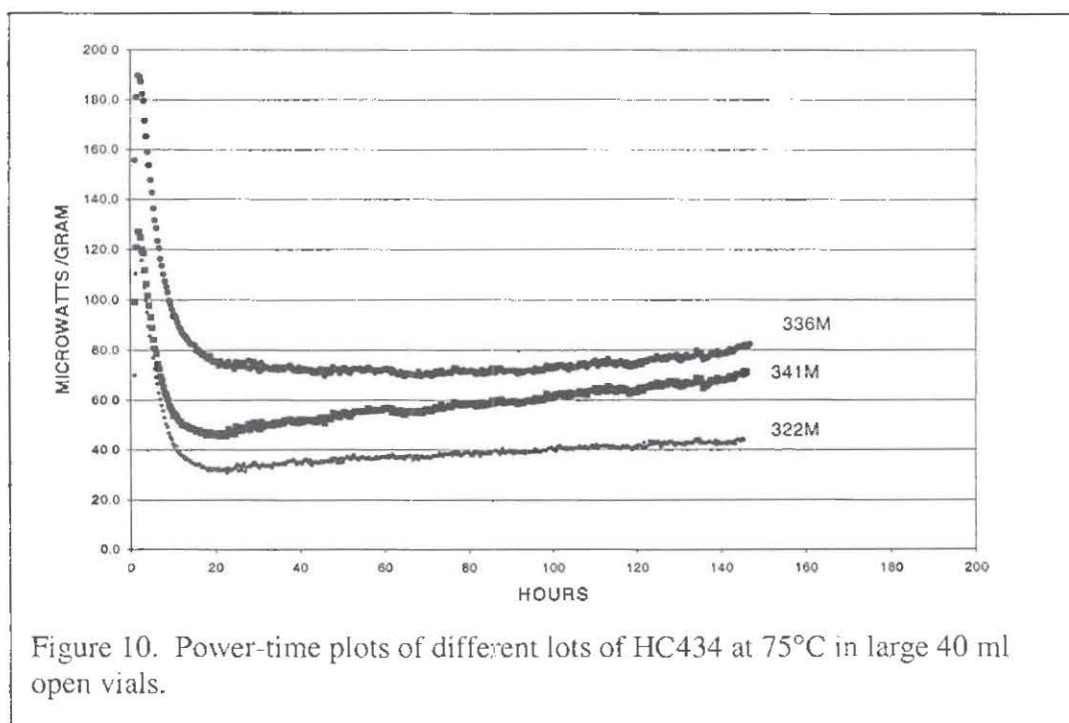
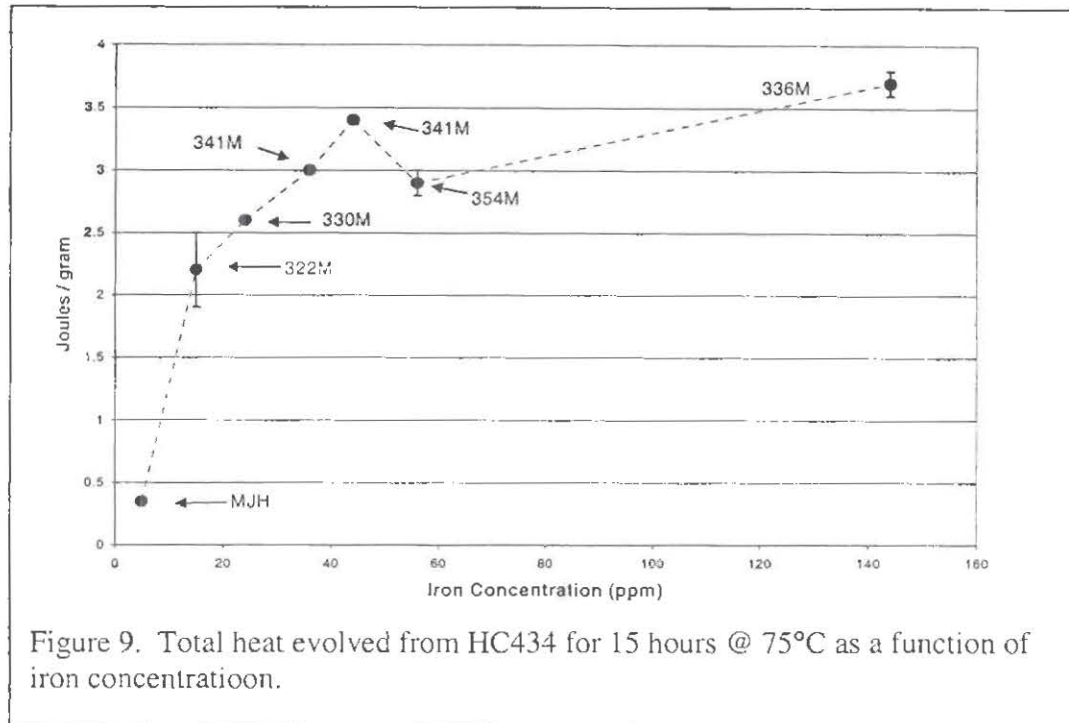
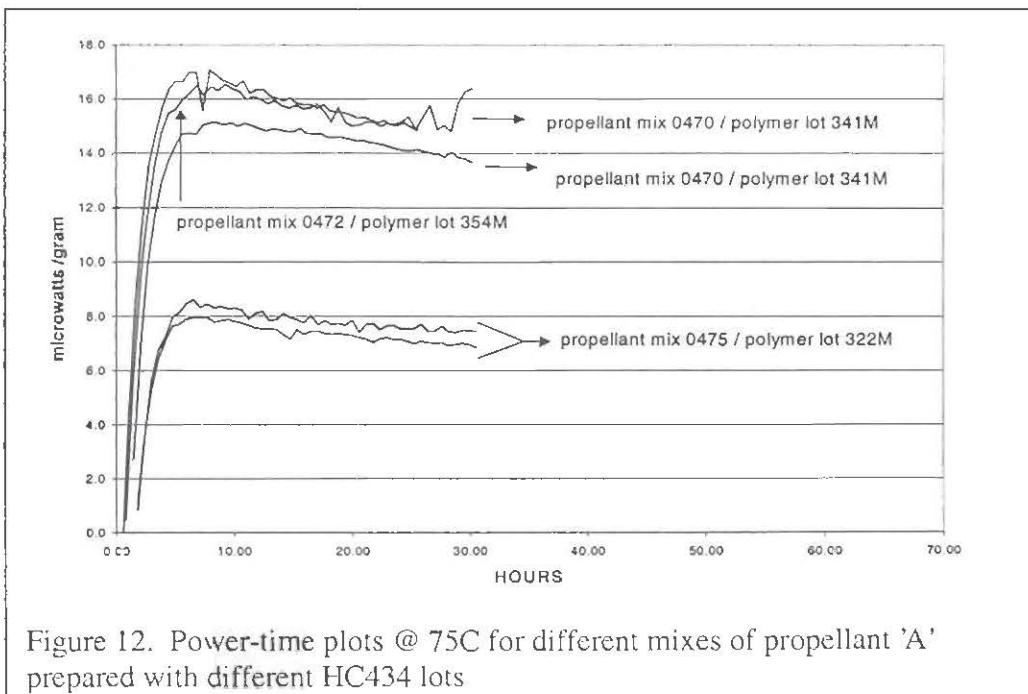
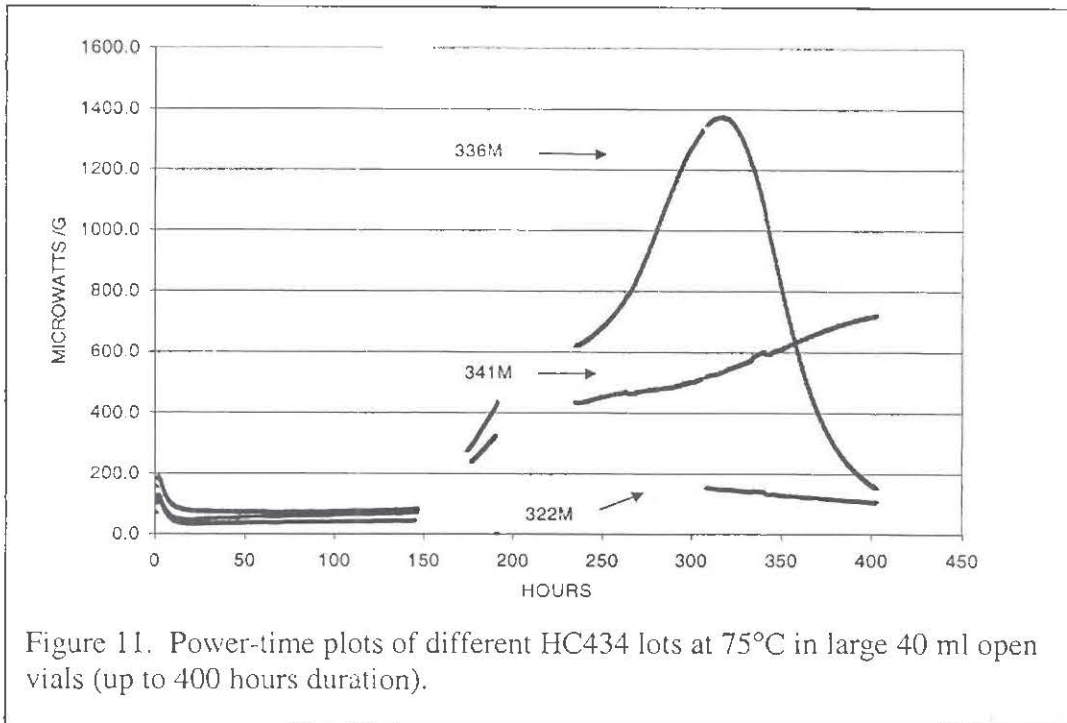


Figure 8. Power-time plots @ 75°C of different lots of HC343 in sealed vials





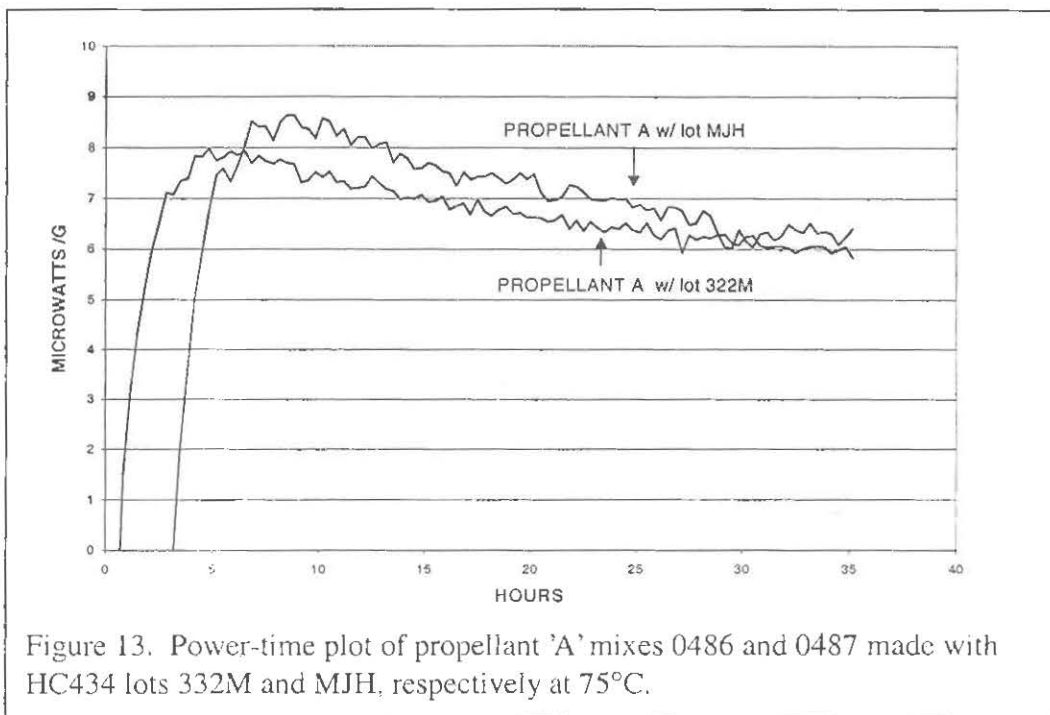


Figure 13. Power-time plot of propellant 'A' mixes 0486 and 0487 made with HC434 lots 332M and MJH, respectively at 75°C.

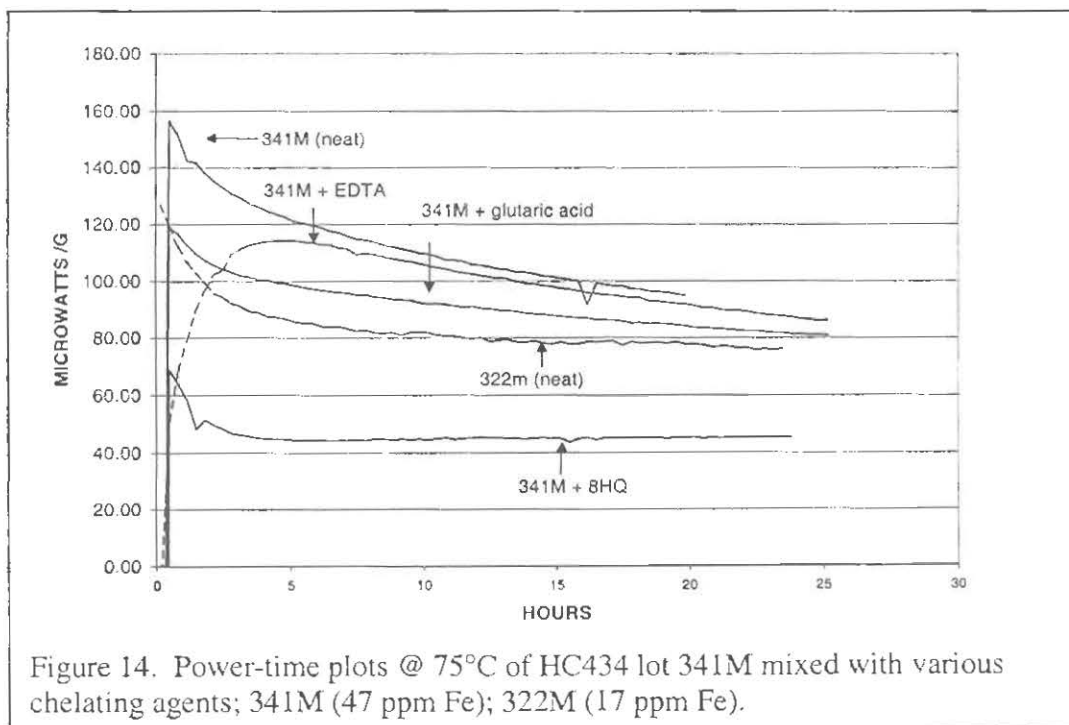


Figure 14. Power-time plots @ 75°C of HC434 lot 341M mixed with various chelating agents; 341M (47 ppm Fe); 322M (17 ppm Fe).

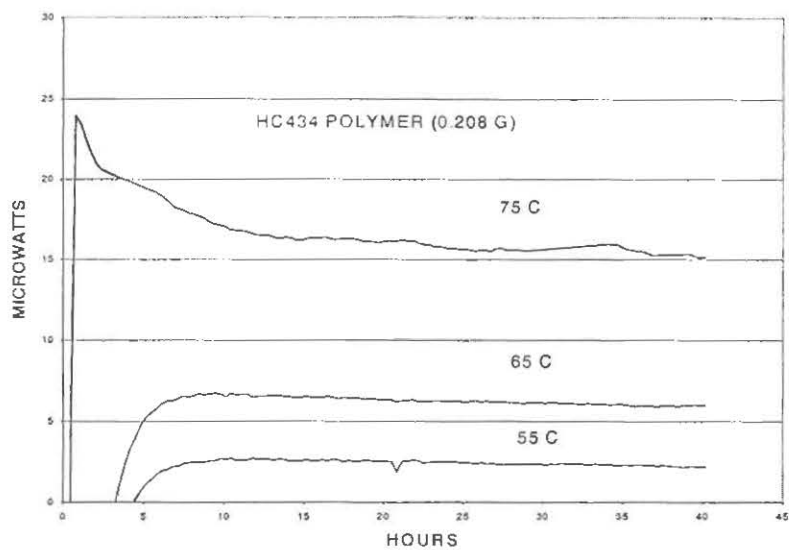


Figure 15. Power-time plots of HC434 lot 322M @ 75°, 65°, and 55°C.

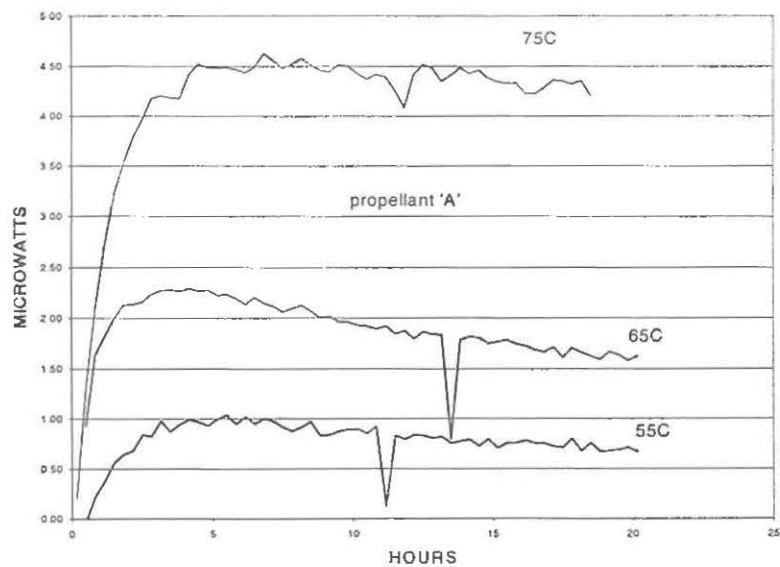


Figure 16. Power-time plots of propellant 'A' prepared with HC434 lot 322M at 75°, 65°, and 55°C.

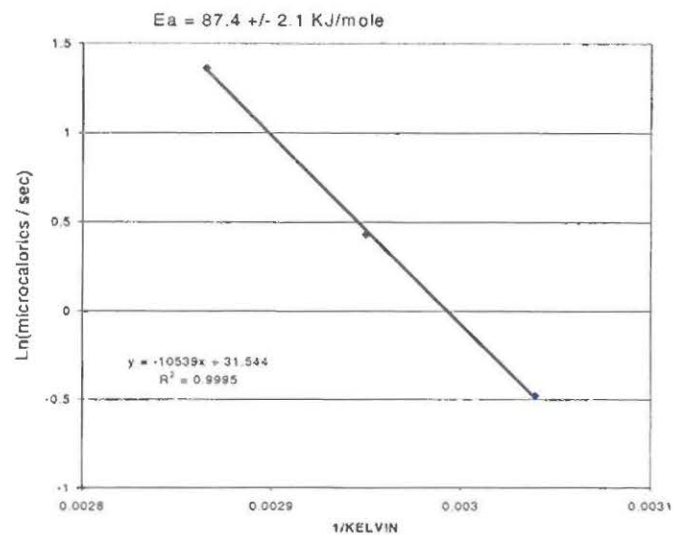


Figure 17. Arrhenius plot for HC434 lot 322M from 75° - 55°C.

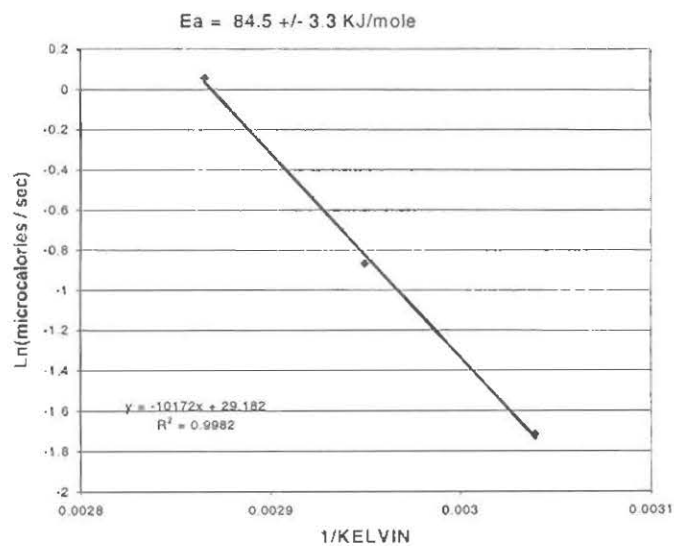


FIGURE 18. ARRHENIUS PLOT FOR PROPELLANT 'A' PREPARED WITH HC434 LOT 322M FROM 75° - 55°C.

Table 1. Percentage of motors showing cracks after hot/cold temperature cycling as a function of age at 75°C a) all historical data; b) more recent data showing motors manufactured and tested during this study.

a)

POLYMER LOT	DAYS AT 75C						NO. OF UNITS TESTED
	0	28	42	56	70	84	
322M	0	1	16	17	21	33	94
341M	0	1	1.5	6.5	34	52	199
336M	25	35	48	94	94	98	99

b)

POLYMER LOT	DAYS AT 75C						NO. OF UNITS TESTED
	0	28	42	56	70	84	
322M	0	0	0	4	20	74	50
341M	0	0	12	47	73	97	34
354M	0	0	0	52	78	91	23
336M	25	35	48	94	94	98	99
MJH	0	5	5	20	65	100	20

Table 2. Induction times obtained from isothermal HPDSC at 125°C and 550 psi and iron concentrations for HC434 polymer lots.

Data Point Label No.	SAMPLE (LOT #)	INDUCTION TIME (MIN.)	RECIPROCAL INDUCTION TIME (1/MIN.)	Fe (PPM)	std. Dev of induction time
1	336M	31	0.0323	140	3
2	336M (1/99)	28	0.0357	140	2
3	336M (THIO)	121	0.0083	26	-
4	341M	44	0.0227	36	1
5	346M	46	0.0217	40	5
6	330M	73	0.0137	24	11
7	330M (1/99)	73	0.0137	24	0
8	354M	31	0.0323	60	5
9	#1(346M)	30	0.0333	63	4
10	#2(336M)	24	0.0417	141	1
11	#3(354M)	38	0.0263	52	2
12	#4(341M)	33	0.0303	44	3
13	#5(322M)	171	0.0058	15	31
14	#5 added Fe	47	0.0213	115	-
15	MJH	906	0.0011	5	485

TABLE 3. ANTIOXIDANT (AO2246) CONCENTRATIONS (AVERAGE OF TWO MEASUREMENTS) IN DIFFERENT HC434 LOT AS MEASURED BY HIGH PERFORMANCE LIQUID CHROMATOGRAPHY.

HC434 SAMPLE	AO2246 CONC. (WT %)
MJH	1.16
322M	0.82
341M	0.50
354M	0.72
336M	0.77

TABLE 4. TOTAL HEAT EVOLVED AFTER 15 HOURS AT 75°C FOR HC434 POLYMER AS A FUNCTION OF IRON CONCENTRATION.

HC434 LOT	FE (PPM)	JOULES /G	STDEV
MJH	5	0.35	0.00
322M	15	2.2	0.30
330M	24	2.6	0.00
341M	36	3	0.00
341M	44	3.4	0.00
354M	56	2.9	0.10
336M	144	3.7	0.10

TABLE 5. ACTIVATION ENERGIES AND HEAT FLOW RATES AT 75, 65, AND 55°C FOR HC434 LOT 322M AND PROPELLANT 'A' MIX PREPARED WITH HC434 LOT 322M.

TEMPERATURE (DEGREES C)	HEAT FLOW RATE AT 15 HOURS (MICROWATTS)	
	HC434 LOT 322M	PROPELLANT 'A' MIX 0475
75	16.3	1.06
65	6.4	0.42
55	2.5	0.18
ACTIVATION ENERGY (KJ/mole)	87.4 +/- 2.1	84.5 +/- 3.3

THIS PAGE LEFT INTENTIONAL BLANK

USES OF CALORIMETRY IN ENERGETIC MATERIALS PROCESS SCALE-UP

Michael W. Lesley

Analytical Laboratories Department
ATK Thiokol Propulsion Corporation
ATK Alliant Techsystems
P.O. Box 707, M/S 245
Brigham City, UT 84302

ABSTRACT

This paper discusses some practical experiences in the thermal hazard evaluation of energetic materials processes prior to trying them out in pilot-scale facilities. Differential scanning calorimetry (DSC), accelerating rate calorimetry (ARC), and/or isothermal microcalorimetry are first used to quantify possible worst-case energy releases. If there is a potential problem on thermodynamic grounds, maximum heat release rates are compared with heat removal capabilities of the reaction vessels to determine if the scaled-up process has enough cooling capacity to keep the reaction under control. If safety margins between cooling capacity and heat generation are small, a numerical simulation of the reactor may be carried out to better understand conditions under which runaway behavior is possible.

Two examples, a process for reclaiming HMX from an aluminized solid propellant by reaction with mineral acid, and synthesis of an energetic polymer with an autocatalytic reaction mechanism, are used to illustrate the principles discussed.

INTRODUCTION

In recent years ATK Thiokol Propulsion/Utah has become increasingly involved in the research, development, and scale-up of energetic materials processing involving liquid-phase or liquid/solid chemical reactions. These include operations such as organic synthesis of new energetic solid propellant or explosive ingredients, and solid propellant disposal operations that rely on chemical degradation and neutralization of energetic ingredients.

Traditionally, our research, development, and production has focused on propellant, explosive, and pyrotechnic formulations made by blending commercially available energetic ingredients and polymers. Safety protocols that verify that no significant exothermic reactions can occur between the ingredients in the formulation under mixing, curing, and storage conditions are sufficient to guarantee the absence of thermal hazards in such situations. Thermal analysis tools that we have found valuable for this sort of assessment include accelerating rate calorimetry (ARC) [1] and a screening test we developed in-house, the simulated bulk autoignition (SBAT) test [2].

In contrast, in organic synthesis of energetic ingredients and similar operations, one must control a liquid-phase chemical reaction that is often quite exothermic. Such reactions will engage in thermal runaway behavior if the reaction vessel is not properly cooled. Usually the result of such a thermal runaway (for a reactor with properly sized vents) is boil-over of the reaction mixture, but when energetic materials are involved, more serious consequences can sometimes ensue.

In this paper we describe some of our early efforts to assess thermal hazards in scaling up liquid-phase or liquid-solid reactions from the laboratory bench to the pilot scale. We made use of various thermal analysis methods that were available to us at the time: differential scanning calorimetry (DSC), accelerating rate calorimetry (ARC), and isothermal heat flow microcalorimetry, which, when using a batch mixing cell accessory, can be used for reaction calorimetry.

Essentially the procedure for thermal hazard evaluation on such systems involves determining if the reaction in question can produce heat at a high enough rate to exceed the cooling capacity of the reaction vessel and lead to a thermal runaway. Proper assessment involves both quantification of heat release rates from the reaction and measurement of the heat removal capacity of the reaction vessel.

Two examples, one a liquid/solid reaction (reaction of aluminized solid propellant with mineral acid) and another a liquid phase reaction (synthesis of an energetic polymer in solvent) are used to illustrate the principles discussed.

EXPERIMENTAL

Differential Scanning Calorimetry

Differential scanning calorimetry (DSC) was used to measure heat generation rates for the energetic polymer synthesis. A Perkin-Elmer DSC-4 Differential Scanning Calorimeter was used for the testing. Freshly mixed (and stored in an ice bath until testing) ~ 60 mg samples of solvent plus reactants were encapsulated in 75 microliter stainless steel capsules with a hermetic O-ring seal. Samples were tested isothermally, at 30, 40, and 50 °C.

Isothermal Microcalorimetry/Reaction Calorimetry

Isothermal microcalorimetry was also performed on samples from both studies. The instrument was a Calorimetry Sciences Corporation model 4400 Isothermal Microcalorimeter. According to the instrument vendor, the unit is capable of measuring heat evolution rates up to 500,000 μ W (0.5 watts).

For the HMX recovery process, a stirred, batch mixing cell was used (essentially as a reaction calorimeter) to measure heat generation rates from mixtures of mineral acid and propellant. In these studies about 0.75 grams of propellant, cut to a uniform sample size, were placed into the calorimeter, thermally equilibrated and then a premeasured amount of acid (same acid/propellant ratio as used in the process) was injected. The rate of heat generation versus time was then recorded for a period of up to 48 hours. Heat generation versus time curves were generated at 25, 29.4, and 35 °C.

For the energetic polymer synthesis, we used isothermal microcalorimetry (on 300 mg samples) at 25 °C as an independent check as to whether the DSC results were reasonable.

Accelerating Rate Calorimetry

Accelerating rate calorimetry (ARC) was performed primarily to support the HMX recovery study. One ARC run was also made on the polymerization reaction starting materials.

The studies were performed using a Columbia Scientific Industries ARC[™] accelerating rate calorimeter, using the original controller and

ARC-WIN[™] version 1.2.1 software. ARC is an adiabatic calorimetric technique that simulates the thermal runaway behavior of bulk quantities of energetic materials.

All ARC experiments were performed using 1-inch (2.54 cm) diameter, spherical titanium bombs.

For HMX recovery, propellant (cut to the same sample size as used for microcalorimetry) was placed in the ARC, heated to 35 °C (in "isothermal age" mode) and allowed to equilibrate there. Then an appropriate quantity of acid was injected into the bomb, using a long, thin needle through the tube in the calorimeter lid, to initiate reaction. (Preliminary experiments had been conducted to prove beyond any doubt that this procedure would not result in an immediate exotherm.) The system was immediately sealed and the sample was allowed to react and self-heat under confined, adiabatic conditions.

For the polymer synthesis a 6.2 gram sample of solvent plus polymerization reactants was tested in a sealed bomb. The ARC run was started at a low temperature (25 °C), which is really below the temperature range in which valid ARC data can be obtained. The sample showed an exotherm (self-heat rate in excess of 0.02 °C per minute) which was sufficient to self-heat it from 25 °C to approximately 40 °C. After this, the exotherm stopped and the sample was step heated to a final temperature of 80 °C in 5 °C increments, with the calorimeter searching for exotherms at each step. This test did not accurately characterize the synthesis reaction, but was useful for verifying that runaway decomposition of the products did not occur in the temperature range of the synthesis reaction.

RESULTS AND DISCUSSION

Method for Thermal Hazard Evaluation

The evaluation of thermal hazards in scaleup from the bench to the pilot scale proceeds in up to three steps with decreasingly conservative assumptions. The overall logic has much in common with that presented in a paper by Gygas [3], which was concerned mainly with control of undesirable side reactions in chemical processes, but many of the principles are applicable here.

Evaluate worst-case energy release. The first step in a thermal hazard evaluation procedure is to evaluate the *potential worst-case energy release* from the reaction. This involves measurement of the total heat evolved by the desired chemical reaction and then considering what might happen if it were released under adiabatic conditions. One can calculate an adiabatic temperature rise from the area under a DSC curve if the heat capacity of the sample is known. Alternatively, the adiabatic temperature rise (or at least a lower bound on it) can be measured directly via ARC experiments.

If this adiabatic temperature rise is not sufficient to heat the sample near the boiling point of the system or to initiate an undesired secondary reaction, generally no thermal hazard exists. If, on the other hand, the desired reaction liberates enough energy to potentially cause a problem, one must next evaluate and compare the reaction energy release rates and process equipment cooling characteristics.

Determine maximum heat generation and removal capacity. If the thermodynamic evaluation indicates that the reaction evolves enough heat to cause a problem under adiabatic conditions, we next compare *maximum heat generation rates* to the *heat removal capacity of the reaction vessel*. This is to determine if the equipment can remove heat as quickly as it is formed and prevent a thermal runaway.

The maximum heat evolution as a function of temperature can be measured by isothermal DSC, isothermal microcalorimetry (reaction calorimetry), or sometimes ARC experiments. It is preferable to select a technique that is sensitive enough to measure heat evolution rates directly in the temperature range where the process will actually be operated. This is done to avoid errors that can occur when high-temperature data are extrapolated to lower temperatures via the Arrhenius equation (because of mechanism changes, etc.).

Heat transfer coefficients of a production reaction vessel will generally be known, so a comparison of heat removal and generation rates can be readily performed. For new pilot-scale vessels that are being set up for the first time, filling the reactor with hot liquid and measuring cooling curves can quantify cooling capacity.

We then compare heat evolution and removal rates in the temperature regime where the chemical reaction will be carried out. If the maximum cooling capacity of the apparatus (e.g. with a cooling water valve wide open) greatly exceeds the measured heat generation rates, we conclude that the reaction can be controlled with the process equipment. If the maximum rates exceed the cooling capacity of the apparatus, we conclude that the reaction cannot be safely carried out in the proposed equipment.

If, on the other hand, the *maximum* heat generation rates are close to heat removal rates, we may wish to take the analysis a step further and do a mathematical reactor model. This will predict the course of a possible thermal runaway and further help define safe operating conditions for the process.

Model reactor. In cases where safety margins in the preceding evaluation are not large, a mathematical model of the reactor can be used to aid in a decision as to whether the reaction should be scaled up in the proposed equipment or not. Additional information about possible thermal runaway time scales and temperature ranges can be obtained from such an analysis.

These models take into account decreases in reaction rate that occur as reactants are consumed. They are more realistic than the simple comparison of maximum heat production and cooling rates. For non-autocatalytic reactions run isothermally, the initial rate is the maximum rate. It then declines as the reactant is depleted. For autocatalytic reactions the rate initially increases with time as the catalytic reaction product is formed, but eventually a maximum is reached and then the rate declines as a result of reactant depletion.

Decisions to scale up are not made solely on the basis of these calculations. They are only part of the information matrix that goes into risk assessment: bench scale process experience, fundamental chemical understanding of the materials and their hazards, etc. Precautions are always taken to protect operators from the consequences of a possible runaway reaction, up to and including barricades or remote operation.

We now proceed to illustrate the above with two examples from actual practice.

HMX Recovery from an Aluminized Solid Propellant

This process involved reacting a solid propellant with mineral acid (identity or concentration of acid will not be revealed here) to digest and decompose all ingredients except HMX. (The reaction between mineral acid and HMX is negligible under the process conditions.) Most of the energy evolved comes from the reaction between aluminum powder and mineral acid.

In the early phases of the program it was desired to process roughly one pound (0.454 kg) of solid propellant in a 2.5 liter, highly stirred, water-jacketed vessel at 25 °C. The vessel was cooled with water from a chiller, its flow rate controlled manually with a valve. The objective was to determine if the reaction could be controlled by manipulation of the cooling water valve.

Evaluation of worst-case energy release.

Adiabatic calorimetry (ARC) results on a mixture of mineral acid and propellant are shown in Figures 1 and 2. The sample size, with a propellant to acid ratio designed to simulate an actual process, yielded a thermal inertia factor below 1.5. Thermal inertia is a measure of the amount of the heat of reaction that goes into heating the bomb instead of self-heating of the sample. A massless bomb (ultimate sensitivity) would yield a thermal inertia factor of one. This run is therefore a reasonable representation of what could occur when mineral acid and propellant are mixed together under confined, bulk conditions.

As described above, the propellant sample was loaded into the ARC, heated to 35 °C, and held under adiabatic conditions, and then the mineral acid was injected.

As shown in Figures 1 and 2, the sample began to exotherm within 20 minutes, with self-heat rates well in excess of the 0.02 °C per minute exotherm threshold. A temperature of 80 °C was reached about 40 minutes after mixing, at which point the run was manually terminated and the cooling air came on. The ARC experiments indicate operating the bulk process at 25 °C without adequate cooling could lead to a thermal runaway and reactor boil-over.

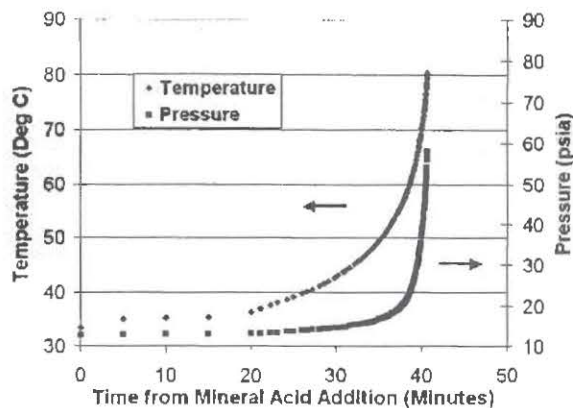


Figure 1. ARC Temperature and Pressure versus Time Plots for Propellant + Mineral Acid

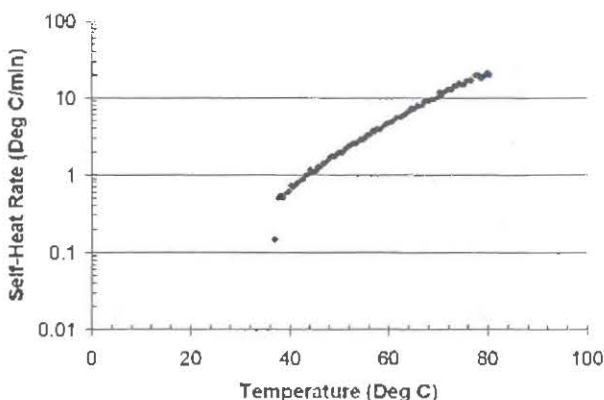


Figure 2. ARC Self-Heat Rate vs. Temperature Plot for Propellant + Mineral Acid

Meanwhile, bench-scale experiments on the 50 grams of propellant level had been carried out successfully at temperatures considerably higher than 25 °C. Consequently a desire was expressed to see if the highly stirred, cooled 2.5-liter vessel could be used to scale up the reaction.

Clearly the reaction is vigorous enough to create a significant thermal runaway under adiabatic conditions. Therefore, more careful measurement of heat production rates and the cooling capacity of the vessel is warranted.

Measurement of maximum heat generation rates. Figure 3 shows isothermal microcalorimetry heat generation curves for the three temperatures. Propellant sample masses were on the order of 0.75 grams. The ratio of acid to propellant was the same as that used in the ARC experiment and the process.

In these curves the initial rate is the maximum rate and the rate of heat evolution decreases monotonically thereafter. The reaction therefore follows ordinary n^{th} order kinetics and is nonautocatalytic.

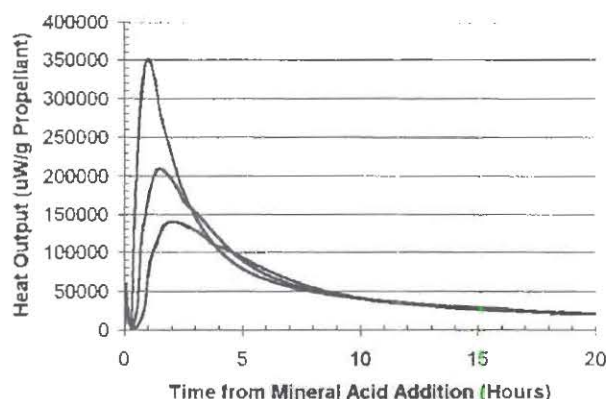


Figure 3. Isothermal Microcalorimetry of Mineral Acid + Propellant Reaction at (Bottom to Top) 25 °C, 29.4 °C, and 35 °C

A zero-order kinetic model, useful for prediction of maximum rates as a function of temperature, can easily be derived from these data. A standard rate expression can be written as follows

$$\frac{d\alpha}{dt} = Ae^{-E/RT}(1-\alpha)^n \quad (1)$$

where α is a fractional conversion, A is a frequency factor in min^{-1} , E is an activation energy in cal/mole , R is the gas constant ($1.987 \text{ cal/(mole K)}$), and T is absolute temperature. At low conversions ($\alpha \sim 0$, $t \sim 0$) this becomes

$$\frac{d\alpha}{dt} = Ae^{-E/RT} \quad (2)$$

Multiplying both sides by the total heat of reaction ΔH (cal/g propellant) yields an

expression for the initial heat generation rate \dot{Q} in $\text{cal/(g propellant min)}$:

$$\dot{Q} = A\Delta He^{-E/RT} \quad (3)$$

Taking logarithms of both sides yields

$$\ln \dot{Q} = \ln(A\Delta H) - \frac{E}{RT} \quad (4)$$

Therefore, a plot of the logarithm of initial (maximum) heat generation rate versus $1/T$ should yield the activation energy from the slope and the product of total heat of reaction and frequency factor from the intercept. The Arrhenius plot from the data in Figure 3 is shown in Figure 4 below.

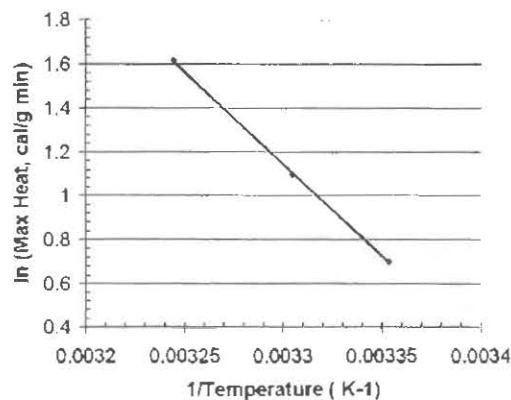


Figure 4. Arrhenius Plot for Mineral Acid + Propellant Reaction

The plot yields an activation energy of 16740.8 cal/mole and a frequency factor - heat of reaction product $A\Delta H$ of $3.736 \times 10^{12} \text{ cal/(g propellant min)}$. These values can be inserted into Equation (3) to predict maximum heat generation rates.

Kinetics can also be developed from ARC to predict maximum heat generation rates. These

will not be as accurate as those obtained with a heat flow calorimeter, owing to temperature gradients in the ARC bomb and lack of stirring, but still provide a "reality check" on the kinetics developed by the other method.

An energy balance on the ARC bomb under adiabatic conditions, at low conversions (zero-order) yields:

$$(m_b C_{pb} + m_p C_{pp} + m_a C_{pa}) \frac{dT}{dt} = Am_p \Delta H e^{-E/RT} \quad (5)$$

where m_b , m_p , and m_a are the masses of the bomb, propellant, and acid respectively, C_{pb} is the heat capacity of the bomb, C_{pp} is the propellant heat capacity, and C_{pa} is the heat capacity of the acid. For the case at hand, the sum $m_b C_{pb} + m_p C_{pp} + m_a C_{pa}$ is equal to 2.5 cal/(g °C). The experimentally measured self-heat rate is dT/dt .

Rearrangement of equation (5) and taking of logarithms yields

$$\ln\left(\frac{dT}{dt}\right) = \ln\left(\frac{(A\Delta H)m_p}{m_b C_{pb} + m_p C_{pp} + m_a C_{pa}}\right) - \frac{E}{RT} \quad (6)$$

Therefore, the parameters E and $A\Delta H$ can be extracted from the slope and intercept of a plot of $\ln(\text{self-heat rate})$ versus $1/T$ at low conversions. This plot is shown in Figure 5 (note that only the initial, low conversion part of the curve is used). An activation energy of 22606.2 cal/mole and a reaction energy-frequency factor product of 1.993×10^{16} cal/(g propellant min) were obtained. These can be inserted into Equation (3) to predict maximum heat release rates.

Experimental evaluation of reactor heat removal capacity. This was accomplished by filling the vessel with hot water, turning on the stirrer, opening the cooling water valve all the way, and measuring the water temperature as a function of time. The cooling curve is shown in Figure 6.

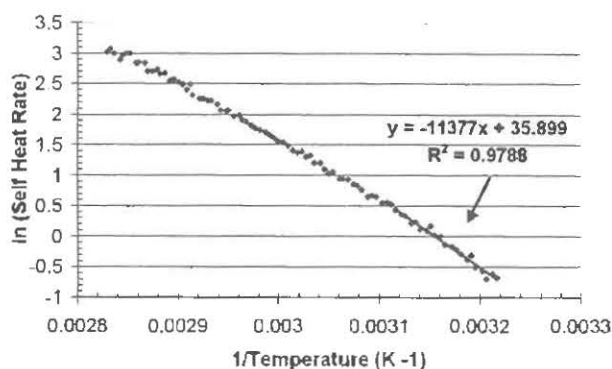


Figure 5. Determination of Zero-Order Kinetic Parameters from ARC Data on Propellant + Mineral Acid

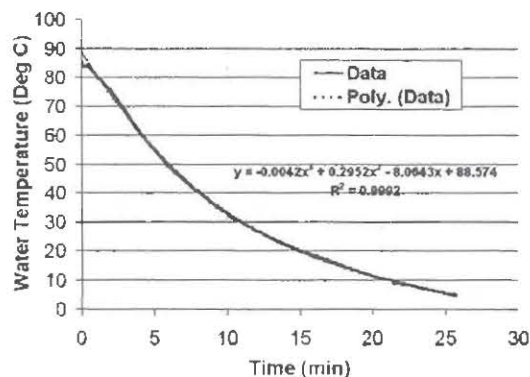


Figure 6. Cooling Curve for Stirred Reaction Vessel, Cooling Water Valve Wide Open

By fitting the cooling curve with a polynomial and then taking the first derivative, the heat removal rate as a function of reactor temperature could be quantified. The removal rate is given by an energy balance on the reactor:

$$q_{loss} = m_w C_{pw} \frac{dT}{dt} \quad (7)$$

where q_{loss} is the rate of heat loss from the reactor in cal/min, m_w is the mass of water in the reactor (1875 grams), C_{pw} is the heat capacity of water (1.0 cal/(g °C)), and dT/dt is the instantaneous rate of temperature change of the water, obtained from the first derivative of the curve fit in Figure 6.

Comparison of maximum cooling and heating rates. Figure 7 shows a comparison of the maximum heat production and removal rates for the reaction vessel, for a one-pound (453.6 grams) batch of propellant and the cooling valve wide open. The heating and cooling rates were obtained by use of Equations (3) and (7) respectively. The data show that, in the vicinity of 25 - 35 °C, the vessel heat removal capacity is several times the maximum heat generation capacity. Therefore, it should be possible to control the reaction with the cooling water valve, even if the propellant is added all at once. Maximum heat generation rates exceed the cooling capacity of the apparatus above the 50 - 60 °C range.

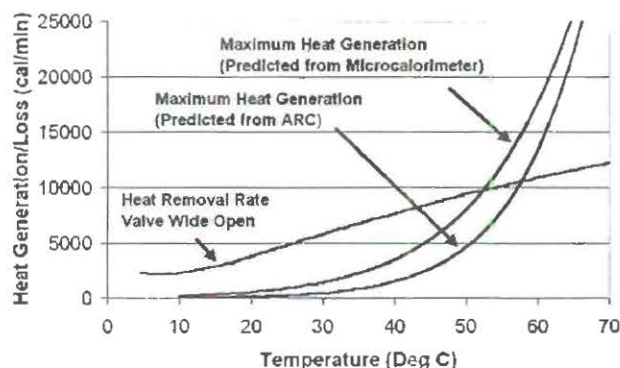


Figure 7. Comparison of Heat Generation and Removal Rates for 2.5 Liter Reactor

Characterization of the aluminum + mineral acid reaction. Finally, some measurement of heat evolution rates from mineral acid + aluminum powder was performed with the idea of using pure aluminum powder for initial reactor checkout instead of propellant. A plot of heat evolution for aluminum powder + mineral acid, plotted on the same coordinates as a propellant run with 0.75 grams of propellant, is presented in Figure 8. The same amount of aluminum as present in 0.75 grams of propellant was used. The quantity of acid was the same in both cases and representative of the process.

Two observations are readily apparent. First, most of the energy evolved from the propellant + mineral acid reaction is from decomposition of the aluminum powder in the propellant. Second, the heat evolution rate from aluminum + mineral

acid is similar to, and maybe a bit higher than, that of propellant + mineral acid. ARC tests on aluminum + mineral acid also support this conclusion. Therefore, we first used pure aluminum powder to verify that the reactor could handle propellant digestion.

Scaleup results. After checking the reactor out with aluminum powder, the propellant + mineral acid reaction was successfully scaled up to the one pound of propellant level in the 2.5 liter reactor. The propellant was not added all at once, but slowly over a period of a few hours. As predicted, the reaction was easily controllable with the process equipment in the 25 - 35 °C range. After the main reaction exotherm was over, the temperature was increased to bring the aluminum powder + mineral acid reaction to completion.

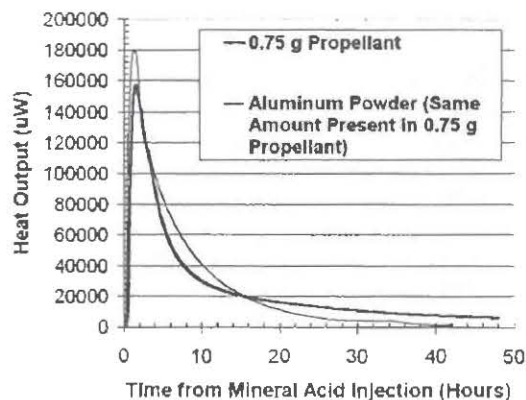


Figure 8. Comparison of Propellant + Mineral Acid and Aluminum Powder + Mineral Acid Heat Generation Rates at 29.4 °C

Obviously, scaling up a reaction scheme such as this to plant scale could be problematic. This is due to the presence of large amounts of unreacted propellant in the initial stages of the digestion.

If a process upset (loss of stirring with propellant settling to the bottom of the reactor, other failure of the cooling system, etc.) were to occur before the digestion was substantially complete, the ARC data indicate that a runaway reaction would probably occur. Therefore, it is preferable from a safety standpoint to operate at a temperature much higher than 25 °C, where the reaction is almost instantaneous, and feed the propellant in

at a rate no greater than the consumption rate. In that event, accumulation of energy in the reactor is avoided. If loss of cooling occurs, heat generation by chemical reaction can be stopped simply by turning off the propellant feed.

Synthesis of an Energetic Polymer

Here we planned to synthesize an energetic polymer in solvent. The reaction was to be carried out on the 2 - 3 kg scale. The reaction vessel in question was a 22 liter round bottom glass flask equipped with a reflux condenser. The flask was immersed in a water bath and was to be charged with several liters of reactants dissolved in the solvent.

The synthesis reaction initially evolves a significant amount of heat. In bench scale syntheses, this initial exotherm is allowed to occur and then progress of the reaction over several hours is followed by nuclear magnetic resonance (NMR) spectroscopy. When the reaction has progressed to the desired extent, reagents are added to the vessel to quench it, and the product polymer is extracted and dried. No external heating is applied to the reaction vessel.

With the larger scale process, it was desired to control the initial reaction exotherm by addition of small amounts of ice to the water bath and by solvent evaporation followed by return of solvent by the reflux condenser. If the reaction began to exotherm out of control, it was planned to pour a large quantity of ice into the water bath to quench the reaction. We were asked to determine if this emergency quenching could really stop the reaction. This reaction, with the ice bath cooling scheme, had previously been carried out many times on the 100 gram to 1 kg scale without incident.

Determination of energy potential. Figure 9 shows isothermal DSC thermograms of the polymerization reactants dissolved in solvent at 30, 40, and 50 °C. The curves show that an autocatalytic reaction mechanism is operative, i.e. in the initial stages the rate increases as reactants are depleted. If baselines are extended backwards from the tail ends of the curves, the total integrated reaction energies are 25 - 30 calories per gram of solution.

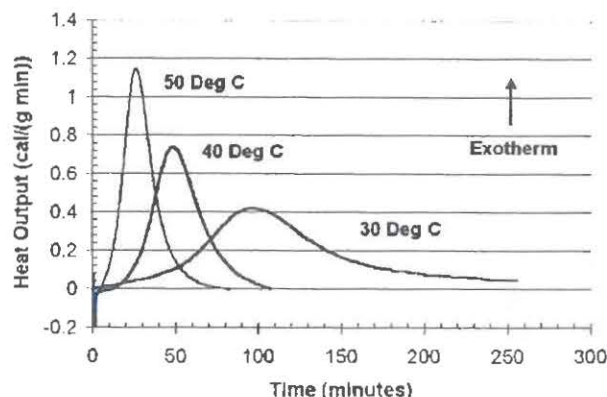


Figure 9. Isothermal DSC Curves for Energetic Polymer Synthesis in Solvent

Isothermal microcalorimetry measurements (not shown) at 25 °C, on approximately 0.3 gram samples, also showed an exothermic, autocatalytic reaction with reaction energy on the order of 30 cal/gram.

Using the heat capacity and latent heat of vaporization of the solvent, the measured heat of reaction is sufficient to raise the temperature of the system beyond the normal boiling point and then evaporate a significant quantity of the solvent. An ARC test, (6.2 grams, thermal inertia less than 1.5), detected no exothermic reactions (other than the one shown in the DSC tests) up to 80 °C, so there is no risk that a runaway reaction will trigger an exothermic decomposition of the polymer itself.

On thermodynamic grounds, there is a risk of reactor boil-over and consequently comparison of reactor cooling and heat production rates is required.

Comparison of heat rates and cooling capacity. The isothermal DSC results in Figure 9 can be used to estimate the maximum rates of heat production for the synthesis reaction. For a reaction that follows an arbitrary rate law the

heat generation rate \dot{Q} (calories per gram solution per minute) is given by

$$\dot{Q} = \Delta H \frac{d\alpha}{dt} = A \Delta H e^{-E/RT} f(\alpha) \quad (8)$$

where $f(\alpha)$ describes the effect of conversion on reaction rate and ΔH is the heat of reaction in calories per gram of solution. Taking logarithms of both sides for any fixed conversion α_f , we get

$$\ln \dot{Q} = \frac{-E}{RT} + \ln(A\Delta Hf(\alpha_f)) \quad (9)$$

If α_f is chosen as the peak conversion, a plot of the natural logarithm of the maximum ordinate of the DSC traces of Figure 9 versus reciprocal temperature should yield a straight line. This equation can be used directly to predict maximum heat generation rates. If desired, an activation energy can be calculated from the slope, and the frequency factor can be extracted from the intercept if an assumption is made about the form of $f(\alpha)$. This plot for the synthesis reaction is shown in Figure 10. The analysis yields an activation energy of 10072.7 cal/mole.

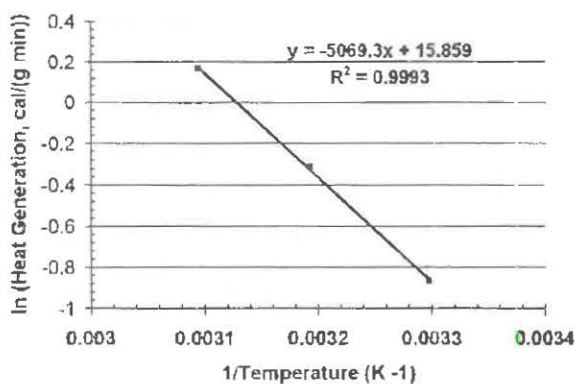


Figure 10. Plot of Maximum Heat Generation Rates from Isothermal DSC versus Reciprocal Temperature

The cooling capacity of the apparatus was established by filling the reactor with hot solvent, turning on the stirrer, and filling the water bath with ice water. The cooling curve is given in Figure 11.

From the cooling curve above one can calculate an overall heat transfer coefficient. An energy

balance on the solvent-filled reaction vessel yields

$$q_{loss} = m_s C_{ps} \frac{dT}{dt} = -U_o A_o (T - T_c) \quad (10)$$

where m_s is the mass of the solvent and C_{ps} is its heat capacity, U_o is the overall heat transfer coefficient based on outside surface area in cal/(cm² min °C), A_o is the (wetted) outside surface area of the reaction vessel. T is the reactor temperature in °C, and T_c is the cooling bath temperature (0 °C in this case). The quantity $A_o/m_s C_{ps}$ was approximately 0.48 cm² °C/cal.

Equation (10) can be integrated from an initial temperature T_i , setting the initial time to zero, to yield

$$\ln\left(\frac{T}{T_i}\right) = -\frac{U_o A_o}{m_s C_{ps}} t \quad (11)$$

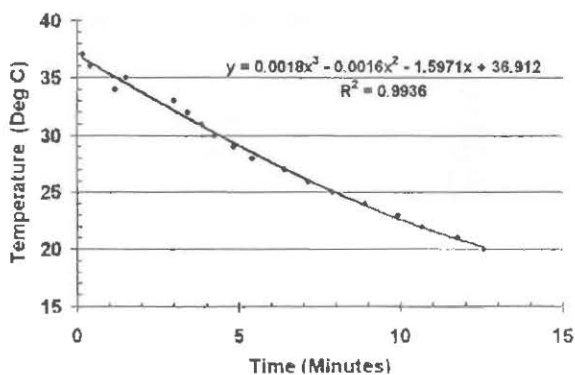


Figure 11. Cooling Curve for Stirred, Solvent-Filled Glass Reaction Vessel, Cooled by Ice Bath

This plot is shown in Figure 12. The heat transfer coefficient U_o can be calculated from the slope of the line. In so doing we obtained a value of 0.102 cal/(cm² min °C).

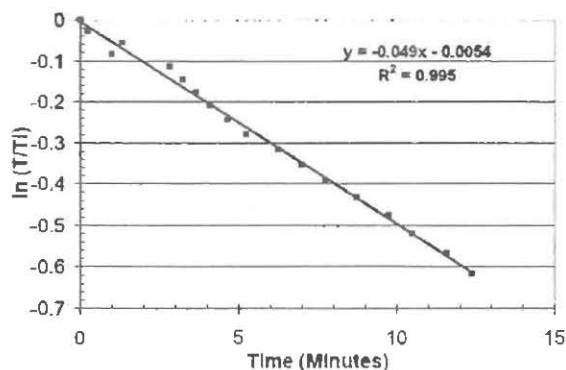


Figure 12. Determination of Overall Heat Transfer Coefficient

Now we can construct a comparison, similar to that shown in Figure 7, of the maximum heat production rate (from Equation 9) and the cooling rate (from Equation 11). This is displayed in Figure 13.

Here it is seen that the maximum heat generation rate begins to exceed the cooling capacity of the of the process equipment at about 30 °C. In contrast with the case of HMX recovery, the heat removal capacities of the apparatus are not comfortably above those of the maximum heat generation rates, especially in the vicinity of 30 °C. We therefore decided to model the reactor, using conservative assumptions, to provide more detailed information on the conditions that might lead to a thermal runaway.

Reactor model. To begin with, we need a kinetic model for the autocatalytic reaction that describes not only the rate maxima but also the dependence on conversion. A common rate law for autocatalytic reactions is

$$\frac{d\alpha}{dt} = k\alpha(1-\alpha) = Ae^{-E/RT}\alpha(1-\alpha) \quad (12)$$

where, as before, α is a fractional conversion (heat evolved up to time t divided by the total heat of reaction). The term k is a rate constant. With such a rate law some reaction product (given by an initial conversion α_o) must be initially present for the reaction to proceed.

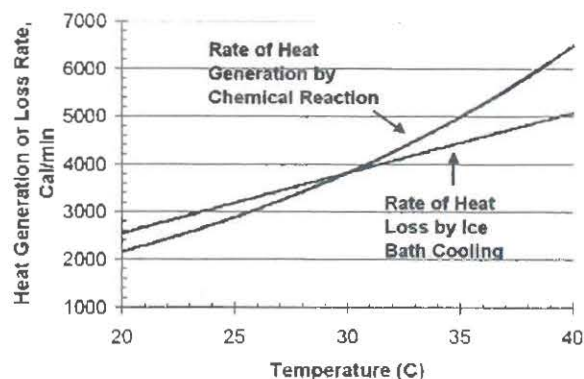


Figure 13. Comparison of Maximum Heat Generation Rate and Reactor Cooling Capacity

For isothermal conditions, Equation (12) has an analytical solution

$$\alpha = \frac{\alpha_o e^{kt}}{1 + \alpha_o(e^{kt} - 1)} \quad (13)$$

the first derivative of which is given by

$$\frac{d\alpha}{dt} = \frac{ke^{kt}\alpha_o(1-\alpha_o)}{[1 + \alpha_o(e^{kt} - 1)]^2} \quad (14)$$

which can be useful for plotting the predictions of an autocatalytic reaction model against the experimental DSC data. The heat production

rate \dot{Q} (cal/(g min)) is obtained by multiplication of $d\alpha/dt$ in Equation (12) or (14) by the total heat of reaction ΔH . Separation of variables and integration of Equation 12 yields the dependence of peak time in isothermal DSC on temperature:

$$\ln t_p = \frac{E}{RT} + \ln \left[\frac{\ln \left(\frac{\alpha_p(1-\alpha_o)}{\alpha_o(1-\alpha_p)} \right)}{A} \right] \quad (14)$$

A plot of $\ln t_p$ versus $1/T$ for the DSC data of Figure 9 should yield a straight line of slope $+E/R$. The frequency factor A can be obtained from the y-intercept if the initial and peak conversions are known. For this model the peak conversion α_p will be 0.5.

Such a plot is shown in Figure 14. The activation energy obtained from the slope is 13194.1 cal/mole. This value is more accurate than the one obtained from peak heights in Figure 10, as uncertainties in placement of the baselines in Figure 9 will have no effect on the peak times.

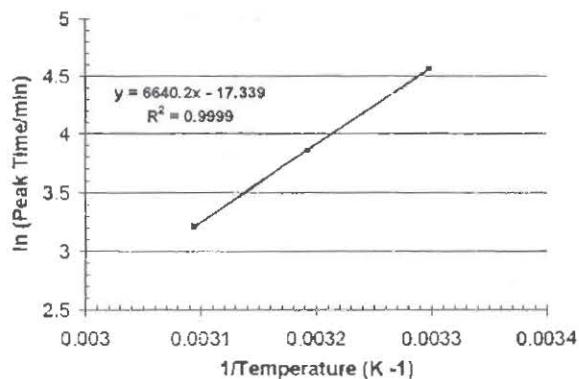


Figure 14. Arrhenius Plot of DSC Peak Times for Polymerization Reaction

To get a value of the frequency factor A for use in a model, various values of α_0 were assumed, used to calculate A from the y-intercept of Figure 14, and then Equation (14) was plotted against the 40 °C isothermal DSC thermogram of Figure 9. This was repeated until the peak width was matched.

Best-fit kinetic parameters obtained were $E=13194.1$ cal/mole, $A=2.05 \times 10^8 \text{ min}^{-1}$, and $\alpha_0 = 0.0025$. (The value of A was adjusted upward by about five percent to improve the quality of the peak time prediction.) The results of the curve fits (using different heat of reaction (ΔH) values, 27 cal/g, 25.7 cal/g, and 24 cal/g for the 30, 40, and 50 °C scans respectively) are shown in Figure 15.

As can be seen, the predictions of the model are

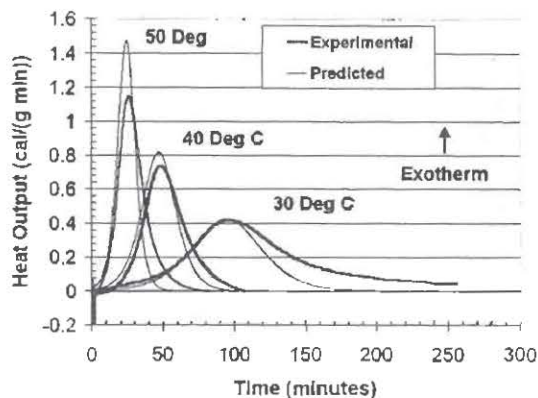


Figure 15. Predictions of Autocatalytic Reaction Model for Isothermal DSC

realistic. To be conservative, however, in all thermal runaway predictions to follow we will assume the heat of reaction ΔH to be 30 calories per gram.

The next step is to write conservation equations for the reactor itself. The progress of the autocatalytic reaction and the reactor temperature (for a well-stirred reactor) can be described by a system of two coupled ordinary differential equations

$$\frac{d\alpha}{dt} = Ae^{-E/RT}\alpha(1-\alpha) \quad (15)$$

$$m_s C_{ps} \frac{dT}{dt} = m_s \Delta H \frac{d\alpha}{dt} - U_o A_o (T - T_c) \quad (16)$$

with initial conditions $\alpha = \alpha_0$ and $T = T_0$ at $t = 0$. The second equation merely states that the rate accumulation of energy in the reactor (left side of the equation) is equal to the rate of heat generation by chemical reaction minus the rate of heat removal by the ice bath.

These equations do not take into account heat absorption by evaporation of solvent, omission of which will make the calculations conservative. Also, we have assumed that the mixture of solvent plus polymerization ingredients has the same heat capacity as pure solvent.

These equations were solved for several initial temperatures T_0 (ranging from 27 - 35 °C) and initial conversions α_0 using *Mathematica* commercial mathematics software. Some typical results are displayed in Figure 16 below.

Generally, for low conversions ($\alpha_0 \leq 0.1$) the calculations showed that addition of ice to the cooling bath will quench the reaction due to the low rate of heat evolution. As the conversion increases, the heat evolution rate goes up (as expected for an autocatalytic reaction) and thermal runaway behavior becomes increasingly possible. At an initial conversion of 0.15 (bottom frame of Figure 16) the initial temperature would have to be 34 °C to permit a reactor boil-over (vicinity of 40 °C). This would take about 30 minutes to occur.

An initial conversion of 0.3 (center frame of Figure 16) represents the worst case as far as initial temperature is concerned: if the ice quench starts after the reaction has progressed to this extent and the temperature is 31 °C, the model predicts boil-over in slightly less than 30 minutes.

As initial conversions approach and exceed 0.5 (where the rate maximum occurs in the autocatalytic reaction model) the initial temperatures required for thermal runaway become increasingly higher. This is illustrated in the top frame of Figure 16 for $\alpha_0 = 0.45$.

Here a temperature in excess of 32 °C is required for reactor boil-over, and the thermal runaway time is on the order of 20 minutes.

These calculations confirm the predictions of the maximum rate comparison of Figure 13 and indicate that, in order to prevent a reactor boil-over, the system temperature should not be allowed to approach 30 °C. Should this threshold be crossed with ice added to the bath, a reactor boil-over, if it occurred at all, would probably take at least 20 – 30 minutes. Again these predictions are likely to be conservative because the model does not take into account heat losses from solvent evaporation during an exotherm.

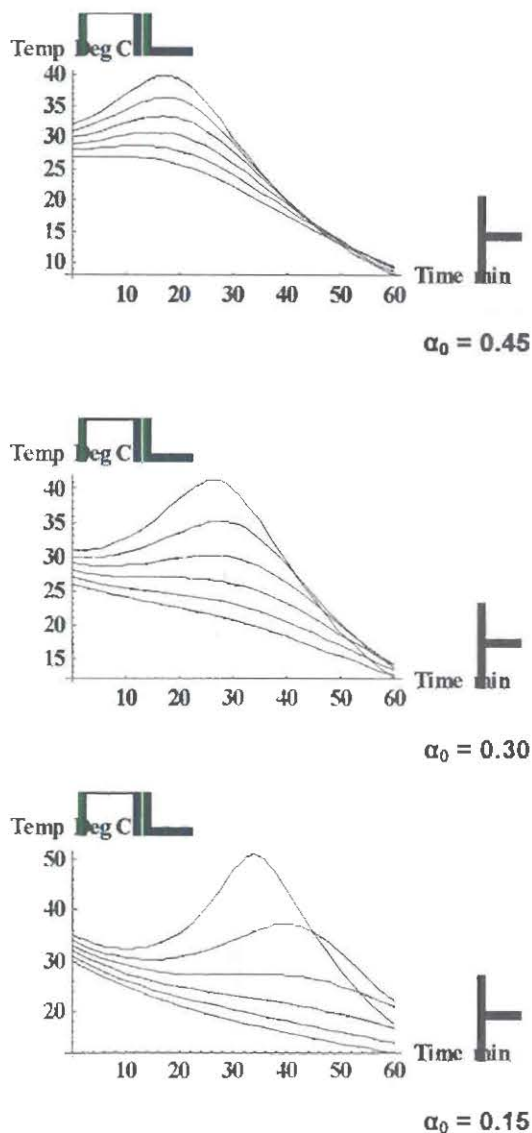


Figure 16. Predicted Temperature versus Time Curves for Reactor, Various Initial Temperatures and Conversions

Scale-up result. The polymerization reaction was carried out successfully, with a directive that the temperatures not be allowed to approach the temperature range (vicinity of 30 °C) for instability defined by the model.

Discussion

The results of this study concern the initial scale-up of chemical reactions involving energetic materials from the lab bench to the pilot scale, in temporary installations. What we have described here is a methodology for making a relatively quick determination as to whether the process equipment has the heat removal capacity to control the reaction in question.

With the HMX recovery process, we were able to demonstrate that, while the system had a sufficient energy potential to cause a violent boil-over of the reactor, the proposed process equipment could easily control it in the vicinity of 25 – 35 °C. The process that was evaluated is not suitable for scale-up beyond the pilot level due to the large amounts of accumulated reactant stored in the vessel during the initial stages of the reaction. It was, however, sufficient for showing, during the early stages of the effort, that mineral acid digestion was a viable method of recovering HMX from propellant.

The energetic polymer synthesis focused on determining the feasibility of preventing a thermal runaway by cooling the reactor with ice water. Here the difference between maximum heat generation rates and cooling capacities was not as great as in the case of the HMX recovery. A reactor simulation, including an autocatalytic reaction model, was used to help define safe operating conditions for the pilot scale process.

Obviously, in scaling up to a plant-sized reactor, a more detailed approach than the one described here needs to be taken. In those cases one should test and evaluate the consequences of a number of possible process upsets, including misformulation of the reaction mixture, loss of stirring, or failure of the reactor cooling system. The heat removal capacities for the reactor under normal and "upset" conditions should be well known, and vents should be sized to accommodate a reactor boil-over.

To accommodate more of this type of testing, ATK Thiokol Propulsion is now acquiring a reaction calorimeter, so heat production data can be routinely obtained during bench- and pilot-scale process development. This type of instrument overcomes the limitations of using a microcalorimeter as a reaction calorimeter (several days to change temperatures, recalibrate and baseline). Also, there can be a long lead

time for getting the analyses done on a microcalorimeter due to its use for other projects, such as long-term aging studies where samples are typically left in the calorimeter for a week or more. The acquisition of a reaction calorimeter should serve to make this type of testing more routine and reduce the risk of runaway reactions in our production facilities.

REFERENCES

- [1] D. I. Townsend and J. C. Tou, "Thermal Hazard Evaluation by an Accelerating Rate Calorimeter," *Thermochim. Acta* **37**, 1 - 30 (1980).
- [2] L. D. Smith, "Easily Test Thermal Stability and Detonability", *Chemical Engineering Progress*, September 1994, page 67.
- [3] R. Gygas, "Explicit and Implicit Use of Scale-Up Principles for the Assessment of Thermal Runaway Risks in Chemical Production," *Proceedings of the International Symposium on Runaway Reactions*, 1989, page 52.

THIS PAGE LEFT INTENTIONAL BLANK

Kinetics of the $\beta \rightarrow \delta$ Solid-Solid Phase Transition of HMX, Octahydro-1,3,5,7-tetranitro-1,3,5,7-tetrazocine

R.K. Weese, J.L. Maienschein and C.T. Perrino*

Lawrence Livermore National Laboratory, Livermore, California 94550

* Chemistry Department, California State University at Hayward, Hayward, CA 94542

We apply Differential Scanning Calorimetry, DSC, to measure the kinetics of the $\beta \rightarrow \delta$ solid-solid phase transition of Octahydro-1,3,5,7-tetranitro-1,3,5,7-tetrazocine, HMX. Integration of the DSC signal gives a direct measurement of degree of conversion. We apply 1st order kinetics, the Ozawa method, and isoconversional analysis to show that the phase transition is not a simple one-step reaction, but instead is a complex combination of steps. The range of activation energies found in this work, centering around 500 kJ/mol, is higher than previously reported values. We discuss possible reasons for the higher activation energies measured here.

INTRODUCTION

The chemical compound Octahydro-1,3,5,7-tetranitro-1,3,5,7-tetrazocine, HMX, is an high-performance nitramine energetic material. HMX exists in four solid phase polymorphs, labeled α , β , γ , δ -HMX,^{1, 2} each of which can reportedly be prepared by a specific cooling rate of a reaction solution.³ The β phase of HMX has the highest density and is stable at room temperature, and is the form in which HMX is normally produced and used. However, when heated to temperatures above 435K, the β -phase converts to δ -phase HMX.^{1, 4-7}

This conversion of the β phase (monoclinic lattice structure) to the δ phase (hexagonal lattice structure) involves a major disruption of the cohesive forces in the HMX crystal lattice and a ring conformation change from β (chair) to δ (chair-chair).^{8, 9} The electrostatic forces created within the HMX lattice produce a potential energy barrier to overcome in the transformation from the $\beta \rightarrow \delta$ phase.⁵ The energy to bring about the change from chair to chair-chair conformation has been reported by Brill⁹ as ring torsion and is essentially a normal mode of the molecule that requires about 4 kJ mol⁻¹. The magnitude of this transformation barrier is indicated by the activation energy of the phase conversion.

The β and δ phases of HMX have quite different behaviors. For example, the volume expansion associated with the $\beta \rightarrow \delta$ phase transition (the density is 1.90 g/cm^3 for β and 1.78 g/cm^3 for δ) produces profound perturbations to the mechanical and combustion characteristics of HMX.^{4, 5, 10, 11} The higher density material shows a higher rate of detonation and maintains greater stability towards shock. In sensitivity to mechanical impact as assessed by a standard dropweight impact test such as described by Dobratz,¹² δ -phase HMX is significantly more sensitive than β -phase HMX.^{1, 10} It is therefore desirable to know the kinetic information associated with this $\beta \rightarrow \delta$ solid phase transition. Data have been reported by Brill^{5, 13, 14} and by Henson^{15, 16} using FTIR and second harmonic generation, respectively, to monitor the transition extent. Here we investigate the kinetics of the $\beta \rightarrow \delta$ solid phase transition in HMX using Differential Scanning Calorimetry, DSC, and determine kinetic rate parameters and an effective activation energy.

EXPERIMENT

DSC measures the difference in the heat flow between a sample and an inert reference as a function of time and temperature. Both the sample and reference are subjected to a controlled environment of time, temperature, and pressure. A linear change of temperature with respect to time is the customary method of operation for DSC, with ramp rates up to $100\text{ }^\circ\text{C/min}$ possible. The instrument design used for making DSC measurements in this work is the heat flux design, TA Instruments Model 2920, shown in Figure 1.

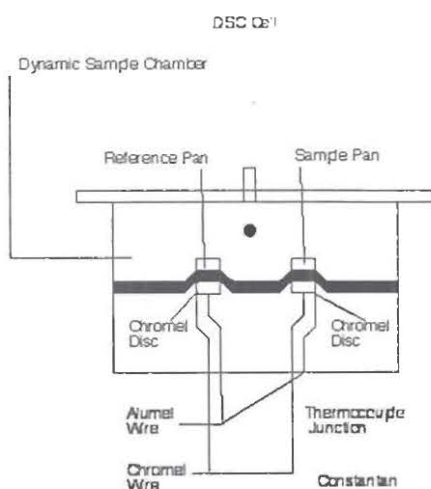


Figure 1: TA Instrument DSC Cell Model 2920¹⁷

In this design, a metallic alloy disk, made of constantan, is the primary means of heat transfer to and from the sample and reference.¹⁷ The sample is contained in a metal pan; it and the reference (an empty metal pan of the same composition as the sample pan) both sit on raised platforms formed in the constantan disc. As heat is transferred through the disc, the differential heat flow between the sample and reference is measured by area thermocouples formed by the junction of the constantan disc and chromel wafers, which cover the underside of the platforms. Chromel and alumel wires attach to the chromel wafers and form thermocouples, which directly measures the voltage difference between the sample and reference and converts to temperature.

The DSC was calibrated at each ramp rate for temperature and heat flow and to reduce baseline drift. Indium, lead, tin, and zinc were used for temperature calibration, and the indium heat of fusion was used for heat flow calibration. The instrumental error was $\leq 1.4^{\circ}\text{C}$ in temperature and $\leq 2.0\%$ in heat flow, typical for this type of measurement.

We recorded DSC data at heating rates of 1, 2, 5, and $10^{\circ}\text{C}/\text{m}$, with sample masses of about 1 mg. The thermal ramp was extended to a temperature sufficient to bring the phase conversion to completion, but was stopped below the temperature where the HMX would exothermically react. We made four runs at each heating rate. The lids of the DSC sample pans were perforated, to maintain the sample at atmospheric pressure. All data reported with exotherm up.

The HMX used in these experiments was recrystallized from standard-grade HMX, and was 99% pure as measured by HPLC. The average particle size was 160 micron with the central 80% being between 30 and 300 micron, and the sample masses ranged from 0.81 – 1.29 mg, with most around 1.1 mg.

RESULTS AND DISCUSSION

The $\beta \rightarrow \delta$ transition in HMX is endothermic, and is readily measured by DSC. Typical data are shown in Figures 2-5 for the different heating rates.

The data in Fig. 2-5 have significant fine structure superimposed on the main thermal event, particularly at the lower heating rates. We conjecture that this is due to uneven contact of the powdered sample with the sample pan, with resulting variations in thermal contact efficiency and therefore heat flow. This would be expected from the change in crystal morphology and density during the phase transition, with different particles undergoing transition at slightly

different times and thereby adding a random structure to the overall thermal signature. The presence of this fine structure does not preclude kinetic analysis of the data, however

The DSC data can be converted to fractional conversion by:

$$\alpha_t = \frac{\Delta H_t}{\Delta H_{\text{tot}}} \quad (2)$$

where: α_t is the reaction extent at time t

- H_t is the total heat of reaction at time t , calculated by integrating the DSC signal up to time t .
- H_{tot} is the total heat of reaction, calculated by integrating the DSC signal over the entire phase transition.

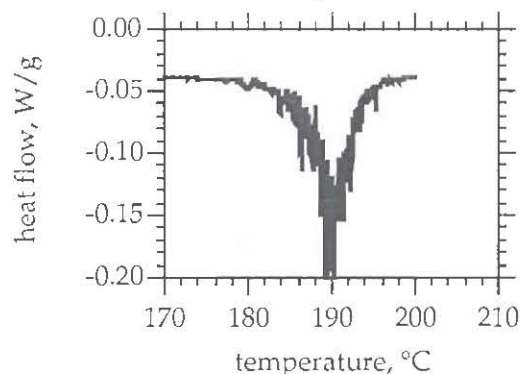


Figure 2. DSC data for 1°C/min.
heating rate, #99-896.01

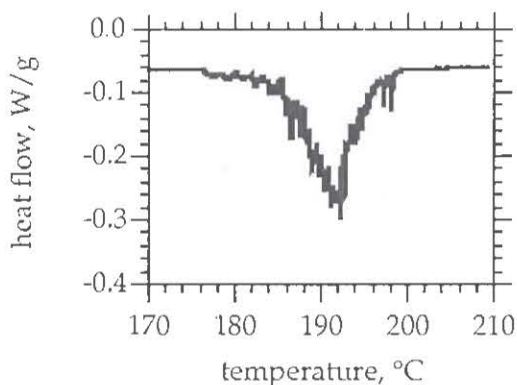


Figure 3. DSC data for 2°C/min.
heating rate, #99-890.01

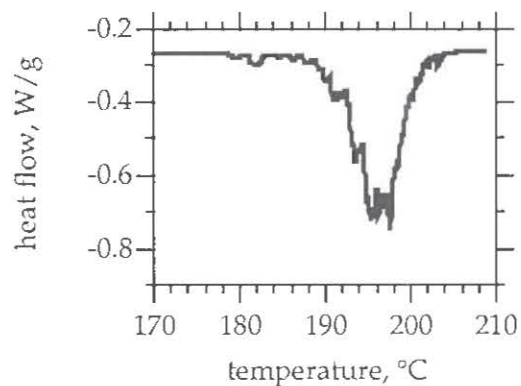


Figure 4. DSC data for 5°C/min.
heating rate, #99-878.01

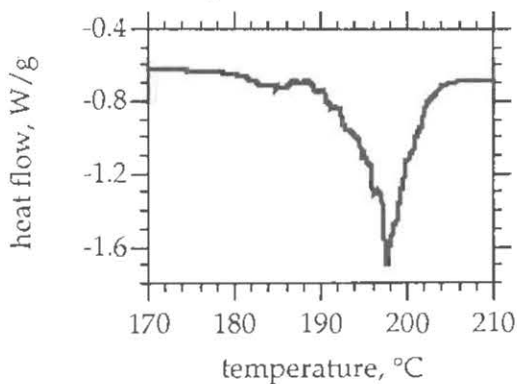


Figure 5. DSC data for 10°C/min.
heating rate, #99-872.01

The reaction rate can then be written as:

$$d\alpha/dt = \left(d(\Delta H_t)/dt \right) \times \left(1/\Delta H_{tot} \right) = dQ/dt \times \left(1/\Delta H_{tot} \right) \quad (3)$$

where: dQ/dt is the heat flow given by the DSC signal.

Calculation of Arrhenius parameters – 1st order assumption

The reaction rate may also be written, for a simple reaction with Arrhenius kinetics, as:

$$d\alpha/dt = k(1-\alpha)^n = Ae^{-E_a/RT}(1-\alpha)^n \quad (4)$$

where: k = reaction rate constant, s^{-1}

A is the Arrhenius pre-exponential, s^{-1}

E_a is the activation energy, kJ/mol

n is the reaction order.

Combining Eqs.(3) and (4), we can calculate the rate constant as a function of temperature for a given DSC run by:

$$k = dQ/dt \times \left(1/\Delta H_{tot} \right) \times (1-\alpha)^{-n} \quad (5)$$

We analyzed each DSC run in the following way. First, we integrated the total phase transition signal to determine the total heat of reaction. Then, the reaction extent as a function of time was calculated using Eq.(2). Finally, the reaction rate constant was calculated as a function of time for reaction extents from 20-80% using Eq.(5), assuming first order kinetics. A representative plot of the rate constant as a function of time for one run is shown in Figure 6. For each run, we calculated an average rate constant for reaction extent from 20 to 80%, and using these values we calculated a mean value were calculated for each thermal ramp rate. These mean values are shown in Table 1, and plotted in Figure 7. The resulting activation energy is 433 ± 13 kJ/mol , and the pre-exponential term is $2 \times 10^{18} s^{-1}$.

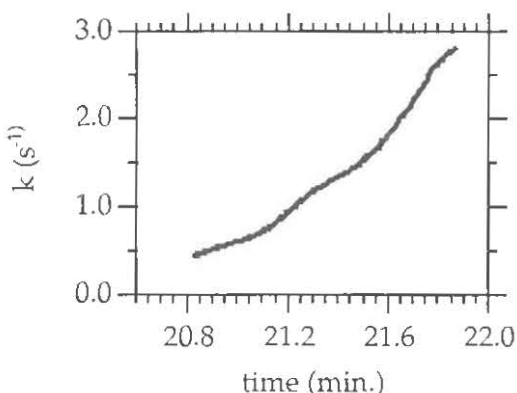


Figure 6. Rate constant calculated from Eq.(5) for run 878.01 at 5°C/min.

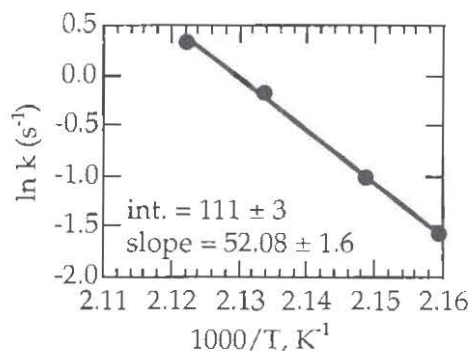


Figure 7. Arrhenius plot of kinetic data from Table 1. Activation energy is 433 kJ/mol, and the pre-exponential term is $2 \times 10^{13} \text{ s}^{-1}$.

From Fig.(6), we see that the rate constant during a DSC run is not actually constant. This could be due to a couple of effects. First, the temperature is not constant during the course of the run, so the rate constant would be expected to change. The data in Fig.(6) span about 1 minute or 5 K. Applying the activation energy of 433 kJ/mol to the minimum and maximum temperatures represented in Fig.(6), 466.2 – 471.2 K, we calculate that the rate constant should vary by a factor of 3.3. This is a significant portion of the overall variation of a factor of 6.5, but does not account for all of the variation. Second, a changing rate constant may indicate that the reaction is not as simple as assumed. We assumed a single first order reaction mechanism in this analysis; zero and second order kinetics also yielded a varying rate constant. It is also possible that the reaction has multiple steps or competing processes, in which case this analysis would not give an invariant rate constant. Our method of using the rate constant at the peak of the endotherm is therefore an approximation, and our kinetic constants calculated in this manner must therefore be considered estimates.

Table 1. Mean rate constants and temperatures for each thermal ramp rate, assuming first order kinetics. Values represent averages of four runs at each ramp rate.

Ramp rate, °C/min	k (s ⁻¹)	T (K)
1	0.208	463.1
2	0.363	465.4
5	0.843	468.7

Calculation of Arrhenius parameters – Ozawa method

An alternate method of calculating kinetic parameters is the method of Ozawa, wherein the thermal ramp rate as a function of the peak temperature is used for conventional Arrhenius analysis.^{18, 25} This gives directly an estimate of the activation energy. The ramp rate and peak temperature data in Table 1 are shown in Arrhenius form in Figure 8. The activation energy, 510 kJ/mol, is significantly higher than that calculated above from the actual reaction rate data.

Calculation of Arrhenius parameters – isoconversional analysis

The above methods for calculating activation energy assume an unchanging reaction mechanism with 1st order reaction. Similar analyses can be made with different reaction orders which lead to different kinetic parameters; it is often difficult if not impossible to determine which is the appropriate reaction order from this type of analysis.¹⁹ Furthermore, if the reaction mechanism changes during the course of the reaction, the above methods can only give a global average that may not truly represent any of the actual mechanistic steps.

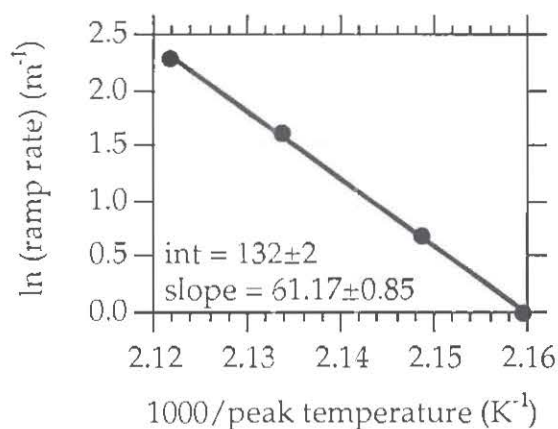


Figure 8. Ramp rate and peak temperature data from Table 1, with a linear fit for calculating activation energy.

Isoconversional analysis is an alternate method of kinetic analysis that avoids these problems.¹⁹⁻²² In isoconversional analysis, data from several different ramp rates are required. For each ramp rate, the reaction rate and temperature is determined for different extents of reaction; then the Arrhenius parameters are calculated from the set of temperature-rate data at each reaction extent assuming

zero-order kinetics (i.e. $n=0$ in Eq.(4)). Changes in the activation energy with reaction extent indicate changes in reaction mechanisms. The pre-exponential parameter lumps together all reaction-order effects, and so its behavior also may give insight into the actual mechanisms. There is no assumption of reaction order inherent in isoconversional analysis, so the activation energies should be representative of the actual reactions taking place.

Steps in the isoconversional analysis were: 1) calculate the reaction extent from integration of the DSC data, using evenly-spaced temperature data over the same temperature range for each run at given ramp rate; 2) interpolate the temperature / reaction extent data sets to give temperature / reaction extent data at evenly spaced reaction extent values ranging from 0.01 to 0.99; 3) calculate the reaction rate for each reaction extent value from the temperature / reaction extent / ramp rate data; 4) for each reaction extent, use rate/temperature data from the four ramp rates to calculate Arrhenius parameters as a function of reaction extent. Typical results at reaction extents of 0.2 and 0.8 are shown in Figure 9, and the resulting Arrhenius activation energy and pre-exponential values are shown in Figure 10 for reaction extents from 0.05 – 0.95.

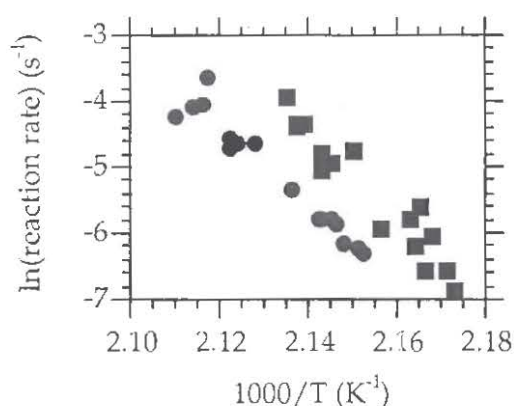


Figure 9. Reaction rates as a function of temperature at reaction extents of 0.2 (square) and 0.8 (circle).

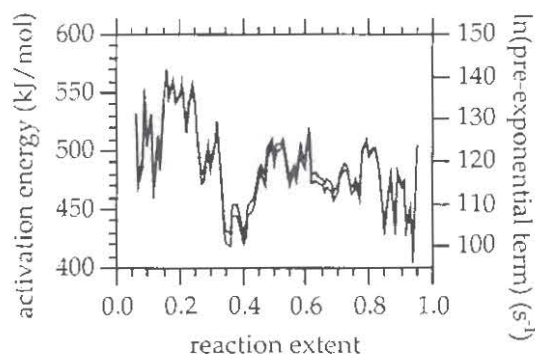


Figure 10. Isoconversional activation energies and pre-exponential values for reaction extents of 0.05 to 0.95.

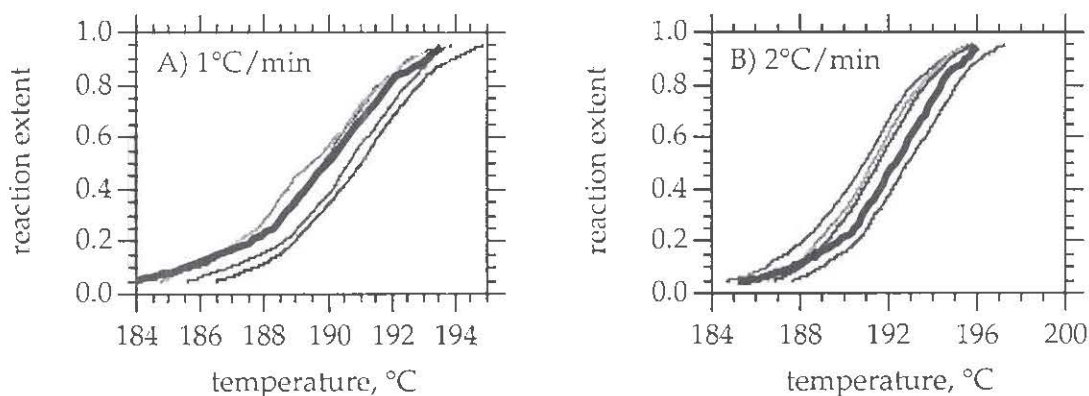
As we see from Figure 10, there is considerable structure in the Arrhenius parameters as the reaction proceeds, with the activation energy and pre-exponential tracking each other very closely. We can capture most of the features by considering seven regions as defined by reaction extent, and determining an activation energy and pre-exponential value for each region. These values, shown in Table 2 below, were determined from the data in Figure 10, with minor

adjustments made as described below in checking the fit of the conversion data to this set of parameters.

Table 2. Arrhenius parameters for the HMX $\beta \rightarrow \delta$ phase transition calculated using isoconversional analysis.

Reaction extent	< 0.15	≤ 0.25	≤ 0.33	≤ 0.47	$\leq .63$	$\leq .81$	≤ 1.0
E_A , kJ/mol	481.5	537.5	491.0	465.0	493.0	471.0	479.0
$\ln(A)$	119.0	133.5	122.0	115.0	122.0	116.0	117.0

As a check of the validity of the values in Table 2, we used these parameters to calculate the reaction extent as a function of temperature for the four experimental ramp rates, and then compared the calculated values with the experimental data. This is shown in Figure 11. The agreement is excellent, with the calculated reaction extent fitting well within the envelope of experimental results for each ramp rate. We note that, to achieve the degree of agreement shown in Figure 11, some of the Arrhenius parameters derived from Figure 10 were adjusted to the nearest 0.5 kJ/mol or sec^{-1} . The adjustments were small in all cases, and the adjusted parameters are still consistent with the data shown in Figure 10.



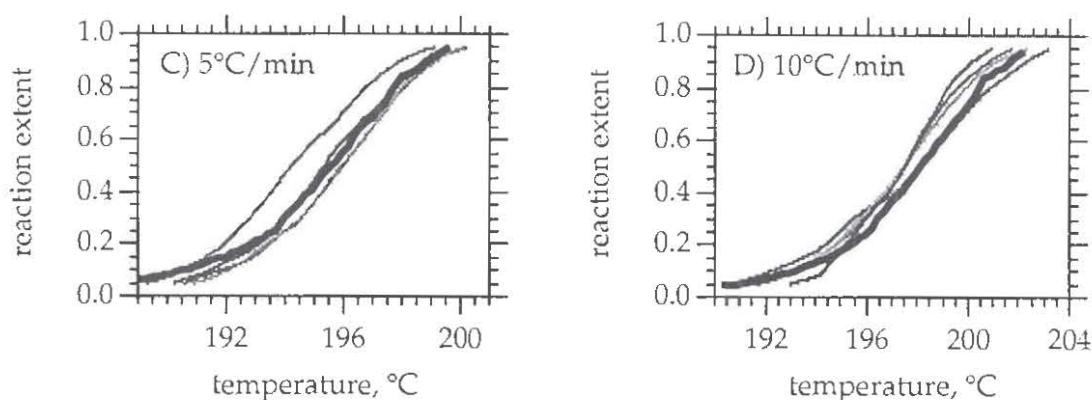


Figure 11. Reaction extent of phase transition. Measured – solid lines. Calculated from Arrhenius parameters in Table 2, thick dotted line. Each plot is for the thermal ramp rate shown on the plot.

From isoconversional analysis results, we conclude that the phase transition kinetics cannot be described by one simple n^{th} order reaction. The range of activation energies at different reaction extents indicates that a more complex set of reactions is taking place. From the data available, we cannot determine a mechanistic scheme, but can deduce that the scheme is not a simple one.

The activation energies for the different steps in the reaction are quite high – 465–538 kJ/mol. These values are consistent with those from our simpler analyses presented earlier – 433 kJ/mol for the 1st order assumption and 510 kJ/mol using the Ozawa method, showing the general validity of the three methods of analysis.

Comparison with literature

With pure HMX and using FTIR spectroscopy to monitor the $\beta \rightarrow \delta$ phase transition, Brill *et al* observed first-order kinetics and determined an activation energy of 204 kJ/mol.²³ Henson *et al* studies HMX mixed with estane and nitroplasticizers (PBX-9501), using second harmonic generation of reflected light to measure the reaction extent.^{15, 16, 24} He built a model for the transition based on a nucleation and growth mechanism with a first order nucleation step and a second order growth step; activation energies were on the order of 200 kJ/mol for each step.

Our results show a complex mechanism, which is consistent with Henson's observation that a multi-step reaction mechanism is required to accurately reproduce the experimental results. The range of activation energies that we find,

around 500 kJ/mol, are significantly higher than those found by Brill and by Henson. The reasons for this are not fully understood. One difference is the measurement method. Our measurements are the first reported using thermal data to monitor the progress of reaction in bulk HMX samples. DSC measures the reaction progress *in situ* integrated across the entire sample, in contrast to the other techniques. The second harmonic generation method observing reflected light used by Henson monitors the surface of the sample; if the surface and bulk kinetics differ, then a difference in results would be expected. The FTIR method used by Brill samples only the sample area interrogated by the FTIR beam, and requires a very thin sample to transmit the IR signal, essentially a surface sampling technique.

A second possible reason for the difference in activation energies is the composition of the samples. Henson's studies used PBX-9501, a mixture of HMX with estane and nitroplasticizers. Brill's work, while done with pure HMX, required the use of a silicone oil for heat transfer. Our experiments used pure HMX with no binder and no additives. It is plausible that the presence of such additives would alter the kinetics of the phase conversion, and we have work underway to study that hypothesis.

CONCLUSIONS

We have monitored the reaction progress of the HMX $\beta \rightarrow \delta$ phase transition using differential scanning calorimetry and pure HMX, and analyzed the results using three methods – assuming 1st order kinetics, the Ozawa method, and isoconversional analysis. Isoconversional analysis shows that the reaction mechanism is not a simple one-step reaction, but instead involves multiple reaction steps; analyses using simple reaction mechanisms must necessarily be approximations that may of limited validity. There are many factors that contribute to an overall reaction mechanism, and our measurements do not define these factors and their relevance, but instead show that such factors are important.

The activation energies with different analytical methods are all around 500 kJ/mol, significantly higher than reported in the literature. As discussed above, this may be the result of other work using experimental methods that monitor surface instead of bulk behaviors, and may also relate to the chemical additives present in many of the samples

ACKNOWLEDGEMENTS

This work was performed under the auspices of the U.S. Department of Energy by the University of California Lawrence Livermore National Laboratory under contract No. W-7405-Eng-48.

REFERENCES

1. H.H. Cady, "Studies on the Polymorphs of HMX", Los Alamos Scientific Laboratory, LAMS-2652 (October 18, 1961).
2. R.E. Cobblestick and R.W.H. Small, "The Crystal Structure of the d-form of 1, 3, 5, 6 - Tetranitro-1, 3, 5, 7-tetraazacyclooctane (d-HMX)", *Acta Cryst.*, **B30**, 1918 (1974).
3. W.C. McCrone, "Crystallographic Data: Cyclotetramethylene Tetranitramine (HMX)", *Analytical Chem.*, **22**, 1225 (1950).
4. M. Herrmann, W. Engel and N. Eisenreich, "Phase Transitions of HMX and their Significance for the Sensitivity of Explosives", in *Proceedings of the Technical Meeting of Specialists MWDDEA AF-71-F/G-7304 - Physics of Explosives*, p. 12 (1990).
5. R.J. Karpowicz and T.B. Brill, "The bæd Transformation of HMX: Its Thermal Analysis and Relationship to Propellants", *AIAA Journal*, **20**, 1586 (1982).
6. A.S. Teetsov and W.C. McCrone, "The Microscopical Study of Polymorph Stability Diagrams", *Microscop. Cryst. Front.*, **15**, 13 (1965).
7. M. Herrmann, W. Engel and N. Eisenreich, "Thermal analysis of the phases of HMX using X-ray diffraction", *Zeitschrift für Kristallographie*, **204**, 121 (1993).
8. T.B. Brill and R.J. Karpowicz, "Solid phase transition kinetics: the role of intermolecular forces in the condensed phase decomposition of octahydro-1,3,5,7-tetranitro-1,3,5,7-tetrazocine", *J. Phys. Chem.*, **86**, 4260 (1982).
9. T.B. Brill and C.O. Reese, "Analysis of intermolecular interactions relating in the thermophysical behavior of alpha, beta, and delta octahydro-1,3,5,7-tetranitro-1,3,5,7-tetrazocine", *J. Phys. Chem.*, **84**, (1980).
10. M. Herrmann, W. Engel and N. Eisenreich, "Thermal Expansion, Transitions, Sensitivities and Burning Rates of HMX", *Propellants, Explosives, Pyrotechnics*, **17**, 190 (1992).
11. J.L. Maienschein and J.B. Chandler, "Burn Rates of Pristine and Degraded Explosives at Elevated Pressures and Temperatures", in *Proceedings of 11th*

International Detonation Symposium, Snowmass, CO, Office of Naval Research, (1998).

12. B.M. Dobratz and P.C. Crawford, "LLNL Explosives Handbook: Properties of Chemical Explosives and Explosive Simulants", Lawrence Livermore National Laboratory, UCRL-52997 change 2 (January 31, 1985).

13. F. Goetz and T.B. Brill, "Laser Raman Spectra of α -, β -, γ -, and δ -Octahydro-1,3,5,7-tetranitro-1,3,5,7-tetrazocine and Their Temperature Dependence", *J. Phys. Chem.*, **83**, 340 (1979).

14. A.G. Landers and T.B. Brill, "Pressure-Temperature Dependence of the β - δ Polymorph Interconversion in Octahydro-1,3,5,7-tetranitro-1,3,5,7-tetrazocine", *J. Phys. Chem.*, **84**, 3573 (1980).

15. B. Henson, L. Smilowitz, B. Asay and P. Dickson, "Thermodynamics of the β to δ phase transition in PBX-9501", in *Proceedings of American Physical Society Topical Group on Shock Compression of Condensed Matter*, Atlanta, GA, American Institute of Physics, (2001).

16. L. Smilowitz, B. Henson, J. Robinson, P. Dickson and B. Asay, "Kinetics of the β to δ phase transition in PBX-9501", in *Proceedings of American Physical Society Topical Group on Shock Compression of Condensed Matter*, Atlanta, GA, American Institute of Physics, (2001).

17. TA Instruments, instrument manual.

18. T. Ozawa, "Kinetic analysis of derivative curves in thermal analysis", *J. Thermal Analysis*, **2**, 301 (1970).

19. S. Vyazovkin and C.A. Wight, "Isothermal and non-isothermal kinetics of thermally stimulated reactions of solids", *Int. Rev. in Phys. Chem.*, **17**, 407 (1998).

20. S. Vyazovkin and C.A. Wight, "Estimating realistic confidence intervals for the activation energy determined from thermoanalytical measurements", *Anal. Chem.*, **72**, 3171 (2000).

21. J.H. Flynn, "The isoconversional method for determination of energy of activation at constant heating rates. Corrections for the Doyle approximation", *J. Thermal Analysis*, **27**, 95 (1983).

22. H.L. Friedman, "Kinetics of thermal degradation of char-forming plastics from thermogravimetry. Application to a phenolic plastic", *J. Polymer Science C*, **6**, 183 (1963).
23. R.J. Karpowicz, L.S. Gelfand and T.B. Brill, "Application of Solid-Phase Transition Kinetics to the Properties of HMX", *AIAA Journal*, (1982).
24. P.M. Dickson, B.W. Asay, B.F. Henson, C.S. Fugard and J. Wong, "Measurement of phase change and thermal decomposition kinetics during cookoff of PBX-9501", in *Proceedings of American Physical Society Topical Group on Shock Compression of Condensed Matter*, Snowbird, UT, American Institute of Physics, (1999).
25. V.A. Bershtein, V.M. Ergorov, *Differential Scanning Calorimetry of Polymers*, Ellis Horwood, Ltd, Chichester (1994)

THIS PAGE LEFT INTENTIONAL BLANK

MICROCALORIMETRIC METHOD TO DETERMINE THE CORROSION RATE OF LIQUID PROPELLANT AND METAL CONTAINER

Harry A. Farmer, Daniel S. Ellison, Anton Chin, and Daniel R. Crowley
Test & Evaluation Department
Ordnance Engineering Directorate
Crane Division, Naval Surface Warfare Center
Crane, Indiana 47522-5001 USA

ABSTRACT

Corrosive liquid propellants such as red fuming nitric acid and hydrazines are often used in the missile propulsion system. During storage at various environmental stimuli, some types of the metal containers may corrode to a point that accidents can occur. In order to accurately test the rate of corrosion, a special metal container was designed and developed to fit the detector of the TAM model 2277 microcalorimeter. The ampoule, made by machining the same alloy metal used for the actual container (17-7 PH stainless steel), was used to determine the compatibility, corrosion rate and safe storage life of metal containers containing liquid propellant IRFNA (Inhibited Red Fuming Nitric Acid).

The compatibility and corrosion rate between the metal and IRFNA were evaluated between 25, 30, 35, 40, 45 and 50EC. The corrosion rate as a function of these temperatures were determined. The safe storage life of the metal container was determined by pressure burst test at 20,000 psi.

In this paper, we will report the modification of the design of the test apparatus and methods used to determine the corrosion rate and the safe storage life of the container will be presented.

I. INTRODUCTION AND BACKGROUND

Liquid propulsion system containing IRFNA (Inhibited Red Fuming Nitric Acid) and MAF-4 (Hydrazine Derivatives) are widely used in the training missiles. Due to the corrosive nature of these ingredients, this system may possess high potential explosion hazard. A spontaneous explosion of one of the IRFNA container was reported during storage in a tropical country in Southeast Asia. Preliminary results from failure analysis indicated that the major cause for the explosion was probably due to the over-pressure from the IRFNA tank. In order to accurately simulate the accident at laboratory scale, a special sample cell was designed to fit the detector of TAM Model 2277 Microcalorimeter. The complete sample cell assembly, including inner cell for holding the sample and outer cell for protecting the microcalorimeter detector in case the inner cell cracks, was made at NSWC, Crane [1]. Machining the same alloy metal used for the actual container (17-7 PH) made both inner and outer cells. The detailed design and methods of testing were reported in the Proceeding of the 1st International Workshop on the Microcalorimetry of Energetic Materials, 1987 [2]. The objective of this project is to determine if the shelf life of

the training missile could be extended to a minimum five years or more at normal storage conditions by determining the compatibility and corrosion rate between the liquid fuel/oxidizer and the PH 17-7 alloy container. A three-way real time temperature, pressure, and degradation rate correlation table will be established to predict the shelf life of the fuel/oxidizer container system at various storage temperatures. The need for an extension of shelf life is due to the two year shelf life restriction that is presently in effect for the training missile due to the early incident. A scientific method was required to extend the shelf life and meet the realistic production or operational requirements of the program.

II. EXPERIMENTAL

1. Sample Identification.

a. Twelve test cell ampoules made from PH 17-7 stainless steel, four from each of the three groups of heat treated and welded test cell ampoules were subjected to a visual inspection, heat flow calorimetry, SEM tests, optical metallography, stress analysis and hydro burst tests. All samples used in the shelf life study are identified below.

b. The manufacturer supplied four plates from standard PH 17-7 stainless steel.

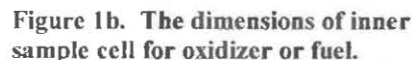
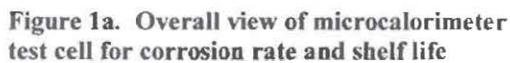
c. A 500ml sample of IRFNA (inhibited red fuming nitric acid) oxidizer in an inert container was provided by the contractor.

d. A premixed 500ml sample of MAF-4 fuel containing 60% 1, 1-dimethylhydrazine, and 40% diethylenetriamine in an inert container was provided by the manufacturer.

2. Evaluation Process.

In this evaluation four plates approximately 1" x 1" x .063" of sheet metal from standard PH 17-7 tank material were provided by the manufacturer. The first two plates were from plain tank metal, which were used as models to calibrate the surface condition of the test cells made at NSWC Crane. The other two plates were two separate pieces of 1" x 0.5" x .063" tank metal welded together by an electron beam and were used in the controlled experiments. Before shipment to NSWC Crane all 4 metal plates were heat-treated using the same process as the full size storage tanks.

All of the test cell ampoules used for this evaluation were machined at NSWC Crane from the same alloy metal block PH 17-7 stainless steel from Allegheny Ludlum) to the dimensions as illustrated in Figures 1a - 1c. The proportion of dimensions of the small-scale sample cell was made as close as possible to that of the actual storage tanks. After completion, the test cell ampoules were sent to the manufacturer for heat treatment and electron beam welding according to manufacturer's specification.



Samples of both the Fuel and Oxidizer were evaluated. Test cell ampoules were filled with both the IRFNA and MAF-4 samples to a point that the volume of ullage to sample ratio is proportional to the storage tanks. In addition some test cell samples were overfilled above the ullage level.

A. Microcalorimetry - Thermometric (TAM Model 2277). Isothermal microcalorimeter was used for the analysis. Measuring the heat flow of an energetic system (i.e. metal + acid) at different temperatures will establish the database for tabulating the accelerating factors. Accelerating factor is defined as the ratio of rate of reaction (k_2/K_1) or degradation (corrosion, etc.) at any two different temperatures (T_2 and T_1). The accelerating factor by far is the most important single number for providing guidelines for an accurate and successful accelerating aging test. To conduct the accelerated aging test at the highest temperature, without compromising safety and/or changing the course of degradation mechanism, microcalorimetry is the best method to achieve the longest aging equivalent within the shortest possible time. Initial tests were conducted at 25, 30, 35, 40, 45 and 50EC. Different temperatures may be used depending upon the initial results. In general, the basic kinetic approach to determine the shelf life of the corrosion process follows the guidelines (a) Define the end of induction time. (b) Establish critical properties at zero aging time. This requires historical information and database analysis. (c) Obtain heat flow (μW) as function of temperature. (d) Identify limiting reactions (Reagents) which control the major aging and degradation processes (rate determining step). (e) Develop a quantitative model for properties as a function of time. (f) Determine orders of reaction and rate constants for property changes. (g) Fit rate constants to the Arrhenius Equation and determine the activation energy and accelerating

factors of the corrosion process in a temperature interval between the natural storage and test temperatures. (h) Define critical property value (end of service life) of the item under test by calculating the maximum acceptable heat flow for the prevailing storage conditions (temperature, material quantity, etc.), using standard models for thermal runaway reactions. (i) Time to reach critical property value at various temperatures (Service life or shelf life) will then be determined.

B. Scanning Electron Microscopy (SEM) Test: An Amray Model 3200S, ECO SEM was used to perform this test. The SEM provides qualitative information on the corrosion by-product during the testing. The morphology information provided by the SEM will allow insight into the growth rate and method of corrosion.

C. Leco Neophot Optical Metallograph (LNOM): The LNOM test was performed on a cross-sectioned sample of the corroded material. The sample was polished and etched in accordance with ASTM procedures. The depth of pitting and corrosion mode, intergranular or transgranular, can show the potential failure mode of the material due to corrosion.

D. Stress Analysis-Hydro-burst Test: A stress analysis and hydro-burst test was performed on the test cells ampoules after exposure to aging. When two pressure cylinders of different size are subjected to the same internal pressure, the distribution of radial and tangential stress to the vessel wall is a function of the ratio of radius to wall thickness. In order to compensate for the differences, high pressures have to be applied to the smaller cell. A computer stress study was conducted to compensate for the difference before the actual hydro-burst test took place. Since the data from the hydro-burst test of the smaller container has to be compensated for by using higher pressure (>20,000 psia), therefore a higher deviation is expected.

E. Three-way Correlation Diagram of Corrosion rate, Temperature and Pressure Charts:

Table (1) is by far the most important information for the responsible safety officer (RSO) to overview the entire relationship of degradation rate as a function of temperature and pressure over a known period of time. In a normal or emergency situation, the RSO will be able to know the exact safety condition of the tank and make a quick judgement.

F. Aging Trend and Shelf Life: Based on the information from these tests the shelf life within the test temperature range (i.e. 25, 30, 35, 40 and 45EC) can be determined. Shelf life beyond this region has to be extrapolated by an Arrhenius Plot (Ln rate vs. reciprocal of test temperatures). The training missile APMML and RSO will determine the final safety margin of extension for shelf life.

There are some limitations involved and some questions may arise about the microcalorimetric data being truly representative of the data from testing the actual storage tank and fuel/oxidizer. The answer is positive for the following three reasons:

- a) corrosion rate is measured in the unit of depth of corrosion per time (mm/year) which is independent of size, shape, and total surface area of the container;
- b) the test cell is nearly a true replica since it was made of the same material as the actual tank and later heat treated according to the manufacturer's specification;
- c) all theories and test methods are based on science and existing procedures.

III. TEST RESULTS

The following paragraphs present the overall test results of all test parameters.

1. **Visual Inspection.** All test samples were subjected to an incoming visual inspection. The inspection revealed that no damage had occurred during shipment and no other defects were observed.
2. **Electron Microscope Inspection.** All twelve samples were subjected to inspection prior to thermal analysis and no major defects were revealed.
3. **Microcalorimetry Analysis of IRFNA.** Twelve samples were subjected to microcalorimetry tests. During the tests the temperature and pressure was monitored and the Microcalorimetry Test set recorded the output data from the test samples. Before the actual data was taken, the sample container was preleached 3 times with IRFNA to assure the surface of the PH 17-7 metal was passivated. The IRFNA was then filled to a point where the volume ratio between IRFNA and ullage are proportional to that of the actual IRFNA container in the training missile. After the pressure transducer was connected, the sample cell was inserted into the micro calorimeter for heat flow measurement after temperature equilibrium was reached. Three micro calorimeters (TAM Model 2277) were used in the analysis. During the test, the temperature and pressure output data from the test samples were recorded by the TAM micro calorimeter. The TAM micro calorimeters are equipped with 4 measuring cells with a sample and a reference heat detector for effective suppression of thermal noise. The measuring cells are all in a constant temperature controlled water bath. The baseline stability over 8 hours at 25 EC is within $\pm 0.05 \Phi W$ in static mode, and $\pm 0.5 \Phi W$ in liquid flow mode. The sample capacity was in between 4 to 25 ml.

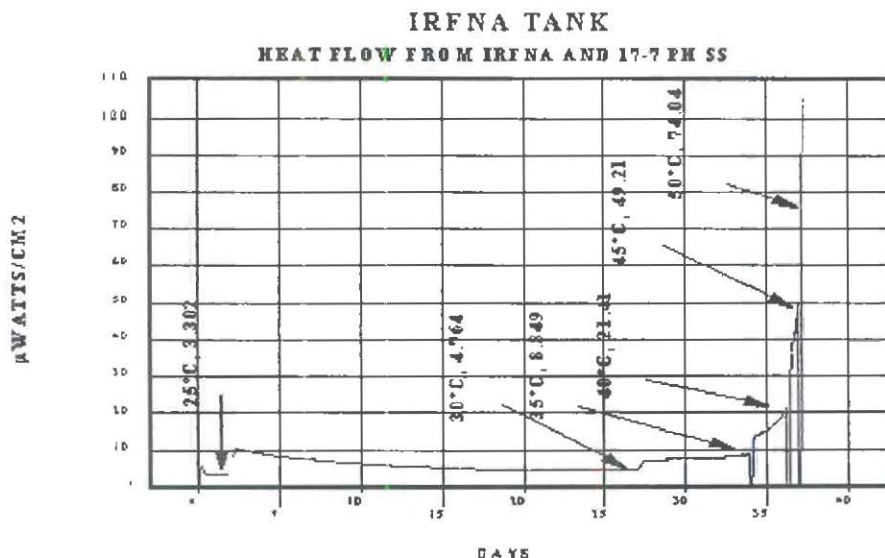


Figure 2. Microcalorimetric heat flow analysis of IRFNA and PH 17-7 stainless steel at 25, 30, 35, 40, 45 and 50°C

The TAM was used to perform the tests between 25 and 50 EC. Based on the data all twelve samples exceeded minimum safety specifications. A typical micro calorimetric heat flow chart is shown in figure 2 and the rate of corrosion as function of temperature and pressure are shown in Table 1. The comparison of corrosion rate and pressure build up in the IRFNA sample cell can be seen in figures 3 and 4.

Table 1. MICROCALORIMETRIC ANALYSIS OF REACTION OF IRFNA WITH PH17-7 STAINLESS STEEL

TEST TEMPERATURE (°C)	STEADY STATE HEAT FLOW ($\mu\text{W}/\text{cm}^2$)	CORROSION RATE		PRESSURE (PSI)
		mm/year	%per year	
25	3.302	0.0165	1.031	3.6
30	4.764	0.0238	1.488	6.0
35	8.849	0.0443	2.769	13
40	21.41	0.1071	6.693	20
45	49.21	0.2461	15.38	56
50	74.04	0.3702	23.13	76

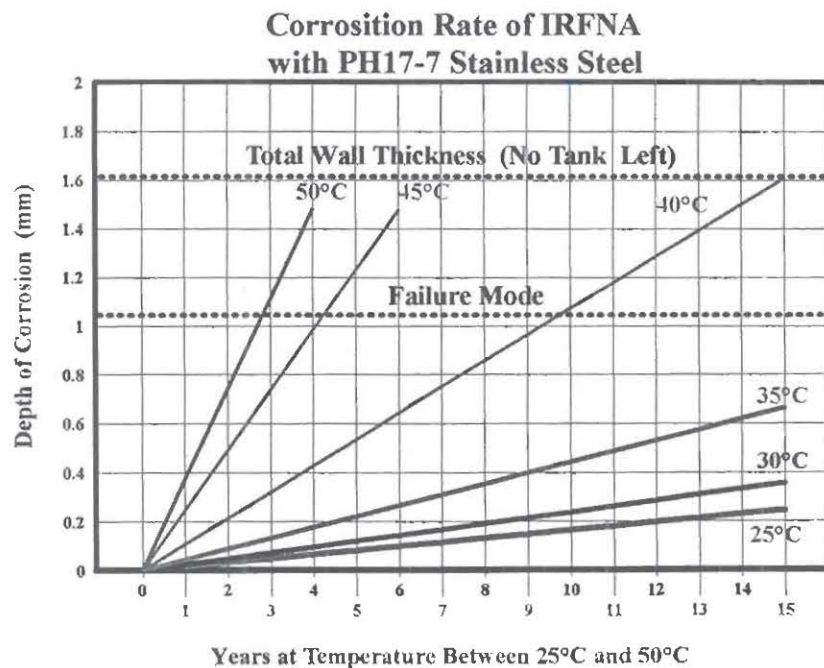


Figure 3. Corrosion rate.

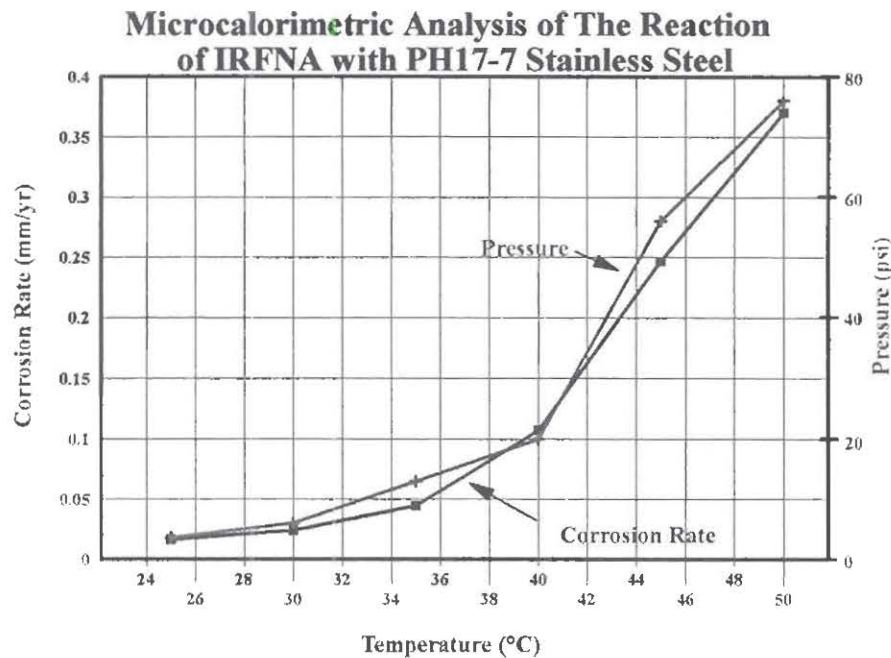


Figure 4. Pressure.

4. Micro calorimetry Analysis of MAF-4

The MAF-4 tests were conducted in the same way the IRFNA was tested. During the tests the temperature was monitored and the output data from the test samples was recorded by the Micro calorimetry Test Set. Before the actual data was taken, the sample container was preleached 3 times with MAF-4 to assure the surface of the PH17-7 metal was passivated. The MAF-4 was then filled to a point where the volume ratio between MAF-4 and ullage are proportional to that of the actual MAF-4 container in the training missile. After the sample cell was inserted into the micro calorimeter for heat flow measurements temperature equilibrium was reached. Three micro calorimeters (TAM Model 2277) were used in the analysis. During the test, the temperature data from the test samples were recorded by the TAM micro calorimeter. A typical MAF-4 micro calorimetric heat flow chart and rate of corrosion as function of temperature is shown in Figure 5. The thermal data collected from the Micro calorimetry test conducted on the MAF-4 indicated the heat flow rate were below 2 μ watts at 40°. A heat flow of 2 μ watts is generally used as the criteria to determine the thermal safety of energetic materials.

This means that the test data indicated the corrosion rate for the MAF-4 was considered low. Overall, the test results indicated the MAF-4 storage tanks should meet the minimum five-year shelf life requirement without jeopardizing safety. If shelf life beyond five years is required additional testing should be conducted.

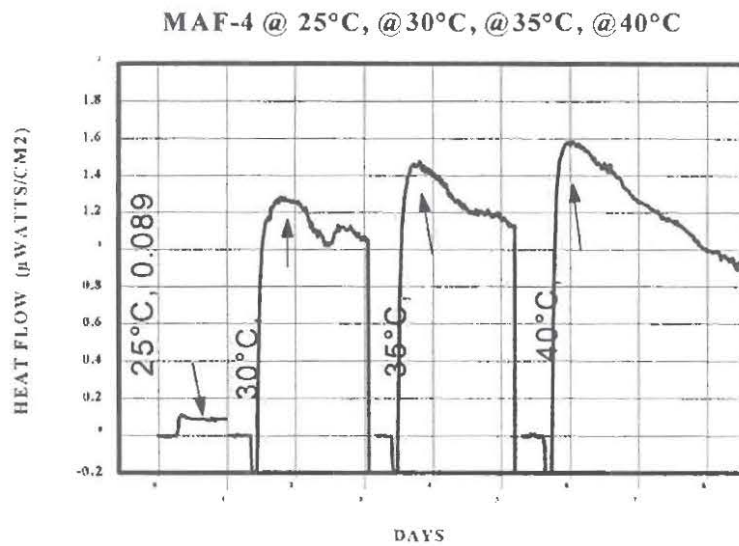


Figure 5. Microcalorimetry analysis on MAF-4.

5. Stress Analysis and Hydro-Burst Test

A stress analysis was conducted to determine the amount of pressure that should be applied to the small-scale test cell ampoules. The analysis determined that 20,000 PSI would be required to equal the same amount of hydrostatic pressure used for the pressure proof test of the actual propellant tank by the manufacturer. Hydro burst tests were performed after accelerated aging and stress analysis of the test samples. All of the Hydro burst tests were conducted by NSWC's Calibration laboratory.

The Micro calorimetry data from the IRFNA tests determined that the rate of corrosion/year was equal to 0.016 millimeters at 25°C, 0.16 millimeters for 10 years and 0.24 millimeters for 15 years. (See Table 1) A large amount of time is consumed for the corrosion rate to etch the same amount of material from the test cell ampoules, therefore, a decision was made to machine away part of the material from the outside of the test cell ampoules. This would provide a verification of the calculated corrosion rates. The calculated corrosion rates (Table 1) determined the amount of material that was machined from the test cell ampoules.

Based on the results of stress analysis the test cell ampoules used to conduct the accelerated aging tests were pressurized to 20,000 PSI for 30 minutes. After passing the 20,000-PSI test the pressure on the test cell ampoules was increased to 22,500 PSI for 1 hour. All of the test cell ampoules withstood the 20,000-PSI test without burst; however, minor deformation of the test cell ampoules began when temperatures reached 35°C.

While machining one of the test cell ampoules for testing at 40°C, which is equal to 10 years of exposure to corrosion, a defect was observed. The defect, as shown in figure 6, indicates this void was in the test cell ampoule before it was machined. It appears that the electron beam welding process caused the defect. This may indicate that the welding process used on the PH 17-7 stainless steel material should be monitored more closely. However, it should be noted that the PH 17-7 stainless steel used to manufacture the test cell ampoules was manufactured from a single piece of stainless steel while the storage tanks used by the training target missile is composed of three separate pieces of PH 17-7 stainless steel. It is not known at this time how this difference may affect the performance of the storage tanks. Perhaps the use of ultrasound may be more helpful to determine if voids or air bubbles are occurring during the welding process. After machining the test cell ampoules Hydro Burst tests were performed at ambient temperature for each of the temperatures shown in Figure 7. Beginning at 25°C which is equal to a corrosion rate of 10 years and also at a corrosion rate of 15 years. Hydro burst tests without ullage were repeated at the 10 and 15-year age equivalent at 30°C and 35°C with no burst. The burst occurred at 40°C test (10 years age equivalent). Testing at 40°C for 15 years was unnecessary because the corrosion rate is greater than 100%.

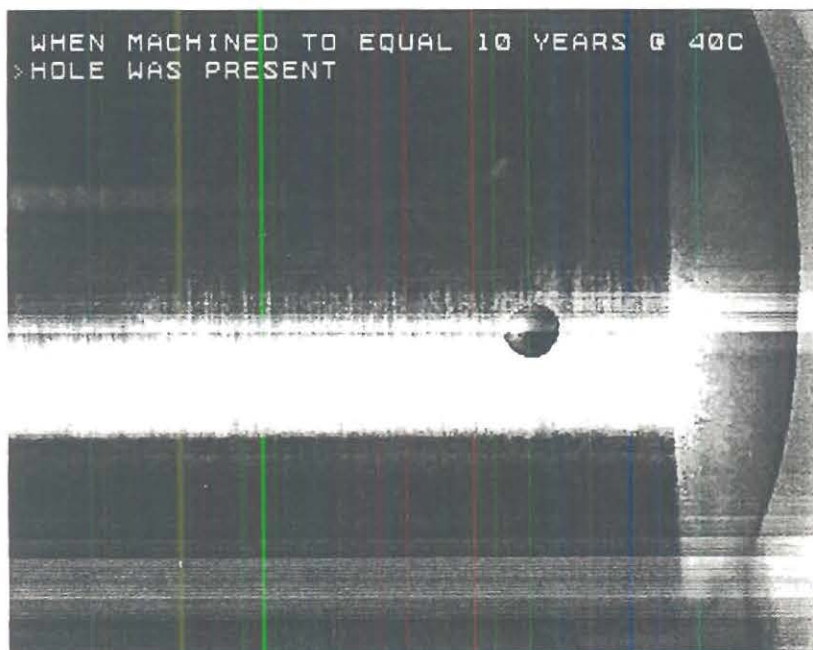


Figure 6. Machined to equal 10 years @40°C

Hydro-Burst on IRFNA Test Ampoules After Aging

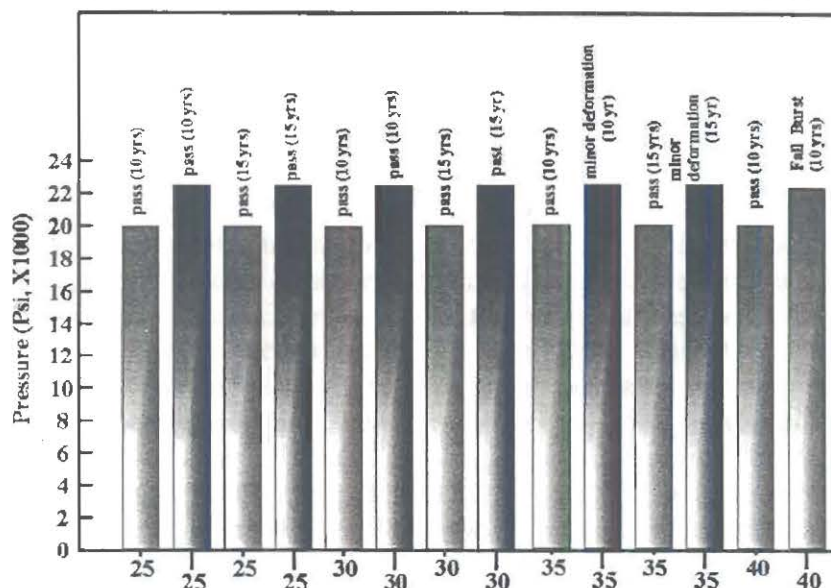


Figure 7. Hydro-burst on IRFNA test ampoules after aging.

To determine when burst would occur, one of the test cell ampoules, shown in figure 8, was machined to equal 40°C at 10 years. The ampoule developed a rupture when the pressure within the test cell ampoule reached only 4,500 PSI. The rupture, as indicated by the small hole along the bottom, occurred at the closed end of the test cell ampoule. The ruptured hole appears next to the intersection of the electron beam welds. One of the 40°C 10 year equivalent test cell ampoules, after being exposed to 20,000 PSI for 30 minutes, burst when the pressure was increased to 22,300 PSI (see figures 9 and 10). This proved that the test cell ampoules might withstand the pressure and corrosion tests up to 40°C at 10 years aging equivalent corrosion before burst would occur. The hydro burst test was considered the final proof the PH 17-7 stainless steel storage tanks used for both the IRFNA oxidizer and MAF-4 fuel could withstand both the corrosion and pressure at 25°C. Based on these test results the PH 17-7 stainless steel storage tanks will meet the necessary requirements needed to extend the shelf life to meet the five years required. However, current hydro burst data indicates that the IRFNA can meet a maximum shelf life of 7 years at 25°C and 5 years at 30°C.

6. Metallographic Microstructure Analysis of Cold-rolled Stainless Steel

A sample of the PH 17-7 cold-rolled stainless steel used in the storage tanks was sent to NSWC Crane Code 4052 for Metallographic Microstructure Analysis. The samples were evaluated to determine its microstructural identification, cold-rolling characteristics and presence of corrosion as a zero time point for future identification. Cutting the samples on a metallographic cut-off saw to enable it to be potted as two separate samples performed the evaluation. Potting and preparing the metallographic samples in this way enabled the pieces at locations ninety degrees to one another to be examined for the purpose of seeing the cold-rolling affects to the microstructure and any corrosion in both these zero time and future samples.

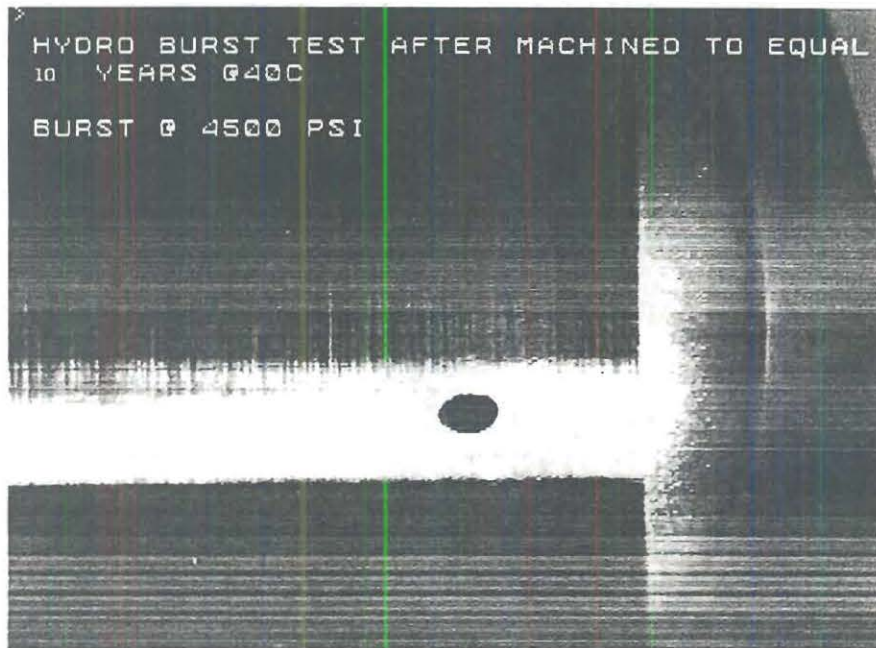


Figure 8. Burst @4, 500 PSI.

The results indicated the samples were a 301 stainless steel, which is a match for the material specified as PH 17-7, stainless. It was also determined that the sample had been cold-rolled. These characteristics were determined by the grain structure when etched. Representative photomicrographs were taken of the grain structure. The grain structure indicates no presence of corrosion development at the time zero point.



Figure 9. Burst @ 22,300 PSI

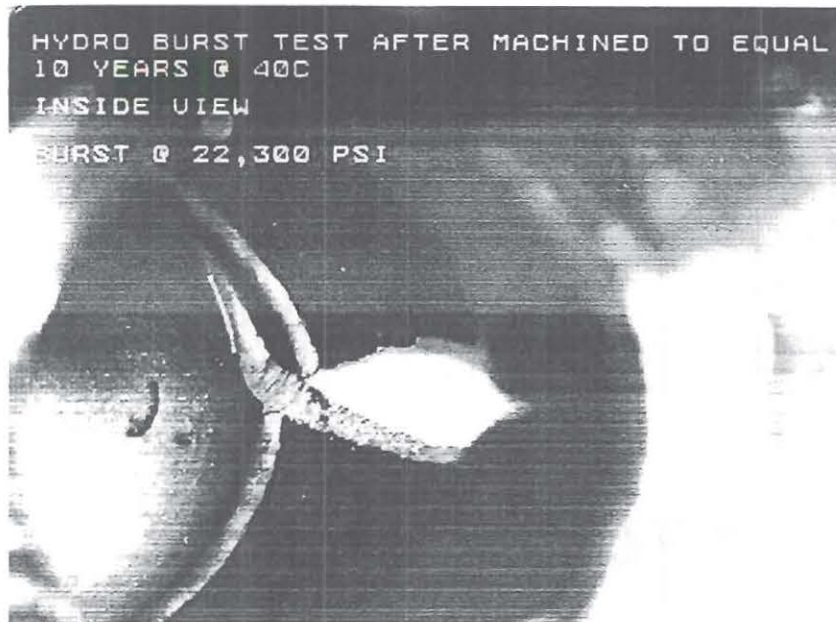


Figure 10. Inside view of burst ampoule.

IV. DISCUSSIONS

Twelve samples from three groups of four were subjected to heat flow calorimetry tests and the data indicated the IRFNA and MAF-4 samples were thermally stable with minimal degradation at ambient temperatures. Testing of both the IRFNA and MAF-4 samples showed no significant variation due to age. Equilibrium occurs rather early once the test cell ampoules are filled. Then the temperature and time in storage determines the corrosion rate.

This was the first time these samples were exposed to Micro calorimetry tests. The reaction rate observed was within the regions expected. The test temperatures were constant at 25°C to 50°C; however, normal temperatures will be variable depending on the location and length of storage. Overall, the data from all of the tests indicate the IRFNA and MAF-4 shelf life should meet the minimum five-year shelf life requirements at ambient temperature.

V. CONCLUSIONS

From the evaluation results the following conclusions have been reached. NSWC Crane manufactured the PH 17-7 stainless steel test cell ampoules, which were used to determine the corrosion rates. The test cell ampoules were heat treated and welded by the manufacturer to simulate the fuel tank construction.

Thermal analysis tests support the finding that the fuel and oxidizer are thermally stable at ambient temperature. However, as temperatures increase in the IRFNA, the degradation increases dramatically. Thermal analysis data, from IRFNA, indicated the rate of degradation and pressure dramatically increased with temperatures above 45°C. Therefore, if the storage temperature is above 45°C, the pressure increases and becomes a safety factor.

Three different groups of PH 17-7 heat-treated and welded samples were evaluated and no significant difference in the heat treating and welding process was observed.

The current quality of the IRFNA and MAF-4 container system is satisfactory for in-service use if stored at temperatures below 30°C. Therefore, handling or storage safety is not considered a hazard provided standard handling instructions are observed.

The shelf life of the IRFNA and MAF-4 container system should meet the minimum five-year requirement provided the materials used meet the weapon specification. The current hydro burst data indicates that the IRENA can meet a maximum shelf life of 7 years at 25°C and 5 years at 30°C.

VI. RECOMMENDATIONS

Based on the test results and an analysis of data the following recommendations are made.

The IRFNA and MAF-4 storage tanks should be retained as serviceable, if stored below 30°C. Storage tanks should not be stored at temperatures above 35°C for prolonged periods to prevent degradation from corrosion and over-pressurization. Temperatures above 30°C should be monitored and recorded closely to ensure safety is not jeopardized.

Future evaluations should include both older and newer production samples of fuel and storage tanks to ensure a sample that is representative of the stockpile. The next shelf life study should be in FY-2001 to monitor the stockpile for aging trends to determine if the safety and serviceability of the fuel/oxidizer container system is continuing to meet specifications.

VII. REFERENCES

1. Naval Surface Warfare Center, 300 Highway 361, Crane. Indiana 47522
2. A. Chin, D. S. Ellison, D. R. Crowley and H. A. Farmer, "Micro calorimetric Criteria For Evaluation of Corrosive Liquid Propellant on Metal Containers". Proceeding of the 1st International Workshop on the Micro calorimetry of Energetic Materials (7-9 April 1997, Leeds, United Kingdom), and references therein. Published by Defense Research Agency (DRUMS), WX3 Pyrotechnics Group, Electro-optic Warfare department, Fort Halstead, Sevenoaks, Kent TN14 7BP, United Kingdom.

HFCS 2001/2 SESSION MINUTES

Session 5

Question asked by: Riza Cruz – St. Marks Powder, Florida

Question directed to: Harry Farmer, NSWC Crane

Question: What actions were taken immediately after explosion of storage tanks in missile propulsion?

Answer: The Shelf-life was restricted to 2 years. This action created safety problems and waivers had to issued before each missile could be used. This action threatened the overall program. Therefore, a scientific method was needed to prove that the storage tanks were safe to use under normal storage conditions. Crane used their microcal facility to establish a temperature, pressure, and corrosion rate which allowed the program to extend the shelf-life to 5 years under proper storage conditions.

THIS PAGE LEFT INTENTIONAL BLANK

Preliminary Assessment of the Superscale Heat Flow Calorimeter (SSHFC)

David G. Sherfick and Steven L. Backer

**Test and Evaluation Branch, Code 4051
Naval Surface Warfare Center, Crane Division
300 Hwy 361
Crane, IN 47522-5001**

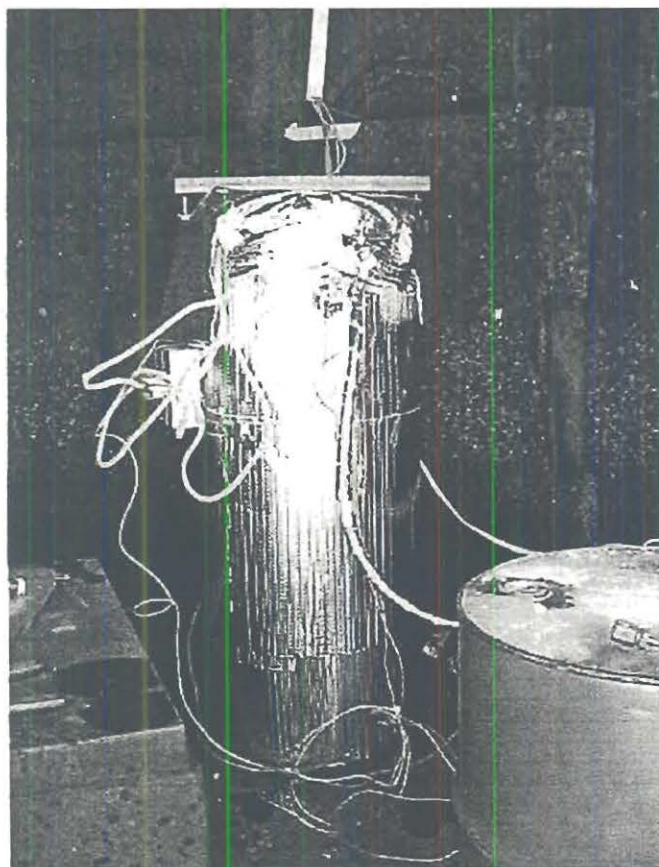


Figure 1. Superscale Heat Flow Calorimeter.

Abstract

The propensity of double based propellants to decompose under normal storage conditions is well known. The possibility of this degradation resulting in the violent autocatalytic reaction given the proper storage conditions is also well known. These storage conditions affecting the possibility of autocatalysis consist of, primarily, storage temperature, physical dimensions of the propellant and the ability of the storage container to transfer heat to its surroundings. Given the results of heat flow calorimetry and a detailed knowledge of the physical conditions of the propelling charge and its storage container, the possibility of autocatalysis can be calculated. However, since the accuracy of these calculations can always be called into question, it was determined that a heat flow calorimeter of sufficient size to hold a propelling charge for a 5 Inch 54 Caliber Projectile could be constructed (see Figure 1). This paper presents the design criteria and the execution of the design.

Acknowledgments

The authors would like to thank Mr. Terry J. Coy and Mr. Luis H. Ortega for their assistance in the preparation of this paper. Design and construction of the SSHFC were also accomplished through the efforts of Messrs. Coy and Ortega. Additional construction assistance was provided by Mr. Paul Fries.

Introduction

Nitrate Ester propellants are utilized in a variety of capacities in a large number of ordnance rounds. The nitrocellulose in these propellants is known to break down by the release of nitrate groups. These groups can further combine to form Nitric Acid (HNO_3). This acid further attacks nitrocellulose which can cause an autocatalytic (or runaway) reaction. In this case, the heat being produced by the inherent breakdown which is occurring in the propellant is further accelerating that reaction. The nature of the reaction rate can take one of two paths. If the combination of heat production, physical size of the propellant and the insulative capacity of the weapon and its shipping container have the capability to release more heat than it produces, the reaction rate will reach a finite peak and proceed at a lower rate until all of the energy in the propellant is consumed. If the weapon characteristics and the storage conditions cannot release more heat than it produces, then the reaction will overwhelm the propellant's stabilizer and then proceed at a higher and higher rate until a runaway reaction occurs.

Since the propensity of a weapon to produce an autocatalytic reaction depends on its physical attributes and storage conditions, the ability to measure the rate of reaction of the propellant of an intact weapon in its storage configuration would provide essential information about its storage safety. The weapons which are more likely to produce autocatalytic reactions are too large to fit into standard calorimeters. Standard calorimeters have measurement cells currently ranging up to 20 ml. It was proposed to construct a much larger calorimeter with the capability to contain much larger weapons. Since the purpose of the SSHFC is to measure the general shape of the

curve (i.e. to determine whether or not the reaction will advance to autocatalysis or not) and not to determine detailed heat flow data (i.e. activation energies or other kinetic data), the measurement would not have to be of the precision of standard calorimeters.

The weapon chosen for this evaluation is the MK 67 MOD 3 propelling charge for 5 Inch 54 Caliber Projectiles (see Figure 2). At the inception of the superscale calorimeter, an investigation of the MK 67 was underway in relation to a hangfire incident aboard the USS Ross (DDG-71).

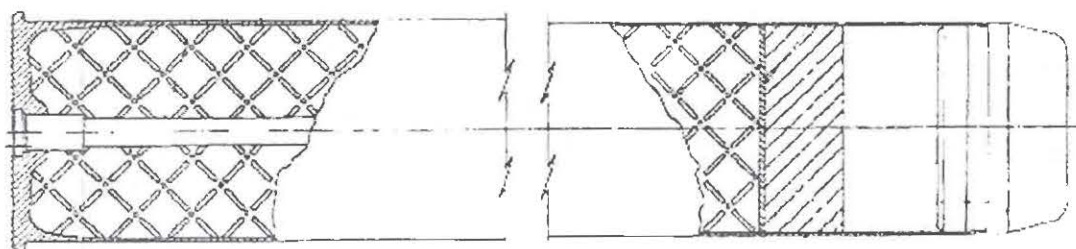


Figure 2. MK 67 Mod 3. Propelling Charge.

The MK 67 Propelling Charge is contained in a MK 15 MOD 1 Storage Tank (see Figure 3). This storage tank is 36.3 inches long and has a maximum diameter of 7.47 inches. The physical dimensions of the SSHFC calorimeter was designed around this storage tank. The SSHFC would consist of a test cell, a temperature controlled bath, an electronic section and associated plumbing and equipment.



Figure 3. MK 15 MOD 1 Propelling Charge Tank.

The rate of reaction would be measured by an array of Peltier cells located in the test cell. The design of the array was intended to have sufficient sensitivity to measure the reaction rate. A personal computer and associated electronics would be utilized to control the bath temperature, ensure proper liquid level in the bath, record and transmit the data. The data recorded would be the Peltier power level, the bath temperature and the temperature of the skin of the propelling charge. These data would be transmitted across the local intranet to personnel who would be tasked to occasionally monitor the data. Additionally, the software would contain algorithms to detect the onset of an autocatalytic event. If such an event is detected, the heating system is shut down, the fluid in the bath is discharged and the bath is refilled with fluid at ambient temperature. Failure to halt an autocatalytic event would likely result in the destruction of the SSHFC. While this would be unfortunate, the possibility of a violent reaction could not be avoided. Therefore, the SSHFC would be located at a remote location, contained in a three-sided gun tub shield and operated remotely in such a manner that no test operator would be required to approach the test site while the test is ongoing. This feature produced other difficulties in that the SSHFC would be located outdoors and exposed to the elements and temperature fluctuations of southern Indiana. While these factors would be crucial in a standard calorimeter, it is hoped that the lack of precision required in the SSHFC will allow the environments to be handled without the expense of building an environmentally controlled structure. However, the fluid was required to remain in the liquid state in temperatures below 0°F (-17.8°C). The temperature requirement was needed because the auxiliary tank, which is used to provide additional bath fluid if the liquid level should drop significantly, is not kept at the test temperature and would be required to remain in the liquid state at ambient outdoor temperatures potentially through the winter.

The Test Cell and Bath

An overview of the system is shown in Figure 4. The test cell and bath were constructed locally (see Figure 5). The goal of the design of the cell was to maximize

the heat transfer rate from the propellant to the bath while passing through the Peltier cells. This was done by creating a heat flow path which transferred the heat through conduction as much as possible. A detail of the heat path is shown in Figure 6. The 60 Peltier were arranged in rows of 15 between the inner cell and the heat sinks (see Figure 7). Figure 8 shows the assembly with all four heat sinks bolted on. The inner assembly was lowered into the stainless steel outer tank

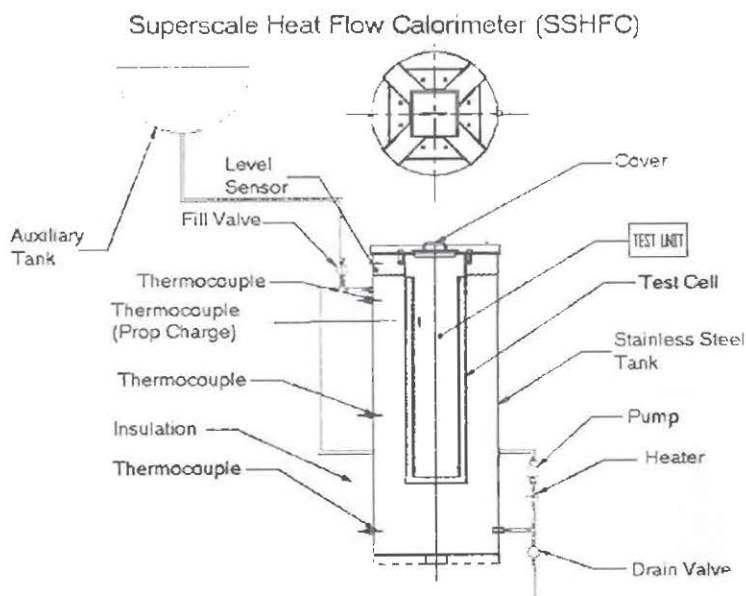


Figure 4. System Overview.

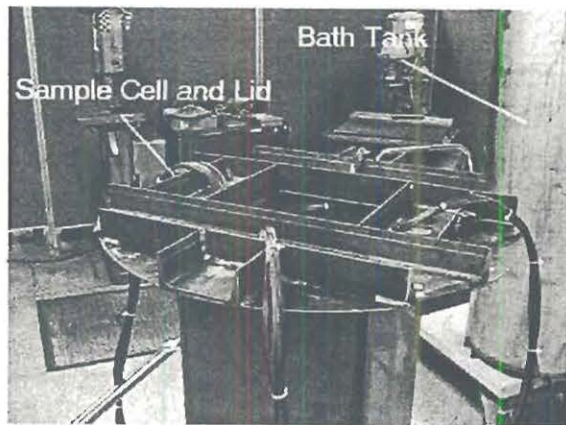


Figure 5. Sample Cell and Tank.

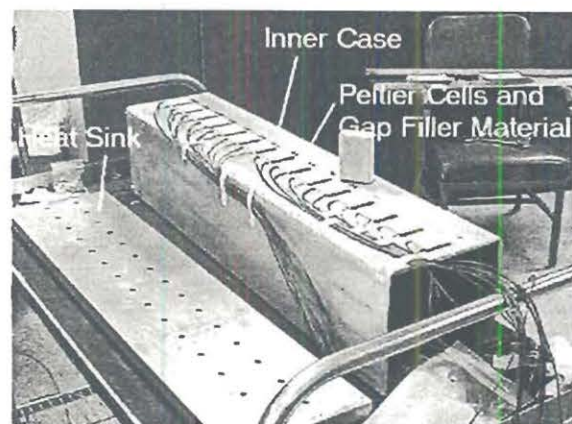


Figure 7. Peltier array arrangement



Figure 9. Outer Case Assembly.

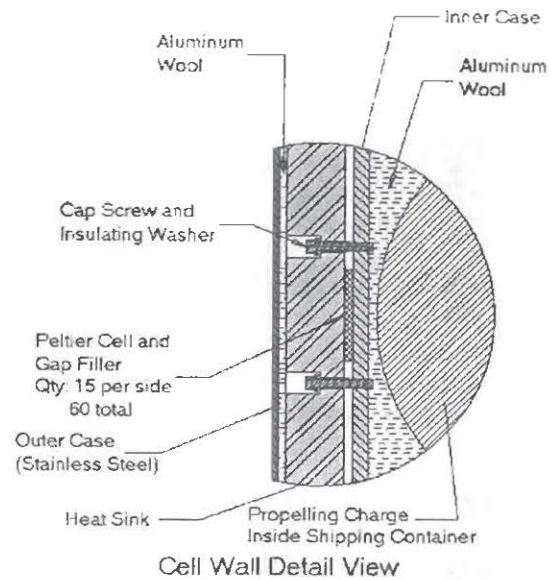


Figure 6. Detail View of Heat Path.

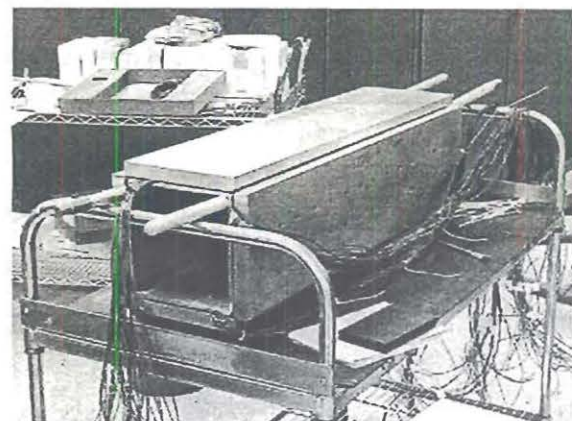


Figure 8. Sample Cell Construction.

while wrapping heat sinks in aluminum wool (see Figure 9.) The aluminum wool was intended to be a heat transfer mechanism so that the heat transfer rate to the bath is maximized and hence the time required to detect a thermal runaway is decreased. A photograph of the assembly is shown in Figure 10.

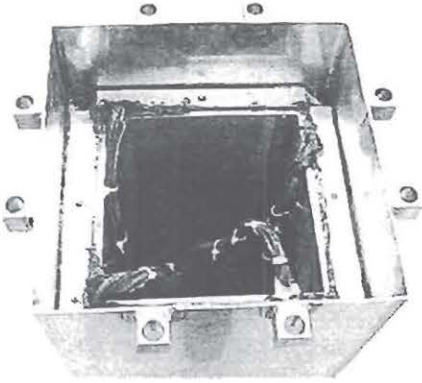


Figure 10. Top view of Sample Cell.

The Data Recording Equipment

The data recording equipment is shown in Figure 11. Analog to Digital Conversion of the data is performed by a Hewlett-Packard Model 34401A Digital Multimeter. The data is digitally transferred to a Personal Computer (PC) via a GPIB cable/card. The PC records data at a rate of one sample per minute. The heat flow is being measured by an array of sixty Peltier cells, Model DT12-6-01-LS, manufactured by Marlow Industries. They have a maximum temperature of 85°C. Bath temperature is being measured by a Omega Model N8501 Temperature Controller connected to an RTD. Case temperature is being measured by a Hart Scientific Model 1502 Thermometer also utilizing an RTD. The data is stored on the PC and is made available to the local area network. The data is read remotely over the network by the program Plotdata.vxe.

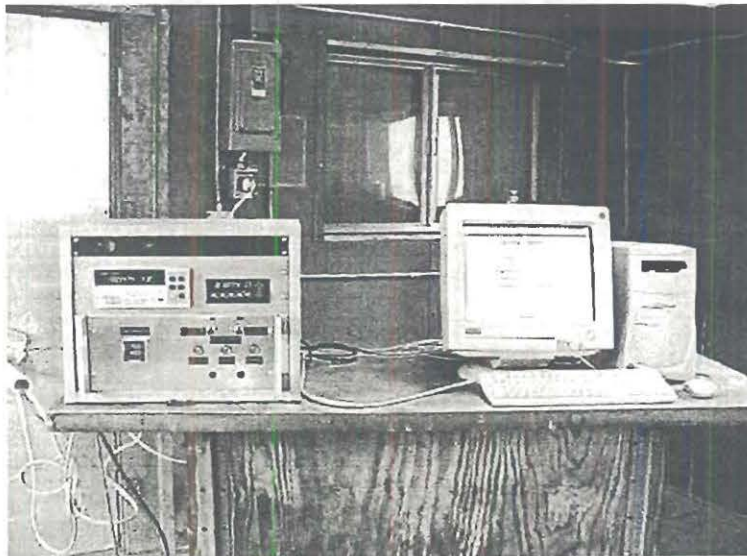


Figure 11. Data Recording Equipment

The Safety Equipment

The safety features of the system consist primarily of the remote operation and monitoring capability of the system. No personnel are required to approach within 100 feet of the SSHFC when it is in operation. Additionally, the SSHFC is located in an armored gun tub which provides approximately 270° protection around the SSHFC which includes the access road and control building (see Figure 12). The software controlling the system contains alarm settings which will automatically shut down the system should the conditions exist which make a runaway reaction appear imminent. Additionally, the software allows remote monitoring of the data being collected. This allows personnel to also begin the shut down sequence should a runaway be identified in a manner not detectable by the alarm algorithms. The shut down sequence consists of the heater being shut down, fluid being drained from the system and replacement fluid at ambient temperature being fed into the system. This would be done in the hopes of arresting an autocatalytic reaction in progress. This may not be possible. Once started, a thermal runaway will progress. It is hoped that the propellant's reaction can be slowed down to the point that the propellant can be removed and destroyed at an adjacent location without the necessity of destroying the SSHFC in the process.

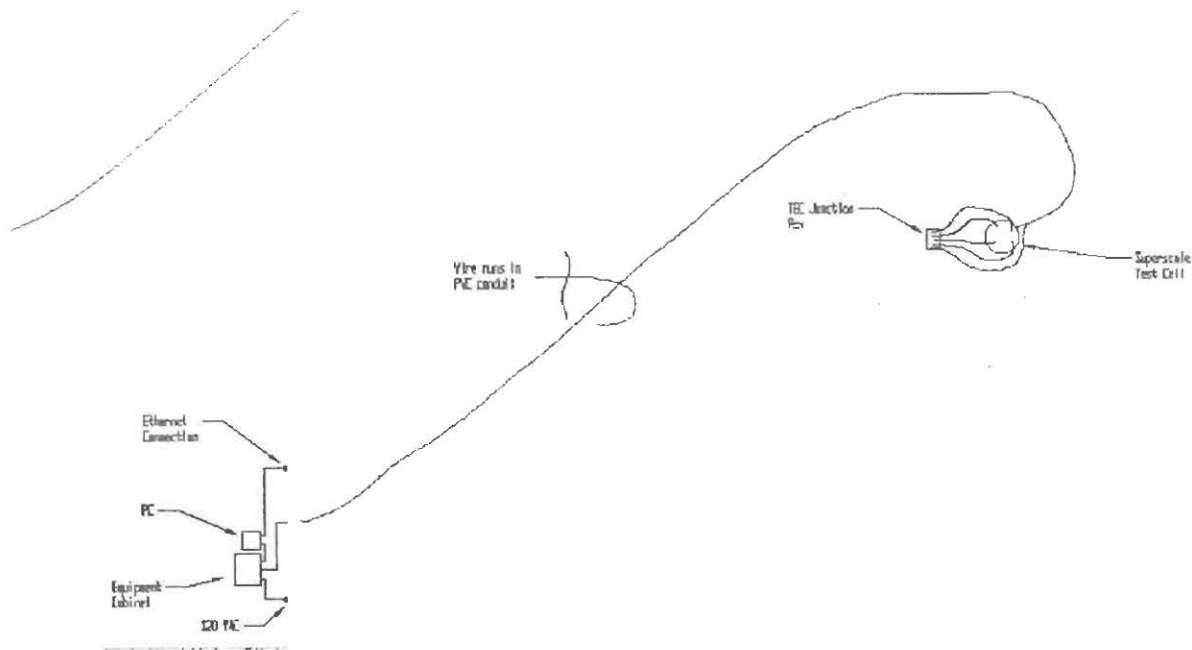


Figure 12. System Location

The Control and Recording Software

Control and data storage/presentation is managed by two locally produced programs called, SaveData.vxe and PlotData.vxe which utilize Hewlett-Packard's HPVEE as a programming base. The software monitors bath temperature, case temperature, the signal from the Peltier cells and the state of the liquid level switch. The software controls the power to the water heater and the valves which feed and release the bath fluid to/from the system. This program contains the algorithms which will determine whether a normal reaction rate is ongoing or whether the reaction has transitioned into a thermal runaway. There are currently two algorithms being utilized to detect thermal runaway. The first is a maximum deviation between internal temperature inside the sample cell and temperature of the bath. The second consists of a maximum slope of the Peltier signal. This maximum slope is yet to be determined. It will be related to data measured in small scale heat flow calorimetry data which will be performed prior to the testing of the propelling charge in the SSHFC. Should the program detect a thermal runaway, it will immediately begin the shut down sequence described above.

Preliminary Data

The data which has been measured at this point consists only of verification tests. Data has been recorded from the Peltier cells. Bath temperature, Case Temperature and Peltier signals have been able to be monitored remotely with PlotData.vxe (see Figure 13). The bath appears to be controllable to within 0.5°C . Calibration data has not been recorded at the time of this presentation. Therefore, whether the system has the sensitivity and stability required to perform its assigned task has not been determined at this time.

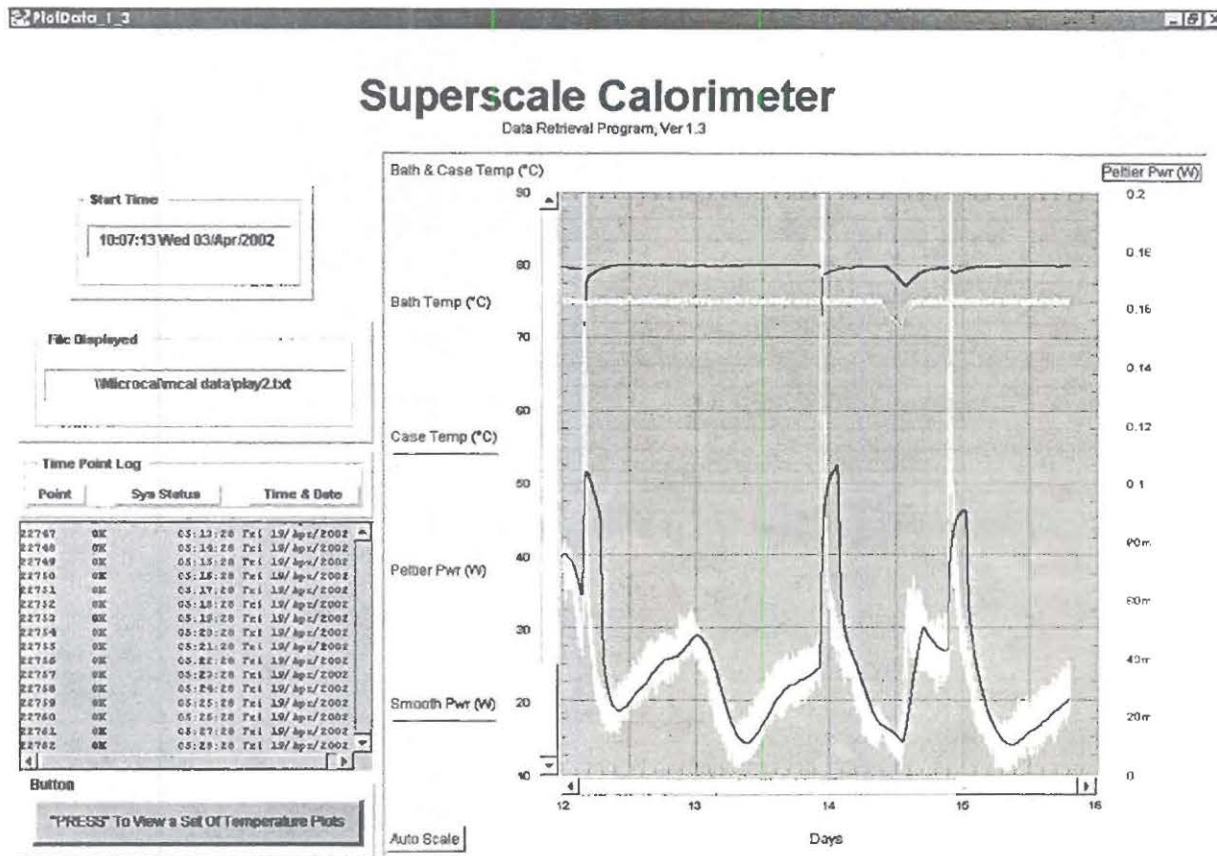


Figure 13. Data collection display.

Conclusions

There are very few conclusions to be drawn at this time. The SSHFC's sensitivity and stability are not known at this time. It is not known whether the system's lack of environmental control and the system's lack of a reference cell are significant issues. It is felt that the SSHFC will prove to be an invaluable tool in the assessment of a variety of propellants in their storage configurations.

THIS PAGE LEFT INTENTIONAL BLANK

THE STATUS OF THE HFC STANAG

Uldis Ticmanis[□], Stephan Wilker[□], Pierre Guillaume[▪], Wim de Klerk[△]

[□] WIWEB, ASt Heimerzheim, Großes Cent, 53913 Swlstaal (Germany)

[▪] PB Clermont SA, Rue de Clermont 176, 4480 Engis (Belgium)

[△] TNO-PML, Postbus 45, 2280AA Rijswijk (Netherlands)

Presentation on the 3rd International symposium on Heat Flow Calorimetry and its applications for Energetic materials, French Lick, Indiana, April 2002

Abstract

The experimental and theoretical work for establishing a STANAG for the estimation of the chemical stability of propellants by heat flow calorimetry is described. The test criteria are derived assuming worst case conditions in ageing and storage. This paper additionally gives a status report about STANAG 4582.

1 Introduction

NATO standardisation agreements (STANAG) for the thermal („chemical“) stability of propellants describe mutually acknowledged test procedures to facilitate cross procurement by avoiding repeated testing in different countries. Already existing STANAGs on this subject are based on stabiliser consumption in isothermal storage at elevated temperatures [1,2,3,4].

Heat flow calorimetry (HFC) offers a more direct treatment of the problem because here just the quantity that causes the danger of thermal explosion is measured. Moreover, interrupting an HFC experiment shortly before autocatalytical reaction starts and analysing the stabiliser content at this stage yields relevant limits for the stabiliser consumption methods.

2 The risk of thermal explosion of propellants

Some examples for heat flow curves of different propellants, measured in a TAM calorimeter at 89°C are shown in figs. 1 to 4. The long time measurements presented in figs. 3 and 4 were performed in glass ampoules. After every gas evolution peak the sample vessel was sealed by a new lid.

Depending on the type of stabiliser and the nitroglycerin (NG) content (both marked in the graphs) the shapes vary from no to extremely autocatalytic characteristics. The double base (DB) propellant („DPA, 40%“) detonated in the calorimeter after 11 days. The last part of the signal was lost, but simulation of the measuring system (a steel ampoule with 11 mm inner diameter) resulted in a heat generation of at least 80 mW/g to cause a thermal explosion. This event shows dramatically that the chemical stability of propellants merits a more deeply consideration.

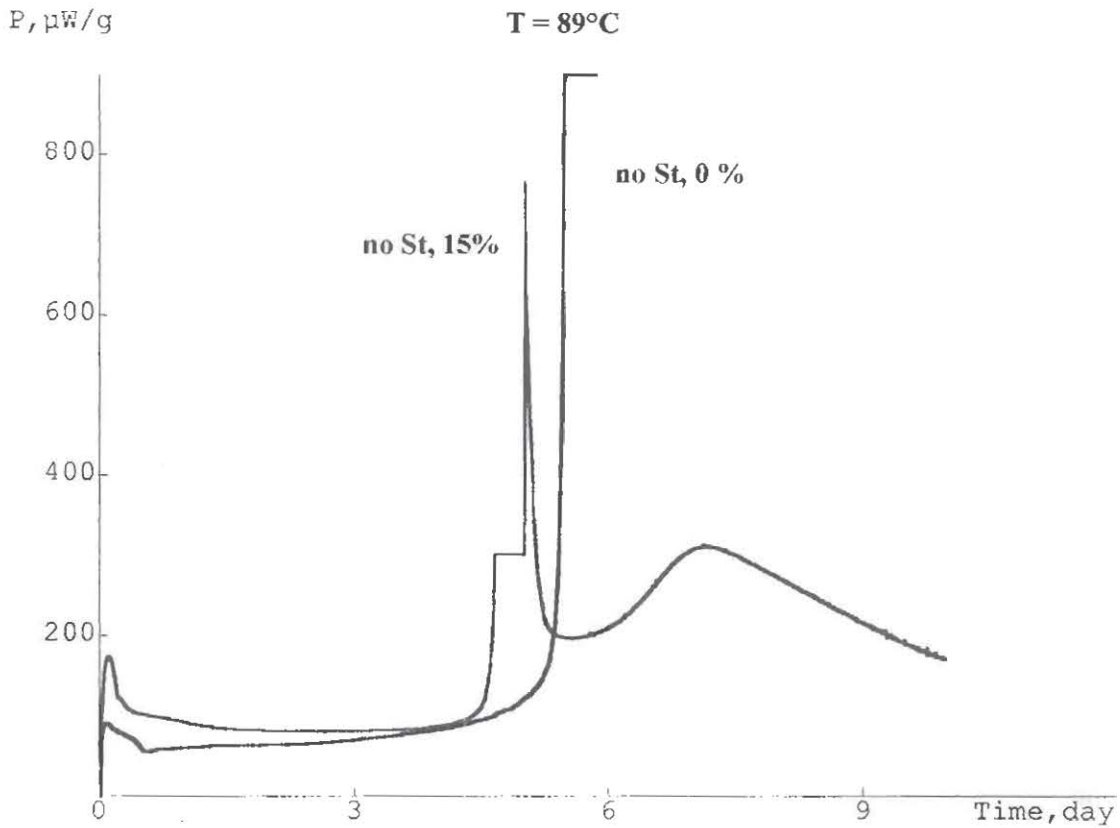


Figure 1. HFC curves of propellants without stabiliser

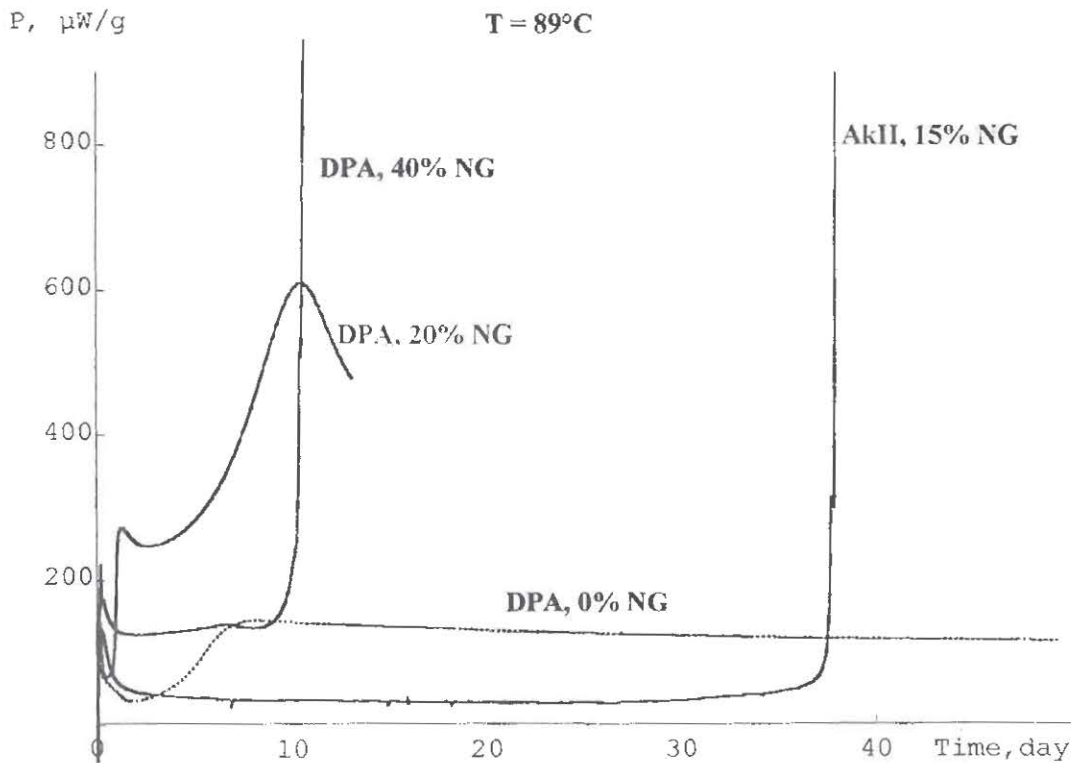


Figure 2. HFC curves of DPA and Akardite II stabilised propellants

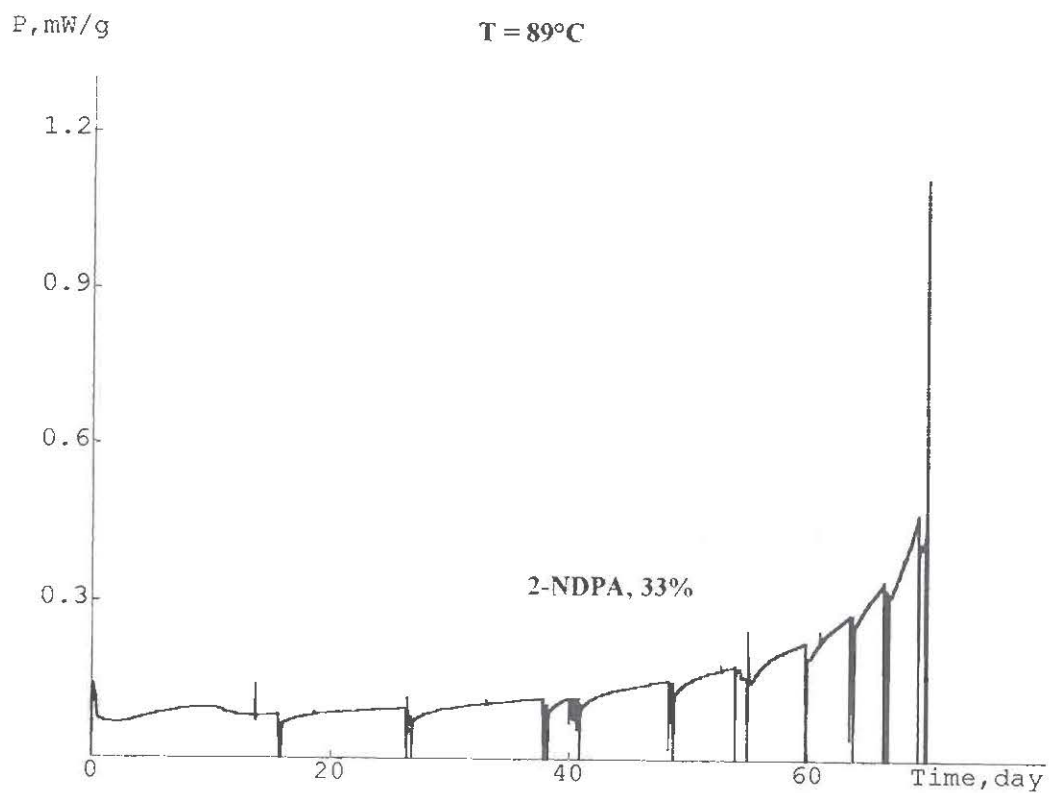


Figure 3. HFC measurement of a 2-NO₂-DPA stabilised propellant

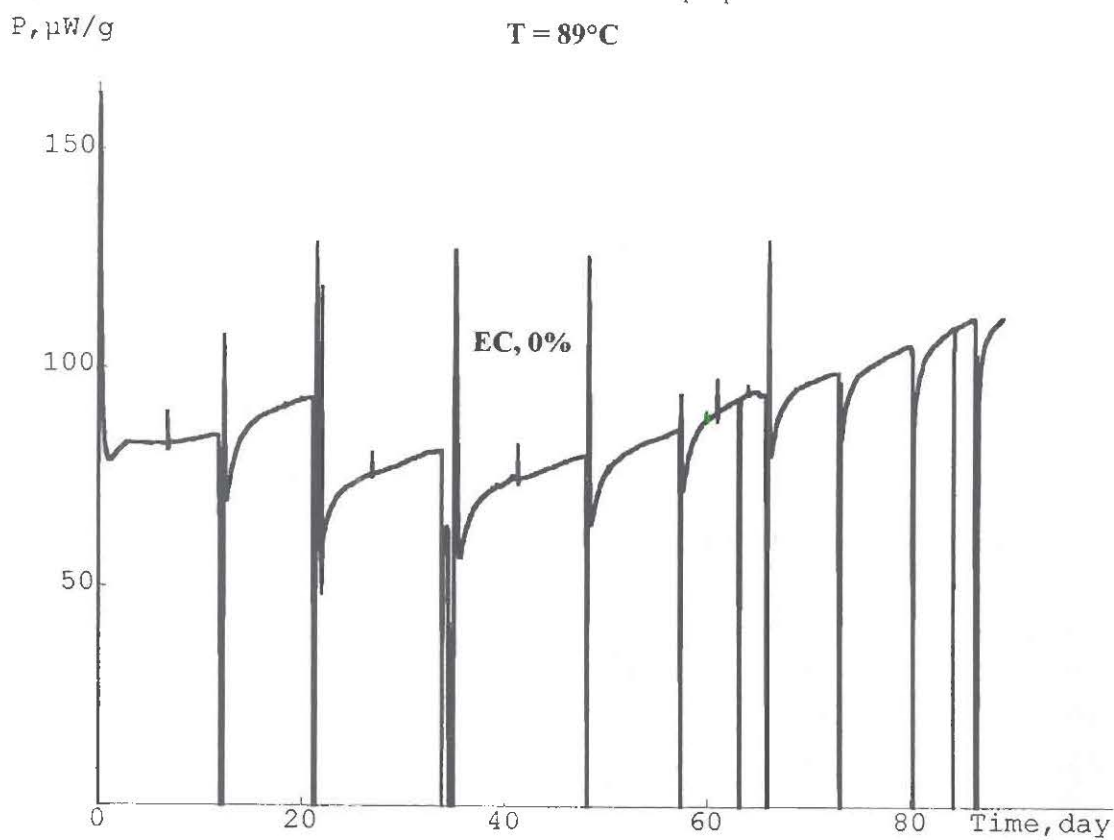


Figure 4. HFC measurement of a propellant stabilised by centralite I.

3 Isothermal ageing theory

The aim of the STANAG [5] is to establish a procedure, based on heat flow calorimetry (HFC), as simple as possible and suitable to ensure chemical stability for a 10-years storage at 25°C. To cover this period in an acceptable measuring duration, the experiments must be performed at elevated temperature. For an extrapolation to ambient conditions we have to consider the temperature dependence of the reactions, characterised by the activation energy (AE). In spite of the quite different shapes of the HFC curves due to nitration and nitrosation of the stabilisers it can be assumed that the temperature dependence will be dominated mainly by the slower decomposition reactions of nitrocellulose and NG. The AE should therefore vary only within a limited range. For the same reason the AE can also be estimated from stabiliser depletion at different storage temperatures.

A lot of storage dates were brought into our NATO "expert working party" while working out the STANAGs based on stabiliser depletion. Former investigations indicated a change in AE in the temperature region around 60°C [6]. Therefore we used the stabiliser depletion dates to test this hypothesis by fitting a n-order reaction below and above this temperature.

$$\ln t = \ln(1/A) + E/RT + \ln[(1 - S/S_0)^{1-n}/(1-n)] \quad (1)$$

t	=	storage time [d]	R	=	gas constant [0.0083143 kJ/(K · mole)]
A	=	frequency factor [d ⁻¹]	n	=	reaction order
E	=	AE [kJ/mole]	S	=	stabiliser content [%]
T	=	storage temperature [K]	S ₀	=	stabiliser content before storage [%]

The results are listed in tables 1, 2 and 3.

Table 1. Activation energy from DPA depletion in DB propellants containing up to 15% NG

Storage temperatures [°C]	Activation energy [kJ/mole]	Storage temperature range [°C]	Activation energy [kJ/mole]
45/50/55	124		
45/50/55	129		
45/50/55	135		
52/60	121	60/65/80	140
52/60	117	60/65/80	153
52/60	109	60/65/80	142
52/60	132	60/65/80	140
52/60	110	60/65/80	140

Table 2. Activation energy from DPA depletion in DB propellants with NG contents from 26 to 43%.

Storage temperatures [°C]	Activation energy [kJ/mole]	Storage temperatures [°C]	Activation energy [kJ/mole]
20/40/50/60	121	20/40/50/60	127
20/40/50/60	131	20/40/50/60	126
20/40/50/60	126	20/40/50/60	100
20/40/50/60	125		

Table 3. Activation energy from 2-NO₂-DPA depletion in DB propellants with NG contents from 20 to 43%.

Storage temperatures [°C]	Activation energy [kJ/mole]	Storage temperature range [°C]	Activation energy [kJ/mole]
50/60	108	60/70	123
50/60	98	60/70	129
50/60	153	60/70	146
50/60	129	60/70/80	167
50/60	144	60/70/80	163
50/60	132	60/70/80	160
50/60	152	60/70	132
50/60	152	60/70/80	128
-	-	60/70/80	134

The overall mean values

$E = 126$ kJ/mole (s.d = 15) for temperatures < 60°C and

$E = 142$ kJ/mole (s.d = 13) for temperatures > 60°C

are not giving a convincing support for a change of AE.

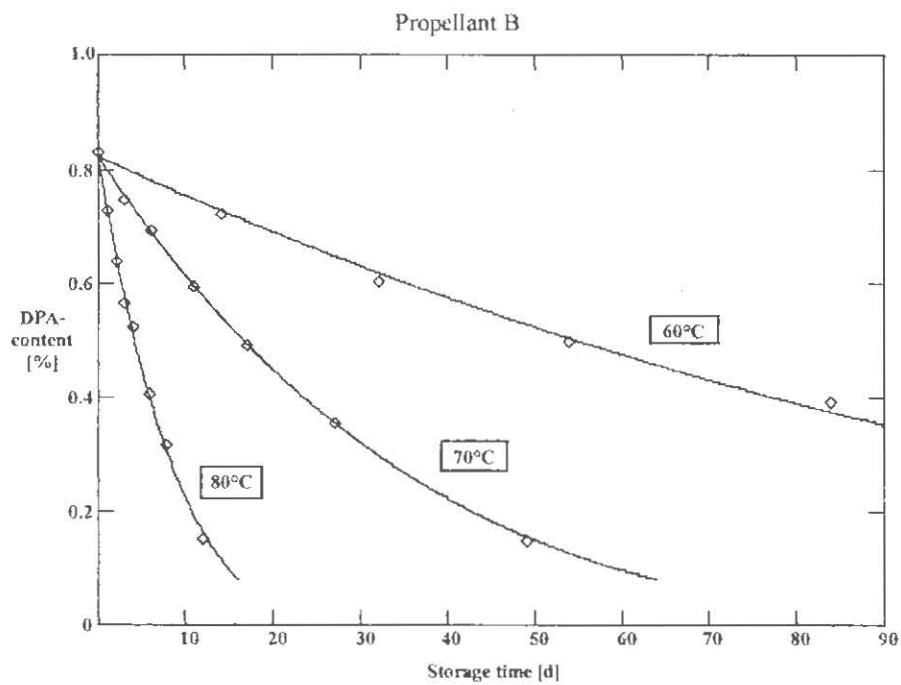
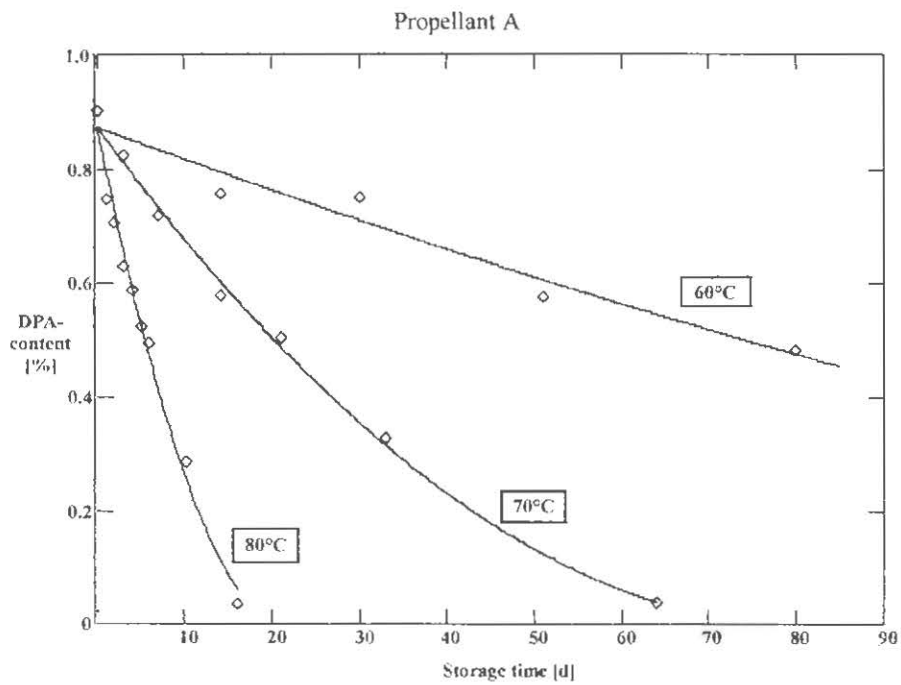
It should however be remarked that the scattering of the dates is high, probably due to unequal sealing of the samples and in consequence a different availability of air. Current investigations in the working group are showing a considerable influence of this factor.

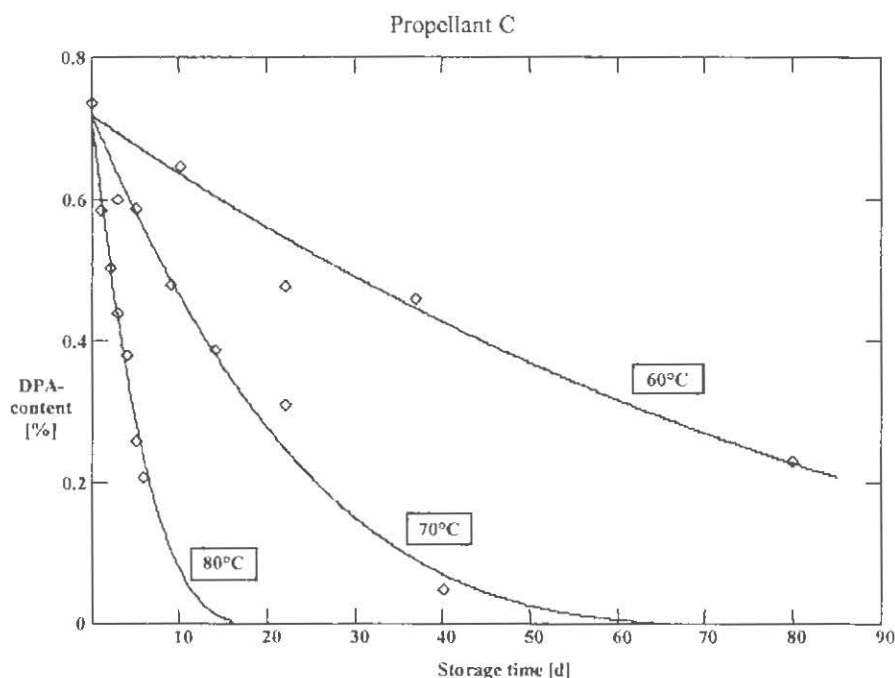
Using hermetically sealed TAM glass ampoules for storage of some DPA stabilised SB propellants we found a continuous change of the AE [6], well described by equation (2):

$$S = S_0 [1 - (1 - n)(A_1 e^{-E_1/RT} + A_2 e^{-E_2/RT}) * t]^{1/(1-n)} \quad (2)$$

E_1 = AE dominating at higher temperatures [kJ/mole]
 E_2 = AE dominating at lower temperatures [kJ/mole]
 A_1, A_2 = frequency factors, corresponding to E_1 and E_2 [d⁻¹]

The fittings are shown in figs. 5, 6 and 7, the kinetic parameters are listed in table 4.





Figures 5-7. Stabiliser (DPA) depletion of some SB propellants in hermetically sealed tubes.

Table 4. Activation energy from DPA depletion in SB propellants using hermetically sealed tubes

Propellant	Lower temperature AE	Higher temperature AE
	[kJ/mole]	[kJ/mole]
A	109	147
B	83	177
C	90	170

From HFC measurements the constance of the AE can be checked using points of equal decomposition degree α (here: equal heat released) at different temperatures and linear regression of

$$\ln t = \ln \left[\frac{1}{\Delta H \cdot A} \star \int_0^Q \frac{dQ}{f(Q/\Delta H)} \right] + \frac{E}{RT} \quad (3)$$

Q = heat released [J/g]
 ΔH = total reaction heat [J/g]
 $f(Q/\Delta H)$ = function describing the dependence of reaction rate from reaction degree ("reaction model")

Some plots of AE against the heat released are shown in the figs. 8, 9 and 10 [11]. The first part is dominated by oxidation reactions with the locked-in air, in the following regions near constant values between 120 and 140 kJ/mole are observed. The most informative long time measurements in a temperature range from 50 to 89°C were realised by GUILLAUME [7]. No transition of AE at lower temperatures can be detected from these dates (fig. 11).

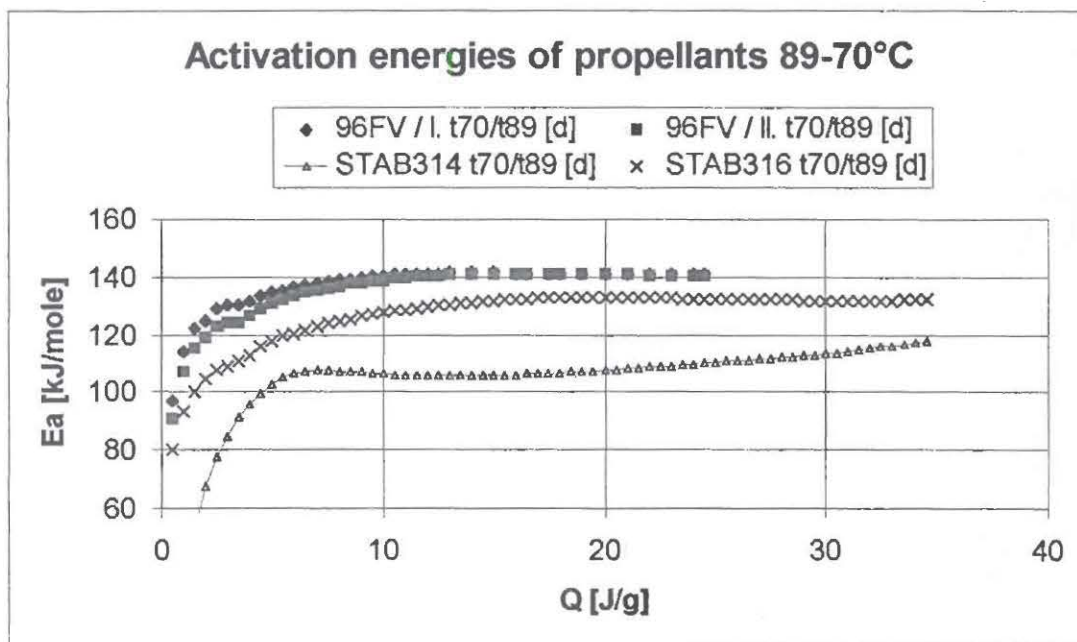


Fig. 8. Activation energies of four DB propellants stabilised with DPA or DPA derivatives.

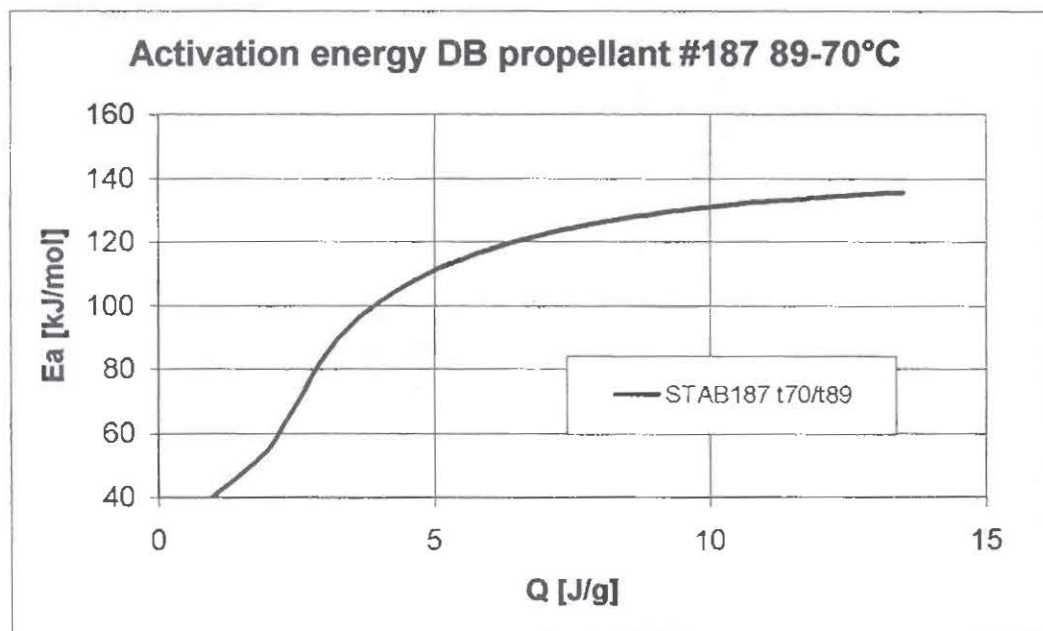


Fig. 9. Activation energy of a DB propellant stabilised by 2-NO₂-DPA [11]

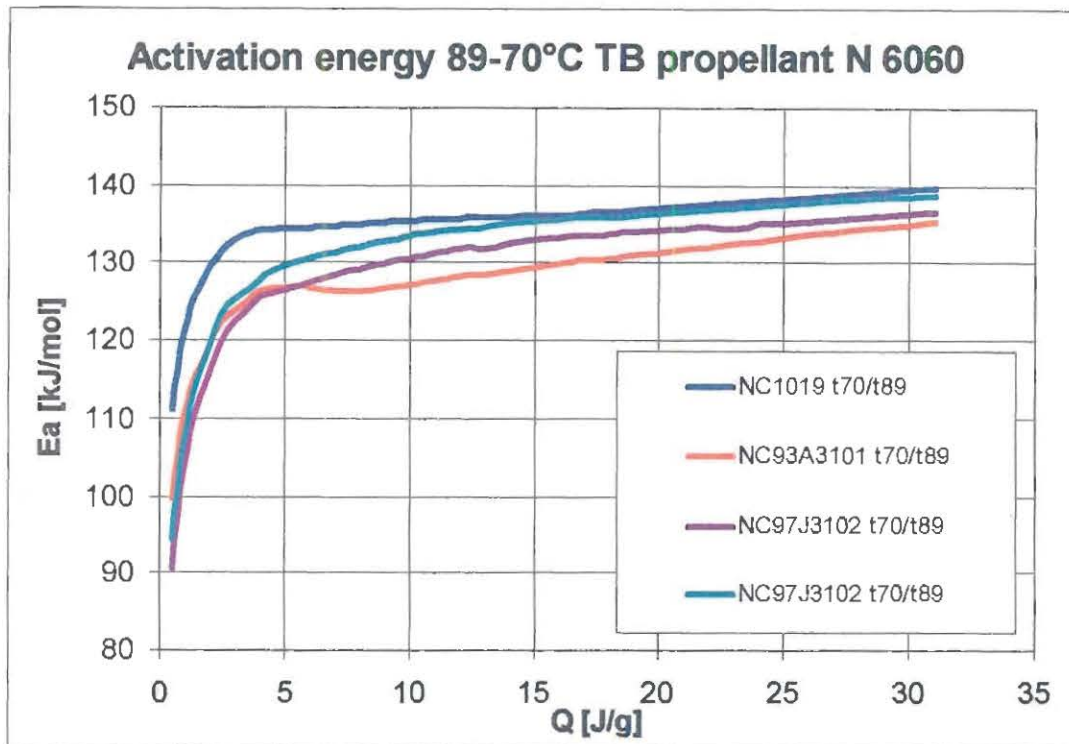


Fig. 10. Activation energy of a TB propellant stabilised by ethyl centralite

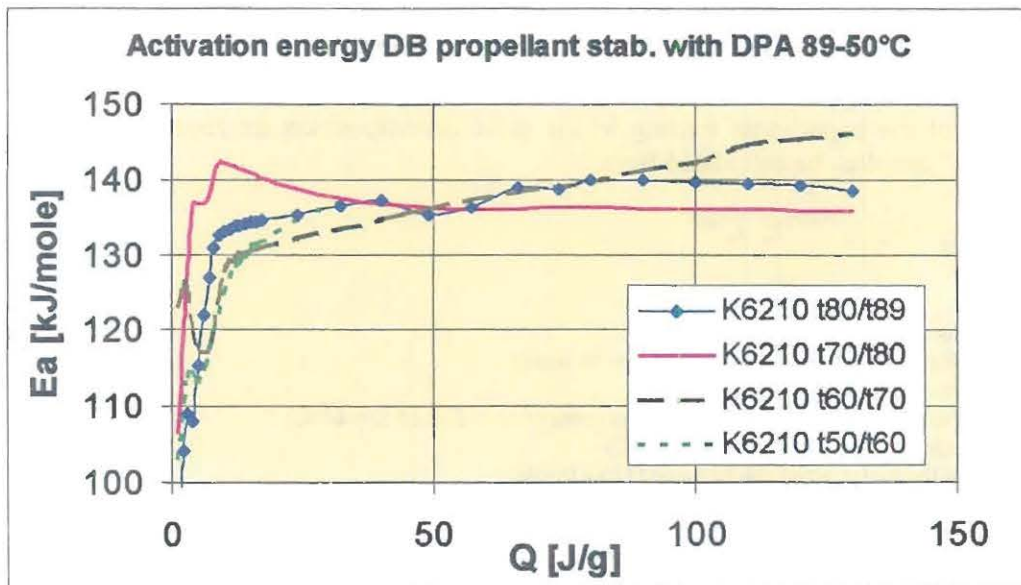


Fig. 11. Activation energy of a DPA stabilised DB propellant between 89°C and 50°C [7]

All HFC measurements reported up to now were carried out starting with fresh samples introduced into the calorimeter at every temperature. Allowing exact "iso- α -evaluation" over a range of decomposition this method is the best. Unfortunately the experiments are extremely time-consuming. An alternative treatment is to age a sample at a higher temperature until a suitable decomposition degree is reached followed by measurements of the same sample at lower temperatures. Since the reaction degree remains nearly constant, the AE can be calculated from temperatures and heat flow values by

$$\ln P = \ln[10^6 * \Delta H * A * f(\frac{Q}{\Delta H})] - \frac{E}{RT} \quad (4)$$

P = heat flow [$\mu\text{W/g}$]
A = frequency factor [s^{-1}]

Measurements of this type with DPA-stabilised SB propellants resulted in two different slopes of the plot (see fig. 12, 13 and 14 and table 5).

Table 5. Activation energy from HFC measurements in SB propellants using hermetically sealed tubes (same samples than in table 4)

Propellant	Lower temperature AE	Higher temperature AE	Temperature of transition ^{a)}
	[kJ/mole]	[kJ/mole]	[°C]
A	88	124	66
B	81	145	65
C	93	136	53

a) Temperature for equal values of both reaction rate constants

Considering all results gained from stabiliser depletion and HFC leads to the conclusion that at least a general transition of AE at lower temperatures is not detectable.

But following the usual philosophy of safety on explosives (If you are not sure, take the worst case) we must assume that a change may exist for some types of propellants. Corresponding to the lowest values found the levels were set at 120 kJ/mole for temperatures above 60°C and at 80 kJ/mole in the range below. Apart from the different temperature dependence the reactions are assumed to be identical below and above 60°C.

The duration of the experiment leading to the same decomposition degree as a ten year's storage at 25°C can then be calculated from ¹

$$t_m = t_{25} * e^{\frac{[E_1 * (\frac{1}{T_m} - \frac{1}{T_{60}}) + E_2 * (\frac{1}{T_{60}} - \frac{1}{T_{25}})]}{R}} \quad (5)$$

t_m = test duration [days]

t_{25} = duration of storage at 25°C (3652.5 d = 10 years)

T_m = test temperature [K]

T_{60} = temperature of change of the activation energy (AE) (333.15 K = 60°C)

T_{25} = storage temperature (298.15 K = 25°C)

E_1 = AE of the higher temperature range (120 kJ/mole)

E_2 = AE of the lower temperature range (80 kJ/mole)

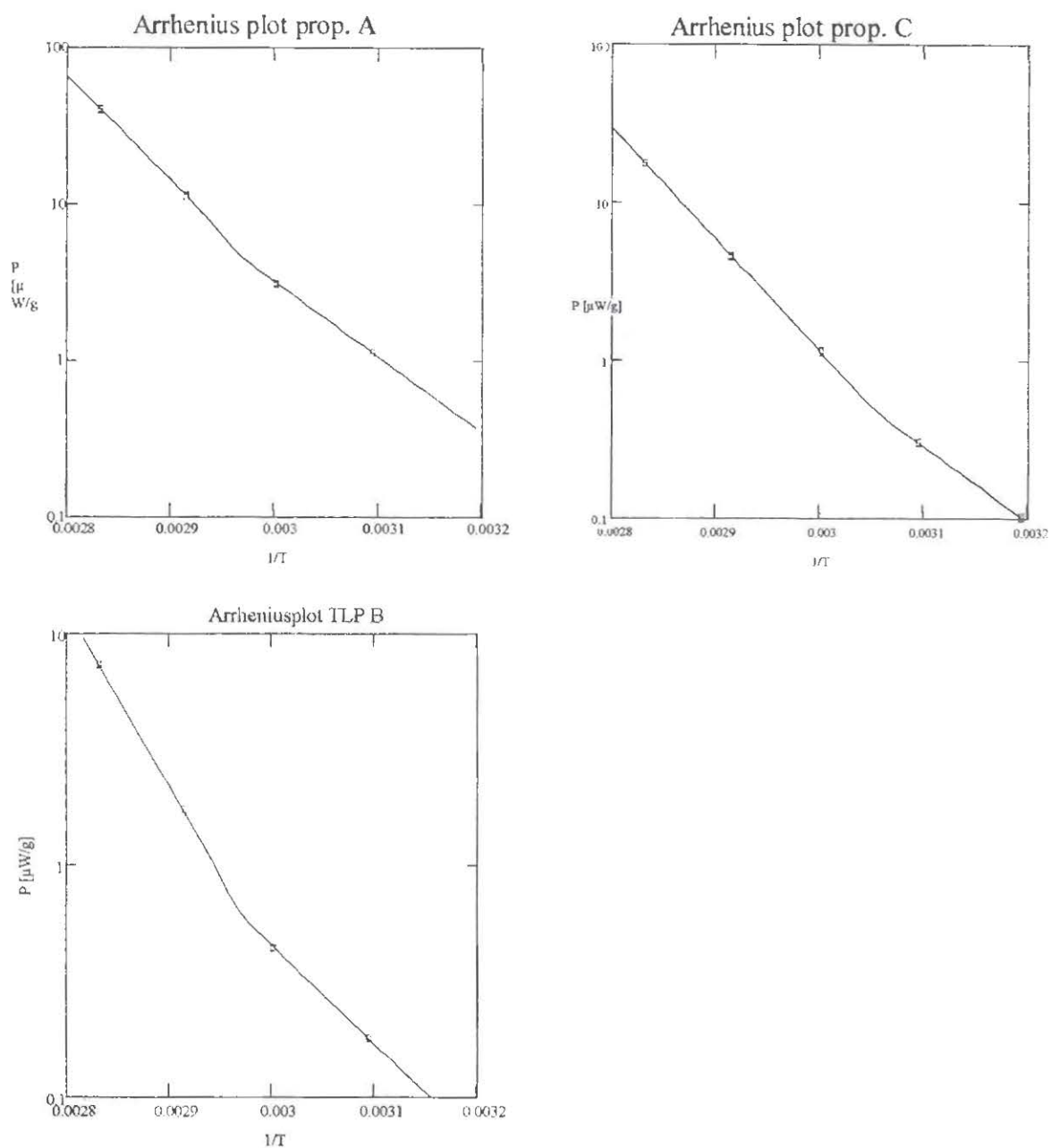
By introduction of the constant values $T_{25} = 298.15$ K, $T_{60} = 333.15$ K and $E_2 = 80$ kJ/mole eq. 5 simplifies to

$$t_m = t_{25} * e^{\frac{E_1}{R} (\frac{1}{T_m} - \frac{1}{T_{60}})} - C \quad (C = 46.713) \quad (6)$$

Taking into consideration different meanings concerning the test temperature the STANAG allows to choose a temperature in the range from 60 to 90°C.

Eq. (6) is used for calculation of the corresponding test duration (see table 6).

¹ For derivation see appendix I



Figures 12-14. Activation energies of three DPA stabilised SB propellants.

Table 6. Test times for different test temperatures

Test temperature [$^{\circ}\text{C}$]	Test time [days]
60	123
65	57,2
70	34,8
80	10,6
89	3,83
90	3,43

4 Assessments for non-isothermal storage

In practice an isothermal storage will never be realised. However, if a temperature and time profile of storage can be predicted, it is possible to check whether the thermal stress will be less or more than a storage at 25°C. For temperatures below 60°C any storage durations can be added up as storage times equivalent to 25°C. An example is given in table 7.

$$t_{25} = t_s * e^{E_2 (1/T_{25} - 1/T_s) / R} \quad (7)$$

T_s = storage temperature [K]
 t_s = storage duration [y]
 t_{25} = storage duration at 298.15 K [y]
 E_2 = 80 kJ/mole

Table 7: Calculation of 25°C times for a storage profile

T_s [°C]	t_s [y]	t_{25} [y]
40	0.1	0.47
35	0.4	1.14
30	1.5	2.55
25	3	3.00
20	4	2.31
15	1	0.33
SUM	10	9.80

5 Limitation of the heat generation

Gained from experiments with very small differences of the test temperature and the temperature in the propellant the extrapolation outlined above is also only valid for a likewise ideal storage. Under unfavourable real conditions however (high temperatures, large diameters and insulating packing material of ammunition) the exothermal decomposition may cause a considerable increase of temperature in the inner parts of the propellant and hence an accelerated ageing. The consequence would be, that the reaction degree might exceed the area controlled in the test and reach probably more dangerous regions. This situation is illustrated in fig. 15.

To prevent this risk a heat generation limit has to be fixed to ensure that the temperature increase in the propellant remains small.

As a most unfavourable system we consider a cartridge of 230 mm diameter, thermally well insulated (thermal transfer 0,001 W/(cm²·K), corresponding for example to a polyethylene package of about 4 cm thickness) and set at a temperature of 71°C. Thermal safety simulations were realised using the heat transfer model of THOMAS [8] in an extended version of OPFERMANN [9,10]. The kinetics were modelled for „strong autocatalysis“ (comparable to propellant „DPA 40%“ in fig. 2), „weak autocatalysis“ (related to propellant „DPA 20%“ in fig. 2) and a zero-order reaction. The equations and parameters used are listed in Appendix 2.

For propellants of the characteristics (strong autocatalysis) a thermal explosion can not be excluded, even at lower temperatures. But the safety is yet guaranteed by the long period of time to reach dangerous conditions. E.g. at 47°C the cartridge needs more than 20 years to explode. For details of the simulations see [12].

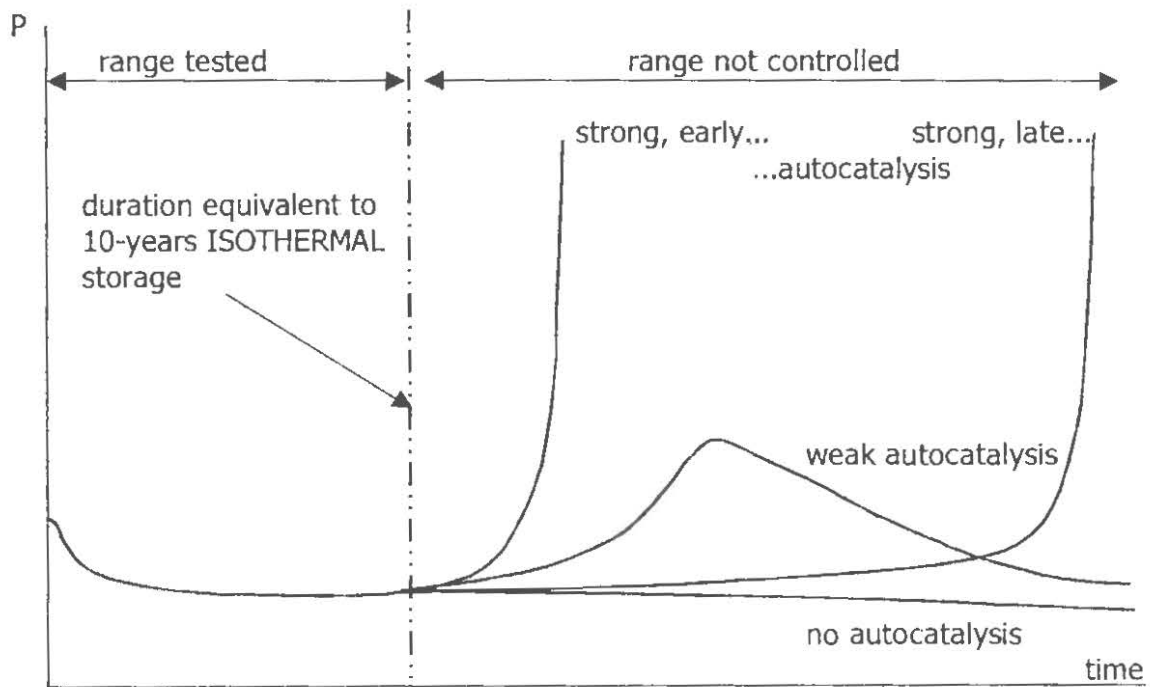


Fig. 15. Possible decomposition mechanisms

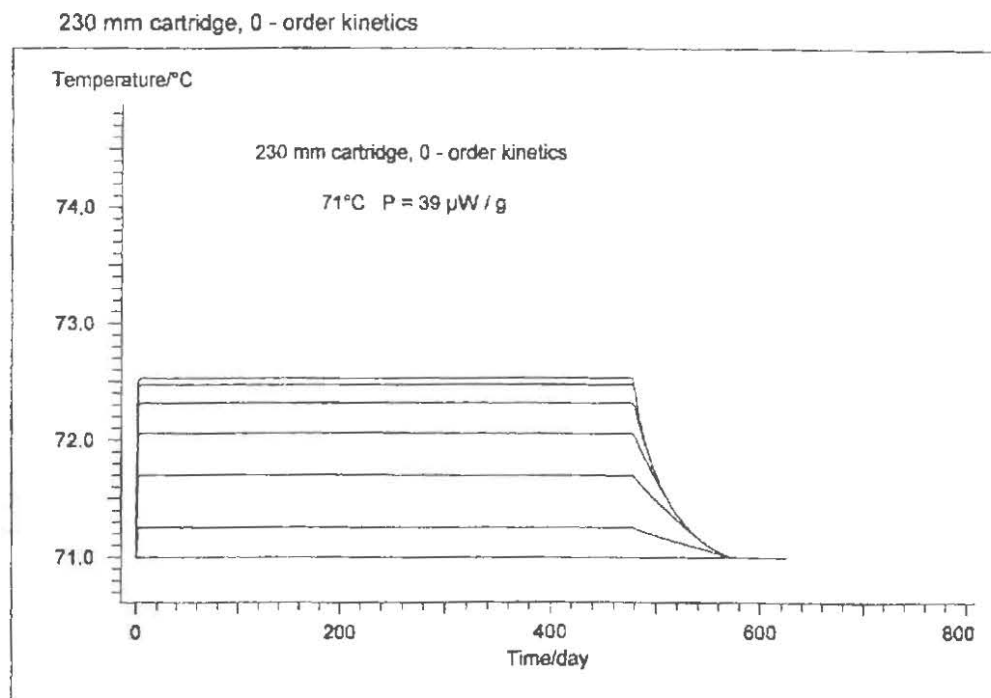


Fig. 16. Simulation of a constant heat generation in a large cartridge

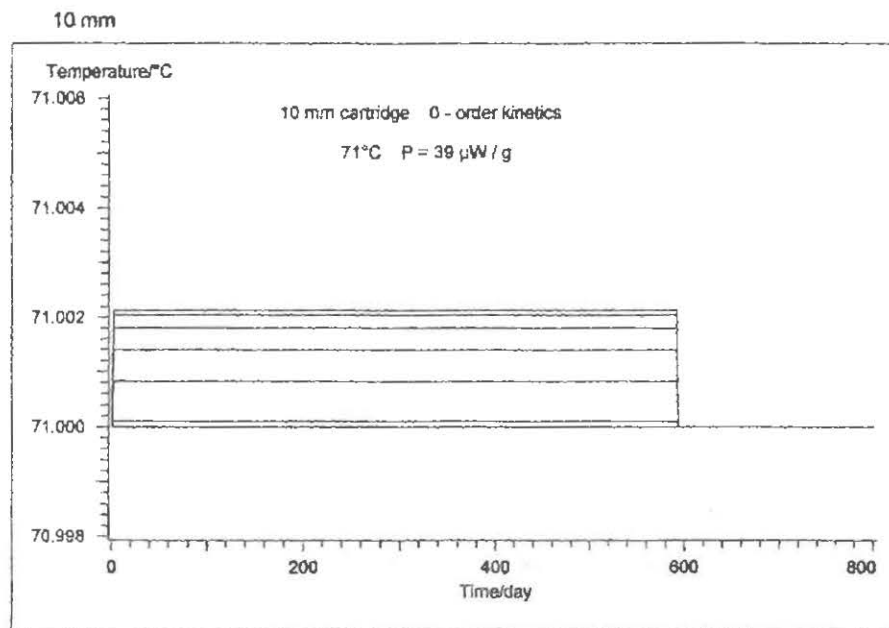


Fig. 17. Simulation of a constant heat generation in a small cartridge

To find a suitable limit for the 230 mm cartridge the heat generation rate was varied by the frequency factor of the zero order reaction. At a level of 39 $\mu\text{W/g}$ the temperature increase in the inner part of the 230 mm cartridge is about 1.5°C, the time for a total reaction is 480 days (fig. 16), in relation to 590 days for an isothermal ageing (fig. 17). This difference is tolerable. Therefore a heat generation limit of 39 $\mu\text{W/g}$ at 71°C can be accepted as sufficient control of ageing in an equilibrium with the ambient temperature even under worst conditions.

An equivalent limit depending on the test temperature chosen is used as a criterion for sufficient chemical stability of a propellant. It can be calculated by

$$P_i = P_{71} * e^{\frac{E_1}{R} \left(\frac{1}{T_{71}} - \frac{1}{T_m} \right)} \quad (8)$$

T_m = test temperature [K]
 $T_{71} = 344.15 \text{ K}$ (= 71°C)
 E_1 = activation energy (120 kJ/mole)
 P_{71} = heat flow limit at 71°C (39 $\mu\text{W/g}$)
 P_i = heat flow limit at T_m [$\mu\text{W/g}$]

Values for some selected temperatures are given in table 8.

Table 8. Heat generation limits for different test temperatures

T_m [°C]	P_i [$\mu\text{W/g}$]	T_m [°C]	P_i [$\mu\text{W/g}$]
60	9.8	80	114
65	18.5	89	314
70	34.5	90	350

In the first part of the measurement some propellants show a fast decreasing exothermic reaction with the locked in air. The total heat of this reaction is small and cannot cause more than a temperature increase of only a few degrees centigrade, even if released momentarily. To disregard this effect the P_i criterion should be used only in the region between the time

corresponding to a heat release of 5 J/g and the test time defined by eq. (6). An example of the evaluation of a test is given in fig. 18.

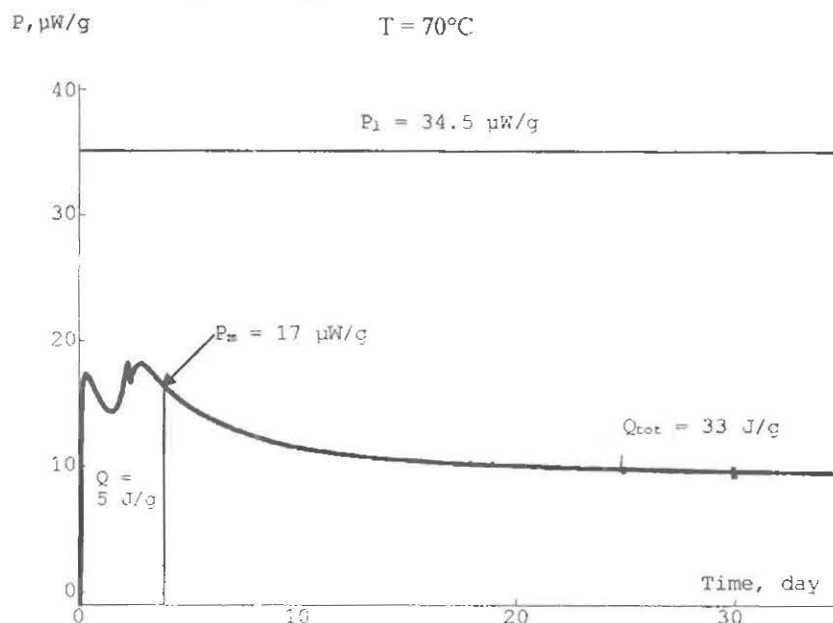


Figure 18. Heat flow curve and evaluation of a DB propellant stabilized with DPA

6 Discussion

While working out this methods some propellants capable of an extremely autocatalytic reaction were found. These propellants can not be expected to remain stable forever, even not if they are used in small calibre ammunition and stored at moderate temperatures. But the safety is guaranteed for a period much longer than usual service life times. To detect certainly the safety life time two parameters were set on very conservative levels:

1. The assumption of a low AE at lower temperatures means that the test duration will be equivalent to a considerably longer storage time at ambient temperatures than the demanded 10 years.
2. The limitation of the tolerable heat generation of the propellant considering a worst case system is a further guarantee that the stress during the service life time will be smaller than in the test.

In consequence the failing criteria of the test are hard, not far away from unfairness. On the other hand until today no qualified propellant ever was found to fail the test, indicating a good quality of manufacture.

7 The actual status of the HFC STANAG 4582

After having laid out the theoretical background [12] and discussed the theory of decomposition kinetics we started to write a draft version of the STANAG in 1999. In permanent discussion with the experts of other countries (many thanks for their contributions) we have finished to complete the draft in September 2000. Some little (most wording) changes have been done since then. The STANAG is now finished in the expert working party and will leave to AC/310 for further discussions. As the theoretical background is very robust and

many recent results of our studies have already been implemented in this draft no big changes of the latest STANAG 4582 draft are to be expected.

8 References and Notes

- [1] STANAG 4527, „Explosives, Chemical Stability, Nitrocellulose based Propellants, Procedure for Assessment of Chemical Life and Temperature Dependence of Stabilizer Consumption“, Draft Edn. 1 (1/98).
- [2] STANAG 4117, „Explosives, Stability Test Procedures and Requirements for Propellants Stabilized with Diphenylamine, Ethyl Centralite or Mixtures of Both“, Edn. 3 (2/98).
- [3] STANAG 4541, „Explosives, Nitrocellulose based Propellants containing Nitroglycerin and Stabilized with Diphenylamine, Stability Test Procedure and Requirements“, Edn. 1 (2/99).
- [4] STANAG 4542, „Explosives, Stability Test Procedure and Requirements for Nitrocellulose based Propellants containing Nitroglycerin and Stabilized with 2-Nitrodiphenylamine“, WG Draft (2/99).
- [5] STANAG 4582, „Explosives, Nitrocellulose Based Propellants, Stability Test Procedure and Requirements using Heat Flow Calorimetry“, WG Draft (2/02).
- [6] U. Ticmanis, G. Pantel, L. Stottmeister, „Stabilitätsuntersuchungen einbasiger Treibladungspulver – Mikrokalorimetrie im Grenzbereich“, *ICT-Jahrestagung* **29**, 27 (1998).
- [7] P. Guillaume, M. Rat, G. Pantel, S. Wilker, „Heat Flow Calorimetry of propellants – Effects of sample preparation and Measuring Conditions“, *Propellants, Explosives, Pyrotechnics* **26**, 51-57 (2001).
- [8] P.H. Thomas, *Trans. Faraday Soc.* **54**, 60-65 (1942).
- [9] J. Opfermann, Manual for the Computer Program „Netzsch Thermal Safety Simulation“, Edn. **1993**.
- [10] U. Ticmanis, G. Pantel, M. Kaiser, „Simulation der chemischen Stabilität eines zwei-basigen Kugelpulvers“, *2. Int. Workshop Mikrokalorimetrie WIWEB*, p. 182-195 (1999).
- [11] J. Petržílek, J. Skládal, S. Wilker, G. Pantel, L. Stottmeister, „Stability analysis of propellants containing new stabilisers – Part I“, *ICT Jahrestagung* **31**, 61 (2000).
- [12] U. Ticmanis, S. Wilker, G. Pantel, M. Kaiser, P. Guillaume, C. Balès, N. v.d.Meer, „Principles of a STANAG for the estimation of the chemical stability of propellants by heat flow calorimetry“, *ICT Jahrestagung* **31**, 2 (2000).

Appendix 1

Calculation of the measuring time

A reaction formulated in the heat flow form is given by

$$\frac{dQ}{dt} = \Delta H * f\left(\frac{Q}{\Delta H}\right) * A * e^{-E/(RT)} \quad (9)$$

Q	= Heat released	ΔH	= Total reaction heat
t	= Reaction time	T	= Temperature of reaction [K]
dQ/dt	= Reaction rate (heat flow)	Q/ ΔH	= Reaction degree
A	= Frequency factor	E	= Activation energy [kJ/mole]
R	= Gas constant		
f(Q/ ΔH)	= Function of describing the dependence of the reaction rate from the reaction degree		

If T_m is the measuring temperature, Q_m the heat released at the end of the measurement, E1 the AE dominating at higher temperatures, then after separation of the variables, integration at constant temperature and rearrangement the reaction time t_m is obtained by

$$t_m = \frac{1}{\Delta H * A} * \int_0^{Q_m} \frac{dQ}{f(Q/\Delta H)} * e^{E_1/(R*T_m)} \quad (10)$$

The time t_{60} to reach the same decomposition Q_m at the assumed temperature (T_{60}) of change of AE can equally be calculated from

$$t_{60} = \frac{1}{\Delta H * A} * \int_0^{Q_m} \frac{dQ}{f(Q/\Delta H)} * e^{E_1/(R*T_{60})} \quad (11)$$

The value of the integral in eqns. 10 and 11 is unknown but equal. Therefore by division and rearrangement eq. 12 results:

$$t_m = t_{60} * e^{[E_1 * (1/T_m - 1/T_{60})]/R} \quad (12)$$

If the change of AE is assumed to occur sharply at 60°C an equation similar to eq. 12 is also valid for E2, the AE dominating the lower temperature range.

$$t_{60} = \frac{1}{\Delta H * A} * \int_0^{Q_m} \frac{dQ}{f(Q/\Delta H)} * e^{E_2/(R*T_{60})} \quad (13)$$

The corresponding time t_{25} for 25°C (T_{25}) is

$$t_{25} = \frac{1}{\Delta H * A} * \int_0^{Q_m} \frac{dQ}{f(Q/\Delta H)} * e^{E_2/(R*T_{25})} \quad (14)$$

Division of eqns. 13 and 14 gives after rearrangement

$$t_{60} = t_{25} * e^{[E_2 * (1/T_{60} - 1/T_{25})]/R} \quad (15)$$

Combination of eq. 12 and 15 results in

$$t_m = t_{25} * e^{[E_1 * (\frac{1}{T_m} - \frac{1}{T_{60}}) + E_2 * (\frac{1}{T_{60}} - \frac{1}{T_{25}})]/R} \quad (5)$$

Appendix 2

Data used for thermal safety simulations

Kinetics for modelling propellant decompositions

$$a) \text{ n - order reaction} \quad P = \Delta H * k * 10^6 * [1 - (1 - n) * kt]^{n/(1-n)} \quad (16)$$

$$b) \text{ 1st order with autocatalysis} \quad P = \Delta H * a^2 * k * 10^6 * \frac{e^{akt}}{(e^{akt} - 1 + a)^2} \quad (17)$$

$$c) \text{ Avrami - Erofeev reaction} \quad P = \Delta H * k * 10^6 * [(1 - p)kt]^{p/(1-p)} * e^{-[(1-p)kt]^{1/(1-p)}} \quad (18)$$

$$d) \text{ Prout - Tompkins reaction} \quad P = \Delta H * 10^6 * \left(\frac{1-Q}{\Delta H}\right)^n * \left(\frac{Q}{\Delta H}\right)^p * k \quad (19)$$

$$k = A * e^{-AE/RT}$$

For 1st and zero-order reaction: n = 1.0001 and n = 0 in eq. (16).

Kinetics for „strong autocatalysis“ were modelled by three independent reactions. For „weak autocatalysis“ four reactions were used. Their parameters are listed below.

Type	Reaction (eq)	log A [A in s ⁻¹]	AE [kJ/mole]	n	log a	p	ΔH [J/g]
„strong	(16)	14,7817	140	1,0001	-	-	46,0
autocata-	(18)	14,9984	140	-	-	0,67	28,7
lytic"	(17)	9,9119	140	-	5	-	61106
	(16)	5,3743	80	1,0001	-	-	46,0
	(18)	5,5910	80	-	-	0,67	28,7
	(17)	0,5045	80	-	5	-	61106
„weak	(16)	14,0776	136	0,6446	-	-	104,9
autocata-	(16)	13,4177	127	0,1583	-	-	-18,3
lytic"	(16)	14,0484	127	0,5372	-	-	2,7
	(19)	14,1993	139	5,4568	-	0,6821	4000
constant	(16)	variable	140	0	-	-	2000

Other propellant data:

Form of reactor: cylindrical
 Specific heat (C_p): 0,205 + 0,00325 T [J/(g·K)]
 Heat conductivity: 0,00122 W/(cm·K)
 Loading density: 1 g/cm³
 Explosion temperature: 170°C

THIS PAGE LEFT INTENTIONAL BLANK

Attendee List

Mr. Eduardo Alvarez

INSTITUTO DE INVESTIGACIONES Y CONTROL
(IDIC)
AV. PEDRO MONTT. N
SANTIAGO, CHILE
SOUTH AMERICA

Phone: 56 - 2 - 5207775
Fax: 56 - 2 - 5207885
E-mail: idic@tnet.cl

Mr. Wong Fun Ark

US ARMY TACOM-ARDEC
BUILDING 3028 AMSTA-AR-WEE-E
PICATINNY ARSENAL NJ 07806-5000

Phone: (973) 724-5053
Fax: (973) 724-3711
E-mail: fark@pica.army.mil

Mr. Juan Arroyo

INSTITUTO DE INVESTIGACIONES Y CONTROL
(IDIC)
AV. PEDRO MONTT. N
SANTIAGO, CHILE
SOUTH AMERICA

Phone: 56 - 2 - 5207775
Fax: 56 - 2 - 5207885
E-mail: idic@tnet.cl

Dr. Robert Babcock

UNIVERSITY OF ARKANSAS
3202 BEC
FAYETTEVILLE AR 72701

Phone: 501-575-5410
Fax: 501-575-7926
E-mail: reb@engr.uark.edu

Mr. Steve Backer

COMMANDER
CRANE DIVISION
300 HWY 361
CRANE IN 47522-5001

Phone: (812) 854-5467
Fax: (812) 854-1198
E-mail: backer_steve@crane.navy.mil

Mr. John Backes

NSWC INDIAN HEAD
PO BOX 0160
BLDG 1346 CODE 702
NAVAL WEAPONS STATION
YORKTOWN, VA 23691-0160

Phone: (757) 887-4683
Fax: (757) 887-4466
E-mail: backesjm@ih.navy.mil

Attendee List

Ms. Carole Baker

DEFENSE ORDNANCE SAFETY GROUP MOD
ABBAY WOOD
BRISTOL
UNITED KINGDOM

Phone: 11791 35816
Fax: 11791 35903
E-mail: dosgst1a1@dpa.mod.uk

Dr. Kai Ballentin

NICO PYROTECHNIK HANNS-JUERGEN
DIEDERICHS GmbH & CO KG
BEI DER FEUERWERKEREI #4
22946 TRITTAU
GERMANY

Phone: +49(0)4154/805-257
Fax: +49(0)4154/805-222
E-mail: k.ballentin@nico-pyro.de

Dr. Peter Barnes

DEFENSE ORDNANCE SAFETY GROUP MOD
ABBAY WOOD
BRISTOL
UNITED KINGDOM

Phone: 44-11791-35437
Fax: 44-11791-31920
E-mail: DOSGST6@dpa.mod.uk

Mr. Juan Berrios

NSWC INDIAN HEAD
101 STRAUSS AVE
BUILDING 1557
INDIAN HEAD MD 20640-5035

Phone: 301-744-2322
Fax: 301-744-4881
E-mail: berriosj@ih.navy.mil

Dr. Manfred Bohn

FRAUNHOFER-INSTITUT FUR CHEMISCHE
TECHNOLOGIE
POSTFACH 1240
D-76318 PFINTAL-BERGHAUSEN
GERMANY

Phone: +49-721-4640-162
Fax: +49-721-4640-111
E-mail: bo@ict.fhg.de

Dr. William Bryant

COMMANDER
INDIAN HEAD DIVISION
NAVAL SURFACE WARFARE CENTER
101 STRAUSS AVENUE
INDIAN HEAD MD 20640-5035

Phone: (301) 744-4580
Fax: (301) 744-4865
E-mail: bryantwf@ih.navy.mil

Attendee List

Prof. Edward Charsley

CENTRE FOR THERMAL STUDIES
SCHOOL OF APPLIED SCIENCES
UNIVERSITY OF HUDDERSFIELD
QUEENSGATE HUDDERSFIELD HD1 3DH
UNITED KINGDOM

Phone: 01484 473178
Fax: 01484 473179
E-mail: e.l.charsley@hud.ac.uk

Mr. Sammy Chevalier

SNPE LEBOUCHET RESEARCH CENTER
917 O VERT LE PETIT
FRANCE

Phone: +33 07 64 99 1369
Fax: (33) 0 64 99 7556
E-mail: s.chevalier@snpe.com

Dr. Anton Chin

COMMANDER
CRANE DIVISION
300 HWY 361
CRANE IN 47522-5001

Phone: (812) 854-6954
Fax: (812) 854-1747
E-mail: chin_anton@crane.navy.mil

Mr. Don Christy

COMMANDER
CRANE DIVISION
300 HWY 361
CRANE IN 47522-500

Phone: 812 854-3828
Fax: 812 854-3930
E-mail: christy_d@crane.navy.mil

Ms. Riza Cruz

ST. MARKS POWDER
A GENERAL DYNAMICS COMPANY
P.O. BOX 222
ST. MARKS, FL
32355

Phone: (850) 577-2315
Fax: (850) 577-2351
E-mail: rcruz@stm.gd-ots.com

Dr. Wim de Klerk

TNO-PRINS MAURITS LABORATORY
PO BOX 45
2280 AA RIJSWIJK
THE NETHERLANDS

Phone: +31 15 284 3580
Fax: +31 15 284 3958
E-mail: klerk@pml.tno.nl

Attendee List

Mr. David Deetz

ARDEC-WECAC
PROPULSION RESEARCH & TECHNOLOGY
BUILDING 3124
PICATINNEY ARSENAL
PICATENNY, NJ 07806-5000

Phone: 973-724-3114
Fax: 973-724-4708
E-mail: ddeetz@pica.army.mil

Ms. Jerrilee deGeus

NATO SEASPARROW PROJECT (CODE N-4051)
727 S. 23rd St.
ARLINGTON, VA 22202

Phone: (703) 607-7200 ext 132
Fax: (703) 607-7203
E-mail: degeusj@navsea.navy.mil

Mr. Joseph Domanico

EDGEWOOD CB CENTER
BLDG E3580 BEACH PT RD
AMSSB-REN-SP
ABERDEEN PROVING GROUND MD 21010-5424

Phone: (410) 436-2180
Fax: (410) 436-4941
E-mail: joseph.domanico@sbccom.apgea.army.mil

Mr. Daniel Ellison

COMMANDER
CRANE DIVISION
300 HWY 361
CRANE IN 47522-5001

Phone: (812) 854-5502
Fax: (812) 854-5054
E-mail: ellison_dan@crane.navy.mil

Mr. Harry Farmer

COMMANDER
CRANE DIVISION
300 HWY 361
CRANE IN 47522-5001

Phone: (812) 854-6950
Fax: (812) 854-3281
E-mail: farmer_harry@crane.navy.mil

Mr. Cabot Faultless

COMMANDER
CRANE DIVISION
300 HWY 361
CRANE IN 47522-5001

Phone: (812) 854-2868
Fax: (812) 854-5054
E-mail: faultless_cabot@crane.navy.mil

Attendee List

Mr. Kevin Fisher

COMMANDER
CRANE DIVISION
300 HWY 361
CRANE IN 47522-6001

Phone: (812) 854-3562
Fax:
E-mail: fisher_kl@crane.navy.mil

Ms. Saw Geok Lay

CHARTERED AMMUNITION INDUSTRIES P/L
601 RIFLE RANGE ROAD
S'PORE 588398

Phone: 65-4665 7 22 EXT 173 OR 165
Fax: 65-4693842
E-mail: sawgl.kinetics@stengg.com

Dr. Lee Gilman

THERMOMETRIC, INC.
9307 MONROE ROAD, SUITE G
CHARLOTTE NC 28270-1485

Phone: 704-841-7230
Fax: 704-841-2128
E-mail: lbg@thetadyne.com

Dr. Trevor Griffiths

QINETIQ, BLD R47
FORT HALSTEAD
SEVENOAKS
KENT TN14 7BP
UNITED KINGDOM

Phone: 44-1959-515347
Fax: 44-1959-516065
E-mail: ttgriffiths@qinetiq.com

Dr. Pierre Guillaume

PB CLERMONT SA
RUE DE CLERMOUT 176
B4480 ENGIS
BELGIUM

Phone: (+32) 4 273 8282
Fax: (+32) 4 273 8250
E-mail: p.guillaume@pbclermont.be

Mr. Jerry Hahin

COMMANDER
CRANE DIVISION
300 HWY 361
CRANE IN 47522-5001

Phone: (812) 854-5652
Fax: (812) 854-5364
E-mail: hahin_jerry@crane.navy.mil

Mr. Darwin Harting

INDIANA ORDNANCE WORKS INC.
11452 HIGHWAY 62
CHARLESTOWN, INDIANA 47111

Phone: 812 256-4478
Fax: 812 256-4617
E-mail: dharting@iglou.com

Attendee List

Dr. Bill Hubble

COMMANDER
CRANE DIVISION
300 HWY 361
CRANE IN 47522-5001

Phone: (812) 854-4053
Fax:
E-mail: hubble_bill@crane.navy.mil

Ms. Heather Hudson

COMMANDER
U.S. ARMY AVIATION & MISSILE COMMAND
ATTN: AMSAM-RD-PS-S
REDSTONE ARSENAL
ALABAMA
35898

Phone: (256)313-6470
Fax: (256) 842-2079
E-mail: heather.hudson@redstone.army.mil

Mr. Jack Johnston

NSWC INDIAN HEAD, YORKTOWN DETACHMENT
P.O. DRAWER 160
CODE 240B
YORKTOWN, VIRGINA, 23691-0160

Phone: 757 887-4763 x20
Fax: 747 887-4766
E-mail: johnstonjl@ih.navy.mil

Dr. David Jones

CANADIAN EXPLOSIVES RESEARCH
LABORATORY
NATURAL RESOURCES CANADA
555 BOOTH ST
OTTAWA
ONTARIO K1A 0G1
CANADA

Phone: (613) 995-2140
Fax: (613) 995-1230
E-mail: djones@nrcan.gc.ca

Ms. Lara Kimble

COMMANDER
CRANE DIVISION
300 HWY 361
CRANE IN 47522-5001

Phone: (812) 854-1543
Fax: (812) 854-3461
E-mail: kimble_l@crane.navy.mil

Dr. Jun-Ichi Kimura

JAPAN KAYAKU RESEARCH: JK RESEARCH
29-45 CHIGUSADAI, AOBA-KU,
YOKOHAMA
227-0051
JAPAN

Phone: +81-45-972-9516
Fax: +81-45-972-9518
E-mail: jkr@ym.catv.ne.jp

Attendee List

Mr. David Lee

NSWC INDIAN HEAD
101 STRAUSS AVE
BUILDING 1865
INDIAN HEAD MD 20640-5035

Phone: (301) 744-4521
Fax: (301) 744-6223
E-mail: leedd@ih.navy.mil

Dr. Michael Lesley

ATK THIOKOL PROPULSION
PO BOX 707
BRIGHAM CITY UT 84302

Phone: (435) 863-5854
Fax: (435) 863-2271
E-mail: michael.lesley@atk.com

Dr. Louis-Simon Lussier

DEFENSE RESEARCH ESTABLISHMENT
VALCARTIER
2459 PIE XI NORTH
VAL-BELAIR QC CANADA G3J1X5

Phone: 418-844-4373 ext. 4373
Fax: 418-844-4646
E-mail: louis-simon.lussier@drev.dnd.ca

Ms. Nancey Maegerlein

COMMANDER
CRANE DIVISION
300 HWY 361
CRANE IN 47522-5001

Phone: (812) 854-5506
Fax: (812) 854-5054
E-mail: maegerlein_nancey@crane.navy.mil

Dr. Robert Maxwell

LAWRENCE LIVERMORE NATIONAL
LABORATORY
MAIL CODE L-091
LIVERMORE CA 94550

Phone: 925 423-4991
Fax: 925 423-8772
E-mail: maxwell7@llnl.gov

Dr. Indu Mishra

CPA, THE JOHNS HOPKINS UNIVERSITY
10630 LITTLE PATUXENT PWY SUITE 202
COLUMBIA MD 21044

Phone: (410) 992-9951 ext 209
Fax: (410) 730-4969
E-mail: imishra@cpia.jhu.edu

Dr. Dietmar Mueller

JOSEPH-VON-FRAUNHOFER-STR. 7
D-76327 PFINTAL (BERGHAUSEN)
GERMANY

Phone: 49-721-4640386 or 0
Fax: 49-721-4640-770
E-mail: mue@ict.fhg.de

Attendee List

Mr. John (JC) Myers

CCI CORP
46915 S. SHANGRI-LA DRIVE
LEXINGTON PARK
MARYLAND
20653

Phone: (301) 866-0078 EXT 266
Fax: (301) 866-1776
E-mail: jmyers@lxpk.cccorp.com

Mr. Greg Nelson

CALORIMETRY SCIENCES CORP
155 WEST 2050 NORTH
SPANISH FORK UT 84660

Phone: 801-794-2600
Fax: 801-794-2600
E-mail: gnelson@calscorp.com

Mr. John Niehaus

COMMANDER
CRANE DIVISION
300 HWY 361
CRANE IN 47522-500

Phone: 812 854-1476
Fax:
E-mail: niehaus_john@crane.navy.mil

Mr. Jesper Nielsen

DANISH ARMY MATERIEL COMMAND
55 ARSENALVEJ
DK-9800 HJOERRING

Phone: 45-99-24-16-41
Fax: 45-99-24-16-29
E-mail: jn.damc@mil.dk

Mr. Miles Olson

COMMANDER
CRANE DIVISION
300 HWY 361
CRANE IN 47522-5001

Phone: 812 854-3917
Fax: 812 854-3930
E-mail: olson_m@crane.navy.mil

Mr. Luis Ortega

COMMANDER
CRANE DIVISION
300 HWY 361
CRANE IN 47522-5001

Phone: (812) 854-6313
Fax: (812) 854-1198
E-mail: ortega_luis@crane.navy.mil

Mr. Jose Ortiz

NSWC INDIAN HEAD
101 STRAUSS AVE
CODE JP11
INDIAN HEAD MD 20640-5035

Phone: (301) 744-6606
Fax: (301) 744-6606
E-mail: ortizje@ih.navy.mil

Attendee List

Mrs. Hazel Schalkwyk

NASCHEM (A DIVISION OF DENEL)
PRIVATE BAG X1254
POTCHEFSTROOM
2520 SOUTH AFRICA

Phone: +27-18-2998917
Fax: +27-18-2981026
E-mail: hazel@naschem.denel.co.za

Mrs. Helge Schimansky

SOMCHEM DIV OF DENEL
PO BOX 187
SOMERSET WEST
7129 SOUTH AFRICA

Phone: +27 +21-850 2889
Fax: +27 +21 - 850 2992
E-mail: helges@somchem.denel.co.za

Mr. David Schulte

COMMANDER
CRANE DIVISION
300 HWY 361
CRANE IN 47522-5001

Phone: 812 854-3418
Fax: (812) 854-3014
E-mail: schulte_david@crane.navy.mil

Ms. Karen Shaw

GEO-CENTERS INC
BUILDING 3028
PICATINNY ARSENAL NJ 07806

Phone: (973) 366-0712
Fax: (973) 366-4552
E-mail: kshaw@pica.army.mil

Mr. David Sherfick

COMMANDER
CRANE DIVISION
300 HWY 361
CRANE IN 47522-5001

Phone: 812 854-6972
Fax:
E-mail: sherfick_dave@crane.navy.mil

Dr. Ahmed "Ed" Soliman

SETARAM, INC.
130 GAITHER DR SUITE 116
MT LAUREL NJ 08054

Phone: 502-253-2226
Fax: 502-253-2228
E-mail: soliman@setaram.com

Mr. Mark Springer

U.S. ARMY PINE BLUFF ARSENAL
PINE BLUFF AR
71602-9500

Phone: 870-540-2960
Fax: 870-540-2964
E-mail: mark.springer@pba.army.mil

Attendee List

Mr. Lars-Gunnar Svensson

BODYCOTE MATERIALS TESTING CMK
GAMMALBACKAVAGEN 6
SE-691 27 KARLSKOGA
SWEDEN

Phone: +46 586 816 05
Fax: +46 586 585 15
E-mail: svensson.l-g@bodycote-mt.com

Ms. Anna Tan

CHARTERED AMMUNITION INDUSTRIES PTE LTD
601 RIFLE RANGE ROAD
S'PORE 588398

Phone: 65-64609165
Fax: 065-64603842
E-mail: tananna.kinetics@stengg.com

Mr. Bill Taylor

COMMANDER
CRANE DIVISION
300 HWY 361
CRANE IN 47522-5001

Phone: 812 854-5192
Fax: 812 854-1198
E-mail: taylor_w@crane.navy.mil

Dr. Uldis Ticmanis

WIWEB AUBENSTELLE HEIMERZHEIM
GROBES CENT
53913 SWISTTAL
GERMANY

Phone: 49 - 2222 - 60081
Fax: 49 - 2222 - 1852
E-mail: uldisticmanis@bwb.org

Mr. Steve Turpen

COMMANDER
CRANE DIVISION
300 HWY 361
CRANE IN 47522-5001

Phone: 812 854-3986
Fax:
E-mail:

Dr. Irmeli Tuukkanen

DEFENSE FORCES MATERIEL COMMAND
HEADQUARTERS
PO BOX 69
FIN-33541 TAMPERE
FINLAND

Phone: +358 3 181 55985
Fax: +358 3 181 55915
E-mail: irmeli.tuukkanen@dme.mil.fi

Attendee List

Mr. Japie Venter

NASCHEM (A DIVISION OF DENEL)
PRIVATE BAG X1254
POTCHEFSTROOM
2520 SOUTH AFRICA

Phone: +27-18-2998920
Fax: +27-18-2981026
E-mail: japiev@naschem.denel.co.za

Dr. Beat Vogelsanger

NITROCHEMIE WIMMIS AG
CH-3752, WIMMIS,
SWITZERLAND

Phone: +41 33 228 12 01
Fax: +41 33 228 13 30
E-mail: beat.vogelsanger@nitrochemie.com

Mr. Randy Weese

LAWRENCE LIVERMORE NATIONAL
LABORATORY
PO BOX 808 BUILDING 191 L-282
LIVERMOORE CA 94551

Phone: (925) 424-3165
Fax: (925) 424-3281
E-mail: weese2@llnl.gov

Ms. Karen Whorral

COMMANDER
CRANE DIVISION
300 HWY 361
CRANE IN 47522-5001

Phone: (812) 854-5420
Fax: (812) 854 5364
E-mail: whorral_karen@crane.navy.mil

Mr. James (JAWS) Wilson

SAIC
RR 6 BOX 28
BLOOMFIELD, INDIANA 47424

Phone: (812) 384-4308
Fax: (812) 384-3744
E-mail: jaws@bluemarble.net

Dr. David Wood

QINETIQ BISHOPTON
STATION ROAD
BISHOPTON
RENFREWSHIRE
PA7 5NJ
SCOTLAND

Phone: 44-1505-832082
Fax: 44-1505-862065
E-mail: djwood2@qinetiq.com

THIS PAGE LEFT INTENTIONAL BLANK